Proceedings of the Second PRC-US Workshop on Seismic Analysis and Design of Special Bridges

Edited by

George Lee
Multidisciplinary Center for Earthquake Engineering Research
University at Buffalo, State University of New York
Buffalo, New York

Lichu Fan
State Key Laboratory for Disaster Reduction in Civil Engineering
Tongji University
Shanghai, China

MCEER
MULTIDISCIPLINARY CENTER FOR EARTHQUAKE ENGINEERING RESEARCH
A National Center of Excellence in Advanced Technology Applications

ISSN 1520-295X

Technical Report MCEER-04-0006
June 25, 2004

This workshop was held December 3-5, 2003 in Buffalo, New York and was supported by the Federal Highway Administration under contract number DTFH61-98-C-00094.

TONGJI UNIVERSITY 1907

NOTICE

This report was jointly prepared by Tongji University and the Multidisciplinary Center for Earthquake Engineering (MCEER) as a result of research sponsored by the Multidisciplinary Center for Earthquake Engineering Research (MCEER) through a contract from the Federal Highway Administration. Neither MCEER, associates of MCEER, its sponsors, Tongji University, nor any person acting on their behalf:

a. makes any warranty, express or implied, with respect to the use of any information, apparatus, method, or process disclosed in this report or that such use may not infringe upon privately owned rights; or

b. assumes any liabilities of whatsoever kind with respect to the use of, or the damage resulting from the use of, any information, apparatus, method, or process disclosed in this report.

Any opinions, findings, and conclusions or recommendations expressed in this publication are those of the author(s) and do not necessarily reflect the views of MCEER or the Federal Highway Administration.

Proceedings of the Second PRC-US Workshop on Seismic Analysis and Design of Special Bridges

Held at
The Marriott Hotel
Buffalo, New York
December 3-5, 2003

Edited by
George C. Lee[1] and Li-Chu Fan[2]

Publication Date: June 25, 2004

Technical Report MCEER-04-0006

Workshop Steering Committee
Lichu Fan, SLDRCE, Tongji University
Mengling Lou, Tongji University
Weigang Bao, PRC Ministry of Communication
George Lee, MCEER, University at Buffalo
Ian Buckle, University of Nevada, Reno
W. Phillip Yen, Federal Highway Administration

FHWA Contract Number DTFH61-98-00094

1 Samuel P. Capen Professor of Civil Engineering, Department of Civil, Structural and Environmental Engineering, and the Multidisciplinary Center for Earthquake Engineering Research, University at Buffalo, State University of New York
2 Professor, State Key Laboratory for Diasaster Reduction in Civil Engineering, Tongji University, Shanghai, PRC

MULTIDISCIPLINARY CENTER FOR EARTHQUAKE ENGINEERING RESEARCH
University at Buffalo, State University of New York
Red Jacket Quadrangle, Buffalo, NY 14261

Participants at the US-PRC Workshop on Earthquake Engineering for Highway Bridges

Preface

This seismic analysis and design of special bridges (SADSB) workshop series is based on a Memorandum of Understanding (MOU) between the Multidisciplinary Center for Earthquake Engineering Research (MCEER), University at Buffalo, State University of New York, Buffalo, New York and the State Key Laboratory for Disaster Reduction in Civil Engineering (SLDRCE), Tongji University, Shanghai China. The MOU was signed by Professor George C. Lee of MCEER and Professor Lichu Fan of SLDRCE on May 26 2001, and resulted from the PRC-US earthquake engineering and earthquake disaster mitigation collaboration project. Four international workshops will be carried out in China and US between 2002-2005, alternating locations each year. In the U.S., the series is sponsored by the Federal Highway Administration.

The purpose of these workshops is to share technical information and construction experience in the seismic design and performance of "special" highway bridges. For the purpose of these meetings, "special" bridges include major long span bridges as well as those with small to moderate spans with complex geometries or sited on particularly hazardous sites. The long-term objective is to develop a knowledge base, from which guidelines for these unique structures can be developed.

The second workshop was held December 3-5, 2003 in Buffalo, New York. A total of 26 participants, 18 from the U.S. and eight from China, attended this workshop. These proceeding contain 23 papers covering a wide range of research fields, and include a summary of research needs and recommendations from the workshop participants. Of the 23 papers, three were not presented orally at the workshop due to scheduling problems.

The first workshop was held on October 8 - 10, 2002 at Tongji University in Shanghai.

Contents

Contents (continued)

Caltrans' Seismic Design Criteria

Mark S. Mahan and Richard D. Land

ABSTRACT

Most of the established design codes tend to be comprehensive in nature and cover as much of the bridge engineering practice as possible. However, the Seismic Design Criteria (SDC, Version 1.2, December 2001) used by the California Department of Transportation (Caltrans) has been published with the unique purpose of addressing only a narrow class of bridge structures, namely "New Ordinary Standard" bridges. By using the SDC the bridge engineer has the opportunity to fit the design within the framework of Ordinary Standard bridges and thus take advantage of the numerous component and system tests performed for Caltrans by various universities. In such bridge systems the structural elements are proportioned such that "plastic hinges" are formed in columns and shafts. All other components of the bridge system are "capacity protected" to create a predictable system with quantifiable energy absorption characteristics. The class of bridges designed to the SDC standards tends to be more uniform. Flexible structural systems such as ductile frames are encouraged, while shear systems, such as pier walls, are discouraged.

Mark. S. Mahan, Ph.D., P.E., (Author), Senior Bridge Engineer, California Department of Transportation, Sacramento, CA, 95816-8041, USA
Richard D. Land, P.E., (Editor), State Bridge Engineer, California Department of Transportation, Sacramento, CA, 95816-8041, USA

INTRODUCTION

Major changes in the California Department of Transportation's (Caltrans) seismic design practice have occurred in the aftermath of the Loma Prieta Earthquake of October 1989. New tools and procedures were developed culminating in new Seismic Design Criteria (SDC), which has been adopted as the seismic code at Caltrans addressing "New Ordinary Standard" bridges. The design engineer typically finds it most expedient to apply the SDC in parallel with service load design as member sizing, stiffness, strength, and frame layout must satisfy both concerns. Other bridge systems not covered by SDC require project specific design criteria. Most project engineers obtain approval of project specific design criteria by providing design requirements that exceed the minimum requirements of the SDC.

Component and system testing at various universities generated a substantial database of bridge component behavior, documented in terms immediately useable by practicing bridge engineers. The SDC takes advantage of this wealth of information and encourages design engineers to follow the rules of "capacity" and "ductility" design. Ongoing research for critical seismic issues such as abutments, connections, and soil-pile interaction continues to enhance the knowledge base, which contributes to the refinement of the SDC.

In general, recent changes in the seismic design practice employed at Caltrans have affected three aspects of ductility design, namely, confinement, continuity, and balance. The purpose of this paper is to describe these requirements and illustrate how they have been applied to engineering practice by providing a design example.

DESIGN EXAMPLE: SALINAS RIVER BRIDGE

The January 1997 flooding along the Salinas River resulted in major damage to the North Bound Salinas River Bridge originally built in 1938. The foundation at Pier 13 was undermined due to excessive scouring causing the pier to uniformly settle approximately 700 mm. This created rotation at Pier 12 as Spans 12 and 13 could not maintain the profile needed for traffic flow. Maintenance and construction engineers determined that Spans 11, 12, and13 and Piers 12 and 13 were unstable, creating a potential hazard to the downstream South Bound Salinas River Bridge. It was therefore decided to replace the upstream structure immediately. The downstream parallel structure was replaced in the subsequent phase.

The soil profile of the riverbed consists of very loose sand for the top 6 m followed by 9 m of loose sand and then 46 m of dense sand. Ground water had been encountered near the surface of the streambed. There is a moderate to high potential for liquefaction. Scour potential is high with local scour at the existing pier supports estimated at 9 m from top of streambed and streambed degradation at an additional 11 m.

The site is located approximately 6 km from the King City-Reliz Fault with a maximum credible earthquake of moment magnitude 7. The peak bedrock acceleration was estimated at 0.5g. The Caltrans Office of Structural Foundations provided a site-specific recommended design ARS curve (Figure 1).

Scour and liquefaction created long pile and column lengths (21 m, total) with minimal lateral soil support. To resolve this problem, one can provide the needed stiffness in the form of large diameter Cast-In-Steel-Shell (CISS) piles extended to the soffit of the bridge structure.

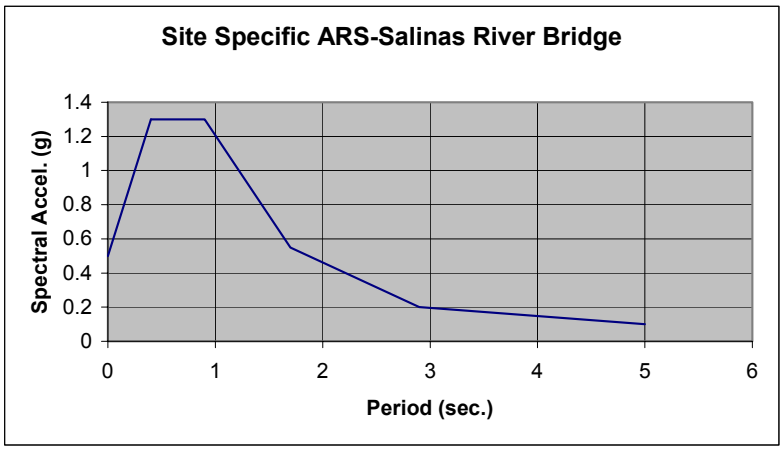

Figure 1- Site Specific ARS Curve

Only the core of CISS was extended into the super-structure to prevent plastic hinging (damage) of the superstructure.

The location, size, and placement of the column supports were determined based on both structural and hydraulic needs to prevent future scour problems (Figure 2).

A two-column bent system on large diameter shaft (CISS) was selected based on the width of the bridge. The CISS pile system was used particularly because of potential channel bed degradation and soil liquefaction.

The CISS concept of placing a reinforced concrete flexural element within a steel pipe element had been used successfully in the past. The pipe is driven to the desired tip elevation and cleaned out, leaving a 3 m soil plug at the tip of the pile. This significantly aids in construction by enhancing the watertight characteristics required to build in the dry condition. The shaft/column rebar cage is then placed within the pipe, followed by the concrete pour (Figure 3).

The pipe and the reinforced concrete element were considered two parallel elements where strength and stiffness is added. Since composite action is not guaranteed, the composite properties of the system were not used.

The yield moment of the pipe was estimated based on a yield stress of 315 MPa and then increased by 25% to represent the plastic moment of the pipe. Since the compression flange of the pipe is continuously supported against buckling, one can use the pipe as a fully compact section.

CONFINEMENT

The need to improve the confinement in bridge columns became evident immediately following the 1989 earthquake. Retrofit techniques of steel jacketing the existing columns and considerable increase in confinement steel in new columns were positive improvements in Caltrans' seismic practice. Figure 4 shows the critical "Plastic Hinge Zone (PHZ)" in a typical single-column bent and the concentration of plastic deformation within this zone. Enhancement of the PHZ results in considerable increases in ductility as shown in extended curvature performance (Figure 5).

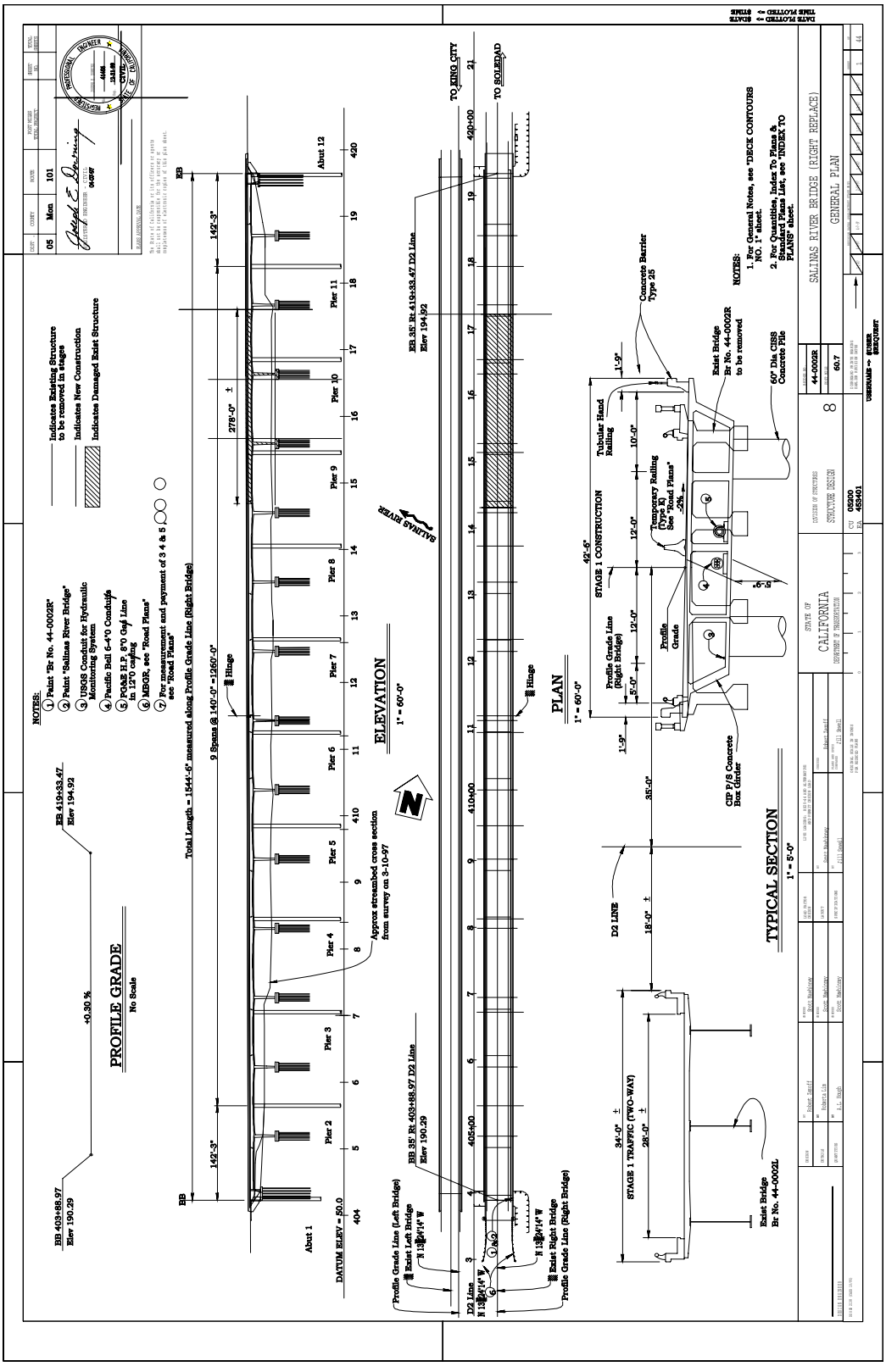

Figure 2 – General Plan for the Salinas River Bridge

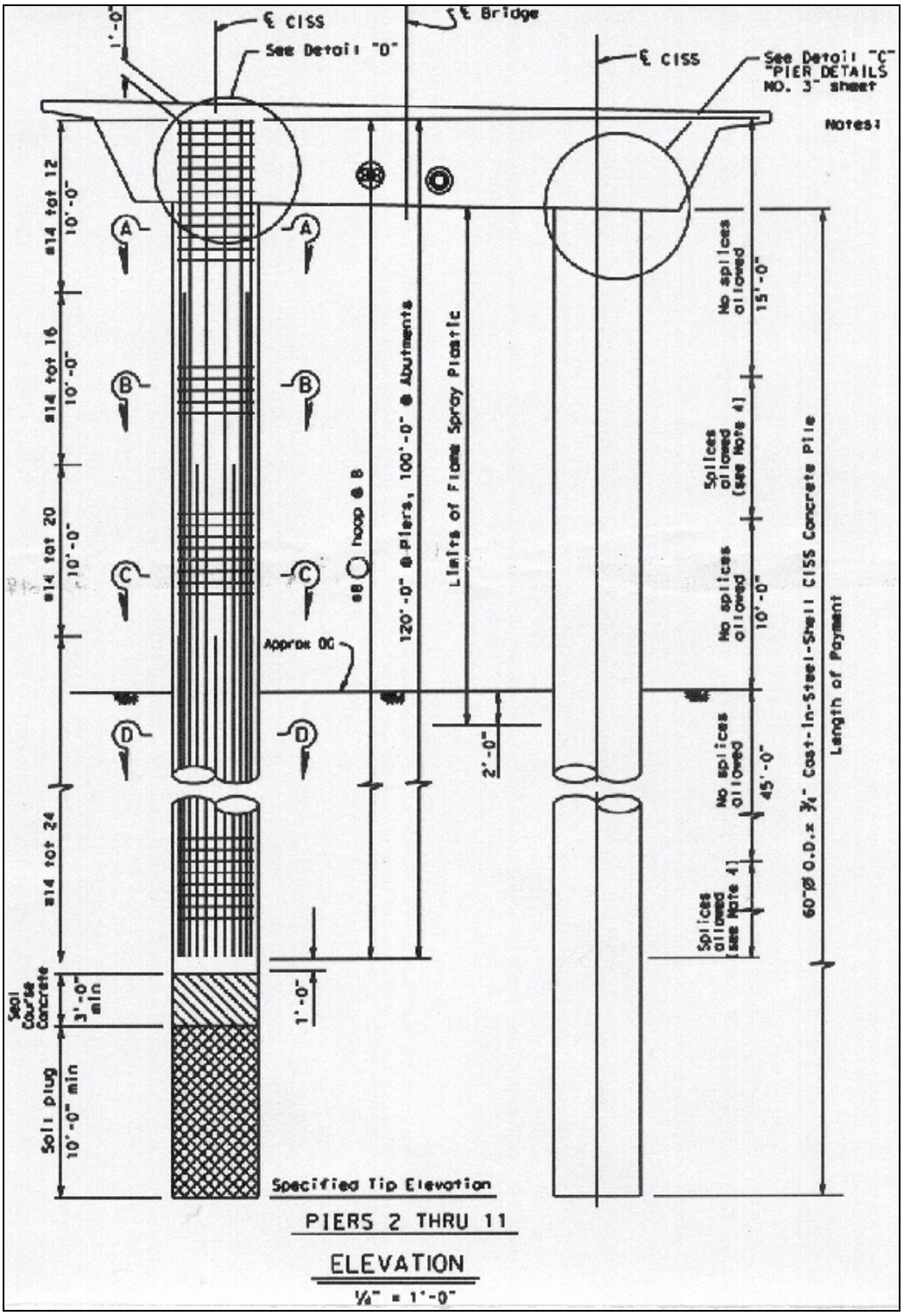

Figure 3 – Bent Details for the Salinas River Bridge

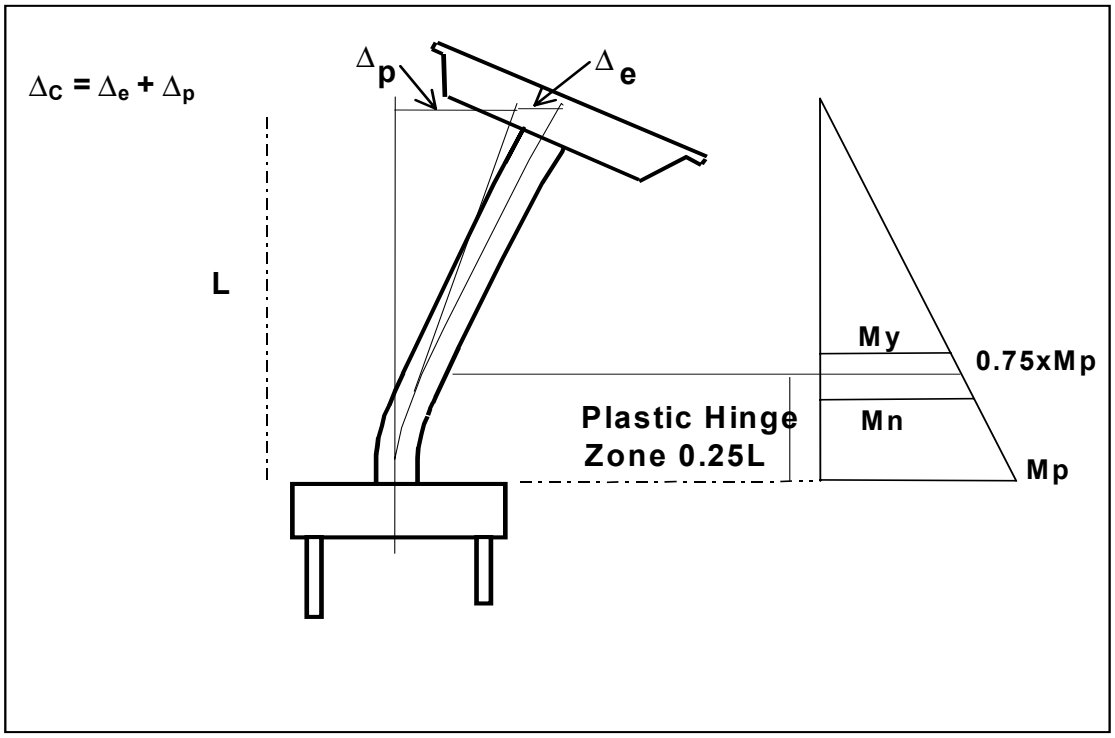

Figure 4 – Moment Demand on a Typical Single Column Bent

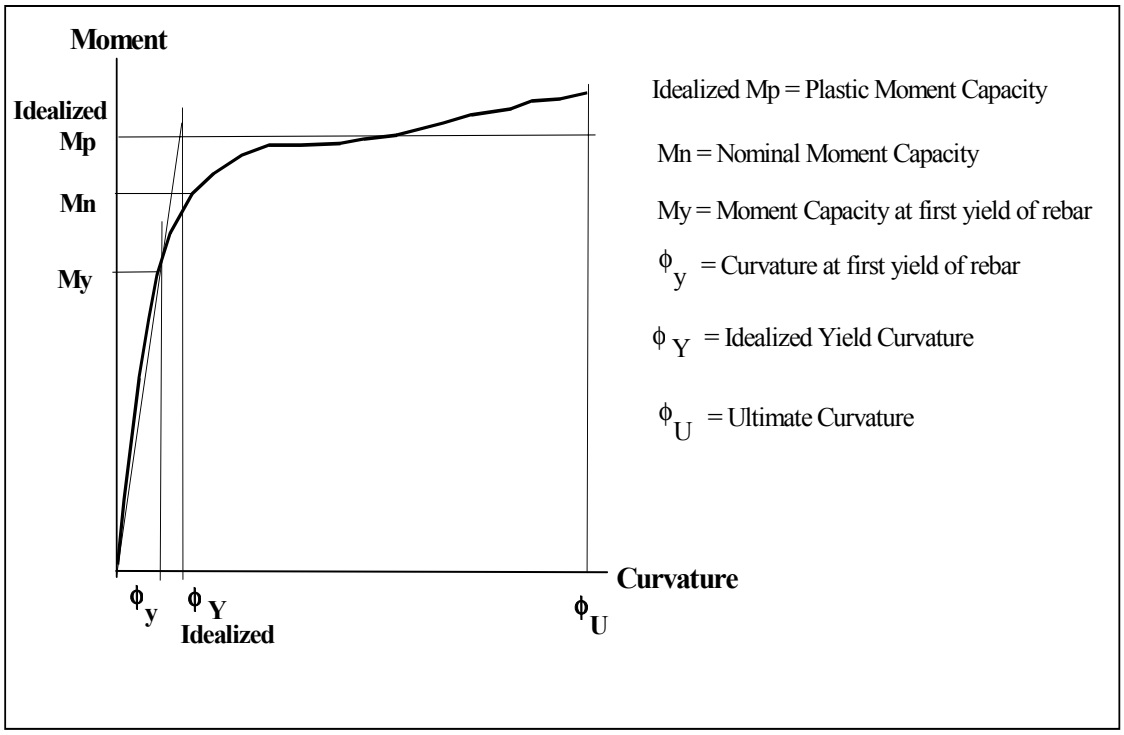

Figure 5 – Typical Moment-Curvature Curve

ASTM A706 reinforcement was selected in the early 1990's to be used in California's bridges because of its ductility and chemical composition limits. This steel was more weldable and showed larger strains at peak (ultimate) stress. ASTM specifically requires a minimum elongation value for various sizes of A706 rebar. The allowance in variation of yield from 420 MPa to 546 MPa is somewhat large, however, a study of 1100 mill reports indicated that an average yield stress value of 476 MPa is appropriate for design purposes. Strain at peak stress values of 6% and 9% were used for #11 and larger and #10 and smaller bars, respectively. A typical steel model is shown in Figure 6.

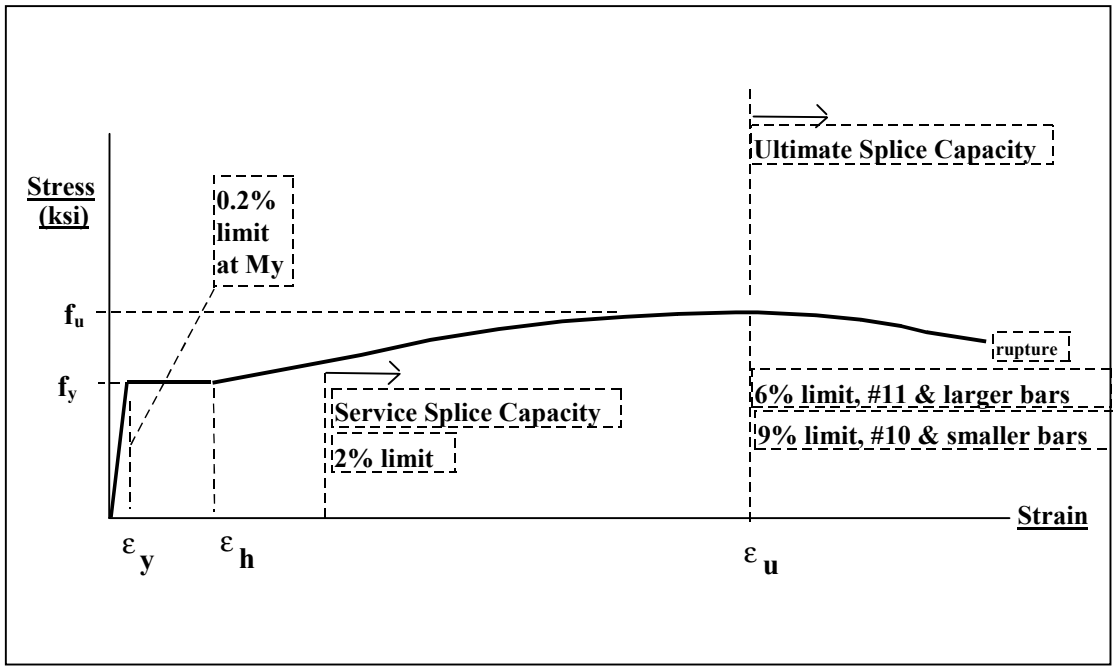

Figure 6 – Typical Stress-Strain Curve for A706 Reinforcing Steel.

Figure 7 shows the confinement reinforcing steel for the Salinas River Bridge. The hoop spacing of # 8 at 200 mm is somewhat larger than the normal 100 to 150 mm spacing used in a typical column. The CISS provides high confinement for the column thereby compensating for the spacing of the hoops. The welding specifications for the pipe do not guarantee a break in the pipe if one were to do a pull test through the weld. Therefore, the combination of the pipe and #8 hoop at 200 mm was judged to be adequate for this design.

CONTINUITY

The need for continuity in bridge frame systems, such as fewer expansion joints in the superstructure and fixed column to super-structure framing was recognized immediately following the 1989 earthquake. Continuity of main reinforcing steel in critical components, columns and shafts, was recognized early as well. The old practice of "starter bars", extending 1.5 m or so from footings, to be lapped with column main bars was proven inadequate. The most

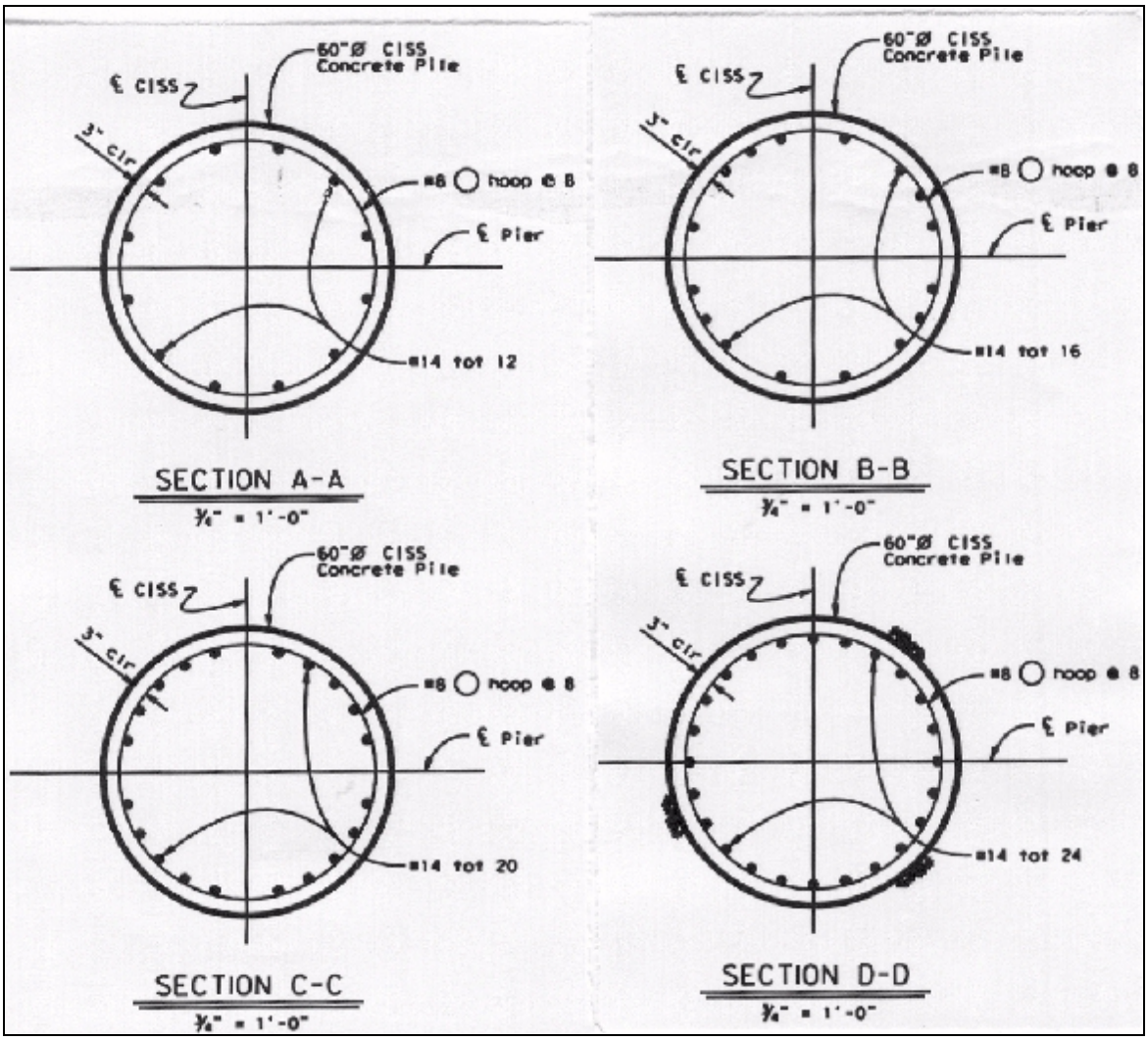

Figure 7 – Column and Shaft Cross Sections (Typical)

recent practice (post 1971 earthquake) of using continuous column cages embedded in footings was reconfirmed. However, tall column cages with rebar lengths greater than 18 m needed splices in the main reinforcement. At the time, full penetration butt-welds and mechanical couplers were the methods used in this splicing task. In 1996 Caltrans initiated a process to improve the quality of these splices and developed the concept of "Ultimate Splices" in reinforcing steel. The old strength requirement of 560 MPa would not be acceptable for Ultimate Splices. Since the earthquake demanded substantial deformation from Seismic-Critical elements, strain was established as the primary parameter to evaluate splices in the Ultimate Splice category. Non-critical splices are now made using Service Splice specifications. Figure 6 shows the strain limits targeted for *Ultimate* and *Service* Splice categories.

Caltrans' Memo-To-Designers (MTD) 20-9 documents the desire and commitment of upgrading and maintaining the quality of splices in rebar as described in the following excerpt:

> *"Seismic-Critical" components are those bridge elements designated to undergo significant post-elastic deformation, dissipate seismic energy, and function through the seismic event. These components are designed and detailed to sustain seismic damage without leading to structural collapse or loss in structural integrity. "Seismic-Critical" elements include, but are not limited to, columns, shafts, and piles in soft or liquefiable soils. Other structural elements such as outrigger bent cap beams, dropped bent cap beams, bent cap beams in "C" bents, and abutment diaphragm walls shall be designed and categorized as "Seismic-Critical" if they are to accept any seismic damage, deliberate or coincidental.*

In accordance with the above requirements Figure 3 shows the details used in the seismic-critical elements, i.e. columns and shafts, of the Salinas River Bridge. Splices in the main column bars were allowed in the middle third of the column. The top 13.7 m of the shaft cage was deemed a no-splice zone since it is a high moment area. The column/shaft reinforcing steel cage totaled 37 m. The hoops were designated as requiring Ultimate Splices.

BALANCE

The most recent effort at Caltrans has been focused on balancing the stiffness and ductility of columns, bents, and frames. The SDC has addressed the issue by making the following recommendations:

> *The best way to increase a structure's likelihood of responding to seismic attack in its fundamental mode of vibration is to balance its stiffness and mass distribution. Irregularities in geometry increase the likelihood of complex nonlinear response that cannot be accurately predicted by elastic modeling or plane frame inelastic static modeling.*

The SDC continues:

> *It is strongly recommended that the ratio of effective stiffness between any two bents within a frame or between any two columns within a bent satisfy Equation 7.1* (see Figures 8, 9, and 10). *It is strongly recommended that the ratio of effective stiffness between adjacent bents within a frame or between adjacent columns within a bent satisfy Equation 7.2. An increase in superstructure mass along the length of the frame should be accompanied by a reasonable increase in column stiffness. For variable width frames the tributary mass supported by each bent or column shall be included in the stiffness comparisons as specified by Equations 7.1(b) and 7.2(b). The simplified analytical technique for calculating frame capacity described in Section 5.4 is only permitted if either 7.1(a) & 7.2(a) or 7.1(b) & 7.2(b) are satisfied.*

Constant Width Frames		Variable Width Frames	
$k_i^e / k_j^e \geq 0.5$	*(7.1a)*	$k_i^e \times m_j / k_j^e \times m_i \geq 0.5$	*(7.1b)*
$k_i^e / k_j^e \geq 0.75$	*(7.2a)*	$k_i^e \times m_j / k_j^e \times m_i \geq 0.75$	*(7.2b)*

k_i^e = *The smaller effective bent or column stiffness*

m_i = *Tributary mass of column or bent i*

k_j^e = *The larger effective bent or column stiffness*

m_j = *Tributary mass of column or bent j*

The SDC emphasizes the following considerations in calculating effective stiffness values:

Framing effects, end conditions, column height, percentage of longitudinal and transverse column steel, column diameter, and foundation flexibility.

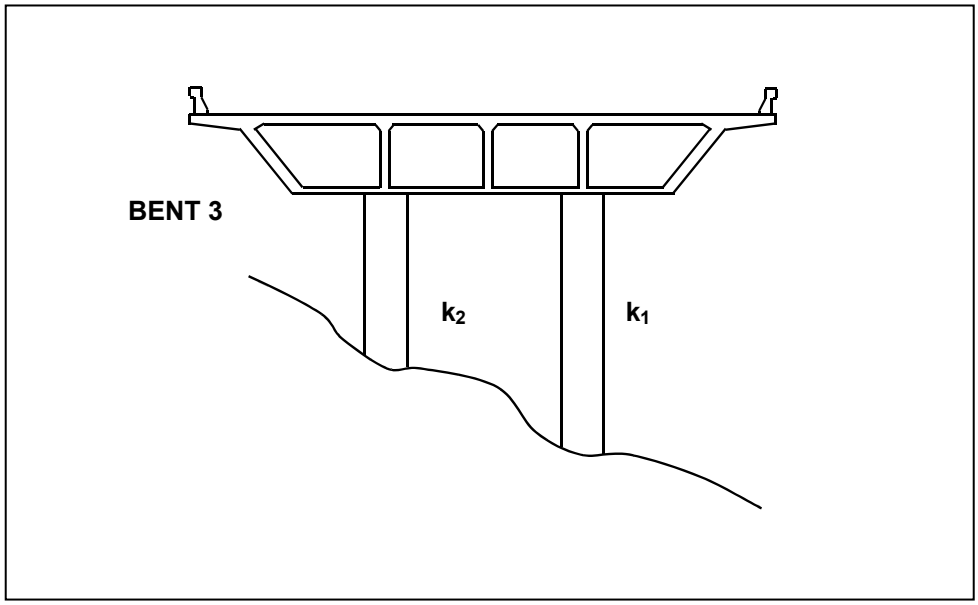

Figure 8- Column Stiffness Balance required within this bent

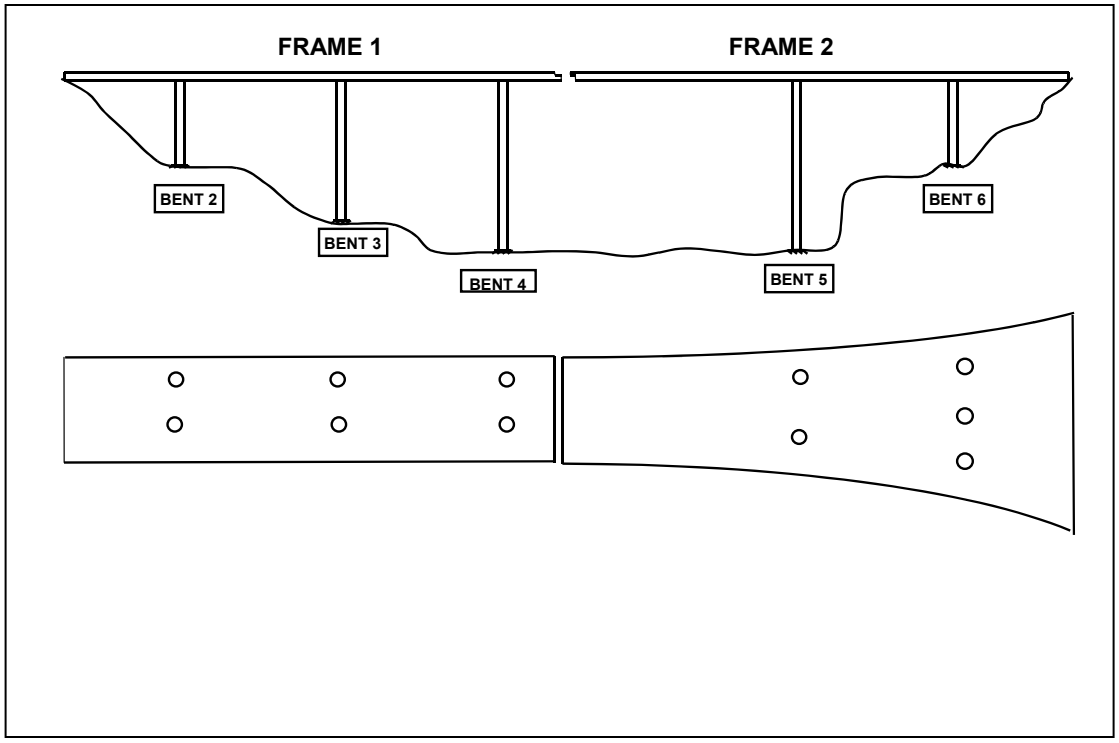

Figure 9- Mass and Stiffness Variations

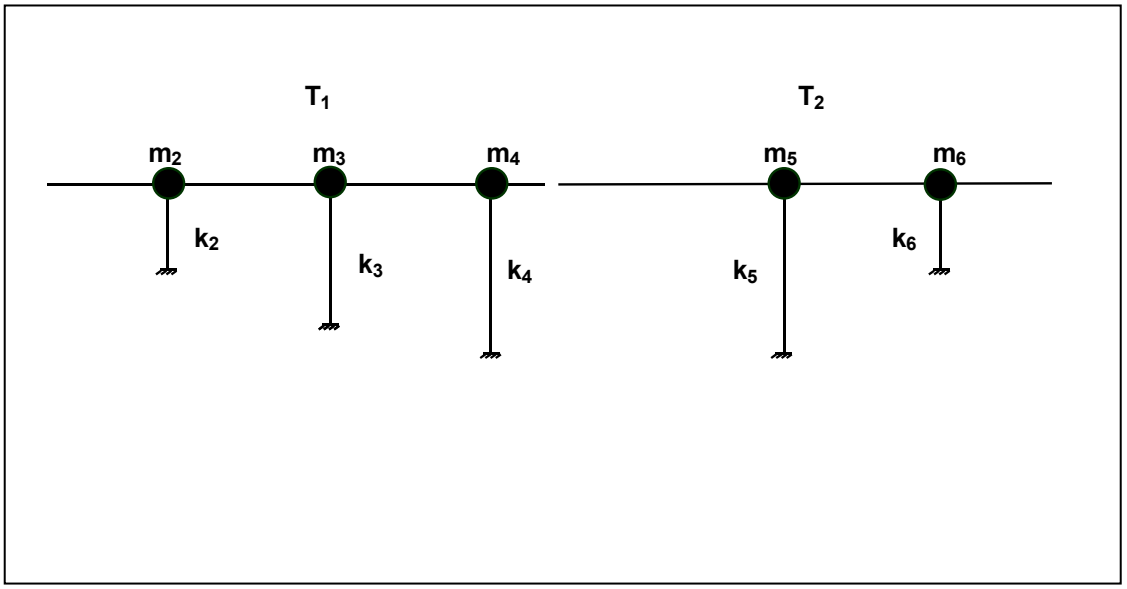

Figure 10- Frame Balance

Some of the consequences of not meeting the relative stiffness recommendations defined by Equations 7.1 and 7.2 include:

- *Increased damage in the stiffer elements*
- *An unbalanced distribution of inelastic response throughout the structure*
- *Increased column torsion generated by rigid body rotation of the superstructure*

It is strongly recommend that the ratio of fundamental periods of vibration for adjacent frames in the longitudinal and transverse direction satisfy Equation 7.3.

$$T_i / T_j \geq 0.7 \qquad (7.3)$$

T_i = Natural period of the less flexible frame
T_j = Natural period of the more flexible frame

The consequences of not meeting the fundamental period requirements of Equation 7.3 include a greater likelihood of out-of-phase response between adjacent frames leading to large relative displacements that increase the probability of longitudinal unseating and collision between frames at the expansion joints. The colliding and relative transverse translation of adjacent frames will transfer the seismic demand from one frame to the next, which can be detrimental to the stand-alone capacity of the frame receiving the additional seismic demand.

The following design parameters have been documented in the SDC to aid the designer in achieving the balance throughout the structure:

- *Oversized pile shafts*
- *Adjustment in effective column lengths (i.e. lower footings, isolation casing)*
- *Modified end fixities*
- *Reduction/redistribution in superstructure mass*
- *Variation in column cross section and longitudinal reinforcement ratios*
- *Addition or relocation of columns*
- *Modification of the hinge/expansion joint layout*
- *Incorporation of isolation bearings or dampers*
- *Redistribution of column reinforcement*

A careful evaluation of the local ductility demands and capacities is required if project constraints make it impractical to satisfy the stiffness and structure period requirements in Equations 7.1, 7.2, and 7.3.

End spans (spans next to abutments) create a challenge of their own due to the reduced height in columns. Shorter columns tend to lose their flexible nature and behave like a shear element as the entire demand from an earthquake is placed on them first. Such a failure occurred in one of the bridges at the I-5/State Route 14 Interchange in Southern California resulting in the loss of three spans during the 1994 Northridge Earthquake.

The mass and the stiffness in the bents and the frames of the Salinas River Bridge has been generally kept to a uniform distribution, as seen in the general plan sheet of Figure 2.

CONCLUSIONS

The most recent design issues facing Caltrans and practical solutions to these problems were presented, including an example bridge. The confinement has been addressed by providing more lateral reinforcement in new bridges and steel jacketing of existing columns. The continuity of structural systems has been addressed by providing "Hinge Restrainers" and larger "seats" in existing and new structures. The continuity of the rebar has become a requirement in new columns and shafts and the columns of existing bridges have been retrofitted with steel jackets to remedy the rebar lap splice problems. The balance of stiffness within a new structure is the current requirement for Caltrans, while solving the problem of unbalanced stiffness in existing structures has been costly and difficult. Most of the above requirements have been met in the Salinas River Bridge, even though it was designed and built prior to the release of the SDC.

The Caltrans SDC addresses many other analysis and design issues such as vertical acceleration, target component ductility values, P-delta effects, and component design recommendations. Issues of confinement, continuity, and balance are viewed as types of "first principles" in the seismic design practice used by the California Department of Transportation.

A Brief Introduction on China Code for Seismic Design of Urban Bridges (2nd Draft)

Lichu Fan[1], Fenghua Zhang[1],Yan Xu[1]

ABSTRACT

The current highway and railway engineering seismic design codes in China are only applicable to the girder bridges and arch bridges with span length less than 150m, but not applicable to the long-span bridges and other bridges. Since 2000 A.C, the new China Code for Seismic Design of Urban Bridges has being compiled by our research group. The second draft of the new code has been completed in summer of 2003 A.C. Some problems in the new code were presented and discussed in this paper.

[1]State Key Laboratory for Disaster Reduction in Civil Engineering, Tongji University, Shanghai 200092, PRC

INTRODUCTION

In China, currently the seismic design codes for highway and railway engineering have been used for more than ten years, which now are under modification to adapt to the new trends for bridge engineering. Considering the specialties of urban bridges, the Department of Construction of China trusted the Division of Bridge Seismic Research of SLDRCE at Tongji University with the compilation of the China Code for seismic design of urban bridges. The 1st draft of the new code had been completed at the end of 2002 A.C. By way of consultation and discussion, now the 2nd draft has also been completed in summer of 2003 A.C.

The key modification to the 1st draft of the new code is about basic criterion for seismic design of bridges. Especially, the new chapter 3 in 2nd draft has broken the old frame and absorbed the concept of performance based design criterion.

MAIN CONTENTS OF THE NEW CODE (2ND DRAFT)

In the 2nd draft of the new code, the main contents include: (1) General Principals; (2) Terms and Notations; (3) Basic Criterion of Bridge Seismic Safety; (4) Seismic Design and Analysis of Bridges; (5) Seismic Action; (6) Performance Criteria and Seismic Checking; (7) Girder Bridges, Viaducts and Interchanges; (8) Long-span Bridges; (9) Isolation; (10) Seismic Measures.

Basically, China natural codes and trade specifications are all obligatory rules. We suggest that the new code for seismic design of urban bridges should not be obligatory rules. Therefore, the seismic design safety criteria of important structures, and the performance criteria of seismic design could be selected and revised by property owners according to acceptable risk level and insurance assessment.

BASIC CRITERION OF BRIDGE SEISMIC SAFETY

Earthquake fortification classification and criterion of bridges

According to "seismic conceptual design based on performance", the definition of guaranteeing bridge seismic safety is that under different earthquake intensities (different earthquake probabilities), the service function of bridges with different importance can attain a group of expected performance objectives.

Urban bridges should be classified into important bridges and ordinary bridges according to the importance of their location in urban transportation network and the traffic volume they carry, as shown in table I.

TABLE I EARTHQUAKE FORTIFICATION CLASSIFICATION OF BRIDGES

Important bridges A		Bay bridges or long-span bridges
Ordinary bridges	B	Bridges at the transportation network hinges
	C	Urban express trunks, railway viaducts and interchanges
	D	Other bridges except for A, B and C

Earthquake fortification criteria of different categories of bridges should comply with the following requirements:

1. When three-level earthquake fortification criterion is adopted to different types of bridges, the annual exceeding probabilities corresponding to different earthquake levels are given in table
2. In regions with fortification intensity of Ⅷ and Ⅸ, earthquake protective measures of first class should be adopted to all types of bridges, and in regions with fortification intensity of Ⅵ and Ⅶ, earthquake protective measures of second class should be adopted to all types of bridges. After approved by authorized government agency, special earthquake protective measures could be adopted to especially important bridges.
3. According to the importance of service function and investment condition, a higher three-level fortification criterion could be adopted to important bridges such as bay bridges, or seismic design guideline could be specially compiled for extremely long-span bridges and very important transportation network engineering under the permission of authorized government agency.

TABLE II THREE-LEVEL EARTHQUAKE FORTIFICATION CRITERIA FOR URBAN BRIDGES

Bridge categories	Ⅰ(Frequently occurred Earthquake)	Ⅱ(Design Earthquake)	Ⅲ(seldom occurred Earthquake)
A		10%(100 years)	2% (100 years)
B	63%(50 years)	10%(50 years)	2% (50 years)
C	63%(50 years)	10%(50 years)	2% (50 years)
D	63%(50 years)	10%(50 years)	

Note: design earthquake is earthquake fortification intensity corresponding to 10% exceeding probability of 50 years in construction site of bridges.

The service requirements, performance requirements and checking criteria

The different service requirements, performance requirements, and checking criteria of bridges after earthquake are defined in table III.

TABLE III THE DIFFERENT SERVICE REQUIREMENTS, PERFORMANCE REQUIREMENTS AND CHECK CRITERIA OF BRIDGES

No.	Service requirements	Performance requirements	Check criteria
S1	Access for emergency traffic within 48 hours, full service within two weeks	No damage to key elements, basically in elastic state	Elastic state
S2	Limited access for emergency traffic within 48 hours, and access after a week; full service after one or two months	No damage to key elements, Minimal damage to non-key elements	Elastic state, local stress could be increased 30%; but foundation should be in elastic state
S3	One or two lanes available for limited access for emergency traffic within 72 hours, full service after two or four months	Minimal damage to key elements, repairable damage to non-key elements	Ultimate state, foundation in elastic state, but stress could be increased 20%
S4	After temporarily retrofitted, one or two lanes available for limited access for emergency traffic within two weeks; full service after two or four months	Repairable damage to key elements,, significant damage to non-key elements	Deformation and ductility requirements
S5	Traffic interrupted and irreparable	Catastrophically damaged, possibly collapse or not	

The service requirements of bridges with different earthquake fortification levels are shown in tableIV

TABLE IV THE SERVICE REQUIREMENTS OF BRIDGES WITH DIFFERENT EARTHQUAKE FORTIFICATION LEVELS

Earthquake fortification levels	Bridge categories			
	A	B	C	D
Frequently occurred Earthquake		S1	S1	S1
Design Earthquake	S1	S2	S3	S4
Seldom occurred Earthquake	S2(or S3)	S3	S4	S5

Earthquake effects

For A, B and C bridges, the ground motion parameters of construction site of bridges must be defined making use of seismic safety evaluation according to<Law of Protecting against and Mitigating Earthquake Disasters in China>; for bridges of D, the design basic seismic acceleration and eigenperiod corresponding to fortification intensity or the design ground motion parameter could be adopted.

Design basic seismic acceleration corresponding to fortification intensity should be determined from table V, according to zoning maps of earthquake intensity and ground motion parameters.

TABLE V BASIC ACCELERATION α_0 FOR DESIGN EARTHQUAKE

Fortification intensity	6	7	8	9
Basic acceleration for design earthquake	0.05g	0.10(0.15)g	0.20(0.30)g	0.40g

Note: 1. g is the acceleration of gravity.

2. Values in brackets are the seismic accelerations of regions specified in Appendix A.

The eigenperiod of response spectrum for Ⅱ soil site can be determined from zoning of eigenperiod of construction sites specified in Appendix A; 0.3s, 0.35s and 0.40s are adopted in Zone Ⅰ, Ⅱ and Ⅲ respectively, and eigenperiods in sites of other categories could be adjusted according to the requirements in 5.1.4 of 2nd Draft.

DESIGN IDEA ON "SEISMIC CONCEPTUAL DESIGN BASED ON PERFORMANCE"

From the perspective of engineering technology, the contents of seismic design based on performance (see figure 1) should include the following items:

1. Defining scientifically earthquake hazard and choosing acceptable risk level;
2. Defining ground motion parameters according to the concerned criteria or earthquake safety evaluation of sites;
3. Defining damage conditions, performance requirements and checking criteria of structures under earthquake;
4. Defining design method, which includes many contents, such as the design new theory based on structural span-life, structural dynamic conceptual design of and earthquake vulnerability analysis, seismic analysis method, the checking criteria of structures and so on.

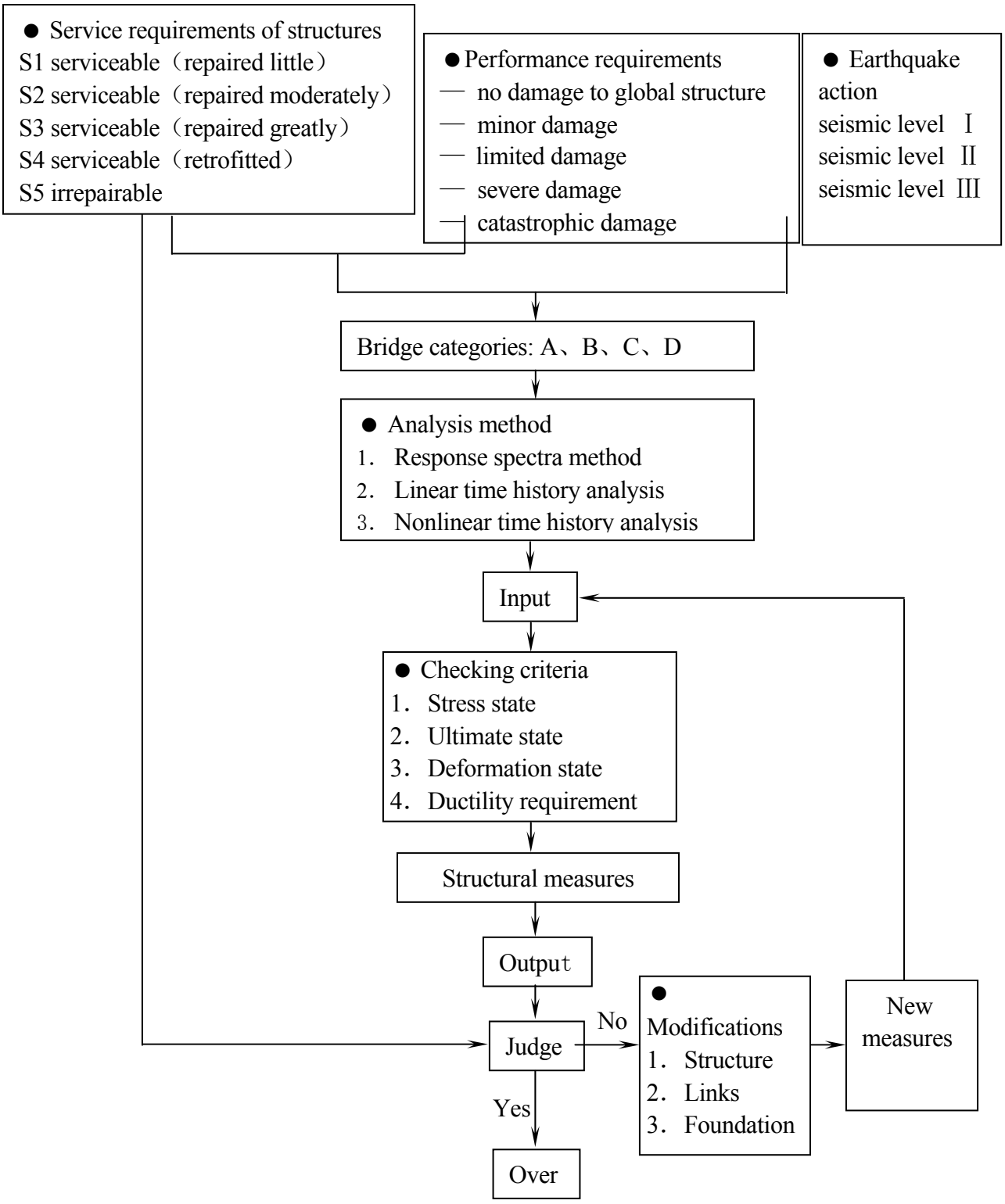

Figure 1　The process of performance based design

PROSPECTIVE OF THE NEW CODE

The 2nd Draft of new code for seismic design of urban bridges will be under revision. The author's view is clear that the code should found on" performance based design method". Most new concepts of the new code would remain. They are as follows.

1. The code provisions will be lowest requirement. Owners can use higher design level according to the acceptable risk level.
2. The earthquake actions will be determined by the following factors: classification and criterion of earthquake fortification of bridges, ground motion parameters, service demand and performance demand of bridges, and the checking criteria of structures.
3. The seismic vulnerability of the bridge structures must be analyzed and then the vulnerable components should be strengthened correspondingly.

REFERENCES

Fan Lichu,1997, Seismic Design of Highway Bridge, Hong Kong, Huajie International Publishing Co. Ltd.

China Code for Seismic Design of Urban Bridges (1st Draft for Seeking Comments), SLDRCE, Tongji University,2001

Fan Lichu, Dec.1998,Some Problems on Shanghai Seismic Design Code for Urban Bridges, Proceedings of International Workshop on Earthquake Engineering for Regions of Moderate Seismicity, p171~176 HongKong China

RECOMMENDED LRFD GUIDELINES FOR THE SEISMIC DESIGN OF HIGHWAY BRIDGES

M. Lee Marsh[1]

ABSTRACT

This paper provides an overview of the proposed seismic design provisions that have been developed to replace those currently in use throughout the United States. The proposed provisions include two-level design procedures, advanced analytical tools such as push-over, updated ground motion data, new site characterizations, simplified methods for lower seismicity regions, and more comprehensive liquefaction provisions. The proposed provisions have been tested in trial designs around the country. The focus of the paper is on the concepts incorporated into the proposed provisions and the issues that arise when attempting to establish appropriate and consistent seismic design criteria and procedures.

BACKGROUND

In the fall of 1998, the AASHTO (American Association of State Highway and Transportation Officials)-sponsored National Cooperative Highway Research Program (NCHRP) initiated a project to develop a new set of seismic design provisions for highway bridges, compatible with the AASHTO *LRFD Bridge Design Specifications* (AASHTO, 2000). NCHRP Project 12-49, which was conducted by a joint venture of the Applied Technology Council and the Multidisciplinary Center for Earthquake Engineering Research (the ATC/MCEER Joint Venture), had as its primary objectives the development of seismic design provisions that reflected the latest design philosophies and design approaches that would result in highway bridges with a high level of seismic performance. Additionally, the provisions were to be nationally applicable.

The current provisions contained in the AASHTO *LRFD Bridge Design Specifications* are, for the most part, based on provisions and approaches carried over from Division I-A, "Seismic Design," of the AASHTO *Standard Specifications for Highway Bridges* (AASHTO, 1996). The Division I-A seismic provisions were originally issued by AASHTO as a Guide Specification in 1983 and were subsequently incorporated with little modification into the *Standard Specifications* in 1991. Thus, the current *LRFD* (Load and Resistance Factor Design) provisions are based on seismic hazard, design criteria and detailing provisions, that are now considered at least 10 years and in many cases nearly 20 years out-of-date. Because AASHTO is in the process of transitioning from the *Standard Specifications* to the *LRFD* specification, it made sense to comprehensively update the seismic provisions.

NCHRP Project 12-49 developed a preliminary set of comprehensive specification provisions and commentary intended for incorporation into the AASHTO *LRFD* specifications. However, due to the amount of detail in the new provisions and the general view that the new provisions were significantly more complex than the existing provisions, the AASHTO Highway

[1] M. Lee Marsh, Senior Project Manager, BERGER/ABAM Engineers Inc, Federal Way, WA, 98003, USA

Subcommittee on Bridges and Structures recommended that the new provisions be considered by AASHTO first as a Guide Specification (MCEER, 2001). This would then allow bridge designers the opportunity to become familiar with the proposed new specifications, and for any problems such as omissions and editorial or technical errors in the new provisions to be identified and rectified, prior to formal adoption into the AASHTO *LRFD* specifications.

BASIC CONCEPTS

The development of these specifications was predicated on the following basic concepts.

- Loss of life and serious injuries due to unacceptable bridge performance should be minimized.
- Bridges may suffer damage and may need to be replaced but they should have low probabilities of collapse due to earthquake motions.
- The function of essential (critical lifeline) bridges should be maintained even after a major earthquake.
- Upper level event ground motions used in design should have a low probability of being exceeded during the approximate 75-year design life of the bridge.
- The provisions should be applicable to all regions of the United States.
- The designer should not be restricted from considering and employing new and ingenious design approaches and details.

In comparison to the current AASHTO *Standard Specifications for Highway Bridges* and the AASHTO *LRFD Bridge Design Specifications,* the recommended Guide Specifications contain a number of new concepts and additions as well as some major modifications to the existing provisions. These are discussed in this paper.

NEW SEISMIC HAZARD MAPS

The national earthquake ground motion map used in the existing AASHTO provisions is a probabilistic map of peak ground acceleration (PGA) on rock that was developed by the U.S. Geological Survey (USGS) in 1990. The map provides contours of PGA for a probability of exceedance (PE) of 10% in 50 years, which corresponds to approximately 15% PE in the 75-year design life assumed by the *LRFD* specifications for a typical highway bridge.

In 1993, the USGS embarked on a major project to prepare updated national earthquake ground motion maps. The result of that project was a set of probabilistic maps first published in 1996 that cover several rock ground motion parameters and three different probability levels or return periods. The maps are available as large-scale paper maps, as small-scale paper maps obtained via the Internet, and as digitized values obtained from the Internet or a CD-ROM published by USGS (Frankel et al., 2000). Parameters of rock ground motions that have been contour mapped by USGS include peak ground acceleration (PGA) and elastic response spectral accelerations for periods of vibration of 0.2, 0.3, and 1.0 second. Contour maps for these parameters have been prepared for three different probabilities of exceedance (PE): 10% PE in

50 years, 5% PE in 50 years, and 2% PE in 50 years (approximately 3% PE in 75 years). In addition to these contour maps, the ground motion values at any specified latitude and longitude in the U.S. can be obtained via the Internet for the aforementioned three probability levels for PGA and spectral accelerations for periods of vibration of 0.2, 0.3, and 1.0 seconds. In addition, the published data contains not only the PGA and spectral acceleration values at three probability levels but also the complete hazard curves (i.e., relationships between the amplitude of a ground motion parameter and its annual frequency of exceedance at each grid point location). Therefore, the ground motion values for all of the aforementioned ground motion parameters can be obtained for any return period or probability of exceedance from the hazard curves. These maps formed the basis for seismic design using these new provisions. Upper bound limits of 1.5 times the median ground motions obtained by deterministic methods have been applied to limit probabilistic ground motions in the western United States.

DESIGN EARTHQUAKES AND PERFORMANCE OBJECTIVES

The existing AASHTO provisions have three implied performance objectives for small, moderate and large earthquakes with detailed design provisions for a 10% PE in 50 year event (approximately 15% PE in 75 year event) to achieve the stated performance objectives. The new provisions provide more definitive performance objectives and damage states for two design earthquakes with explicit design checks for each earthquake to ensure the performance objectives are met (Table 1). This approach provides designers with choices of performance levels. For major structures, most agencies prefer the flexibility to select an enhanced performance objective over that used for typical structures. However, permitting such a choice for the more common structures has raised concerns over liability. Users would naturally prefer the highest level of performance, but as a matter of economics the seismic design of bridges has largely been based on permitting limited damage. Thus, the preference of many state agencies was to eliminate the Operational Performance Level from consideration for typical designs and include the option for such enhanced design as non-mandatory. Thus, the selection of performance objective was removed in the later balloted drafts of the provisions.

The upper-level event, termed the ‘rare earthquake’ or Maximum Considered Earthquake (MCE), describes ground motions that, for most locations, are defined probabilistically and have a probability of exceedance of 3% in 75 years. However, for locations close to highly active faults, the MCE ground motions are deterministically bounded so that the levels of ground motions do not become unreasonably high. Deterministic bound ground motions are calculated assuming the occurrence of maximum magnitude earthquakes on the highly active faults and are equal to 1.5 times median ground motions for the maximum magnitude earthquake but not less than 1.5g for the short-period spectral acceleration plateau and 0.6g for 1.0-second spectra acceleration. On the current MCE maps, deterministic bounds are applied in high-seismicity portions of the western U.S. In areas where deterministic bounds are imposed, ground motions are lower than ground motions for 3% PE in 75 years. The MCE earthquake governs the limits on the inelastic deformation in the substructures and the design displacements for the support of the superstructure.

Table 1. Design Earthquakes and Seismic Performance Objectives

Probability of Exceedance For Design Earthquake Ground Motions		Performance Level	
		Life Safety	Operational
Rare Earthquake (MCE) 3% in 75 years	Service	Significant Disruption	Immediate
	Damage	Significant	Minimal
Expected Earthquake 50% in 75 years	Service	Immediate	Immediate
	Damage	Minimal	Minimal to None

The lower level design event, termed the 'expected earthquake', has ground motions corresponding to 50% PE in 75 years. This event ensures that essentially elastic response is achieved in the substructures for the more frequent or expected earthquake. This design level is similar to the 100-year flood and has similar performance objectives. An explicit check on the strength capacity of the substructures is required. Parameter studies performed as part of the development of the provisions show that the lower level event will only impact the strength of the columns in parts of the western United States. Background on the choice of the two design events is provided in Appendix A of the Guide Specification.

The return period or frequency of exceedence of the rare event has become one of the most controversial elements of the proposed provisions. The rare event was selected to roughly bound scientifically credible ground motions for the country. The methodology was calibrated such that for design to Life Safety collapse was prevented in the rare event and service was maintained in the expected event. The rare event design methodology was also set to provide a similar margin against collapse as that provided by the current specifications. The goal was that designs developed using the current provisions and those by the proposed provisions would not be significantly different from one another, even though the design earthquake shaking is significantly larger. This was confirmed in the parameter study and later by a trial design study done by approximately 20 states. However, the change in the return period coupled with the approach to minimum protection levels led to more bridges geographically being included in the higher categories. This led to resistance to adoption because of the concern that design costs will rise due to the larger geographic area included in the higher seismic hazard zones. In the most recent consideration of adoption, a lower return period, approximately 1000 years (7% PE in 75 years), was considered by AASHTO.

NEW SOIL FACTORS

The site classes and site factors incorporated in the new provisions are the same as those adopted in the Seismic Design Criteria of Caltrans (1999), the 1997 NEHRP Provisions (BSSC,

1998), the 1997 Uniform Building Code (UBC) (ICBO, 1997), and the 2000 and 2003 International Building Code (IBC) (ICC, 2000 and 2003). This is one of the most significant changes with regard to its impact on the level of seismic design forces and more importantly on the classification of the bridge for seismic design. The increase in site factors with decreasing accelerations is due to the nonlinear response effects of soils. Soils are more linear in their response to lower acceleration events and display more nonlinear response as the acceleration levels increase. The effects of soil nonlinearity are also more significant for soft soils than for stiff soils.

The new site class is significant for classification of the structure for design, because bridges typically are founded on sites with poor soils, which have higher site coefficients. This that more bridges tend to fall into the higher design categories. It also means that a single acceleration map no longer can be used to classify bridges for design in a given jurisdiction. While technically a rational approach, practically this feature makes consistent design enforcement difficult, and it has increased the number of bridges that need to be designed for higher seismic forces.

EARTHQUAKE RESISTING SYSTEMS AND ELEMENTS (ERS AND ERE)

The provisions provide a mechanism to permit the use of some seismic resisting systems and elements that were not permitted for use in the current AASHTO provisions. Selection of an appropriate ERS is fundamental to achieving adequate seismic performance. Seismic performance is typically better in systems with regular configurations and evenly distributed stiffness and strength. Thus, typical geometric configuration constraints, such as skew, unequal pier heights, and sharp curves, conflict, to some degree, with the seismic design goals. For this reason, it is advisable to resolve potential conflicts between configuration and seismic performance early in the design effort. The classification of ERS and ERE into the categories of (1) permissible, (2) permissible with owner's approval, and (3) not recommended is done to trigger due consideration of seismic performance that leads to the most desirable outcome — that is, seismic performance that ensures wherever possible post-earthquake serviceability. It is not the objective of the provisions to discourage the use of systems that require owner approval. Instead, such systems may be used, but additional design effort and consensus between the designer and owner are required to implement such systems. Common examples from first two categories of systems are shown in the Figures 1 and 2.

NO ANALYSIS DESIGN CONCEPT

The no analysis design procedure is an important new addition to the recommended provisions. It applies to regular bridges in the lower seismic hazard areas, including the expanded areas now requiring more detailed seismic design. A bridge is designed for all non-seismic loads and does not require a seismic demand analysis. Capacity design procedures are used to determine detailing requirements in columns and in the connection forces of columns to the footing and superstructure. There are no seismic design requirements for abutments, except that integral abutments need to be designed for passive pressure.

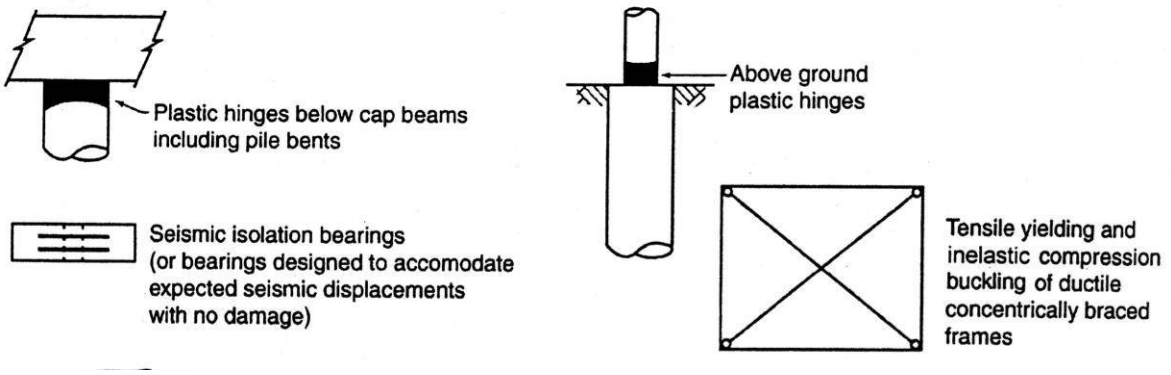

Figure 1. Permissible Earthquake Resisting Elements (ERE)

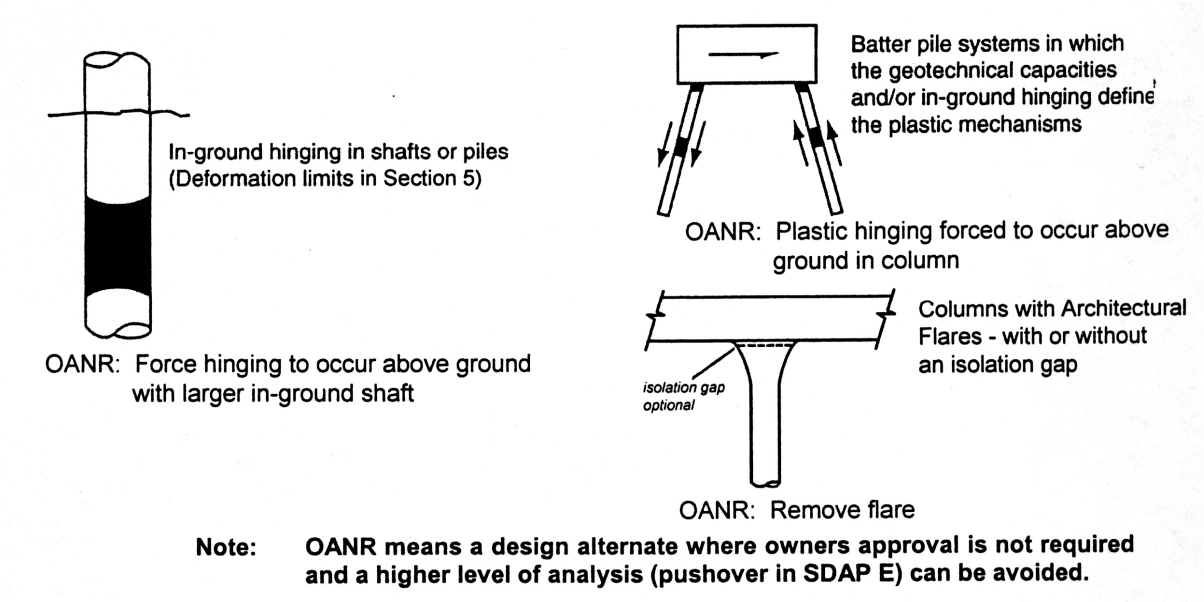

Figure 2. Earthquake Resisting Elements (ERE) that Require Owner's Approval

The No Analysis feature of the provisions is important because the limits for the use of the approach also establish the extent of application of the more rigorous provisions in lower seismic hazard portions of the country. Regularity of the bridge configuration also is a factor in establishing whether a bridge can be designed by the no-analysis procedure. Thus the regularity

limits are likewise important. From a code development perspective, conservative limits should be set until more is understood about the effects of irregularity. From a bridge management perspective, more conservative limits mean more bridges must be considered in design, and this may lead to increased design costs for state and local agencies.

CAPACITY SPECTRUM DESIGN PROCEDURE

The capacity spectrum design method is a new addition to the provisions and is conceptually similar to the new Caltrans' displacement design method. The primary difference is that the capacity spectrum design procedure begins with the non-seismic capacity of the columns and then assesses the adequacy of the resulting displacements. At this time, the capacity spectrum method may be used for 'very regular' bridges that respond essentially as single-degree-of-freedom systems, although future research should expand the range of applicability. The capacity spectrum approach uses the elastic response spectrum for the site, and this spectrum is appropriately reduced to account for the dissipation of energy in the earthquake resisting elements. The advantage of the approach is that the designer sees the explicit trade-off between the design forces and displacements.

As with the No Analysis procedure, the cut off limits for regularity have an impact on the number of bridges within a jurisdiction that will qualify for the benefits of the method. Thus, practically it would be desirable to allow as many bridges as possible to be designed by the method; however, current knowledge and experience levels with the method do not yet support overly liberal use of the procedure.

DISPLACEMENT CAPACITY VERIFICATION ("PUSHOVER") ANALYSIS

The pushover method of performance assessment has seen increasing use since the early 1990's, and is employed in the both the building industry and transportation industry. It is also regularly used for more important and longer span bridges for which the additional analytical and design costs are warranted. This analysis method provides additional information on the expected deformation demands of columns and foundations and, as such, provides the designer with a greater understanding of the expected performance of the bridge. The method was used for two different purposes in these new provisions. First, it provided a mechanism under which the highest R-Factor for preliminary design of a column could be justified, because there are additional limits on the column plastic rotations that the results of the pushover analysis must satisfy. Second, it provided a mechanism to allow incorporation of earthquake resisting elements (ERE) that require owner's approval. The trade-off was the need for a more sophisticated analysis so that the expected deformations in critical elements could be assessed. Then EREs requiring owners approval could be used, provided that the appropriate plastic deformation limits were met.

FOUNDATIONS

The new provisions are an update of the existing AASHTO LRFD provisions incorporating explicit material that was referenced in the existing specifications and to incorporate recent research. The changes include specific guidance for the development of spring constants for spread footings and deep foundations (i.e., driven piles and drilled shafts.), as well as approaches for defining the capacity of the foundation system under overturning moments. The capacity provisions specifically address issues such as uplift and plunging (or yield) limits within the foundation. Procedures for including the pile cap in the lateral capacity and displacement evaluation are also provided. The implications of liquefaction of the soil, either below or around the foundation system, are also described. This treatment of liquefaction effects is a major technical addition to the provisions.

ABUTMENTS

The new provisions incorporate much of the research that has been performed on abutments over the past ten years. Current design practice varies considerably on the use of the abutments as part of the ERS. Some agencies design a bridge so that the substructures are capable of resisting all of the seismic loads without any contribution from the abutment. Other agencies use the abutment as a key component of the ERS. Both design approaches are permitted in these provisions. The abutments can be designed as part of the ERS and become an additional source for dissipating the earthquake energy. In the longitudinal direction, the abutment may be designed to resist the forces elastically utilizing the passive pressure of the backfill or, in some cases, passive pressure at the abutment is exceeded, resulting in larger soil movements in the abutment backfill. This requires a more refined analysis to determine the amount of expected movement, and procedures are provided herein to incorporate this nonlinear behavior. In the transverse direction, the abutment is generally designed to resist loads elastically. These provisions therefore recognize that the abutment can be an important part of the ERS and considerable attention is given to abutment impacts on the global response of the bridge. For the abutments to be able to effectively contribute to the ERS, a continuous superstructure is required.

LIQUEFACTION

Liquefaction has been one of the most significant causes of damage to bridge structures during past earthquakes. Most of the damage has been related to lateral movement of soil at the bridge abutments. However, cases involving the loss of lateral and vertical bearing support of foundations for central piers of a bridge have also occurred. Considerable research and development have occurred over the past decade in the areas of liquefaction potential and effects, and much of this information has been incorporated in these new provisions. For example, the new provisions outline procedures for estimating liquefaction potential using methods developed in 1997, as part of a national workshop on the evaluation of liquefaction. Procedures for quantifying the consequences of liquefaction, such as lateral spreading of approach fills and settlement and potential flow of liquefied soils, are also given. The provisions also provide

specific reference to methods for treating deep foundations extending through soils that are spreading or flowing laterally as a result of liquefaction.

For sites with mean earthquake magnitudes less than 6.0, the effects of liquefaction on dynamic response can be neglected. For higher magnitudes the potential for liquefaction must be considered. When liquefaction occurs both structure vibration and lateral soil movement may occur. The recommended methodology in these provisions is to consider the two effects independently; i.e., de-coupled.

If lateral flow or spreading occurs, significant movement of the abutment and foundation systems can result and this can be a difficult problem to mitigate. The range of design options include (1) designing the piles for the flow forces to (2) an acceptance of the predicted lateral flow movements, provided inelastic hinge rotations in the piles remain within a specified limit. Figure 3 shows a case where spreading movements will cause yielding in both the abutment and pier foundations. The acceptance of plastic hinging in the piles is a deviation from past provisions in that damage to piles is accepted when lateral flow occurs, thereby acknowledging that the bridge may need to be replaced if this option is selected.

Structural or soil mitigation measures to minimize the amount of movement to meet higher performance objectives are also outlined in the new provisions. Due to the concerns about the potential cost impact of liquefaction coupled with the impact of higher level design events, two detailed case studies on the application of the recommended design methods for both liquefaction and lateral flow design were performed (NCHRP, 2001). The results are also summarized in Appendix H of the provisions. These examples demonstrated that for some soil profiles application of the new provisions would not be significantly more costly than the application of the more conservative current provisions.

BEARING DESIGN REQUIREMENTS

One of the significant issues that arose during development of the steel provisions, and was subsequently endorsed by the NCHRP Project Panel and the ATC/MCEER Joint Venture Project Team (PT) and Project Engineering Panel (PEP), was the critical importance of bearings as part of the overall bridge load path. The 1995 Kobe, Japan earthquake (and other more recent earthquakes) clearly showed the very poor performance of some bearing types and the disastrous consequence that a bearing failure can have on the overall performance of the bridge. Three design options are included to address the issue; these are (1) testing of the bearings, (2) ensuring restraint of the bearings, and (3) a design concept that permits the girders to slide on a flat surface if the bearings fail.

COST IMPLICATIONS

A parameter study was performed as part of the project, and following completion of the guideline form of the provisions a number of state departments of transportation undertook trial design efforts to evaluate the cost impacts of the provisions. In brief, the studies showed that the sizes of substructure produced and the costs were similar to those produced using the current Division I-A provisions. These costs, of course, are related to the seismic design costs in the higher seismic zones where seismic design was already required with the current specifications.

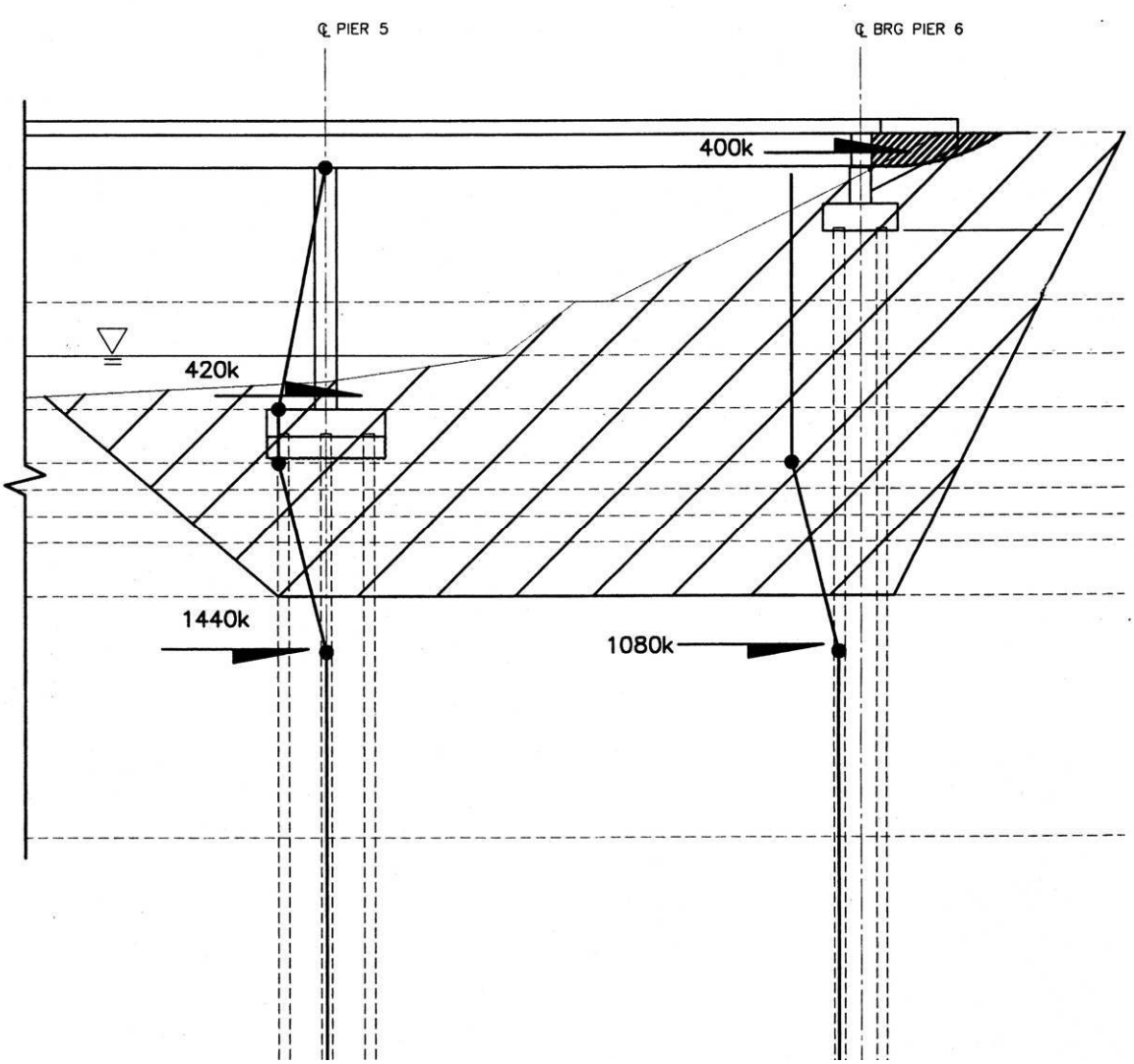

Figure 3. Foundation Movements and Resisting Forces from Lateral Spreading

In some areas of the country, the new provisions would require seismic design where similar levels of seismic design were not previously required. This occurred as the result of such features as improved site classification and increased return periods.

CONCLUSIONS

The proposed provisions have not been adopted by AASHTO as either new LRFD provisions or as a Guide Specification. The reasons for not adopting the provisions have largely been due to concerns regarding the longer return periods, concerns regarding the numbers of

bridges affected, concerns regarding the complexity of the provisions, and uncertainty regarding the provisions' potential impact on the existing bridge inventory. While these concerns have delayed adoption of the provisions, the features of the provisions have made their way into bridge practice as engineers augment the existing specifications with more up to date technologies. Some agencies have elected to use the provisions for important and/or major structures either verbatim or as a starting point for a project-specific basis of design. It is likely that the return period will be reduced, the limits on the more liberal design methods will be made less restrictive, and a revised document will be developed that retains much of what was proposed by the NCHRP 12-49 effort. This project serves to illustrate the challenges of developing a nationally-applicable, effective, and versatile seismic design specification for highway bridges.

ACKNOWLEDGMENTS

Development of the original NCHRP Project 12-49 provisions (from which the Guide Specification was generated) was by the ATC/MCEER Joint Venture. Ian Friedland of FHWA (formerly ATC and MCEER) was the project principal investigator and Ronald Mayes of Simpson, Gumpertz and Heger was the project technical director. Christopher Rojahn of ATC was the project administrative officer on behalf of the ATC/MCEER Joint Venture. The Project team members for NCHRP Project 12-49 included:

- Donald Anderson, CH2M Hill, Inc.,
- Michel Bruneau, University at Buffalo,
- Gregory Fenves, University of California at Berkeley,
- John Kulicki, Modjeski and Masters, Inc.,
- John Mander, University of Canterbury (formerly with the University at Buffalo),
- Lee Marsh, BERGER/ABAM Engineers,
- Ronald Mayes, Simpson, Gumpertz and Heger,
- Geoffrey Martin, University of Southern California,
- Andrzej Nowak, University of Michigan,
- Richard Nutt, bridge consultant,
- Maurice Power, Geomatrix Consultants, Inc.,
- Andrei Reinhorn, University at Buffalo.

The project also included a distinguished advisory committee through ATC (the Project Engineering Panel); Ian Buckle, of the University of Nevada at Reno, co-chaired this committee with Christopher Rojahn of ATC. The NCHRP Project Panel C12-49, under the direction of NCHRP Senior Program Officer David Beal and chaired by Harry Capers of the New Jersey Department of Transportation, also provided significant input and guidance during the project. Three drafts of the specifications and commentary were prepared and reviewed by these panels and the AASHTO Highway Subcommittee on Bridges and Structures seismic design technical committee (T-3), which was chaired by James Roberts and later by Richard Land of Caltrans.

REFERENCES

AASHTO, 2000, *LRFD Bridge Design Specifications*, American Association of State Highway and Transportation Officials, Second Edition with Interims, Washington, D.C. www.aashto.org.

AASHTO, 1999, *Guide Specifications for Seismic Isolation Design,* Association of State Highway and Transportation Officials, Washington, D.C.

AASHTO, 1996, *Standard Specifications for Highway Bridges*, American Association of State Highway and Transportation Officials, Sixteenth Edition with Interims, Washington, D.C. www.aashto.org.

BSSC, 1998, *NEHRP Recommended Provisions for Seismic Regulations for New Buildings and Other Structures*, Report FEMA 302, Building Seismic Safety Council, Washington, D.C.

Caltrans, 1999, *Seismic Design Criteria*, Version 1.1, California Department of Transportation, Sacramento, CA. July.

Frankel, A.D. and Leyendecker, E.V., 2000, "Uniform Hazard Response Spectra and Seismic Hazard Curves for the United States": CD-ROM Published by the U.S. Geological Survey National Seismic Hazard Mapping Project, March. http://geohazards.cr.usgs.gov/eq/

ICBO, 1997, *Uniform Building Code*, Structural Engineering Design Provisions, Volume 2, International Conference of Building Officials, Whittier, CA.

ICC, 2000 and 2003, *International Building Code*, International Code Council, Inc. Falls Church, VA.

MCEER, 2001, *Recommended LRFD Guidelines for the Seismic Design of Highway Bridges*, Multidisciplinary Center for Earthquake Engineering Research, NCHRP Project 12-49, MCEER Highway Project 094, Task F3-1, Buffalo, NY.

NCHRP, 2001, *Liquefaction Study Report*, National Cooperative Highway Research Program, Project 12-49, Transportation Research Board, National Research Council, Washington, D.C.

Impacts of Seismic Requirements on the Design of the I-70 Cable-Stayed Bridge at St. Louis

John M. Kulicki, Ph.D., S.E.
Thomas P. Murphy, Ph.D., P.E.

ABSTRACT

Design of the new I-70 Mississippi River Bridge at St. Louis is currently nearing completion. This 2,000 foot long, 222 foot wide, 12 lane bridge is located near the New Madrid Seismic Zone. A two level performance-based design is being considered with the high level event having a 2,500 year return frequency. The aesthetic requirement to use towers that incline towards the banks of the river introduced structural articulation that places special demands on the end side span piers. This paper introduces the bridge, summarizes dynamic response, presents the site-specific seismic spectrum developed for the bridge, and summarizes the design ramifications of the seismic requirements.

John M. Kulicki, President/CEO and Chief Engineer, Modjeski and Masters, Inc., P. O. Box 2345, Harrisburg, PA 17055
Thomas P. Murphy, Structural Engineer, Modjeski and Masters, Inc., P. O. Box 2345, Harrisburg, PA 17055

Figure 1. The New Mississippi River Bridge.

INTRODUCTION

This paper describes the seismic design of the proposed New Mississippi River Bridge (NMRB) at St. Louis as shown in Figure 1. Situated north of the Eads and south of the McKinnley bridges, this bridge will carry eight lanes of interstate I-70 and I-64 across the Mississippi river just north of downtown St. Louis, Missouri. Figure 2 shows the project location on a seismic hazard map of the United States. Note the New Madrid Seismic Zone south of the project location.

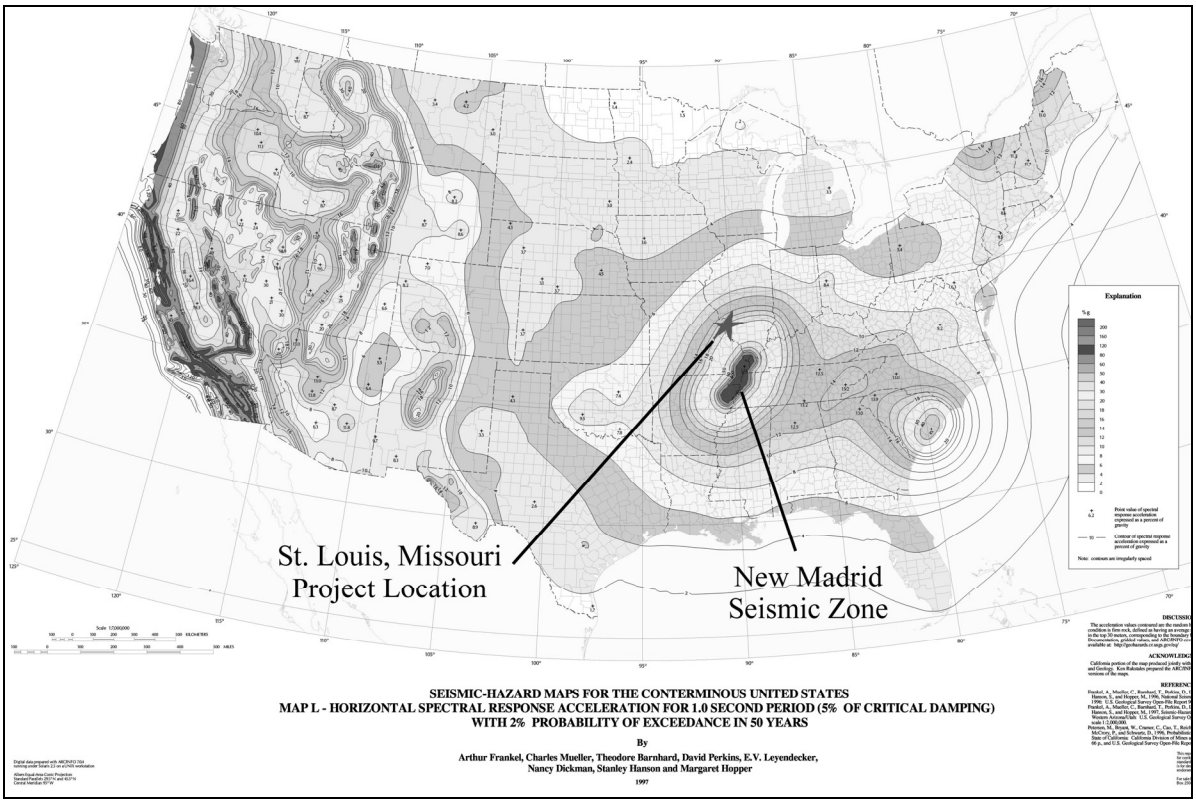

Figure 2. Project Location and Seismicity.

General Description

The design is for a cable-stayed bridge with two main single pylon towers located at the edges of the river, as shown in Figure 3. The main span is 610 m (2,000 ft), which will make it the longest bridge of its type in the western hemisphere when completed. The bridge type and major appearance features resulted from extensive public involvement, the participation of the owners, and an integrated engineering-architecture design team. The side spans are pier supported, and consist of three spans (45.0 m-62.2 m-69.0 m [147.5 ft-204.0 ft-226.5 ft]). The towers are single pylons with centroids inclined 7 degrees from the vertical away from the river. They are situated between the two travel directions, in a 12.1 m (40 ft) slot down the middle of the bridge. The Missouri tower is supported by a spread footing on rock; the depth to rock at this location is only approximately 7.6 m (25 ft). The Illinois tower will be supported by a dredge well caisson sunk nearly 30.5 m (100 ft) to rock. The superstructure is constructed integrally with the tower, and also supported by curved struts at the tower centerline. There are three cable planes in the main span arranged in the semi-fan pattern, anchoring at the center and both edges of the deck. While four cable planes may have some structural efficiency, the additional visual interferences were seen as an aesthetic drawback. The majority of the main span is a composite steel-concrete superstructure, while the side spans are a combination of cast-in-place cellular concrete box girders, referred to as tower integral deck units herein, and conventional plate girder construction. The anchor cables are arranged in two parallel planes along the center of the concrete box girder, and are splayed longitudinally along the ends of the side spans.

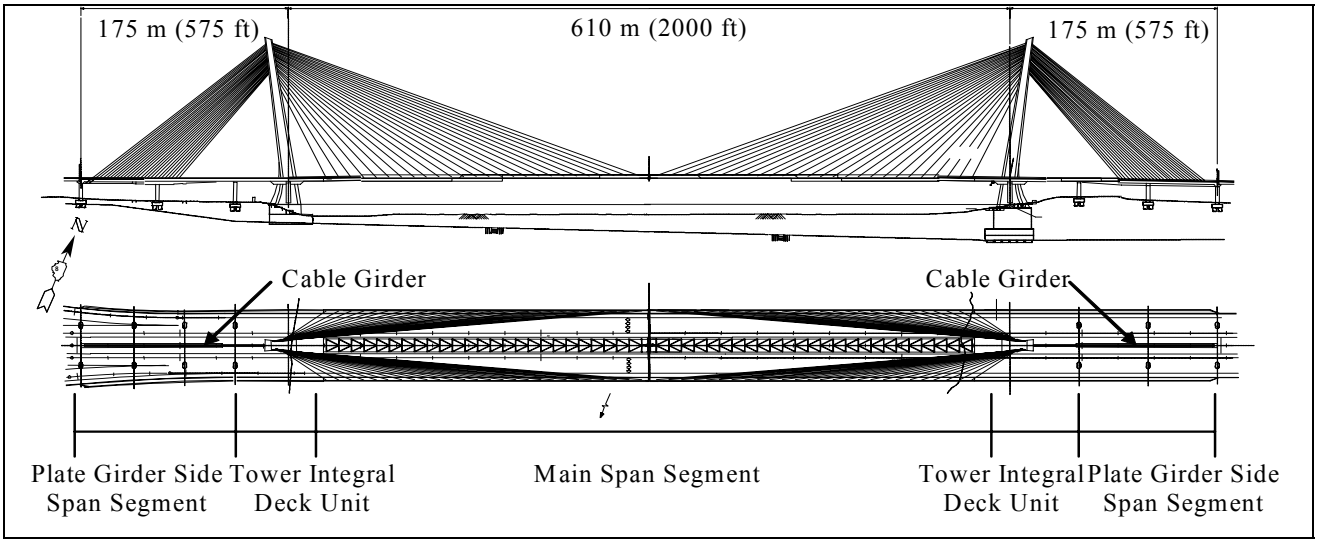

Figure 3. General Plan and Elevation.

Cross-section

The out-to-out width of the main span is an extraordinary 67.6 m (222 ft), the extra width occurring due to the passage of the tower up through the center of the cross-section, as well as the provision for full-width shoulders along both sides of each roadway. With full-width shoulders, the bridge can be expanded to carry a total of 12 lanes in the future, if need be. The main span cross-section, shown in Figure 4, may be thought of as consisting of two individual cross-sections, one for each direction of traffic, straddling the towers and joined along the center gap. Each cross-section consists of an interior I-girder and an exterior steel box girder arranged along the edges, the interior I-girder is on the side of the center gap. Steel floorbeams span between girders and support the post-tensioned concrete deck.

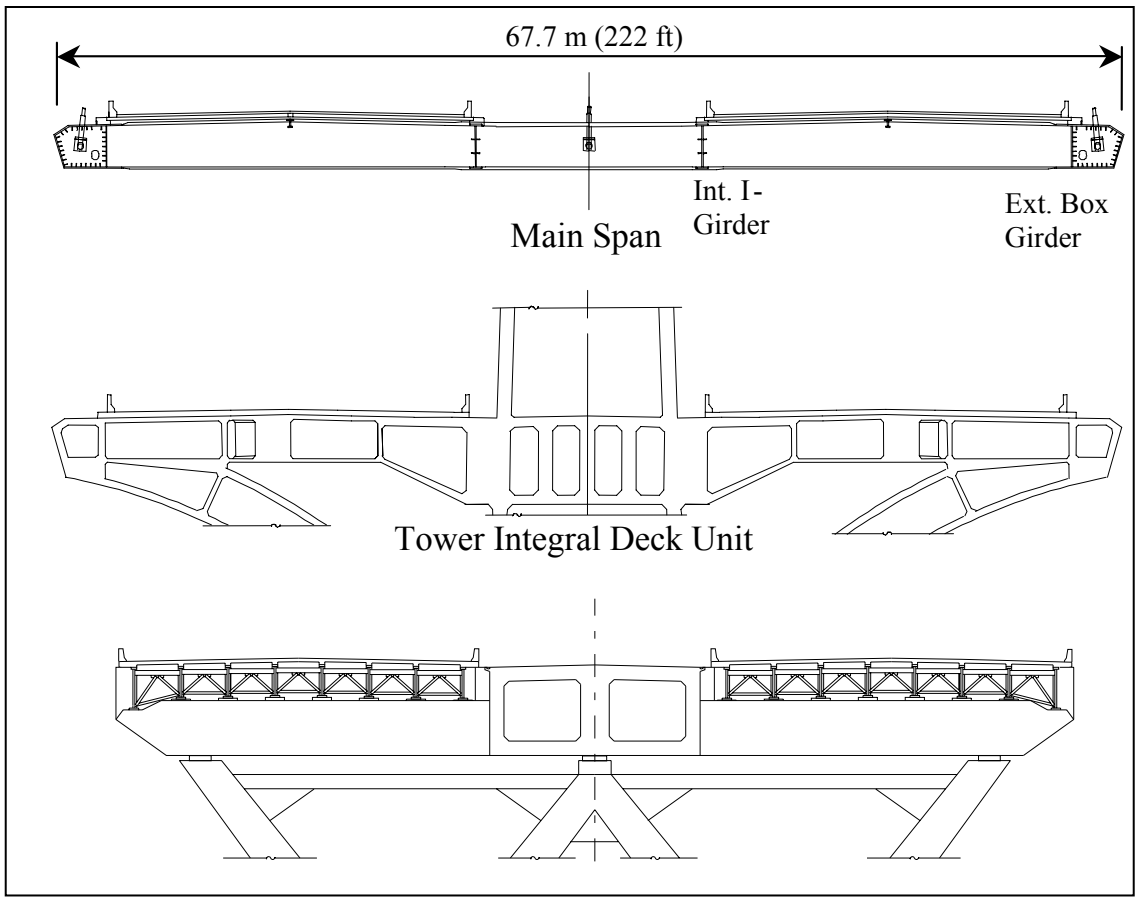

Figure 4. Main Span, Tower Integral Unit and Side Span Cross-sections.

The exterior box girders are 2.7 m (9 ft) deep, 3.4 m (11 ft) wide and are shaped to improve the aerodynamic performance of the bridge. The shape has not been finalized at this writing, aerodynamic studies are ongoing. The inner I-girders along the sides of the slot are 2.7 m (9 ft) deep and the flanges are 0.9 m (3 ft) wide. The box girders are constructed of stiffened steel plates. HPS Grade 70 steel is used extensively. The side planes of cables are anchored within the exterior box girders for improved aesthetics.

The typical floorbeams are approximately 1.5 m (5 ft) deep and span 20.7 m (68 ft) between the longitudinal girders. They are spaced at 3.6 m (11.7 ft) and have widened top flanges to accommodate the erection of precast deck panels. A small longitudinal beam, spanning between floorbeams, also serves as an edge support for precast panels. At each cable anchorage location, a main floorbeam spans between the box girders and across the center gap. These are full-depth steel beams, moment connected to the box girders. In addition to supporting the concrete deck, they carry the transverse bending moments and anchor the central plane of cables.

The concrete deck consists of precast panels, two per half bridge, which will be post-tensioned together after erection. Due to the long main span of the NMRB, the efficiency of the deck will have a large impact on the magnitude of the forces in the cables and tower.

In addition to the main floorbeams, the center gap contains two planes of bracing, one in the top plane of the boxes, one in the bottom plane. These struts resolve the longitudinal components of the cables anchored in the main floorbeams. In addition, they carry shear forces due to transverse bending in the main span.

Towers

The single pylon inclined towers, approximately 158.5 m (520 ft) tall from high water elevation, are perhaps the most distinctive visual feature of the bridge. Figure 5 shows the towers in elevation and cross-section. They are constructed of 44.8 MPa (6,500 psi) concrete and maintain an approximately rectangular cross-section through most of their height. The front face is inclined at a constant 9 degrees from the vertical, while the back and

side faces vary over the height to allow for changes in the cross-section dimensions. The cross-section of the tower is a concrete box with interior cross walls and exterior spurs that start and end along the height. In the cable nest area, the cross-section transitions to a solid H-shape with steel skin plates on the webs to facilitate controlling anchorage geometry. The cables, three planes from the main span and two planes from the side spans, pass through the web of the H and anchor across from each other. Facia panels are used to cover the anchorage areas in this region.

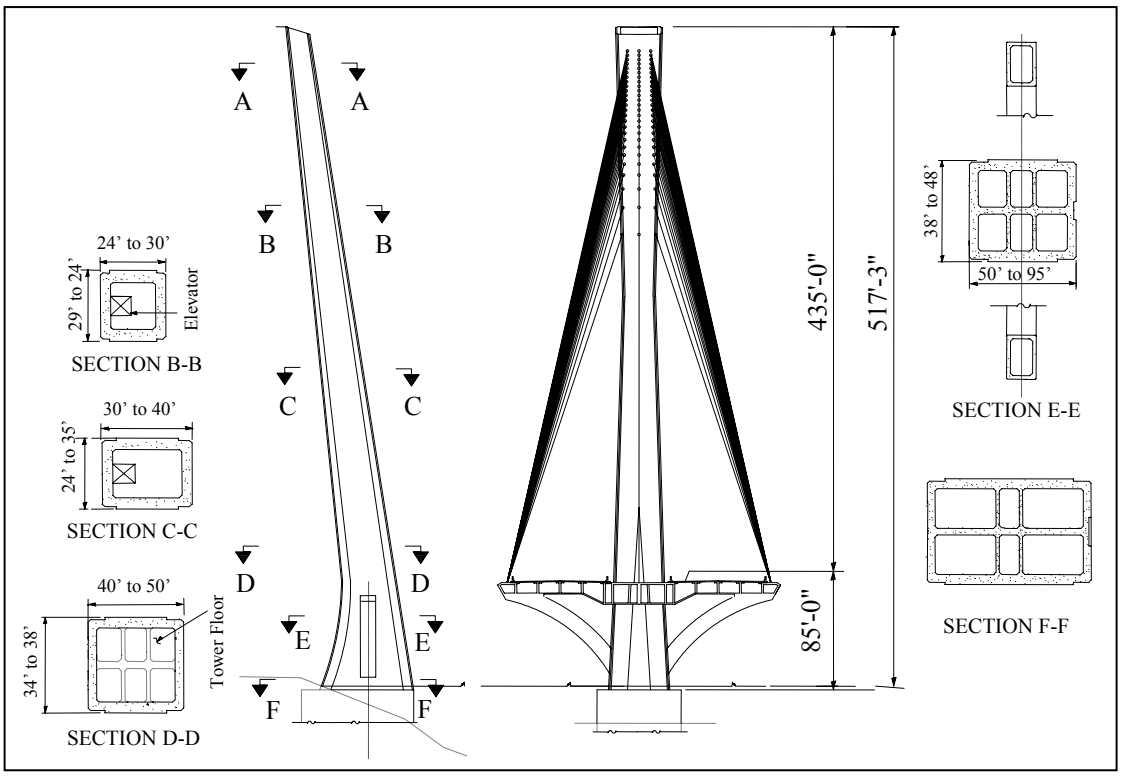

Figure 5. Tower Elevations and Cross-sections.

Tower Integral Deck Unit

The concrete superstructure is made integral with the tower where the two intersect. The depth of the superstructure is locally increased around the tower to reduce the post-tensioning required to resist live and dead load moments. This region resembles a column capital from building construction. 44.8 MPa (6,500 psi) concrete will also be used in this area. The box girders are longitudinally post-tensioned to resist local dead and live loads. The box girders match the approximately 2.7 m (9 ft) depth and shape of the steel main span and are continuous over their full length from the end of the conventional I-girder side span cross-section to the interface with the steel main span approximately 18.3 m (60 ft) into the main span.

Side Spans

The superstructure cross-section for the side spans consists of conventional I-girders as shown in Figure 4.

Cable Girder

The 26 cable-stay pairs anchor into a centrally located, massive, hollow concrete cable girder shown in Figure 4. Roadway geometrics of ramp structures made the use of centrally located cables desirable. This longitudinally post-tensioned cable girder is 13.4 m (44 ft) wide and varies in depth from 5.6 m (18 ft) to 7 m (23 ft). The hollow chamber inside the cable girder will be filled with counterweight, concrete and scrap steel, as the cables

are installed and tensioned so as to balance the weight of the main span. The use of a structurally independent cable girder between the side span roadway clarifies the structural behavior, eliminates numerous heavily post-tensioned transverse diaphragms needed to engage a fully integral back span structure and simplifies the erection of the side span roadways, making construction without shoring possible in a site replete with ground level and underground interferences. It does, however, create a large concentration of mass which has seismic implications to be discussed below.

SEISMIC HAZARD

The most important seismic zone in the central United States is the New Madrid Seismic Zone (NMSZ). The New Madrid zone is located about 225 km (140 miles) south of St. Louis. The fault system extends 241 km (150 miles) southward from Charleston, Missouri, and Cairo, Illinois, through New Madrid and Caruthersville, Missouri, following I-55 to Blytheville and Marked Tree, Arkansas. It crosses five state lines, the Mississippi River three times and the Ohio River twice.

The largest earthquake recorded on this system of faults was the series of quakes and aftershocks that occurred during the winter of 1811-1812. Of the hundreds of earthquakes that occurred at this time, three were of very large magnitude, the largest estimated at greater than 7.5. These events all but destroyed the small town of New Madrid (population 400) and caused widespread destruction.

Only recently has the full potential of the NMSZ to produce damaging earthquakes been realized. In the 1970's, widespread monitoring of the region was instituted. Since that time, thousands of earthquakes have been recorded, although most are too small to be felt. A magnitude 4.0 or greater event occurs almost annually, magnitude 5.0 or greater events occur nearly every decade, and magnitude 6.0 or greater about once every century. The return period for events of the magnitude of the 1811-1812 quakes is estimated at somewhere between 300 to 1,200 years. Obviously, the small amount of data available about larger events results in high uncertainties in their predictions.

Aside from the NMSZ, earthquakes can occur virtually anywhere in the St. Louis region. The probability of such an event is relatively low, but must be considered when identifying the seismic hazard. The possible existence of as yet unknown faults which can produce earthquakes is termed "background hazard." The size of such hypothetical quakes is expected to be relatively small to moderate. However, even a small quake can cause damage if the epicenter is close to the structure.

Site Hazard

Current AASHTO seismic design procedures use a hazard level of 10% in 50 years (i.e., a return period of 475 years, commonly stated as 500 years), meaning the design earthquake has a 10% probability of being exceeded in a time window of 50 years. Only one hazard level is considered.

Recent draft seismic provisions, i.e., ATC-32 and NCHRP 12-49, recommend a two level design process, where a lower hazard level is used to represent a frequently occurring event during which the structure is expected to sustain very low damage levels, and a higher hazard level representing a rare, strong earthquake. The exceedence probabilities for these two levels are 40% in 50 years (return period of 100 years) for the frequent event and 2% in 50 years (2,500 year return period) for the rare earthquake. Performance levels are selected to be appropriate for each of the two design events.

Early in the project, a desire to design the bridge to a high level of seismic safety was expressed. The bridge will be an important lifeline for the St. Louis area, and it is essential that it remains functioning after a major disaster, such as an earthquake, in order to accommodate emergency response efforts. In addition, the anticipated 150-year life span of the bridge is two to three times longer than normally expected from a bridge. It would be very undesirable to design the bridge to a currently acceptable standard only to have more stringent requirements come into effect in the near future which would require retrofitting of the bridge. Because of the above, the design hazard level for the bridge has been chosen as 2% in 50 years (i.e., an earthquake with a return period of 2,500 years), the service level has been identified as "immediate", and the damage level has been chosen as "minimal to none." An "immediate" service level is defined as allowing full access to normal traffic after a seismic event, with perhaps a short period of closure while the bridge is visually inspected. The "minimal to none" damage level means that there should be no apparent deformations, although narrow cracking of the concrete may occur. In order to achieve these goals, the R factor for the main bridge has been set at 1.5 for the 2,500-year event.

Rock Spectra

The NCHRP 12-49 Draft LRFD Design Specifications utilize uniform hazard maps developed by the USGS. A spectrum is developed using the two point method, where two values of the spectrum are obtained from the maps at periods of 0.2 and 1.0 seconds and the remainder of the spectrum is obtained by fitting standard curves to the two points. Figure 2 shows the 1.0 second values of spectral acceleration. Previous methods used only the peak ground acceleration and a spectrum shape that was the same for all locations in the country.

In order to more accurately identify the hazard level at the site, synthetic ground motions representative of those expected at St. Louis were used to develop a site-specific design spectrum. Researchers at the Mid-America Earthquake Center have developed a suite of ten time histories representative of the motions expected in St. Louis due to large earthquakes from the NMSZ and due to smaller earthquakes generated by the background hazard. These motions, along with the spectra from NCHRP 12-49, developed from the USGS data, were used to develop a site-specific spectrum for this project.

Figure 6 shows the maximum, minimum, and median rock response spectra from the suite of synthetic motions along with the NCHRP 12-49 Soil Class B spectrum. At longer periods, the maximum of the suite of motions exceeds the design spectrum. Therefore, a modification to the design spectrum is shown which has slightly higher values at periods exceeding two seconds. This is the design spectrum specified in the project design guidelines for structures with foundations providing direct lateral connection with the bedrock, such as dredge well caissons.

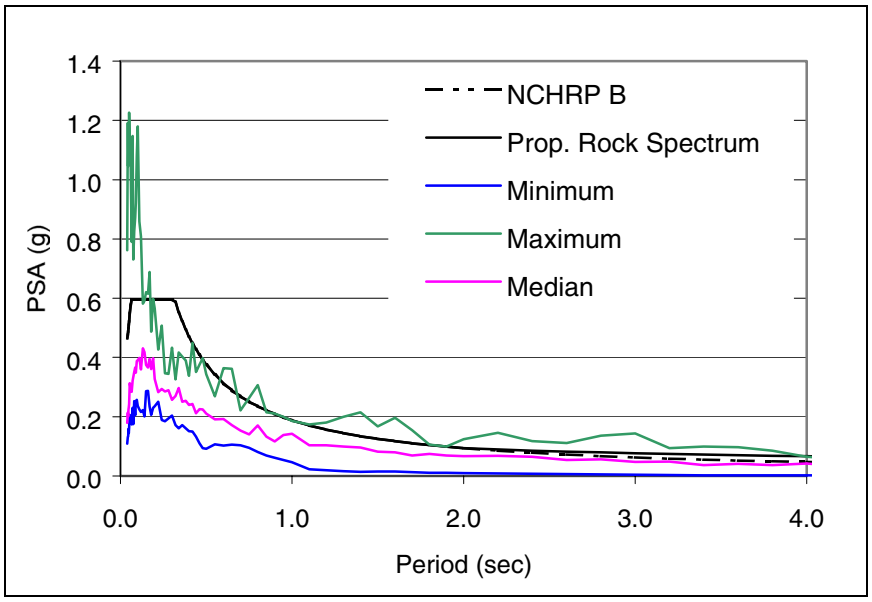

Figure 6. Design Spectra.

Liquefaction-Induced Lateral Spread

In addition to the inertial forces due to the earthquake accelerations defined by the above spectra, the foundations of the main span will be subjected to significant lateral spread forces arising from the susceptibility of the local soils to liquifaction. Preliminary investigations identified potential liquifaction zones as deep as 15 m (50 ft) below grade on the Illinois side of the river and extending hundreds of meters eastward into Illinois. These liquefaction zones, along with the cut formed by the Mississippi River, presents a potential for gross soil movements toward the river. As the foundations to the bridge will present obstructions to the flow of soil, large riverward horizontal forces could be induced.

A study of in-situ soil improvement techniques by geotechnical consultant Hanson Professional Services identified a combination of vibro compaction and stone column installation as a cost effective means of significantly reducing the threat of liquefaction and, therefore, lateral spread. The region around each of the Illinois piers in a zone of soil extending approximately 600 m (2,000 ft) eastward from the Illinois Levee will be treated with vibro compaction to a depth of about 20 m (60 ft). Additionally, the middle one-third of this zone will have stone columns installed in the top half of the soil by vibro replacement.

STRUCTURAL BEHAVIOR

The behavior of the bridge in the longitudinal direction under seismic loads is in large part determined by the articulation option chosen. For the NMRB, the use of inclined towers introduces additional constraints which affect the articulation of the main span, and thus the seismic behavior.

Articulation

In most self-anchored cable-stayed bridges, the permanent force horizontal components of the main span cables and the anchor cables balance each other quite closely. The towers supply primarily vertical support. Unless structural actions are taken, an inclined tower has the potential to create enormous moments due to the centroid of the tower at the base having a large eccentricity from the vertical cable forces.

One way to reduce this bending moment is to turn the resultant of the cable forces to the inclination of the tower. This is achieved by releasing some load from the side span cables through the selection of cable camber and creating an imbalance in the horizontal component of the cable force. However, the imbalance in cable forces is reflected in an imbalance in the deck forces in the main span and side spans.

There are two different approaches for dealing with the unbalanced forces in the deck. One option is to use the deck as a tension tie, allowing the two towers to pull against each other. The other approach is to fix the deck to both towers, using the unbalanced force in the deck to equilibrate the horizontal component of the inclined tower force. In this case, an expansion joint will need to be introduced at mid-span to allow for thermal movements of the superstructure.

It was found that the second option, utilizing and expansion joint at mid-span and integrally connecting the superstructure to the tower, possessed significant advantages. They are:

- Vertical loads to the foundations. The resultant of the inclined force in the tower and the unbalanced horizontal thrust in the deck is vertical below the deck level, resulting in no dead load shear on the foundations, unlike the other approach.

- Minimal thermal tower moments. By essentially de-coupling the towers by the introduction of the mid-span expansion joint, the thermal moments induced in the towers drop to a negligible level.

- Elimination of bearings. The removal of the requirement of the superstructure to slide at one or both towers, as would be required in the other approach, allows an integral connection between the superstructure and the tower, eliminating the need for sliding bearings at the tower, albeit requiring expansion relief at mid-span.

- Simplified construction. Because the state of the bridge during construction and in service are the same, no redistribution of forces is required during construction, eliminating a potentially difficult erection step.

The expansion joint at mid-span will be able to transmit both vertical and transverse shears between the two halves of the bridge, and also torsional moments. The bending moments in the remaining two directions, along with axial thrusts, will not be transmitted. This type of joint has been used in previous cable-stayed bridges, most notably the Dame Point Bridge in Florida and the Barrios de Luna Bridge in Spain. Additionally, prestressed segmental concrete bridges often use similar in span hinges.

Mode Shapes

The dynamic properties of the bridge are best evaluated by examining the modal shapes and periods. Cable-stayed bridges are characterized by having a relatively large number of closely spaced modes which contribute to the dynamic properties. It is instructive to categorize as much as possible the modes as vertical, longitudinal, or transverse in nature.

Vertical Modes

Because of the long span length of the bridge, the first modal periods are relatively long. Figure 7 shows three important vertical modes of the bridge. Mode 1 is a symmetrical bending mode with a period of 3.93 sec. This is the longest period of the bridge. The action of the center expansion joint is clearly visible. Mode 6 is the next symmetrical bending mode with a period of 2.52 sec. Both of these modes primarily involve movement in only the main span. The towers do not become active until Mode 103, a vertical vibration mode of primarily the towers, with a period of only 0.17 sec.

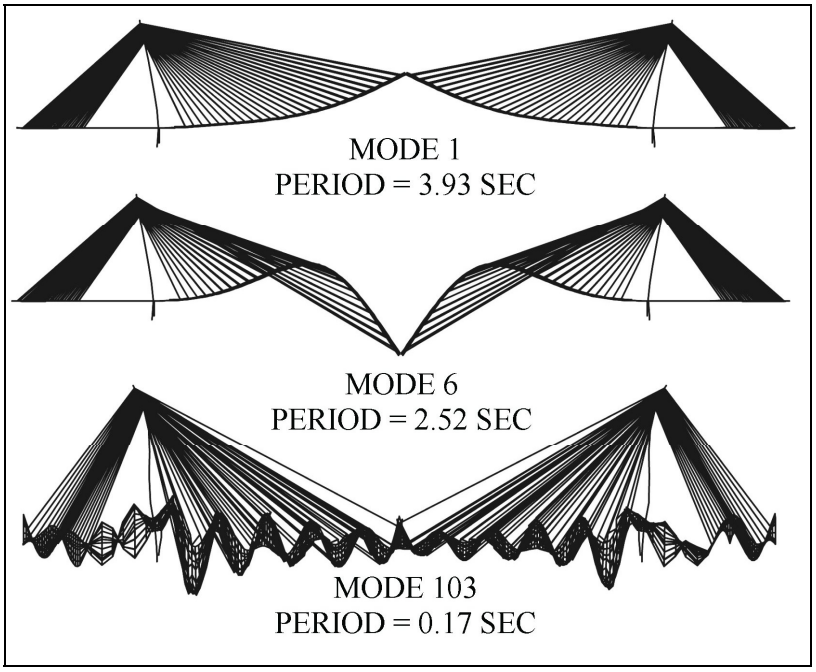

Figure 7. Vertical Mode Shapes.

Transverse Modes

Due to the large structural width of the bridge, and the three-dimensional arrangement of the cable stays, the transverse modal periods are relatively short for a bridge of this span. The first transverse mode, Mode 4, shown in Figure 8, has a period of 2.73 sec., much less than the first vertical mode. It is a symmetric, simple transverse bending mode. The next important transverse mode is mode 19 with a period of 0.95 sec. In this mode, the side spans have become activated due to the transverse flexibility of their supporting piers. This is an unsymmetrical mode shape, due in part to the differing side span arrangements. Mode 31, another symmetric lateral mode, has a period of only 0.59 sec.

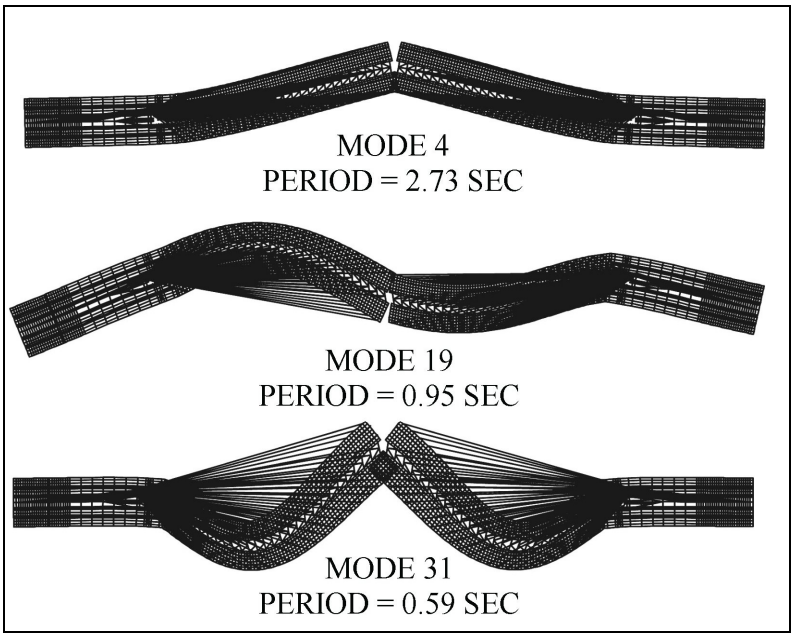

Figure 8. Lateral Mode Shapes.

Longitudinal Modes

Because the superstructure is integrally connected to both towers, and because the tower sections below deck level are very stiff, the longitudinal periods of the bridge are much shorter than in the previous directions. The first longitudinal mode has a period of only 0.73 sec. Figure 9 shows three important longitudinal modes. Because of the different tower foundation stiffnesses, and the differences in side span roadway widths needed to accommodate ramps on the Missouri side, all of the longitudinal modes are unsymmetrical. Some of the longitudinal modes, e.g., Mode 27, clearly show the influence of the center hinge. The movements in this area have been extensively studied and are well within the capability of the swivel joint being specified for that location. The swivel joint accommodates the rotations implied by the modes shown in Figure 8, as well as the longitudinal displacement.

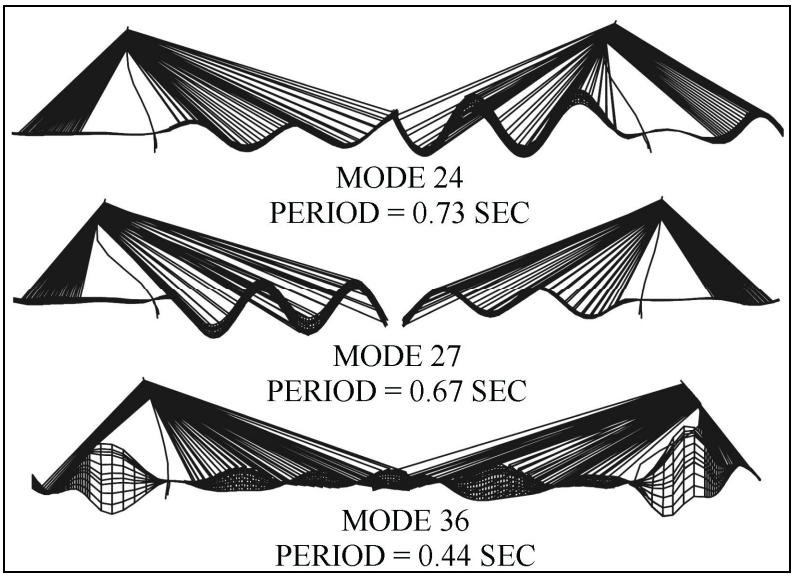

Figure 9. Longitudinal Mode Shapes.

Other Modes

Because of the unique features of this bridge, there is a large amount of coupling between mode shapes, such that many modes have significant components in one or more of the bridge axes. In addition, there exist also a number of torsional modes. However, these do not have much impact on the seismic response of the bridge.

SEISMIC LOADS

For this preliminary analysis, the multi-modal response spectrum analysis was used. The design spectra was applied in both horizontal directions, along with 2/3 of the spectrum in the vertical direction. Of interest at present is the determination of the global response of the structure, and not the demands on the individual components of the structure. The global response will be characterized by examining the base reactions, the global displacements, and the tower moment diagram.

Reactions

Table 1 lists the reactions at the bases of the Missouri and Illinois towers due to the seismic loads. Forces are given in kN and moments in kN-m. The longitudinal direction is parallel to the direction of traffic, while the transverse is perpendicular. For the moments, the longitudinal moment acts about the longitudinal axis, as does the transverse moment about the transverse axis, while the torsional moment acts about the vertical axis.

Examining the reaction forces, the longitudinal forces are nearly twice those from the other two directions. This occurs due to the much stiffer, and hence shorter period, behavior of the bridge in this direction. In general, as the period decreases, the seismic demands increase, as is shown in the design spectrum. This large longitudinal force then induces the large moment about the transverse axis.

The torsional moments come from two sources; inertia of the tower, and transverse bending of the superstructure. Because the tower is inclined, transverse forces will induce a torsional moment about a vertical axis. This is equally valid for transverse inertia forces such as those induced by seismic ground accelerations. The second source of torsion comes from the fixed nature of the integral connection between the superstructure and the tower. The rotational restraint provided by the tower to the deck against rotation about a vertical axis creates the torsional moment. This is evident in the lateral mode shapes presented in Figure 8. Initially, it was thought that these modes and the integral connection of deck and tower, discussed above, could result in unacceptable torques in the tower below the deck. As final design progressed, it was found that these torques, while much larger than torque arising from other design loads, were well within the capability of the tower. This fortuitous finding is a direct outcome of the architectural shape of the tower which flares out below the deck and, therefore, has much larger torque capacity than the tower cross-section above the deck, where the torque is small. The situation was further helped by the large compressive force in the tower resulting primarily from the composite suspended span.

The lateral modes were found to excite the large mass of the cable girder resulting in such large lateral forces that configuration of the side span piers had to be changed. It was originally intended to support the side spans and the cable girder on three independent columns as shown in Figure 10. The high horizontal shears resulted in such large cantilever bending moments that reinforcing or prestressing was impractical. Wall piers were not aesthetically acceptable. The solution was the “W-pier”, shown in Figure 11, which carries the shear through structurally efficient truss action utilizing the two middle arms. Very little seismic shear is transmitted to the external arms. As the design evolved, the exterior arms were curved to be aesthetically compatible with the curved deck supports at the tower, which are shown in Figure 4.

Table 1. Seismic Reactions at Tower Base

Tower	Longitudinal Force	Transverse Force	Vertical Force	Longitudinal Moment	Transverse Moment	Torsion
Missouri	181,000	93,900	78,300	1,680,000	4,340,000	515,000
Illinois	173,000	95,600	83,200	1,750,000	4,200,000	393,000

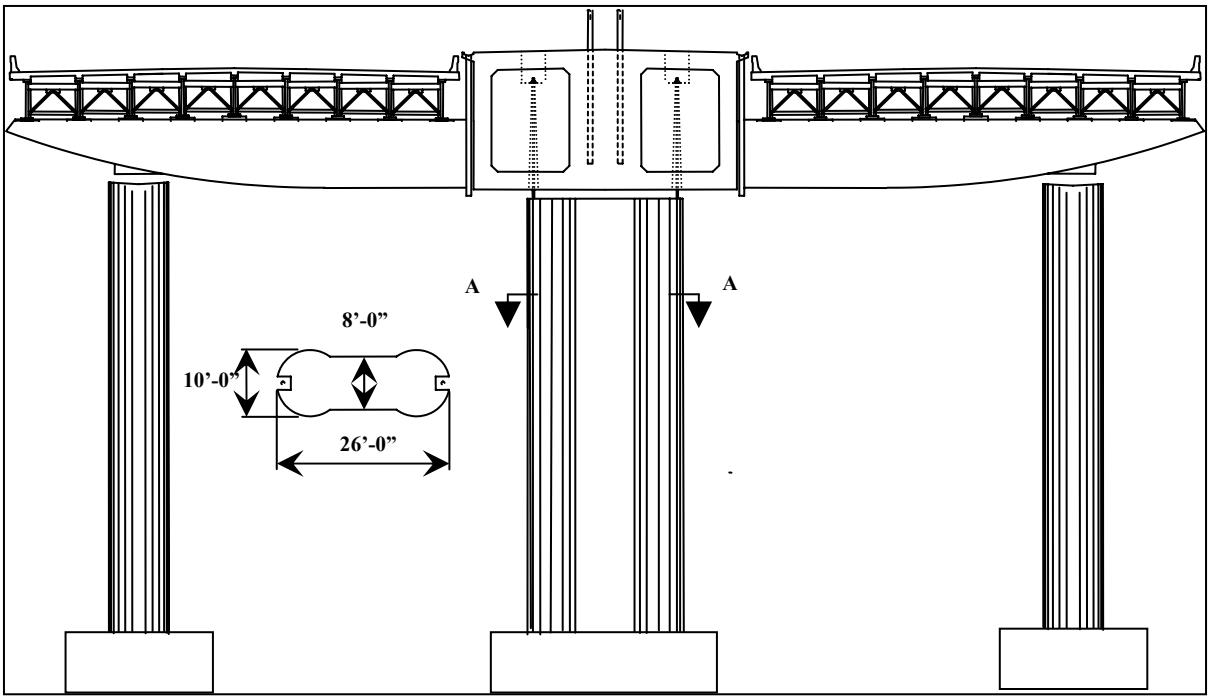

Figure 10. Tower Seismic Moments.

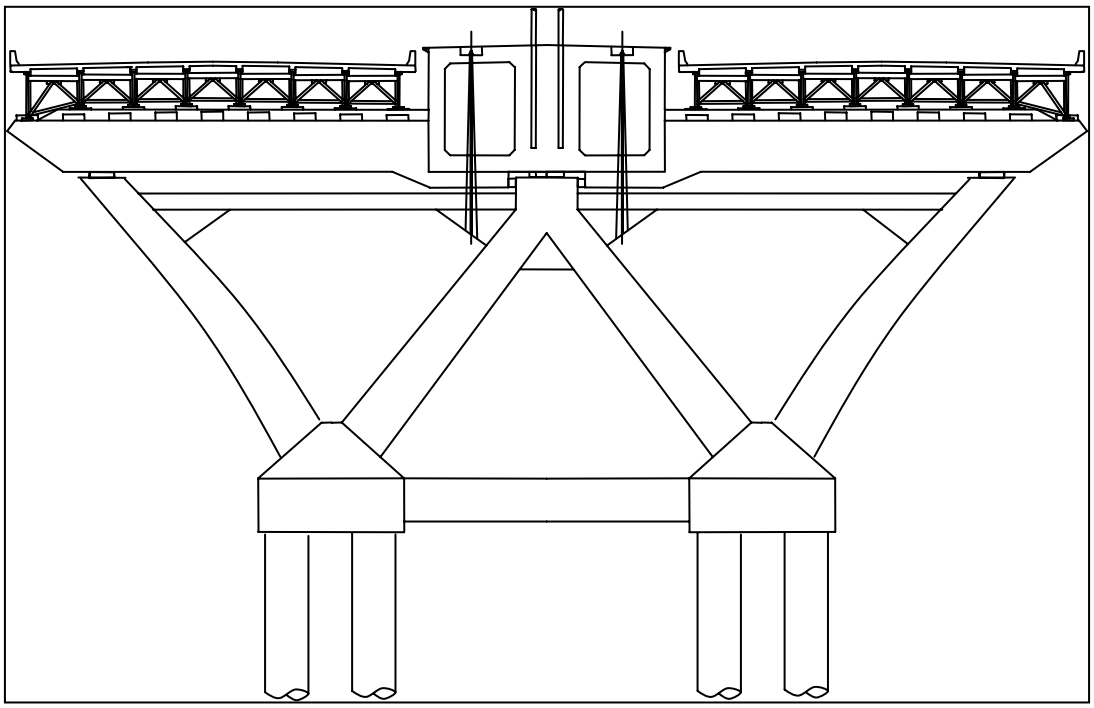

Figure 11. Column C/D Ratios.

Displacements

Despite the large magnitudes of the seismic base reactions, the displacements remain relatively small.

Table 2 shows the seismic displacements at mid-span and at the tower top in meters. The maximum displacements of the deck occur at mid-span. The order of the displacement values follows that displayed in the modal periods. The longitudinal direction is stiffest, and has the smallest displacements, followed by the transverse and the vertical directions. The vertical displacements, although the largest, is still very small when compared to the length of the main span. Expressed as fraction of the span length, the displacement is roughly equal to L/2000.

The tower top displacements show a similar trend, only in this case the vertical displacement is the smallest. Again, this agrees with the modal results, as the first vertical mode that includes vertical tower motions has a very short period. In evaluating the magnitudes of the tower displacements, it is useful to note that the maximum displacement is roughly only 0.1% of the tower height.

Table 2. Seismic Displacements

Location	Longitudinal	Transverse	Vertical
Mid-span	0.024	0.177	0.305
Tower top	0.078	0.146	0.011

Tower Moments

The moments in one tower due to seismic loads are shown in Figure 12. The moments are plotted versus elevation, where zero corresponds to deck level. Nomenclature is the same as for base reactions. From the graph, it is clear that the majority of the transverse moment at the base is due to the inertia forces from the deck. For the longitudinal moments, this is still true although the contribution of the tower above deck level is somewhat higher. The flat slope of the moment diagram below deck elevation indicates a very high shear force. The forces from the tower above the deck, either due to the vibration of the tower itself or to load entering the tower through the cables, are small in comparison to the large shears at deck level.

A comparison of column interaction values for the governing non-seismic load case and the seismic load are shown in Figure 13. It can be readily seen that the tower above the deck is controlled by the non-seismic loads. Below the deck, the seismic loads control near the base, but the architectural shape mentioned previously results in such high capacity/demand ratios that the tower behaves essentially elastically.

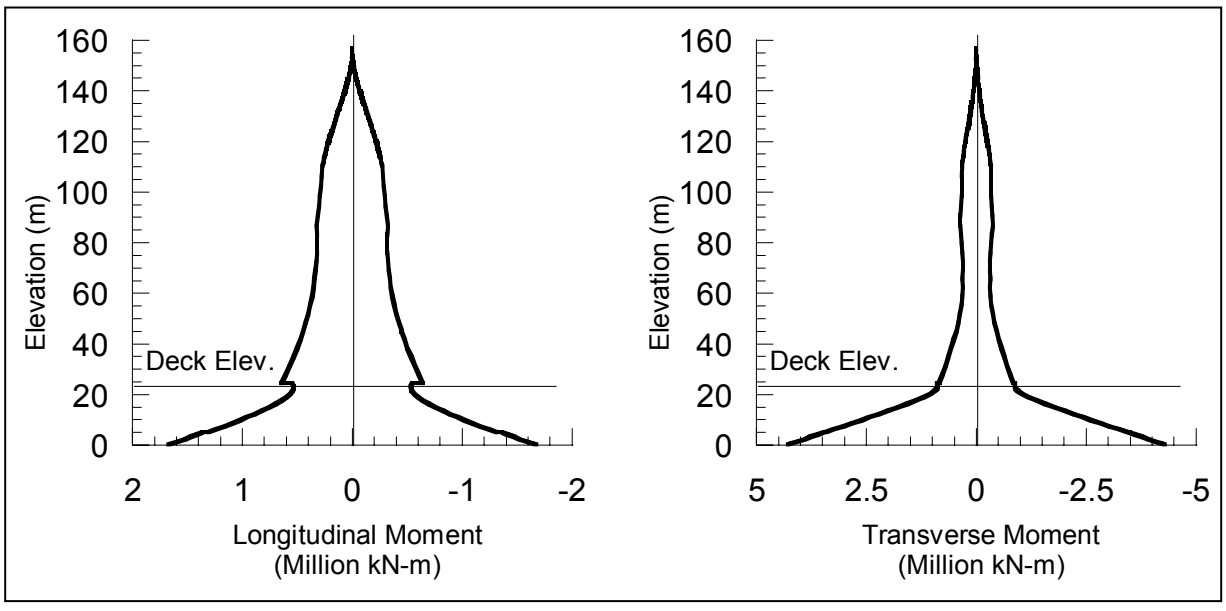

Figure 12. Tower Seismic Moments.

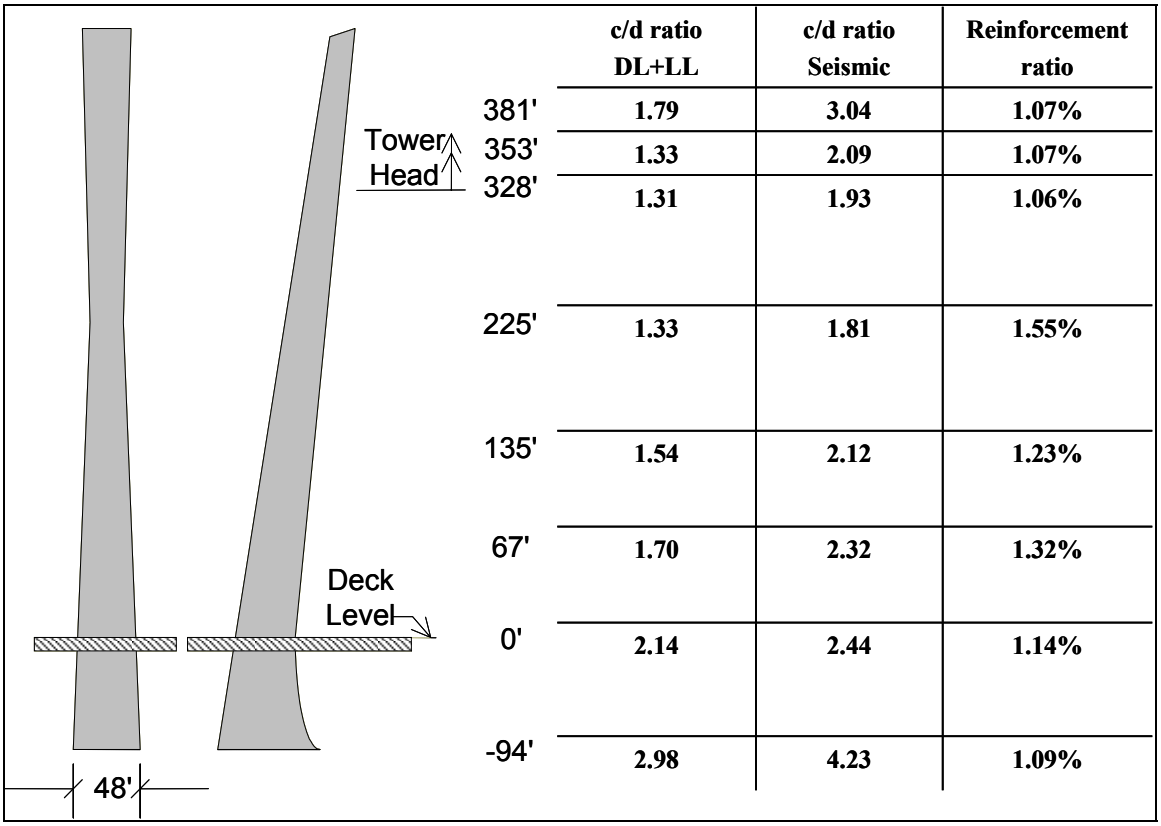

	c/d ratio DL+LL	c/d ratio Seismic	Reinforcement ratio
381'	1.79	3.04	1.07%
353'	1.33	2.09	1.07%
328'	1.31	1.93	1.06%
225'	1.33	1.81	1.55%
135'	1.54	2.12	1.23%
67'	1.70	2.32	1.32%
0'	2.14	2.44	1.14%
-94'	2.98	4.23	1.09%

Figure 13. Column Interaction Values.

SUMMARY

The NMRB is an inclined tower cable-stayed bridge with a main span of 610 m (2,000 ft), which will make it the longest bridge of its type in the Western Hemisphere. It crosses the Mississippi River just north of downtown St. Louis. The seismic design is based on a 2,500-year return period event, with the performance objectives of minimal damage and immediate serviceability.

The bridge articulation consists of integrally connecting the superstructure to the towers and providing expansion joints at mid-span and at the connections to the approaches. This creates relatively short period modes of vibration in the longitudinal direction of the bridge. The transverse modes are also shorter due to the width of the superstructure. The seismic base reactions in the longitudinal direction are roughly twice those in the transverse direction. Most of the seismic moments in the lower portion of the towers comes from the superstructure and not from the tower itself or through the cables.

Despite being located near the New Madrid Seismic Zone, and using a 2,500-year return period design spectrum, very few bridge components are controlled by seismic loads. This occurs due to other factors, including aesthetics, controlling the geometry of bridge components. The choice to utilize a cable girder in the short-end spans resulted in such a large concentration of mass that a unique pier shape was required to react the loads while still maintaining the required aesthetics.

ACKNOWLEDGEMENTS

The NMRB project is a collaboration between the Missouri and Illinois Departments of Transportation, with Illinois as the lead owner. HNTB, Inc. is the Project Management Consultant. The preliminary engineering phase of the design of the NMRB was conducted by a team of consultants. The major team members during the

Bridge Type Study phase of work were:

Modjeski and Masters, Inc.	Prime Consultant - Design of main bridge
Alfred Benesch & Co., Inc.	Design of approach spans and main bridge foundations
Hanson Professional Services, Inc.	Geotechnical consultant
TRC	Side span consultant
H2L2, Inc.	Lead Architects, preliminary plans
Rosales Gottemoeller & Associates, Inc.	Architectural consultant
KAI, Inc.	Architectural consultant
Jacobs Facilities	Architectural consultant

REFERENCES

[1] ATC/MCEER 2000. "NCHRP 12-49: Comprehensive Specifications for the Seismic Design of Highway Bridges - Draft," National Cooperative Highway Research Program, Washington, D.C.

[2] Hanson Engineers 2001. "Preliminary Geotechnical Report I-70 Mississippi River Bridge St. Louis County, Missouri, St. Clair County, Illinois," Hanson Engineers Inc., Springfield, Illinois.

[3] Wen, Y.D. and Wu, C.L. 2002. "Uniform Hazard Ground Motions for Mid-America Cities," *Earthquake Spectra* 17(2):359-384.

Seismic performance of a Double-deck viaduct

Tianbo Peng [1], Jiangzhong Li [1], Shide Hu [1], Lichu Fan [1]

ABSTRACT

In this paper, pseudodynamic test (PSD test) and numerical analytical results of a double-deck viaduct were conducted. The restoring force model, ductility capacity, strength, stiffness characteristics and collapse mechanism of the viaduct are analyzed and discussed. It's shown that test results can be predicted approximately through an equivalent bilinear restoring force model, and if the double-deck viaduct is designed appropriately, satisfactory seismic performance can be achieved.

[1]State Key Laboratory for Disaster Reduction in Civil Engineering, Tongji University, Shanghai 200092, PRC

INTRODUCTION

To resolve serious traffic problems in congested urban area, seven continuous double-deck viaduct structures were built in the San Francisco Bay Area during 1950s and 1960s. But six of these were damaged during the 1989 Loma Prieta earthquake [1], therefore seismic design for double-deck viaducts has been undergoing a critical reappraisal.

The first viaduct with a double deck in China was constructed in Shanghai. The pier is Y shape with an upper deck of six lanes for urban highway and a lower deck with two lanes for urban light railway system. The upper deck is simple concrete hollow plate girders and the lower deck simple box girders, supported on the elastomeric bearings with a span of 30m. Both of upper and lower columns of the pier are of rectangular section with initial cross section 1.3m ×3.0m.

In order to investigate the seismic performance of the double deck viaduct, PSD test and numerical analysis were carried out by State Key Laboratory for Disaster Reduction of Civil Engineering at Tongji University. In this paper, analytical and test methods are introduced first, and then their results are compared.

TEST AND ANALYSIS METHODS

Test method and model

PSD test method [2,3], which is developed in the last 30 years, is used to simulate the seismic behavior of the viaduct with a double-deck. The method integrates the advantages of quasi-static test method and shaking table test method, and can be applied to investigate nonlinear seismic behavior of a large-scale model.

A one-fifth-scale model based on the viaduct with a double-deck in Shanghai, as shown in figure 1, was selected. Distance between the bottom of lower columns and top of upper cap beam is 3.74m, and distance between the centerlines of the two cap beams is 1.80m. Longitudinal reinforcement ratios of the upper and lower columns equal to 1.359% and 1.661%, respectively. Axial load ratios of the upper and lower columns are 0.075 and 0.108, respectively. Because the columns of prototype are designed to be ductile members, and cap beams and joints are capacity protected members, the investigation focuses on the seismic response of columns.

Numerical analysis methods

Pushover analysis (nonlinear static analysis) method and nonlinear dynamic time history analysis method are both adopted to check the test results. The program DRAIN-3D [4] is used to carry out the seismic numerical analysis, where columns are simulated with fiber beam-column elements and joints are assumed to be rigid. The Mander model [5], which has been widely used in analyzing columns with both circular and rectangular cross sections, is adopted for confined concrete, and the elastic perfectly plastic model is for reinforcement. Lumped mass model is adopted, and damp ratio of concrete is set to 0.05.

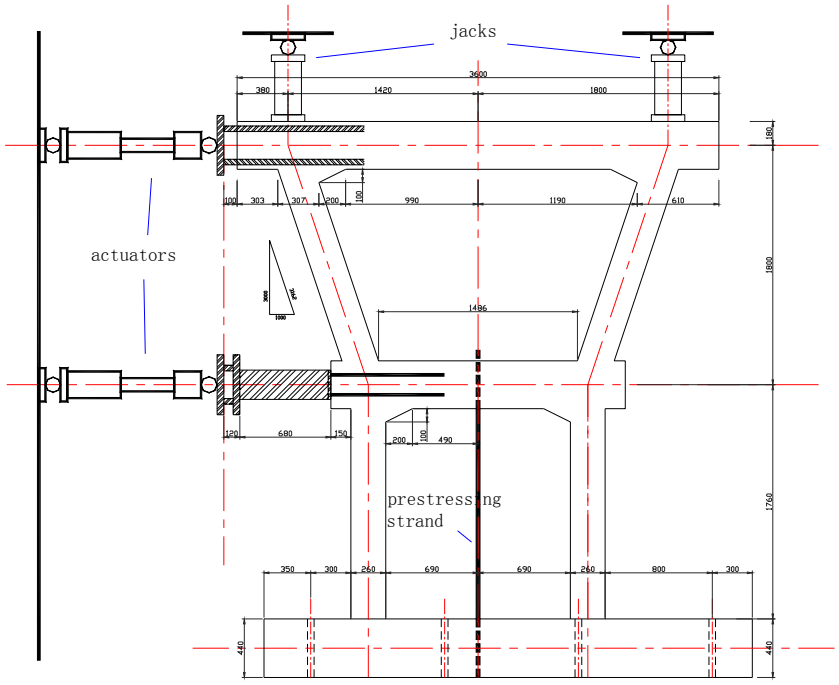

Figure 1. Elevation of the specimen

Earthquake inputs and test cases

A site specific time history of input acceleration, called Gong2 wave, is shown in figure 2. The seismic behavior of the prototype structure is investigated systematically by increasing the maximum of the acceleration history progressively (form 0.04g to 1.00g). 20 cases are arranged in sequence in the PSD test and numerical analysis.

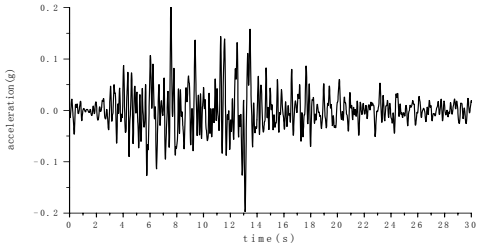

Figure 2. The earthquake input - Gong2 wave

COMPARISON OF TEST AND ANALYSIS RESULTS

The PSD test phenomena and preliminary analysis have been introduced in reference [6]. The problems, which have been investigated and compared, are as follows.

Restoring force model

"Skeleton curves" can be formed according to interstory hysteresis loops, which is constructed by the data of interstory drifts and the corresponding interstory shears. The structural restoring force model can be deduced if the skeleton curves are equivalently bilinearized, which is shown in figure 3. Where Δ_y and Q_y are the first yield displacement and corresponding shear force, Δ_u is the ultimate displacement, and E_c is the area between the skeleton curve and abscissa axis, which reveals the energy dissipated. The equivalent yield displacement Δ_e and yield strength Q_e for bilinear model can be deduced according to the equal energy-dissipated principle. In figure 3, solid line and dash line represent the equivalent bilinear model and the skeleton curve respectively.

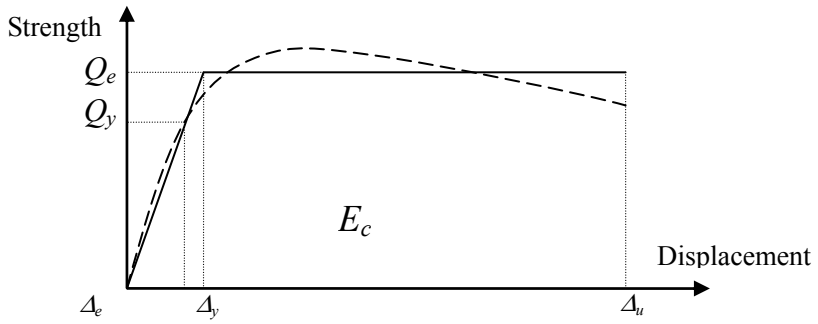

Figure 3. Equivalent bilinear model of skeleton curve

The comparison of the equivalent bilinear model parameters from test and analysis results is given in table I. It's shown that difference from test and analysis are small, and the difference is in the range of 1.03% to 27.07%.

The displacement ductility capacity shown in table I is obtained by dividing the ultimate displacement by equivalent yield displacement. As shown in table I, all the ductility capacities are approximate to 10 and sufficient to meet the seismic demands. The lower structural capacity is less than the upper one because the lower columns are subjected to more axial forces, which not only increases the yield displacement, but also decreases the ultimate displacement.

Strength and stiffness characteristics

The equivalent yield strength and maximum strength of the upper, lower and total structure are tabulated in table II. It's shown that all the test strengths are close to the corresponding analysis results, and the difference is in the range of 0.08 %to 16.16%, and the fiber element can simulate the structural performance and overstrength phenomena.98

The structural stiffness kept declining during PSD test and the relationships of stiffness and cases are shown in figure 4. Initial tangent stiffness and secant stiffness from test and analysis results are compared. As shown, serious stiffness degradations take place in two cases, which should correspond to the structural cracking state and yielding state, respectively. Consequently the

stiffness curves can be divided into three phases: initial stiffness, descending stiffness and residual stiffness.

TABLE I. COMPARISON OF PARAMETERS OF THE TWO MODELS FROM TEST AND ANALYSIS

Structure	Parameters	Test results	Analysis results	Difference (%)
Upper	Δ_u(mm)	136.78	150.62	-10.12
	Δ_e(mm)	12.47	10.32	17.24
	Q_e(kN)	232.73	245.51	-5.49
	Displacement ductility capacity	10.97	14.59	-33.00
Lower	Δ_u(mm)	80.47	81.30	-1.03
	Δ_e(mm)	8.20	9.65	-17.68
	Q_e(kN)	295.86	343.68	-16.16
	Displacement ductility capacity	9.81	8.42	14.17
Total	Δ_u(mm)	166.33	169.99	-2.20
	Δ_e(mm)	14.04	17.84	-27.07
	Q_e(kN)	285.33	300.98	-5.48
	Displacement ductility capacity	11.85	9.53	19.58

TABLE II. STRENGTH CHARACTERISTICS

Structure	Strengths	Test results	Analysis results	Difference (%)
Upper	Q_e (kN)	232.73	245.51	-5.49
	Q_m (kN)	246.54	260.31	-5.59
Lower	Q_e (kN)	295.86	343.68	-16.16
	Q_m (kN)	318.58	350.79	-10.11
Total	Q_e (kN)	285.33	300.98	-5.48
	Q_m (kN)	318.58	318.82	-0.08

In figure 5, relationships of the interstory secant stiffness and interstory displacement amplitude from test and analysis results are compared. As shown, the upper secant stiffness from test results is greater, but the lower secant stiffness from test results is lesser, because the equipments used in PSD test to simulate the dead load acting on the upper cap beam might restrict the upper structural deformation and then increase the restoring force measured.

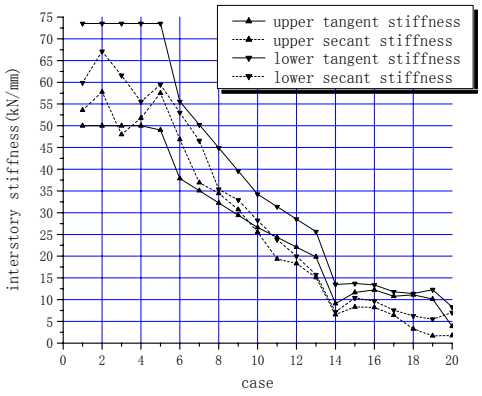

Figure 4. Relationships of stiffness and cases

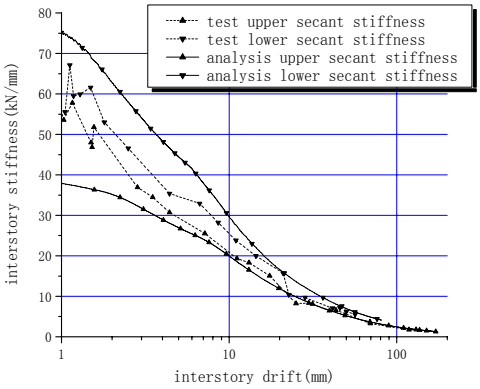

Figure 5. Comparison of secant stiffness

Collapse mechanism

In the double-deck viaduct, four columns are selected as ductile members. In the PSD test and dynamic analysis, all the columns' ends yielded before the bottoms of upper columns are destroyed as expected. It's shown from the common feature of test and analysis that structural deformation is concentrated in the upper structure, and the structural damage is concentrated in the bottoms of upper columns. The collapse mechanism of the model after PSD test is shown in figure 6.

Figure 6. The collapse mechanism of the model after PSD test

Time history comparison of three typical cases

The absolute displacement time histories of the two cap beams from test and analysis results are compared, and the results of three typical cases, whose acceleration peaks correspond to 0.04g, 0.10g and 0.20g respectively, are shown in figure 7 and 8. In the figures, all the lines above are from test results and all the below are from analysis results. It's shown that the shape of each curve approximates to the corresponding one, therefore PSD test and time history analysis method are both credible.

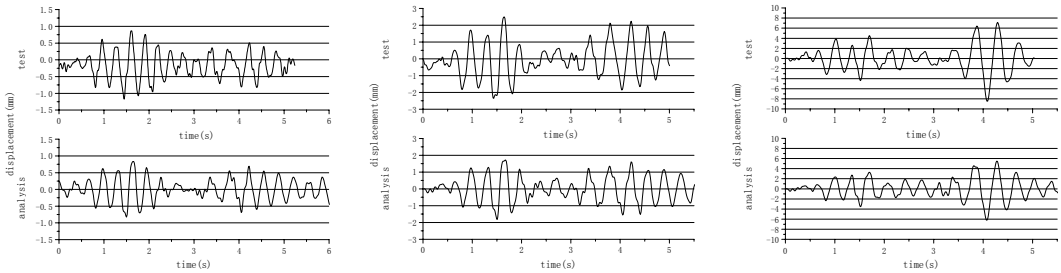

a) a_g=0.04g b) a_g=0.10g c) a_g=0.20g

Figure 7. Comparison of lower cap beam displacement time histories

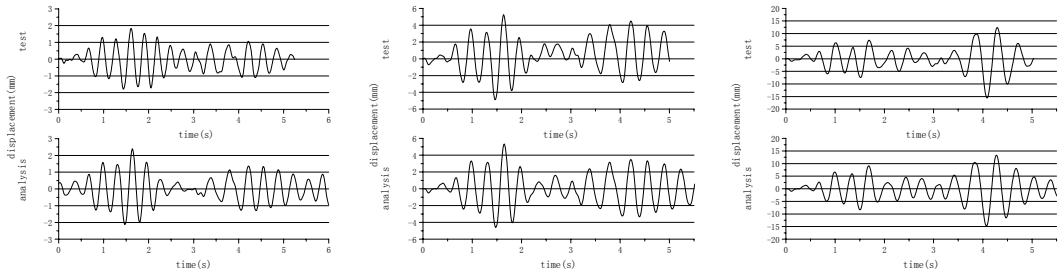

a) a_g=0.04g b) a_g=0.10g c) a_g=0.20g

Figure 8. Comparison of upper cap beam displacement time histories

CONCLUSION

In this paper, PSD test and numerical analysis results are compared, and conclusions are drawn as follows:

1. Both restoring force models are approximately equal;
2. All the ductility capacities are sufficient to meet the seismic demands;
3. All the test strengths are close to the corresponding analysis results;
4. The stiffness curves can be divided into three phases, equipments may increase the restoring force measured;
5. The shape of each time history curve approximates to the corresponding one.
6. According to the seismic investigation of double-deck viaduct, it's shown that PSD test method and numerical analysis method using nonlinear fiber beam-column element for structural elements are reliable and satisfactory.

REFERENCES

F. Zayati, S. A. Mahin, 'Experimental and analytical evaluation of a retrofit double-deck viaduct structure', UCB/EERC 96/03, University of California, 1996.

S. A. Mahin, P. B. Shing, ‘Pseudodynamic test method-Current status and future directions’, Journal of Structural Engineering, ASCE 1989(8), 2113-2128.

K. Takanashi, M. Nakashima, ‘Japanese activity on on-line testing’, Journal of Engineering Mechanics, ASCE 1987(7), 1014-1032.

V. Prakash, G. H. Powell and S. Cambell, ‘Drain-3DX base program description and user guide’, UCB/SEMM 94/07, University of California, 1994.

J. B. Mander, M. J. N. Priestley, R. Park, ‘Theoretical Stress-Strain Model for Confined Concrete’, J. Struct. Eng., ASCE, 1988, 114(8), p. 1804-1849

Peng tianbo, ‘Pseudodynamic test investigation of double-deck viaduct’, doctoral dissertation, 2003.3.

Chongqing CaiYuanBa Yangtze River Crossing

John Sun, Ph.D, PE; the Project Chief Engineer; T. Y. Lin International
Man-.Chung Tang, Ph.D, PE; the Project Technical Director; T. Y. Lin International

Approved by the National Council and Office of Prime Minister of China, 2.2 Billion RMB ($300 millions) Chongqing CaiYuanBa Yangtze River Crossing is currently the single most important infrastructure improvement project in this ever-expanding City of Chongqing. Bridging the great Yangtze in the heart of two busiest business districts of Chongqing city, it will carry six lanes of highways and two pedestrian walkways on its upper deck as well as two mono-rails on its lower deck, serving as one of the transportation backbones for the City of Chongqing. In Feburary, 2003, the joint venture between T.Y.Lin International and Chongqing Transportation Research and Design institute were officially commitioned to perform the design of the entire project which include a main arch span, two approaches (or skyways), two massive four-level interchanges and two parks within the project limits.

In addition to design for its basic function as the transportation “life-line” and extremely demanding construction schedule and conditions, the designers must also address the bridge’s impacts on the great Yangtze navigation line and respect the city’s civil and natural landscapes, as well as consider the budgetary restraints. With extensive comparative studies and evaluations, the 420-meter tie-arch, shown in the rendering, was recommended for the final design as the signature main span of the Chongqing CaiYuanBa Yangtze River Crossing. When completed by the end year 2005, it most will be the longest arch for rail and highway dual crossings in the world.

This paper presents key issues, the design philosophy, major innovative design concept, critical details of the main arch span of the CaiYuanBa Yangtze River Crossing.

Rendering of Chongqing CaiYuanBa Yangtze River Crossing Main Span

Effect of Retrofit, Skew and Number of Spans on Bridge Fragility

Masanobu Shinozuka, Sang-Hoon Kim and Youwei Zhou

ABSTRACT

The Northridge Earthquake inflicted various levels of damage upon a large number of Caltrans' bridges not retrofitted by column jacketing. In this respect, this study particularly investigates the effect of retrofit on the seismic fragility of bridges strengthened by steel jacketing of columns, and also of the skew and number of spans of bridges. Monte Carlo simulation is performed to study nonlinear dynamic response of the bridges before and after column retrofit. Fragility curves in this study are represented by lognormal distribution functions with two parameters (fragility parameters consisting of median and log-standard deviation) and developed as a function of peak ground acceleration (PGA). The sixty (60) ground acceleration time histories for Los Angeles area developed for FEMA SAC project are used for the dynamic analysis of the bridges. In addition, a computer code is developed and used to calculate hysterestic parameters of bridge columns before and after steel jacketing for nonlinear dynamic analysis of bridges. From the nonlinear response analysis performed on five bridges typical in California, analytical fragility curves are derived in accordance with prescribed ductility-based damage condition. The comparison of the analytical fragility curves of the bridges before and after column retrofit demonstrates that the improvement of the bridges with steel jacketing on the seismic performance is excellent for the damage states prescribed in this study. The improvement is expressed in terms of the fragility enhancement factor defined as the ratio of the median value of the fragility curve after the retrofit to the median value before. The empirical fragility curves obtained for bridges not retrofitted are adjusted by the enhancement factor evaluated from analytical fragility curves in order to obtain empirical fragility curves associated with the retrofitted bridges. The effect of skew and number of span on bridge fragility is investigated by comparing empirical fragility curves of bridges classified into several categories based on the bridge damage data from the Northridge Earthquake. On the one hand, the results demonstrate the adverse effect increases as the skew angle and the number of spans become larger, just as FEMA HAZUS bridge fragility formula shows. On the other hand, compared with the developed empirical fragility curves, FEMA HAZUS formula tends to be unconservatively underestimating the negative effect of both skew and number of spans on bridge fragility.

Masanobu Shinozuka, Department of Civil and Environmental Engineering, University of California, Irvine, CA 92697
Sang Hoon Kim, Department of Civil and Environmental Engineering, University of California, Irvine, CA 92697
Youwei Zhou, Department of Civil and Environmental Engineering, University of California, Irvine, CA 92697

INTRODUCTION

Several recent destructive earthquakes, particularly the 1989 Loma Prieta and 1994 Northridge earthquakes in California, and the 1995 Kobe earthquake in Japan, have caused significant damage to a large number of highway structures. The investigation on these negative consequences gave rise to serious review of seismic design philosophy and lead to extensive research activities on the retrofit of existing bridges as well as the seismic design method of new bridges.

The first objective of the study is to evaluate the effects of column retrofit with steel jacketing on increasing the ductility capacity of bridge columns and hence improving the bridge fragility characteristics. These analytical fragility curves developed in this study are used to adjust the empirical fragility curves obtained for the bridges not retrofitted on the basis of seismic damage data on Caltrans' freeway bridges under the 1994 Northridge Earthquake. The adjustment is carried out by multiplying the medians of the empirical curves before the retrofit by corresponding fragility enhancement factor obtained analytically.

The second objective of this study is to investigate the effect of two important structural attributes of bridges, skew and number of spans, on their fragility. For this objective, the same empirical fragility curves of bridges based on the 1994 Northridge Earthquake damage are used. The empirical modification factors are then evaluated and compared with FEMA HAZUS bridge fragility models.

RESEARCH APPROACH

Fragility Curves for Seismically Retrofitted Bridges

This study represents results of fragility analysis of example bridges (Figs. 1-5) typical in California strengthened for seismic retrofit by means of steel jacketing of bridge columns. A computer code is developed and used to calculate bilinear hysterestic parameters of bridge columns before and after steel jacketing. These parameters are used for nonlinear dynamic time history analysis to evaluate responses of the bridges before and after column retrofit under the sixty (60) ground acceleration time histories for Los Angeles area developed for FEMA SAC project. Monte Carlo simulation is performed to study fragility curves represented by lognormal distribution functions with two parameters (fragility parameters consisting of median and log-standard deviation) and developed as a function of peak ground acceleration (PGA). The comparison of fragility curves of the bridges before and after column retrofit demonstrates that the improvement of the bridges with steel jacketing on the seismic performance is excellent for the damage states defined in this study.

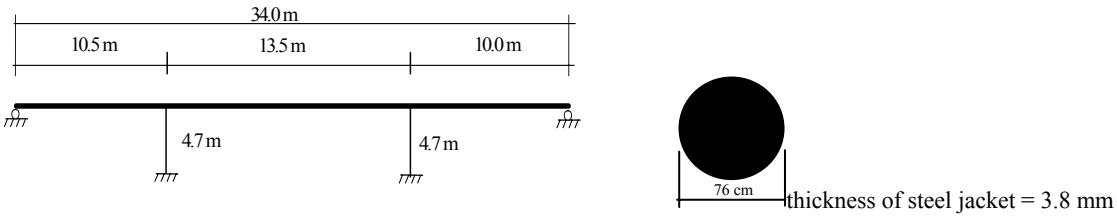

Figure 1. Elevation and Column Section of Bridge 1

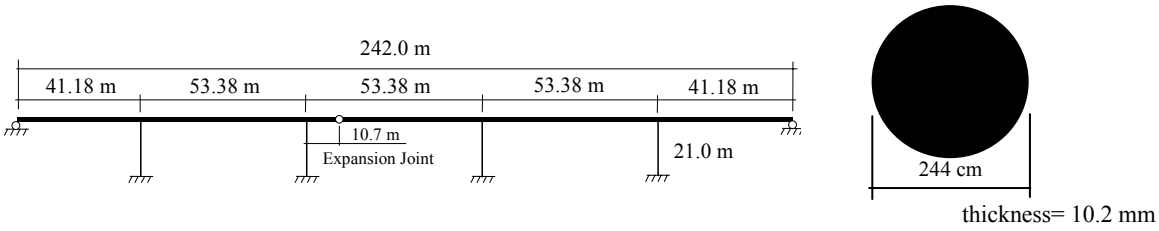

Figure 2. Elevation and Column Section of Bridge 2

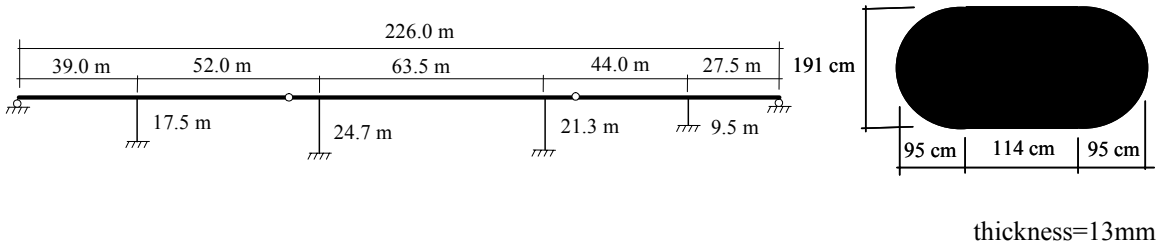

Figure 3. Elevation and Column Section of Bridge 3

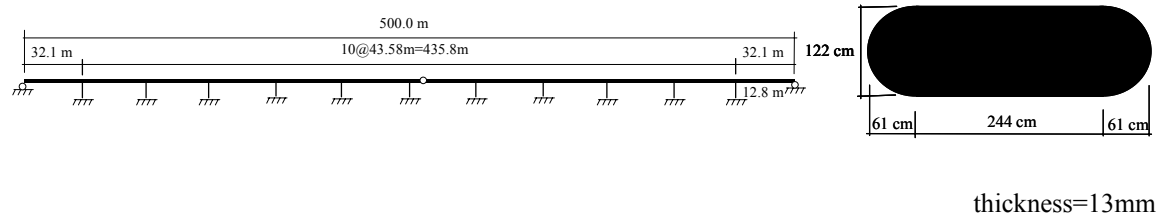

Figure 4. Elevation and Column Section of Bridge 4

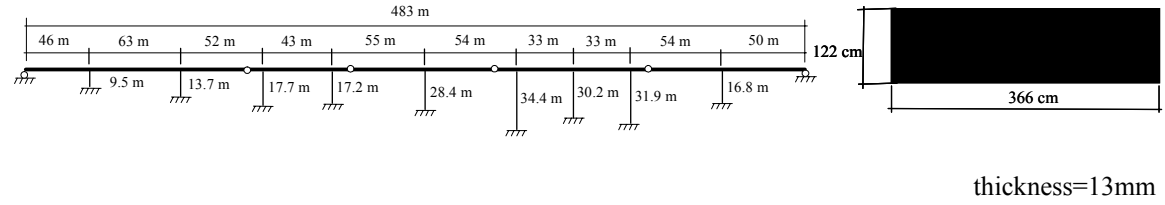

Figure 5. Elevation and Column Section of Bridge 5

The moment-curvature curves for a column of Bridge 1 are plotted together in Fig. 6. In the present study, Kushiyama's (Kushiyama 2002) curves are used for the dynamic analysis. The result shows that the curve after retrofit gives a much better performance than that before retrofit by 2.6 times based on curvature at the ultimate compressive strain.

The parameter used to describe the nonlinear structural response in this study is the ductility demand. The ductility demand is defined as θ/θ_y, where θ is the rotation of a bridge column in its plastic hinge under earthquake ground motion considered and θ_y is the corresponding rotation at the yield point. Ductility demand suggested by Dutta and Mander (Dutta and Mander 1999) shown in Table 1 is used for determining the state

of damage for a column in question. Then, a bridge reaches the state of no, at least slight, at least moderate, at least extensive or collapse damage if at least one hinge at any of the columns sustains no, at least minor, at least moderate, at least major or collapse damage, respectively.

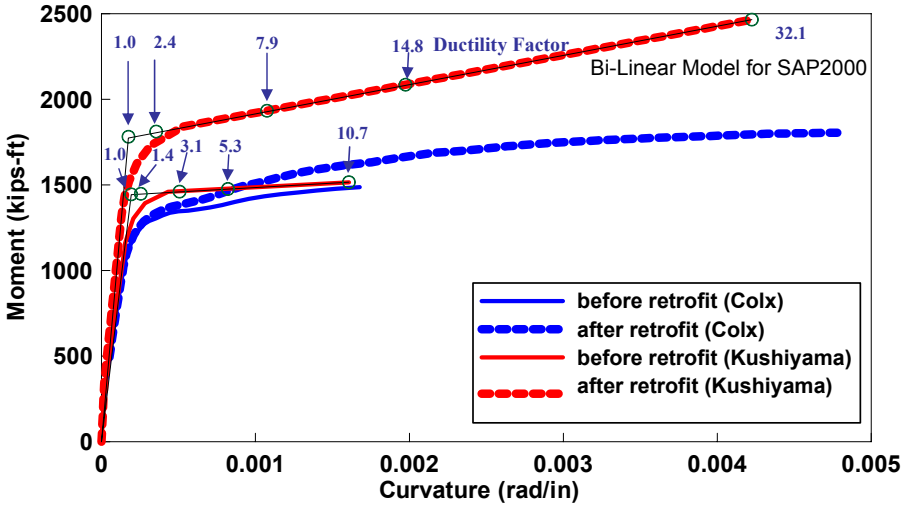

Figure 6. Moment-curvature curves for column of Bridge 1

Damage State	Description	Drift Limits	Ductility
No Damage	First Yield	0.008	1.0
Slight Damage	Cracking & Spalling	0.010	2.01
Moderate Damage	Loss of Anchorage	0.025	6.03
Extensive Damage	Incipient Pier	0.050	11.07
Complete Collapse	Pier Collapse	0.075	23.65

Table 1. Damage States Definition of Bridge Column

RESEARCH RESULTS

Fragility Curves for Seismically Retrofitted Bridges

The effect of column retrofit on the seismic performance is excellent in that the bridges are up to three times less fragile (complete damage) for Bridge 1 and 2.5 times (extensive damage) for Bridge 2 after retrofit compared to the case before retrofit in terms of the median values (Figs. 7 and 8). The effect of retrofit is demonstrated by means of the ratio of the median value of the fragility curve for retrofitted column to that of the column before retrofit. This ratio is referred to as fragility "enhancement". Considering Bridges 1 and 2 with circular columns and corresponding sets of fragility curves before and after retrofit, the average fragility enhancement over these bridges at each state of damage is computed and plotted as a function of the state of damage. An

analytical function is interpolated as "enhancement curve" and it is plotted through curve fitting as shown in Fig. 9. This curve shows enhancement factor 0f 1.2, 1.34, 1.58, 1.98 and 2.67 for each damage state described on the *x* axis in Fig. 9.

It is assumed that the fragility enhancement obtained from this function also applies to the development of the fragility curves after the retrofit for the empirical fragility curves (Fig. 10) associated with the expressway bridges in Los Angeles and Orange County, California subjected to the Northridge earthquake. Under the assumption that Dutta and Mander's damage states (1999) are interchangeable with Caltrans definition so that "slight=minor", "moderate=moderate", "extensive=major" and "complete=collapse", three enhanced empirical fragility curves after retrofit for minor, moderate and major damage are plotted in Figs. 11, 12 and 13 respectively to be used in expressway network performance analysis.

The fragility curves for Bridge 2 are also developed to demonstrate the effect of retrofit at expansion joints by extending seat width in Fig. 14 and installing restrainers designed for anchor force capacity in Fig 15. These two figures show excellent improvement for both retrofit methods at expansion joints.

Table 2 Number of damaged Bridge 1

sample size=60

Damage states	before retrofit	after retrofit
Almost no	56	53
Slight	51	44
Moderate	41	28
Extensive	34	15
Complete	17	2

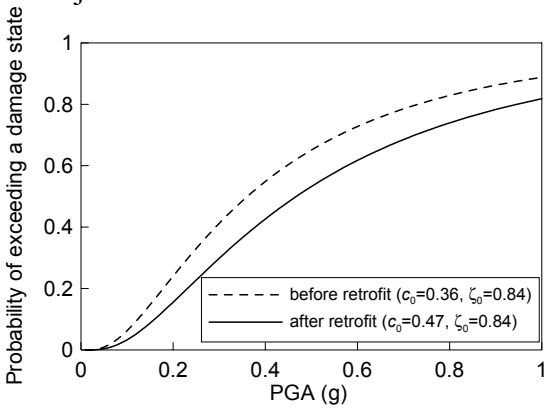

(a) Almost no damage

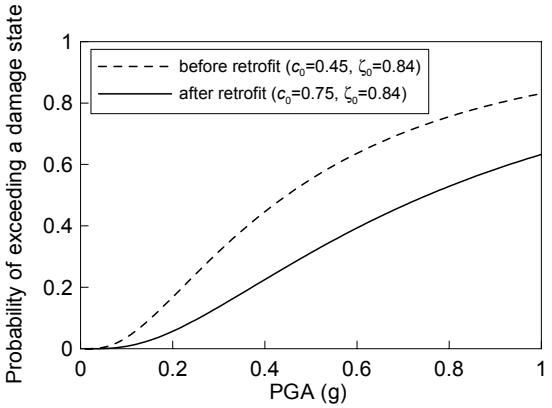

(b) Slight damage

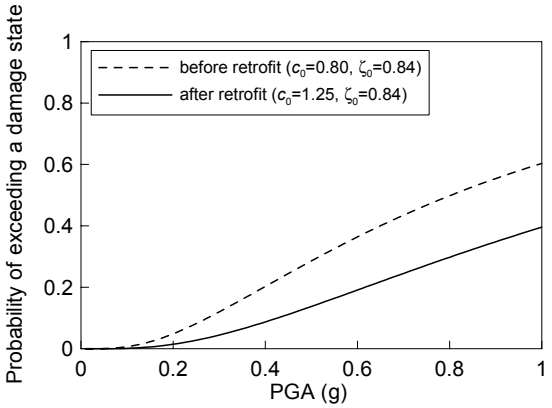

(c) Moderate damage

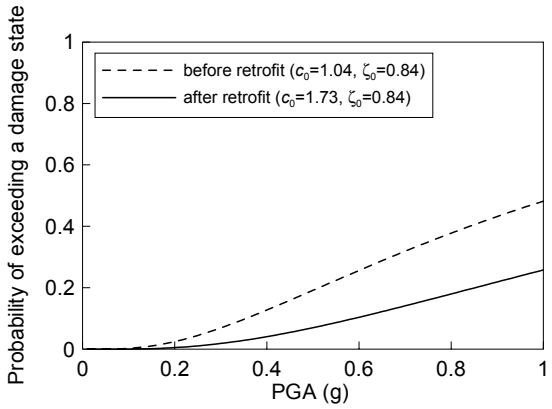

(d) Extensive damage

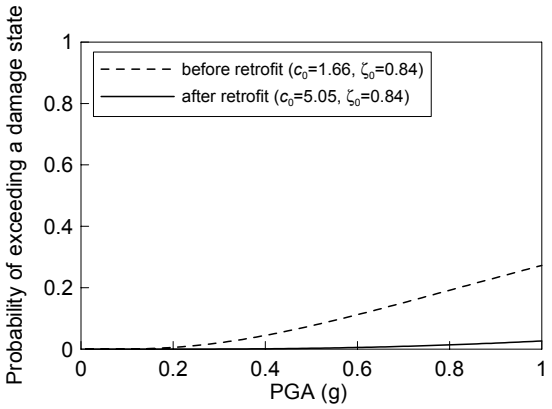

(e) Complete collapse

Figure 7. Fragility Curves of Bridge 1

Table 3. Number of damaged Bridge 2

sample size=60

Damage states	before retrofit	after retrofit
Almost no	51	50
Slight	47	41
Moderate	37	22
Extensive	30	10
Complete	14	4

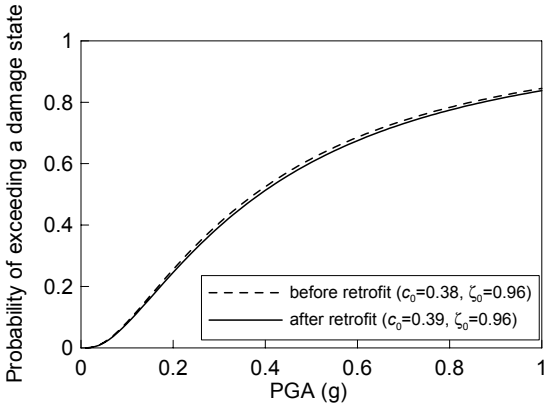

(a) Almost no damage

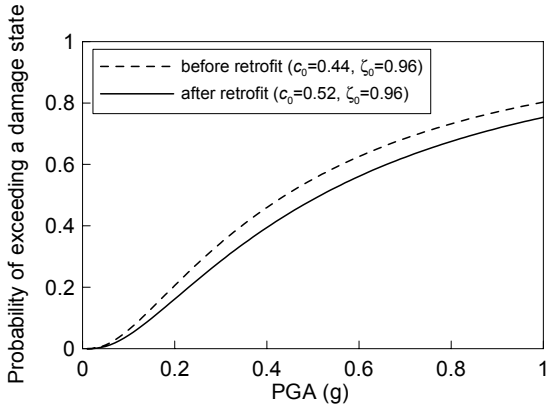

(b) Slight damage

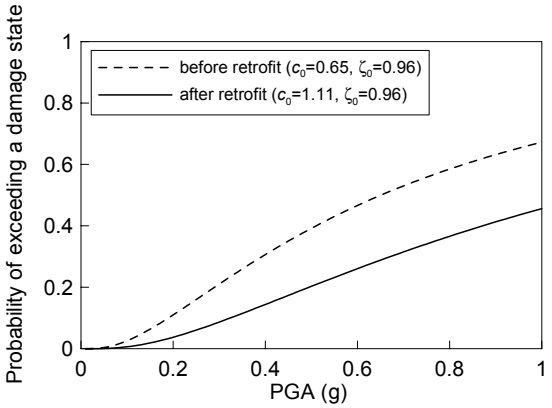

(c) Moderate damage

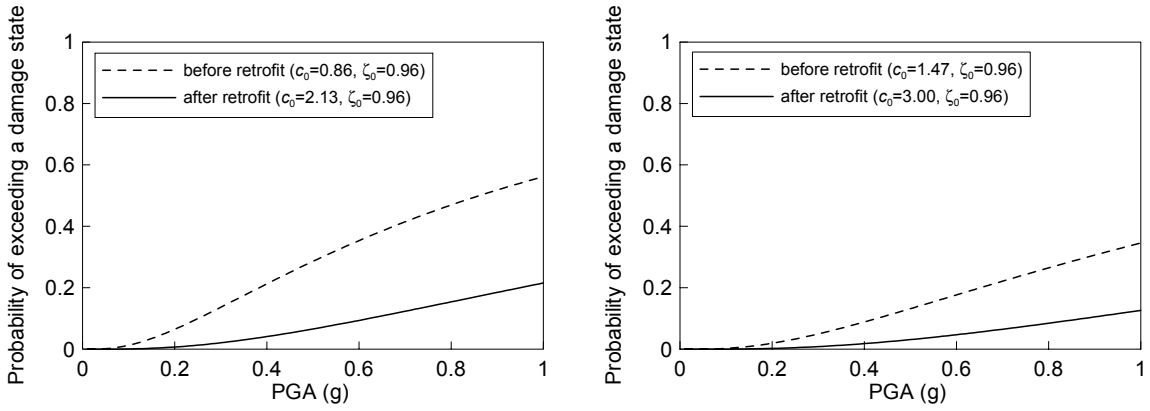

(d) Extensive damage (e) Complete collapse

Figure 8. Fragility Curves of Bridge 2

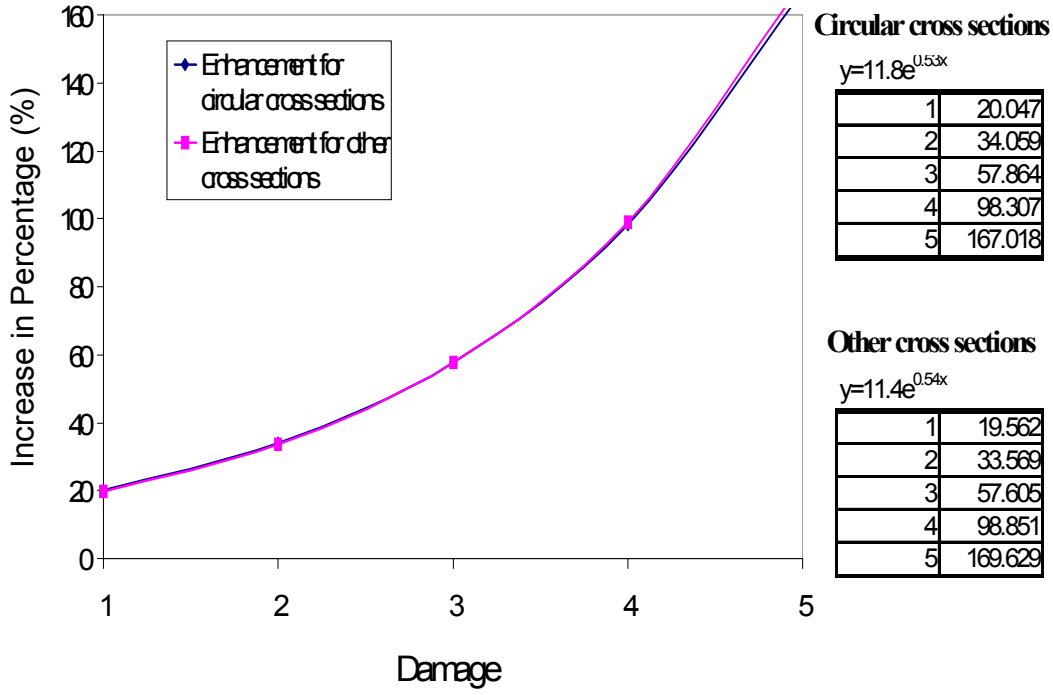

Figure 9. Enhancement Curve for Circular Columns with Steel Jacketing

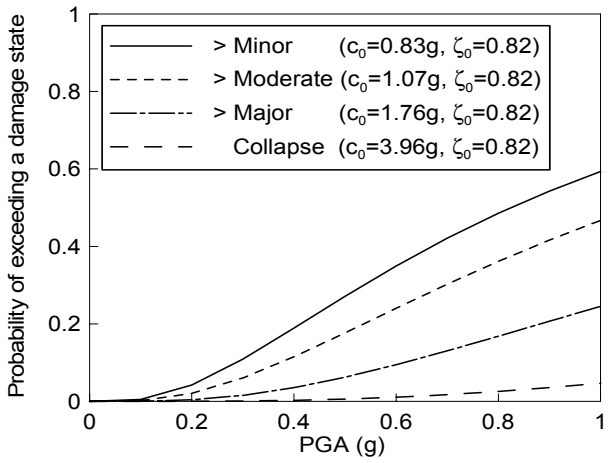

Figure 10. Empirical Fragility Curves of Caltarns' Bridges (developed by Shinozuka et al. 2001)

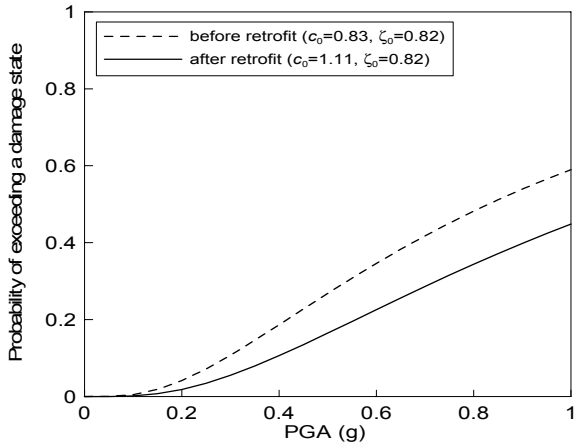

Figure 11. Enhanced Empirical Fragility Curves for Minor Damage after Retrofit

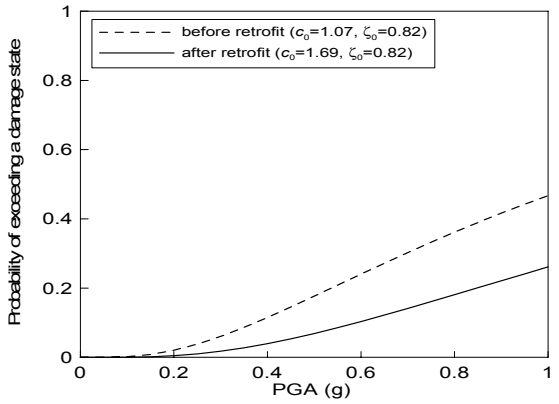

Figure 12. Enhanced Empirical Fragility Curves for Moderate Damage after Retrofit

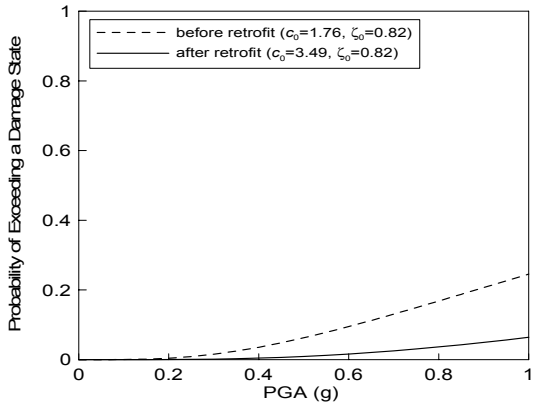

Figure 13. Enhanced Empirical Fragility Curves for Major Damage after Retrofit

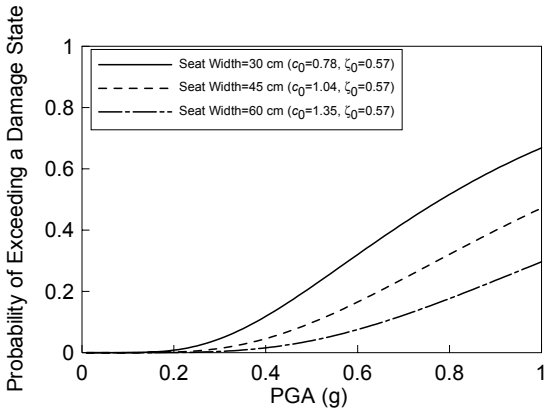

Figure 14. Fragility Curves for Expansion Joint Retrofit by Extension of Seat Width

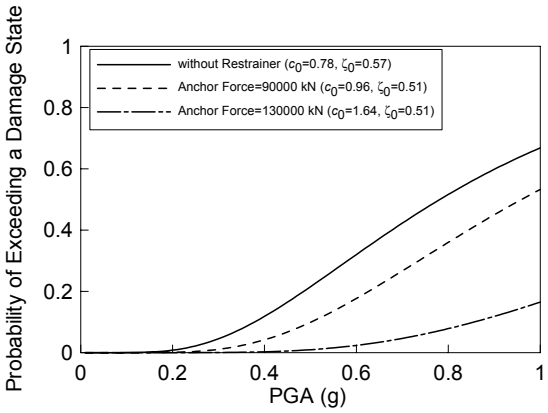

Figure 15. Fragility Curves for Expansion Joint Retrofit by Restrainers

Effects of Skew and Number of Spans

Two structural attributes, skew angle and number of span will also affect the seismic performance of a bridge. In Figure 16, the empirical fragility curves with single or multiple spans are compared. The comparison shows that the single span bridge is much seismically stronger than the multi-span bridge. The effect of the skew angle is demonstrated in Figure 17 and as the skew angle increases, the bridge tends to be more seismically vulnerable.

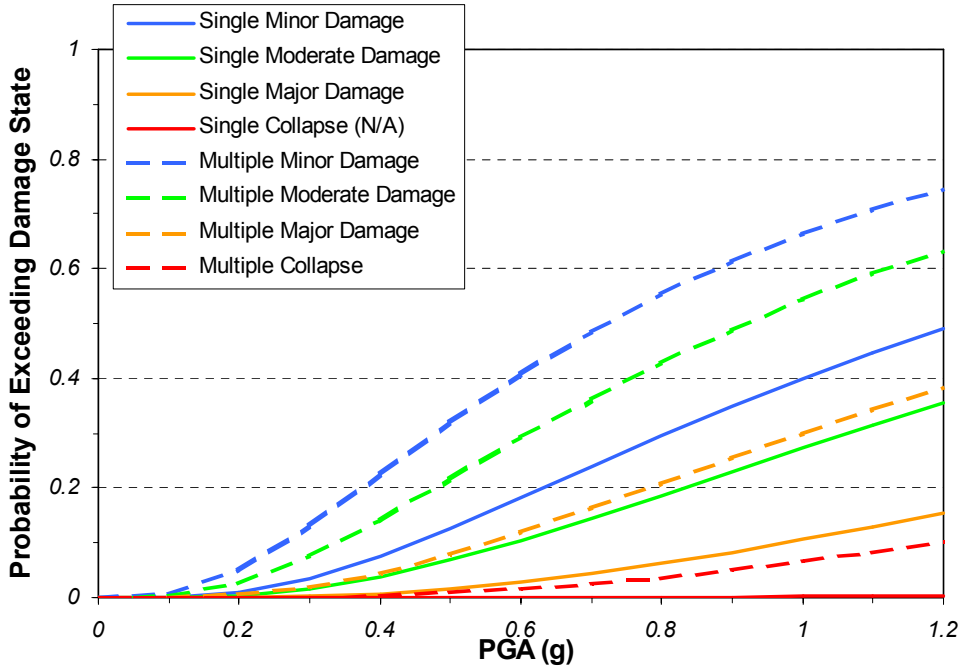

Figure 16. Effect of Number of Span (Single or Multiple)

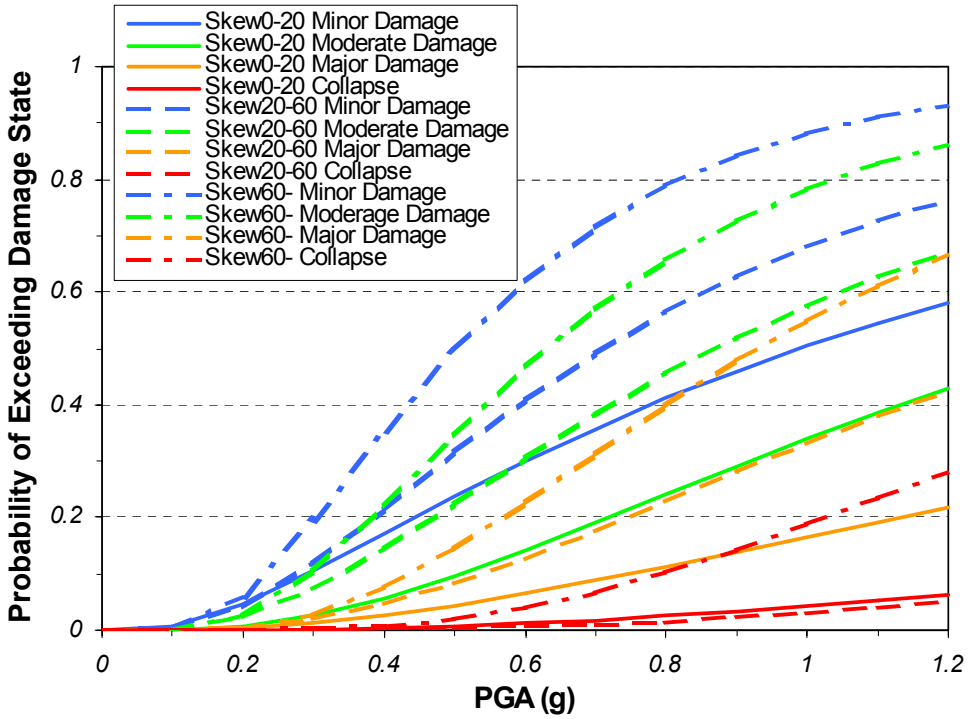

Figure 17. Effect of Skew Angle

Comparison with HAZUS Fragility Model

In HAZUS (NIBS, 1999 and, Basoz and Mander, 1999), the effect of skew is considered by a factor $F_{skew} = \sqrt{\sin(90^\circ - skew)}$, which is used to modify the median value of fragility curves associated with damage states of at least moderate(C2), at least extensive(C3) and collapse(C4). To compare with HAZUS formula, empirical fragility curves of bridges classified into more categories based on the skew angle are developed with maximum likelihood method (Shinozuka and etc., 2001) in Table 4 where parameters of fragility curves are given with C1, C2, C3 and C4 being the median value, and Log. S.D. the log standard deviation. Divided by median value of the fragility curve of bridges with skew=0, the empirical modification factor related with skew angle is obtained. Figure 18 compares the skew modification factor in FEMA HAZAUS bridge fragility model and the developed empirical fragility curves. It can be seen that HAZUS modification factor is larger and tends to result in unconservative estimation of bridge seismic capacity.

HAZUS also considers the effect of the number of span by the modification factor

$$F_{3D} = 1 + A/(N - B) \quad (1)$$

N is the number of span, A and B depend on the bearing type and structural type. B adopts 1 or 0 and A is between 0.10 and 0.33. So the range of F_{3D} is between 1 and 1.33 For seismically designed continuous concrete bridge,

$$F_{3D} = 1 + 0.33/N. \quad (2)$$

The parameters of empirical fragility curves of bridges with different spans are shown in Table 5. With the median value of each damage state divided by the median value of the bridge with number of spans =1, the empirical modification factor related

with number of spans is obtained, which is then compared with equation (2) divided by 1.33 in Figure 19. For small number of spans (up to 3), empirical results agree with the HAZUS model except for the state of extensive damage. However, for bridges with number of spans larger than 3, HAZUS formula is greater than empirical value and thus overestimate the seismic performance of bridges.

Table 4. Parameters of Fragility Curves of Bridges with Different Skew

SKEW	0	1-20	21-40	41-60	>60
C1 (g)	1.18	0.88	0.60	0.77	0.49
C2 (g)	1.66	1.14	0.74	0.86	0.65
C3 (g)	3.17	1.61	1.12	1.36	0.83
C4 (g)	5.94	-----	-----	4.03	1.00
Log. S.D.	1.00	0.71	0.58	0.86	0.53

Table 5. Parameters of Fragility Curves of Bridges with Different Number of Span

SPAN	1	2	3	4	5,6,7	8,9,10	>10
C1 (g)	0.93	0.80	0.77	0.63	0.46	0.37	0.34
C2 (g)	1.14	0.95	1.02	0.80	0.60	0.42	0.39
C3 (g)	1.51	1.50	1.52	1.22	0.88	0.59	0.69
C4 (g)	-----	-----	-----	2.89	1.43	1.13	-----
Log. S.D.	0.63	0.62	0.77	0.74	0.54	0.55	0.36

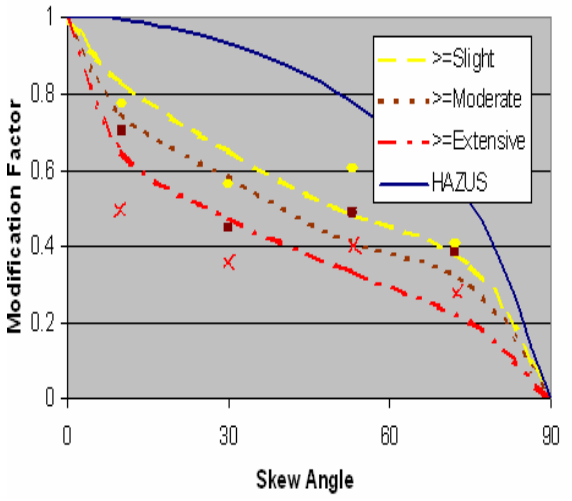

Figure 18. Effect of Skew Angle

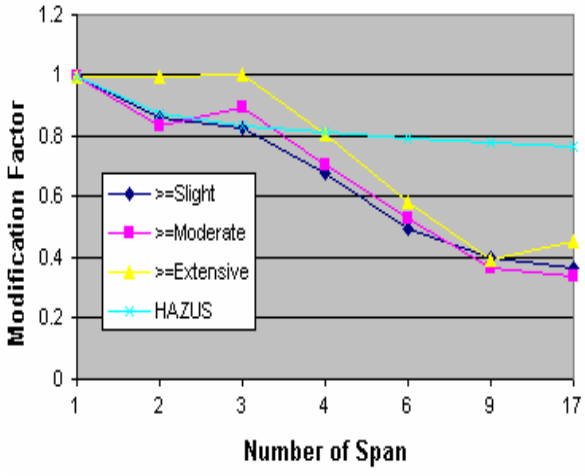

Figure 19. Effect of Number of Spans

CONCLUSION

The following conclusions are drawn from the results of this study.

(1) The simulated fragility curves after column retrofit with steel jacketing show excellent improvement (less fragile) compared to those before retrofit by as much as three times based on median PGA values.

(2) After retrofit, the number of damaged bridges substantially decreases especially for severe damage states defined in this study.

(3) An "enhancement curve" is proposed and applied to develop fragility curves after retrofit on the basis of empirical fragility curves. This is done for the reason that empirical fragility curves are expected to be significantly more reliable than those derived otherwise.

(4) Regarding the effect of skew and number of spans on bridge fragility, the empirical fragility curves of bridges classified into several categories are developed based on the historical damage data and compared with FEMA HAZUS bridge fragility model. Similar to HAZUS formula, the results show the adverse effect increases as skew and number of spans become larger, but HAZUS formula tends to underestimate their negative effects.

ACKNOLEDGEMENT

This study was supported by the MCEER/FHWA under Contract No. DTFH 61-98-C-00094 and Caltrans under Contract No. 59A0304.

REFERENCES

Basoz Nesrin and Mander John, 1999, "Enhancement of the Highway Transportation Lifeline Module in HAZUS", report prepared for National Institute of Building Sciences, 1999.

Chai, Y.H., Priestley, M.J.N. & Seible F. 1991. "Seismic Retrofit of Circular Bridge Columns for Enhanced Flexural Performance ". ACI Structural Journal V. 88 (No. 5): 572-584.

Dutta, A. and Mander, J.B. 1999. "Seismic Fragility Aanalysis of Highway Bridges," Proceedings of the Center-to-Center Project Workshop on Earthquake Engineering in Transportation Systems, Tokyo.

Kushiyama, S. 2002. Calculation Moment-Rotation Relationship of Reinforced Concrete Member with/without Steel Jacket. Unpublished Report at University of Southern California, CA, USA.

National Institute of Building Sciences, (1999), *Earthquake Loss Estimation Methodology: HAZUS 99 (SR2) Technical Manu*al, Developed by Federal Emergency Management Agency, Washington D.C., http://www.fema.gov/hazus.

Priestley, M.J.N., Seible, F. & Calvi, G.M. 1996. Seismic Design and Retrofit of Bridges. John Wiley & Sons, Inc.: 270-273.

SAP2000 v.7.44 User Manual. 2002. Computer and Structures Inc., CA, USA.

Shinozuka, M., Feng. M.Q., Kim, H.-K., Uzawa, T. & Ueda, T. 2001. Statistical Analysis of Fragility Curves. Technical Report at Multidisciplinary Center for Earthquake Engineering. (http://shino8.eng.uci.edu/techniclpapers.htm).

Shinozuka, M., Kim, S.-H., Yi, J.-H. & Kushiyama, S. 2002. Fragility Curves of Concrete Bridges Retrofitted by Column Jacketing. Earthquake Engineering and Engineering Vibration. V. 01 (No. 2). (http://shino8.eng.uci.edu/journalpapers.htm).

Shinozuka, M. & Kim, H.-K. 2003a. Effects of Seismically Induced Pounding at Expansion Joints of Concrete Bridges. Accepted for Publication. Journal of Engineering Mechanics, ASCE. (http://shino8.eng.uci.edu/journalpapers.htm).

Shinozuka, M., Kim, S.-H., Kushiyama, S. 2003b. Fragility Curves of Seismically Retrofitted Bridges with Column Jacketing. To be submitted for Publication. Journal of Engineering Mechanics, ASCE. (http://shino8.eng.uci.edu/journalpapers.htm).

Seismic pounding behavior of simply supported girder bridges

Xi Zhu[1] and GangYi Shuai[1]

ABSTRACT

The characters of the pounding response of the simple supported bridges under earthquake excitations are studied. For short span bridges, a number of different actual earthquake waves are selected to investigate the factors that affected the bridge pounding response, such as the earthquake excitations, the gap size between the girder segments, the friction coefficient of the Teflon sliding bearing and the foundation soil conditions. The pounding responses of bridges are influenced by different earthquake excitations and gap sizes of girder segments .When the increasing of fraction coefficient of Teflon sliding bearings, the bending moments and shear forces at the bottom of the bridge pier and the pounding forces of the adjacent girders will be decreased to different extent. When the groundsill, which is not rock , the influence of soil deformation can't be neglected. But the seismic responses of bridges are not sensitive to the groundsill coefficient in the Chinese railway and highway design codes.

[1] College of Civil Engineering & Architecture Beijing Jiaotong University, Beijing, P.R.China,100044

INTRODUCTION

Pounding between adjacent segments of bridges during major earthquakes has often been reported. It has also been identified as one of the main causes for structural damages or for complete collapse of bridges. There is however a consensus that the existing bridge-code provisions for seismic poundings are not enough.

Simply supported concrete bridges usually are provided with an expansion bearing at one end of the girder and a fixed bearing at another end to minimize temperature-induced stresses. The expansion bearings have a 5-10cm gap to allow free longitudinal movement. In past earthquake, extensive damage has been sustained at the joints because of impact spalling of concrete, failure of bearings, and collapse caused by the loss of support failure. Because the interaction between adjacent girders plays a key role in the seismic response of bridges, it should be investigated thoroughly and considered rationally in dynamic analysis models.

In this paper, the gap element essentially consists of a spring , a damper and a gap . The spring ensures impact duration and the damper accounts for the loss of energy by impact. Usually, very large spring stiffness is assumed to prevent overlapping between adjacent segments and to ensure small impact duration(Liu et al,1996).

ANALYTICAL MODEL

A three-span bridge was modeled as shown in Fig.1. The geometry data of the bridge pier is shown in Fig.2. When the difference of natural frequencies for adjacent members is larger, the seismic pounding reaction is larger, so a three-span simply supported bridge was selected. The height of left pier is 14m and that of the right pier is 8m. The length of each girder span is 16.5m. The simply supported bridge is consisted of 4 T-concrete girders in translation. Concrete with Young's modules, E, for piers was assumed to be equal to 2.35×10 kN/m^2. The specific weight of concrete 2.5t/m was used for computing the mass and rotary inertia. The area of beam cross section was taken as A=4.8996m^2. The vertical inertia moment I=1.4879m^4. Standard rubber bearings with shear stiffness in horizontal direction k=5.3MN/m. Teflon sliding bearings with initial shear stiffness in horizontal direction k=5.3MN/m. The collisions of girder-to-girder and girder-to-abutment are simulated by the GAP element shown in Fig.3. The stiffness and damping of the pounding element are $k=1.0718\times10^{10}$ N/m and $c=9.075\times10^{6}$kg/s. The spring stiffness to simulate abutment was 3.91×10^{8}N/m (almost 7-8times pier stiffness) . The depth of pier foundation is 1m, the cross section size is $9.8\text{m}\times3.2\text{m}$.

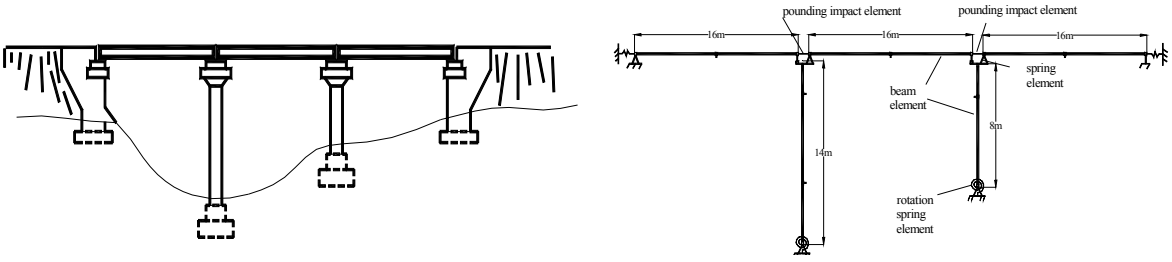

Fig.1. Dimension of the three-span simply supported viaduct

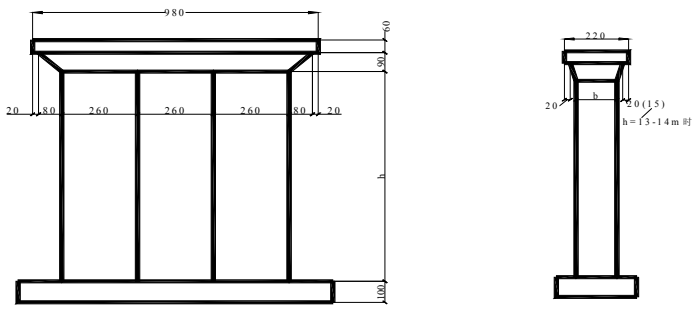

Fig.2 Cross section of typical pier in longitudinal and transversal direction

Pounding is a boundary nonlinear physics as is changed from one state to another state. At the beginning, the adjacent beam bodies move each other as free motion. Once the relative displacement of adjacent bodies exceeds over the size of beam gap the collision occurs. At this time, the GAP element will be worked. The value of element stiffness is taken as beam stiffness in axis direction[10]. The damping value can calculate as

$$c = 2\xi\sqrt{k\frac{m_1 m_2}{m_1 + m_2}} \qquad \xi = \frac{-\ln e}{\sqrt{\pi^2 + (\ln e)^2}}$$

in which, k is pounding stiffness of adjacent two girders, m1,m2 is the mass for adjacent two girders respectively, ξ is damping ratio, e is recover factor which describes energy-loss procedure. e=1(ξ=0) means perfect elastic collision; e=0 (ξ=1) means perfect plastic collision. For concrete, generally, e=0.65(ξ=0.14).

Pounding for two adjacent beams is usually controlled by the displacements of adjacent beam and the size of the gap between two adjacent girders.

Pounding condition: $\delta_{i-1,i}(t)=u_{i-1}(t)-u_i(t)-d\geqslant 0$

Pounding force: $F=K\,\delta_{i-1,i}(t)+C\,\dot{\delta}_{i-1,i}(t)$

The analysis model of GAP element and the force-displacement relationship of impact spring are shown as Fig.3.

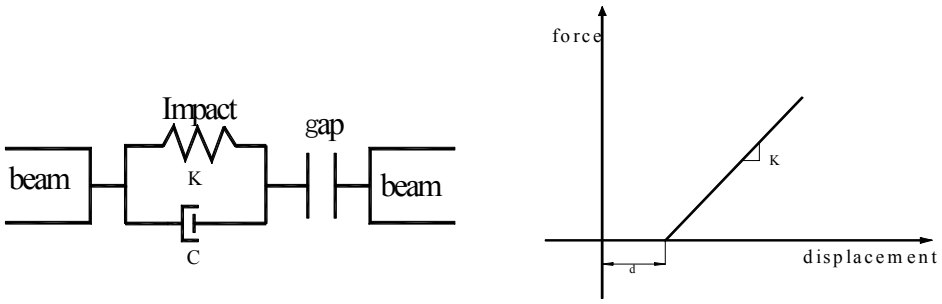

Fig.3 GAP element

NUMERICAL ANALYSIS RESULT

Pounding Force with Various Earthquake Excitation

Seismic pounding response of simply supported bridge is greatly influenced by the waves of earthquake excitation. The structure response of same bridge is different with different earthquake excitation. The basic character of six seismic waves selected by this paper is shown in TABLE 1. The peak value of acceleration of Kobe earthquake was adjusted to 0.2g to approach the intensity of another two compared earthquake waves in Fig.4 .

TABLE I BASIC CHARACTER OF EARTHQUAKE RECORDS AT VARIOUS SITE

Earthquake name	Site Type	Direction	Station Intensity	Epi-centre Inten-sity	M_s	Acc (cm/s^2)	Time
Kobe	1	N00E	8	8	6.0	817.82	1995.10.21
W.Washington	1	S04E	8	8	7.1	161.6	1949.4.13
El-Centro	2	S00E	8	10	6.3	341.7	1940.5.18
San Fernando	2	N37E	7	11	6.4	195.6	1971.2.9
Imperial Valley	3	S90W	8	10	6.3	210.1	1940.5.18
San Fernando	3	S00W	7	11	6.4	267.3	1971.2.9

When the longitudinal gap sizes of girder-to-girder and girder-to-abutment are same, under El- Centro wave, if all gap sizes are same to take as d□17cm in whole bridge, the collision will not be occurred under the El Centro wave and if the gap size d=12cm the pounding forces approach the maximum value. If the gap sizes are taken as d□13cm in whole bridge, under the Kobe earthquake the collision will not be occurred and if the gap size yield d=8cm, the pounding forces approach the maximum value .Excited by three different earthquake waves the maximum pounding forces are changed with the gap size as shown in Fig.4.

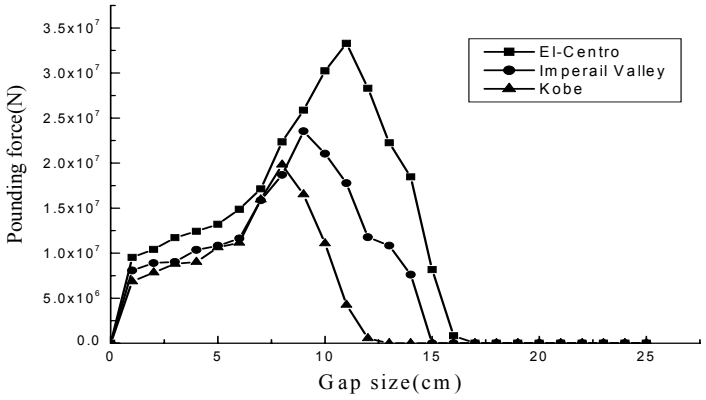

Fig.4 Pounding forces changed with the girder gaps

TABLE II THE GIRDER GAPS OF MAX.OR MIN. POUNDING FORCES

Earthquake Wave	Kobe	W.Washiongton	El-Centro	San FernandoN37E	Imperial Valley	San FernandoS00W
$a_{gmax}(cm/s^2)$	196	161.6	341.7	195.6	210.1	167.3
Gap Size for no Collision(cm)	13	14	17	10	15	12
Gap Size for Max.Pounding force(cm)	8	9	12	6	9	6

Structure Response by Seismic Pounding with Difference Gap Sizes

The time history curves of displacement at span center of middle girder excited by El Centro or Kobe wave are shown in Fig.5 and Fig.6. All girder gap sizes are taken as one value, d=1cm or12cm. It is shown that when gap size is very small (as d=1cm) the girder displacement is small too. The reason is that poundings impose the girders moved forward opposite directions, respectively. When gap size is increased then the girder displacements are increased too, because the pounding impose the girders moved forward same direction.

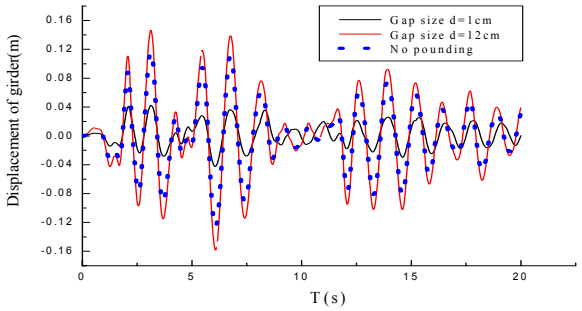

Fig.5 Time history curves of displacement at middle girder excited by El Centro Wave

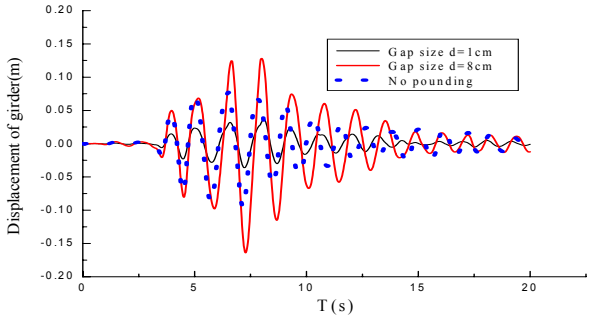

Fig.6 Time history curves of displacement at middle girder excited by Kobe Wave

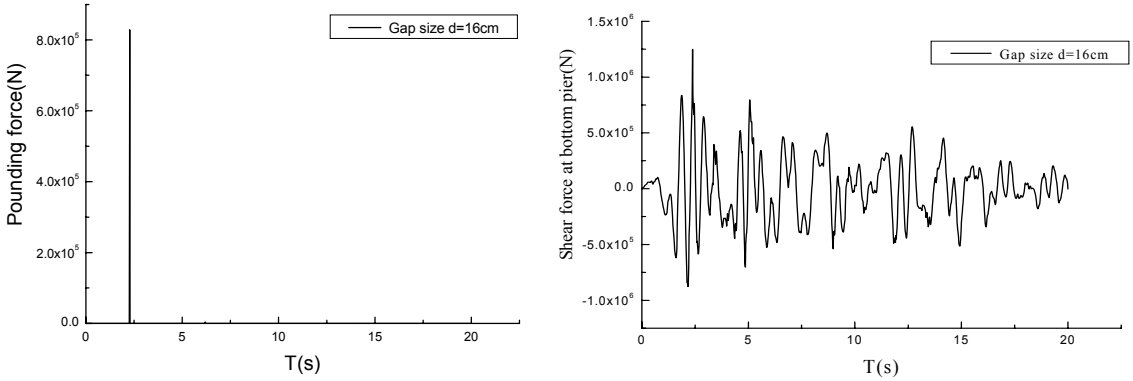

Fig.7 Pounding force and Moment of left pier bottom time history

curves of gap=16cm excited by El Centro

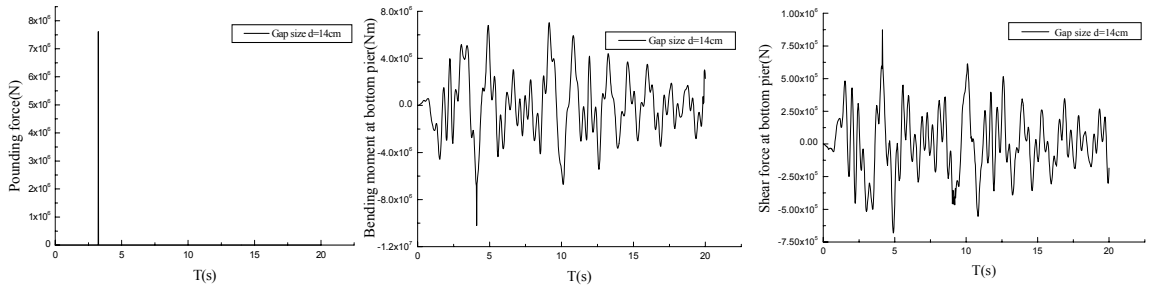

Fig.8 Pounding force and Moment ,shear force of left pier bottom time history curves of gap=14cm excited by Imperial Valley

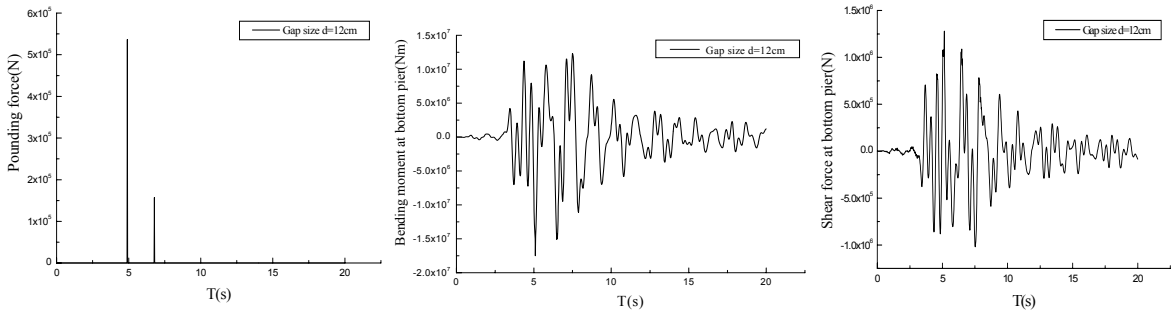

Fig.9 Pounding force and Moment, shear force of left pier bottom time history curves of gap=12cm excited by Kobe Wave

From Fig.7 ,8,9, there are the time history curves of pounding force and bending moment, shear force at pier bottom of left pier, respectively excited by El Centro wave, Imperial valley wave or Kobe wave, and the same girder gap size is d=16cm, 14cm or 12cm. The increased amplitudes of structure response excited by different earthquake wave are different. The bending moment and shear force at pier bottom after poundings are increased almost 60% for El Centro wave, are increased almost 55% for Imperial Valley wave, almost 30% for Kobe wave. There is same performance for right pier and other earthquake waves.

Pounding response of simply supported bridge influenced by girder gap size

The criterions of girder gap size for simply supported bridges in Chinese railway bridge technical code are as following: when girder span L≦16m, gap size d=6cm; when girder span L□20m, gap size d=10cm. This criterion was made for considering the requirement of error of construction and temperature deformation. There did not consider seismic poundings. The pounding force time history curves of middle girder impacted with left or right girder respectively under one of three kind waves such as El Centro, Imperial valley and Kobe taken different girder gap size are shown in Fig.10-Fig.12.

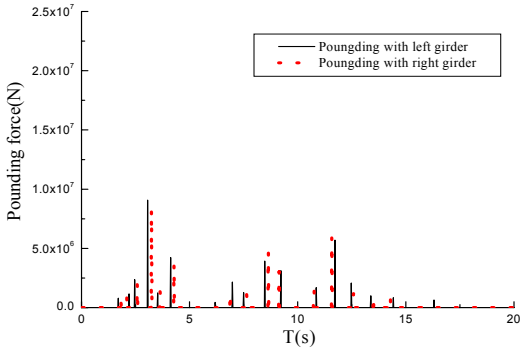

Fig.10 Time history curve of pounding force excited by El Centro wave

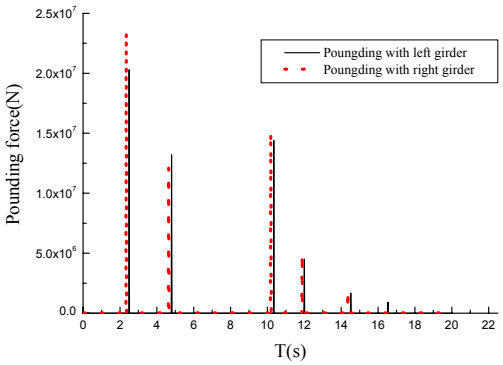

Fig.11 Pounding force time history curve for gap size d=1cm or d=9cm excited by Imperial Valley Wave

It is indicated by figures and calculation results, when gap size between girders is very small, the number of impact is large, arrived 30, but the pounding forces are very small, the maximum pounding force is not exceeded 10000KN, and the displacement of girder is small too, is not exceeded 6cm; when gap size between girders d=6cm, the impact number of adjacent girders is decreased, but the pounding forces are large and the displacements of girders are large too; when gap size of girder is increased at d=12cm (for the excitation is El Centro wave), though the impact number is very smaller than d=1cm or 6cm, but the pounding force is increased at the maximum value fmax=33170KN. The gap size is increased continually, the pounding force will be decreased, until d>=17cm, there will be no impacted, because the gap size is enough large. The maximum bend moment and shear force at pier bottom were changed due to pounding between girders with different gap size of girders, as shown in Fig.13-Fig15 for three different excited earthquake waves.

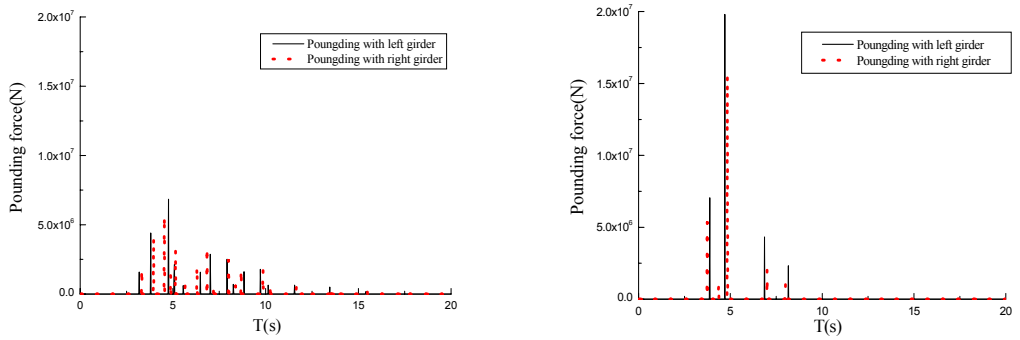

Fig.12 Pounding forces time history curve of d=1cm and d=8cm excited by Kobe Wave

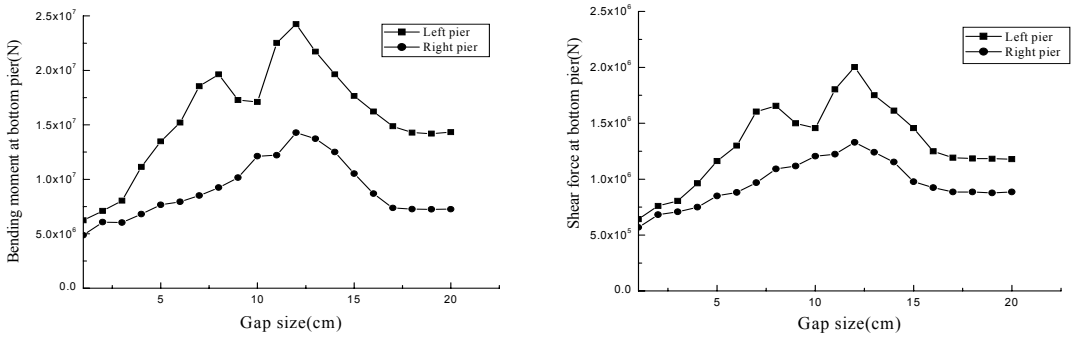

Fig.13 Bending moment and shear force at pier bottom changed with gap size excited by El Centro Wave

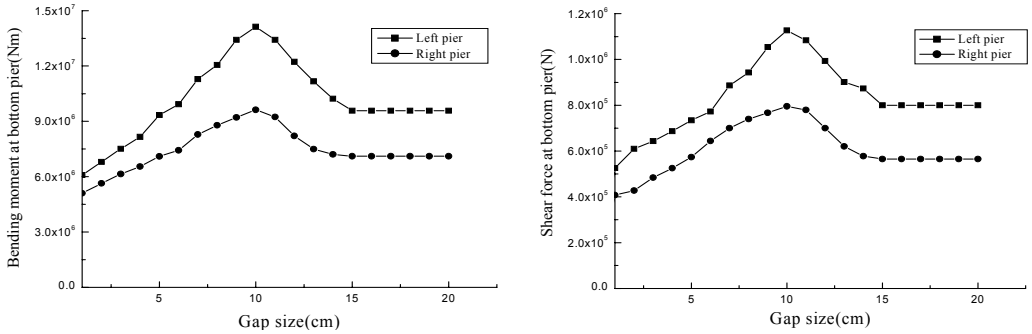

Fig.14 Bending moment and shear force at pier bottom changed with gap size under Imperial Valley Wave

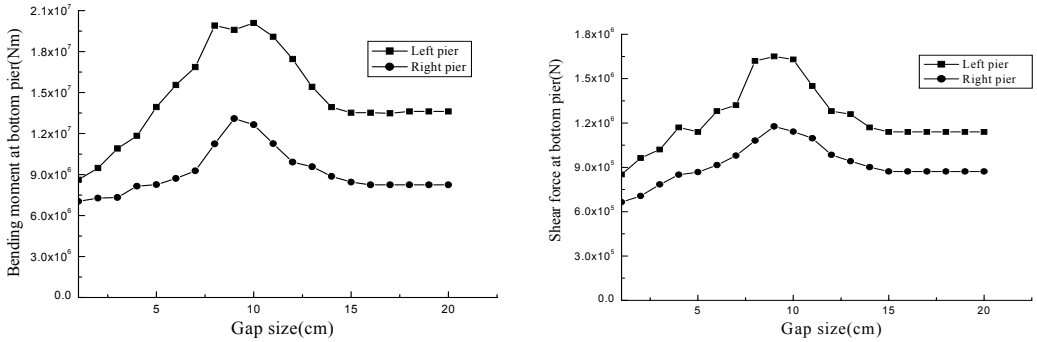

Fig.15 Bending moment and shear force at pier bottom changed with gap size under Kobe Wave

The Influence of Bearing Character

It was changed the coefficient of friction of slide plate bearings to investigate the influence for pounding of superstructure in this paper. The coefficient of friction was changed from 0.02 to 0.08, because the coefficient of friction between Teflon and stainless steel is usually less than 0.08. Bending moment and shear force at pier bottom changed with friction coefficient.

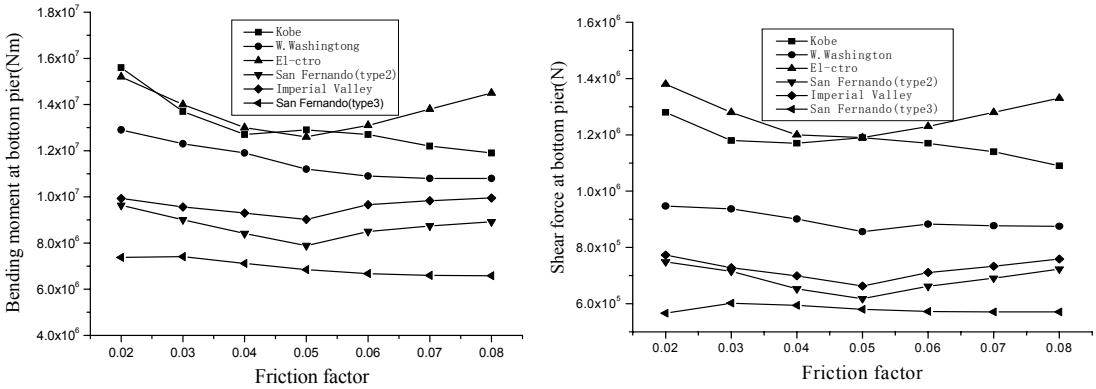

Fig.16 Bending moment and shear force at pier bottom changed with friction coefficient excited by various earthquake waves

The curves of bending moment and shear force at pier bottom of left pier are shown in Fig.16, if the friction coefficients were changed. It is found that the bending moment and shear force will be decreased when the friction factor is increased.

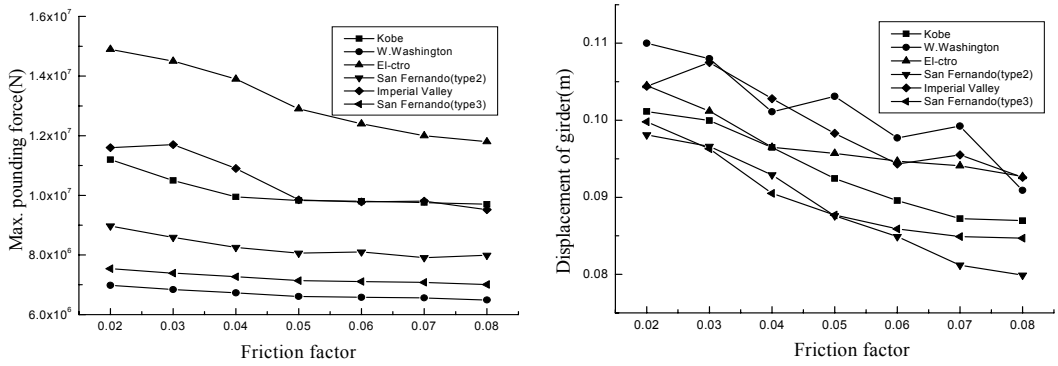

Fig.17 Curves of Max. pounding force and displacement of girder changed with friction coefficient

The curves of maximum pounding force and displacement of middle girder are shown in Fig.17. It was excited by various earthquake wave with different friction factors. It is found that the pounding forces will be decreased with the increased friction factor.s

The Influence of Groundsill Deformation

To groundsills which are not rocks, the influence of subgrade deformation can't be neglected. But the seismic pounding response is not very sensitive to subgrade proportion coefficient m defined by Chinese bridge design code as shown in TABLE 4 and TABLE 5 .

TABLE IV STRUCTURE RESPONSE EFFECTED BY COEFFICIENT OF SUBGRADE(TYPE 2)

Subgrade coef. / Struct. Response	El-Centro m(KN/m^4)			San Fernando(type2) m(KN/m^4)		
	10^4	3×10^4	Rock subgrade	10^4	3×10^4	Rock subgrade
Structural period(s)	0.93035	0.67134	0.4121	0.93035	0.67134	0.4121
Left pier bottom moment (KN)	1.33E+07	1.52E+07	2.16E+07	7.95E+06	8.97E+06	1.18E+07
Right pier bottom moment（KN）	7.06E+06	7.94E+06	1.09E+07	5.30E+06	6.27E+06	7.88E+06
Left pier bottom shear force（KN）	1.21E+06	1.38E+06	1.86E+06	5.69E+05	6.45E+05	8.54E+05
Right pier bottom shear force(KN)	7.80E+05	8.82E+05	1.15E+06	4.83E+05	5.52E+05	7.01E+05
Max.pounding force(KN)	1.66E+07	1.49E+07	8.93E+06	9.93E+07	8.97E+06	5.93E+06
Left beam disp.(cm)	8.07E-02	7.54E-02	6.26E-02	6.90E-02	6.70E-02	5.91E-02
Middle beam disp.(cm)	0.1069	0.1045	8.58E-02	0.1033	9.81E-02	8.25E-02
Right beam disp（cm）	9.05E-02	9.02E-02	7.49E-02	6.86E-02	6.26E-02	5.78E-02

TABLE V STRUCTURE RESPONSE EFFECTED BY COEFFICIENT OF SUBGRADE (TYPE3)

Subgrade coef. / Struct. Response	Imperial Valley m(KN/m^4)			San Fernando(type3) m(KN/m^4)		
	3×10^3	10^4	Rock subgrade	3×10^3	10^4	Rock subgrade
Struct.period(s)	1.4485	0.93035	0.4121	1.4485	0.93035	0.4121
Left pier bottom moment（KNm）	8.54E+06	9.93E+06	1.32E+07	6.94E+06	8.09E+06	1.08E+07
Right pier bottom moment（KN）	6.60E+06	7.53E+06	9.79E+06	5.12E+06	6.18E+06	8.20E+06
Left pier bottom share force（KN）	6.54E+05	7.73E+05	1.05E+06	5.49E+05	6.32E+05	8.25E+05
Right pier bottom share force(KN)	5.43E+05	6.44E+05	8.75E+05	4.82E+05	5.78E+05	7.88E+05
Max.pounding force(KN)	1.33E+07	1.16E+07	8.54E+06	9.13E+06	7.54E+06	5.54E+06
Left beam disp.(cm)	8.62E-02	8.19E-02	6.91E-02	7.03E-02	6.85E-02	5.83E-02
Middle beam disp.(cm)	0.1085	0.1044	9.47E-02	0.1006	9.98E-02	8.72E-02
Right beam disp.(cm)	0.1015	9.98E-02	8.37E-02	8.25E-02	8.07E-02	7.00E-02

CONCLUSIONS

This paper is investigated seismic pounding behavior for 16m span simply supported girder bridges. The principal conclusions are as follows.

1. The pounding response for simple supported bridges is related with the earthquake ground motion of the site on which is constructed the bridge.
2. The significant influence for structure response is produced by seismic interaction at separation joints of girder bridges.
3. With the increasing of fraction coefficient of Teflon sliding bearings, the bending moments and shear forces at the pier bottom and the pounding forces between the adjacent superstructures will be decreased to some extent.
4. To groundsills which is not rock, the influence of soil deformation cannot be neglected.

ACKNOWLEDGMENTS

This research is supported by the National Natural Science Foundation of China under grant No.50278002 .This support is gratefully acknowledged.

REFERENCES

Robert Jamkowski, Kezysztof Wilde and Yozo Fujino, “Pounding of superstructure segments in isolated elevated bridge during earthquakes”, *Earthquake Engineering and Structural Dynamics* V27, 487-502 (1998)

Robert Jamkowski, Kezysztof Wilde and Yozo Fujino, “Reduction of pounding effects in elevated bridges during earthquakes”, *Earthquake Engineering and Structural Dynamics* V 29, 195-212 (2000)

Praveen K. Malhotra, “Dynamics of Seismic Pounding at Expansion Joints of Concrete Bridges ”, *Journal of Engineering Mechanics* (1998), 794-802

Joseph Penzien , “Evaluation of Building Separation Distance Required to Prevent Pounding during Strong Earthquakes”, *Earthquake Engineering and Structural Dynamics* V26,849-858 (1997)

Implications of Seismic Pounding on the Longitudinal Response of Multi-Span Bridges – An Analytical Perspective

Reginald DesRoches and Susendar Muthukumar

ABSTRACT

Seismic pounding between adjacent frames in multiple-frame bridges and girder ends in multi-span simply supported bridges has been commonly observed in several recent earthquakes. The consequences of pounding include damage to piers, abutments, shear keys, bearings and restrainers, and possible collapse of deck spans. This paper investigates pounding in bridges from an analytical perspective. A simplified nonlinear model of a multiple-frame bridge is developed including the effects of inelastic frame action and nonlinear hinge behavior, to study the seismic response to longitudinal ground motion. Pounding is implemented using the contact force-based Kelvin model, as well as the momentum-based stereomechanical approach. Parameter studies are conducted to determine the effects of frame period ratio, column hysteretic behavior, energy dissipation during impact and near source ground motions on the pounding response of the bridge. The results indicate that pounding is most critical for highly out-of-phase frames and is not significant for frame period ratios greater than 0.7. Impact models without energy dissipation overestimate the displacement and acceleration amplifications due to impact, especially for elastic behavior of the frames. Representation of stiffness degradation in bridge columns is essential in capturing the accurate response of pounding frames subjected to far field ground motion. Finally, it is shown that strength degradation and pounding can result in significant damage to the stiffer frames of the bridge when subjected to large acceleration pulses from near field ground motion records.

Reginald DesRoches, Associate Professor, Georgia Institute of Technology, School of Civil and Environmental Engineering, Atlanta, GA 30332-0355
Susendar Muthukumar, Graduate Research Assistant, Georgia Institute of Technology, School of Civil and Environmental Engineering, Atlanta, GA 30332-0355

INTRODUCTION

The advent of an earthquake can induce out-of-phase vibrations in adjacent structures due to differences in dynamic characteristics, which can result in impact if their at-rest separation is insufficient to accommodate the relative displacements. This impact, commonly referred to as seismic pounding, generates high magnitude and short duration acceleration pulses that can cause structural damage. Furthermore, seismic pounding can amplify the global response of the participating structural systems. The multiple-frame bridge and multi-span simply supported bridges are most vulnerable to pounding damage due to numerous independent components and lack of continuity in the superstructure. In a multiple-frame bridge, the interaction between adjacent frames can result in pounding of the deck at the intermediate hinge or abutment locations. Pounding of girder ends at piers and end abutments can occur in a multi-span simply supported bridge.

Bridge damage from seismic pounding has been observed in several earthquakes during the last decade. After the 1994 Northridge earthquake, significant pounding damage was observed at the expansion hinges and abutments of standing portions of the connectors at the Interstate 5 and State road 14 interchange, which was located approximately 12 km north-northeast of the epicenter (Hall, 1995). Reconnaissance reports from the 1995 Hyogo-Ken Nanbu earthquake in Japan identify pounding as a major cause of fracture of bearing supports and potential contributor to the collapse of several bridge decks (Comartin et al., 1995). The 1999 Chi-Chi earthquake in Taiwan revealed hammering at the expansion joints in some bridges which resulted in damage to shear keys, bearings and anchor bolts (Usarski et al., 2001). Failure of girder ends and bearing damage due to pounding of adjacent simply supported spans were reported after the 2001 Bhuj earthquake in Gujarat, India (Jain et al., 2002). Based on observations from past earthquakes, pounding can cause crushing and spalling of concrete at the impact locations, result in damage to column bents, abutments, shear keys, bearing pads and restrainers, and possibly contribute to the collapse of deck spans.

Pounding is a highly nonlinear phenomenon and two analytical techniques are available for modeling - the contact element method and the stereomechanical approach. In the former approach, a contact element is activated when the structures come into contact. A spring with stiffness proportional to the axial stiffness of the colliding bodies is used, sometimes in conjunction with a damper. The contact elements used in the past include the linear spring (Maison and Kasai, 1990), the energy-dissipating Kelvin-Voigt (Anagnostopoulos, 1988; Jankowski et al., 1998) and the nonlinear Hertz contact element (Pantelides and Ma, 1998; Chau et al., 2003). The stereomechanical approach assumes instantaneous impact and uses momentum balance and the coefficient of restitution to modify velocities of the colliding bodies after impact. This approach has been used by Papadrakakis et al. (1991), Athanassiadou et al. (1994) and Malhotra (1998).

Past research has focused on certain aspects of the pounding problem in bridges. Maragakis et al. (1991) studied the effect of impact between the bridge deck and abutments on the dynamic response of the bridge during strong ground motion. The parameters affecting the pounding response were identified as the abutment gap, mass ratio between bridge deck and abutment, abutment stiffness and the coefficient of restitution. Jankowski et al. (1998) performed an analysis of pounding in an isolated bridge superstructure subject to a propagating seismic wave. The authors concluded that the optimal separation gap between superstructure segments should be either too small (less than 10 mm) or large enough to avoid collisions. Malhotra (1998) investigated seismic pounding at the expansion joints of multi-span concrete bridges by

formulating the problem as collinear impact between concrete rods of the same cross section but different lengths. The findings indicated that pounding reduced the column deformations, and that impact forces generated in the superstructure were not transmitted to the columns and foundations. Pounding between adjacent bridge segments was found to amplify the relative displacement, resulting in the requirement of a longer seat width to support the deck (Ruangrassamee and Kawashima, 2001). Other studies have assessed pounding mitigation techniques in bridges. Shock absorbers, connectors with high damping or stiffness, energy dissipating restrainers and friction-type dampers were found effective in reducing the deck responses, relative hinge displacements and impact forces from pounding (Jankowski et al., 2000; Kawashima and Shoji, 2000; Kim et al., 2000; Ruangrassamee and Kawashima, 2003)

This paper presents a broad overview on the implications of pounding in bridges from an analytical stand point. The multiple-frame bridge is considered as the representative bridge structure. Two adjacent bridge frames are isolated to study the effects of pounding on the longitudinal response of the frames. A simplified two degree-of-freedom (DOF) planar model is developed incorporating the effects of inelastic frame action and nonlinear hinge behavior. Pounding is implemented using the contact force-based Kelvin model, as well as the momentum-based stereomechanical approach to compare the impact performance of the two techniques. A comprehensive study is then performed to investigate the effects of frame dynamic characteristics, column hysteretic behavior, energy loss during impact and ground motion characteristics on the global response of the adjacent bridge frames. The effects of skewed hinges, non-uniform support motion and soil-structure interaction are beyond the scope of this study.

SIMPLIFIED ANALYTICAL MODEL

The interaction between adjacent frames of a multiple-frame bridge plays an important role in its seismic response. Two adjacent frames of a typical multiple-frame bridge shown in Figure 1(a) are isolated to investigate the effects of pounding. A planar two-DOF nonlinear model is developed, as shown in Figure 1(b). Each bridge frame is idealized as a single DOF yielding element with mass m_i, initial stiffness k_i, and a viscous damping coefficient c_i. Several hysteretic models are considered for the frame response including elasto-plastic, bilinear, stiffness-degrading and strength-degrading models. The Q-Hyst model is selected for representing stiffness-degradation in the columns (Saiidi and Sozen, 1979). The pivot hysteresis model is chosen for representing strength degradation with increased cycles of loading (Dowell et al., 1998). The inelastic restoring force for each frame is obtained from the assumed frame force-deformation relationship. For representing pounding, the contact force-based Kelvin model and the momentum-based stereomechanical approach are considered, to evaluate the performance of different impact methodologies. The effects of restrainers and bearings at the hinge locations are not considered, since the focus of the study is on seismic pounding.

The equations of motion for the two-DOF system subject to horizontal ground motion can be expressed as:

$$\begin{bmatrix} m_1 & 0 \\ 0 & m_2 \end{bmatrix} \begin{Bmatrix} \ddot{u}_1 \\ \ddot{u}_2 \end{Bmatrix} + \begin{bmatrix} c_1 & 0 \\ 0 & c_2 \end{bmatrix} \begin{Bmatrix} \dot{u}_1 \\ \dot{u}_2 \end{Bmatrix} + \begin{Bmatrix} F_{F_1}(u_1) \\ F_{F_2}(u_2) \end{Bmatrix} + \begin{Bmatrix} F_I(u_2 - u_1 - g_p) \\ -F_I(u_2 - u_1 - g_p) \end{Bmatrix} = -\begin{bmatrix} m_1 & 0 \\ 0 & m_2 \end{bmatrix} \begin{Bmatrix} 1 \\ 1 \end{Bmatrix} \ddot{u}_g \quad (1)$$

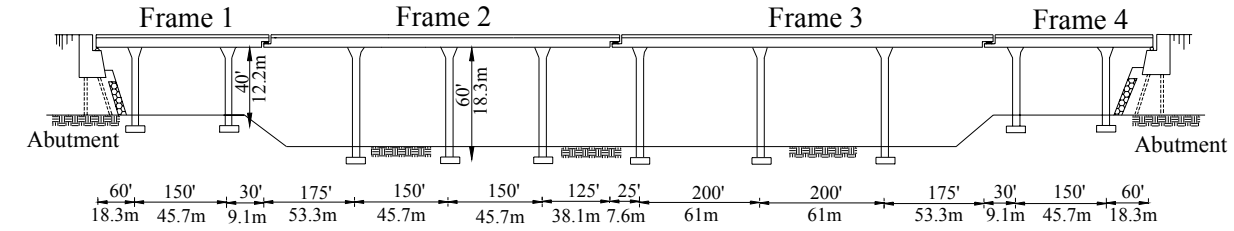

(a)

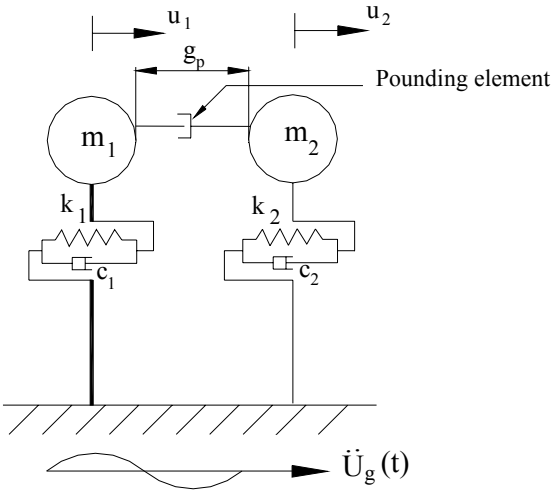

(b)

Figure 1. (a) Typical multiple-frame bridge; (b) simplified model of adjacent frames

where m_i is the mass of each frame, c_i is the frame damping coefficient, F_{Fi} is the inelastic restoring force for each frame based on the hysteretic relation chosen, and F_I is the force due to pounding (for Kelvin model); $\ddot{u}_i$, $\dot{u}_i$ and u_i (i = 1 to 2) represent the frame acceleration, velocity and displacement relative to the ground, and $\ddot{u}_g$ represents the horizontal ground motion applied to the bridge.

Seismic pounding occurs when the gap between adjacent frames closes ($u_2 - u_1 < -g_p$). The contact force (F_I) for the Kelvin model is given below:

$$F_I = k_k\left(u_i - u_j - g_p\right) + c_k\left(\dot{u}_i - \dot{u}_j\right) \;;\; u_1 - u_2 - g_p \geq 0 \tag{3}$$

where k_k is the impact spring stiffness and c_k is the damping coefficient, which can be related to the coefficient of restitution as follows:

$$c_k = 2\xi\sqrt{k_k\left(\frac{m_1 m_2}{m_1 + m_2}\right)} \quad ; \quad \xi = -\frac{\ln e}{\sqrt{\pi^2 + (\ln e)^2}} \tag{4}$$

The contact force (F_I) for the stereomechanical model is taken as zero, since it is not a force based approach. However, the velocities of the colliding masses are adjusted after impact, as shown in equations (5) and (6).

$$v_1^{'} = v_1 - (1+e)\frac{m_2(v_1 - v_2)}{m_1 + m_2} \tag{5}$$

$$v_2^{'} = v_2 + (1+e)\frac{m_1(v_1 - v_2)}{m_1 + m_2} \tag{6}$$

where $v_1^{'}$ and $v_2^{'}$ are the velocities of adjacent frames after impact; v_1, v_2 are the frame velocities before impact and e is the coefficient of restitution. The solution to equation (1) is obtained numerically using the fourth order Runge-Kutta method (Kreyzig, 1999).

EFFECT OF FRAME PERIOD RATIO

Past research has shown that the critical parameters affecting seismic pounding include the system configuration, gap between adjacent structures and ground motion characteristics (Athanassiadou et al., 1994; DesRoches and Fenves, 1997). The mass ratio between adjacent frames is not significant as long as the differences in frame periods result from the differences in frame stiffnesses (Trochalakis, 1997). An in-depth investigation is conducted herein to determine the effect of frame period ratio on the pounding response of the bridge. The mass ratio of adjacent frames is taken as unity and four values of the frame stiffness ratio (K_1/K_2) are considered, K_1/K_2 = 2, 4, 8, 10. The hinge gap, g_p is normalized with respect to the maximum relative hinge displacement when pounding of the frames does not occur (D_{np}), as follows:

$$\chi = \frac{g_p}{D_{np}} \tag{7}$$

where χ is the gap ratio parameter. A value of $\chi < 1$ results in pounding between the frames and $\chi > 1$ corresponds to the case when pounding does not occur.

Five ground motion records scaled to 0.7g peak ground acceleration are used for analysis. The inelastic response of the frames is governed by the Q-Hyst force-deformation relation. The ground motion characteristics are related to the frame period through the effective ground motion period ratio, T_{eff}/T_g, as shown below:

$$\frac{T_{eff}}{T_g} = \frac{2\pi}{T_g}\sqrt{\frac{m}{K_{eff}}} = \frac{2\pi}{T_g}\sqrt{\frac{m}{K/\mu}} = \frac{T\sqrt{\mu}}{T_g} \tag{8}$$

where T is the elastic frame period and T_g is the characteristic period of the ground motion. T_g is defined as the period at which the input energy of a 5% damped linear elastic system is maximum (Miranda and Bertero, 1994). The ground motion effective period ratio for the flexible frame (T_{2eff}/T_g) is varied from 0.20 to 5.0 s in increments of 0.05 s. An iterative procedure is used

to determine the reduction factors required to give μ = 4 for the individual frame response. Pounding is modeled using the stereomechanical approach, with e = 0.8. The effect of pounding is expressed in terms of the displacement amplification ratio (γ), which is the ratio of the maximum pounding displacement to the maximum frame displacement if pounding does not occur.

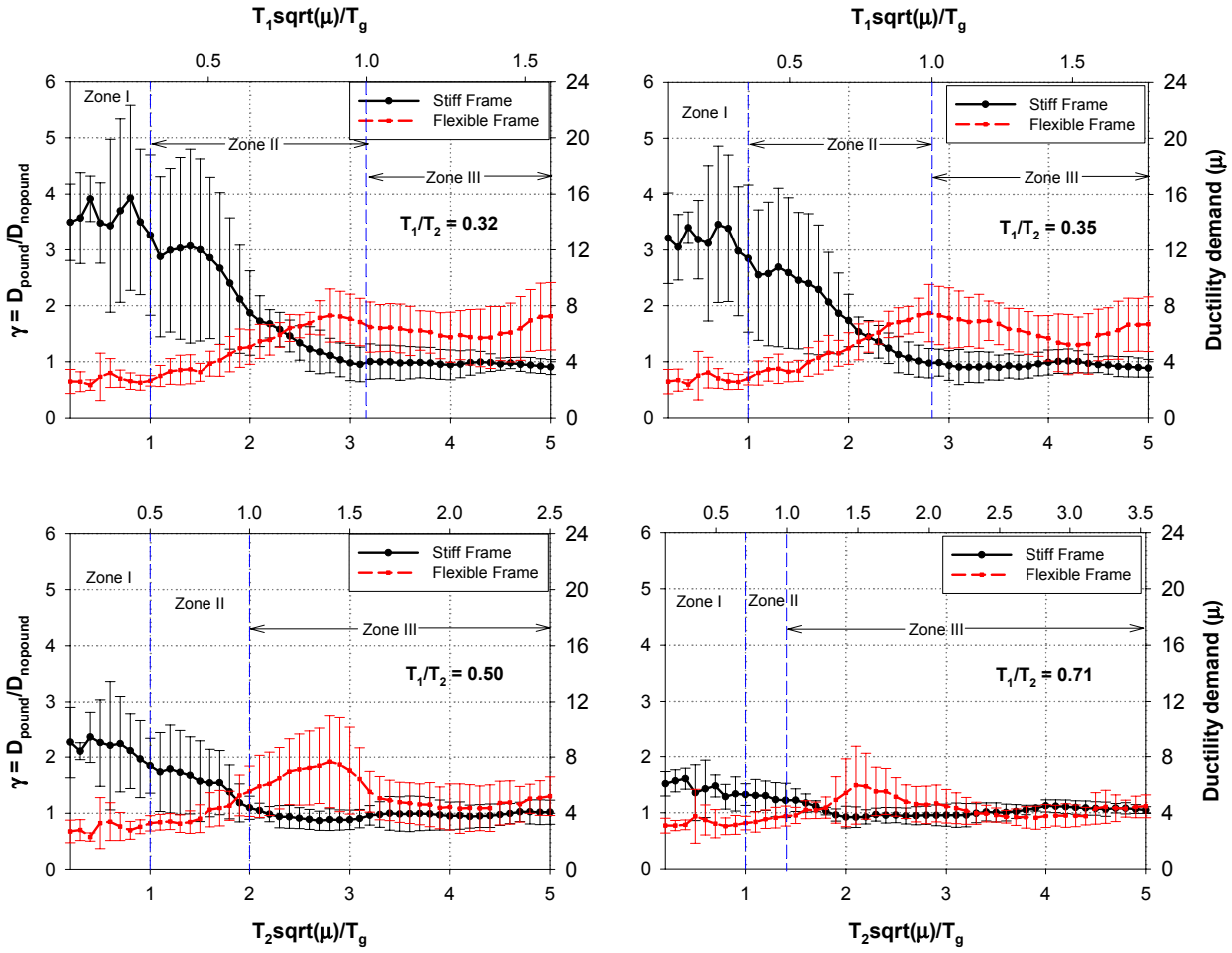

Figure 2. Mean displacement amplification (with error bars) for inelastic frames (χ = 0.02); five earthquake records (scaled to 0.7g) – stereomechanical approach (e = 0.8)

Figure 2 presents the mean amplification in displacement and ductility demand as a function of T_{1eff}/T_g and T_{2eff}/T_g, for χ = 0.02. The variability in response is indicated by the error bars. The effect of pounding is more critical for highly out-of-phase frames (T_1/T_2 = 0.32 or K_1/K_2 = 10). Pounding reduces the frame response when the effective frame period (T_{eff}) is near the characteristic period of the ground motion (T_g). The displacement amplification curves due to pounding can be classified into three zones depending on the effective ground motion period ratio.

In Zone I, where $T_{2eff}/T_g < 1$, the stiff frame amplification is greater than one and the flexible frame amplification is less than one. The stiff frame ductility demand is increased by as much as

300% and the flexible frame ductility demand is reduced by approximately 40%, when T_1/T_2 = 0.32. The coefficient of variation (COV) defined as the ratio of the standard deviation to the mean can be as high as 57% for the stiff frame and 58% for the flexible frame. In Zone II, $T_{1eff}/T_g < 1 < T_{2eff}/T_g$, pounding increases the displacement demand of both the frames. In Zone III ($T_{1eff}/T_g > 1$), the flexible frame response is increased and the stiff frame response is reduced due to pounding. In general, the displacement amplification decreases as the frame period ratio (T_1/T_2) approaches unity, for all values of T_{2eff}/T_g. The effects of pounding are less pronounced when K_1/K_2 = 2.0 (T_1/T_2 = 0.71). The maximum increase in the mean stiff frame demand is 60% (Zone I) and the maximum increase in the mean flexible frame demand is 50% (Zone II). These values are much lower than the corresponding increases of 300% (Zone I) and 83% (Zone II), for the stiff and flexible frames, respectively, at T_1/T_2 = 0.32.

EFFECT OF ENERGY DISSIPATION DURING IMPACT

In this section, the contact element method and the stereoemechanical approach are evaluated to determine differences in the frame pounding response, when subjected to horizontal ground motion. The Kelvin model consisting of a linear spring in parallel with a damper is chosen as the contact element. The effect of energy loss during pounding is explored by selecting two values of the coefficient of restitution, e = 1.0 (no energy loss) and e = 0.6 (some energy loss). Equal frame masses of 7.8 kip-s^2/in are considered with 5% modal damping assigned to each frame. The frame response is assumed elastic and the period ratio is taken as 0.3 (highly out-of-phase frames). An impact spring stiffness of 25000 kip/in is assumed for the Kelvin model.

A suite of thirty ground motion records with peak ground accelerations (PGAs) varying from 0.1g to 1.0g are used in analysis. The characteristic periods of the records ensure that the ground motion period ratio (T_2/T_g) falls within Zone I ($T_2/T_g < 1$). The hinge gap is set very large for the no-pounding analysis and assumed as ½ inch for the pounding analysis. Figure 3 presents the mean values of stiff frame displacement and acceleration amplifications due to pounding, as a function of PGA, for different values of e. Three ground motion records are used at each PGA level. The results indicate that the stereomechanical and Kelvin models predict similar displacement responses, even though they use different methodologies to account for impact. The largest difference between the displacement amplifications is 18%, when PGA = 0.9g and e = 1.0. The Kelvin model, being a contact force-based approach generates acceleration spikes during impact, which result in higher frame accelerations when compared to the stereomechanical model. Considering energy dissipation (e = 0.6) reduces both the displacement and acceleration responses for the stiff frame. On the average, energy loss during impact reduces the frame displacements by 20% and 15% for the stereomechanical and Kelvin models, respectively. The corresponding reductions in the frame accelerations are 25% and 20%.

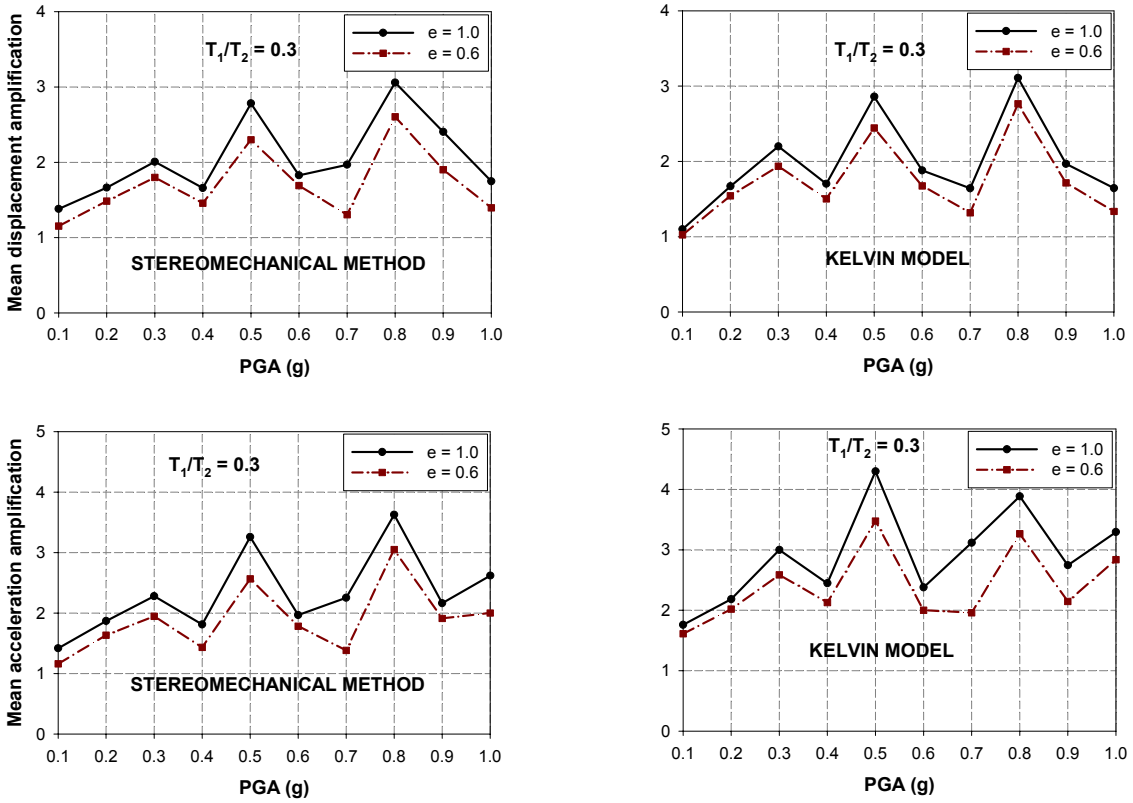

Figure 3. Effect of energy dissipation during pounding on the stiff frame response – elastic frames subjected to 30 ground motion records

EFFECT OF COLUMN HYSTERETIC BEHAVIOR

Previous research studies have typically used bilinear or stiffness-degrading models for the participating structural systems, while analyzing the effects of pounding. Strength degradation in bridge columns has not been considered so far. In this section, the influence of column hysteretic characteristics, such as stiffness degradation, strength deterioration and pinching on the pounding response is studied. Several analytical models are considered including the bilinear, Q-Hyst (stiffness degrading) and pivot hysteresis (strength degrading) models. Three frame period ratios are considered, T_1/T_2 = 0.3, 0.5 and 0.7. The flexible frame period is fixed at 0.40 seconds and the stiff frame period is varied to get the desired period ratio. The initial stiffness, yield strength and strain hardening ratio (if applicable) are assumed to be the same for all hysteretic models. Ten far-field ground motions recorded on medium soil (T_g = 0.6 – 1.2 sec) are selected for analysis, as listed in Table 1.

Each record is scaled such that the spectral acceleration at fundamental period equals the mean spectral acceleration of the suite of records at the fundamental period of the system (S_{amean} = 0.69g). The yield strengths of the hysteretic models are selected such that the stand-alone ductility of each frame (μ) equals 4, when the Q-Hyst model is used as the force-deformation relation. An iterative scheme is used to obtain the requisite yield strengths for each ground motion record at the various system periods. The characteristic periods of the records ensure that the effective ground motion period ratio, T_{2eff}/T_g lies in Zone I. The stereomechanical method,

with a coefficient of restitution, e = 0.8, is used for simulating impact. The hinge gap is set very large for the no-pounding analysis and is taken as ½ inch for the pounding analysis. The hysteretic parameters of the Q-Hyst and pivot models are correlated to get good agreement in the maximum displacement responses of the system, when strength degradation does not occur. The pivot model parameters are carefully chosen such that strength degradation occurs only during the pounding analysis. Thus, differences in displacement amplifications between the Q-Hyst and pivot models can be directly related to the effects of strength degradation.

Table 1: Suite of far-field records used in parameter study comparing hysteretic models

No	Earthquake	M_w	Station	Φ°	PGA (g)	T_g (s)
1	San Fernando, 1971	6.6	Pasadena	000	0.09	0.85
2	Morgan Hill, 1984	6.2	Gilroy Array #3	000	0.19	1.10
3	Morgan Hill, 1984	6.2	Gilroy Array #6	090	0.29	1.20
4	N. Palm Springs, 1986	6.0	5070 N Palm Springs	210	0.59	1.10
5	Loma Prieta, 1989	6.9	WAHO	000	0.37	0.85
6	Loma Prieta, 1989	6.9	Saratoga – W Valley Coll.	270	0.33	1.20
7	Loma Prieta, 1989	6.9	16 LGPC	090	0.61	0.80
8	Northridge, 1994	6.7	LA - Wonderland Avenue	095	0.11	0.80
9	Northridge, 1994	6.7	LA – Hollywood Stor	360	0.36	0.85
10	Northridge, 1994	6.7	Old Ridge Route	090	0.57	0.80

M_w – Moment magnitude; Φ° - Component; PGA – Peak Ground Acceleration; T_g – Characteristic period

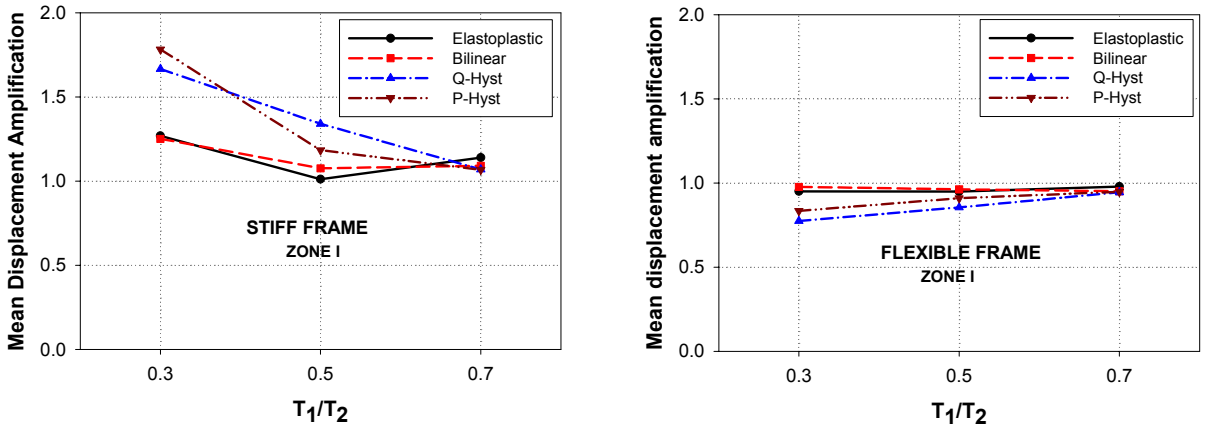

Figure 4. Mean displacement amplification due to pounding from various hysteresis models – 10 far-field ground motion records

The mean displacement amplification due to pounding is presented in Figure 4, for the various hysteretic models. In general, the elasto-plastic and bilinear models (traditional models) underestimate the stiff frame amplification and overestimate the flexible frame amplification, when compared to the Q-Hyst and pivot models (sophisticated models). For instance, at T_1/T_2 =

0.3, the stiff frame mean displacement amplification predicted by the sophisticated models is 30% more than that predicted by the traditional models. The traditional models underestimate the flexible frame displacement amplification by 20%, when T_1/T_2 = 0.3. The differences become smaller with increasing period ratio. All the hysteretic models predict similar impact responses when the frames are essentially in-phase (T_1/T_2 = 0.7). While comparing the Q-Hyst and pivot models, the strength degradation effect imposes no additional demands on the response of the system. The pivot model shows only a 7% increase in the mean displacement amplification when compared to the stiffness degrading only (Q-Hyst) model, for T_1/T_2 = 0.3. In fact, at T_1/T_2 = 0.5, the stiff system amplification from the pivot model is smaller than the Q-Hyst model response by around 12%. Thus, as long as stiffness degradation is modeled, the impact responses in the presence of far-field records can be correctly predicted.

EFFECT OF NEAR-FIELD GROUND MOTIONS

Near field earthquake motions are characterized by high peak ground accelerations and velocity pulses with a long period component (Yang and Agrawal, 2002). Such characteristics can greatly amplify the dynamic response of multiple-frame bridges, resulting in severe damage. To study the effects of near field ground motion on the pounding response of adjacent frames, ten near-source records (T_g = 0.6 – 1.2 sec) are selected for analysis, as listed in Table 2. The parameter study conducted in the earlier section is repeated with all records being scaled to the mean spectral acceleration at the fundamental period of the system (S_{amean} = 0.83g).

Table 2: Suite of records used to study the effect of near-field ground motions

No.	Earthquake	M_w	Station	Φ°	EPD (km)	PGA (g)	T_g (s)
1	Gazli, USSR, 1976	6.8	Karakyr	000	3.0	0.61	1.10
2	Coyote Lake, 1979	5.7	Gilroy Array #6	230	1.2	0.43	0.85
3	Imperial Valley, 1979	6.5	El Centro Array #7	140	0.6	0.34	1.10
4	Imperial Valley, 1979	6.5	Bonds Corner	140	2.5	0.59	0.85
5	Morgan Hill, 1984	6.2	Halls Valley	240	3.4	0.31	0.85
6	Northridge, 1994	6.7	Arleta	090	3.9	0.34	0.85
7	Northridge, 1994	6.7	Sylmar	052	0.2	0.61	1.10
8	Chi-Chi, Taiwan, 1999	7.6	TCU072	N	0.24	0.40	0.90
9	Chi-Chi, Taiwan, 1999	7.6	TCU129	N	1.18	0.63	0.80
10	Chi-Chi, Taiwan, 1999	7.6	TCU076	N	1.95	0.42	0.80

M_w – Moment magnitude; Φ° - Component; EPD – Epicentral distance; PGA - Peak Ground Acceleration; T_g – Characteristic period.

Figure 5 presents the mean displacement amplification due to pounding for the various hysteresis models. As observed for the far-field records, the traditional models (elasto-plastic and bilinear models) underestimate the stiff frame amplification and overestimate the flexible frame amplification, when compared to the more sophisticated models (Q-Hyst and pivot models). However, when using near source records, the differences between the traditional and

sophisticated models persist even when the frames are essentially in-phase, unlike earlier. At $T_1/T_2 = 0.7$, the traditional models underestimate the stiff frame displacement amplification by 20% and overestimate the flexible frame amplification by 15% when compared to the more rigorous models.

The biggest difference in using near-field records is that strength degradation and pounding significantly affect the system response, especially when the system is highly out-of-phase. For example, the pivot model results in a mean stiff frame displacement amplification of 5.8 as opposed to 2.6 for the Q-Hyst model. Thus, accounting for strength degradation increases the stiff frame demand by 125%. This implies that utilizing a bilinear or stiffness-degrading only model while analyzing pounding effects will grossly underestimate the displacement demands when compared with a strength degrading model for near field ground motion.

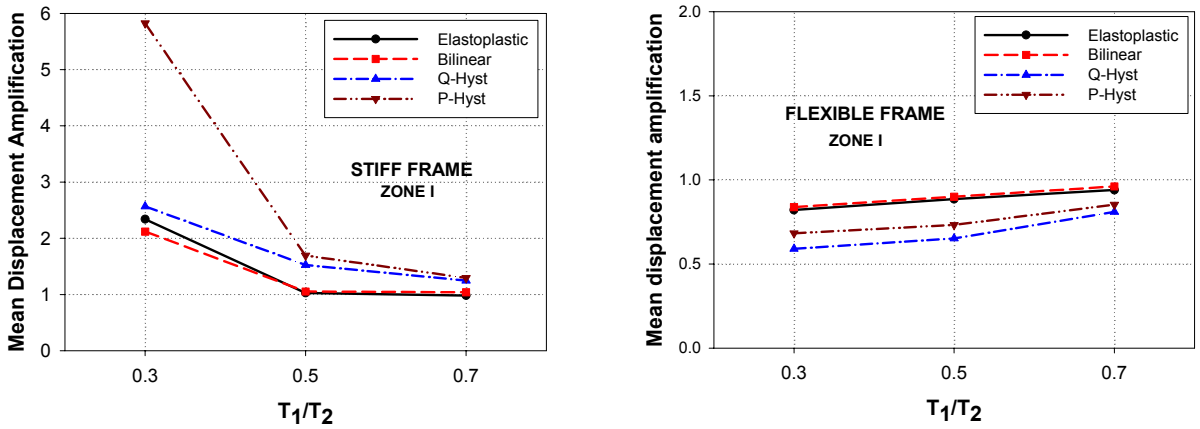

Figure 5. Mean displacement amplification due to pounding from various hysteretic models – 10 near-field records.

CONCLUSIONS

Seismic pounding in multiple-span and multiple-frame bridges has been commonly observed in several recent earthquakes. The consequences of pounding range from localized deck damage, bearing failure, damage to shear keys and abutments to possible collapse of bridge spans. This paper investigates the effect of pounding on the global demand of bridge frames in a multiple-frame bridge. A simplified, planar, nonlinear model of two adjacent bridge frames is developed. Several hysteresis models are considered for representing inelastic frame action, including the elasto-plastic, bilinear, Q-Hyst (stiffness-degrading) and pivot hysteresis (strength degrading) models. Pounding at the intermediate hinge is modeled using the contact force-based Kelvin model, as well as the coefficient of restitution-based stereomechanical approach. A comprehensive analytical study is conducted to investigate the effects of frame period ratio, energy dissipation during pounding, frame hysteretic behavior and ground motion characteristics on the global pounding response of adjacent bridge frames.

The results indicate that pounding is critical for highly out-of-phase frames ($T_1/T_2 = 0.3$) and less pronounced for essentially in-phase frames ($T_1/T_2 = 0.7$). A comparison of the contact element and stereomechanical approaches reveals that both techniques predict similar impact

responses, in spite of differences in impact methodology. Neglecting energy dissipation during impact overestimates the stiff frame displacements by 20% when the stereomechanical approach is used and 15% when the contact force-based Kelvin model is employed. The acceleration responses are reduced by 25% and 20% for the stereomechanical and Kelvin models, respectively, on lowering e from 1.0 to 0.6. Modeling stiffness degradation in bridge columns is essential in capturing the accurate responses of pounding frames subjected to far-field records. However in the presence of near-source records, strength degradation in the columns along with pounding can impose severe demands on the stiff frame displacements, especially for highly out-of-phase frames.

REFERENCES

Anagnostopoulos, S.A., 1988, "Pounding of Buildings in Series during Earthquakes," *Earthquake Engineering and Structural Dynamics*, 16(3):443 – 456.

Athanassiadou, C.J., G. G. Penelis, and A. J. Kappos, 1994, "Seismic Response of Adjacent Buildings with Similar or Different Dynamic Characteristics," *Earthquake Spectra*, 10(2):293 – 317.

Chau, K. T., X. X. Wei, X. Guo, and C. Y. Shen, 2003, "Experimental and Theoretical Simulations of Seismic Poundings between Two Adjacent Structures," *Earthquake Engineering and Structural Dynamics*, 32(4):537 - 554.

Comartin, C. D., M. Greene, and S. K. Tubbesing, 1995, "The Hyogo-Ken Nanbu Earthquake Reconnaissance Report," *Rep. No. 95-04*, EERI, Oakland, CA.

DesRoches, R. and G. L. Fenves, 1997, "New Design and Analysis Procedures for Intermediate Hinges in Multiple Frame Bridges," *Rep. No. UCB/EERC-97/12*, University of California, Berkeley.

Dowell, R. K., F. Seible, and E. L. Wilson, 1998, "Pivot Hysteresis Model for Reinforced Concrete Members," *ACI Structural Journal*, 95(5):607-617.

Hall, J. F., 1995, "Northridge Earthquake of January 17, 1994 - Reconnaissance Report, Vol. 1," *Rep. No. 95-03*, EERI, Oakland, CA.

Jain, S. K., W. R. Lettis, C. V. R. Murty, and J. P. Bardet, 2002, "Bhuj, India Earthquake of January 26, 2001 Reconnaissance Report." *Publ. No 02-01*, EERI, Oakland, CA.

Jankowski, R., K. Wilde, and Y. Fuzino, 1998, "Pounding of Superstructure Segments in Isolated Elevated Bridge During Earthquakes," *Earthquake Engineering and Structural Dynamics*, 27(5):487 – 502.

Jankowski, R., K. Wilde, and Y. Fuzino, 2000, "Reduction of Pounding Effects in Elevated Bridges during Earthquakes," *Earthquake Engineering and Structural Dynamics*, 29(2):195-212.

Kawashima, K., and G. Shoji, 2000, "Effect of Shock Absorber to Mitigate Pounding Effect between Bridge Decks," *Proceedings, International Workshop on Mitigation of Seismic Effects on Transportation Structures*, National Center for Research on Earthquake Engineering, Taipei, Taiwan, R.O.C:207-218.

Kim, J.-M., M. Q. Feng, M. Shinozuka, 2000, "Energy Dissipating Restrainers for Highway Bridges," *Soil Dynamics and Earthquake Engineering*, 19(1):65-69.

Kreyzig E., 1999, *Advanced Engineering Mathematics*, 8th Edition, New York: John Wiley & Sons, pp. 942-952.

Maison, B. F., and K. Kasai, 1990, "Analysis for Type of Structural Pounding," *J. Structural Engineering*, ASCE, 116(4):957 - 975.

Malhotra, P. K., 1998, "Dynamics of Seismic Pounding at Expansion Joints of Concrete Bridges," *J .Engineering Mechanics*, ASCE, 124(7):794–802.

Maragakis, E., B. Douglas, and S. Vrontinos, 1991, "Classical Formulation of the Impact between Bridge Deck and Abutments during Strong Earthquakes," *Proceedings of the 6th Canadian Conference on Earthquake Engineering*, Toronto, Canada: 205 – 212.

Miranda, E., and V. V. Bertero, 1994, "Evaluation of Strength Reduction Factors for Earthquake-Resistant Design," *Earthquake Spectra*, 10(2):357-379.

Pantelides. C. P., and X. Ma, 1998, "Linear and Nonlinear Pounding of Structural Systems," *Computers & Structures*, 66(1):79 – 92.

Papadrakakis, M., H. Mouzakis, N. Plevris, and S. Bitzarakis, 1991, "A Lagrange Multiplier Solution Method for Pounding of Buildings During Earthquakes," *Earthquake Engineering and Structural Dynamics*, 20(11):981 – 998.

Ruangrassamee, A., and K. Kawashima, 2001, "Relative Displacement Response Spectra with Pounding Effect," *Earthquake Engineering and Structural Dynamics*, 30(10):1511-1538.

Ruangrassamee, A., and K. Kawashima, 2003, "Control of Nonlinear Bridge Response with Pounding Effect by Variable Dampers," *Engineering Structures*, 25(5):593-606.

Saiidi, M., and M. A. Sozen, 1979, "Simple and Complex Models for Nonlinear Seismic Response of Reinforced Concrete Structures," *Rep. No. UILU-ENG-79-2013*, Struct. Res. Series No. 465, University of Illinois, Urbana.

Trochalakis, P., M. Eberhard, and J. Stanton, 1997, "Evaluation and Design of Seismic Restrainers for In-Span Hinges," *J. Structural Engineering*, ASCE, 123(4):103 – 113.

Uzarski, J., and C. Arnold, 2001, "Chi-Chi, Taiwan, Earthquake of September 21, 1999 - Reconnaissance Report," *Publ. No. 01-02*, EERI, Oakland, CA.

Yang, J. N., and A. K. Agrawal, 2002, "Semi-Active Hybrid Control Systems for Nonlinear Buildings Against Near-Field Earthquakes," *Engineering Structures*, 24(3):271-280.

Analysis Models and Methods for Structural Response of Spatially Varying Ground Motions

Qingshan Yang[1] Yuji Tian[1]

ABSTRACT

Two Models, Displacement Input Model and Acceleration Input Model, for analyzing the structural response of earthquake ground motions are discussed. The approaches of using direct integration methods to these models are analyzed. The numerical results presented here illustrate the Displacement Input Model is more accurate than the generally used Acceleration Input Model, given the same direct integration method and time step. This is contrary to the conclusions of Wilson (2000) that there are several new sources of numerical errors associated with the direct application of earthquake displacement loading and a very small time step is required to define the displacement record and to integrate the dynamic equilibrium equation. It is believed in the present paper that Displacement Input Model is more accurate and suitable for analyzing the response of ground motions, especially the response of nonlinear structures subjected to spatially varying ground motions.

[1] College of Civil Engineering & Architecture Beijing Jiaotong University, Beijing, P.R.China,100044

INTRODUCTION

There are two analysis models for the structural response of earthquake ground motions. One is that the excitation of the dynamic equilibrium equation is the displacement of earthquake ground motions (Displacement Input Model, DIM), and the other is the generally used Acceleration Input Model (AIM), in which the absolute response is decomposed as pseudo-static response induced by static displacement and dynamic response induced by the dynamic inertial force.

In earthquake response analysis traditionally it has been assumed that all points of the ground surface beneath the foundation are excited synchronously and experience the same ground motion. In which the structural pseudo-static displacement is the same as the displacement of the ground motion and the dynamic response is the relative response of the structure. Then the dynamic response becomes the one relevant to the structural inner forces, and is the only concerned response of the cases with uniform excitation.

It has been well known from real earthquake records that the earthquake ground motions vary both temporally and spatially and it has been believed that the spatial variability of seismic ground motions can have an important effect on the response of multi-support structures and the pseudo-static response in AIM can not be neglected (Yang 2000, 2002). As superposition is not able to be applied to nonlinear system, AIM can not be considered a general method which can be used for all structural systems. With the development of structural engineering, more and more structures subjected to spatially varying ground motions are needed to be analyzed as a nonlinear system. DIM becomes to be attractive, sometimes even the only approach, for analyzing the nonlinear response of spatially varying ground motions (Wilson 2000).

Unfortunately, it is concluded in Wilson (2000) that there are several new sources of numerical errors associated with the direct application of earthquake displacement loading and a very small time step is required to define the excitation record and to integrate the dynamic equilibrium equation if the DIM is applied. If this conclusion is true, the analysis of nonlinear response of spatial varying ground motions will be disturbed greatly. Reanalysis is conducted by the authors and it is fortunately our results show that DIM is more accurate than the generally used AIM for response analysis of both uniform and spatially varying ground motions, given the same direct integration method and time step are applied. It is believed in this paper that Displacement Input Model is suitable for the response analysis of earthquake ground motions, especially for the nonlinear response of spatially varying ground motions.

DISPLACEMENT INPUT MODEL AND ACCELERATION INPUT MODEL

If a structure is excited by earthquake ground motion, the degrees of freedom in an inertia coordinate system may be classified as the degrees of upper structure and bottom foundation in the finite element model, and the equation of motion is:

$$\begin{bmatrix} \mathbf{M}_{aa} & \mathbf{M}_{ab} \\ \mathbf{M}_{ba} & \mathbf{M}_{bb} \end{bmatrix} \begin{Bmatrix} \ddot{\mathbf{X}}_a \\ \ddot{\mathbf{X}}_b \end{Bmatrix} + \begin{bmatrix} \mathbf{C}_{aa} & \mathbf{C}_{ab} \\ \mathbf{C}_{ba} & \mathbf{C}_{bb} \end{bmatrix} \begin{Bmatrix} \dot{\mathbf{X}}_a \\ \dot{\mathbf{X}}_b \end{Bmatrix} + \begin{bmatrix} \mathbf{K}_{aa} & \mathbf{K}_{ab} \\ \mathbf{K}_{ba} & \mathbf{K}_{bb} \end{bmatrix} \begin{Bmatrix} \mathbf{X}_a \\ \mathbf{X}_b \end{Bmatrix} = \begin{Bmatrix} \mathbf{0} \\ \mathbf{R}_b \end{Bmatrix} \tag{1}$$

in which $\mathbf{M}$, $\mathbf{C}$, $\mathbf{K}$ are mass, damping and stiffness matrices; $\ddot{\mathbf{X}}_b$, $\dot{\mathbf{X}}_b$, $\mathbf{X}_b$ are the absolute acceleration, velocity and displacement responses relative to the inertia coordinate system, respectively. The subscripts aa, bb and ab are attached to the structure, foundation and coupling terms. $\mathbf{R}_b$ is the reaction forces of the supports.

Eq.(1) may be written as:

$$\mathbf{M}_{aa}\ddot{\mathbf{X}}_a + \mathbf{C}_{aa}\dot{\mathbf{X}}_a + \mathbf{K}_{aa}\mathbf{X}_a = -\left(\mathbf{M}_{ab}\ddot{\mathbf{X}}_b + \mathbf{C}_{ab}\dot{\mathbf{X}}_b + \mathbf{K}_{ab}\mathbf{X}_b\right) \tag{2}$$

Since the physical damping matrix on the right-hand side of the equation is almost impossible to define, the part of the damping force is normally neglected (Wilson, 2001); and for lumped-mass system, $\mathbf{M}_{ab} = \mathbf{0}$; there is

$$\mathbf{M}_{aa}\ddot{\mathbf{X}}_a + \mathbf{C}_{aa}\dot{\mathbf{X}}_a + \mathbf{K}_{aa}\mathbf{X}_a = -\mathbf{K}_{ab}\mathbf{X}_b \tag{3}$$

where $\mathbf{X}_b$ is the displacements of the ground motions and $-\mathbf{K}_{ab}\mathbf{X}_b$ is the force in the inertia coordinate system acting on the structure induced by the ground motions. Eq.(3) becomes the fundamental formula of Displacement Input Model.

For a linear structure, the response $\mathbf{X}_a$ may be described as the sum of two components:

$$\mathbf{X}_a = \mathbf{X}_d + \mathbf{X}_p \tag{4}$$

where $\mathbf{X}_d$ is known as the dynamic response and $\mathbf{X}_p$ the pseudo-static response which results from the differential support displacements. And from the definition of stiffness matrix, there is

$$\mathbf{K}_{aa}\mathbf{X}_p + \mathbf{K}_{ab}\mathbf{X}_b = \mathbf{0} \quad \text{or} \quad \mathbf{X}_p = -\mathbf{K}_{aa}^{-1}\mathbf{K}_{ab}\mathbf{X}_b = \mathbf{T}_{ab}\mathbf{X}_b \tag{5}$$

and $\mathbf{T}_{ab}$ is called influence matrix.

Substitute Eqs.(4), (5) into Eq.(2) and obtain:

$$\mathbf{M}_{aa}\ddot{\mathbf{X}}_d + \mathbf{C}_{aa}\dot{\mathbf{X}}_d + \mathbf{K}_{aa}\mathbf{X}_d = -\left(\mathbf{M}_{ab}\ddot{\mathbf{X}}_b + \mathbf{M}_{aa}\mathbf{T}_{ab}\ddot{\mathbf{X}}_b + \mathbf{C}_{ab}\dot{\mathbf{X}}_b + \mathbf{C}_{aa}\mathbf{T}_{ab}\dot{\mathbf{X}}_b\right) \tag{6}$$

The same as Eq.(2), $-\mathbf{C}_{ab}\dot{\mathbf{X}}_b$ may be neglected and $\mathbf{M}_{ab}$ may be let to be zero, so, Eq.(6) can be rewritten as:

$$\mathbf{M}_{aa}\ddot{\mathbf{X}}_d + \mathbf{C}_{aa}\dot{\mathbf{X}}_d + \mathbf{K}_{aa}\mathbf{X}_d = -\mathbf{M}_{aa}\mathbf{T}_{ab}\ddot{\mathbf{X}}_b - \mathbf{C}_{aa}\mathbf{T}_{ab}\dot{\mathbf{X}}_b \tag{7}$$

The combination of Eqs.(4), (5) and (7) becomes the Acceleration Input Model (AIM) for analyzing the structural response of ground motions. The derivation shows that the response obtained from Eqs.(4), (5) and (7) should be the same as that from Eq.(3).

The damping force on the right-hand side of Eq.(7) is less than the inertia force and may usually be neglected and then Eq.(7) becomes

$$\mathbf{M}_{aa}\ddot{\mathbf{X}}_d + \mathbf{C}_{aa}\dot{\mathbf{X}}_d + \mathbf{K}_{aa}\mathbf{X}_d = -\mathbf{M}_{aa}\mathbf{T}_{ab}\ddot{\mathbf{X}}_b \,. \tag{8}$$

To avoid solving the inverse of a large matrix, a practical form of Eq.(8) may be obtained by left times $\mathbf{K}_{aa}\mathbf{M}_{aa}^{-1}$ to Eq.(8):

$$\mathbf{K}_{aa}\ddot{\mathbf{X}}_d + \mathbf{K}_{aa}\mathbf{M}_{aa}^{-1}\mathbf{C}_{aa}\dot{\mathbf{X}}_d + \mathbf{K}_{aa}\mathbf{M}_{aa}^{-1}\mathbf{K}_{aa}\mathbf{X}_d = -\mathbf{K}_{ab}\ddot{\mathbf{X}}_b \tag{9}$$

If ground motion is uniform, the pseudo-static structural displacement is the same as the displacement of ground motion, i.e. $\mathbf{X}_p = \mathbf{X}_b$, $\mathbf{T}_{ab} = \mathbf{I}$. Then Eq.(7) becomes

$$\mathbf{M}_a\ddot{\mathbf{X}}_d + \mathbf{C}_{aa}\dot{\mathbf{X}}_d + \mathbf{K}_{aa}\mathbf{X}_d = -\mathbf{M}_a\ddot{\mathbf{X}}_b - \mathbf{C}_{aa}\dot{\mathbf{X}}_b \tag{10}$$

The same as Eq.(7), the damping force on the right-hand side of Eq.(10) may be neglected and Eq.(10) becomes:

$$\mathbf{M}_a\ddot{\mathbf{X}}_d + \mathbf{C}_{aa}\dot{\mathbf{X}}_d + \mathbf{K}_{aa}\mathbf{X}_d = -\mathbf{M}_a\ddot{\mathbf{X}}_b \tag{11}$$

This is the generally used dynamic equilibrium equation for uniform excitation. As the force in this case is related to dynamic displacement and with no relevance to the pseudo-static displacement, Eq.(11) may be applied to both linear and nonlinear structures.

Based on the discussion above, it is concluded that Displacement Input Model (DIM) is the fundamental, accurate and simple model for analyzing structural response of earthquake ground motions, which may be applied to both linear and nonlinear structures and both uniform and spatially varying ground motions; AIM and its derived equations are the special cases of DIM for different conditions.

Eqs.(4), (5) and (7), and Eqs.(4), (5) and (8) are for linear structures. They may be applied both uniform and spatially varying ground motions. For the accuracy, Eqs.(4), (5) and (7) are the same as DIM, while Eqs.(4), (5) and (8) are less than DIM.

Eqs.(10) and Eq(11) are for uniform excitation. They may be applied to both linear and nonlinear structures. For the accuracy, Eq.(10) is the same as DIM, while Eq.(11) is less than DIM .

COMMENTS ON DIM AND AIM OF WILSON (2000)

Normally, discrete points are used to define an acceleration record and it is assumed that the acceleration function is linear within each time interval. Ground velocities and displacements can then be calculated from the integration of the accelerations within each time interval:

$$\dddot{X} = \frac{1}{\Delta t}(\ddot{X}_i - \ddot{X}_{i-1}) \tag{12}$$

$$\ddot{X}_i = \ddot{X}_{i-1} + \Delta t \dddot{X} \tag{13}$$

$$\dot{X}_i = \dot{X}_{i-1} + \Delta t \ddot{X}_{i-1} + \frac{\Delta t^2}{2}\ddot{X} \tag{14}$$

$$X_i = X_{i-1} + \Delta t \dot{X}_{i-1} + \frac{\Delta t^2}{2}\ddot{X}_{i-1} + \frac{\Delta t^3}{6}\ddot{X} \tag{15}$$

It is shown in Eq.(15) that the displacements are cubic functions within each time interval, illustrated in Fig.1b. Therefore, it is believed in Wilson (2000) that if displacement records are used as the specified earthquake loading, e.g. DIM, smaller time steps or a higher-order solution method based on cubic displacements must be used for the dynamic structural analysis. On the other hand, if acceleration records are used as the basic loading, a lower-order solution method, based on linear functions, may be used to solve the dynamic response problem.

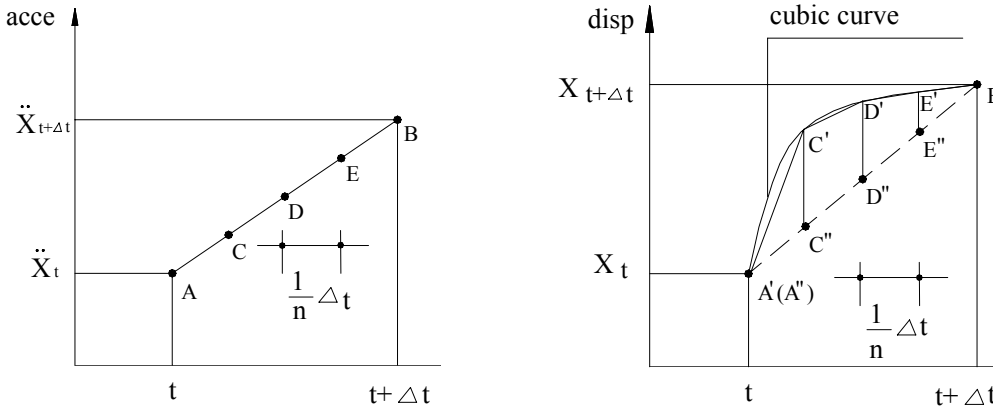

(a) Acceleration (b) Displacement

Fig.1 Acceleration record and displacement record

REANALYSIS OF DIM AND AIM

It is well known from structural dynamics that the structural response of dynamic excitation is controlled by the frequencies of the structures and the excitation, dominantly, in addition to the excitation magnitude. Denote the frequencies of the structure and the excitation as ω_0 and ω, respectively. The dynamic response is about the same as the static if $\omega < \omega_0/4$ and can be neglected if $\omega > 4\omega_0$. The dynamic response should be considered when $\omega_0/4 < \omega < 4\omega_0$ and satisfied accurate solution may be obtained from numerical direct integration methods, such as Newmark method, Wilson-θ method, etc., if time step Δt is less than $T_{\min}/10$ (where $T_{\min} = \min\left(\frac{2\pi}{\omega_0}, \frac{2\pi}{\omega}\right)$) (Bathe, 1982).

The comments above of Bathe (1982) are true for any sorts of excitations, no matter what the excitation is acceleration, displacement or dynamic force. If the frequency is the same, the time step should not change with physical nature of the excitations. For an instance, a SDOF system is subjected to a ground motion with displacement, $A\sin\omega t$, velocity, $A\omega\cos\omega t$, and acceleration, $-A\omega^2\sin\omega t$, then the equation of the SDOF system is

$$M_{aa}\ddot{X}_a + C_{aa}\dot{X}_a + K_{aa}X_a = -K_{ab}A\sin\omega t = A^*\sin\omega t \tag{16}$$

for DIM and

$$\begin{aligned} M_{aa}\ddot{X}_d + C_{aa}\dot{X}_d + K_{aa}X_d &= -M_{aa}T_{ab}\left(-A\omega^2\sin\omega t\right) - C_{aa}T_{ab}\left(A\omega\cos\omega t\right) \\ &= B^*\sin\omega t + C^*\cos\omega t \end{aligned} \tag{17}$$

for the dynamic response of AIM.

It is apparent that Eqs. (16) and (17) will reach the same accuracy given the same integration method and time step are applied, even though $\sin\omega t$ represents displacement in Eq.(16) and Acceleration in Eq.(17).

Real earthquake ground motion is the sum of a series of harmonic functions, and denote the displacement of ground motion as $d = \sum A_i \sin\omega_i t$, and the acceleration $a = -\sum A_i\omega_i^2 \sin\omega_i t$. If the dominant frequency of a is ω_I, there is $A_i < A_I$ for $i > I$ as $\omega_i > \omega_I$, which implies that the dominant frequency of the displacement d, ω_I^*, will not be bigger than ω_I (Fig. 2).

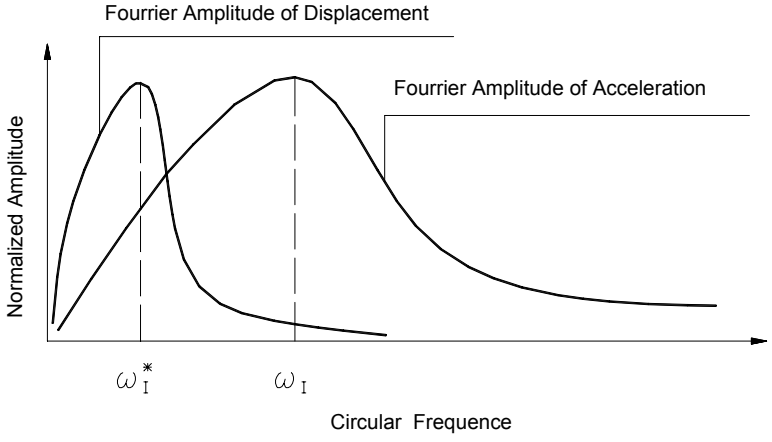

Fig.2 Dominant frequencies of acceleration and displacement

Let the truncated frequency of acceleration be noted as $\alpha\omega_1$, then the time step for calculating Eq.(17), Δt_a, may be determined by $T_{\min} = \min\left(\frac{2\pi}{\omega_0}, \frac{2\pi}{\alpha\omega_1}\right)$; meanwhile, denote the truncated frequency of displacement as $\alpha\omega_I^*$, the time step for Eq.(16), Δt_d, may be determined by $T_{\min} = \min\left(\frac{2\pi}{\omega_0}, \frac{2\omega}{\alpha\omega_I^*}\right)$. If Δt_a is determined by $\frac{2\pi}{\omega_0}$, it is sure Δt_d will be determined by $\frac{2\pi}{\omega_0}$, and $\Delta t_a = \Delta t_d$. Provided Δt_a is determined by $\frac{2\pi}{\alpha\omega_1}$, there will be $\Delta t_d = \Delta t_a$ for $\omega_1^* = \omega_1$ and $\Delta t_d > \Delta t_a$ for $\omega_1^* < \omega_1$, where Δt_d is determined by $T_{\min} = \min\left(\frac{2\pi}{\omega_0}, \frac{2\pi}{\alpha\omega_1^*}\right)$.

It may be concluded from the discussion above that the time step for DIM, Δt_d, is less than or equal to the time step for AIM, Δt_a, given the same integration method is applied. It is sure that this conclusion is also true for MDOF, if ω_0 is defined as the truncated natural frequency.

From this view point, the comments of Wilson (2000) may be reanalyzed. The interpolated points of the acceleration and displacement record (Fig. 1) improve the truncated frequencies of the input excitations. The promotion of the truncated frequencies do not improve the accuracy of the integration as the promoted frequencies from the original truncated frequencies to the news are much higher than the natural frequency if the original time step Δt has satisfied Bathe's requirement. If the original time step Δt does not satisfy Bathe's requirement, a smaller time step will be helpful for both AIM and DIM to obtain a more accurate solution. The following numerical example will illustrate there is no big differences for the accuracy among loading paths $ACDEB$, $A'C'D'E'B'$ and $A^*C^*D^*E^*B^*$, shown in Fig.1. Linear loading paths, $ACDEB$, for AIM, and $A^*C^*D^*E^*B^*$, for DIM, instead of the cubic path $A'C'D'E'B'$, are recommended, as they are simple and convenient.

The analyses above and the numerical examples following will show that the direct integral methods fitting for the Acceleration Input Model are suitable for the Displacement Input Model, also. Time step satisfying the accuracy requirement of AIM may make DIM obtain the same or even more accurate solution given the same numerical method is applied; i.e., time step for DIM is bigger than or equal to the time step for AIM to get a same accurate result. It is not necessary to apply a smaller time step and/or cubic loading path to DIM.

NUMERICAL EXAMPLES

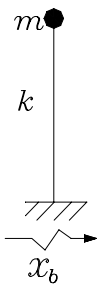

Fig.3 A SDOF system

Example 1

A SDOF system, sketched in Figure 3, is subjected to ground motion with acceleration, $\ddot{x}_{\mathrm{b}} = A\omega^2 \sin\omega t$, velocity, $\dot{x}_{\mathrm{b}} = -A\omega\cos\omega t$, and displacement $x_{\mathrm{b}} = -A\sin\omega t$.

The parameters in Eq.(3) for this system is $M_{\mathrm{aa}} = m$, $K_{\mathrm{aa}} = k$, $K_{\mathrm{ab}} = -k$, $T_{\mathrm{ab}} = -K_{\mathrm{aa}}^{-1}K_{\mathrm{ab}} = 1$ and denote $\omega_0 = \sqrt{k/m}$ and $C_{\mathrm{aa}} = 2\zeta\omega_0 m$, then Eq.(3) becomes

$$\ddot{x}_{\mathrm{a}} + 2\zeta\omega_0\dot{x}_{\mathrm{a}} + \omega_0^2 x_{\mathrm{a}} = -A\omega_0^2\sin\omega t \tag{18}$$

and Eqs.(4), (5) and (7) may be written as

$$x_{\mathrm{a}} = x_{\mathrm{p}} + x_{\mathrm{d}} \tag{19}$$

$$x_{\mathrm{p}} = x_{\mathrm{b}} = -A\sin\omega t \tag{20}$$

$$\ddot{x}_{\mathrm{d}} + 2\zeta\omega_0\dot{x}_{\mathrm{d}} + \omega_0^2 x_{\mathrm{d}} = -\omega^2 A\sin\omega t + 2\zeta\omega_0\omega A\cos\omega t \tag{21}$$

The absolute displacement and velocity responses obtained from Eq.(18) are

$$\begin{aligned} x_{\mathrm{a}}^{\mathrm{DIM}} &= e^{-\zeta\omega_0 t}\left(B_1\cos(\omega_0\sqrt{1-\zeta^2}\,t) + \frac{B_2+\zeta\omega_0 B_1}{\omega_0\sqrt{1-\zeta^2}}\sin(\omega_0\sqrt{1-\zeta^2}\,t)\right) \\ &+ \frac{-\omega_0^2\left(\omega_0^2-\omega^2\right)A}{\left(\omega_0^2-\omega^2\right)^2+4\zeta^2\omega_0^2\omega^2}\sin\omega t + \frac{2\zeta\omega_0^3\omega A}{\left(\omega_0^2-\omega^2\right)^2+4\zeta^2\omega_0^2\omega^2}\cos\omega t \end{aligned} \tag{22a}$$

$$\begin{aligned} \dot{x}_{\mathrm{a}}^{\mathrm{DIM}} &= -\zeta\omega_0 e^{-\zeta\omega_0 t}\left(B_1\cos(\omega_0\sqrt{1-\zeta^2}\,t) + \frac{B_2+\zeta\omega_0 B_1}{\omega_0\sqrt{1-\zeta^2}}\sin(\omega_0\sqrt{1-\zeta^2}\,t)\right) \\ &+ e^{-\zeta\omega_0 t}\left(-\omega_0\sqrt{1-\zeta^2}B_1\sin(\omega_0\sqrt{1-\zeta^2}\,t) + \left(B_2+\zeta\omega_0 B_1\right)\cos(\omega_0\sqrt{1-\zeta^2}\,t)\right) \\ &+ \frac{-\omega_0^2\left(\omega_0^2-\omega^2\right)\omega A}{\left(\omega_0^2-\omega^2\right)^2+4\zeta^2\omega_0^2\omega^2}\cos\omega t + \frac{-2\zeta\omega_0^3\omega^2 A}{\left(\omega_0^2-\omega^2\right)^2+4\zeta^2\omega_0^2\omega^2}\sin\omega t \end{aligned} \tag{22b}$$

where B_1 and B_2 are two parameters determined by the initial conditions of absolute displacement and velocity $x_{\mathrm{a}}^{\mathrm{DIM}}|_{t=0}$, $\dot{x}_{\mathrm{a}}^{\mathrm{DIM}}|_{t=0}$. If it is assumed $x_{\mathrm{a}}^{\mathrm{DIM}}|_{t=0} = \dot{x}_{\mathrm{a}}^{\mathrm{DIM}}|_{t=0} = 0$, then

$$\begin{cases} B_1 = -\dfrac{2\zeta\omega_0^3\omega A}{\left(\omega_0^2-\omega^2\right)^2+4\zeta^2\omega_0^2\omega^2} \\ B_2 = \dfrac{\omega_0^2\left(\omega_0^2-\omega^2\right)\omega A}{\left(\omega_0^2-\omega^2\right)^2+4\zeta^2\omega_0^2\omega^2} \end{cases}$$

The dynamic displacement and velocity may be got from Eq.(21) as

$$\begin{aligned} x_{\mathrm{d}}^{\mathrm{AIM}} &= e^{-\zeta\omega_0 t}\left(B_3\cos(\omega_0\sqrt{1-\zeta^2}\,t) + \frac{B_4+\zeta\omega_0 B_3}{\omega_0\sqrt{1-\zeta^2}}\sin(\omega_0\sqrt{1-\zeta^2}\,t)\right) \\ &+ \frac{-\omega^2\left(\omega_0^2-\omega^2\right)A + 4\zeta^2\omega_0^2\omega^2 A}{\left(\omega_0^2-\omega^2\right)^2+4\zeta^2\omega_0^2\omega^2}\sin\omega t + \frac{2\zeta\omega_0^3\omega A}{\left(\omega_0^2-\omega^2\right)^2+4\zeta^2\omega_0^2\omega^2}\cos\omega t \end{aligned} \tag{23a}$$

$$\dot{x}_{\mathrm{d}}^{\mathrm{AIM}} = -\zeta\omega_0 e^{-\zeta\omega_0 t}\left(B_3\cos(\omega_0\sqrt{1-\zeta^2}\,t)+\frac{B_4+\zeta\omega_0 B_3}{\omega_0\sqrt{1-\zeta^2}}\sin(\omega_0\sqrt{1-\zeta^2}\,t)\right)$$
$$+e^{-\zeta\omega_0 t}\left(-\omega_0\sqrt{1-\zeta^2}\,B_3\sin(\omega_0\sqrt{1-\zeta^2}\,t)+\left(B_4+\zeta\omega_0 B_3\right)\cos(\omega_0\sqrt{1-\zeta^2}\,t)\right) \tag{23b}$$
$$+\frac{\left(-\omega^2\left(\omega_0^2-\omega^2\right)+4\zeta^2\omega_0^2\omega^2\right)\omega A}{\left(\omega_0^2-\omega^2\right)^2+4\zeta^2\omega_0^2\omega^2}\cos\omega t+\frac{-2\zeta\omega_0^3\omega^2 A}{\left(\omega_0^2-\omega^2\right)^2+4\zeta^2\omega_0^2\omega^2}\sin\omega t$$

where parameters B_3 and B_4 are determined by the initial conditions of dynamics displacement and velocity, i.e., $x_{\mathrm{d}}^{\mathrm{AIM}}|_{t=0}$ and $\dot{x}_{\mathrm{d}}^{\mathrm{AIM}}|_{t=0}$.

The absolute displacement and velocity may be obtained by substituting Eqs.(23) and (20) into Eq.(19), and shown as:

$$x_{\mathrm{a}}^{\mathrm{AIM}} = e^{-\zeta\omega_0 t}\left(B_3\cos(\omega_0\sqrt{1-\zeta^2}\,t)+\frac{B_4+\zeta\omega_0 B_3}{\omega_0\sqrt{1-\zeta^2}}\sin(\omega_0\sqrt{1-\zeta^2}\,t)\right)$$
$$+\frac{-\omega_0^2\left(\omega_0^2-\omega^2\right)A}{\left(\omega_0^2-\omega^2\right)^2+4\zeta^2\omega_0^2\omega^2}\sin\omega t+\frac{2\zeta\omega_0^3\omega A}{\left(\omega_0^2-\omega^2\right)^2+4\zeta^2\omega_0^2\omega^2}\cos\omega t \tag{24a}$$

$$\dot{x}_{\mathrm{a}}^{\mathrm{AIM}} = -\zeta\omega_0 e^{-\zeta\omega_0 t}\left(B_3\cos(\omega_0\sqrt{1-\zeta^2}\,t)+\frac{B_4+\zeta\omega_0 B_3}{\omega_0\sqrt{1-\zeta^2}}\sin(\omega_0\sqrt{1-\zeta^2}\,t)\right)$$
$$+e^{-\zeta\omega_0 t}\left(-\omega_0\sqrt{1-\zeta^2}\,B_3\sin(\omega_0\sqrt{1-\zeta^2}\,t)+\left(B_4+\zeta\omega_0 B_3\right)\cos(\omega_0\sqrt{1-\zeta^2}\,t)\right) \tag{24b}$$
$$+\frac{-\omega_0^2\left(\omega_0^2-\omega^2\right)\omega A}{\left(\omega_0^2-\omega^2\right)^2+4\zeta^2\omega_0^2\omega^2}\cos\omega t+\frac{-2\zeta\omega_0^3\omega^2 A}{\left(\omega_0^2-\omega^2\right)^2+4\zeta^2\omega_0^2\omega^2}\sin\omega t$$

It is sure that Eq.(23) equals Eq.(24), i.e.,

$x_{\mathrm{a}}^{\mathrm{DIM}} = x_{\mathrm{a}}^{\mathrm{AIM}}$ $\quad$ $\dot{x}_{\mathrm{a}}^{\mathrm{DIM}} = \dot{x}_{\mathrm{a}}^{\mathrm{AIM}}$

and

$B_1 = B_3$ $\quad$ $B_2 = B_4$

can be resulted.

Substitute $B_3 = B_1$, $B_4 = B_2$ and $t = 0$ into Eq.(23), it is obtained that

$x_{\mathrm{d}}^{\mathrm{AIM}}|_{t=0} = 0$ $\quad$ $\dot{x}_{\mathrm{d}}^{\mathrm{AIM}}|_{t=0} = \omega A$

This result can also be obtained from Eqs.(19) and (20) for $t = 0$.

Now, let $\omega_0 = 5\pi\,\mathrm{rad/s}$, $\zeta = 0.05$, $A = 10$, $\Delta t = 0.01\mathrm{s}$ and $x_{\mathrm{a}}^{\mathrm{A}}|_{t=0} = \dot{x}_{\mathrm{a}}^{\mathrm{A}}|_{t=0} = 0$, and it is assumed that ω is $0.25\omega_0$, $0.8\omega_0$, $2\omega_0$ and $4\omega_0$, i.e., 1.25π、4π、10π and 20π respectively. Numerical responses are got for $\Delta t = (\frac{1}{10},\ \frac{1}{20},\ \frac{1}{40})T_{\min}$ by applying Newmark method and some of the results are presented in Fig.4, 5. A large difference between DIM and AIM is not observed for the response of SDOF under harmonic excitation when the same time step is applied.

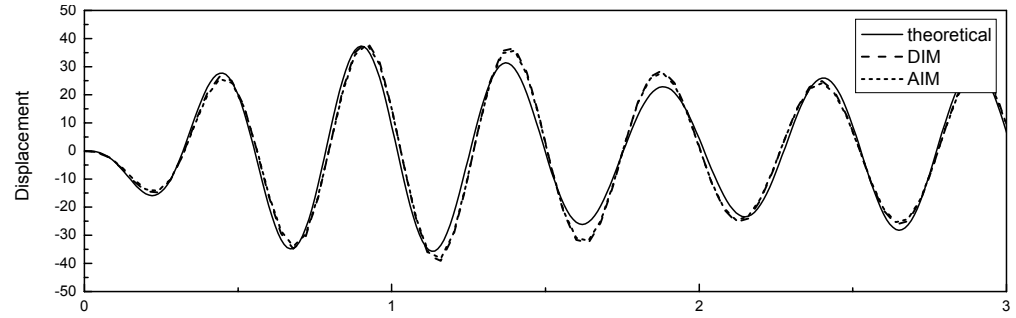

Fig.4 Absolute displacement for $\omega = 4\pi$rad/s and $\Delta t = T_{\min}/10 = 0.04$s

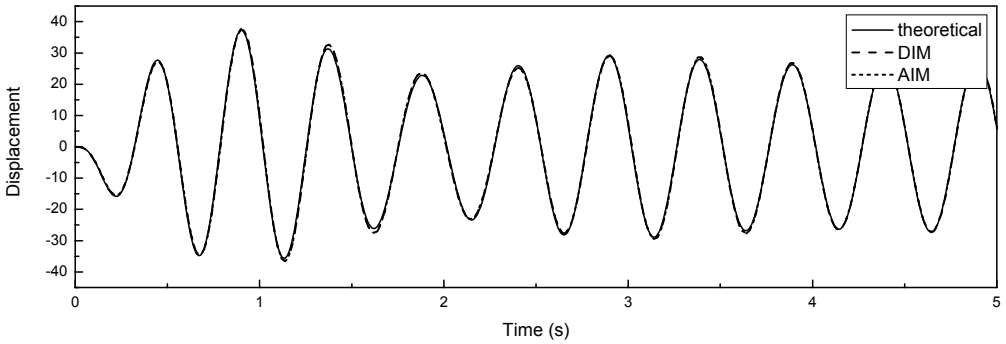

Fig.5 Absolute displacement for $\omega = 4\pi$rad/s and $\Delta t = T_{\min}/20 = 0.02$s

Example 2

It is assumed that the system, illustrated in Figure 3, excited by a ground motion with acceleration, $\ddot{x}_b = A\omega^2 \sin\omega t$, and displacement, $x_b = -A\sin\omega t$ (where $A = 10$ and $\omega = 4\pi$rad/s), recorded with time step $\Delta t = 0.08$s （ $\Delta t > T_{\min}/10$ ）. The structural responses under loading paths AB and $A'B'$ are illustrated in Fig.6. It is apparent that there is a great difference between them and the theoretical result. Numerical results for loading paths $ACDEB$, $A'C'D'E'B'$, $A''C''D''E''B''$, where three equal-spaced interpolate points are added and the time step becomes $\Delta t/4$, are shown in Fig.7. Figs.6 and 7 indicate when the time step is bigger than $T_{\min}/10$, to add interpolate point is an effective approach to improve the accuracy of numerical results, while there is not big difference between linear and cubic loading paths for displacement excitation.

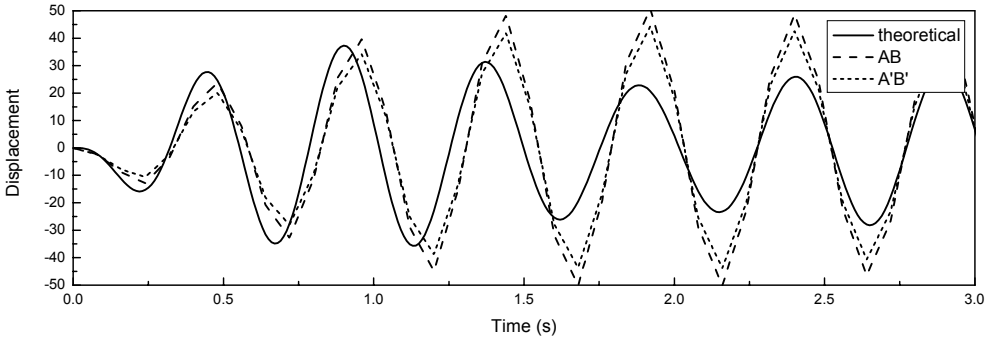

Fig.6 Absolute displacement for $\omega = 4\pi$rad/s and $\Delta t = 0.08\text{s} = T_{\min}/5$

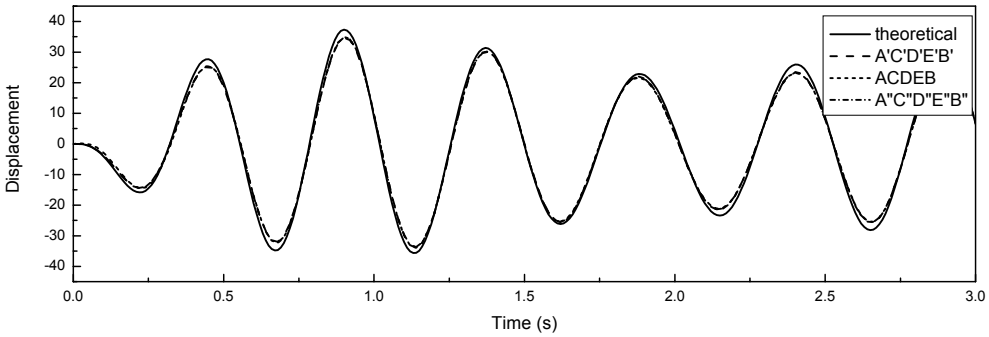

Fig.7 Absolute displacement for $\omega = 4\pi \text{rad/s}$ and $\Delta t = T_{\min}/20 = 0.02\text{s}$

Example 3

The SDOF with natural frequency $\pi \text{rad/s}$, presented in Fig.3, is subjected to earthquake ground motion of EL Centro record. The time history ($\Delta t = 0.01\text{s}$) of acceleration is illustrated in Fig.8 and the integrated displacement in Fig.9. The normalized Fourier amplitude spectra of acceleration and displacement are presented in Fig.10.

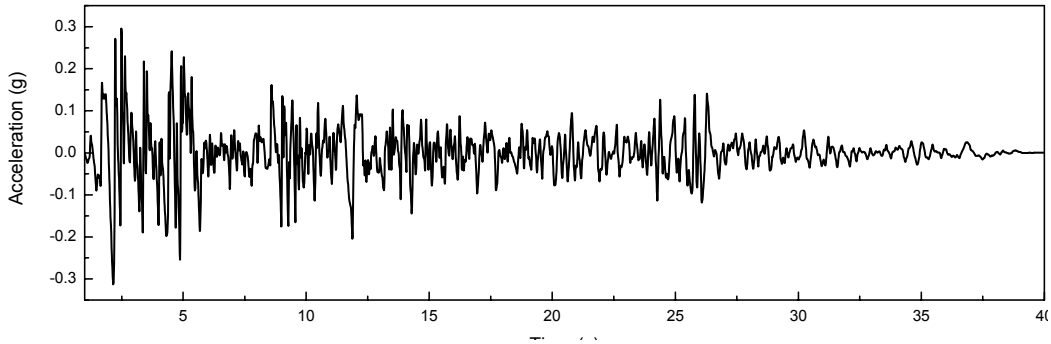

Fig.8 Acceleration of EL Centro earthquake wave

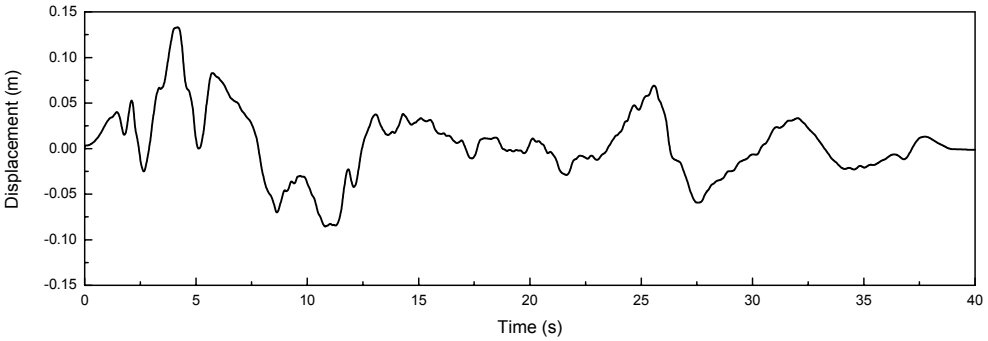

Fig.9 Displacement of EL Centro earthquake wave

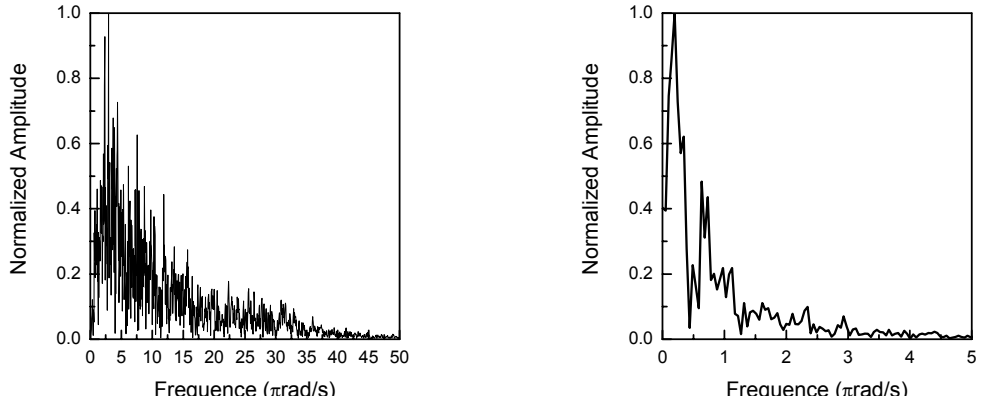

(a) Acceleration (b) Displacement

Fig.10 Fourier amplitude spectra of El Centro earthquake wave

Fig.10a indicates the dominant frequency of the acceleration is $\omega_1 = 2.9\pi \text{rad/s}$, and the truncated frequency can be $\alpha\omega_1 = 20\pi \text{rad/s}$, the value of amplitude spectrum at this frequency is less than 5% of that at the dominant frequency, i.e., $\alpha \approx 7$. The maximum time step for AIM may be calculated by

$$\Delta t_{\text{a,max}} = \frac{T_{\min}}{10} = \frac{1}{10}\min(\frac{2\pi}{\pi}, \frac{2\pi}{20\pi}) = 0.01\text{s}$$

The dominant frequency of the displacement is $\omega_1^* = 0.2\pi \text{rad/s}$ and its truncated frequency may be $\alpha\omega_1^* = 1.4\pi$ rad/s at which the spectra value is also less than 5% of that at the dominant frequency. The maximum time step for DIM is

$$\Delta t_{\text{d,max}} = \frac{T_{\min}}{10} = \frac{1}{10}\min(\frac{2\pi}{\pi}, \frac{2\pi}{1.4\pi}) = 0.14\text{s}$$

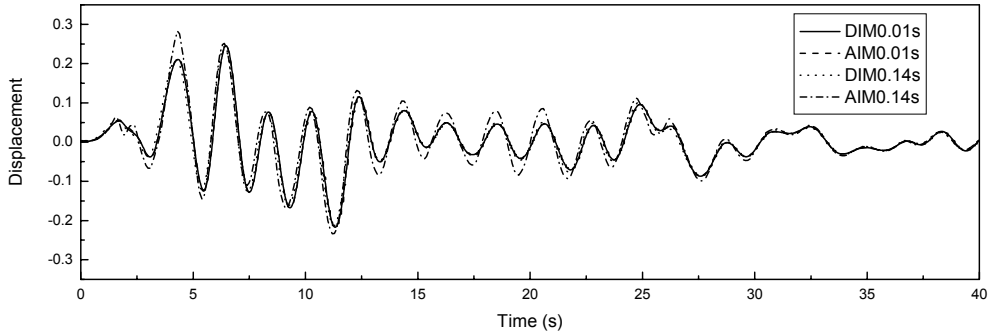

Fig.11 Absolute displacement response

The numerical results of DIM and AIM for $\Delta t = 0.01\text{s}$ and $\Delta t = 0.14\text{s}$, presented in Fig.11, indicate DIM can reach a satisfied accuracy for both $\Delta t = \Delta t_{\text{a,max}} = 0.01\text{s}$ and $\Delta t = \Delta t_{\text{d,max}} = 0.14\text{s}$, while AIM may reach only when $\Delta t = \Delta t_{\text{a,max}} = 0.01\text{s}$. It may be conclude from this example that the time step may be larger for DIM than that for AIM to reach the same accuracy of the response of earthquake ground motion.

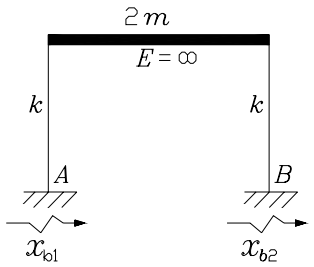

Fig.12 Multi-support structure

Example 4

A two-support SDOF system with natural frequency $\omega_0 = \pi$rad/s , shown in Fig.12 is subjected to EL Centro earthquake ground motion（1940 NS）. It is assumed that the time delay the wave propagates from Support A to Support B is 1.5s，and the numerical response of DIM and AIM with $\Delta t = 0.01$s and $\Delta t = 0.14$s are presented in Fig.13 respectively. The same conclusion as Example 3 may be drawn.

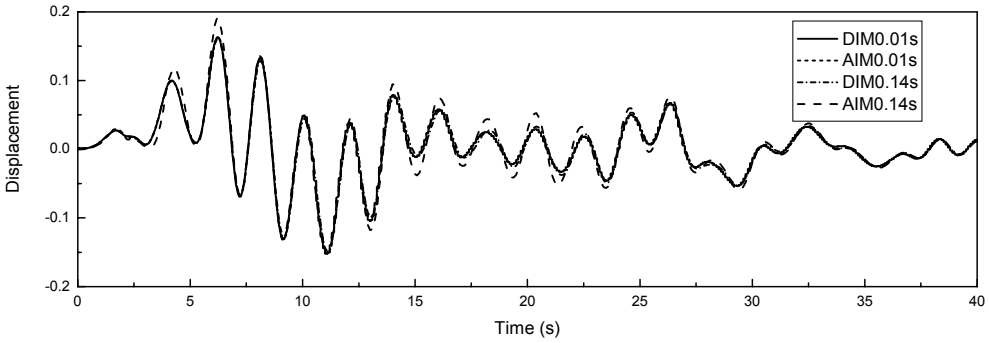

Fig.13 Absolute displacement of the beam

COMMENTS AND CONCLUSIONS

Some comments and conclusions may be drawn from the theoretical analysis and numerical results as follows:

(1) Displacement Input Model, able to be applied both to uniform and spatially varying ground motions, and both to linear and nonlinear structures, is the fundamental and general model for analyzing the structural response of earthquake ground motions.

(2) Acceleration Input Model, which fits to the linear response analysis of spatially varying ground motions and the linear and nonlinear response analysis of, can be considered a special form of Displacement Input Model.

(3) Direct integration methods fitting AIM, Such as Newmark method and Wilson-θ method, are suitable for the DIM, too.

(4) DIM and AIM can reach the same accuracy for the response of a single-frequency harmonic excitation.

(5) DIM are more accurate than AIM for the response analysis of earthquake ground motions given the same integration method and same time step.

(6) Decrease the time step by linear interpolation may promote the accuracy of both DIM and AIM when the original time step is too large, while cubic interpolation can not make a big difference.

(7) DIM is the only suitable model for the nonlinear response analysis of spatially varying ground motions.

REFERENCES

Bathe, K. (1982) "Finite Element Procedures in Engineering Analysis", Prentice-Hall, Inc., Englewood Cliffs. New Jersey

Wilson, E.L. (2000) "Three Dimensional Static and Dynamic Analysis of Structures: A Physical Approach with Emphasis on Earthquake Engineering", Computers and Structures, Inc., Berkley, California.

Yang Qingshan, Saiidi M.S.,et al (2002), "Influence of Earthquake Ground Motion Incoherency on Multi-support Structures", *Earthquake Engineering and Engineering Vibration*, 1(2), 167-180.

Yang Qingshan (2000), "A Practical Coherency Model for Spatially Varying Ground Motions", *Struc. Eng. & Mech.*, 9(2), 141-152.

Controlled Rocking System for Seismic Retrofit of Steel Truss Bridge Piers

Michael Pollino[1] and Michel Bruneau[2]

ABSTRACT

In assessments of the seismic adequacy of existing steel bridges, the steel-to-concrete anchorage connections typically found at the base of steel truss piers can be potentially vulnerable, having little to no ductility and inadequate strength to resist seismic demands. Many other non-ductile failure locations may also exist along the seismic load path. Failure would result in unacceptable performance, especially for bridges deemed critical for response and recovery efforts following an earthquake.

While strengthening is an option, this approach may only transfer damage to another location. An alternative solution could be to release the anchorage connection, allowing development of a rocking bridge pier system that can partially isolate the structure. An improvement on this approach, and the retrofit solution proposed here, allows this rocking mechanism to develop, but complements it by adding passive energy dissipation devices across the anchorage interface to control the rocking response. These specially detailed hysteretic energy dissipating elements (unbonded braces) act as easily replaceable, ductile structural "fuses". This system also provides an inherent restoring force capability that allows for automatic re-centering of the tower, leaving the bridge with no residual displacements after an earthquake.

A similar controlled rocking approach to seismic resistance was implemented into the design of the South Rangitikei Rail Bridge, located in Mangaweka, New Zealand (Priestley et. al. 1996) and was used as a seismic retrofit technique in the Lions' Gate Bridge located in Vancouver, British Colombia (Dowdell & Hamersley 2001). Both bridges use steel yielding devices across the anchorage interface. The Lions' Gate Bridge retrofit utilized time history analysis to size the device and assess the adequacy of existing elements.

This paper investigates the dynamic characteristics of the above proposed controlled rocking/energy dissipation system in order to formulate a capacity design procedure that can reliably predict response using simplified methods of analysis. Design constraints are established that attempt to satisfy performance objectives. Nonlinear time history analyses are used to assess the seismic behavior of the bridges retrofitted per this strategy.

[1] Michael Pollino, Graduate Research Assistant, Department of Civil, Structural and Environmental Engineering, University at Buffalo, Buffalo, NY.

[2] Michel Bruneau, Professor, Department of Civil, Structural and Environmental Engineering, Director of Multidisciplinary Center for Earthquake Engineering Research, University at Buffalo, Buffalo, NY.

INTRODUCTION

Recent earthquakes, such as the 1989 Loma Prieta, 1994 Northridge, and 1995 Kobe earthquake in Japan have demonstrated the need for improved methods for the design and construction of highway bridges to withstand seismic force and displacement demands. While collapse is rare, undesirable damage can leave the bridge unusable until repairs can be made. Highway bridges deemed critical in the response and recovery efforts following a major earthquake need to remain operational after an earthquake requiring the bridge to respond in a mostly elastic manner with little to no residual displacements.

Many existing steel truss bridges consist of riveted construction with built-up, lattice type members supporting a slab-on-girder bridge deck. Truss piers are typically in an x- or v-braced configuration. Steel truss bridges are found in nearly every region of the U.S. A typical steel truss bridge with this type of construction is shown in Figure 1.

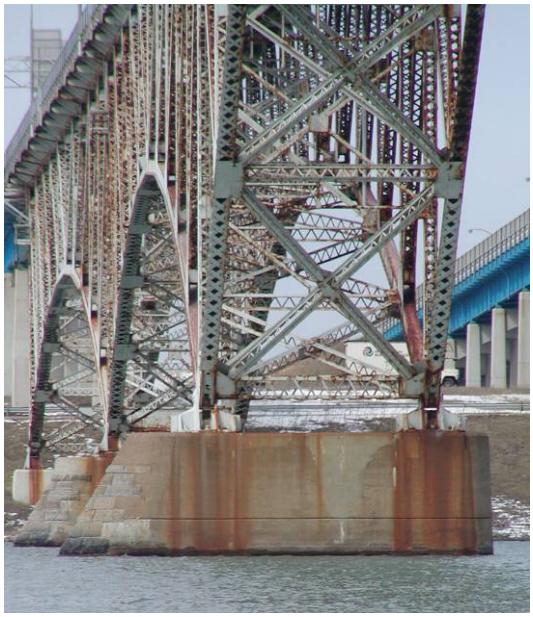

Figure 1. Typical Steel Truss Pier

These built-up lattice type members and their connections can be the weak link in the seismic load path. Recent experimental testing of these members revealed that they suffer global and local buckling causing significant member strength and stiffness degradation resulting in loss of pier lateral strength and major structural damage during an earthquake (Lee & Bruneau 2003). Existing, riveted connections and deck diaphragm bracing members typically possess little to no ductility (Ritchie et. al. 1999). Another possible non-ductile failure location is the anchorage connection at the pier-to-foundation interface. Analysis of "typical" steel-concrete connections suggests it may be unable to resist even moderate seismic demands.

While strengthening these existing, vulnerable elements to resist seismic demands elastically is an option, this method can be expensive and also gives no assurance of performance beyond the elastic limit. Therefore it is desirable to have structures able to deform inelastically, limiting damage to easily replaceable, ductile structural "fuses" able to produce stable hysteretic behavior

while protecting existing non-ductile elements and preventing residual deformations using a capacity-based design procedure.

Failure of or releasing the anchorage connection allows a steel truss pier to step back-and-forth or rock on its foundation, partially isolating the pier. Addition of passive energy dissipation devices at the uplifting location can control the rocking response while providing energy dissipation. An inherent restoring force is provided by gravity, allowing the rocking system to recover plastic rotational deformations at the base and possible re-centering of the pier. The device used in this application is the unbonded brace. An unbonded brace consists of a steel core surrounded by a restraining part, allowing the brace to reach full yield in tension and compression. Experimental testing of the braces can be found in Iwata & Kato (2000). Also, this strategy limits the retrofit effort by working at a fairly accessible location. A sketch of a retrofitted bridge pier is shown in Figure 2.

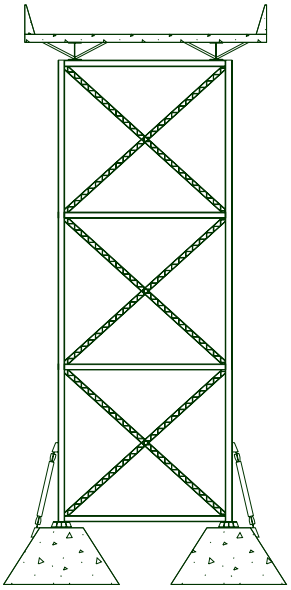

Figure 2. Sketch of Retrofitted Bridge Pier

The dynamic characteristics of the above proposed rocking/energy dissipation system are investigated to develop a design procedure that can size the passive energy dissipation elements while capacity protecting the existing pier. Simple, existing methods of analysis are evaluated for predicting response of this type of system and nonlinear time history analyses are used to assess the seismic behavior.

CONTROLLED ROCKING SYSTEM FOR SEISMIC RETROFIT

Existing Rocking Bridges

A controlled rocking approach to seismic resistance was implemented into the design of the South Rangitikei Rail Bridge (shown in Figure 3), Mangaweka, New Zealand in the early 1970's (Priestley et. al. 1996) and was later used as a seismic retrofit technique in the Lions' Gate Bridge located in Vancouver, British Colombia (Dowdell & Hamersley 2001) as shown in Figure 4. The

South Rangitikei Rail Bridge used torsion yielding, mild steel bars as the energy dissipation device implemented at the anchorage interface while the Lion's Gate Bridge used a triangular shaped flexural yielding device at the anchorage interface.

Figure 3. South Rangitikei Rail Bridge (courtesy of Ian Buckle)

Figure 4. Lions' Gate Bridge, North Approach (courtesy of Bruce Hamersley)

Hysteretic Behavior

The controlled rocking bridge pier system considered can be shown to develop a flag-shaped hysteresis. This is due to the combination of pure rocking response from the restoring moment provided by the bridge deck weight and energy dissipation provided by yielding of the unbonded braces. The key parameters for the hysteretic response of the rocking bridge pier system considered here include the fixed-base lateral stiffness of the existing steel truss pier (k_o), the aspect ratio of the pier (h/d) and the cross-sectional area (A_{ub}), effective length (L_{ub}) and yield strength of the unbonded brace (F_{yub}). Also, the weight excited by horizontally imposed accelerations (W_h) and the vertical gravity weight carried by a pier (W_v) are assumed equal here and expressed as W. The

various steps and physical behaviors that develop through a typical half-cycle of the controlled rocking response, along with the corresponding actions of the unbonded brace are shown in Figure 5. By symmetry, the behavior repeats itself for movement in the other direction.

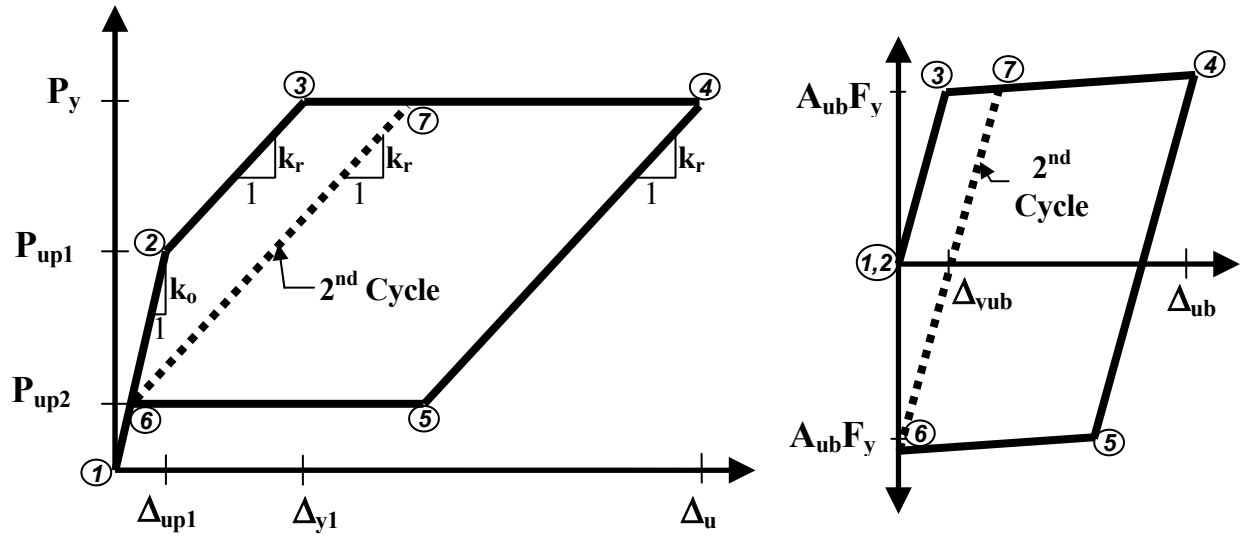

Figure 5. (a) Global Hysteretic Behavior, (b) Response of Unbonded Brace

Transition from 1st to 2nd cycle response occurs when the unbonded braces yield in compression and the braces carry a portion of the weight after the system comes to rest upon completion of the cycle. Ignoring strain hardening in the brace and any difference in compressive and tensile yield strengths of the brace, a displacement of $2\Delta_{yub}$ within the brace will result in the brace carrying an amount of the gravity load equal to the unbonded brace strength. This transfer of gravity load from the pier leg to the unbonded brace reduces the base shear, P, required to initiate uplift ($P_{up2}<P_{up1}$, Figure 5.(a)) resulting in a more flexible system due to the earlier transition to the smaller lateral stiffness k_r.

Re-centering of Pier

By limiting the unbonded brace yield strength to the pier leg's tributary gravity load, the plastic deformations accommodated at the base can be returned to the undeformed positions. Assuming a symmetrical, two-legged pier the limit to allow for pier re-centering is W/2. A local strength ratio, η_L, is defined here as:

$$\eta_L = \frac{A_{ub}F_{yub}}{W/2} \tag{1}$$

Thus $\eta_L<1$ allows for pier re-centering. This ratio is also a measure of the system's energy dissipation per cycle.

Proposed Capacity Based Design Procedure

In the perspective of seismic retrofit, a capacity based design procedure is proposed here to protect non-ductile elements while dissipating energy in specially detailed steel yielding devices. A large number of constraints exist and thus a systematic design procedure that attempts to obey all constraints is desirable. The proposed design procedure uses a graphical approach to size the two key design parameters, the effective length and cross-sectional area of the unbonded brace, L_{ub} and A_{ub} respectively.

Deck-level Displacement

To the writer's knowledge, there exists no solidly established rule of determining maximum allowable displacements for bridges. There likely exist structural elements for which deformations must be limited to prevent their damage or damage of their connections. Such deformation limits vary from bridge to bridge. Here, the deformation limits considered are those that attempt to prevent P-Δ effects from affecting the seismic behavior and a limit based on overturning stability. The smaller of these two limits is used.

A requirement shown to be adequate to prevent excessive P-Δ effects can be found in the NCHRP 12-49 (ATC/MCEER 2003) document. This limit is:

$$\Delta_G \leq 0.25 \frac{V}{W} h \tag{2}$$

where V is the lateral strength of the pier.

Another limit is set based on preventing displacement of the center of mass beyond half of the base width ($^{d}/_{2}$), with a large factor of safety since this is the point of overturning. This limit is defined by:

$$\Delta_G \leq \frac{d}{2FS} \tag{3}$$

A factor of safety (FS) of 5 is recommended.

Ductility Demand on Unbonded Brace

Limits on the inelastic strain demands are set in order to ensure that the brace behaves in a stable, predictable manner. These limits should be based on engineering judgment and experimental test data. Experimental test data of the inelastic cyclic response of an unbonded brace, adapted from Iwata & Kato, is shown in Figure 6. A strain of 1.5% has been selected for a "maximum considered" type earthquake, as appropriate for unbonded braces based on many reported experimental results. Therefore this constraint can be established in terms of brace elongation by:

$$\Delta_{ub} \leq 0.015 L_{ub} \tag{4}$$

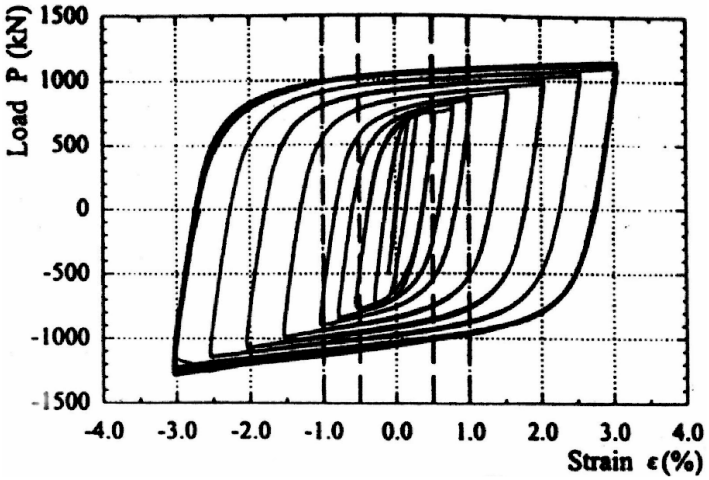

Figure 6. Experimental Test Results (adapted from Iwata and Kato 2000)

Forces to Existing Members and Connections

Capacity design procedures are used to conservatively predict the maximum force demand such that the non-ductile elements can remain elastic, forcing all inelastic action to the specially detailed, ductile structural elements.

After a tower leg uplifts from the foundation it eventually returns to the foundation with a velocity upon impact. Assuming that the maximum velocity of the bridge deck to be equal to the inelastic pseudo spectral velocity and the maximum to occur the moment before impact, the impact velocity can be taken for design purposes as:

$$v_d = PS_{vi}\left(\frac{d}{h}\right) \tag{5}$$

where the inelastic pseudo-spectral velocity, PS_{vi}, can be determined using a ductility reduction strategy.

As the rocking motion continues the structures weight and other loads are transferred to the compressive side as it becomes the new axis of rotation. The hysteretic behavior shown in Figure 5 was determined assuming static response of the controlled rocking pier. However, analysis has revealed that the dynamic response is quite different with the maximum horizontal base shear significantly exceeding the yield force, P_y. Vertical modes of vibration of the controlled rocking system are excited even when subjected solely to horizontal excitation. A sample response of the dynamic hysteresis is shown in Figure 7.

Dynamic effects occur as a result of impact to and uplift from the foundation. Two amplification factors are assigned to the static forces such that members can be capacity protected. The demands placed on a pier leg and a general foundation element, resulting from the impact velocity and dynamic loads, are determined using the conservation of energy. Modification of the key design parameters, A_{ub} and L_{ub}, to limit forces to an acceptable level or strengthening of the non-ductile elements along the lateral load path can satisfy this constraint.

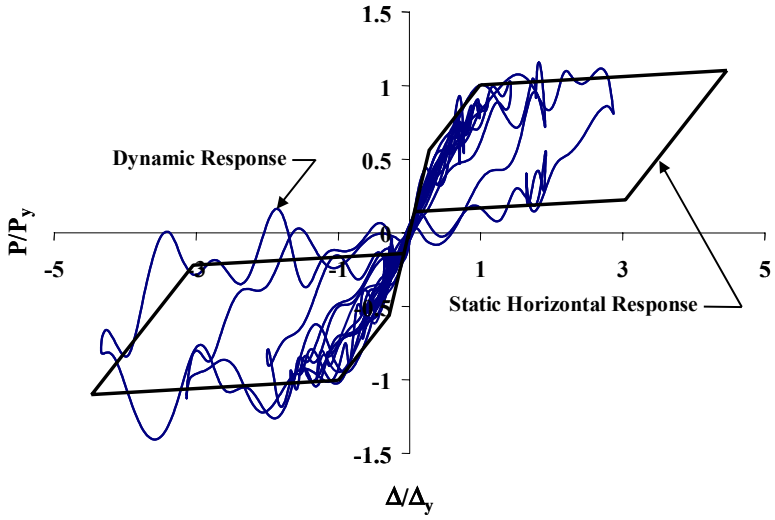

Figure 7. Dynamic Hysteretic Behavior

With appropriate constraints assigned for a particular bridge, the key design parameters (A_{ub} and L_{ub}) can be selected using an iterative analysis and design procedure or a graphical approach, similar to that proposed by Sarraf and Bruneau (1998) could be used to determine the range of A_{ub} and L_{ub} which satisfy the constraints. The procedure determines boundaries of compliance and non-compliance of the design constraints with respect to the key design parameters. A sample graphical design plot is shown in Figure 8.

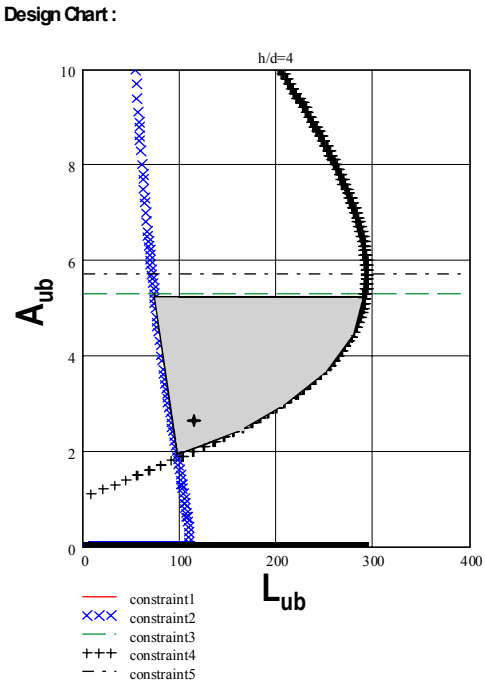

Figure 8. Graphical Design Plot

Simplified Methods of Analysis

To determine the seismically imposed demands to a self-centering, flag-shaped hysteretic system, a number of simple methods of analysis were considered to verify their accuracy in predicting response for design purposes. A first method of analysis considered to characterize system response is similar to the nonlinear static procedure (NSP) in FEMA 356 (FEMA 2000) while a second is similar to the nonlinear static procedure for passive energy dissipation systems found in FEMA 274 (FEMA 1997). An analysis procedure similar to the second one can be found in the NCHRP 12-49 document (ATC/MCEER 2003).

The NSP uses the unbonded brace's stiffness properties to determine the retrofitted effective system stiffness and then calculates a displacement demand using a 2% damped spectrum with some rational coefficients. A conservative estimate of the effective stiffness can be taken as the rocking stiffness (k_r), as shown in Figure 5. A rational expression for the effective stiffness can also be taken as:

$$k_{eff} = k_o\left(\frac{\Delta_{up2}}{\Delta_{y2}}\right) + k_r\left(\frac{\Delta_{y2} - \Delta_{up2}}{\Delta_{y2}}\right) \tag{6}$$

This characterization of the effective stiffness is similar to that in FEMA 356 for systems that experience progressive yielding and do not have a definite yield point and is referred to as Method 1.

The capacity spectrum method for the design of passive energy dissipation systems uses spectral capacity and demand curves to represent the response in a graphical format. The added energy dissipation from the unbonded braces is converted to equivalent viscous damping thus reducing the seismic demand curve from the 2% damped spectrum. This is referred to as Method 2.

Time history analysis is used to verify the adequacy of the simplified methods of analysis and to observe dynamic behavior. Analytical models were developed of the representative piers subjected to a horizontal excitation applied in a primary orthogonal direction. Each pier is assumed to carry an equal mass both vertically and horizontally. The pier itself is modeled with its elastic properties and all nonlinear action occurs at the foundation interface. "Gap" and hysteretic elements are placed in parallel across the anchorage interface to model the rocking mechanism. The hysteretic element is based on the model proposed by Wen (1976). Braces are aligned vertically in the analytical model however they may be implemented inclined to the pier. Restraints are provided at the anchorage level that prevent movement in the horizontal direction but pro-vide no resistance to vertical movements. Inherent structural damping is approximated by assigning 2% equivalent viscous damping to each mode. The Target Acceleration Spectra Compatible Time Histories (TARSCTHS) software developed by the Engineering Seismology Laboratory (ESL) at the State University of New York (SUNY) at Buffalo is used to generate synthetic ground motions attempting to match elastic response spectra defined by the NCHRP 12-49 (ATC/MCEER 2003) spectrum. These motions are applied to the analytical model.

With this type of system (flag-shaped hysteretic), it was shown (including results not presented here) that Method 2 will be more reliable for all possible designs. Method 1 uses a design philosophy that was initially established for elasto-plastic systems however it appears to work reasonably well for systems with $\eta_L > 0.6$. Sample results are shown in Figure 9, for an aspect ratio of 4 and strength ratios, η_L, of 0.25 and 0.5. The deck-level displacement from time history analysis (Δ_{TH}) is normalized by the displacement predicted from analysis methods 1 and 2 (Δ_{design}).

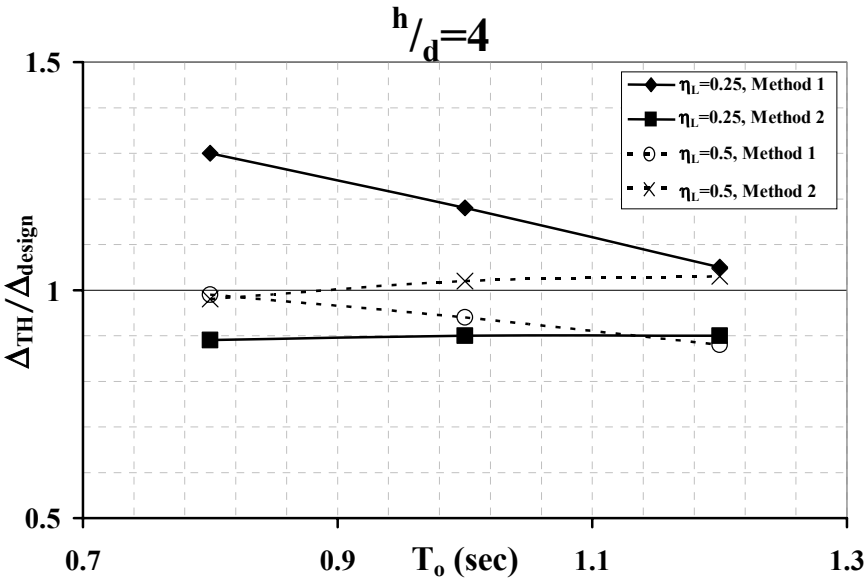

Figure 9. Normalized Displacement Results

Example Time History Results

An example set of time history analysis results obtained following the above design procedure are presented in Figures 10 to 13. Results are normalized by their respective allowable values determined from the design constraints presented in Section 4.1. It can be seen that the displacement of the bridge deck (Figure 10) oscillates about the undeformed position as it comes to rest due to the self-centering ability of the system. The values obtained are less than 1.0, indicating that the resulting system response complied with the design intent.

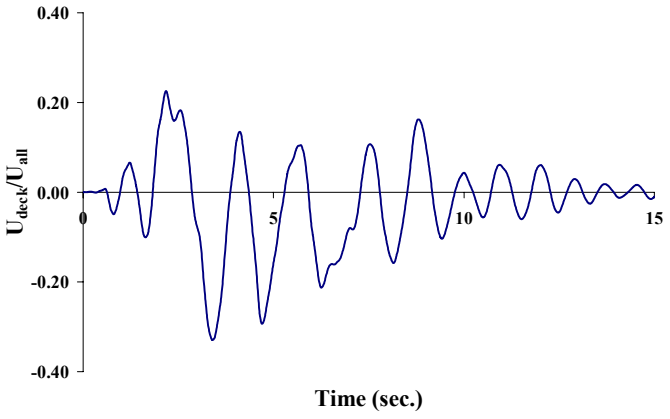

Figure 10. Deck-level Displacement

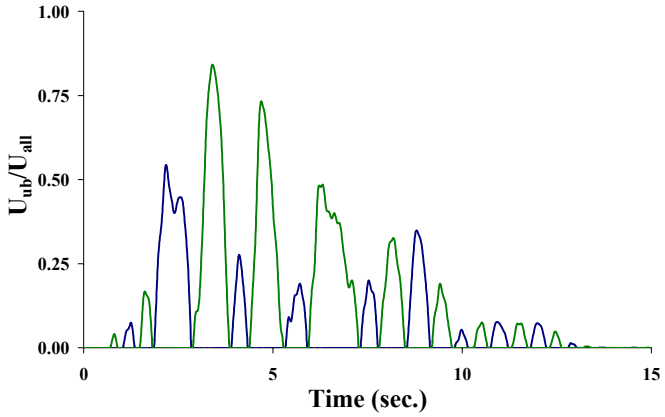

Figure 11. Uplift Displacements

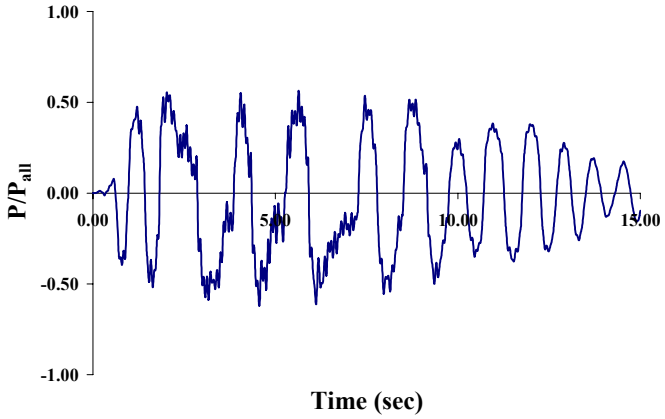

Figure 12. Base Shear

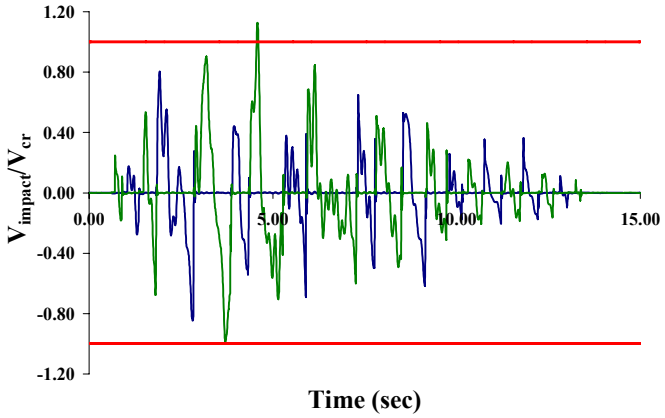

Figure 13. Deck-level Velocity

Conclusions

A new retrofit strategy relying on controlled rocking has been proposed to achieve ductile seismic performance of steel truss bridge piers. Unbonded braces are used to provide energy dissipation to the system while limiting the base overturning moment. This retrofit strategy allows the existing pier and superstructure to remain elastic, and provide self-recentering of the structure following earthquakes, providing a higher level of performance during earthquake motions and increasing the probability that the bridge will remain operational for response and recovery efforts following an earthquake. Results suggest that the proposed retrofit strategy using the capacity design procedure can predict response such that desired performance is achieved. Further analytical research is needed to investigate response of the rocking system subjected to bi-directional and vertical excitation, refine the existing design procedure and develop details for the implementation of the system. Dynamic experimental testing of rocking steel truss piers with passive energy dissipation devices implemented at the anchorage location is expected in the near future.

References

ATC/MCEER (2003), NCHRP 12-49 Recommended LRFD Guidelines for the Seismic Design of High-way Bridges, Part I: Specifications, ATC/MCEER Joint Venture.

Dowdell, D. and Hamersley, B. (2001) "Lions' Gate Bridge North Approach: Seismic Retrofit", Behaviour Steel Structures in Seismic Areas: Proceedings of the Third International Conference: STESSA 2000; Montreal, Canada, August 21-24, 2000, pp.319-326

FEMA (1997), FEMA 274 NEHRP Recommended Provisions for Seismic Regulations for New Buildings and Other Structures, Part-2-Commentary, Building Seismic Safety Council for the Federal Emergency Management Agency, Washington, D.C.

FEMA (2000), FEMA 356 NEHRP Recommended Provisions for Seismic Regulations for New Buildings and Other Structures, Building Seismic Safety Council for the Federal Emergency Management Agency, Washington, D.C.

Iwata, M., Kato, T., Wada, A., (2000) "Buckling-restrained braces as hysteretic dampers" Behaviour of Steel Structures in Seismic Areas, STESSA 2000, pp. 33-38.

Lee, K. and Bruneau, M., (2003) "Review of Energy Dissipation of Compression Members in Concentrically Braced Frames", Technical Report MCEER-02-0005, Multidisciplinary Center for Earthquake Engineering Research, State University of New York at Buffalo, Buffalo, NY.

Priestley, M.J.N., Seible, F. and Calvi, G.M. (1996). Seismic Design and Retrofit of Bridges, John Wiley & Sons, New York.

Ritchie, P., Kauhl, N. and Kulicki, J. (1999) "Critical Seismic Issues for Existing Steel Bridges", Technical Report MCEER-99-0013, Multidisciplinary Center for Earthquake Engineering Research, State University of New York at Buffalo, Buffalo, NY.

Sarraf, M., and Bruneau, M. (1998). "Ductile seismic retrofit of steel deck-truss bridges. II: Design applications." J. Struct. Engrg., ASCE, 124(11), 1263-1271.

Wen, Y. K. (1976). "Method for Random Vibration of Hysteretic Systems," Journal of the Engineering Mechanics Division, ASCE, Vol. 102, No. EM2.

Development of Built-up Shear Links as Energy Dissipators for the Seismic Protection of Long Span Bridges

Ian Buckle, Peter Dusicka, and Ahmad Itani[1]

ABSTRACT

The proposed new east bay crossing of the San Francisco-Oakland Bay Bridge (SFOBB) will use steel shear links as energy dissipators for added protection during strong earthquakes. These large-capacity, built-up shear links are embedded at various heights in the tower, which comprises four vertical steel shafts that are cantilevered from the pile cap. Although A709 HPS 70 steel is used throughout the bridge, the shear links use A709 Grade 50 steel, due to a lack of data regarding the inelastic performance of the HPS 70 steel at large plastic strains.

Inelastic shear links have been used in building construction for many years but their application to bridge structures is still in its infancy. For this reason the California Department of Transportation (Caltrans) funded both full-scale and half-scale tests of the proposed SFOBB shear links. The full-scale test was carried out at University of California in San Diego, and the half-scale test, which included sections of the adjacent tower shafts, was carried out at University of Nevada in Reno (UNR). Both tests demonstrated the adequacy of the design by T.Y. Lin, with rupture occurring at about 11% shear strain, well above the minimum required value of 3%.

This paper presents the results of the UNR tests and describes a subsequent study which compares this performance with that obtained from a series of follow-on experiments using links fabricated from a high performance steel (HPS 70) and two different low yield point steels (LYP 100 and LYP 225).

It is shown that the HPS link performed as well as the Grade 50 link with less overstrength at high inelastic strains (1.5 vs 2.2). Failure in both cases was initiated at the welds between the stiffeners and the web. It was also found that the stiffeners may be eliminated altogether if thicker webs and low yield point steels are used (for the same nominal shear capacity). These LYP links demonstrated a very high capacity for inelastic strain, due to the significant reduction in welding in areas with high plastic yield strains. Failure occurred at about 20% strain. These results also appeared to be independent of the load sequence used to reach failure. Overstrength was observed to be of the same order of magnitude as for the Grade 50 links.

The paper concludes that inelastic shear links are very efficient energy dissipators and can designed to have a high tolerance for inelastic strain. Applications to long span bridges are attractive because of their low cost and negligible maintenance requirements.

[1] Department of Civil Engineering, University of Nevada Reno, MS 258, Reno NV 89557

INTRODUCTION

The pros and cons of using mechanical energy dissipators for the improvement of the seismic performance of buildings and bridges have been argued for many years. From a theoretical viewpoint the advantages clearly outweigh the disadvantages, but the practical difficulties of developing reliable and robust devices, that need little or no maintenance, have slowed their application to real structures. Examples of such dissipators include fluid dampers, viscoelastic devices, friction dampers, and hysteretic devices. Of these, the last named seem to have the greatest promise because of negligible maintenance requirements and low cost. Hysteretic dissipators include flexural, torsional and shear devices usually constructed from steel, but lead has also been used to advantage in various kinds of dampers including an extrusion damper. This paper focuses on the development of a new class of shear device for application to large bridge structures.

Inelastic shear links have been used to improve the performance of steel buildings for many years. Usually part of an eccentrically braced frame, substantial research in the late 1970s and early 1980s demonstrated both the advantages and practicality of such systems (Hjelmstad and Popov, 1986; Engelhardt and Popov, 1989). Most seismic building codes permit the use of these devices and design guidelines are well developed (ICBO, 2002). Rolled steel sections are commonly used for the link itself, provided certain requirements on section compactness are satisfied. But the force capacity at yield is limited by available section sizes and if a large device is required, built up sections must be used. This situation is rarely found in buildings but is common in bridges, especially in long-span bridges. However experience with large capacity shear links using built-up sections is limited (Itani, 1997) and very little is known about how performance might be optimized by choice of, say, material strength (Grade 50 vs a high performance steel, HPS 70, for example), geometry, and stiffener layout.

Triggered by the proposal to use inelastic shear links in the new east bay spans of the San Francisco – Oakland Bay Bridge (SFOBB), an experimental study has been undertaken to examine some of these issues. This paper summarizes the results of this study.

SAN FRANCISCO - OAKLAND BAY BRIDGE

The San Francisco - Oakland Bay Bridge (SFOBB) is a major crossing between the cities of San Francisco and Oakland across San Francisco Bay. Opened in 1936**,** the bridge has a total length 13.4 km (8.3 mi). It comprises back-to-back suspension spans across the west side of the Bay from San Francisco to Yerba Buena Island, and cantilever and simply supported truss spans from the Island to Oakland. The double deck structure carries about 280,000 vehicles per day forming a vital link between the two cities. The collapse of the link span over Tower E9 during the 1989 Loma Prieta earthquake (M7.1), led to an assessment of the vulnerability of the eastern spans of bridge and the conclusion by the California Department of Transportation (Caltrans), that a new east bay crossing was more cost effective than retrofitting the old one.

The new east bay crossing is being designed by a joint venture of T.Y. Lin International and Moffatt & Nichol Engineers, under contract to Caltrans (Tang et al, 2002). The new bridge is 3.7 km (2.3 mi) long and consists of a number of continuous, reinforced concrete approach spans and a single 565 m (1854 ft) suspension span over the navigation channel on the east side of Yerba Buena Island. The self-anchored suspension span comprises a single tower and a number

of innovative design concepts (Figure 1). Of particular interest is the configuration of the tower and the
resisting system for lateral loads, such as wind and earthquake. It is noted that the seismicity of the site is high due to the close proximity of the Hayward and San Andreas faults, 12 km (6.5 mi) and 25 km (15.5 mi) from the bridge respectively. The 160 m (525 ft) tall tower consists of four hollow shafts connected by links as illustrated in the enlarged section of Figures 1 and 2. Each steel shaft is made from stiffened skin plates to form an asymmetrical pentagon. The shafts are inter-connected both transversely and

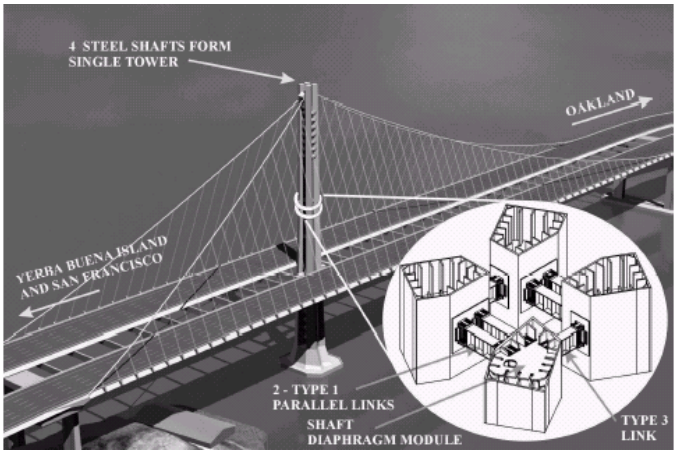

Figure 1: Suspension span of proposed east bay crossing of the San Francisco - Oakland Bay Bridge. (Rendering by T.Y. Lin International)

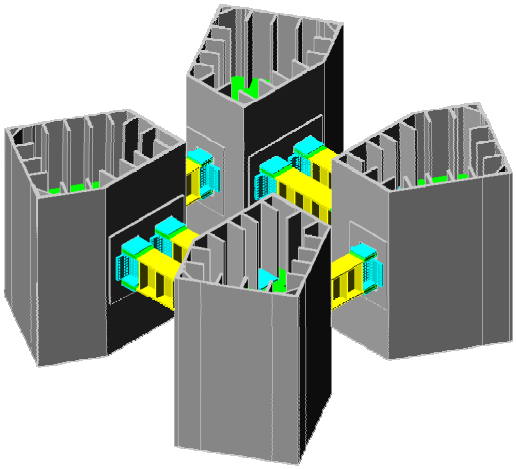

Figure 2: Cross section through tower of proposed east bay crossing of the San Francisco - Oakland Bay Bridge.

longitudinally at various heights by steel linkage beams. These links are engaged in shear as the tower deforms laterally due to transverse and longitudinal loads. Internal diaphragms provide the load path between the membrane forces in the shaft walls and the flexure and shear forces in the links. In the transverse direction, two parallel beams make up each link, to provide sufficient strength and stiffness for transverse loads. In the longitudinal direction each link is a single beam.

In order to satisfy rigorous performance requirements for the bridge, the tower shafts are required to remain elastic under the maximum considered earthquake (MCE). To help achieve this level of performance the links are intended to yield in shear and dissipate energy, thus reducing the demand on the towers and foundations. As a consequence, the tower is designed using capacity-design principles, which includes the connections between the tower diaphragms and the shear links. It is noted that these connections are bolted to facilitate replacement should the need arise after a large earthquake.

EXPERIMENTAL PROGRAM

The primary objective of the experimental program was to quantify the cyclic behavior of the shear links proposed for the SFOBB and investigate alternative materials and configurations. In addition, the link-to-shaft connection detail was studied using boundary conditions in the experiment that represented the as-designed condition. Accordingly a half-scale model of two of the four shafts, including the bolted connections, was constructed and used as the test bed for this project.

Materials studied include A709 Grade 50 steel (as specified by the designers and owners), A709 HPS 70 steel, and two low yield point steels (LYP 100 and LYP 225). No experimental data is known to exist on the performance of HPS70 steel at large plastic strains and seismic applications of this material are not encouraged pending the availability of this data. The low yield point steels offer the potential for reducing the number of web stiffeners (or their complete elimination) with consequential savings in cost and a marked increase in plastic capacity. Two sets of experiments were therefore conducted involving a total of 9 links. Web stiffeners are provided in specimens A1, A2, and A3, but not in specimens B1, B2, and B3. Table 1 summarizes the links tested.

Table 1. Shear Link Summary.

Set	Number	Material	Nominal Yield (ksi)	Link Type	Single/Dual Beam	Web Stiffeners	Number Tested
A	A1	A709 G50	50	3	Single	Yes	1
	A2	A709 G50	50	1	Dual	Yes	1
	A3	A709 HPS70W	70	3	Single	Yes	1
B	B1	LYP 100	15	3	Single	No	2
	B2	LYP 225	33	3	Single	No	2
	B3	LYP100/225	15/33	Hybrid	Single	No	2

For each material, cyclic tests were used to identify the

- plastic rotational capacity (shear strain)
- overstrength ratio, and
- ultimate failure mode.

In addition to the above objectives, the construction of a half-scale replica of the complex shaft / link assembly gave fabricators and design engineers the opportunity to verify and refine the sequence of fabrication prior to finalizing the design.

SPECIMEN DETAILS

Replicas of the shear links and corresponding sections of the tower shafts were built at one-half scale. The dimensions were based on the design drawings for the bridge including the details of the adjacent shaft, to ensure the correct boundary conditions were provided for the links.

Shear Links

The shear links were I-beams, built up from steel plates of different thickness and material properties. As shown in Table 1, two representative shear links from the bridge tower were chosen for study. In the actual structure, the links vary with height and the ones studied in this project were from tower at elevation 89 m (292ft). A Type1 link is located transversely and a Type 3 link longitudinally with respect to the bridge orientation. As shown in Figure 3, two distinct regions in the link can be identified: the deformable region in the middle, which for link 1 was fabricated from A709 grade 50, and the connection region at the ends which for all links (1-6) was fabricated from A709 grade HPS 70W steel. In addition to the higher strength material, the connection region also has increased thickness of plates in both the flange as well as in the web to accommodate the bolt holes. For the transition to the thicker plates, complete joint penetration (CJP) welds were used. In the case of the flange, these welds are located in zones of high moment and close to the deformable length and thus an area of potential failure.

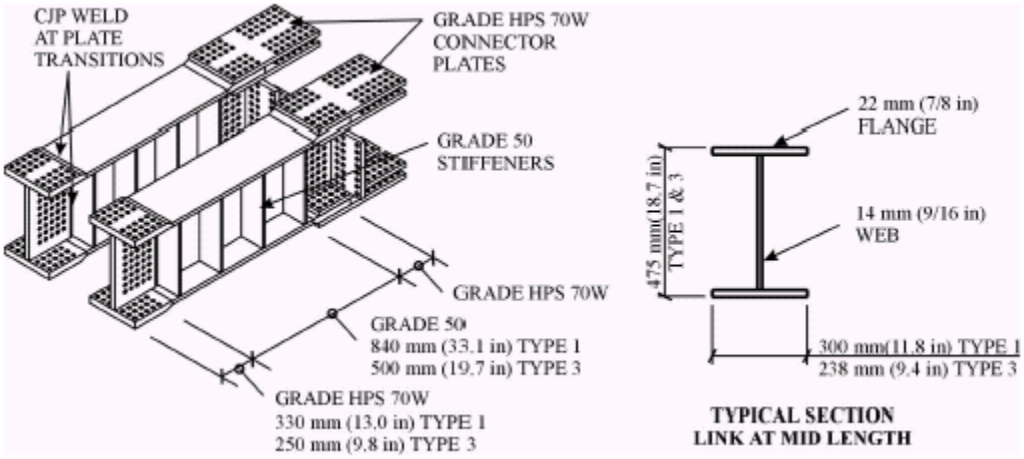

Figure 3: Type 1 shear link (dual beam, half-scale dimensions shown).

The nominal seismic capacity of the shear link can be computed using American Institute of Steel Construction (AISC) seismic specifications as:

$$V_p = 0.6\, F_y\, A_w \qquad (1)$$

where F_y = nominal yield stress, and
A_w = sectional area of the web.

Equation 1 gives a nominal shear strength of 1250 kN (281 kip) for both Type 1 and 3 links. Assuming a constant shear distribution, the moment demand at the end of the deformable link is 526 kNm (387 kip ft) and 312 kNm (230 kip ft) for Types 1 and 3 respectively. Comparing these values to the respective nominal plastic moment capacity of 1256 kNm (926 kip ft) and 1042 kNm (768 kip ft), the links should yield in shear before flexure, as required.

As noted above, one of the main objectives of the experimental program was to quantify the overstrength ratio. This ratio dictates the strength required for adjacent connections and members in order that these components remain elastic, as required by the performance criteria for the bridge. The AISC seismic provisions, which are intended for rolled shapes, recommend this ratio be calculated from a combination of yield overstrength ($R_y = 1.1$) and strain hardening, giving a total of $1.25R_yV_p$ ($= 1.375V_p$). For large-scale built-up shear links, with high flange-to-web thickness ratios such as those used in this bridge, the overstrength ratio could be significantly higher.

Tower Shafts and Connection

As noted above, the shear links are bolt-connected to the shafts using connector plates for the flanges and angles for the web, all fabricated from A709 grade HPS 70W. The flange connector plates bolt to a diaphragm, also made from A709 grade HPS 70W, inside the shaft as illustrated in Figure 4. The diaphragm transfers load from the shear links to the tower shafts. The shafts are pentagonal in shape and have stiffened skin plates as shown.

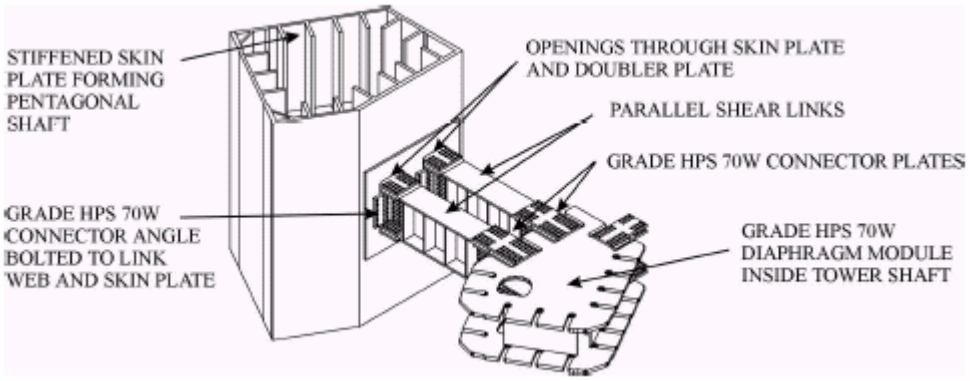

Figure 4: Schematic of link - diaphragm - shaft connection (Type 1 link shown).

The flexibility of the connection zone contributes to the overall rotational capacity of the shear link and thus affects its ductility capacity. Bolt slippage is expected to also contribute, along with possible additional flexibility within the tower shaft. The distribution of in-plane stresses within the diaphragm was monitored during these experiments to gain an understanding of the load transfer mechanism within the asymmetric cross section of the shaft.

EXPERIMENTAL SETUP

For practical purposes, the vertical tower shafts and link assembly are tested horizontally on the strong floor of the laboratory, as shown in Figures 5 and 6. The shaft sections are pinned at the base. A pinned stiff link redistributes the actuator force between the two shafts. An actuator capable ±3100 kN (±700 kip) force with ±610 mm (±24 inch) stroke was used to apply the lateral load to the shafts. Reaction blocks, stressed to the laboratory floor, act as buttresses and distribute the loads to the strong floor.

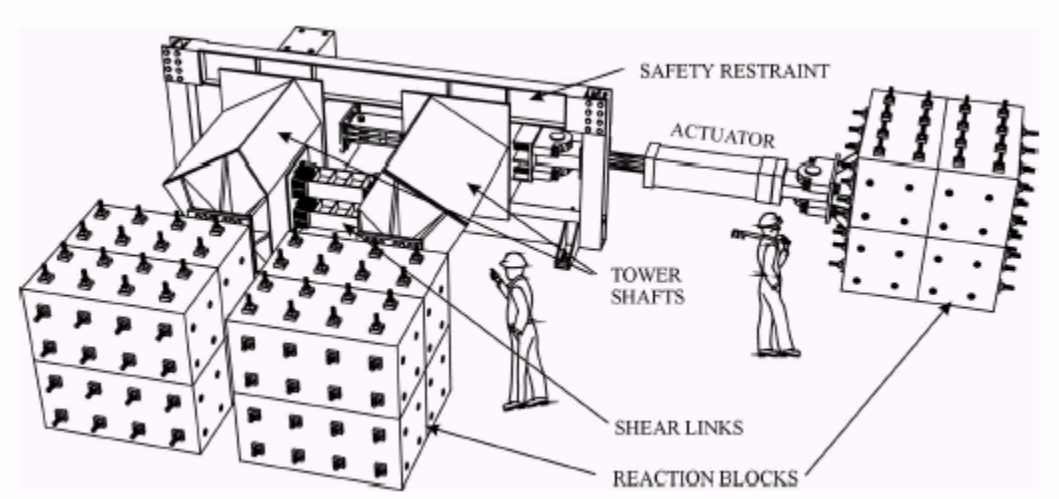

Figure 5: Schematic of test assembly (Type 1 link shown).

Figure 6: Test assembly in Large-Scale Structures Laboratory
at University of Nevada Reno (Type 1 link shown).

INSTRUMENTATION AND LOAD HISTORY

The instrumentation was chosen to monitor the behavior of the shear link-to-shaft assembly, as partly illustrated in Figure 7. Displacement transducers were used to measure the deformation in the link. Both the deformable and connection region were monitored. From these transducers the rotational capacity, or shear deformation (γ), was calculated. The strain distribution along the diaphragm was measured using the strategically placed strain gages. The actuator displacement and load was also recorded. For Set A (Table 1), the loading history was a set of reversed cycles at increasing shear strain (rotation) to failure (Figure 8a). For Set B, in which two identical specimens were available, one specimen was tested using monotonically increasing strain as for Set A, and the other was tested to failure using a load history representative of near-fault response (Figure 8b). Results were calculated and presented as plots of shear strength versus shear deformation. Overstrength ratios were also measured and recorded.

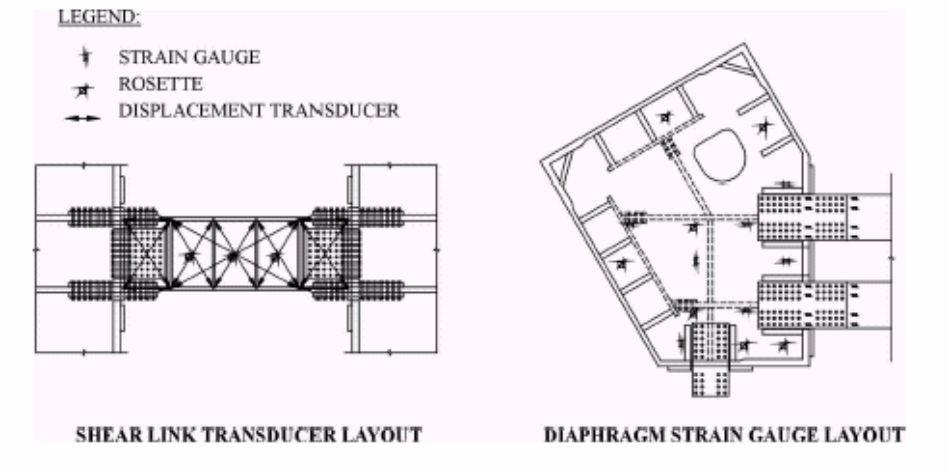

Figure 7. Instrumentation layout for typical link (left: side view) and diaphragm (right: plan view) partially shown for clarity.

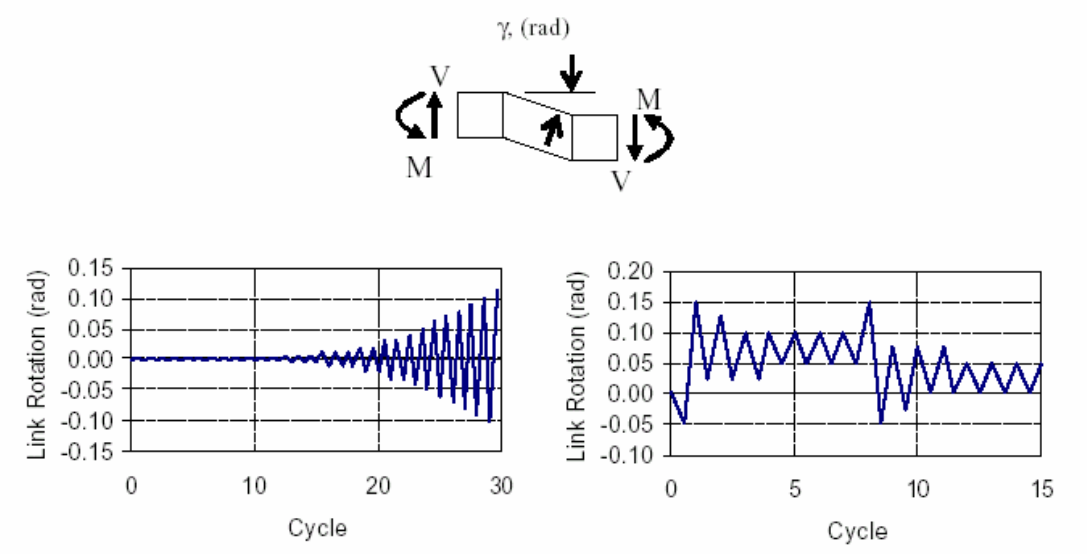

Figure 8. Test load histories: monotonically increasing (left) and near-fault (right).

RESULTS

Tests on the Grade 50 links (A1 and A2, Table 1) demonstrated the adequacy of the design by T.Y. Lin, with rupture occurring at about 13% shear strain (Figure 9), well above he minimum required design value of 3% and the AISC minimum value of 8% (AISC 1997).

In addition an HPS 70 link (A3, Table 1) with the same nominal yield capacity performed equally well, with respect to the ultimate shear strain. Figure 9 shows a comparison of the results obtained for the Grade 50 and HPS 70 links and the stable hysteretic loops up to failure. It is also clear in Figure 9 that the overstrength in the Grade 50 link is substantial (about 2.2 at failure) whereas the HPS 70 link shows considerably less overstrength (1.5 at failure). The number for the Grade 50 link is much higher than expected and needs further evaluation. In both the Grade 50 and HPS 70 links, failure was initiated by rupture at the welds between the stiffeners and webs (Dusicka et al, 2002).

As noted above, links in Set B do not have web stiffeners to reduce the likelihood of weld rupture and increase rotational capacity. To prevent web buckling and maintain the same nominal capacity as in Set A, the web was thickened and yield strength decreased accordingly. Two low-yield-point steels were studied, one with a 15 ksi (LYP 100) and the other a 33 ksi yield point (LYP 225).

Figure 10 shows the hysteretic loops for the LYP 225 link where it is clear that, for the same strength, this link has considerably greater ductility. Rupture occurred at 20% strain and demonstrated an overstrength of 2.0 (about the same as the Grade 50 link). Figure 11 shows the failed specimen. Considerable warping of the web has occurred (to accommodate substantial changes in geometry) and failures have occurred in the welds at the right hand end of the lower web-to-flange connection and up along the right hand edge of the web to connection plate.

Figures 12a and b show the hysteretic loops for the both the LYP links subject to increasing strain levels (Figure 8a) until failure. Failure occurred at 20% strain for the LYP 225 (33 ksi) link and at 17% strain for the LYP 100 (15 ksi) link. Overstrength for the LYP 100 link was however considerably greater than for the LYP 225 link (3.1 vs 2.1). In fact the high overstrength observed in the LYP 100 link caused failure in the connection plates for this link leading to the premature termination of this experiment before the full capacity of the link itself was reached.

Figures 13a and b show similar results for the near-fault load sequence (Figure 8b). The maximum shear strain before degradation was again 20% for the LYP 225 link, and in order to protect the connections for the LYP 100 link, the test was terminated at 15% before failure of the connection occurred (due to exceptional overstrength). It is however clear that performance up to 15% strain is very similar to that seen in Figure12b.

CONCLUSIONS

It has been shown that the HPS 70 link performed as well as the Grade 50 link with less overstrength at high inelastic strains (1.5 vs 2.2). Failure in both cases was initiated at the welds between the stiffeners and the web. It was also found that the stiffeners may be eliminated altogether if thicker webs and low yield point steels are used (for the same nominal shear capacity). These LYP links demonstrated a very high capacity for inelastic strain, due to the significant reduction in welding in areas with high plastic yield strains. Failure occurred at about 20% strain. These results also appeared to be independent of the load sequence used to reach

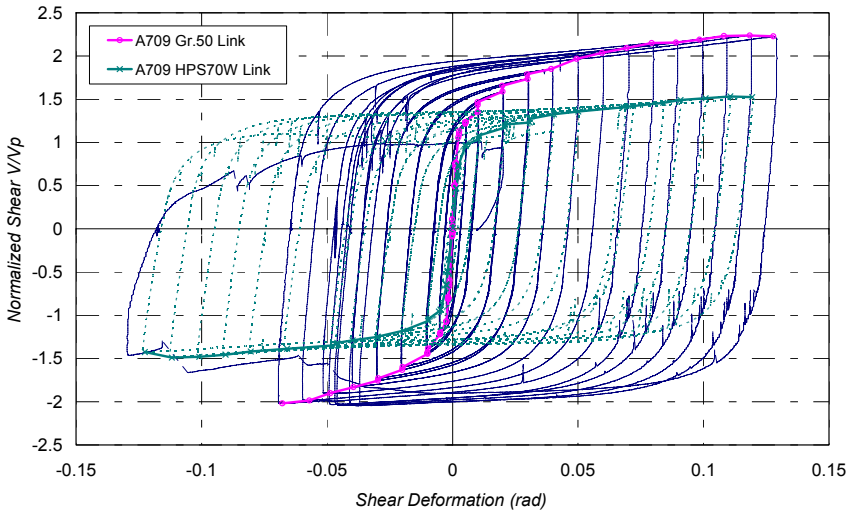

Figure 9. Hysteretic loops for the Grade 50 and HPS 70 shear links (A1 and A3).

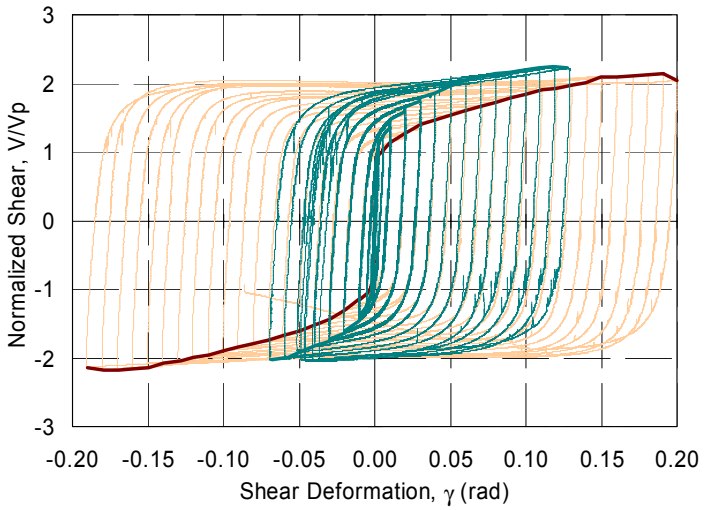

Figure 10. Hysteretic loops for the Grade 50 and LYP 225 (33 ksi) shear links (A1 and B2: A1 envelope is lighter line to +13% strain; B2 envelope is darker line to +20% strain).

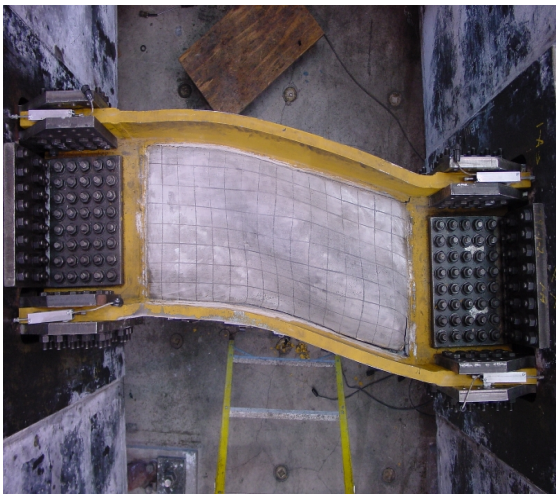

Figure 11. Failure of LYP 225 (33ksi) shear link (B2) at 20% strain.

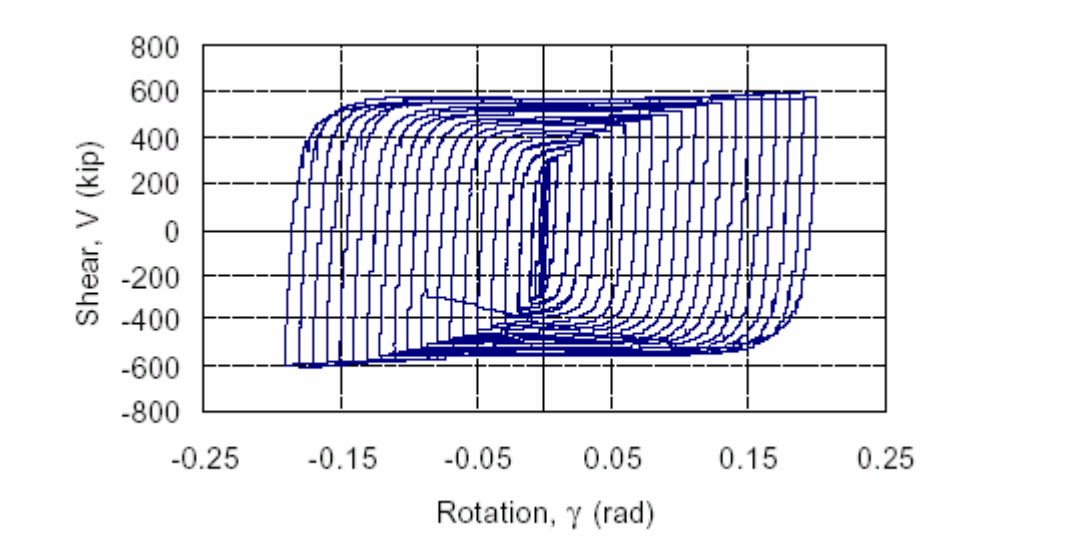

Figure 12a. Hysteretic loops for LYP 225 (33 ksi) link (B2) subject to increasing levels of cyclic strain.

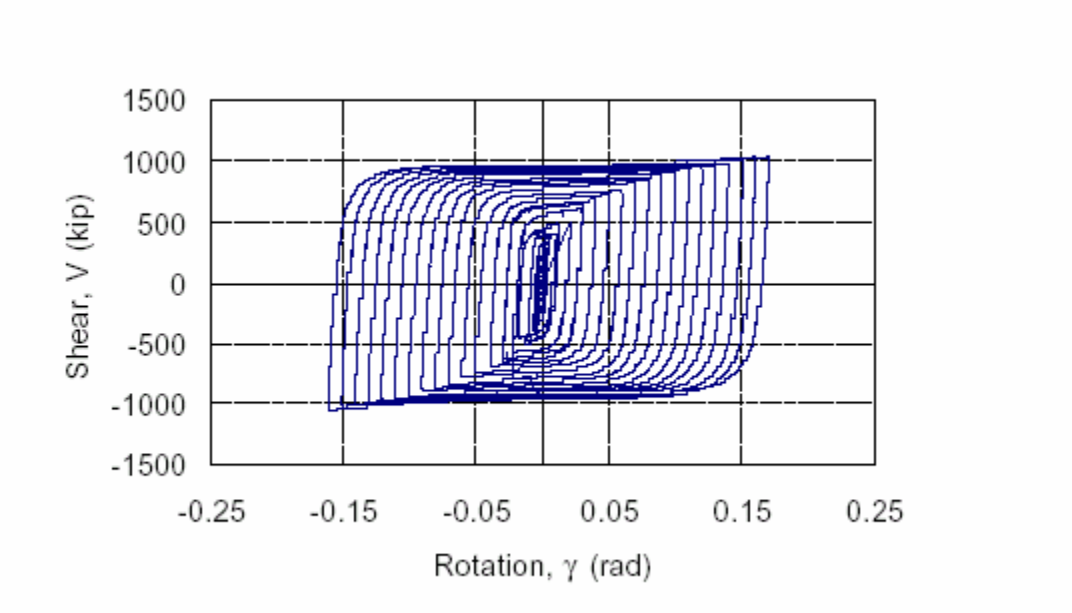

Figure 12b. Hysteretic loops for LYP 100 (15 ksi) link (B1) subject to increasing levels of cyclic strain.

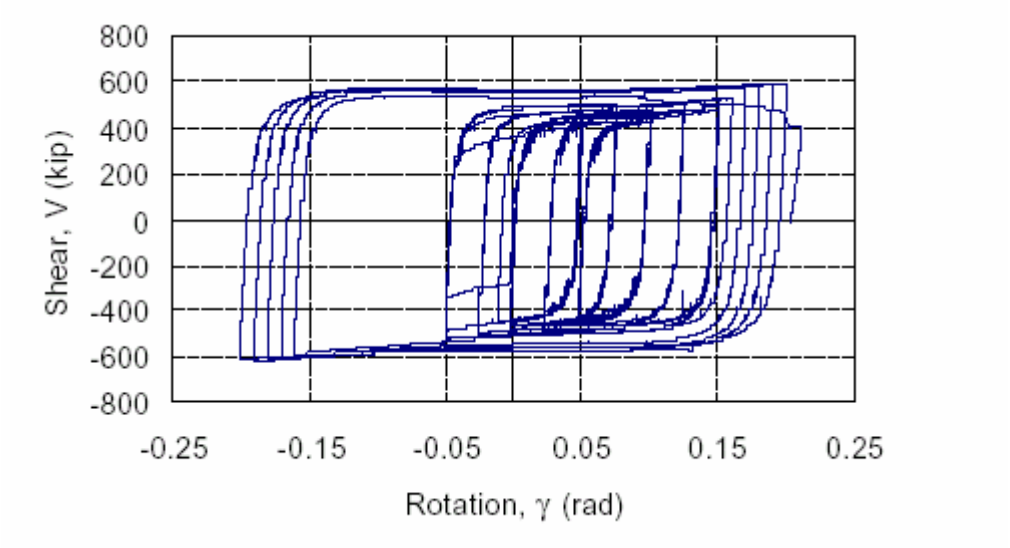

Figure 13a. Hysteretic loops for LYP 225 (33 ksi) link (B2) subject to a simulated near-field strain history.

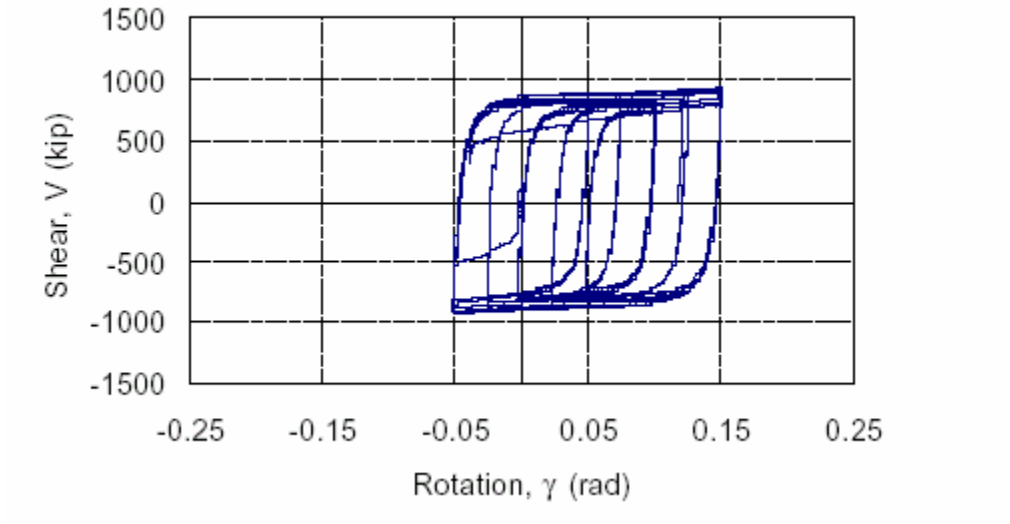

Figure 13b. Hysteretic loops for LYP 100 (15 ksi) link (B1) subject to a simulated near-field strain history.

failure. Overstrength was observed to be of the same order of magnitude as for the Grade 50 links.

It is concluded that inelastic shear links are very efficient energy dissipators and can designed to have a high tolerance for inelastic strain. Applications to long span bridges are attractive because of their low cost and negligible maintenance requirements. The elimination of web stiffeners using LYP steels appears practical with advantages of reduced cost and increased deformation capacity. The relatively high overstrength (compared to an HPS steel) is similar to that observed for the Grade 50 steel.

ACKNOWLEDGEMENTS

The research described above was funded by both the California Department of Transportation (Caltrans), through the toll bridge retrofit program, and the Federal Highway Administration through the Highway Project at the Multidisciplinary Center for Earthquake Engineering Research (MCEER) at the University at Buffalo, NY. Acknowledgement is also made of the constructive contributions received from T.Y. Lin International (designers of the new east bay crossing, SFOBB), Christie Constructors (Richmond CA) and Remarc (Reno NV), fabricators of the test specimens. The LYP shear links were provided by Nippon Steel (Japan), and the generous assistance of Dr Ian Aiken (SIE, Oakland CA) and Dr Isao Kimura (Nippon Steel) is gratefully acknowledged.

REFERENCES

AISC, 1997, *Seismic Provisions for Structural Steel Buildings*, American Institute of Steel Construction, Chicago, IL.

Dusicka, P., Itani, A.M. and Buckle, I.G., 2002, 'Cyclic behavior of shear links and tower shaft assembly of San Francisco - Oakland Bay Bridge Tower', Report CCEER 02-06, Center for Civil Engineering Earthquake Research, University of Nevada, Reno, NV.

Engelhardt, M.D. and Popov, E.P., 1989, 'Behavior of long links in eccentrically braced frames', Report UCB/EERC-89/01, Earthquake Engineering Research Center, University of California, Berkeley, CA

Hjelmstad, K.D. and Popov, E.P., 1986, 'Seismic behavior of active beam links in eccentrically braced frames', Report UCB/EERC-86/01, Earthquake Engineering Research Center, University of California, Berkeley, CA

ICBO, 2002, 'Seismic Design Manual' Vol. III, International Conference of Building Officials, Whittier CA.

Itani, A.M., 2003, 'Cyclic behavior of Richmond San Rafael Tower Links', Report CCEER 97-4, Center for Civil Engineering Earthquake Research, University of Nevada Reno, NV

Tang, M., Manzanarez, R., Nader, M., Abbas, S. and Baker, G., 2000, 'Replacing the East Bay Bridge', *Civil Engineering*, American Society of Civil Engineering, Washington DC.

The Implementation of Dampers on Several Large Bridges in China

Aijun Ye [1], Zhi-qiang Wang[1] and Li-chu Fan[1]

ABSTRACT

Viscous damper is a way to add energy dissipation to a structure, and its many applications have been found in the seismic protection of bridges around the world. This paper introduces seismic applications of viscous dampers on four long-span bridges in China. The first one is Egongyan Bridge (a three span suspension bridge with a main span of 600m), the second one is Lu-Pu Bridge (a tied through arch bridge with a main span of 550m), the third is Su-Tong Bridge under construction (a cable-stayed bridge with a main span of 1088m), and the forth is Dong-Hai Bridge under construction (a cable-stayed bridge with main span of 420m).

[1]State Key Laboratory for Disaster Reduction in Civil Engineering, Tongji University, Shanghai 200092, PRC

INTRODUCTION

Energy dissipation devices have been widely used in the world since 1970s for the seismic protection of bridges. Viscous damping is a way to add energy dissipation to a structure, and viscous damper has lately emerged as one of the alternative technology device that is available for seismic design of bridge structures. Up to now, many applications of viscous dampers have been found for the seismic protection of bridges around the world.

In China, large numbers of long-span bridges have been constructed or under construction, or in the design and planning stage. In order to improve the earthquake resistance behavior of long-span bridges, some researchers and engineers began to do researches on the application of viscous dampers for the seismic protection of bridges.

The mechanical behavior of viscous dampers can be described by the following equation:

$$F = C|V|^{\xi}\,\mathrm{sgn}(V) \tag{1}$$

where F is the damping force, V is the velocity across the device; C is a damping coefficient and ξ is an velocity exponent in the range of 0.1 to 2.0. These damping devices can be manufactured with a wide range of C and ξ values. The cost of the devices is generally proportional to the maximum damping force required.

Different types of bridges and site conditions may result in significantly different strategy in applying the seismic protection concept with viscous dampers. This paper introduces seismic applications of viscous dampers on four long-span bridges in China. The four bridges are:

1) Egongyan Bridge over Yangtze River in Chongqing a three span suspension bridge with a main span of 600m. Viscous dampers have been installed between the anchor blocks and the bridge girders to keep the girder movements within the working range of the expansion joints.

2) Lu-Pu Bridge in Shanghai, a tied through arch bridge with a main span of 550m. Viscous dampers are installed at expansion joints to reduce the relative displacements between the adjacent decks.

3) Su-Tong Bridge over Yangtze River in Jiangsu Province (under construction), a cable-stayed bridge with a main span of 1088m. The viscous dampers will be located between the box girder and the towers.

4) Dong-Hai Bridge in Shanghai, a cable-stayed bridge with a main span of 420m. It is proposed to set viscous dampers only between the girder and towers, or set the viscous damper both in towers and auxiliary piers as alternative.

APPLICATION IN EGONGYAN BRIDGE

Bridge description

Egongyan Bridge, as shown in Figure 1, is a suspension bridge with a main span of 600m and two side spans of 211m each. The continuous steel box girder deck is 6-lane and 35.5m wide. The design speed of is 80km/h. Moreover, Light railroad tracks will be set on the deck in the future.

Figure 1 Egongyan Bridge

Figure 2. Setting viscous dampers

Floating system is adopted, that is, there is no bearing between deck and crossbeam of each tower. The floating system will reduce seismic forces of each tower, but might result in large displacement of deck under wind, braking force, and earthquake etc.

Setting of viscous dampers

Four viscous dampers have been installed between the anchor blocks and the bridge girders (see Figure 2) to restrain the movements of bridge girder under wind, braking force, and earthquake etc., so that the displacement demands on the bridge expansion joints could be reduced. However, viscous dampers will not restrain the thermal movements of the girder.

The installation of the viscous damper is illustrated in Figure.3.

Damper parameters

Based on an optimization study, dampers were chosen for the bridge with a force-velocity relationship of

$$F = (460kN.s/mm) \cdot V^{0.21} \tag{2}$$

At a peak velocity of 1000mm/s, a damper will produce a control-peak force of 2000kN between the girder and the anchor block. The maximum displacement allowance for the damper is ±550mm.

The theoretical and testing force-velocity relationship are compared in Figure 4, from which one can see that the damper acts in accord with the design behavior.

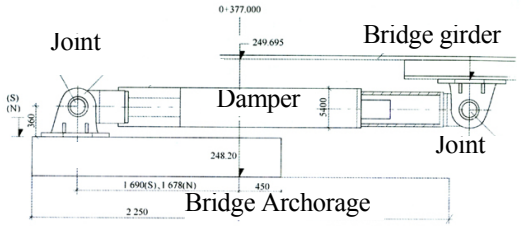

Figure 3. Installation of viscous dampers

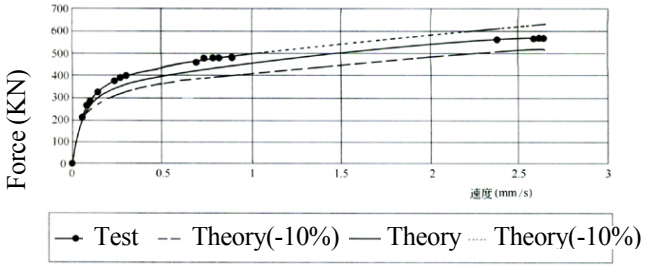

Figure 4 Force-velocity curves

APPLICATION IN LU-PU BRIDGE

Bridge description

LuPu bridge, the largest steel arch bridge in the world at present, is a half through tied arch bridge with a 550m main span and 2×100m side spans. The major components of the arch bridge are steel arch ribs, and orthogonal anisotropic steel deck with separate steel boxes, as shown in Figure 5. The width of the bridge deck is 37m.

Setting of viscous dampers

At the intersections of the arch rib and deck, crossbeams are designed, and the deck is supported by longitudinal sliding pot rubber bearings on the crossbeam. Investigations on seismic response of Lupu Bridge revealed that relative displacements at expansion joints are large. Impact might occur under earthquake. Therefore, longitudinal viscous dampers are installed at expansion joints. Locations of longitudinal dampers installed are shown in Figure 6.

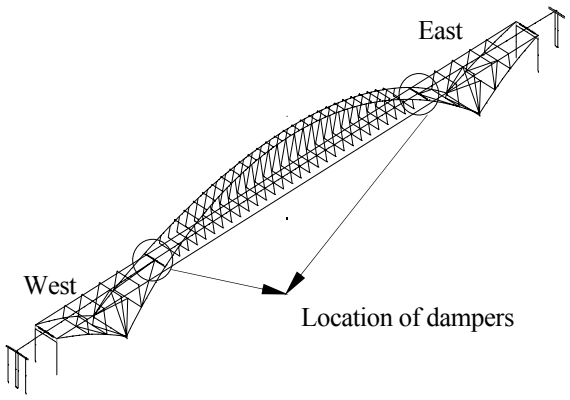

Figure 6 Locations of dampers

Two viscous dampers will be installed at each of the expansion joints between the main span deck and the transverse girder that connects the two ribs. The main purpose is to reduce the relative displacements at the expansion joints, thus to eliminate the possibility of impact due to longitudinal movements. At the same time, viscous damper can accommodate slow temperature displacements without forces in the dampers.

Damper parameters

The properties of the dampers were optimized to achieve an appropriate reduction of the relative displacements and stresses, keeping the damper force within reasonable limit. Different values of the exponent ξ were evaluated. Exponents ξ from 0.15 to 1.0 were considered. For each of these exponents, several values of C were examined in a parametric study aimed to identify the optimum dampers. This study was carried out by calculating the seismic response

subjected to the site ground motions with three-dimensional elastic models of the bridge. The same damper properties were assumed for all dampers. Cases of parametric analysis are listed in table I.

TABLE I CASES OF PARAMETERS ANALYSIS

C	230	330	460	560	660
ξ	0.15	0.15	0.15	0.15	0.15
	0.21	0.21	0.21	0.21	0.21
	0.3	0.3	0.3	0.3	0.3
	0.5	0.5	0.5	0.5	0.5
	0.7	0.7	0.7	0.7	0.7
	1.0	1.0	1.0	1.0	1.0

The parametric study shows that the velocity exponent and damping coefficient can have an effect on the optimum seismic design, the force, relative displacements, and the damping force. At last, exponent ξ was selected as 0.21, and damping coefficient 520kN.mm/s for LU-PU Bridge. The effect of viscous dampers (with C=520, α=0.21) is shown in Table II.

TABLE II. EFFECT OF VISCOUS DAMPERS

Section Position	Axial force (kN×10^4)		Bending moment (kN.m×10^4)	
	west	east	west	east
Side arch base	3.248 (3.949)	3.605 (4.266)	18.57 (25.32)	19.96 (20.61)
main arch base	2.487 (2.963)	2.965 (2.960)	17.42 (17.61)	25.09 (27.04)
deck joint Disp.(mm)	107.7 (160.7)	133.5 (169.1)		

Where values in brackets correspond to response without damper.

Damper tests

In order to investigate the dynamic performance of the damper, a comprehensive testing program was designed and undertaken at State Key Laboratory for Disaster Reduction in Civil Engineering of Tongji University, specifically to validate the assumed mechanical characteristics of scaled viscous damper (see Figure 7).

Figure 7. Testing damper

The damper tested is designed for a force-velocity relationship of

$$F = 92 \cdot V^{0.21} \quad \text{kN} \tag{3}$$

The tested damper is designed to produce approximately 200kN at a velocity of 200mm/s, and to have a displacement range of ± 70 mm. These values represent scale factors of 1:10 for force, 1:2.857 for displacement, and 1:3.2 for velocity.

A typical damper force-displacement relationship for a constant-velocity test is shown in Figure 8. The plot is for a five-cycle test with a target constant velocity of 35.2mm/s. It can be seen that the damper force output was very stable and repeatable in this test. Note that the damper force is a function of velocity and that the applied velocity was approximately constant, the damper force is therefore also approximately constant across the test displacement range. For each of the constant velocity tests, an "average" value of damper force as a function of velocity was determined, and then compared to the target force-velocity relationship. Figure 9 summarizes all of the constant-velocity tests. The solid line shown in the figure is the target force-velocity law. It can be seen that in general, there is a good agreement between the actual and target damper behavior.

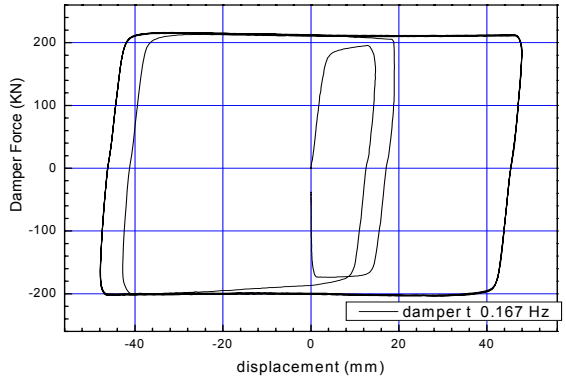

Figure 8. Typical damper force verus displacement plot for a cvclic constant-velocitv test

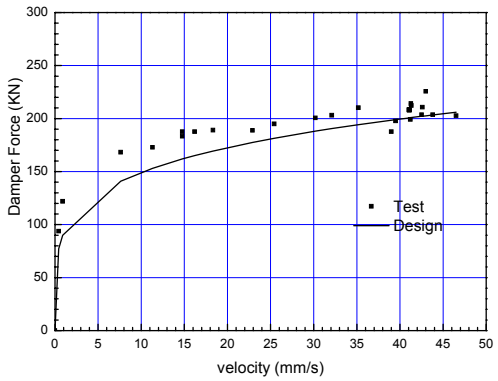

Figure 9. Damper force verus velocity for all cyclic constant-velocitv tests

Other damper characteristics that were evaluated in the test program include: the predictability of the damper behavior under seismic loading and sinusoidal Tests.

APPLICATION IN SU-TONG BRIDGE

Bridge description

The Su-Tong Bridge will be the longest cable-stayed bridge in the world with its completion. It has a steel box girder deck of 40.6m wide and 4.0m high. The layout of spans is 100+100+300+1088+300+100+100m (see Figure 10). The inverted Y shape reinforced concrete tower is 300m high. The deck is supported by sliding bearings sitting on the top of each auxiliary pier and anchored pier, and there is no bearing between deck and crossbeam of each tower. The sectional area of the first cable away from tower is 0.01134 m^2, and 0.00518m^2 near the tower.

Setting of viscous dampers

Figure 10 Su-Tong Bridge

Figure 11 Locations of viscous dampers

The investigation on seismic response using response spectrum method reveals that the maximum displacement of the girder might exceed 1.0m, therefore efficient devices should be adopted to restrain the movements of the deck. Viscous damper is one of the devices under investigation. It is proposed to set viscous dampers between the girder and towers, as shown in Figure 11.

Parameter sensitivity analysis of dampers

Key parameters of a viscous damper are damping coefficient C and velocity exponent ξ, which determine the damper's dynamic behavior under earthquake. In order to choose optimum values for C and ξ, parameter study was carried out using nonlinear time-history response analysis method. The value of ξ is 0.3, 0.4, 0.5, 0.7, 1.0 respectively, and value of C ranges from 0 to 25000.

The study was carried out based on ten site ground motions and three-dimensional elastic models considering the energy dissipation of sliding bearing sitting on the top of each side pier. Among the voluminous results from a transient dynamic analysis, the displacement of bridge girder, the bending moment at the base of tower, the damper force, the relative displacement between girder and tower are monitored. The effects of damper parameters on response of the above components are illustrated in figure 12 to figure 14.

From figure 12 to figure 14, one can see that viscous dampers can reduce the earthquake response notably, especially for displacement. With a view to get balance between force and displacement, a velocity exponent ξ of 0.4, and a damping coefficient of 15000 were proposed.

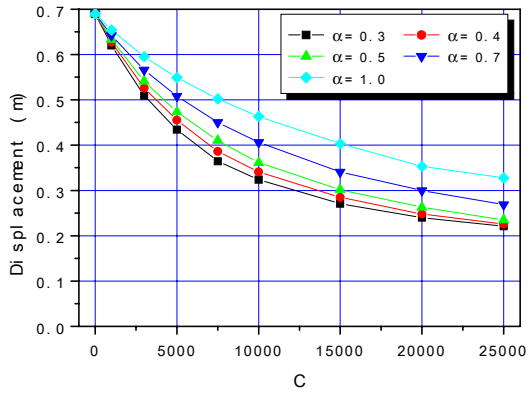

Figure 12 Displacement of deck

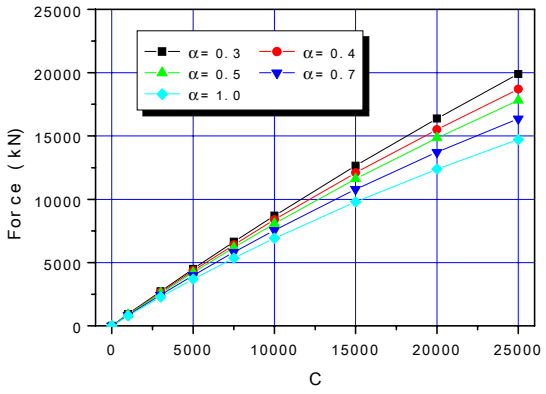

Figure 13 Force of the damper

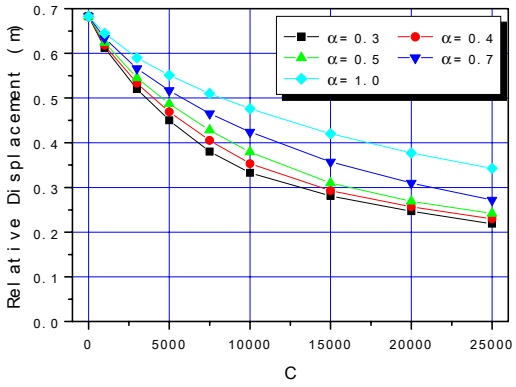

Figure 14 Relative displacement between girder and tower

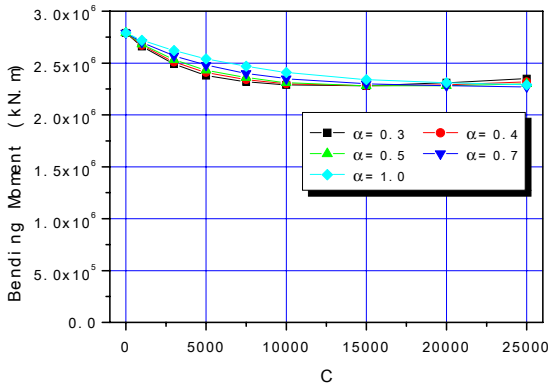

Figure 15 Bending moment at the base of tower

APPLICATION IN DONG-HAI BRIDGE

Bridge description

The Dong-Hai Bridge has a steel box girder deck of 33.0m wide and 4.0m high. The layout of spans is 73+132+420+132+73m (see Figure 16). The inverted Y shape reinforced concrete tower is 147.9m high. The deck is supported by sliding bearings, sitting on the top of each auxiliary pier and anchored pier, and between the deck and crossbeam of each pylon.

Setting of viscous dampers

The investigation on seismic response reveals that the maximum displacement of expansion joint might exceed 0.5m, therefore efficient devices should be adopted to restrain the movements of the deck. Viscous damper is investigated. It is proposed to set viscous dampers only between the girder and towers , or set the viscous damper both in towers and auxiliary piers as alternative shown in Figure 17.

Figure 16 Dong-Hai Bridge

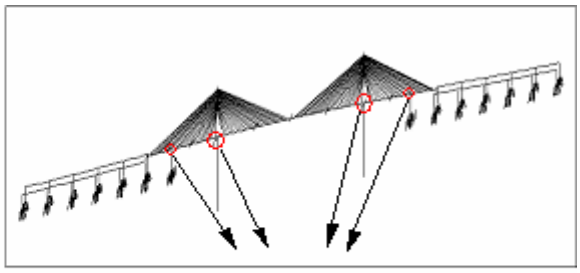

Figure 17 Damper locations

Viscous dampers will be used to absorb energy, to reduce seismic impacting forces between the stiffening girder and approach girder, and to control displacements at the critical location. These dampers are adopted because they will not restrain the thermal-induced movements of the bridge, and can be designed with large capacity if needed.

Based on an optimization study of damper parameters, if setting damper only between towers and stiffening girder, dampers were chosen with a force-relationship of:

$$F = (13000kN \cdot \sec^{0.3}/\mathrm{m}^{0.3}) \cdot V^{0.3} \tag{4}$$

At a peak velocity of 64.0 cm/sec, the dampers will produce a control-peak force of 11340 kN between the stiffening girder and the towers.

If setting damper not only between towers and stiffening girder, but also in auxiliary piers, dampers in towers were chosen with a force-relationship of:

$$F = (10000kN \cdot \sec^{0.3}/\mathrm{m}^{0.3}) \cdot V^{0.3} \tag{5}$$

And dampers in auxiliary piers were chosen with a force-relationship of:

$$F = (4000kN \cdot \sec^{1.0}/\mathrm{m}^{1.0}) \cdot V^{1.0} \tag{6}$$

The dampers will produce a control-peak force of 8798 kN between the stiffening girder and the towers, and 4240 kN between the stiffening girder and auxiliary piers.

This two schemes of setting dampers all dramatically reduce the displacement demands on the bridge and expansion joints, and eliminate the actual impact between the stiffening girder and approach girder, and reduce force of tower base as well.

Results of analysis show that scheme of setting dampers in auxiliary piers have two advantages: one is that the dampers could be designed with lower tonnages and which can have the same mitigation effect on the displacement as that of the latter scheme which needs 1000-1500 tons dampers. The other is that with the dampers set in the auxiliary piers, the mechanical behavior of which can be effectively improved.（if without dampers, the mechanical behavior of which is hardly effected by the dampers set between towers and stiffening girder）。

CONCLUSIONS

Although this investigation has been far from thorough, the following conclusions can be drawn:

Placing dampers in long-span bridges can effectively reduce the seismic response of the bridge.

Different types of bridges and site conditions may result in significantly different strategy in applying the seismic protection concept with viscous dampers.

The parameter sensitivity study should be performed to obtain the optimum design of dampers.

Besides seismic excitation, the damper will be subjected to thermal movements, wind excitation and small amplitude, high frequency vibrations caused by traffic on the bridge. The final damper design must be able to perform well under all these conditions.

REFERENCES

Lichu, Fan, 1997. *Seismic design for highway bridge*, Huajie International Publishing Co. Limited, Hong Kong,

Priestley, M.J.N., Seible, F., and Calvi, G.M.. 1996. *Seismic design and retrofit of bridges.* John Wiley & Sons, Inc., New York.

Zhiqiang WANG, Shide HU, Lichu FAN, 2002. *Analytical investigation of the response of bridges with added viscous dampers*, Proceedings, Fifteenth China conference on bridge engineering, Tongji University Publishing House (in Chinese).

Zenghuan Zhang, Hongwei Zhou, Xinfang Wang, 2002. A*pplication and study of viscous dampers in Egongyan suspension bridge in Chongqing*. Proceedings, 2002 China National conference on bridge engineering, People's Communication Publishing House, (in Chinese).

Aiken, I.D. and Kelly, J.M., 1996. *Cyclic dynamic testing of fluid viscous dampers*, Proceedings, Caltrans; Fourth Seismic Research Workshop, California Department of Transportation, Sacramento, California.

Parvin, A. and Ma, Z., 2001. *The use of helical spring and fluid damper isolation systems for bridge structures subjected to vertical ground acceleration*, Electronic Journal of Structural Engineering, (2),98-110.

Murphy, T.P. and Collins, K.R., 2000. *Retrofit of suspension bridges subjected to long period earthquake motion*, Proceedings of the 12th world conference on earthquake engineering, Auckland, New Zealand.

Seismic Performance of Bolu Viaduct's Isolation System in the 1999 Duzce Earthquake

Michael C. Constantinou and Panayiotis C. Roussis

ABSTRACT

Part of the Trans-European Motorway, the 2.3-km long seismically isolated Bolu viaduct was approximately 95% complete when it was hit by the devastating 1999 Duzce earthquake in Turkey. The viaduct suffered complete failure of the seismic isolation system and narrowly avoided total collapse due to excessive superstructure movement. This paper presents an evaluation of the design of the viaduct's seismic isolation system and an assessment of its performance in the Duzce earthquake. Evaluation of the seismic isolation system design has revealed that it did not meet the requirements of AASHTO Guide Specifications for Seismic Isolation Design. Analysis of the viaduct with motions scaled in accordance to the AASHTO Guide Specifications resulted in a required displacement capacity of over 1000 mm, a figure much higher than the 210 mm displacement capacity of the existing isolation system. Analysis of the viaduct for a simulated near-fault motion with characteristics consistent with the site conditions resulted in isolation system displacement demand of 1400 mm. This indicates that even if the isolation system had been designed in compliance with the AASHTO, it would have still suffered some damage in the earthquake. The evaluation of design and assessment of performance of the viaduct are important in developing experience in the design of seismically isolated structures and in validating analysis and design specifications.

Michael C. Constantinou, Professor and Chair, Department of Civil, Structural and Environmental Engineering, University at Buffalo, State University of New York, Buffalo, N.Y. 14260, USA.
Panayiotis C. Roussis, Graduate Research Assistant, Department of Civil, Structural and Environmental Engineering, University at Buffalo, State University of New York, Buffalo, N.Y. 14260, USA.

INTRODUCTION

On November 12, 1999, an earthquake with a moment magnitude of 7.2 struck north-central part of Turkey (Erdik 2000). The earthquake caused nearly 1000 fatalities and 5000 injuries. In addition to many buildings, a tunnel, a bridge, and the seismically isolated Bolu viaduct 1, which was under construction at the time of the earthquake, suffered considerable damage. Bolu viaduct 1 is the subject of this study.

Viaduct 1 is part of the Bolu Mountain Project that was initiated to improve transportation in the mountainous terrain to the west of Bolu province. It forms a small segment of the Trans European Motorway (TEM), which runs from the nation's capital Ankara to Europe parallel to the North Anatolian Fault (NAF). The seismically isolated viaduct was approximately 95% complete at the time of the earthquake. It suffered complete failure of the seismic isolation system and narrowly avoided total collapse due to excessive superstructure movement.

The earthquake was centered near the town of Duzce within the territories of Bolu province. Figure 1 presents a general map of the region and illustrates the location of Viaduct 1, the epicenter of the earthquake, the extent of the fault rupture, and the location of strong ground motion stations that produced significant records. The earthquake was caused by a right lateral strike-slip rupture along a significant part of the fault. The length of the fault is estimated as 40 km with an average lateral offset of 4 m (Ghasemi et al. 2000) and it crossed the viaduct at 25-degree angle with respect to the viaduct's longitudinal direction.

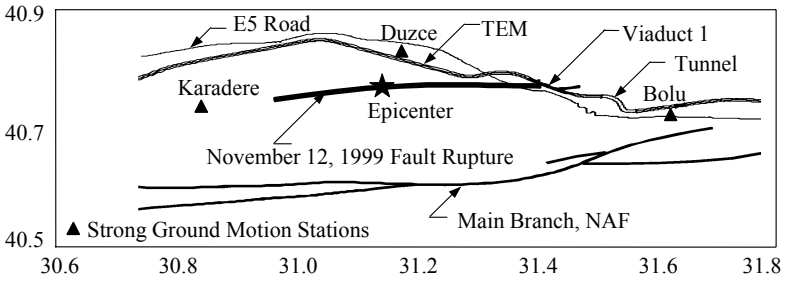

Figure 1. Map of Region Showing Location of Viaduct 1 and Surface Rupture in Duzce Earthquake

This paper presents an evaluation of the design of the viaduct's seismic isolation system and an assessment of its performance in the Duzce earthquake. For more details, the reader is referred to the report of Roussis et al. (2002). The outcome of this study becomes important in validating the AASHTO specifications (AASHTO 1991, 1999) and in developing experience in the seismic behavior of this type of structures.

DESCRIPTION OF THE VIADUCT

Viaduct 1 is 2.3 km long and has dual 59 spans supported by 58 piers as shown in Figure 2. The superstructure consists of seven lines of simply-supported prestressed concrete box girders seated on sliding pot bearings with stainless steel-polytetrafluoroethylene (PTFE) sliding interfaces. The slab is continued over the piers to form a continuous superstructure over 10-span segment of the structure. A typical segment of the viaduct between Pier 10 and Pier 20 is illustrated in Figure 3 (piers are numbered from 1 to 58 from west to east). Each segment is

392.2 m long and comprises 11 piers. The piers are single, octagonal, hollow-core reinforced concrete columns, 4.5 by 8.0 m in plan dimension, with heights varying along the structure. They rest on 3-meter thick reinforced concrete pile caps, which are supported on twelve 1.8m-diameter cast-in-drilled-hole reinforced concrete piles in alluvium. The piles extend up to 37.5 m below the ground surface.

Figure 2. General View of Bolu Viaduct 1

The viaduct incorporates an energy dissipation system in the form of yielding steel devices installed on each pier cap to form together with the sliding bearings a seismic isolation system (Ghasemi et al. 2000; Marioni 1997, 2000) as illustrated in Figure 3. Details of the yielding steel devices are displayed in Figure 4. A yielding steel device is composed of an

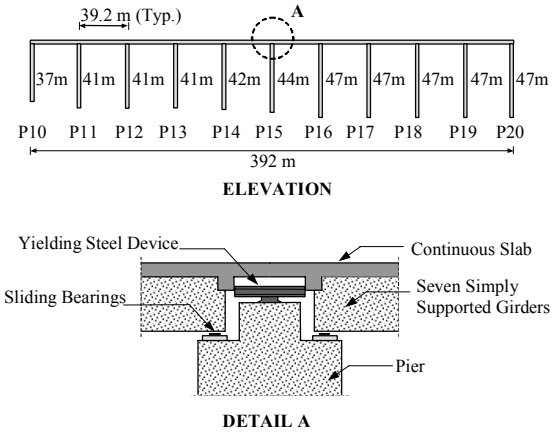

Figure 3. Elevation of Viaduct at Piers

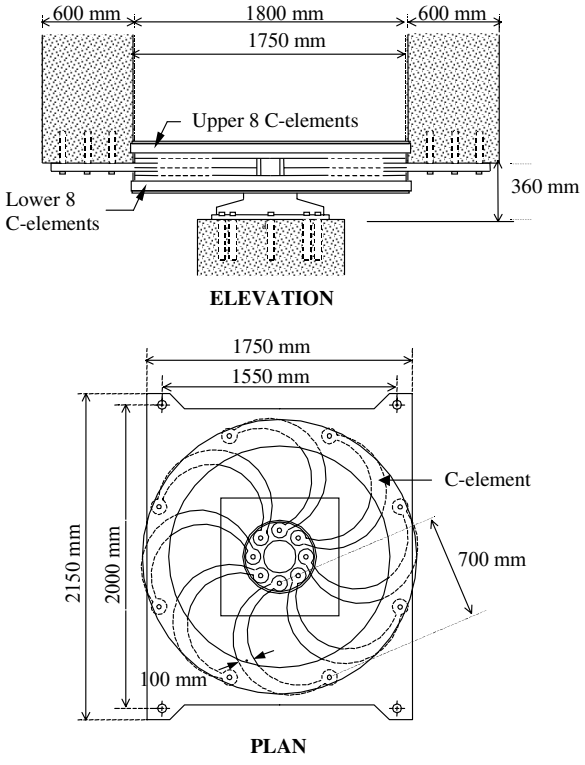

Figure 4. Details of Yielding Steel Device

inner and an outer ring interconnected by sixteen steel C-elements in a radial configuration. The inner and outer rings are connected to the substructure and superstructure, respectively. As the superstructure moves relative to the substructure, the C-elements deform, yield and dissipate energy. Moreover, shock transmission devices are incorporated between the yielding steel devices and the substructure in the longitudinal viaduct direction. This system allows free longitudinal movement of the superstructure relative to the substructure due to creep, shrinkage, and temperature change, and locks up under high-speed movement to engage the yielding steel devices (Ciampi and Marioni 1991; Tsopelas and Constantinou 1997).

Moreover, cable restrainers were used at the expansion joints (Ghasemi et al. 2000). These restrainers may have been instrumental in preventing the girders from falling off the piers.

DESIGN OF THE STRUCTURE

Turkey is an affiliate AASHTO State. However, the design concept for the viaduct involved the application of mixed criteria using the then applicable AASHTO Standard Specifications (AASHTO 1992) and seismic isolation guidelines developed by the designer. The design seismic forces and displacements were determined by means of nonlinear time history analyses performed using seven uni-directional artificial accelerograms. The 5% damped acceleration spectra of the artificial accelerograms matched the AASHTO soil-type-II spectrum scaled to 0.4g peak ground acceleration (AASHTO 1992). The design of the structure was based on the mean values of the maximum forces and displacements obtained from the seven analyses (Marioni 1997, 2000).

The stiffness of the reinforced concrete substructure elements was calculated assuming uncracked conditions. The stiffness of the foundation was modeled using translational and rotational elastic springs with linear stiffness calculated using the field test results. Based on test results of the yielding steel devices, the seismic isolation system was modeled assuming a bilinear hysteretic behavior as shown in Figure 5 (Astaldi S.p.A. 2000). This behavior is the combination of the inelastic behavior of the yielding steel devices and of the sliding bearings. The 1520-kN yield force of the isolation system primarily consists of 1400-kN yield strength of the yielding steel devices, with the remaining being the force generated due to friction in the lubricated sliding bearings. The post-elastic stiffness of the seismic isolation system is 1080 kN/m.

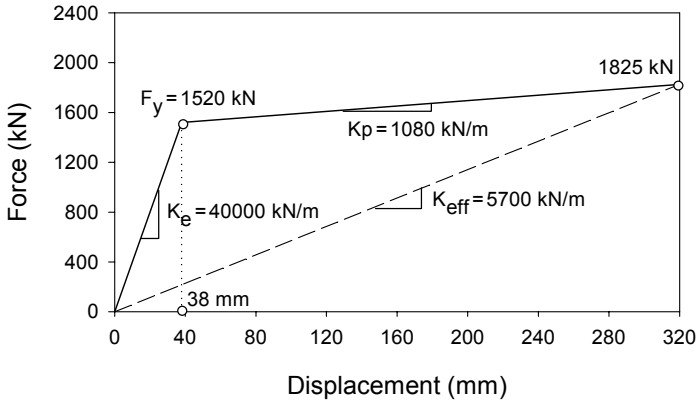

Figure 5. Assumed Bilinear Hysteretic Behavior of Seismic Isolation System

REMARKS ON THE SEISMIC ISOLATION DESIGN OF THE STRUCTURE

The design displacement of the seismic isolation system was calculated as 320 mm. However, the bearings had a displacement capacity of only 210 mm and the yielding steel devices had an ultimate deformation capacity of 480 mm (Marioni 1997, 2000). Clearly, there is an apparent inconsistency in the design of the seismic isolation system as the displacement capacity of the bearings is much smaller than the design displacement while the ultimate deformation capacity of yielding steel devices is larger.

The 1991 AASHTO Guide Specifications for Seismic Isolation Design (AASHTO 1991), which could have been used in the design of this structure, require that the difference between the magnitude of the restoring force at design displacement and at 50% of the design displacement is larger than 2.5% of the tributary weight acting on the isolation bearings. The main purpose of this requirement is to ensure a minimum restoring force level to limit the magnitude of the cumulative isolator displacements. Using the post-elastic stiffness of 1080 kN/m and the design displacement of 320 mm, this difference is calculated as 1.2% of the 14200-kN tributary weight acting on the bearings. A larger post-elastic stiffness should have been provided to the seismic isolation system to satisfy the above criterion. For cases where this criterion is not met, the isolation system must be capable of accommodating displacements equal to the greater of three times the displacement calculated by single mode analysis method, or $36AS_i$ inches, where A and S_i are respectively the acceleration and site coefficients (AASHTO 1991). Analysis utilizing the characteristics of Figure 5 results in a displacement of 263 mm. Using A=0.4 and S_i=1.5 for the viaduct's site, $36AS_i$ is calculated as 550 mm. Therefore, the isolation system should have been designed to have a minimum displacement capacity of three times 263 mm or 790 mm. This figure is greater than both the 210 mm displacement capacity of the installed system and the calculated response of 320 mm (Marioni 2000).

Using the post-elastic stiffness of 1080 kN/m and tributary weight of 14200 kN, the period of the system is calculated as 7.27 seconds. The 1999 AASHTO Guide Specifications (AASHTO 1999) limit this period to a maximum of 6 seconds. Accordingly, the use of this system would not be permitted by the 1999 AASHTO Guide Specifications.

In summary, the low value of the post-elastic stiffness does not meet the criteria for the lateral restoring force of either the 1991 or the 1999 AASHTO Guide Specifications for Seismic Isolation Design. Although the 1991 AASHTO Guide Specifications allow the use of this system, the 1999 AASHTO Guide Specifications prohibit its use.

Moreover, the 1999 AASHTO Guide Specifications for Seismic Isolation Design require that, three-dimensional nonlinear dynamic analysis must be used if the seismic isolation system has insufficient restoring force capability. Such an analysis requires at least three pairs of horizontal ground motion histories selected from recorded events and scaled to represent the applicable response spectrum. Yet, the design of the structure was performed using only uni-directional ground motion inputs ignoring the three-dimensional effect of pairs of ground motion components simultaneously applied on the structure.

DAMAGE TO SEISMIC ISOLATION SYSTEM IN THE 1999 DUZCE EARTHQUAKE

The viaduct was subjected to a near-fault, pulse-type ground motion since the ruptured fault crossed the viaduct at 25-degree angle with respect to the viaduct's longitudinal direction. Thus, the structure may have been exposed to significant directivity and fling effects with

associated large velocity pulses and permanent tectonic deformations. Consequently, the viaduct superstructure experienced a westward permanent displacement relative to the piers, leaving all the ends of the girders offset from their supports in the order of 1000 mm longitudinally and 500 mm transversely. At nearly all locations, the sliding bearings suffered complete failure with their parts dislocated and ejected from the bearing pedestals as shown in Figure 6. The observed scratch signs on the surface of bearing's stainless steel plates resembled the number six. This indicates that the bearings slid off probably in a very early stage before any significant cyclic movement. This also supports the scenario that the bridge was subjected to a near-fault pulse-type motion (Ghasemi et al. 2000). Figure 7 shows a view of failed connections of the yielding steel devices at an expansion joint. All 1638 sliding bearings failed and the beams sled on the plinths below. Some beams fell off their plinths onto the pier tops below. Cable restrainers at the expansion joints and 468 lateral shear keys (of which 176 were severely damaged) at the piers were instrumental in preventing beams from falling off the piers.

Figure 6. Failed Sliding Bearings

Figure 7. Failure of Yielding Steel Device Connections at Expansion Joint

STRUCTURE MODEL FOR ASSESSING THE VIADUCT'S PERFORMANCE

A typical ten-span segment of the viaduct (Figure 3) was analyzed using the finite element program ANSYS (ANSYS 1996). The analysis was based on a three-dimensional finite element model. The model's cross-section over a typical pier is illustrated in Figure 8. The piers and the deck were modeled using three-dimensional beam elements. Rigid elements were introduced at each pier top to model the height difference between the deck's centroid and the top of each bearing. The sliding bearings were modeled as vertical stiff truss elements. Their length was set equal to the height of the bearings (0.2 m). The small friction force in these bearings was lumped and included in the hysteretic behavior of the yielding steel devices. The yielding steel devices were modeled using the fixed-pinned, thin-walled pipe element in ANSYS, which is capable of describing bilinear hysteretic behavior of the type shown in Figure 5. Table 1 presents the material and geometric properties of the elements used in the model. Moreover, elastic translational and rotational springs were used at each pier base to model the foundation stiffness. The stiffness of these springs are tabulated in Table 2. To properly model the bridge continuity at the expansion joints, pier stiffness, foundation spring stiffness, masses, and isolator properties at the end piers were modeled with half of their full values.

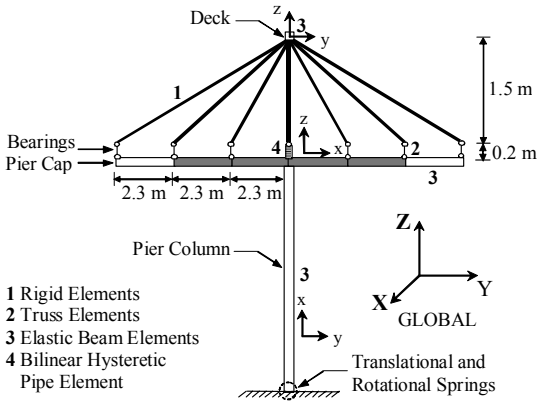

Figure 8. Schematic of Pier Top in Finite Element Model

Table 1. Material and Geometric Properties of Pier and Deck Elements

Properties	Piers	Pier Cap		Deck	Rigid Elements
		Flexible	Rigid Portion		
A (m^2)	14.30	7.50	100	12.88	100
I_{yy} (m^4)	38.30	1.40	1000	0.581	1000
I_{zz} (m^4)	106.30	15.60	1000	328	1000
I_{xx} (m^4)	88.50	4.60	1000	2.33	1000
E (GN/m^2)	23.60	23.60	23.60	31.20	23.60
ν	0.17	0.17	0.17	0.17	0.17
ρ (kg/m^3)	2502	2502	250	2867	0
A=area; I_{yy},I_{zz}=moments of inertia; I_{xx}=torsional constant; E=elasticity modulus; ν=Poisson's ratio; ρ=density.					

Table 2. Pier Foundation Spring Stiffnesses

Pier	Height (m)	Rotational Stiffness (GN-m)	Translational Stiffness (GN/m)
P10	37	340	2.8
P11	41	340	2.8
P12	41	340	2.8
P13	41	380	3.9
P14	42	380	3.9
P15	44	380	3.9
P16	47	380	3.9
P17	47	350	3.5
P18	47	320	3.1
P19	47	290	2.6
P20	47	260	2.2

ANALYSIS OF THE VIADUCT

A modal analysis was conducted to understand the dynamic behavior of the structural system and to determine the parameters required for defining Rayleigh damping in a subsequent nonlinear time history analysis. The linear character of the modal analysis dictates the use of linear elements and material properties. Accordingly, the bilinear behavior of the seismic isolation system was approximated by considering an effective stiffness of 5700 kN/m at the reported design displacement of 320 mm (Marioni 1997, 2000) as shown in Figure 5. The structure vibration periods obtained from modal analysis ranged between 3.52 and 0.85 sec in the first twenty modes.

Nonlinear time history analysis was carried out in ANSYS using the Newmark integration scheme with a time step of 0.002 sec. Furthermore, a Newton-Raphson iteration procedure was used in each time step for the equilibrium iteration process. Viscous damping in the system was specified to be of the Rayleigh type, yielding a structural damping equal to 2% to 3% of critical in the first twenty modes.

SELECTION OF MOTIONS FOR TIME HISTORY ANALYSIS

Motions for Assessing Performance in the 1999 Duzce Earthquake

The strong ground motion stations operated by the General Directory of Disaster Affairs in Turkey produced 20 records of the 1999 Duzce earthquake. Among these, the Bolu and Duzce station records are significant for the assessment of the performance of the viaduct. In addition, two temporary stations installed at Karadere for aftershock investigation of the August 17 earthquake yielded relevant records. The location of the stations is shown in Figure 1.

Table 3 presents the peak ground acceleration (PGA), velocity (PGV), and displacement (PGD) of the Bolu, Duzce and the two Karadere records. These values were obtained following correction of the recorded ground accelerations. Figure 9 presents the 5% damped response spectra of the horizontal components of the aforementioned records and compares them to the AASHTO design spectrum. It is evident that the spectral values of the recorded components far exceed the design spectral values in the period range of less than about 0.6 sec. With the

Table 3. Peak Ground Motion Values of Records at Stations Near the Bolu Viaduct

Station	Component	PGA (g)	PGV (cm/sec)	PGD (cm)
Bolu [1]	NS	0.728	56.4	23.1
	EW	0.822	62.1	13.6
Duzce [1]	NS	0.348	60.0	42.1
	EW	0.535	83.5	51.6
Karadere 496 [2]	NS	0.750	39	17
	EW	0.750	38	11
Karadere 375 [2]	NS	1.097	47	8
	EW	0.641	21	4

[1] Based on data at PEER Strong Motion Database (http://peer.berkeley.edu/smcat/)
[2] Based on analysis performed at Kandilli Observatory and Earthquake Research Institute, Bogazici University, Istanbul, Turkey.

exception of the Duzce records, they are all below the design spectral values in period ranges larger than about 1.5 sec. Particularly the Karadere records exhibit very low spectral acceleration values at long periods. Since these records cannot be critical in the analysis of the seismically isolated viaduct, no further analysis with Karadere records was performed.

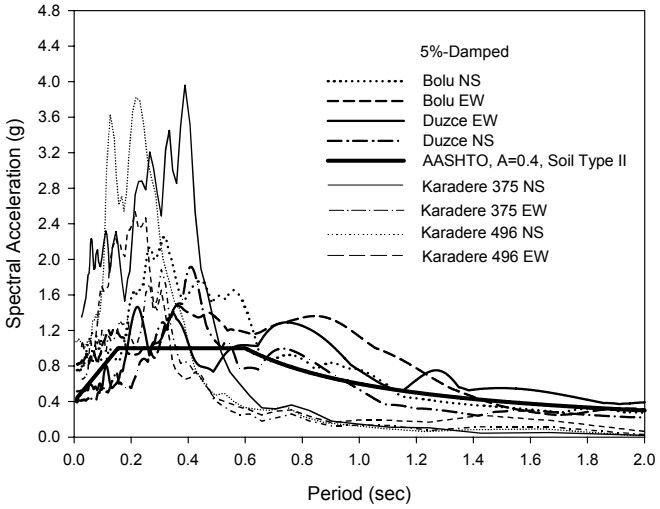

Figure 9. Response Spectra of Horizontal Components of Records at Bolu, Duzce and Karadere Stations in 1999 Duzce Earthquake

Figure 10 presents the acceleration time histories recorded at Bolu and Duzce stations. The Duzce station is located in a basin with alluvium up to a depth of about 100 meters. The Duzce records contain long duration and long period energy content, which are indicative of basin response and softening of soil media. The Bolu station is located in a building founded on soft, deep sediment. The Bolu records are high-intensity ground motions with characteristics indicating effects of directivity and sudden stopping phase of rupture.

The two records at Bolu and Duzce were first used to assess the performance of the viaduct during the Duzce earthquake. However, it was recognized that neither of the two records truly represent the conditions experienced by the viaduct in the vicinity of the fault. Accordingly, the ground motion at the viaduct's site was simulated based on stipulated earthquake source parameters and used for the assessment of the performance of the viaduct.

Simulated Near-Fault Ground Motion in the Vicinity of the Bolu Viaduct

The simulation of the ground motion near the viaduct followed the so-called hybrid methodology. In this methodology, a deterministic approach (Anderson and Luco 1983; Luco and Anderson 1983) is utilized to simulate the ground motion in the low frequency range and a stochastic process (Boore 1983; Silva and Green 1989) is utilized to simulate the high frequency components of the motion.

The following parameters were used to obtain the low frequency components of the simulated ground motion:

i. Moving ramp-type dislocation function with maximum displacement of 5.6 m and rise time of 1 sec.
ii. P-wave, S-wave, and rupture velocities of 5, 2.9 and 2.6 km/sec, respectively; 18 km wide

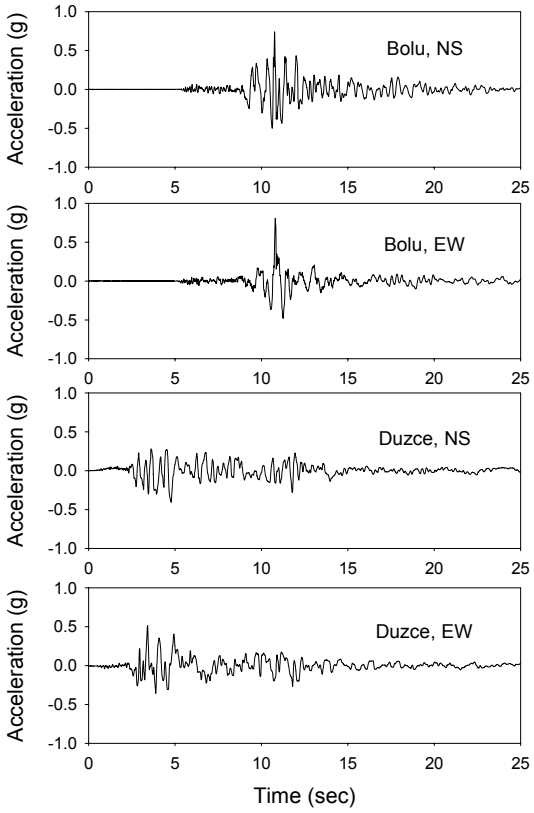

Figure 10. Ground Acceleration Histories for Bolu and Duzce Records

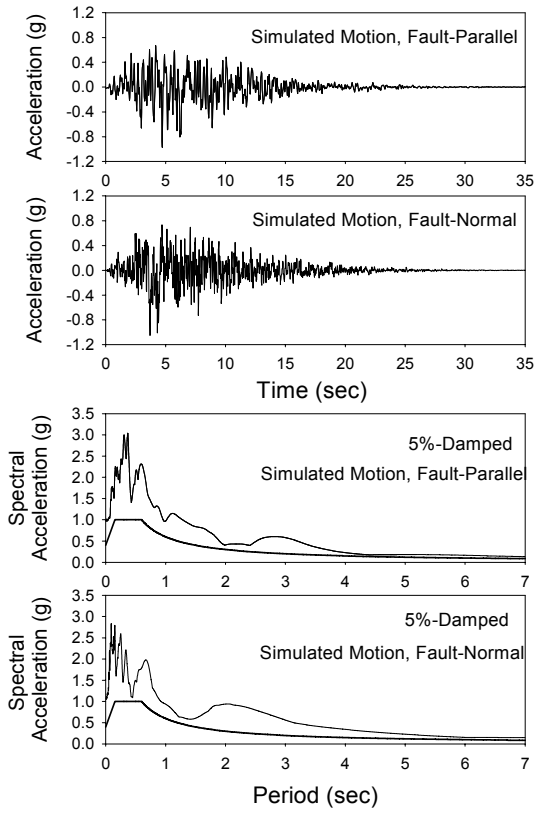

Figure 11. Ground Acceleration Histories and Response Spectra for Simulated Motion

vertical fault plane.

iii. The simulation was performed for a point at a distance of 500 m from the fault trace and the parameters were based on the information available from Duzce earthquake data.

The simulation of the high frequency content of the motion was performed using a moment magnitude of 7.2, a fault distance of 1 km, and good soil conditions.

Figure 11 presents the simulated ground acceleration histories parallel and normal to the fault directions and their response spectra alongside the AASHTO design spectrum for the viaduct site. The simulated motion exhibits clear near-fault characteristics, including forward directivity effects in the fault-normal direction and fling effects in the fault-parallel direction. The response spectra of the two simulated components are substantially larger than the design spectrum.

Motions for Determining Isolation System Design Displacements in Compliance with AASHTO Guide Specifications

Nonlinear time history analyses were also performed to calculate the design displacements for the isolation system in compliance with AASHTO Guide Specifications. The calculated displacements are used to determine whether the structure would have survived the earthquake if it had been designed in compliance with AASHTO Guide Specifications. The analyses were conducted using three pairs of scaled horizontal ground motions selected from different recorded events. These ground motions are: (i) 360 and 270 components of 1992

Landers earthquake recorded at Yermo station; (ii) 90 and 0 components of 1989 Loma Prieta earthquake recorded at Hollister station; and (iii) S00W and S90W components of 1971 San Fernando earthquake recorded at station 458. The ground motions were scaled in compliance with the 1999 AASHTO Guide Specifications. First, the 5% damped response spectrum was obtained for each orthogonal component of the pair of horizontal ground motions. The square root of the sum of the squares (SRSS) of the 5% damped spectra of the two orthogonal components was calculated for each pair of horizontal ground motions. The ground motions were then scaled by a factor of 1.5 so that the average of the SRSS spectra of the three ground motions does not fall below 1.3 times the AASHTO design spectrum for the period range of 1 to 5 seconds.

ANALYSIS RESULTS

Isolation System Displacement Demand in the 1999 Duzce Earthquake

Nonlinear dynamic analyses were carried out to estimate the response of the viaduct in the 1999 Duzce earthquake. The analyses were performed using the recorded motions at the Bolu and Duzce stations and the simulated near-fault motion.

Three cases of direction of the seismic excitations were considered in the analyses using the Bolu and Duzce stations ground motions: (i) the EW component of the ground motion was applied in the longitudinal direction and the NS component applied in the transverse direction of the viaduct; (ii) the NS component of the ground motion was applied in the longitudinal direction and the EW component applied in the transverse direction of the viaduct; and (iii) the EW and NS components of the ground motion were applied at 25-degree angle with respect to the longitudinal and transverse directions of the viaduct, respectively. The simulated ground motion was applied in directions parallel and normal to the fault crossing the viaduct at an angle of 25^{o} with respect to viaduct's longitudinal direction. In addition, a time history analysis was performed where the ground motion recorded at the Bolu station was used after truncation of peak accelerations exceeding 0.4g. This analysis was conducted to study the effect of large accelerations on the seismic response of the viaduct.

Table 4 presents the calculated maximum resultant displacement of the isolation system at each pier. Furthermore, Figure 12 presents graphs of the calculated displacement paths of the isolation bearings at Pier 15 during the initial portion of movement for the simulated, the Bolu station, and Duzce station ground motions. Displacement paths at other piers are similar. The results in Table 4 and Figure 12 reveal the following:

(1) The calculated paths of the isolation system displacement for the Bolu station and the simulated near-fault motions consist of a half cycle of displacement with amplitude of about 100 to 150 mm followed by movement in the opposite direction that exceed the displacement capacity of the bearings. Observations of the scoring on the stainless steel plates of the sliding bearings of the viaduct are consistent with the calculated displacement paths.

(2) The calculated paths of the isolation system displacement for the Duzce station motion show no resemblance to the observed traces on the stainless steel plates of the bearings of the viaduct. This observation, along with the aforementioned characteristics of the Duzce station record, suggests that this record is likely not representative of the ground motion at the location of the viaduct.

Table 4. Calculated Maximum Isolation System Resultant Displacements

Ground Motion	Application Direction		Maximum Isolation System Resultant Displacement (mm)											
			P10	P11	P12	P13	P14	P15	P16	P17	P18	P19	P20	Max
Bolu	EW	NS												
	Longitudinal	Transverse	325	325	329	337	344	346	342	355	367	380	393	393
	Transverse	Longitudinal	296	311	316	311	317	334	363	358	354	352	353	363
	25° wrt Long.	25° wrt Trans.	321	348	347	344	349	353	349	355	361	368	375	375
Bolu Truncated	EW	NS												
	Longitudinal	Transverse	333	335	339	346	352	353	348	361	373	386	399	399
	Transverse	Longitudinal	293	291	291	290	288	281	266	269	275	282	289	293
	25° wrt Long.	25° wrt Trans.	330	357	355	351	356	360	355	360	367	374	381	381
Duzce	EW	NS												
	Longitudinal	Transverse	441	463	463	463	462	448	401	405	407	404	398	463
	Transverse	Longitudinal	530	525	521	516	515	514	504	511	513	511	509	530
	25° wrt Long.	25° wrt Trans.	439	436	437	438	437	432	412	415	420	424	426	439
Simulated	Fault Parallel	Fault Normal												
	25° wrt Long.	25° wrt Trans.	1297	1291	1302	1308	1322	1336	1354	1375	1391	1409	1425	1425
Scaled Yermo	360	270												
	Longitudinal	Transverse	487	489	496	506	514	522	531	543	557	569	581	581
	Transverse	Longitudinal	523	519	521	525	527	531	524	521	518	516	515	531
Scaled Hollister	0	90												
	Longitudinal	Transverse	644	743	742	734	756	790	820	818	815	812	810	820
	Transverse	Longitudinal	587	603	611	615	617	617	612	635	664	687	700	700
Scaled S. Fernando	0	90												
	Longitudinal	Transverse	363	356	357	361	357	355	355	362	365	367	367	367
	Transverse	Longitudinal	325	341	353	363	372	379	379	385	388	392	397	397

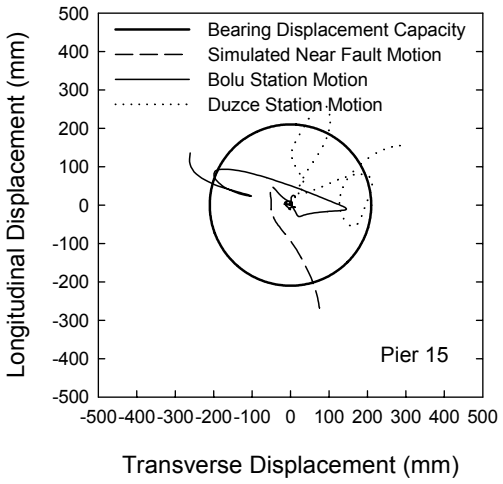

Figure 12. Isolation System Displacement Paths at Pier 15 During Initial Portion of Movement for the Simulated Near-Fault, Bolu and Duzce Motions

(3) The peak isolation system resultant displacement obtained using the Bolu station motion does not exceed 400 mm. Analysis using the Bolu station motion truncated to a peak acceleration of 0.4g did not appreciably change the peak response, thus demonstrating that the large accelerations of the Bolu station record are not intrinsically responsible for the response of the viaduct.
(4) The calculated peak displacement response of the isolation system in the simulated near-fault motion is in the order of 1400 mm. While this figure may be a conservative estimate, it demonstrates that the demand in the Duzce earthquake far exceeded the capacity of the isolation system of the viaduct.

Isolation System Design Displacements in Compliance with AASHTO Guide Specifications

Nonlinear time history analyses were performed in compliance with the 1999 AASHTO Guide Specifications using the three pairs of scaled ground motions. Each pair of ground motions was applied simultaneously to the model in the longitudinal and transverse directions of the viaduct. Two analyses were performed for each pair of records by switching the directions of application of the two components. The maximum displacement obtained from these analyses is used as the design displacement in compliance with AASHTO Guide Specifications. The peak resultant displacement at each pier location is presented in Table 4.

The analyses results demonstrated that the displacement capacity of the isolation system should have been at least 1000 mm (1.25 times the calculated demand of 820 mm). This value is substantially larger than the 210 mm capacity provided to the isolated viaduct.

CONCLUSIONS

The results of this study serve to demonstrate the following:

(1) The seismic isolation system for the Bolu Viaduct 1 did not meet the requirements of either the 1991 or the 1999 AASHTO Guide Specifications for Seismic Isolation Design.
(2) Analysis of the seismically isolated viaduct with motions scaled in accordance to the 1999 AASHTO Guide Specifications resulted in a displacement demand of 820 mm. Moreover, a direct application of the minimum requirements of the 1991 AASHTO Guide Specifications resulted in a displacement demand of 790 mm. The displacement capacity should have been 1.25 times the demand in the Design Basis Earthquake, or just over 1000 mm. This value of the displacement capacity is substantially larger than the 210 mm capacity provided.
(3) Analysis of the viaduct for the motions recorded at the nearby Duzce and Bolu stations resulted in isolation system displacements that exceeded the capacity by a factor of two or more. The Duzce record was deemed not representative of the actual conditions at the viaduct's site primarily due to the lack of resemblance of the calculated displacement paths to those observed. Collaborating evidence was provided by the characteristics of the record indicating basin response rather than near fault characteristics. The Bolu record contained clear near-fault characteristics and the calculated displacement paths using this record closely resembled the observed paths. However, the motion was recorded at a distance of approximately 25 km away from the viaduct and, therefore, cannot be deemed representative of the conditions experienced at the viaduct site.
(4) Analysis of the viaduct for a simulated near-fault ground motion with characteristics

consistent with the identified fault rupture mechanism and conditions at the viaduct's site resulted in isolation system displacement demand of up to 1400 mm, thus far exceeding the capacity.

(5) It appears that, had the isolation system been designed in accordance with the AASHTO Guide Specifications to have a displacement capacity of over 1000 mm, it would have still suffered some damage in the Duzce earthquake given that the displacement demand was likely of the order of 1400 mm.

ACKNOWLEDGEMENTS

Financial support for this project was provided by the Multidisciplinary Center for Earthquake Engineering Research (MCEER), Highway Project, Task D3-1. MCEER is, in turn, supported by the Federal Highway Administration.

REFERENCES

AASHTO Guide Specifications for Seismic Isolation Design, 1991, American Association State Highway Transportation Officials, Washington, D.C.

AASHTO Guide Specifications for Seismic Isolation Design, 1999, American Association State Highway Transportation Officials, Washington, D.C.

AASHTO Standard Specifications for Highway Bridges, 1992, American Association State Highway Transportation Officials, 15th Edition, Washington, D.C.

Anderson, J., and Luco, J., 1983, "Parametric Study of Near-Field Ground Motion for a Strike Slip Dislocation Model", *Bulletin of Seismological Society of America*, 73, 23-43.

ANSYS User's Manual, 1996, Version 5.3, Swanson Analysis Systems, Inc., Houston, PA.

Astaldi S.p.A, 2000, Miscellaneous documents and diagrams related to the Bolu Viaduct, Duzce, Turkey.

Boore, D., 1983, "Stochastic Simulation of High-Frequency Ground Motions Based on Seismological Models of the Radiated Spectra", *Bulletin of Seismological Society of America*, 73(6), 1865-1894.

Ciampi, V., and Marioni, A., 1991, "New Types of Energy Dissipating Devices for Seismic Protection of Bridges", Proceedings, *Third World Congress on Joint Sealing and Bearing Systems for Concrete Structures*, Vol. 2, National Center for Earthquake Engineering Research, State Univ. of New York at Buffalo, N.Y., 1225-1245.

Erdik, M., 2000, "Report on 1999 Kocaeli and Duzce (Turkey) Earthquakes", Department of Earthquake Engineering, Bosphorous University, Istanbul, Turkey.
<http://www.iiasa.ac.at/Research/RMS/july2000/Papers/erdik.pdf> (Jul. 03, 2002).

Ghasemi, H., Cooper, J., Imbsen, R., Piskin, H., Inal, F., and Tiras, A., 2000, "The November 1999 Duzce Earthquake: Post-Earthquake Investigation of the Structures on the TEM", Report FHWA-RD-00-146, Department of Transportation, Washington, D.C.
<http://www.tfhrc.gov/structur/00-146.pdf> (Jul. 03, 2002).

Luco, J., and Anderson, J., 1983, "Steady State Response of an elastic half-space to a Moving Dislocation of Finite Width", *Bulletin of Seismological Society of America*, 73, 1-22.

Marioni, A., 1997, “Development of a New Type of Hysteretic Damper for the Seismic Protection of Bridges”, Proceedings, *Fourth World Congress on Joint Sealants and Bearing Systems for Concrete Structures*, SP-164, Vol. 2, American Concrete Institute, 955-976.

Marioni, A., 2000, “Behaviour of Large Base Isolated Prestressed Concrete Bridges During the Recent Exceptional Earthquakes in Turkey”, ENEA-Divisione Sistemi Energetici Ecosostenibili, Bologna, Italy. <http://192.107.65.2/GLIS/HTML/gn/turchi/g5turchi.htm> (Jul. 03, 2002).

Roussis, P.C., Constantinou, M.C., Erdik, M., Durukal, E., and Dicleli, M., 2002, “Assessment of Performance of Bolu Viaduct in the 1999 Duzce Earthquake in Turkey”, Technical Report MCEER-02-0001, Multidisciplinary Center of Earthquake Engineering Research, University at Buffalo, State University of New York, Buffalo, NY.

Silva, W., and Green, R., 1989, “Magnitude and Distance Scaling of Response Spectral Shapes for Rock Sites with Applications to North American Tectonic Environment”, *Earthquake Spectra*, 5, 591-623.

Tsopelas, P., and Constantinou, M., 1997, “Study of Elastoplastic Bridge Seismic Isolation System”, *Journal of Structural Engineering*, ASCE, 123(4), 489-498.

Instrumentation and Baseline Modeling for Long-Term Performance Monitoring of Highway Bridges

Maria Q. Feng[1], Doo Kie Kim[2], Jin-Hak Yi[3], and Yangbo Chen[4]

ABSTRACT

Sensor systems were installed on two highway bridges for vibration-based long-term performance monitoring. In the structural performance and health evaluation, a baseline model is essential. This study represents the first effort in applying a neural network-based system identification technique to establish and update a baseline finite element model of an instrumented highway bridge based on the measurement of its traffic-induced vibrations. The neural network approach is particularly effective in dealing with measurement of a large-scale structure by a limited number of sensors. In this study, extensive vibration data were collected, based on which modal parameters including natural frequencies and mode shapes of the bridges were extracted using the frequency domain decomposition method as well as the conventional peak picking method. Then an innovative neural network is designed with the input being the modal parameters and the output being the structural parameters of a 3-dimensional finite element model of the bridge such as element stiffness. After extensively training and testing, the neural network became capable to identify the structural parameter values based on the measured modal parameters, and thus the finite element model of the bridge was successfully updated to a baseline. The neural network developed in this study can be used for future baseline updates as the bridge being monitored periodically over its lifetime.

INTRODUCTION

As the state of the art in bridge design is advancing toward the performance-based design, it becomes increasingly important to monitor and evaluate the long-term structural performance of bridges. Such information is essential in developing performance criteria for design. Meanwhile, long-term monitoring can produce valuable knowledge regarding the structural health condition, which can potentially minimize maintenance cost and enhance longevity of highway bridges. While there are many techniques involved in the structural performance monitoring, they can be broadly

1 Professor, Dept. of Civil and Environmental Engineering, University of California, Irvine, CA92697-2175. E-mail: mfeng@uci.edu

2 Assistant Professor, Kunsan National University, Kunsan 573-701, Korea. E-mail: kim2kie@kunsan.ac.kr. Formerly he was a visiting post-doctoral researcher at University of California, Irvine.

3 Research Assistant Professor, Smart Infrastructure Technology Center, Korea Advanced Institute of Science and Technology. Daejeon 305-701, Korea. E-mail: yijh@kaist.ac.kr. Formerly he was a visiting post-doctoral researcher at University of California, Irvine

4 Graduate Student, Dept. of Civil and Environmental Engineering, University of California, Irvine, CA92697-2175. E-mail: yangboc@uci.edu

categorized as a local or global approach. The former is to obtain information about a relatively small region of a structure by utilizing local non-destructive evaluation (NDE), while the latter uses measurements from a dispersed set of sensors to obtain global information about the condition of the structural system. The global structural performance monitoring involves: (1) instrumentation of a structure with sensors and more importantly, (2) methodologies for interpreting the measured data to obtain meaningful information and knowledge concerning the structural performance and integrity. Numerous studies have focused on methodologies based on vibration tests. Structural deterioration or damage causes stiffness degradation that can be reflected, to certain extent, in the changes of structural dynamic characteristics such as frequencies, mode shapes, and mode shape curvatures.

The authors recently installed sensor systems including accelerometers, pressure sensors, displacement sensors, and embedded strain sensors, on two new highway bridges in Orange County, California. Taking advantage of these permanently instrumented bridges, a methodology is being developed for long-term structural performance/integrity evaluation. Integrating the global and local monitoring approaches, this methodology involves the following steps: (I) developing a three-dimensional (3-D) baseline finite element model of the bridge through ambient and/or forced vibration measurements carried out preferably at the very beginning of the bridge life, with a database containing the element stiffness values corresponding to different weather and traffic conditions, (II) periodically updating the baseline model by performing vibration tests, (III) carrying out vibration measurement after a major earthquake or vehicle overloading to globally assess the structural integrity by identifying the change in the baseline model, particularly in the element stiffness, and (IV) executing visual and NDE inspection (e.g., Feng et al. 2002) at the identified damage location for more accurate local damage assessment.

In this methodology, a reliable 3-D baseline model is essential for successful assessment of the structural performance/integrity. This paper focuses on the development of the baseline model using neural network-based system identification technique and vibration data measured at the instrumented bridges. To be more specific, instrumentation of the two new highway bridges with sensors is first presented, then vibration testing and extraction of bridge dynamic characteristics (modal parameters) using different techniques are discussed, and finally the neural network-based system identification technique is presented to develop a 3-D baseline model for one of the instrumented bridges based on its measured dynamic characteristics.

INSTRUMENTATION OF TWO BRIDGES

In order to study long-term structural performance of highway bridges, the authors recently instrumented two new highway bridges, the Jamboree Road Overcrossing and the West Street On-Ramp.

The Jamboree Road Overcrossing, as shown in Figure 1, is a typical three-span continuous cast-in-place prestressed post-tension box-girder bridge of the Eastern Transportation Corridor, located in Irvine, CA. The total length of the bridge is 110.9 m with each span length of 35.5, 46.1, and 30.3 m. The bridge is supported on two monolithic single columns and sliding bearings on both abutments. The sliding bearings allow creep, shrinkage, and thermal expansion or contraction.

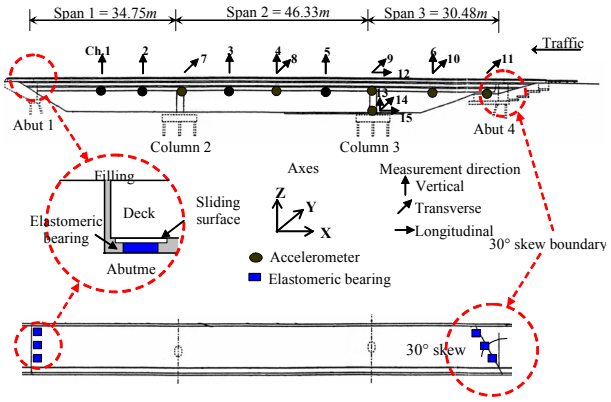

Figure 1. Jamboree Road Overcrossing and accelerometer arrangement

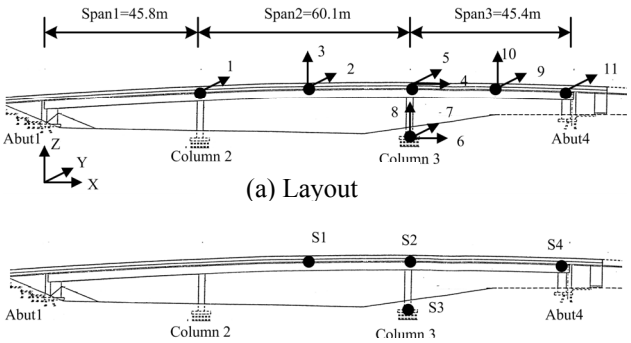

Figure 2. West Street On-Ramp

The West Street On-Ramp, as shown in Figure 2, is a three-span continuous and curved cast-in-place prestressed post-tension box-girder bridge. The total length of the bridge is 151.3m with the span lengths of 45.8, 60.1, and 45.4m. The bridge is supported by two fixed columns and sliding bearings on both abutments similar to the Jamboree Road Overcrossing. This bridge is highly curved and inclined with a 12% super-elevation.

These two bridges represent two types of typical highway bridges in California, one is over- or under- crossing which is usually straight, and the other is on-ramp which is curved in plane.

Monitoring systems involving not only accelerometers but also strain gauges were installed at both super- and sub-structures. Monitoring vibration of the sub-structures is also of importance since the columns turned out to be one of the most vulnerable structural components of highway bridges under damaging earthquakes. Uni-axial, bi-axial, and tri-axial force-balance servo-type accelerometers were permanently installed on both of the bridges. The locations of the accelerometers at Jamboree Road Overcrossing are shown in Figure 1, and they are placed along the centerline of the bottom of the girder to minimize the torsional effect of the bridge box girder. Strain gauges, which are micro-displacement sensors, were permanently embedded in concrete members of the West Street On-Ramp to measure dynamic strains. In order to measure the movement of the super-structure with respect to the abutment due to shortening, creep, shrinkage, as well as seismic excitations, a displacement sensor was installed at an abutment for each bridge. To measure the soil pressures at the abutment during earthquakes, a soil pressure sensor was installed on the back wall of the abutment at the West Street On-Ramp. Uninterruptible power supply systems were installed at the bridges to prevent power failure due to unexpected events such as earthquakes. In the Jamboree Road Overcrossing, a solar power supply system was also installed as a backup to power the monitoring system.

VIBRATION TESTS

With the sensors installed on the bridges, traffic-induced vibrations were measured, based on which the dynamic characteristics (modal parameters) were extracted using the signal processing techniques discussed as follow.

Signal processing techniques

For traffic-induced vibration, the input loads are normally difficult to measure, and thus the dynamic characteristics are estimated based on the responses only. The peak picking (PP) and the frequency domain decomposition (FDD) (Otte et al. 1990; Brinker et al. 2001) methods were used to derive modal parameters from the vibration measurements without requiring information about input loads.

The PP method widely used in practice gives reasonable estimates of natural frequencies and mode shapes if the vibration modes are well separated. The FDD method may be used to separate close modes, thus obtaining better estimates. In the FDD technique, taking the singular value decomposition (SVD), the spectral density matrix $\mathbf{S}_{\mathbf{YY}}(\omega)$ of the response vector $\mathbf{Y}(t)$ is decomposed into:

$$\mathbf{S}_{\mathbf{YY}}(\omega) = \mathbf{U}(\omega)\mathbf{\Sigma}(\omega)\mathbf{U}^{H}(\omega) \tag{1}$$

where, $\mathbf{\Sigma}(\omega)$ is the diagonal matrix of the singular values, $\mathbf{U}(\omega)$ is the unitary matrix of the singular vectors and the superscript H denotes the complex conjugate and transpose. It has been shown by Brinker et al. (2001) that, when the structure is loaded with broad-band excitation, near the natural frequencies of the modes, $\mathbf{\Sigma}(\omega)$ contains a set of functions which are approximations of the auto-spectral density functions of the modes' normal coordinates, while the vectors in $\mathbf{U}(\omega)$ hold the mode shapes of the corresponding modes. The approximation becomes exact in the case where the loading is white noise, the structure is lightly damped, and the mode shapes of the close modes are geometrically orthogonal. If these assumptions are not satisfied, the decomposition is still expected to be more accurate than those of the classical approaches including PP.

The random decrement (RD) technique, sometimes referred to as randomdec, was used to average the measured data in order to reduce the noises (Yang et al. 1985; Asmussen and Brinker 1996). The fundamental concept of the RD technique is based on the fact that the response of a structure under random excitation is composed of a deterministic part (associated with the initial conditions) and a random part (associated with the random excitation). By averaging sufficient sample responses, the random part associated with the zero mean random excitation will average out, leaving only the deterministic part. The RD signature vector $\mathbf{z}(\tau,x)$ can be obtained as

$$\mathbf{z}(\tau,x)=\frac{1}{N}\sum_{i=1}^{N}\mathbf{y}(\tau+t_{\mathrm{i}},x) \tag{2}$$

where $\mathbf{y}(t,x)$ is the measurement at x, t_i's are the time instances satisfying a prescribed triggering condition at a leading station, N is the number of triggering points, and τ is the time variable. Therefore, the RD signature will exhibit the free vibration decay associated with the initial condition same to the prescribed triggering condition. In this study, the PP technique is then apply to the RD signature in frequency domain to obtain the modal parameters. The combination of PP and RD is hereafter referred to as the PP/RD method.

Ambient vibration tests

Ambient vibration tests were carried out for the Jamboree Road Overcrossing. The accelerations at the various locations on the box-girder and a column (shown in Figure 1) were measured with a sampling frequency of 100 Hz, with the corresponding Nyquist frequency being 50Hz, which is sufficient for identifying the major lower modes of the bridges. Typical time histories of

accelerations measured in the middle of span 2 in the vertical and in the transverse directions are shown in Figure 3. The amplitudes of accelerations in the transverse direction are approximately half of those in the vertical direction, as the traffic loads mainly induce vibrations in the vertical direction.

Totally, 82 sets of data measured in the daytime were processed, in which the time length of each data set is 10 minutes. The PP/RD method and the FDD method were used to extract modal parameters. The RD signature in the PP/RD method was obtained with a prescribed initial condition of positive zero crossing. In the FDD method, the spectral density matrix $\mathbf{S}_{\mathbf{YY}}(\omega)$ was obtained from the averaged vibration data with 25 percent overlapping. Figure 4 shows the time histories of the RD signature and the averaged acceleration in the middle of span 2. A 0.5 Hz high-pass filter was used to reduce bias errors, and extensive averaging contributed to reducing random errors.

The natural frequencies of the bridge derived using the two different methods are shown together in Table 1, in which the in-plane modes are the modes in the vertical and longitudinal directions, while the out-of-plane modes are the modes in the transverse direction. The table also shows the natural frequencies calculated from a preliminary finite element (FE) analysis using a model based on the bridge's design drawings (to be described later). There are not much differences between the frequencies derived from the two methods based on the measured data, but the calculated frequencies do not agree with the measured ones.

Figure 5 shows the mode shapes corresponding to the natural frequencies. It is observed that the high and the horizontal modes contain more noises than the low and the vertical modes, as traffic loads mainly excite vertical vibration and the frequency contents of the loads are relatively low. The measurement on the top of column 3 in the longitudinal direction was important to distinguish the second and the third vertical modes, because the two modes are very similar in the vertical direction but different in the longitudinal direction. As shown in Figure 5, the longitudinal displacement of the second vertical mode at column 3 was to the right, whereas that of the third mode was to the left. This is because that the maximum vertical modal displacement of span 2 is larger than that of span 3 in the second mode, and vice versa in the third mode.

In Figure 5, the mode shapes estimated from the PP/RD and FDD methods were also compared with those from the preliminary FE analysis. Observing the mode shapes, those estimated by the FDD method agree better with those from the FE analysis than those estimated by the PP/RD methods. The mode shapes estimated by the FDD method appear more reasonable than those by the PP/RD method.

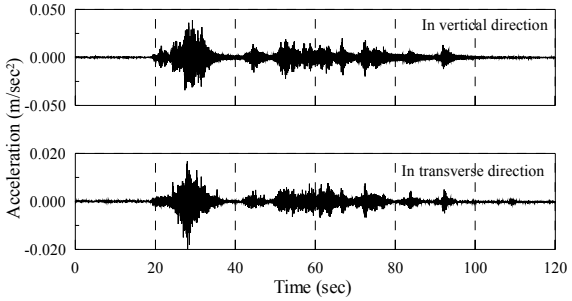

Figure 3. Typical accelerations in the middle of span 2

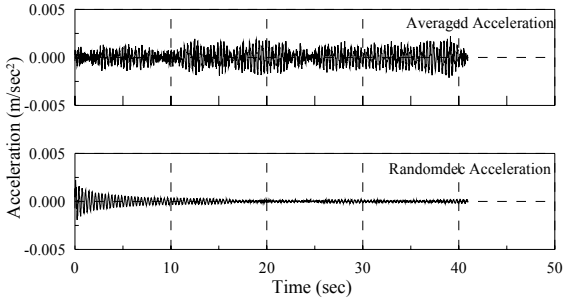

Figure 4. Processed accelerations in the middle of span 2

Table 1. Comparison of Natural Frequencies of Jamboree Road Overcrossing (Hz)

Mode Number	In-plane mode				Out-of-plane mode			
	Measured		Numerical		Measured		Numerical	
	PP/RD	FDD	Preliminary FE	Baseline FE	PP/RD	FDD	Preliminary FE	Baseline FE
1	2.954	2.954	2.889 (2.20)	2.947 (0.24)	2.612	2.612	3.126 (19.7)	2.633 (0.80)
2	4.077	3.979	3.716 (6.61)	3.955 (0.60)	5.004	5.004	4.535 (9.37)	4.982 (0.44)
3	4.638	4.638	4.654 (0.35)	4.798 (3.45)	9.940	9.936	10.509 (5.77)	9.745 (1.92)
4	6.323	6.250	5.721(8.46)	5.831 (6.70)				
5	8.813	8.911	9.400 (5.49)	9.565 (7.34)				

Note: The values in the parentheses are the differences (%) between the numerical and the experimental natural frequencies (obtained from FDD).

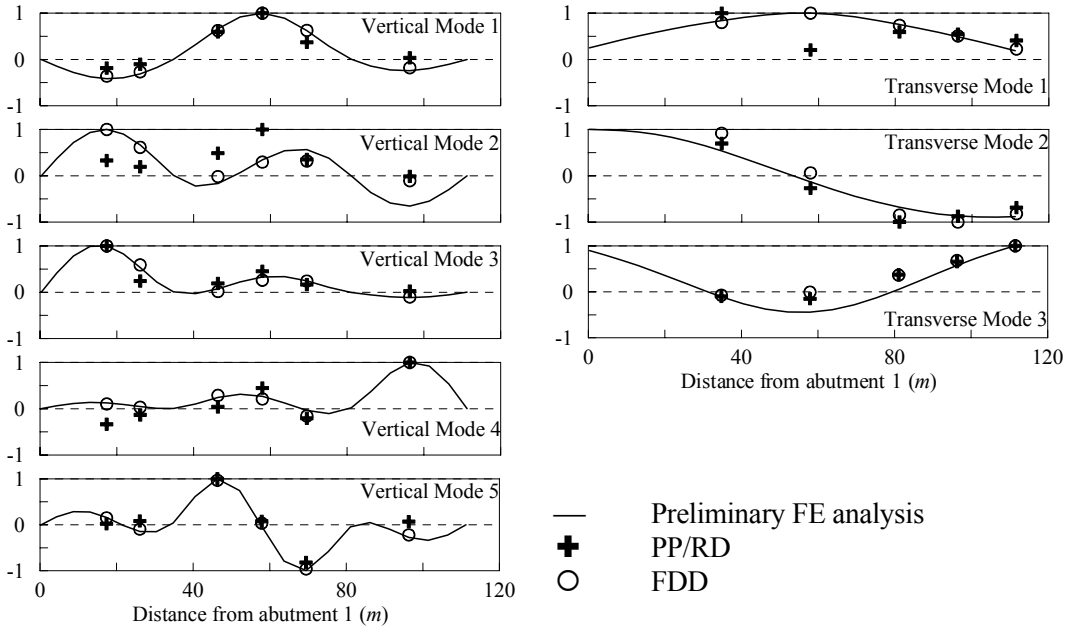

(a) In-plane Modes (b) Out-of-plane Modes

Figure 5. Comparison of mode shapes

Forced vibration tests

Braking and bumping vibration tests were carried out using a water truck at the final constructional stages of the West Street On-Ramp before it opened to traffic. Braking and bumping forces applied by the water truck at the middle point of each span induced bridge vibration in the longitudinal and vertical directions. The bumping force was applied vertically using a bumper, and the braking force was created by sudden stoppage during traveling. The fully loaded water truck weighed approximately 15000 kg. Typical time histories of accelerations of the super-structure are shown in Figure 6. The amplitudes of accelerations in the transverse direction are relatively smaller than those in the vertical direction. More importantly, the amplitudes of the accelerations in the bumping vibration tests were greater than those in the braking vibration tests.

Four sets of data from the braking vibration tests and three sets from the bumping vibration tests were processed, in which the time length of each data set is 10 minutes and all the data were collected

at night with little traffic in the neighboring freeways and the bridge blocked. The FDD method was used to extract modal parameters from the averaged vibration data with 25 percent overlapping. The sampling frequency is 100Hz and the time length of the averaged data 40.96 sec. Since the vertical and the transverse modes are coupled together due to the curved shape of the bridge, the first two modes were estimated utilizing simultaneously the vertical and transverse vibration signals. The resulting natural frequencies are shown in Table 2. It is observed that the natural frequencies estimated from the bumping tests are 3.4 percent smaller than those from the braking tests, although these tests were performed with the same water truck and at the same loading locations. The difference in vibration amplitudes caused by the bumping and breaking tests may have contributed to the difference in the natural frequencies. This suggests a need for further study on the nonlinear effect associated with different excitation levels on the modal parameters.

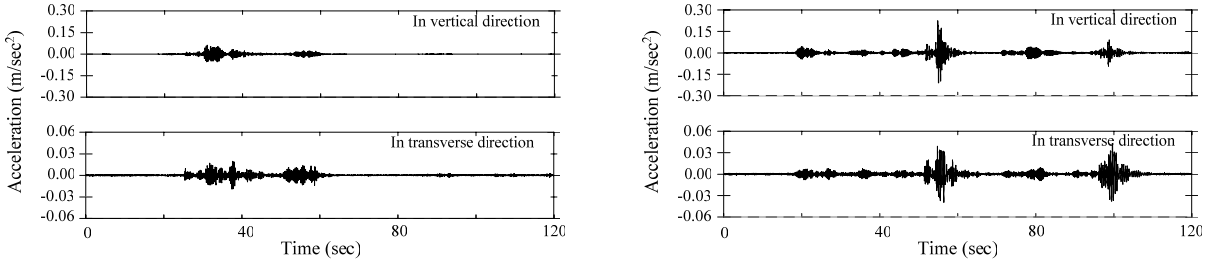

(a) Braking tests (b) Bumping tests

Figure 6. Typical acceleration time history by braking and bumping tests

Table 2. Comparison of Natural Frequencies of West Street On-Ramp (Hz)

Test	Braking Vibration Test		Bumping Vibration Test	
Mode	Vertical	Transverse	Vertical	Transverse
1	2.148	2.148	2.075 (3.40)	2.124 (1.12)
2	2.465	2.465	2.441 (0.97)	2.441 (0.97)

Note: The values in the parentheses are the differences (%) between breaking and bumping results.

DEVELOPMENT OF BASELINE MODEL

A baseline model has been developed using the Jamboree Road Overcrossing as an example. A preliminary FE model was first developed based on the bridge design drawing, and then updated to the baseline based on the measured dynamic characteristics by applying a the neural network-based system identification technique.

Preliminary finite element analysis

A 3-D preliminary FE model, as shown in Figure 7, was developed for the bridge. The super- and sub-structures were modeled as 3-D frame elements by using SAP2000 (1999). The cross-section area and moment of inertia for each element were calculated from the design drawings and listed in Table 3. Usually the abutments are assumed as hinged or fixed supporting conditions. However, recent research reports reveal that they are neither hinged nor fixed and the stiffness affects the behavior of bridges (Sanayei et al. 1999; Yun et al. 2002). In this study, considering that the model is

for analyzing bridge response to operational (traffic) loads, the abutment was modeled as linear longitudinal and transverse rotational springs with the stiffness values determined based on the FHWA recommendation (1996) and listed in Table 3. The natural frequencies and the mode shapes computed using this preliminary FE model are shown in Table 1 and Figure 5. The difference as shown in the parentheses between the calculated and the measured natural frequencies suggests the need for updating the preliminary FE model using the measurement results.

Sensitivity of the modal parameters to column damage was analyzed. The damage is defined as the decrease of flexural stiffness. Seismic damage often occurs at the plastic hinge zones that are at the top and bottom sections of the columns in the longitudinal direction and at the bottom sections of the columns for the transverse direction considering the maximum bending moments. Figure 8 shows the column damage decreases the lower natural frequencies and increases the rotations of columns in the mode shape. Therefore, installing accelerometers in the longitudinal and transverse directions at the top of columns is important for seismic damage detection.

Sensitivity analyses of the modal parameters with respect to the abutment spring stiffness were also performed. The spring stiffness at abutment 4 changed from 10 to 190 percent of the original value. As shown in Figure 9, the modal parameters are not sensitive to the rotational stiffness.

Table 3. Structural Parameters for Jamboree Road Overcrossing

Element	Area (m^2)	Moments of inertia (m^4)			Spring Stiffness	
		I_X	I_Y	I_Y	k_{l1}^{abut}, k_{l4}^{abut} (N/m)	k_{r1}^{abut}, k_{r4}^{abut} ($N{\cdot}m$)
Deck	5.94	7.63	3.01	3.01	N/A	N/A
Column	3.53	2.51	0.72	0.72	N/A	N/A
Abutment	N/A	N/A	N/A	N/A	1.996×10^8	7.582×10^8

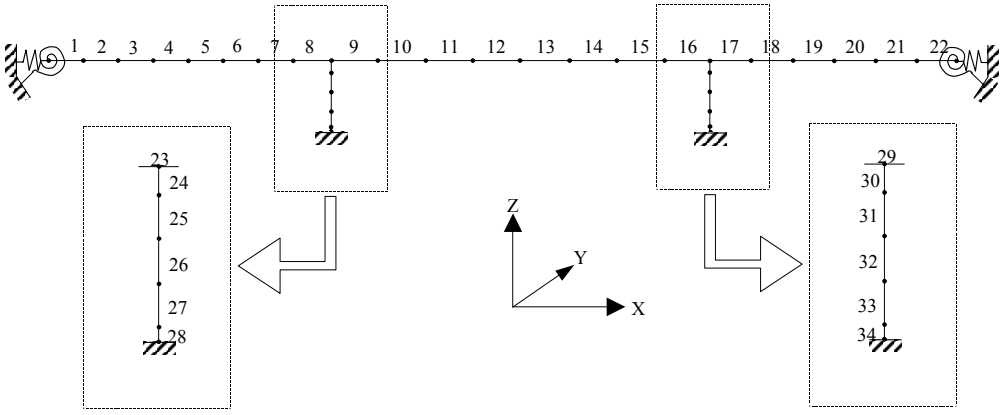

Figure 7. Finite element model of Jamboree Road Overcrossing

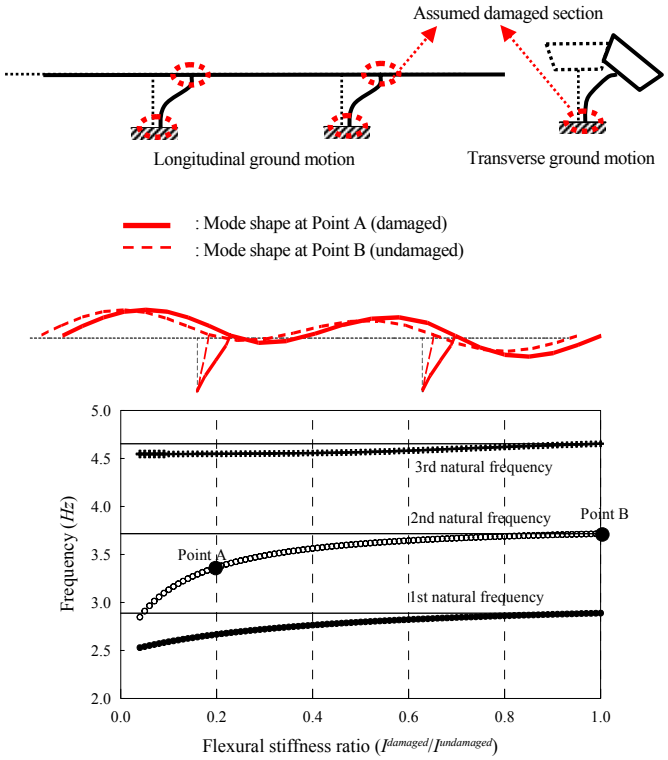

(a) In-plane mode by longitudinal ground motion

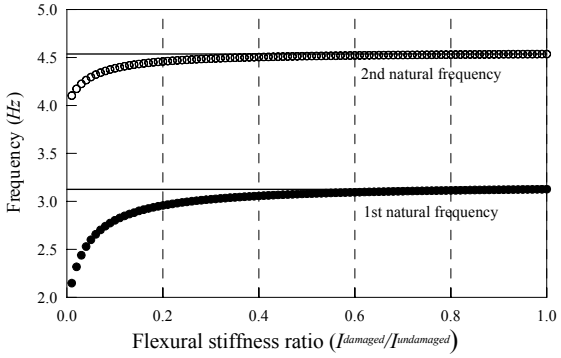

(b) Out-of-plane mode by transverse ground motion

Figure 8. Sensitivity of natural frequency for column damages

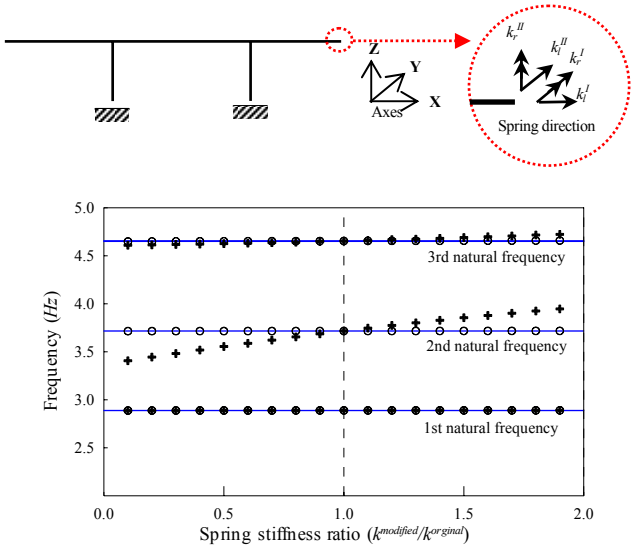

(a) In-plane mode (✚ : longitudinal (k_l^I) ○: rotational (k_r^I))

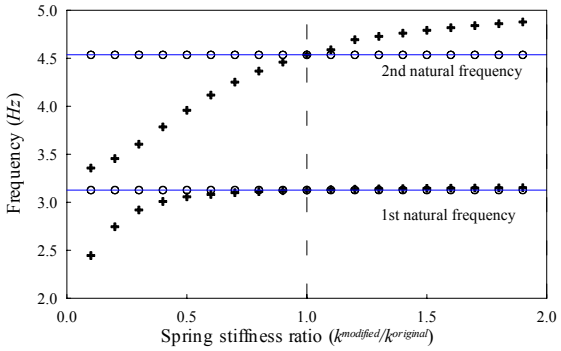

(b) Out-of-plane mode (✚ : transverse (k_l^{II}) ○: rotational (k_r^{II}))

Figure 9. Sensitivity of natural frequency to spring stiffness

Neural network-based system identification

The back propagation neural network was applied to update the preliminary FE model to the baseline model based on the measured dynamic characteristics of the bridge. The neural network-based system identification method has several advantages compared with conventional system identification methods. The neural network approach is more capable to build a baseline FE model based on the partially and incompletely measured components of the mode shapes due to the limited sensor number, and on only a few lower modes extractable from the vibration signals. Furthermore, it is very convenient to use the neural network to parameterize any properties of the structures, such as the effective shear area, as the unknowns to be identified. Different from many system identification methods in which the sensitivity matrix may become unstable especially for complex structural systems, the neural network approach does not require the calculation of sensitivity matrix, and thus can be applied to the complex civil engineering structures avoiding the numerical difficulty.

As shown in Figure 10, the neural network consists of an input layer, hidden layers, and an output layer. The relationship between input and output of a neural network can be nonlinear or linear, and its characteristics are determined by the weights assigned to the connections between the neurons in two adjacent layers. Changing these weights will change the input/output relationship of the network. A systematic way of determining the weights of the network to achieve a desired input/output relationship is referred to as a training or learning algorithm. The standard back propagation algorithm was used in this study, for training the neural network to identify structural parameters (the stiffness and the mass matrices of the bridge, and the spring stiffness at the abutments) from measured natural frequencies and mode shapes.

The procedure of the neural network-based identification involves the following steps: (1) determining the types of input and output patterns; (2) preparing the training and testing patterns through FE analyses; (3) training the neural network using the back propagation algorithm; and finally (4) estimating the structural parameters of the baseline FE model by inputting the measured natural frequencies and mode shapes to the well trained neural network.

In the present study, the input pattern consists of the natural frequencies and the mode shapes :

$$Input\ \ Pattern\ \ Vector = \{f_1, \cdots, f_i, \cdots, f_l, [(\phi_{1i}, \cdots, \phi_{ji}, \cdots \phi_{ki}),\ i = 1, \cdots, m]\} \tag{3}$$

where f_i is the i-th natural frequency, ϕ_{ji} denotes the j-th component of the i-th mode shape $\boldsymbol{\varphi}_i$ which is normalized as $\boldsymbol{\varphi}_i^T \boldsymbol{\varphi}_i = 1$. k is the number of accelerometers installed on a structure, and l and m are the number of natural frequencies and mode shapes considered, respectively. The output pattern consists of correction coefficients of structural parameters,

$$Output\ \ Pattern\ Vector = \{\ c_1,\ \cdots,\ c_n\ \} \tag{4}$$

where $c_1,\ \cdots,\ c_n$ are the correction coefficients for the FE model's structural parameters (described as a portion of the original values in the preliminary FE model). Training input-output data sets were obtained by extensive FE analyses with different sets of correction coefficients randomly assumed using the Latin hypercube sampling technique (Press et al. 1992; Olsson and Sandberg 2002).

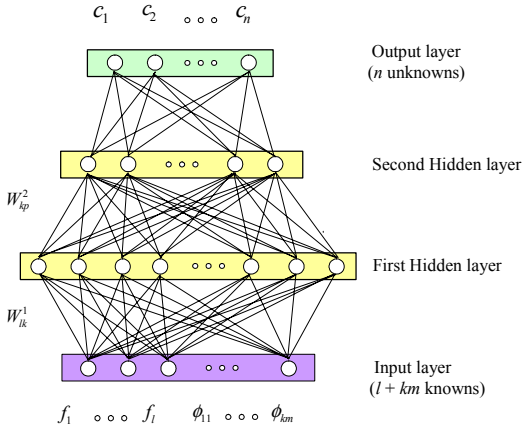

Figure 10. Back propagation neural network

Development of 3-D baseline model based on vibration tests

The baseline model of the bridge was developed using the approach described above, which particularly involves: step (1) updating the in-plane structural parameters of the 3-D preliminary FE model based on the measured vertical and longitudinal modes, and then step (2) identifying the out-of-plane structural parameters of the 3-D baseline FE model based on the measured transverse modes.

The natural frequencies for the lower five modes and the first mode shape of the in-plane modes, and the natural frequencies for the lower three modes and the first mode shape of the out-of-plane modes were used in the neural network in step (1) and (2) respectively. Although more natural frequencies and mode shapes could be included, higher mode shapes were ignored due to noise contamination. The correction coefficients are related with the mass and the stiffness matrices of the super- and sub-structures, and the abutment spring stiffness as follows:

Step 1 (in-plane motion)

$$\mathbf{M} = \{c_1^I A^{super}, c_2^I A^{sub}\} \tag{5a}$$

$$\mathbf{K} = \{c_3^I I_Y^{super}, c_4^I I_Y^{sub}\} \tag{5b}$$

$$k = \{c_5^I k_{l1}^{abut}, c_6^I k_{r1}^{abut}, c_7^I k_{l4}^{abut}, c_8^I k_{r4}^{abut}\} \tag{5c}$$

Step 2 (out-of-plane motion)

$$\mathbf{K} = \{c_1^{II} I_Z^{super}, c_2^{II} I_Z^{sub}\} \tag{6a}$$

$$k = \{c_3^{II} k_{l1}^{abut}, c_4^{II} k_{r1}^{abut}, c_5^{II} k_{l4}^{abut}, c_6^{II} k_{r4}^{abut}\} \tag{6b}$$

in which A^{super} and I^{super} are the effective shear area and the moment of inertia of the cross-section in super-structure; A^{sub} and I^{sub} are those in sub-structures; k_{li}^{abut} and k_{ri}^{abut} are linear spring stiffness in the longitudinal and rotational directions at abutment i; and c^I and c^{II} are correction coefficients at each step for these parameters. The shear areas of the super- and sub-structures are common parameters for both in-plane and out-of-plane motions of the bridge. In this study, the shear areas were identified from step (1), since the in-plane motions are more dominant and accurately measured than the out-of-plane motions under traffic loads.

Five thousand training patterns numerically obtained by FE analyses were used for the training of the neural network, and 1000 iterations were performed. An output-input pair in the training patterns is obtained by assuming a set of correction coefficients c's with the corresponding frequencies and mode shapes being calculated through FE analysis. The ranges of the correction coefficients in the training process of the neural network were chosen from 0.5 to 1.5 for the super- and sub-structures, and from 0.1 to 1.9 for the abutment spring stiffness values considering their relatively high uncertainties.

In order to verify the performance of the trained neural network, a set of correction coefficients c's were assumed and the frequencies and mode shapes were calculated through FE analysis. By inputting the calculated mode parameters into the trained neural network, a set of correction coefficients were resulted and compared with the assumed ones. The verification results are shown in Table 4 where the assumed (target) correction coefficients are compared with those identified from the neural network. It is observed that structural parameters, except the stiffness of the rotational springs at abutments, are well identified. The lack of correlation between the rotational springs and the modal parameters (as shown in Figure 10) make it difficult to identify the rotational

spring stiffness. Therefore, the stiffness of the rotational springs at the abutments were not updated in the baseline FE model.

Table 4. Neural Network Output for Verification

Correction Coefficient		Target			Output with Identification of Rotational Stiffness			MSE (%)	Output without Identification of Rotational Stiffness			MSE (%)
		1	2	3	1	2	3		1	2	3	
In-plane mode	c_1^I	1.2	1.2	1.3	1.34	1.22	1.32	6.00	1.19	1.20	1.32	1.00
	c_2^I	0.5	1.3	1.4	0.55	1.26	1.41	3.33	0.51	1.31	1.40	0.67
	c_3^I	0.7	0.7	0.5	0.76	0.71	0.57	4.67	0.70	0.70	0.50	0.00
	c_4^I	0.9	0.5	1.3	0.97	0.56	1.27	5.33	0.90	0.50	1.31	0.33
	c_5^I	1.1	1.6	1.0	1.21	1.56	0.97	6.00	1.09	1.58	1.00	1.00
	c_6^I	1.5	1.4	1.5	1.38	1.05	0.97	33.33				
	c_7^I	0.1	0.6	1.1	0.15	0.72	1.12	6.33	0.15	0.56	1.12	3.67
	c_8^I	0.2	1.8	0.3	0.26	1.80	0.74	16.67				
Out-of-plane mode	c_1^{II}	1.2	1.2	1.3	1.16	1.11	1.35	6.00	1.20	1.20	1.30	0.00
	c_2^{II}	1.1	1.0	1.0	1.08	0.91	0.95	5.33	1.10	1.01	1.00	0.33
	c_3^{II}	0.6	0.5	0.1	0.60	0.49	0.13	1.33	0.59	0.51	0.12	1.33
	c_4^{II}	0.6	1.7	0.3	0.97	0.81	0.8	58.67				
	c_5^{II}	0.8	0.4	0.9	0.81	0.43	0.83	3.67	0.81	0.41	0.90	0.67
	c_6^{II}	0.6	1.5	0.1	0.99	1.07	1.15	62.33				

Note: MSE (mean sizing error) is the average value of the absolute estimation errors for correction coefficients.

After the trained neural network was accepted based on the above testing and verification procedure, the modal parameters measured in the field (shown in Table 1 and Figure 5) were used as the input in the neural network to identify the structural correction coefficients for the Jamboree Road Overcrosssing. The results are shown in Table 5, indicating that the structural parameters are corrected by up to 84% of the original values in the preliminary FE model.

Using these correction coefficients, the preliminary FE model was updated to the baseline model. The modal parameters measured in the field (using only the results by the FDD method) are compared with those computed by the baseline model in Table 1. It was demonstrated that the natural frequencies of the baseline model better agree with the reality than those of the preliminary FE model.

Table 5. Neural Network Output Using Measurement Data

In-Plane Structural Parameters								Out-of-Plane Structural Parameters					
c_1^I	c_2^I	c_3^I	c_4^I	c_5^I	c_6^I	c_7^I	c_8^I	c_1^{II}	c_2^{II}	c_3^{II}	c_4^{II}	c_5^{II}	c_6^{II}
0.93	0.99	0.96	1.00	1.25	N/A	1.24	N/A	1.00	0.99	0.16	N/A	0.67	N/A

CONCLUSIONS

This paper presents the application of a neural network technique for developing a baseline model of a bridge structure, based on vibration tests. This is an essential step in the methodology currently being established by the authors for long-term structural performance monitoring of bridges. Based on the vibration tests on two instrumented highway bridges, the data analysis and the baseline development, the following observations or conclusions can be made:

1. Sensitivity analysis indicates that it is important to measure vibration on the top of a column in both transverse and longitudinal directions in order to detect seismic damage on the columns.
2. The traffic-induced vibration in the vertical direction is twice intensive than that in the transverse direction. The higher modes and the horizontal modes are more noise-contaminated than the lower modes and vertical modes.
3. The natural frequencies of the bridge estimated from the bumping test are lower than those from the braking test, indicating the need to study the effect of excitation level on the vibration characteristics of the bridge.
4. The mode shapes estimated by the FDD method appear more reasonable than those by the PP/RD method.
5. The neural network technique is effective in identifying the structural parameters based on vibration measurement, despite the incomplete measurement of the mode shapes due to the limited senor number.
6. The lack of correlation between the rotational stiffness of the bridge abutments and the modal parameters makes it difficult to identify these stiffness values.

With the sensor systems permanently installed on the highway bridges and their baselines established in this study, the long-term structural performance of the bridges will be continuously monitored and evaluated in the future. The effects of environmental conditions (e.g. temperature and moisture) and the level of exciting forces on the baseline parameters will be studied.

ACKNOWLEDGMENTS

This research was supported by the California Department of Transportation (Caltrans), the Korea Science and Engineering Foundation (KOSEF) and UC-SMART. The authors would like to thank Caltrans District 12, Tokyo Sokushin Co., FCI Constructors, and Silverado Constructors for their generous support in traffic control and sensor installation.

REFERENCES

Asmussen, J. C., and Brincker, R. (1996). "Estimation of frequency response function by random decrement." *Proc., 14th Int. Modal Analysis Conference*, Society for Experimental Mechanics, Dearborn, Michigan, 246-252.

Brinker, R., Zhang, L., and Andersen, P. (2001). "Modal identification of output-only system using frequency domain decomposition." *Smart Mater. Struct.*, 10(3), 441-455.

Federal Highway Administration. (1996). *Seismic Design of Bridges Design Example No. 6: Three-Span Continuous CIP Concrete Box Bridge*, Report FHWA-SA-97-011, Federal Highway Administration.

Feng, M. Q., De Flaviis, F., and Kim, Y. J. (2002). "Use of microwaves for damage detection of fiber reinforced polymer-wrapped concrete structures." *J. Eng. Mech.* 128(2), 172-183.

Olsson, A. M., and Sandberg, G. E., (2002), "Latin hypercube sampling for stochastic finite element analysis." *J. Eng. Mech*., 128(1), 121-125.

Otte, D., Ponseele, P. V. D., and Leuridan, J. (1990). "Operational shapes estimation as a function of dynamic loads." *Proc., 8th Int. Modal Analysis Conference*, Society for Experimental Mechanics, Orlando, Florida, 413-421.

Press, W., Teukolsky, S. A., Vetterling, W. T., and Flannery, B. P. (1992). *Numerical recipes in C-the art of scientific computing*, Cambridge University Press, New York.

Sanayei, M., McClain J. A. S., Wadia-Fascetti, S., and Santini, E. M. (1999). "Parameter estimation incorporating modal data and boundary conditions." *J. Struct. Eng.*, 125(9), 1048-1055.

SAP2000 User's manual-Nonlinear Version 7.1. (1999). Computers and Structures, Inc., Berkeley, California.

Yang, J. C. S., Chen, J., and Dagalakis, (1985). "Damage detection in offshore structures by the random decremental technique." *J. Energy Resources Tech.*, ASME, 106, 38-42.

Yun, C.B., Lee, J.J., Lee, J.W., Yi, J.H., and Jung, H.Y. (2002). "Ambient vibration tests for structural integrity assessment of bridges." *Proc. 1st International Conf. on Bridge Maintenance, Safety and Management*, International Association for Bridge Maintenance and Safety, Barcelona , Spain.

.

SEISMIC DESIGN OF THE NEW SAN FRANCISCO OAKLAND BAY BRIDGE SELF ANCHORED SUSPENSION SPAN

Marwan Nader Ph.D., PE, Brian Maroney Ph.D., PE and Man-Chung Tang Ph.D., PE

BACKGROUND

Introduction

The seismically vulnerable East Span of the San Francisco-Oakland Bay Bridge will be replaced with a dual east bound and west bound 3.6 km long parallel structure. The cost of the Replacement Bridge is estimated at $2.5 billion and the bridge will be constructed by the year 2006. The Bay Bridge lies between the Hayward and the San Andreas faults which can generate magnitude 7.5 M and 8.1 M earthquakes, respectively. Performance criteria require that the bridge must be operational immediately following a 1500-year return period earthquake from either of these two faults. Four distinct structures will make up the bridge crossing: a low rise post-tensioned concrete box girder near the Oakland shore; a 2.4 km long segmental concrete box girder; a self-anchored suspension signature span; and a post-tensioned concrete box girder that connects to the east portal of the Yerba Buena Island tunnel (Figure 1).

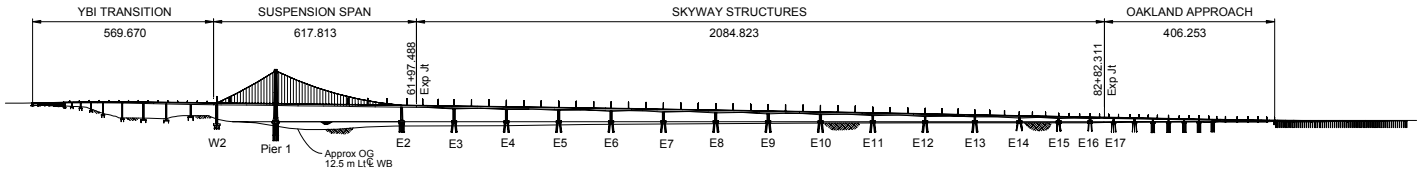

Figure 1. The new San Francisco Oakland Bay Bridge

The San Francisco-Oakland Bay Bridge was constructed in the mid-1930s. At 8 miles long, it was one of the longest high-level bridges in the world at the time. Today, the bridge is a primary route between the San Francisco Peninsula and the East Bay, carrying nearly 280,000 vehicles daily. A variety of bridges span the waterways of the San Francisco Bay. There are suspension bridges such as the Golden Gate Bridge, long skyway bridges such as the San Mateo-Hayward Bridge, and truss bridges such as the Richmond-San Rafael Bridge. Figure 2 is a map of the San Francisco Bay Area showing the location of these bridges.

Comparable to the levels specified in the 1930 Uniform Building Code for buildings, the Bay Bridge was designed for only 10 percent gravity (0.1g) earthquake accelerations. In 1989, the Loma Prieta earthquake measuring 7.1 on the Ritcher scale with an epicenter 70 miles to the south of San Francisco caused a 15 m section of the upper deck of the East Span of the San Francisco-Oakland Bay Bridge to collapse as shown in Figure 3. A more severe earthquake is expected to occur in the next 50 years and will cause significant damage and possibly the collapse of the existing East Span's truss structures. Retrofitting the structure was not only determined to be expensive and unreliable but also very difficult to implement while the bridge is under heavy use.

Figure 2. Geographical Location of Bridge

Figure 3. Damage to Bay Bridge after Loma Prieta Earthquake

Geotechnical Conditions

The limits of the potential bridge locations were defined by alignments designated N1 and N2 as shown on Figure 4. The selected alignment, N6, is shown in white.

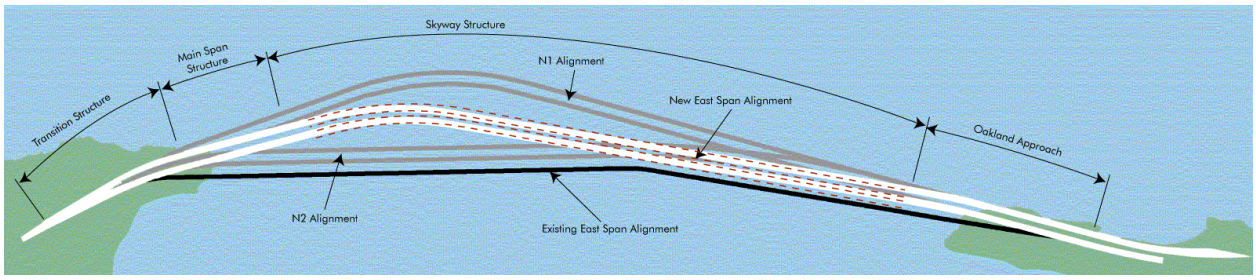

Figure 4 – Bridge Alignment

The site geology varies dramatically along the length of the bridge. Figure 5 is a geological profile at the bridge alignment. At the western end of the bridge (YBI), the piers will be founded on rock. As the bridge alignment progresses east towards Oakland, the bedrock Franciscan Formation drops abruptly and the remaining piers overlie deep Bay muds, followed by the interlayered clays and sands of the Alameda Formation. The main span tower structure will be sited on relatively shallow, sloping bedrock. The remainder of the skyway will be founded on a significant thickness of sediment.

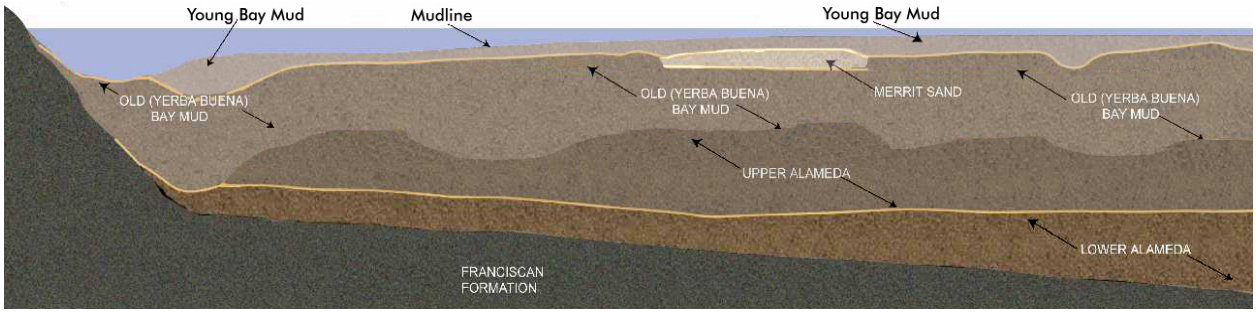

Figure 5 – Soil Profile

Seismic Hazard

Seismic hazard evaluations were performed to define the safety-evaluation earthquakes (SEE) and the functional-evaluation earthquakes (FEE). The SEE corresponds to an earthquake with a return period of 1,500 years while the FEE corresponds to an earthquake with a return period of 450 years. Both deterministic and probabilistic approaches were used to set the appropriate seismic criteria for the site. The seismic risk is dominated by the San Andreas Fault and the Hayward Fault. The bridge design is controlled by the SEE events. Six seismic ground motions were developed and used to determine the structural deformation, strength demands and drifts.

Seismic Performance Criteria

The bridge is designed to provide a high level of seismic performance. It is designed to resist two levels of earthquake, a functional evaluation earthquake (FEE) and a safety evaluation earthquake (SEE). After a functional evaluation earthquake, the bridge will provide full service almost immediately and there will be minimal damage to the structure. Minimal damage implies essentially elastic performance and is characterized by minor inelastic response, narrow cracking in concrete, no apparent permanent deformations, and damage to expansion joints. After a safety evaluation earthquake, the bridge will provide full service almost immediately and will sustain repairable damage to the structure. Repairable damage is damage that can be repaired with minimum risk of losing functionality; it is characterized by yielding of reinforcement, spalling of concrete cover and limited yielding of structural steel.

Bridge Type Selection

The Engineering and Design Advisory Panel (EDAP) appointed by Metropolitan Transportation Committee evaluated various design alternatives for the signature span and skyway. The single-tower, self-anchored, asymmetrical suspension span with a steel tower and a steel orthotropic deck was selected from a total of four design alternatives that were developed for the signature main span. These included two cable-stayed bridges and two self-anchored suspension bridges (each bridge type included single tower and dual portal tower alternatives; see Figure 6). The Panel also selected the segmental concrete haunched girder with spans of 160 m for the skyway from a total of three design alternatives; these included a concrete haunched girder with a 160 m typical span, a 6 m constant depth concrete girder with a typical span of 120 m, and a 6 m constant depth steel box girder with a 160 m span. In addition, the Panel recommended that a single pedestrian and bicycle path be built on the south side of the EB structure and that the bridge should be designed to carry Light Rail Transit in the future.

Suspension Bridge Alternatives

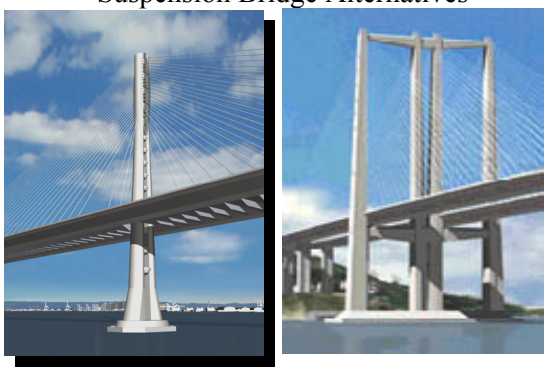

Cable Stayed Alternatives

Figure 6 – Design Alternatives for Main Span

SELF ANCHORDED SUSPENSION BRIDGE

The Self-Anchored Suspension (SAS) portion of the new East Span of the San Francisco-Oakland Bay Bridge consists dual box girders suspended from cables which are supported on the 160 m tower located off of the eastern shore of the Yerba Buena Island. The SAS spans 565 m between the piers E2 and W2, with a 385m main span, over the navigational channel, and a 180 m back span (Figure 7).

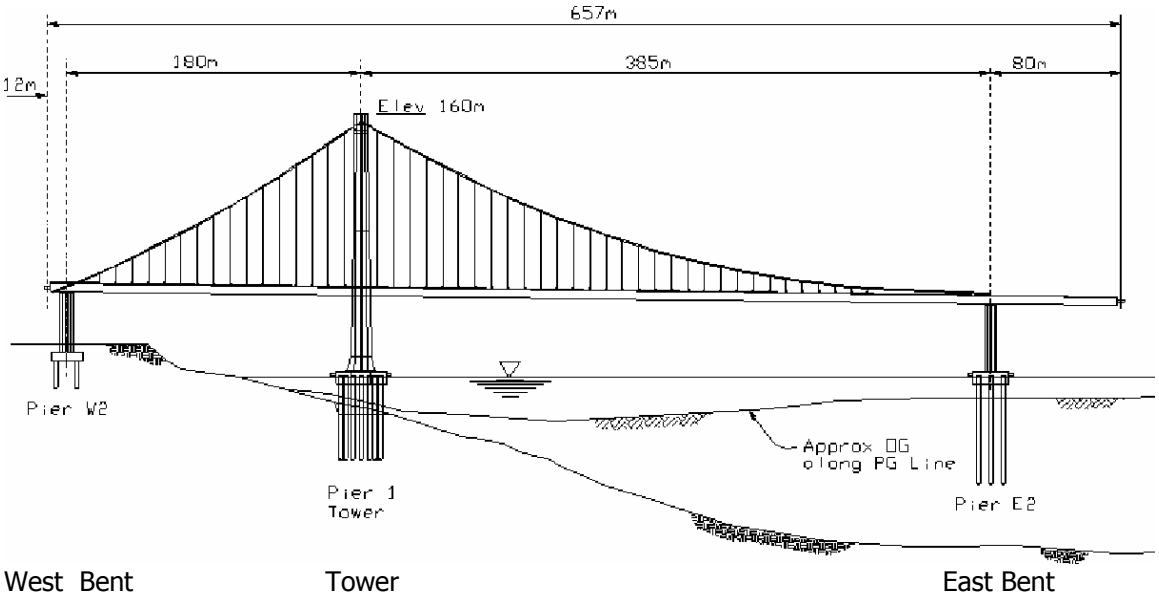

Figure 7. Elevation of the Self Anchored Suspension Bridge

The asymmetry of the bridge subjects pier W2 to a vertical uplift while the bridge is lightly supported on pier E2. The main tower therefore carries most of the bridge dead load. The uplift at pier W2 is fully counterbalanced by the pre-stressed concrete cap beam at pier W2. This ensures that the bridge is always balanced without relying on the pier to carry any tension. In order to balance the moments in the box girder caused by the 45 m cantilever at the east anchorage, suspenders do not support a 35 m segment of eastern end of the main span.

The box girders are not supported by the tower and are therefore "floating" at the tower with the suspenders providing the only connection between the box girders and the tower. This implies that while the tower carries most of the bridge dead load, the tower is not the primary element that carries the bridge seismic loads. The tower seismic response is mainly governed by its own mass and stiffness (the tower acts as a propped cantilever with a spring support at the tower saddle). The gap between the tower and the deck is designed to be large enough to prevent any impact during a Safety Evaluation Earthquake. Piers E2 and W2 are designed to provide the main lateral seismic support of the bridge.

The 0.78 m diameter cable is anchored to the east anchorage and is looped around the west bent through deviation saddles. Unlike traditional suspension bridges, these deviation saddles are fixed

to the west bent and the cable force on either side is balanced during construction using a jacking saddle. The pre-stressed cap beam supporting these saddles carries any differential stresses arising due to service and seismic loads (Figure 8).

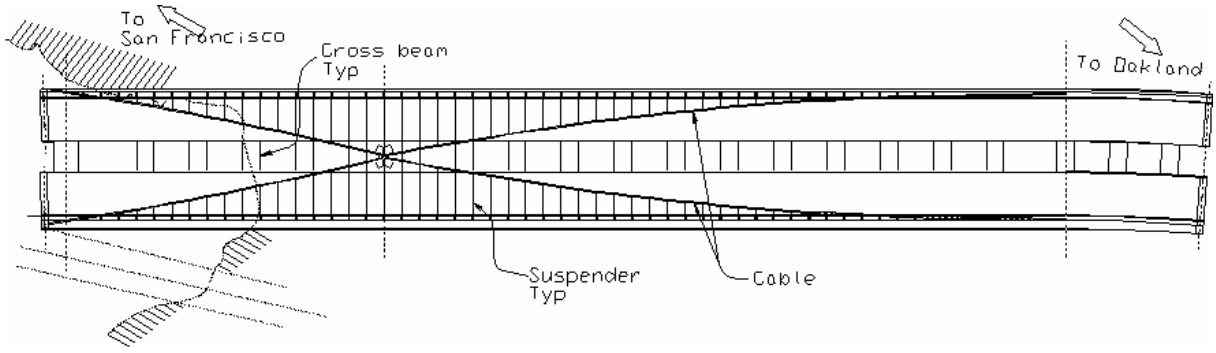

Figure 8. Plan of the Self Anchored Suspension Bridge

The cables do not cross at the main tower and are secured in a single saddle. The east saddles are supported on a set of rockers. These rockers bear on a grillage which is embedded into specially reinforced bulkheads in the box girders. The alignment of the grillage is tied to both the cable and the highway profiles. The rockers are designed to allow an adequate rotation angle to accommodate movement of the saddle in response to cable deformations due to service loads and seismic loads. The suspenders are splayed to the exterior sides of the box girders and are spaced at 10 m.

The superstructure consists of dual hollow orthotropic steel box girders (Figure 9). These girders are in longitudinal compression (reacting against the cable tension force) and are a part of the gravity load system. Transverse diaphragms spaced at 5 m support the orthotropic deck and distribute the suspender loads to the entire box. The box girders are connected together by 10 m wide by 5.5 m deep crossbeams spaced at 30 m on center. These cross beams carry the transverse loads between the suspenders (span of 72 m) and ensure that the dual boxes act composite during wind and seismic loads (Verendeel truss action).

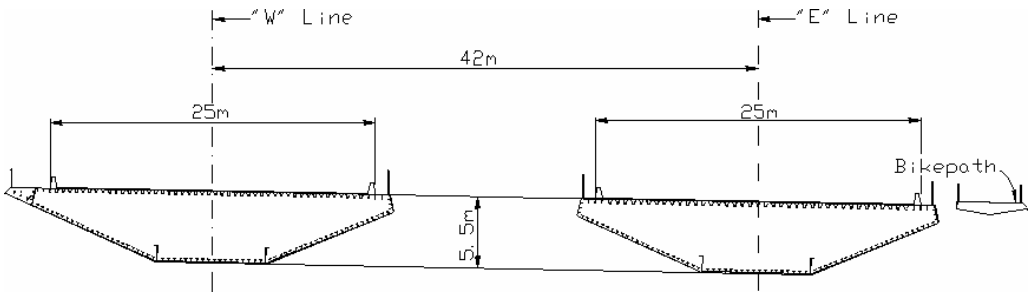

Figure 9. Typical Cross Section of Bridge – Dual Box Girders with Cross Beam

The bridge carries a pedestrian path on the south side of the eastbound deck. The pedestrian path eccentric load is balanced by a counter-weight on the north side. At the west bent, the steel box girders frame into the prestressed cap beam. The connection between the orthotropic steel box girders and concrete cap beam is subjected to the compressive reaction forces to the cables. Additional prestress is added through post-tension strands connected at each steel orthotropic rib.

The 160 m main tower is composed of four shafts interconnected with shear links along its height. The tower shafts are stiffened pentagonal steel box sections which taper along the height. The tower shafts are provided with diaphragms spaced at 4 m. The tower shafts are rigidly connected at the top and bottom by tower saddle grillage and tower base grillage, respectively (Figure 10).

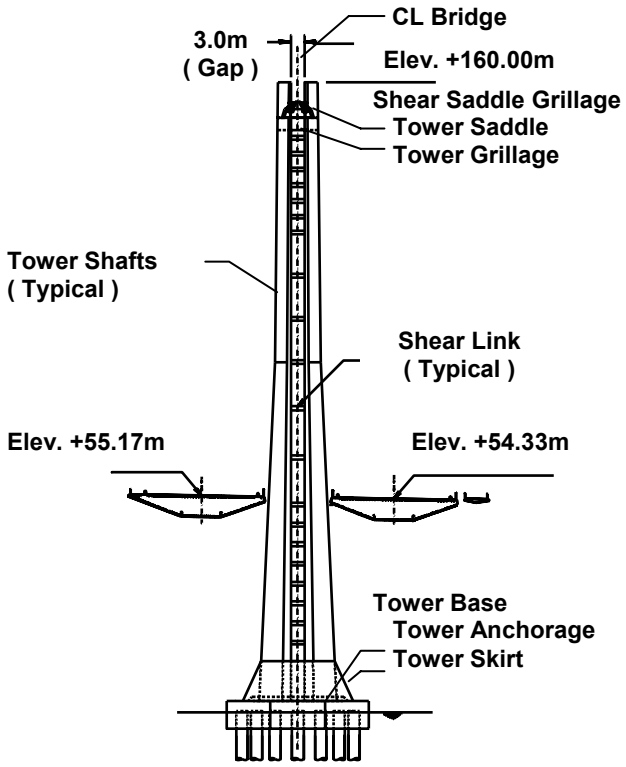

Figure 10 - Single Tower – Four Shafts Interconnected with Shear Links

The tower is fixed to a 6.5 m deep pile cap with anchor rods and dowels. The pile cap consists of a steel moment resisting frame encased with concrete and is supported on thirteen (13) 70 m long 2.5 m diameter steel shell pipe piles filled with concrete and embedded into rock (Figure 11). The rock slope is benched to give the piles equal lateral stiffness and to reduce torsional response (approximate clear length is 20 m), see Figure 12.

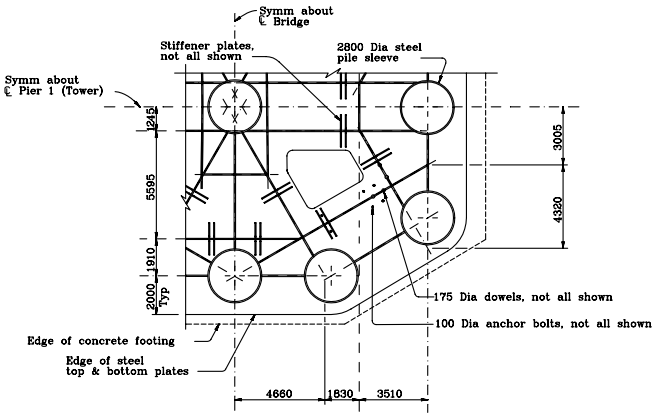

Figure 11. Partial Plan View of the Tower Pile Cap Steel Frame

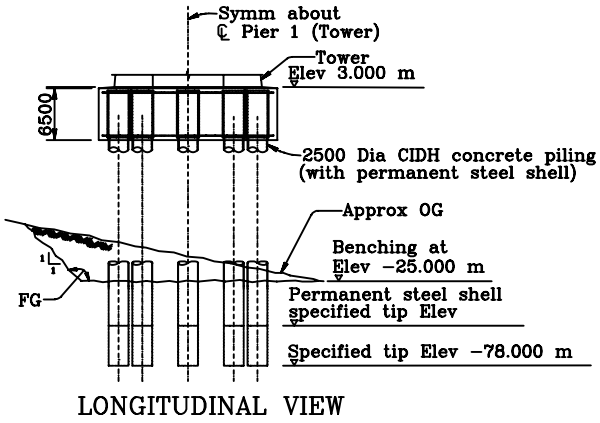

Figure 12. Elevation View of Tower Foundation Benching

Figure 13 shows the east bent which is comprised of two reinforced concrete piers and a prestressed concrete cap beam. The prestressed cap beam is introduced to protect the bearings and shear keys which connect the box girders to the east bent. The bearings are designed to carry the vertical loads (with the capacity to carry the lateral loads) while the shear keys are designed to carry all the lateral loads. The bearings are made of a spherical bushing assembly capable of large rotations about the transverse axis of the bridge; thus providing an almost true pin connection (Figure 14). Sixteen (16) 2.5 m diameter cast-in steel shell concrete piles support the east bent. These vertical piles are about 100 m long and are founded on bedrock.

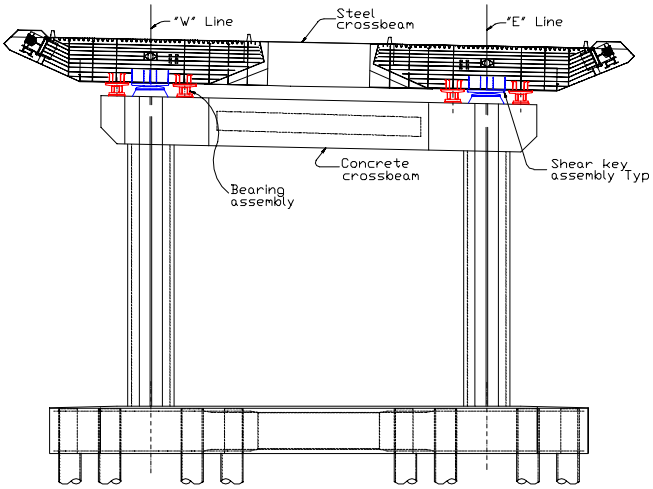

Figure 13. Elevation of the East Bent

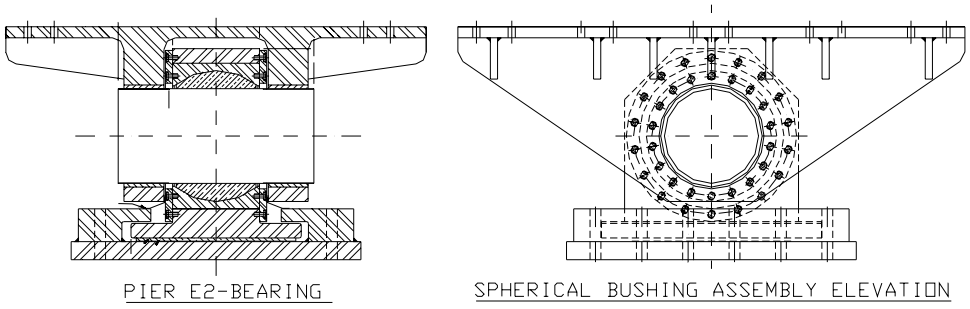

Figure 14. East Pier Bearing - Spherical Bushing Assembly

The west piers are reinforced concrete columns which are monolithically connected to the prestressed cap beam forming the west bent. The west bent is supported on gravity footings which in turn are anchored into rock with 10 m long corner piles. A tie-down system, designed to ensure that the west piers remain in compression during a seismic event connect the west bent cap beam to the gravity footings (Figure 15).

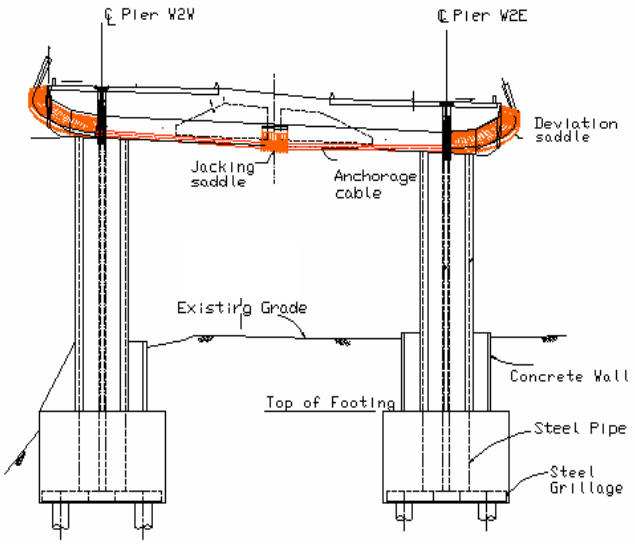

Figure 15. Elevation of the West Bent

The hinges in the transition spans between the SAS and Skyway as well as the SAS and YBI structures are designed to allow the structures to move relative to each other in the longitudinal direction and to rotate about the longitudinal axis of the bridge. The hinges are comprised of compact steel beam pipe section capable of transferring live loads and seismic loads. These hinge pipes are designed to fuse before any other bridge components in case of an overload (Figure 16).

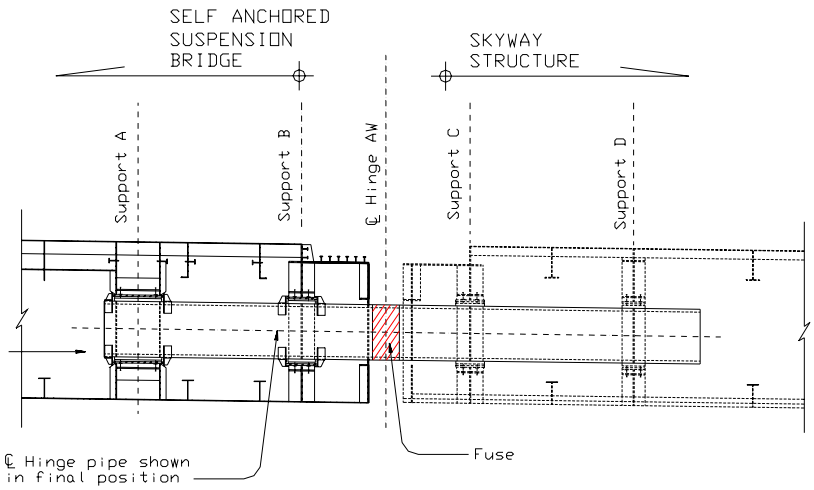

Figure 16. SAS to Skyway Hinge

SINGLE TOWER DESIGN

Structural System

Figure 17 shows three tower configurations that were evaluated in the 30% design stage, these are:

- *Dual Portal Towers:* In this design the bridge is split into two separate and parallel self anchored suspension bridges. Each bridge is supported by two cables which are individually anchored into the box girders. The cables lie in a vertical plane like most traditional suspension bridges.
- *Three legged Tower:* In this design the bridge is supported with three separate cables with the middle cable carrying half the bridge load. Each cable is individually anchored within the box girders. The box girders are connected at the east and west anchorages where the cables are anchored. The cables lie in a vertical plane like most traditional suspension bridges.
- *Single Tower:* In this design the bridge decks are connected with cross beams. The bridge is supported with a single cable which is anchored into the box girder at the eastern end and is looped around the west bent. The suspenders are splay out to the exterior edge of the box girders and lie in an inclined plane giving a three dimensional effect to the bridge.

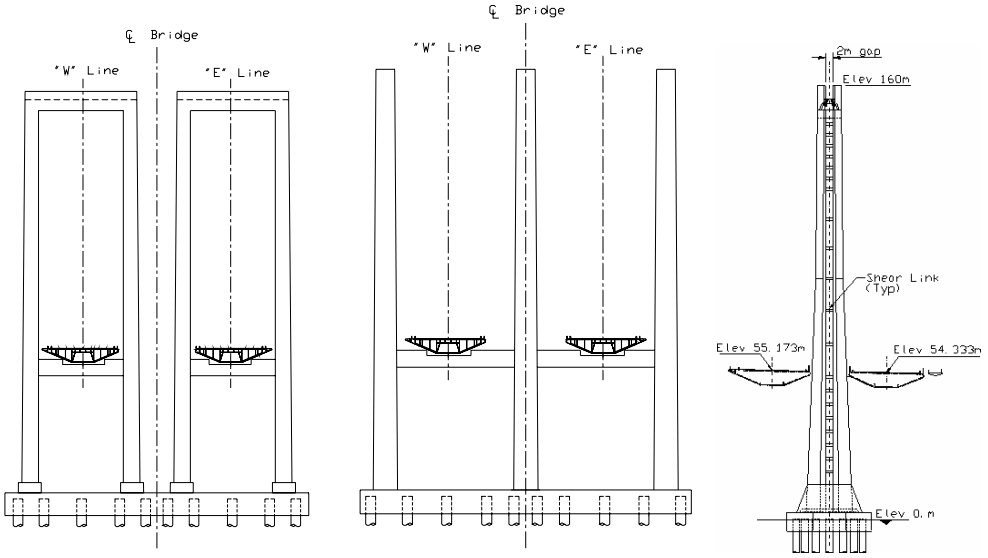

Dual Portal Towers Three Legged Tower Single Tower

Figure 17. Tower Alternatives Evaluated

The criteria used to evaluate the tower alternatives were seismic performance, aesthetics and cost. While the single tower alternative was the most appealing aesthetically, it was the most controversial in terms of its seismic performance. This was mainly due to the fact that the single tower is a pure cantilever that has no redundancy in the event of a major earthquake (in comparison with the dual portal towers and three legged tower alternatives which have horizontal struts which can be designed to yield in the event of an earthquake).

To improve the seismic performance of the single tower, the following measures were incorporated in the design, these are:

- Divide the tower into four shafts and introduce struts (shear links) to connect the shafts intermittently along its height. The shear links provide redundancy to the tower and can be designed to fuse during SEE.

- Remove the connection between the tower and the box girders; thus providing a "floating" deck which is supported laterally at the east and west bents. Having a "floating" deck at the tower provided two distinct load paths for gravity and seismic loads. While the tower carries most of the bridge dead load, the east and west bents resist most of the seismic bridge loads.

Figure 10 shows the elevation of the tower while Figure 18 shows the tower cross section. Each shaft is a stiffened pentagonal box section (A709 Grade 50 steel) which tapers along the height of the tower. The shaft skin plate thickness varies from 45 mm to 100 mm while the longitudinal stiffeners vary from 400x60 mm to 520x75 mm. Transverse diaphragms are spaced at 4m.

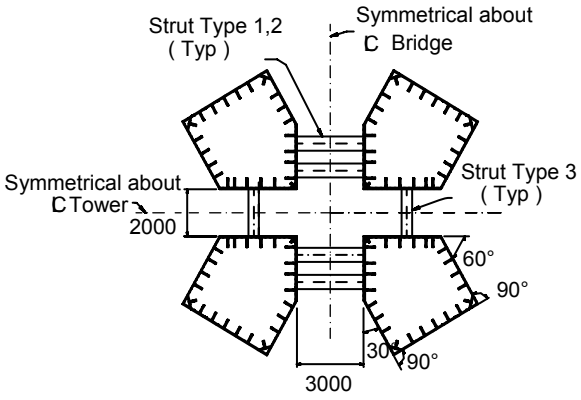

Figure 18. Tower Cross Section

Although the tower shafts are designed to remain elastic during SEE, the shafts were designed as stiffened box section per ATC-32. This insured that the shafts could undergo large inelastic compressive strains without locally buckling.

Shear Links

As discussed previously, the tower shear links play a significant role in resisting the seismic loads as well as to supply the tower with the proper stiffness during service load conditions. The tower shear links are designed to satisfy the following criteria:

- supply the tower with the required stiffness for service load conditions.
- remain almost elastic during a functional evaluation earthquake (FEE)
- plastify during a safety evaluation earthquake (SEE); thus dissipating energy and limiting the damage in the tower shafts (shafts are designed to remain almost elastic).
- to be replaceable after an SEE, if necessary

In order to satisfy the above requirements, various configurations of the tower were evaluated where the strength and stiffness of the shear links as well as their location along the height of the tower were varied. These studies were primarily done in the form of static pushovers to determine the response of the tower during service loads, wind loads, FEE and SEE loads. An optimal

layout of these links was then established (shown in Figures 10 and 18) as well as the stiffness and yield strength of the shear links.

Figure 19 shows a typical Shear Link (type 1). As noted, the shear link is connected to the tower shafts with bolts (A490) so that it may be replaced, if necessary. As in typical design of shear links, the web is designed to yield in shear; thus providing the ductility to the member. The flanges are designed to brace the webs along with vertical stiffeners. The yielding zone of the web is made of A709 Gr. 50 steel with additional requirements to limit the Fy and Fu. This requirement is mainly intended to insure that the yield strength (and overstrength) of these links is accurately bounded. As shown, the shear link connection zone uses thicker plates made of HPS70W steel to insure that this zone remains elastic while the shear link web yields.

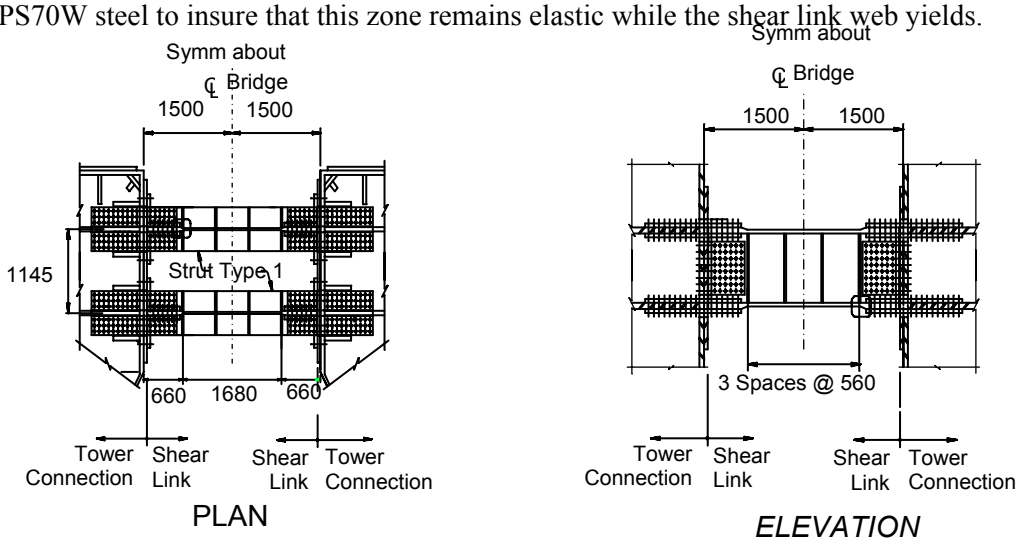

Figure 19. Tower Shear Link Type 1

A pushover analysis of tower is shown in Figure 20. This analysis was performed to evaluate the base shear versus top of tower displacement relationship; to optimize the design of the tower shear link and shaft; to evaluate the lateral ductility of the tower before collapse; and to evaluate the ductility demands on the shear links and tower shafts at various levels of displacement demand. Figure 20 shows the effects of using shear links on the lateral behavior of the tower. As noted the tower has stable behavior for displacements much larger than the SEE displacement demands (1 m).

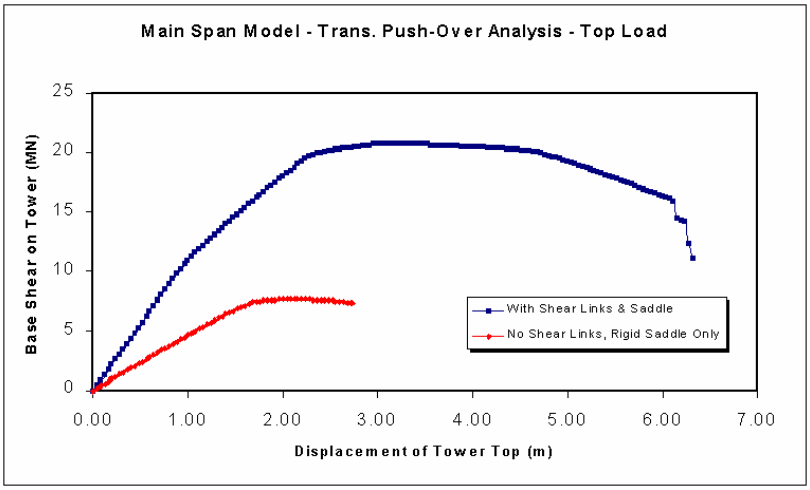

Figure 20. Pushover Analysis of the Single Tower

Figure 21 shows the stress contours and the deformed shape of a typical shear link at a rotational demand of 0.08 radians. The maximum SEE rotational demand on these links is in the order of 0.04 radians. Figure 22 shows a full-scale test specimen tested at the University of California at San Diego at a rotation of 0.07 radians.

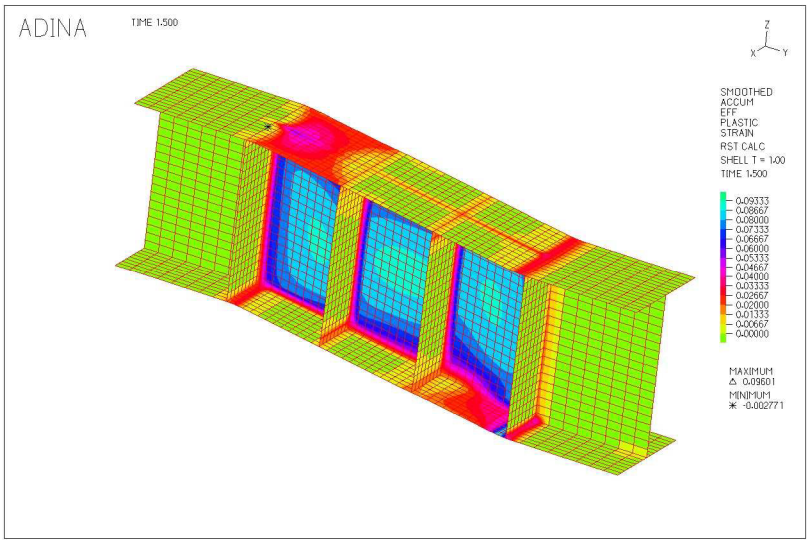

Figure 21. Finite Element Analysis of the Tower Shear Link Typ1

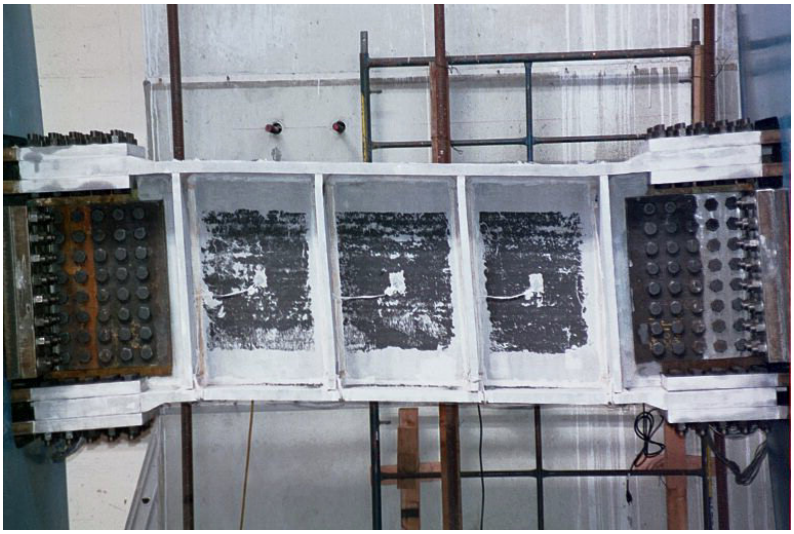

Figure 22. Full Scale Test of Shear Link Type 1 at UCSD

Tower Anchorage

At the base the tower shafts are connected with shear plates to form a grillage comprised of 11 cells. This grillage is designed to insure that the tower shafts act compositely, thereby reducing the seismic demands at the interface between the tower and the pile cap. The tower is anchored to the steel pile cap with 100-mm diameter anchor bolts (to resist tensile forces) and with 175-mm dowels (to resist shear forces). The anchor bolts are anchored to the bottom flange of the pile cap steel frame providing a direct transfer of forces. Similarly, the dowels are connected directly to the tower shaft skin plates and the web of the pile cap steel frame (see Figures 23 and 24).

The tower skirt (shown in Figure 10) at the base has several functions, these are: aesthetics, protection against ship collision and corrosion protection of the tower anchorage (tower base will be dehumidified).

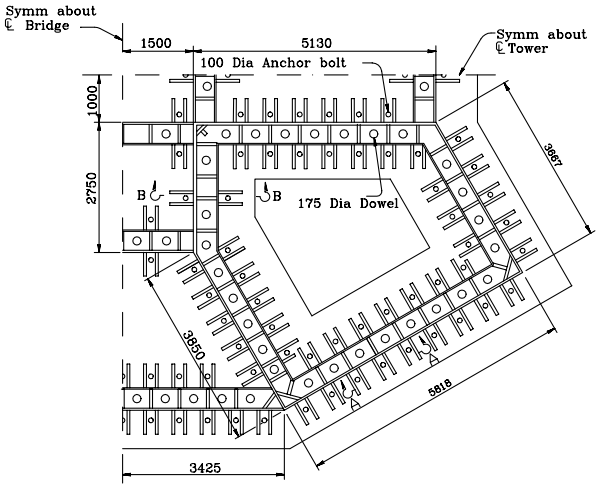

Figure 23. Tower Anchorage Layout

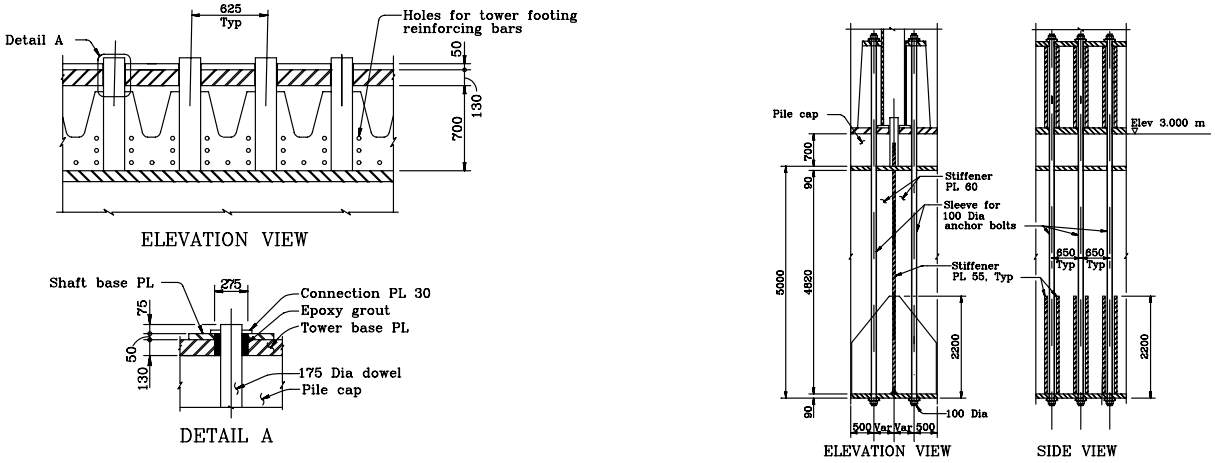

Figure 24. Tower Anchorage Details

SUPERSTRUCTURE DESIGN

Structural System

The single tower design presented a unique set of design requirements for the design of the super structure, these are:

- The two box girders have to be connected transversely for gravity loads. Given the cable and suspender layout, the transverse span is in the order of 72 m with 12 traffic lanes (6 East Bound and 6 West Bound)
- The two box girders have to act compositely to resist seismic and wind loads. The Design Criteria requires the bridge to be open to traffic almost immediately after and an SEE event. This requirement means that the box girders as well as the crossbeams shall remain almost elastic during SEE.
- The superstructure weight should not increase significantly (relative to two separate self-anchored suspension bridges). The weight of the cross beams directly impact the size of the cables, suspenders, anchorages, and tower.

In order to satisfy these requirements the 5.5 m deep box girders were connected with 10 m wide by 5.5 m deep cross beams spaced at 30 m on center. Figures 8 and 9 show the superstructure of the SFOBB-SAS. The following sections describe some of the salient features of this design.

Box Girder

Figure 25 shows a typical cross section of the box girder. The perimeter of the box girder is designed as a set of ten stiffened plates. The design of these plates satisfies the compactness requirements of Caltrans BDS, with the further requirement that wall stability conditions of ATC32 be met. The girders are designed to remain almost elastic under all combinations of the design loads. As noted, closed ribs were used for the top deck plate while open ribs were used for the remainder skin plates. This was mainly governed by the fact that orthotropic ribs are needed for fatigue while open ribs are more economical to satisfy the seismic codes.

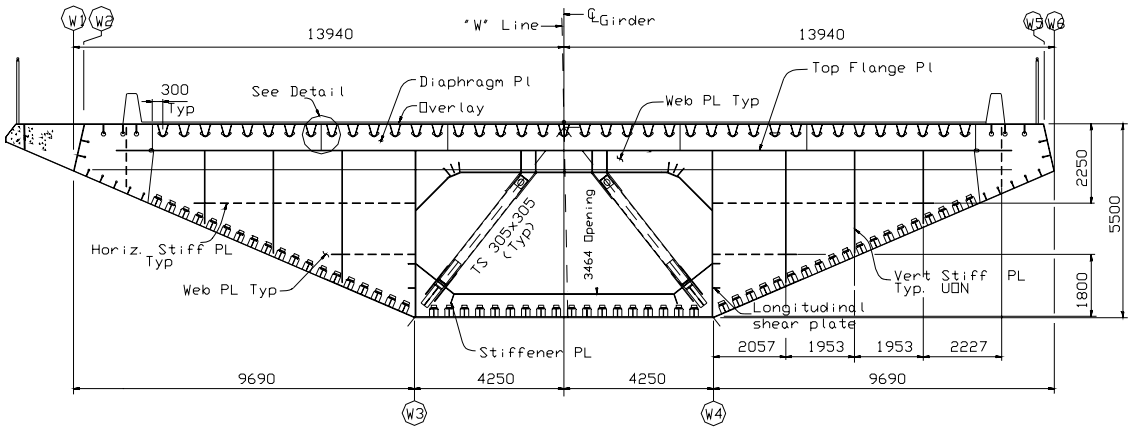

Figure 25. Typical Cross Section of the Box Girder

The self-anchored structural system requires the box girders to carry a compressive force that is equal to the horizontal component of the cable tension. Each box girder of the SFOBB-SAS is subjected to 200 MN compression or about 100 MPa (for a typical cross section). While this compressive force is good for fatigue, it made the design of the top deck more challenging. This is because the top deck is subjected to:

- compressive force to resist cable tension
- compressive force due to service global bending
- compressive force due to local bending

In order to reduce these compressive stresses, a target dead load "hogging" moment of about 100MN-m (about 40 MPa for a typical section) was included in the design of the bridge. This was particularly advantageous, since the 45 m cantilever at the East End produced a "hogging" moment which produced tension at the top deck.

Floor beams spaced at 5 m support the perimeter plates and their stiffeners. Figure 25 shows a typical floor beam. As noted, K-braces were introduced at the middle (instead of full depth webs) to economize and reduce the suspended weight.

Detailed Local Analysis and Design

It is unfeasible to perform an analysis using a sufficiently fine mesh without the use of submodeling. The technique was used extensively in these studies. As the ultimate goal of the local model was to evaluate stresses in the unusually complex system, all typical details were submodeled with a very fine mesh. For critically sensitive details, such as the orthotropic deck ribs and diaphragm cutouts, suspender brackets, and the intersections of crossbeams with the box girder, the submodel mesh was fine enough to study the fatigue stresses at the welds and cutouts. For simple plates and rolled sections not near connections, the mesh was coarser.

As the full local model could not accommodate all degrees of freedom of all submodels, each submodel was given a counterpart submodel with a coarser mesh. All submodels were calibrated for stiffness using proprietary programs. The coarse submodel was calibrated in all its properties, such that at its boundaries its stiffness matrix was identical to that of the fine mesh submodel. Thus, any analysis of the larger model preserves all details of the stress states at any point. By applying the displacements obtained at the boundaries of the coarse submodel, the fine submodel is analyzed to obtain the results at the fine mesh points. The ANSYS program automates these sequential computations, and facilitates the nesting of submodels at many levels. Thus, one submodel may itself contain yet finer submodels.

Figure 26 shows a local model representing a 30-meter segment of one deck girder and one half of one crossbeam. The crossbeam was centered in the segment, and the entire unit is symmetrical about the crossbeam. The centerline of the bridge was modeled as a symmetric boundary plane. The local model was created in the program ANSYS, and consisted entirely of finite element plates. All plates, ribs, flanges, and access cutouts were modeled.

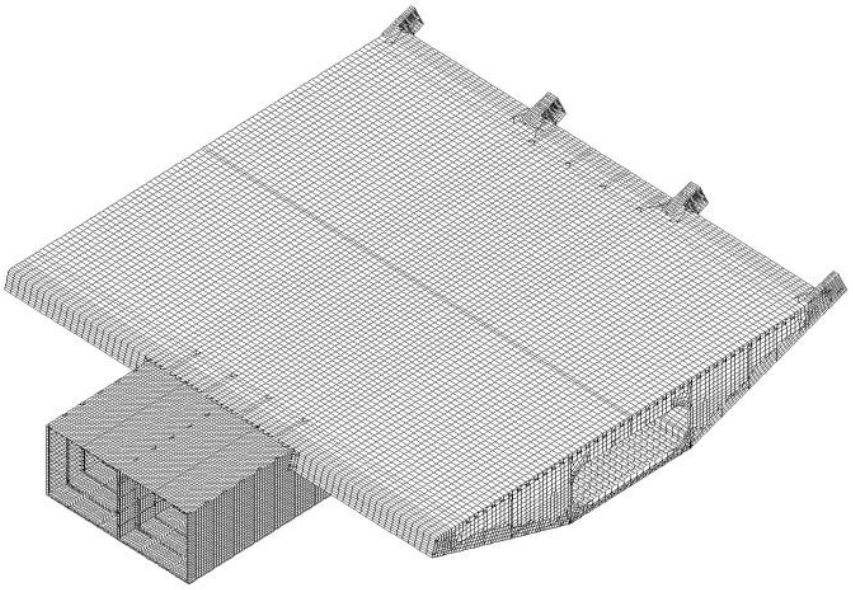

Figure 26. Finite Elemenet Model of a Typical Segment of the Superstructure

Orthotropic Deck

A typical orthotropic deck rib is shown in Figure 27. As noted the deck plate thickness is 14 mm and the rib depth is 345 mm. A 50 mm thick Epoxy Asphalt overlay is recommended for the SFOBB-SAS.

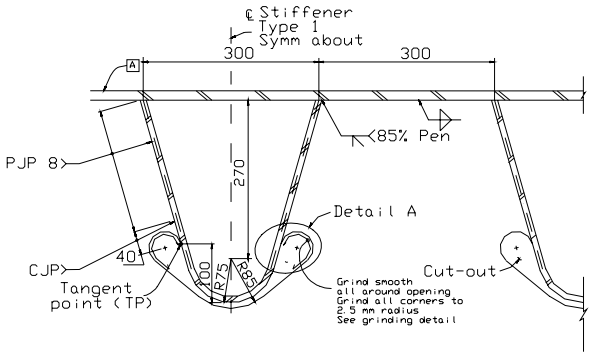

Figure 27. Typical Orthotropic Deck Rib

While the design of the orthotropic deck is mainly governed by service loads and fatigue requirements, all sections had to satisfy compact section requirements and stiffened section design per Caltrans BDS and ATC32.

The fatigue evaluation considered the effects of a single fatigue vehicle. Based on current accepted practice, the fatigue range for design was taken to be the maximum range due the passage of a single vehicle along any single travel lane. AASHTO LFRD specifications were used. The design aim was to limit fatigue stress ranges to a level 2.5 times less than the specified propagation threshold. In some cases this was not possible, however fatigue stress ranges were always limited to 2.0 times less than the threshold, in accordance with the code.

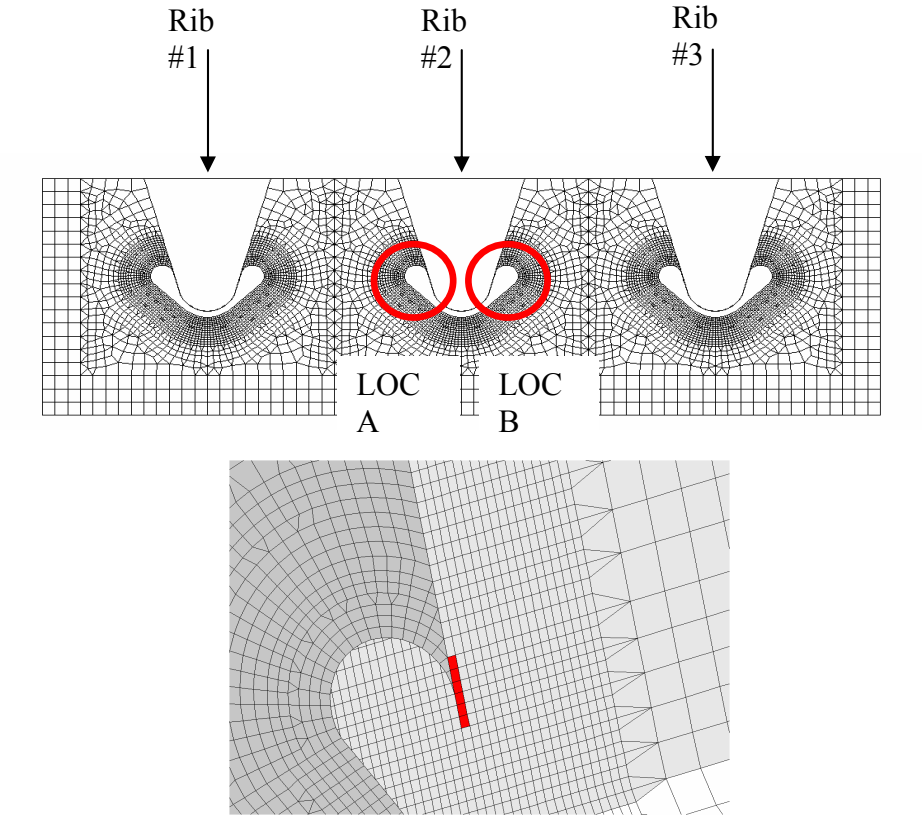

Figure 28. Finite Element Analysis Model of a typical Orthotropic Deck Rib in ANSYS

Figure 28 shows a local FEM analysis performed to evaluate the fatigue service stresses in the orthotropic deck ribs and the deck plate. The recommended details differ from the most current design details as follows:

- The interior diaphragm plate will be eliminated from the typical rib section
- A CJP weld will be specified for a length of 40 mm above the tangent point of the cutout
- The remaining weld will be specified as PJP with 5 mm penetration and 3 mm reinforcement.
- The cutout and the grinding cannot be eliminated. The analyzed fatigue stresses are such that a category B connection is needed to remain within AASHTO limits. A finish number will be specified with the grinding detail to ensure an adequate fatigue category.

Cross Beams

Various configurations were evaluated for the crossbeams. These configurations varied in terms of depth, width, spacing and detailing. The following give a brief summary of the alternatives evaluated:

- 3 m deep by 2 m wide spaced at 10 m: While it was aesthetically appealing to have the cross beams shallower than the box girder it was very difficult from a detailing point of view to have the flange of the cross beam frame into the middle of the box girder.
- 5.5 m deep by 2 m wide spaced at 10 m: While this alternative showed potential, it was not easy to detail the web connection between the cross beams and the floor beams which were not aligned
- 5.5 m deep by 5 m wide spaced at 30 m: This alternative solved the detailing conflicts presented by the previous alternatives; however the flanges of the cross beams were very thick which in turn required a thick deck plate (which was not acceptable)
- 5.5 m deep by 10 m wide spaced at 30 m: This alternative required a 22 mm thick flange and the transverse stresses in the box girder deck plates were acceptable. This alternative was selected for the design of the SFOBB-SAS.

Figure 29 shows a typical crossbeam section. As noted the crossbeam plates are stiffened box sections which are supported by transverse diaphragms spaced at about 3 m.

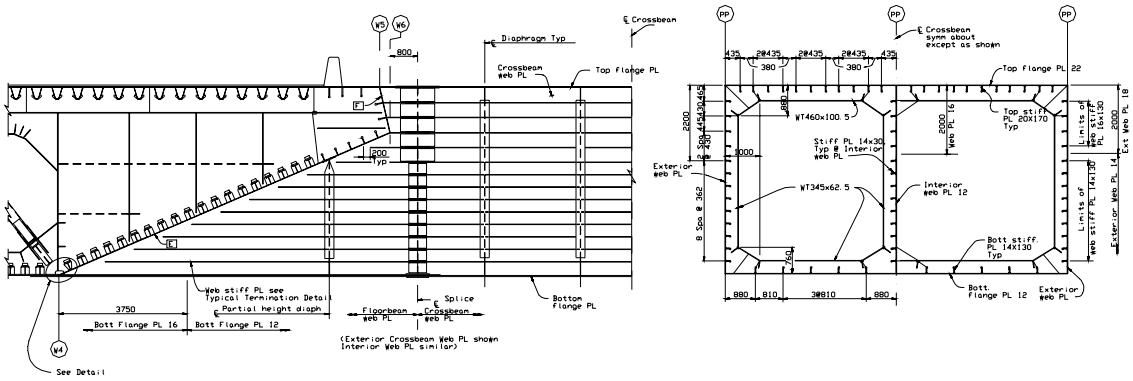

Figure 29. Typical Cross Beam Section

The connection between the crossbeam plates and the box girder plates required that one of these plates had to be discontinued. Local analysis of this juncture showed that it was more important to have the web plates of the cross beams continuous (and have a through thickness weld for the inclined face of the box girder), than to have the internal face of the box girder continuous. This was mainly due to the fact that the box girders were under compression while the crossbeams (and floor beams) were under tension during service loads. The flange plates of the crossbeams are bolted to the top and bottom box girder plates. Figure 30 shows the detail of the bottom bolted connection between the crossbeam and the box girders.

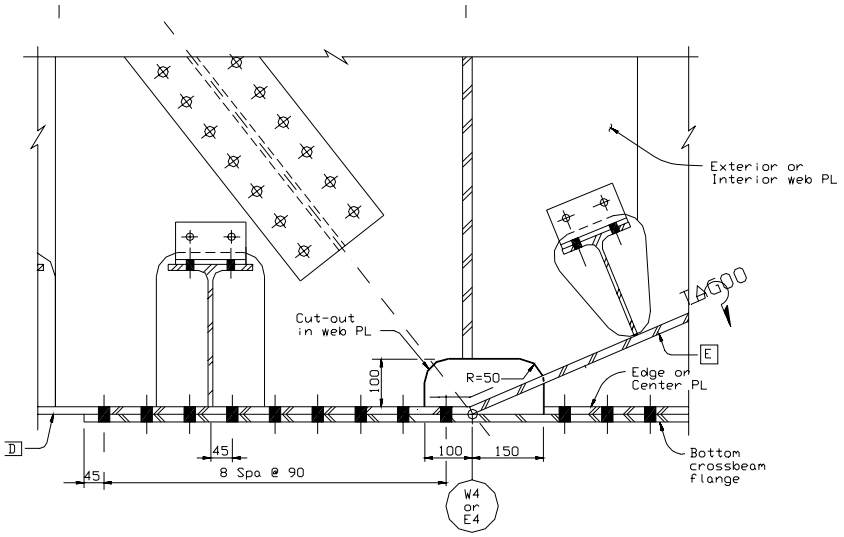

Figure 30. Cross Beam Connection to the Box Girders (bottom flange)

West Bent Closure Joint

The box girders frame into the West Bent as shown in Figures15 and 31. The mating between the steel and concrete at the Closure joint presented a series of design requirements for the design of this joint, these are:

- the joint is subjected to the box girder compressive forces (200 MN)
- the joint is subject to high bending moments about both axes due to seismic loads
- the joint must be designed to insure that it can resist the plastic hinge capacity of the West Pier (using overstrength materials)
- the orthotropic deck must be detailed to have a service design life of 150 years

Figure 31 shows the details of the West Bent Closure Joint. Additional prestress tendons are added around the perimeter of the box girders to insure that the joint moment capacity exceeds the box girder capacity. The box girder has a 38 mm thick bulkhead (reinforced with 45 mm thick by 2100 mm deep vertical stiffeners) to avoid local stresses due to carry shear lag. A series of vertical ribs are designed to carry the shear (without depending on the shear friction which is capable of carrying the entire shear).

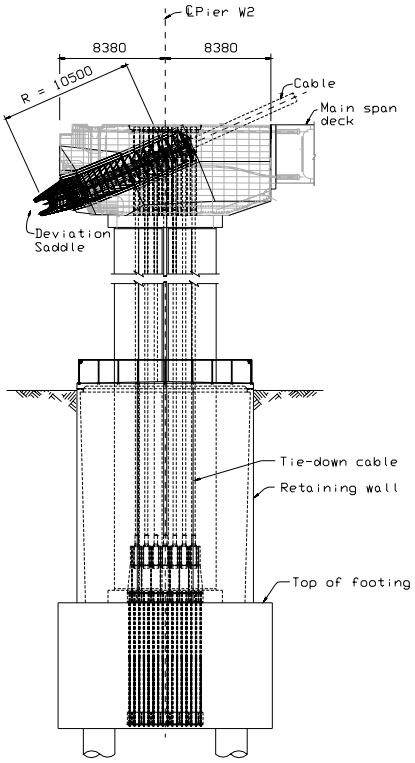

Figure 31. West Bent Closure Joint

SUSPENSION STRUCTURAL SYSTEM DESIGN

Structural System

As discussed earlier, various cable and suspender layouts were evaluated in the preliminary stages of design. These included:

- Multiple parallel cables with vertical suspenders (similar to traditional suspension bridges). This layout was used with the dual portal towers and the three legged tower alternatives.
- Mono-cable with a single line of suspenders at the bridge centerline. This layout was used with the single tower alternative
- A single cable which is anchored into the box girder at the eastern end and is looped around the west bent. This layout was used with the single tower alternative. In this design the suspenders are splayed to the exterior edge of the box girders.

The suspension structural system is comprised of the main cable, suspenders, west cable anchorage (cable loop) and east anchorage. The following sections present some of the salient features of the suspension structural system of the SFOBB-SAS.

Main Cable and Suspenders

The main design features of the cable are shown in Figure 32. The design of the main cable included the following main considerations:

- cable geometry
- allowable cable stresses
- cable construction method
- corrosion protection system

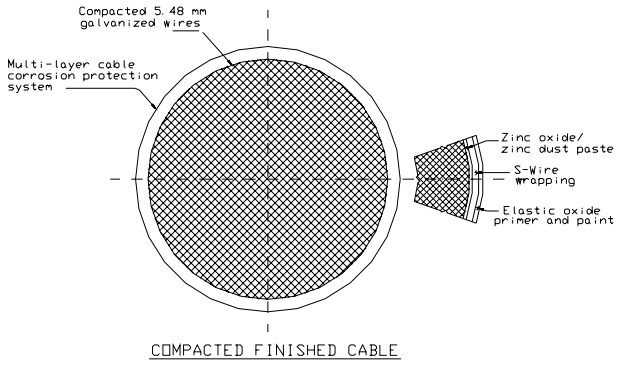

CABLE DATA @ 27° C	
Cable Diameter (20% Void Ratio)(m)	0.792
Steel Wire Diameter (mm)	5.4
Number of Wires	17399
Number of Strands	137
Number of Wires per Strand	127
Net Cable Area (Steel) (m^2)	0.39848

Figure 32. Main Suspension Cable

Due to the complex three-dimensional geometry of the cable, the trough orientations of the tower saddle, west anchorage deviation saddles and the east splay saddles are different. Large cable twist (in access of 90 degrees) will result if a conventional hexagon cable strand layout is adopted. This twist could lead to unacceptable strand tangling during cable construction, unacceptable secondary stresses and poor cable compaction. To address this problem, a modified

octagonal strand layout was developed. This layout eliminates most of the twist of the main cable by cutting 90 degrees off the total twist (Figure 33).

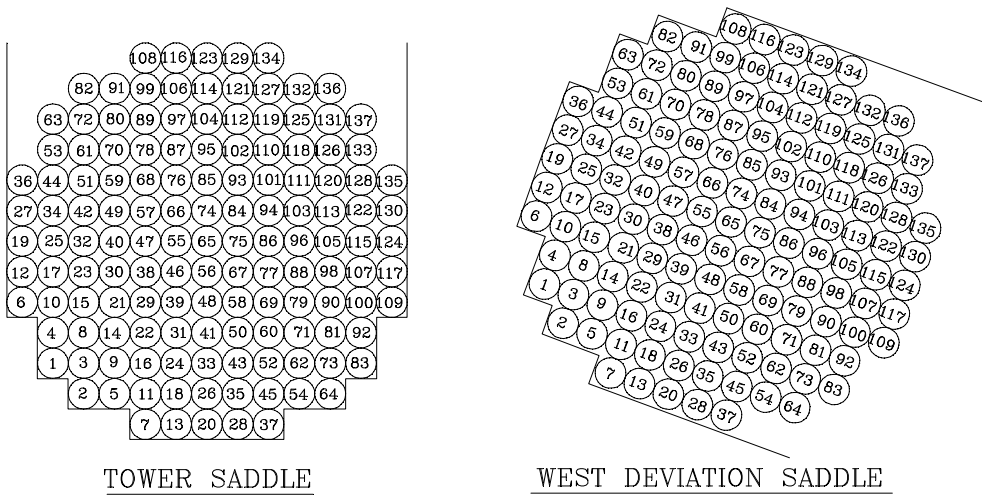

Figure 33. Tower Saddle and West Deviation Saddle Orientations

The cable is made of 17399 5.4 mm wires with an ultimate strength of 1760 MPa (Figure 32). The SFOBB-SAS design criteria give an allowable stress for this wire of 689 MPa. This allowable stress is much higher than the allowable stress of most "older" suspension bridges. This higher allowable stress is based on two factors:

- the capability to produce a much stronger wires relative to 50 years ago
- the state-of-the-art wire fabrication method which insures that there is minimal residual stresses in the wire

Both the Aerial-Spun Method (AS) and the Prefabricated Parallel Wire method (PWS) were studied for the construction of main cable. While the main cable can be erected using either method, the PWS method was recommended for the construction of the main cable. This recommendation is based on the fact that the PWS strands will result in a better cable in terms of strand manufacturing and cable erection; thus reducing the vulnerability of the wires to stress corrosion and water-induced corrosion. Using the PWS strands almost eliminates cross wires, provides a lower void ratio, produces a lower stress at the strand anchors and at the spliced ferrets; in comparison to a cable made up of individual wires and erected by the AS method.

A multi-layer corrosion protection system is recommended for main cable. This protection system consists of the following corrosion protective components:

- Zinc galvanization of each steel wire that composes the main cable
- Grease application to each individual cable wire during PWS manufacturing
- A paste composed of a blend of zinc oxide with zinc dust and a non-dry thermoplastic polymer base to protect the outer perimeter of the main cable
- S-wire wrapping
- Elastic Noxide primer and paint
- Dehumidification of the cable sections at locations of East Anchorage, West Loop Cable Anchorage, and the Tower Saddle.

Dehumidification of the entire cable may be recommended pending further evaluation of data on the use of this cable corrosion protection system.

The suspenders are made of galvanized steel wire structural rope with a metallic area ranging between of 3000 and 4460 mm2 (Figure 34)

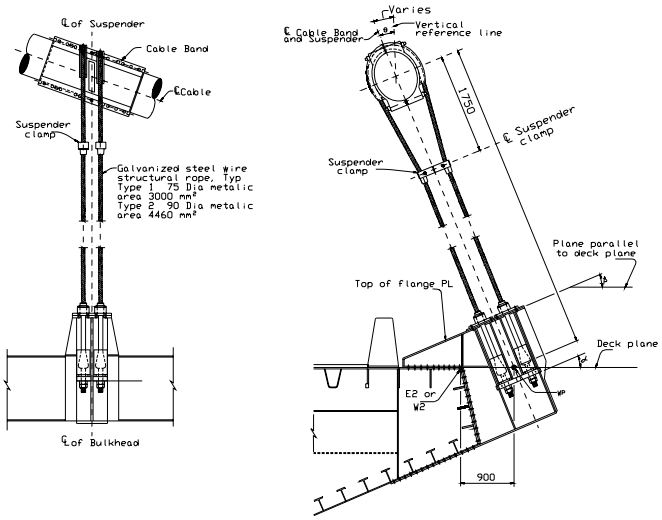

Figure 34. Typical Suspender Layout

West Anchorage (Cable Loop)

Various alternatives were evaluated for the West Anchorage, these are:

- *Deck Anchor:* In this alternative the cable is anchored inside the box girder to a grillage using anchor rods. This alternative is used in traditional self-anchored suspension bridges.
- *Tied-Down Cable:* In this alternative the cable deviated (turned downwards) and is anchored directly into a gravity foundation. The details to anchor the cable strands to the gravity footing are similar to typical suspension bridge anchorages.
- *Earth Anchor:* In this alternative the cable is anchored into a separate anchorage. This anchorage is similar to typical suspension bridge anchorages except for the fact that it would also be required to support the compressive forces that are in the box girder.
- Looped Cable Anchorage: In this alternative a single cable is used which is anchored at the East Anchorage and is looped around the west bent using deviation saddles.

The Looped Cable Anchorage was selected for the final design of Bay Bridge West Anchorage. The plan and a side elevation of this unique anchorage system are shown in Figures 35 and 15.

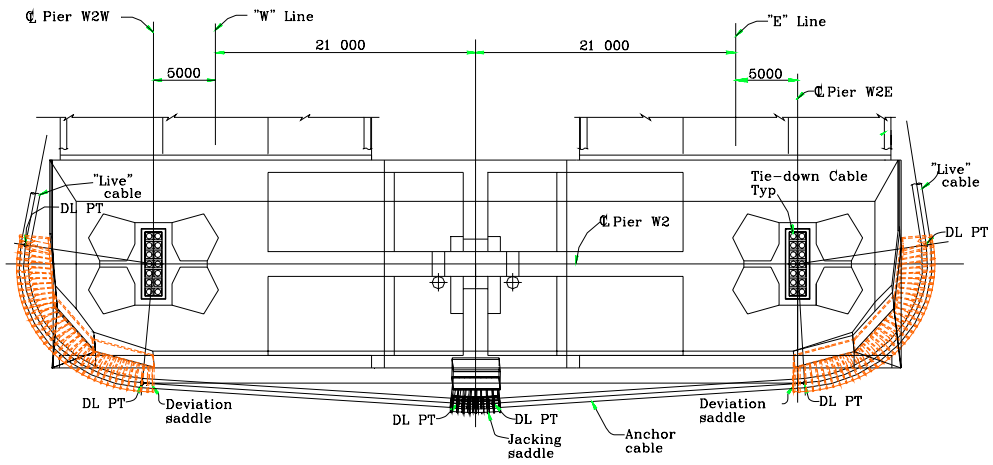

Figure 35. Plan of the Looped Cable West Anchorage

The Looping Cable Anchorage system essentially consists of a prestressed concrete frame bent, a looping anchor cable, two deviation saddles, a jacking saddle, and independent tie-down systems.

In this anchorage system, strands of the main cable are not splayed at the west piers. Instead, the cable is looped around the prestressed concrete cap beam. The cable looping is achieved using a pair of deviation saddles at the outer edges of both roadways, and a jacking saddle located at the rear center of the cap beam. The massive tension forces in the main cable are balanced by the distributed compression stress behind the deviation saddles. The three-dimensional compression thrusts behind the deviation saddles are resisted by bridge box girders in the bridge longitudinal direction, cap beam in the transverse direction, and cap beam gravity in the vertical direction. The independent tie-downs serve as redundant elements to resist the unbalanced vertical loading in the unexpected event that both east and west piers are severely damaged under a seismic action beyond the design SEE.

The merits of having fixed vs. sliding deviation saddles were evaluated for all load conditions including erection, service, and seismic events. Based on this evaluation, it was concluded that a fixed deviation saddle alternative combined with a jacking saddle best suits the overall performance and safety requirements of the SFOBB-SAS. The primary function of the jacking saddle is to jack the cable outward at critical deck erection stages such that the main cable forces in the “anchor cable” and “live cable” are balanced within the design limits.

East Anchorage

In the preliminary stages of the design of the East Anchorage three alternatives were considered, these are:

- *Center Anchorage:* In this alternative center line of the east anchorage grillage was aligned with the centerline of the box girder. This alternative was most appealing aesthetically, however it posed a challenge geometrically and structurally.
- *Side Anchorage:* In this alternative the cable was not deviated transversely and the centerline of the east anchorage grillage was external to the box girder. While this alternative was the simplest because it had the least interference with the box girder webs and did not require

complex analysis of the strand layout, it was not acceptable aesthetically since it required a 5m x 5m extension to the side of the box girder cross section at the East Anchorage.

- *Mid Anchorage:* In this alternative the center line of the grillage of the East Anchorage was placed such that it would have the least visual impact to the shape of the box girder while having less interference with the box girder webs.

The East Anchorage is shown in Figures 36 and 37. The cable is almost horizontal at the East Saddle which is supported on rollers to allow for movement in the plane of the cable. The saddle is in turn supported on specially designed bulkheads which are part of the crossbeam that connects the box girders at the East Pier. As the cable exits the east saddle towards the east anchorage a splay saddle is used to minimize the size of the required cutout in the box girder.

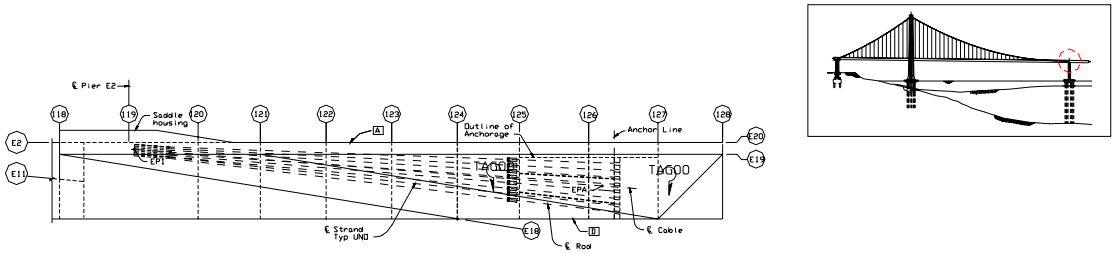

Figure 36. Elevation of the southern East Anchorage

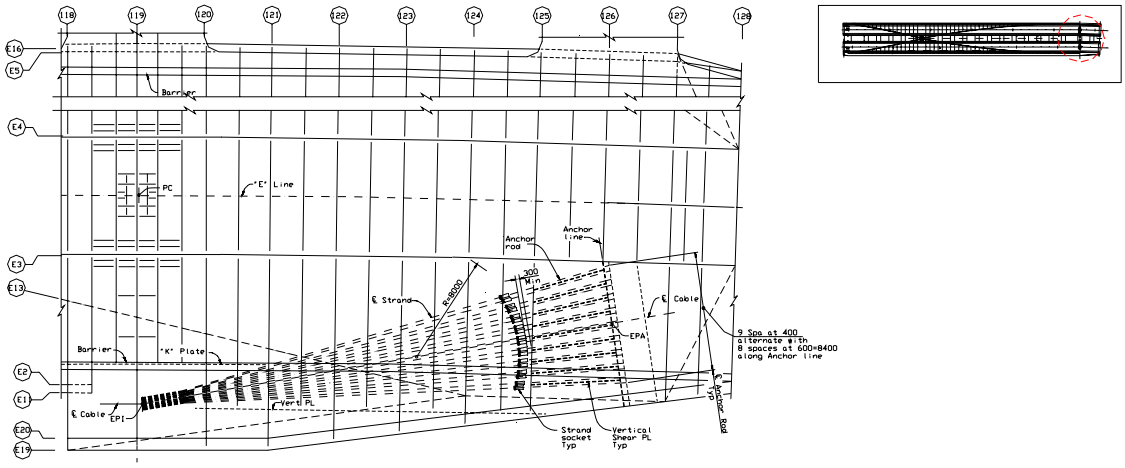

Figure 37. Plan of the southern East Anchorage Plan

The cable is then splayed out into 137 strands each of which is anchored into a grillage about 40m away from the east saddle. High strength anchor rods with cast steel sockets are used to anchor the strands into the grillage. The 137 strands are arranged in an array of eight rows and eighteen columns, allowing seven redundant spaces (Figure 38). The layout of the sockets has been determined to maintain the symmetry of reactions in an unsymmetrical box girder, and to allow the use of the same saddle casting for both “E” Line and “W” Line anchorages. At the east anchorage a specially reinforced crossbeam connects the two box girders. This cross beam carries the resulting tension that arises from the cable forces.

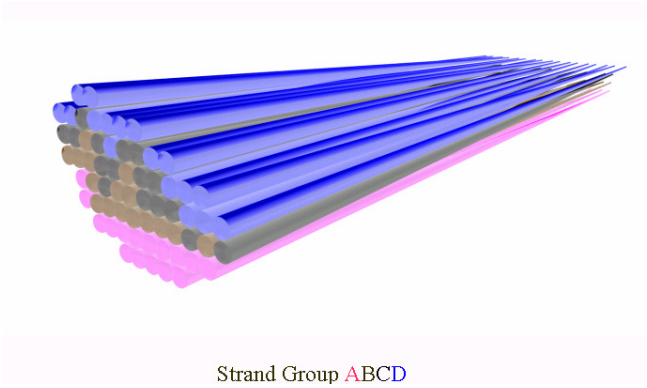

Figure 38. Schematic Cable Strand Layout at the East Anchorage

Figure 39 shows a three dimensional view of the finite element mesh used to evaluate the East Anchorage (note that the actual mesh size is not shown for clarity).

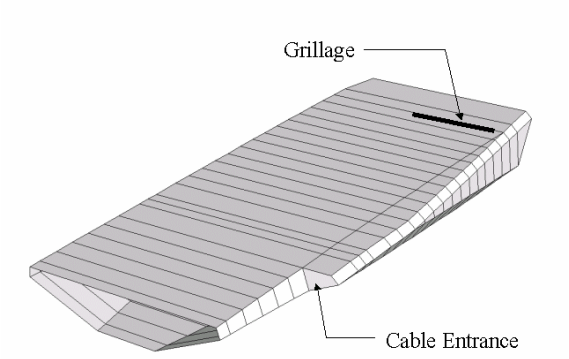

Figure 39. Finite Element Mesh for the East Anchorage using ANSYS

Figure 40 shows a schematic view of the East Anchorage with the Top Deck Plate Removed

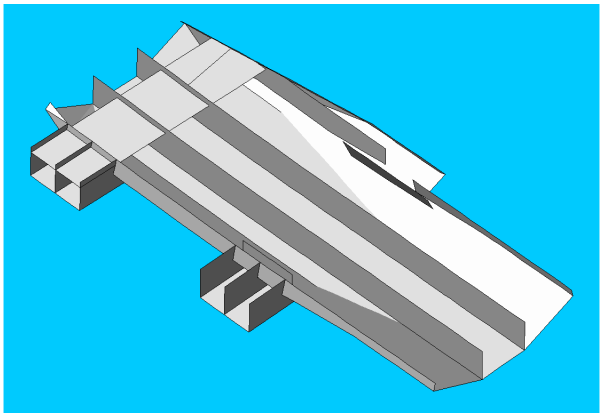

Figure 40. Finite Element Mesh for the East Anchorage using ANSYS

Tower Saddle

Given the cable layout and the single tower head geometry, various design alternatives were considered for the tower saddle, these are:

- *Two Separate Saddles:* In this design alternative prestress anchor rods would be used to carry the splitting forces in the north and south cables.
- Single Saddle *w/ Crossing Troughs:* In this alternative the troughs were designed such that the cables would cross over each other. This was mainly intended to reduce the cable splitting forces.
- *Single Saddle w/ twin troughs:* In this design the troughs were designed to be side by side with the saddle ribs designed to carry the vertical as well as the transverse cable force. Tower alternatives were evaluated for the orientation of the trough for this design.
    - *Inclined trough:* The troughs would be tilted to fall in the cable plane. This design would require a much larger saddle given the geometry of the cable.
    - *Vertical troughs:* The troughs would be vertical to avoid complex cable erection as well as to reduce the cable twist between the west deviation saddle and the tower saddle.

The single saddle with twin vertical trough was selected for the design of the tower saddle of the SFOBB-SAS, see Figure 41. This decision was based on the complex geometry of the cable, the limited space required for the saddle at the tower head, the cable erection method, cable twist and stress analysis.

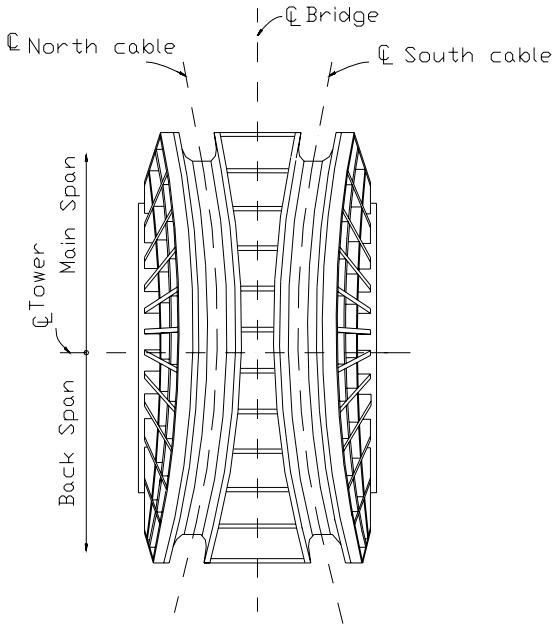

Figure 41. Plan View of the Tower Saddle

Figure 42 shows the stress contours due to the dead loads on the tower saddle. The maximum stress was limited to o.55 Fy during service loads and 0.9 Fy during seismic loads.

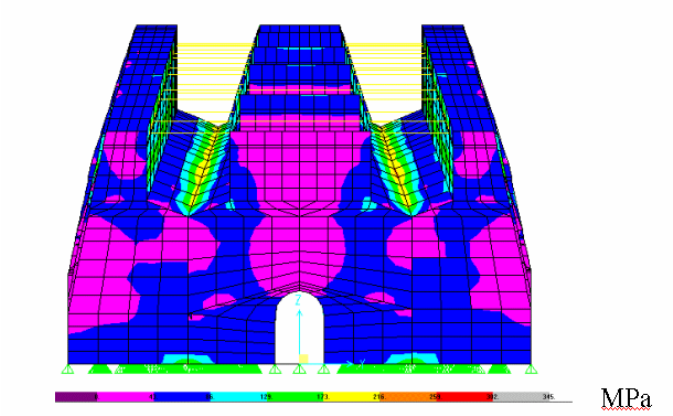

Figure 42. Finite Element Analysis Using SAP2000

SEISMIC PERFORMANCE

Analysis Methodology

Seismic analysis was performed using the ADINA general-purpose finite element program. Three forms of analysis were employed: time history analysis (global model), pushover analysis and local detailed analysis. Time history analysis was used as the primary means of analysis for several reasons. Foremost among these is that the bridge foundations are subjected to different excitations. The tower and west pier of the bridge are founded on rock while the east pier is supported in deep soil. The ground motions at these supports are completely different in character and intensity. This was reflected in the analysis by applying different time histories of ground displacement at the supports. A large displacement analysis and the use of nonlinear material where necessary to allow the designers to capture the true behavior of the bridge (geometric stiffness of bridge, P-delta effects, slacking of suspenders, plastic hinging of piers, tower shear links, etc.). The model was ”built” in a single step, in the dead load state. Initial strains in the deck, cables and suspenders were applied in this single step rather than simulating the construction sequence of the bridge. Time history analyses were done as restart analyses from the dead load state. Push Over analysis was primarily used to evaluate ductility of critical elements and to establish failure mode sequence. Local detailed analysis was used to establish local strain/stress demands and to evaluate the modeling used for the global model.

Site Conditions and Seismicity

The Bay Bridge lies between the Hayward and the San Andreas faults which are capable of producing magnitude 7.5M and 8M earthquakes, respectively. The proposed bridge alignment is underlain by variable subsurface conditions. While the west pier sits on Yerba Buena Island and the tower is located on relatively shallow sloping bedrock, the east piers and the remainder of the skyway will be founded in deep soils. Spectrum compatible ground motions were generated for this site (three for Hayward and three for San Andreas). Figure 43 illustrates the fault normal spectral accelerations for San Andreas ground motion number 3. As noted, the character of these motions is very distinct.

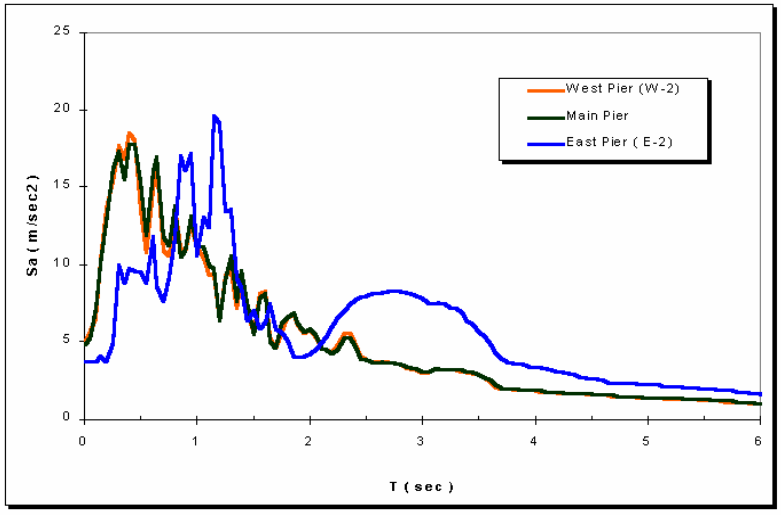

Figure 43. Fault Normal Response Spectrum of the San Andreas Ground Motion No. 3

Description of the Analysis Model

The ADINA global model of the Self-Anchored Suspension Bridge is shown in Figure 44. In addition to the main span structure, the model includes boundary frames representing the skyway and the transition structure on Yerba Buena Island. The model is largely inelastic and consists of nonlinear truss and beam elements. The bridge deck is modeled with two parallel spines of beam elements representing the axial, bending, and torsional properties of the suspended structure. Stiff beam elements extending to the edge of the bridge deck provided nodes for connection of the suspenders (these elements captured the deck stiffness for vertical deformations and were rigid for transverse deformations). The suspenders were modeled with several truss elements in series. This was done to allow the suspenders to go slack during the time history analysis (large displacement formulation).

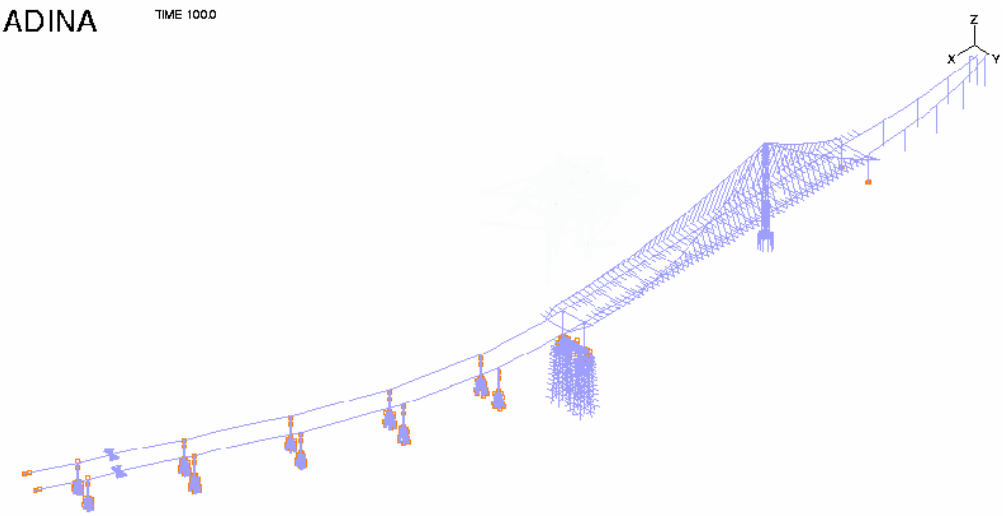

Figure 44. Adina Model of the Suspension Bridge

The dead load stress in the main cables and suspenders was modeled by means of an initial strain applied when the model was built. The tower shafts were modeled with nonlinear beam elements. The shear links between the shafts were also modeled with inelastic moment-curvature beam elements. The yield moment of these elements was set to obtain the desired plastic shear capacity of the links. The rotation of the beam plastic hinges serves as a measure of the shear deformation of the links. Each pile in the tower foundations was modeled directly with several nonlinear beam elements from the bottom of the pile cap to the rock surface. The ground motion was applied directly to the bottoms of the piles assuming the piles to be fixed at the rock surface. The mass of the foundation was lumped at a node at the center of gravity of the pile cap. The east and west piers were modeled with nonlinear beam elements. The west pier was assumed to be founded on rock and the ground motions were applied directly to the bottom of the pier.

The east pier piles were modeled using nonlinear beam elements which modeled each pile from the pile cap to the pile tip. Each pile was supported with nonlinear p-y and t-z springs along its height. The model also included t-z dampers to account for viscous damping. Depth varying ground motions were applied to the p-y and t-z springs of the piles.

Seismic Response

As discussed earlier the bridge is designed based on a limited ductility design in which plastic deformations are clearly defined and predetermined. Figure 45 summarizes the seismic response of the bridge. As noted the bridge is designed to remain largely elastic with the exception of the east and west piers which are designed to form plastic hinges. The plastic strain in these piers is limited to 2/3 the ultimate strains based on Manders equation for confined concrete columns. The shear links between the tower shafts are also designed to yield in shear during the SEE earthquake. The maximum rotation demand on these links is 0.03 radians compared with an ultimate rotation of 0.09 radians. The piles were designed to sustain minimal damage (strains less than 0.01 for concrete and 0.02 for steel) when subjected to the SEE displacement demands. The tie down at the west pier was designed with a factor of safety of two. Figure 46 summarizes the displacement demands on the bridge. The bridge is a long period structure and is mainly in the region of constant displacement demand. This improves the reliability of the structural response.

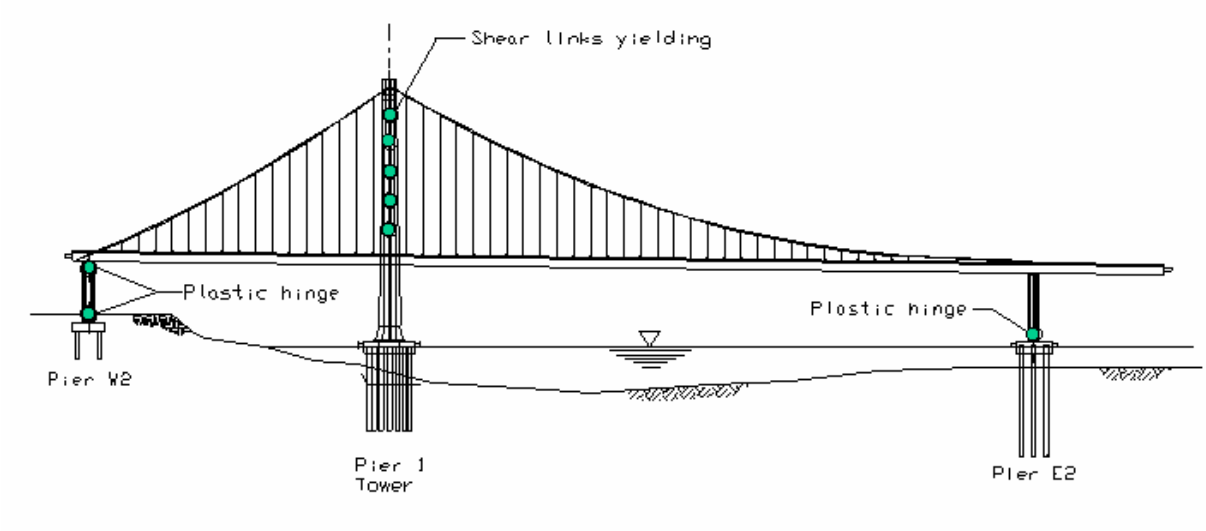

Figure 45. Seismic Response of the Bridge

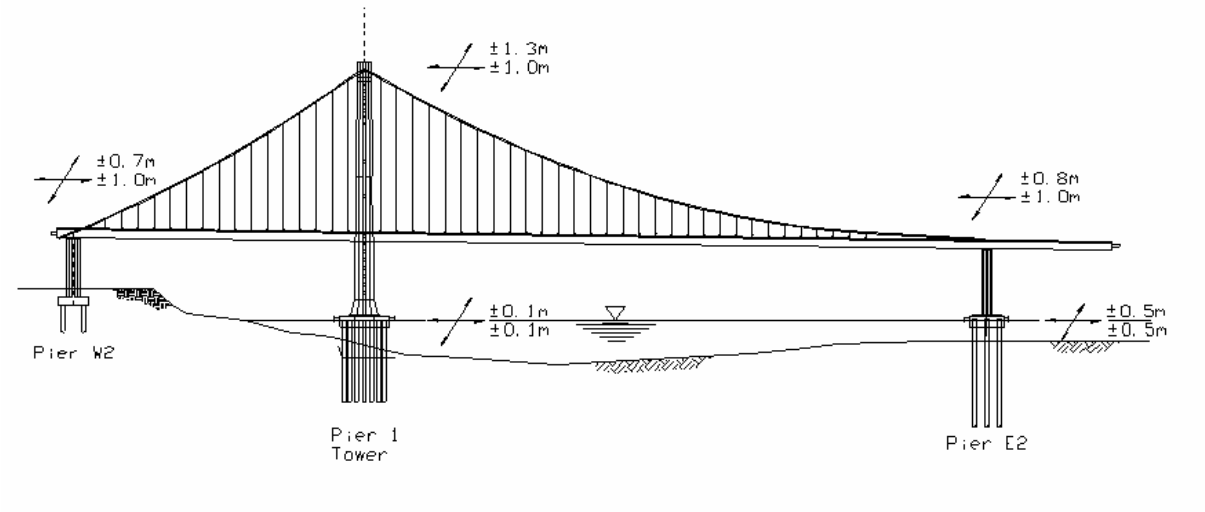

Figure 46. Seismic Displacement Demands

PROJECT STATUS

The San Francisco-Oakland Bay Bridge Self Anchored Suspension Bridge is currently at the 85% Design Stage. It is expected to go out for bid in mid year 2002.

ACKNOWLEDGEMENTS

The authors would like to acknowledge the invaluable contribution of the California Department of Transportation personnel, namely: Denis Mulligan, Brian Maroney and Ade Akinsanya.

REFERENCES

(1) The San Francisco-Oakland Bay Bridge East Span Seismic Safety Project, 30% Design Report, May 11, 1998—Prepared by TYLin International – Moffatt & Nichol Joint Venture – Prepared for the State of California Business, Transportation, and Housing agency.
(2) The San Francisco – Oakland Bay Bridge East Span Seismic Safety Project, Supplement to Final 30% Design Report, June 22, 1998 – Prepared by TY Lin International – Moffatt & Nichol Joint Venture – Prepared for the State of California Business, Transportation, and Housing Agency
(3) Design Criteria of the San Francisco-Oakland Bay Bridge East Span Seismic Safety Project (1999), TY Lin International – Moffatt & Nichol Joint Venture
(4) First Annual Progress Report San Francisco-Oakland Bay Bridge, July 1934
(5) Fugro/EMI Geotechnical & Seismic Report May 1999
(6) Vulnerability Reports on the Seismic Performance of the Existing East Span of the San Francisco Oakland Bay Bridge, California Department of Transportation
(7) Design of the New San Francisco-Oakland Bay Bridge, Rafael Manzanarez et al, 16th International Bridge Conference, Pittsburgh Pennsylvania, 1999.
(8) Seismic Design Strategy for the New San Francisco-Oakland Bay Bridge Suspension Span, Marwan Nader et al, 12th World Conference on Earthquake Engineering, New Zealand, 2000.
(9) Design Concepts of the New San Francisco-Oakland Bay Bridge, Man-Chung Tang et al, 17th International Bridge Conference, Pittsburgh Pennsylvania, 2000.
(10) Design of the Superstructure of the New San Francisco-Oakland Bay Bridge Self-Anchored Suspension Bridge, George Baker et al, 17th International Bridge Conference, Pittsburgh Pennsylvania, 2000.
(11) Design of the Substructure of the New San Francisco-Oakland Bay Bridge Self-Anchored Suspension Bridge, Marwan Nader et al, 17th International Bridge Conference, Pittsburgh Pennsylvania, 2000.
(12) AASHTO LRFD Specifications for Highway Bridge Design, 2nd Edition, 1998
(13) ATC-32, Improved Seismic Design Criteria for Californmia Bridges, Provisional Recommendations, Applied Technology Council, 1996
(14) AISC Manual of Steel Construction, Load and Resistance Factor Design, 2nd Edition, 1998
(15) BDS, Caltrans Bridge Design Specifications Manual, 1995
(16) ADINA, Automatic Dynamic Incremental Nonlinear Analysis, ADINA R&D Inc, Watertown, MA
(17) SAP2000, Structural Analysis Programs, Computers and Structures Inc, Berkeley, CA

Seismic Retrofit Strategies for Substandard Single-Column Bents Supported on Pedestals

Nathan Johnson[1], M. Saiid Saiidi[2], and Ahmad Itani[3]
Civil Engineering Department, University of Nevada, Reno

ABSTRACT

The ramp structures of a major freeway bridge in Las Vegas, Nevada, are supported on octagonal columns, many of which are supported on pedestals with one-way hinges at the pedestal base. Because the bridge was designed in the late 60's, its members lack the necessary details that are needed to withstand strong earthquakes. This study focused on the development of retrofit methods for these piers. Three identical quarter-scale column specimens were built for shake table testing. One column was tested in the as-built form while the others were tested after they were strengthened. The columns were subjected to the 1994 Northridge Sylmar earthquake in the strong direction until failure. The pedestal in the as-built column cracked vertically even under small earthquakes. Under larger motions, the column and the pedestal separated and no longer acted as integral members. The damage in the column above the pedestal was minimal. It was felt that the pedestal needs substantial strengthening. The first of the retrofitted columns was tested with a pedestal extension and glass fiber reinforced plastic (GFRP) used as additional pedestal reinforcement. The second was tested with the same retrofit as the first but several of the column bars were severed at the base of the column to reduce plastic shear demand. It was determined that the pedestal retrofit was successful to strengthen the pedestal sufficiently to shift the plastic hinging into the column. The severed column bars lowered the plastic shear demand and increased the plastic deformation. Results led to retrofit design recommendations that included the experimentally verified methods.

1. PhD Candidate
2. Professor
3. Associate Professor

INTRODUCTION

Recent earthquakes in California (1994 Northridge earthquake), Japan (1995 Kobe earthquake), and Turkey (1999 Izmit earthquake) have generally shown response of retrofitted bridges to be successful. However, many seismically deficient bridges still remain. Because of the strong nature of bridge superstructures, the substructure is expected to be the primary outlet for dissipating seismic energy. Substructure deficiencies for concrete bridges include the column shear strength, confinement, and structural detailing. These deficits usually cause non-ductile and unexpected modes of failure. Though methods to address typical insufficiencies have been developed, retrofit methods are still lacking for unusual details.

The main issues concerning this study are column retrofit, pedestal retrofit, and performance of one-way hinges. Extensive research has been done in the field of column retrofit. However, limited work has been conducted on one-way hinges, and no available literature addresses seismic retrofit of octagonal columns or columns with pedestals.

PROTOTYPE SELECTION

The primary objective of this study was to identify seismic vulnerability and develop retrofit strategies for single-column piers in three ramp structures that are part of the 24-span Las Vegas Downtown Viaduct, a freeway bridge in Las Vegas, Nevada. The most critical structure was Ramp DW. The structure was built in the late 1960's when seismic detailing was not considered. Ramp DW is a reinforced concrete box girder structure containing six single column bents with octagonal columns. Four of the six columns are supported on a pedestal with a one-way hinge at the pedestal base. Others are directly connected to the footing with a one-way hinge at the column base. Both the pedestals and columns were found to be highly deficient with respect to lateral steel. The mean unconfined compressive strength of the concrete based on cylinder tests in 1968 during construction was 33.8 MPa (4900 psi). Considering the over strength of the concrete to current times, a compressive strength of 41.3 MPa (6000 psi) was assumed. The reinforcing steel had an average yield and ultimate stress of 303 MPa (44 ksi) and 524 MPa (76 ksi), respectively.

Selection of the prototype column for testing was based on susceptibility to shear failure in the strong direction. The prototype column was the shortest of the columns with a pedestal at the base. The total height from top of footing to superstructure centerline is 7.04m (23.1 ft). The column height above the pedestal is 5.21 m (17.1 ft) providing an aspect ratio in the strong direction of approximately 2. Based on current AASHTO (Ref. 1) guidelines, all development lengths in the column are adequate. According to current Caltrans (Ref. 2) and AASHTO guidelines, the column confinement inside the plastic hinge region is deficient by 87% and 74%, respectively.

Lateral force demand and capacities of the prototype were calculated for shear and flexure. Shear capacities were calculated from Caltrans Seismic Design Criteria equations (Ref. 2). Caltrans equations for nominal shear capacity are based on axial load and displacement ductility. The axial load on the column was based on the superstructure tributary loading. For ductility up to 1.5 the Shear Capacity is approximately 4960 kN (1120 k). For ductility greater than 4.2 the Capacity is approximately 1410 kN (320 k). Between a ductility of approximately 1.5 and 4.2 the concrete shear capacity varies linearly with ductility. Before testing the column it

was not known how well the Caltrans equations would apply to an octagonal column with very small lateral steel. The values obtained from Caltrans equations were noted and compared the plastic shear demand at the base of the column and the base of the pedestal. These values are 3870 kN (870 k) and 3287 kN (739 k), respectively. Assuming flexural failure, the first yield is at the pedestal base, followed by yielding at the base of the column, then failure at the pedestal base

TEST SPECIMENS

Three identical quarter-scale as-built specimens of column 8DW were created for shake table testing. One specimen, OLVA (octagonal Las Vegas column, as-built) was created for as-built testing, the other two for retrofit testing. The specimens were designed to be as large as possible and possess material and geometric properties very similar to the prototype. The scale was governed by the capacities of the shake table. Moment-curvature analysis was performed on flexural sections to assure the response of the specimen matched that of the prototype. Details of the specimen are shown in Fig. 1. The footing of the specimens was designed to be strong and stiff to avoid footing damage. The longitudinal bars from the pedestal to the footing were sufficiently embedded for full development.

The material properties for the scaled specimen were very similar to that of the prototype. The concrete had a 9.5 mm (3/8 in) maximum aggregate size and a 28-day strength of approximately 39.3 MPa (5700 psi). The longitudinal steel used in the column and pedestal was annealed to match the steel properties of the prototype. Due to the unavailability of Grade 40 steel in #3 bar, Grade 60 steel was used and subjected to heat ramps to obtain the target yield stress of 303 MPa (44 ksi).

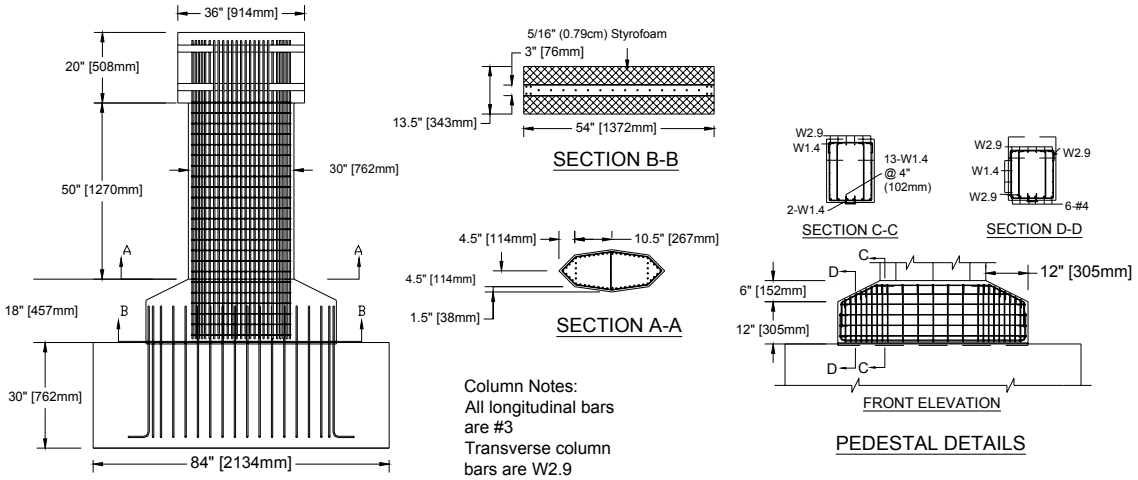

Figure 1. Details of as-built specimen.

INSTRUMENTATION

Instrumentation was nearly the same for all of the specimens. Full details of the instrumentation layouts are presented in Ref. 3. The specimens were extensively instrumented

with strain gauges, displacement transducers, load cells, and accelerometers. The data were recorded at a rate of 160 samples per second.

Strain gauges for the longitudinal steel were placed at the two critical sections, the column to pedestal, and the pedestal to footing connections. Gauges were also placed at 12.7 cm (5 in) above and below these sections to measure bar pullout and strain variation. Strain gauges were placed on the column ties at 14.0 cm (5.5 in) level increments from the top of the pedestal to approximately one column depth above the pedestal.

Column curvature, pedestal uplift and horizontal pedestal slippage were measured with displacement transducers. For pedestal slippage and uplift, transducers were located on both sides of the weak and strong axis of the pedestal. For curvature measurement, transducers were located in pairs at five 12.7 cm (5 in) intervals from the base of the column on either side of the strong axis of the column.

Displacement transducers were used to measure column displacements in the direction of testing and in the transverse lateral direction. Load cells measured the column axial loads and the link force between the column and the inertial mass on the mass rig. Acceleration was measured by an accelerometer at the top of the stub head and by the internal table accelerometer.

TEST PROCEDURE

A drawing of the shake table setup is shown in Fig. 2. Scaled masses of the tributary loading on the actual structure were applied through an inertial mass rig and vertical hydraulic jacks. The mass rig design is covered in Ref. 5. The hydraulic jack system was two jacks connected in series to an accumulator and pump. Hydraulic jacks supplied the axial load to the specimen through a steel spreader beam bolted to the top of the column. The axial load rods went through the footing and were bolted into the table. An axial load of 218 kN (49 k) was applied to the specimen with the jacks, which produced the same level of axial stress as that of the prototype. A steel frame for lateral stability was included to test the retrofitted columns because of the large out of plane movement observed in OLVA due to damage of the pedestal. Use of stability frame was important because a significant transverse deflection during the tests could have required testing to end prematurely.

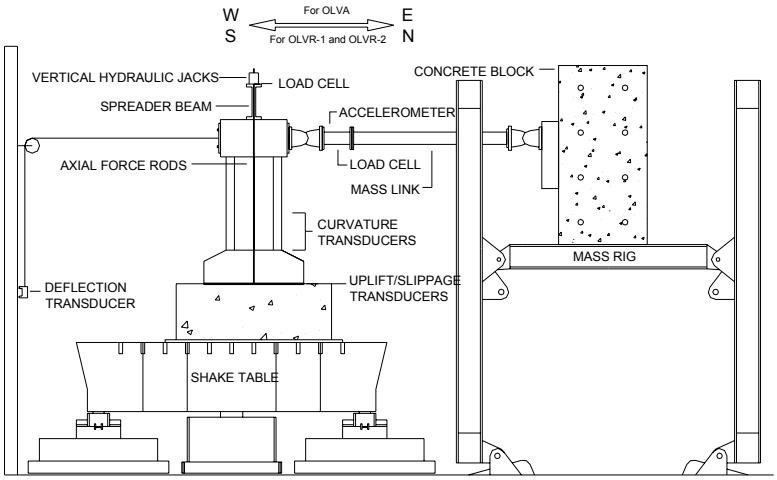

Figure 2. Shake table test setup.

The acceleration record used to drive the shake table was the 90-degree component of the 1994 Northridge earthquake as recorded at the Sylmar Hospital parking lot. The Sylmar record was chosen because through preliminary analysis it was established that the Sylmar record would demand the largest ductility on the column. It is also representative of an earthquake in the western United States, and is widely used in structural research. The record was applied to the

columns in 0.25x acceleration increments until failure. To scale the acceleration record for use on the specimen, the timescale of the record was compressed by the square root of 0.25 for the quarter scale dimension and the square root of fraction of inertial load over axial load. The timescale adjustment for a small difference of inertial and axial load was required because the mass rig blocks could only be added in 89 kN (20 k) increments. The timescale used for testing was 0.476.

TEST RESULTS

As-Built (OLVA)

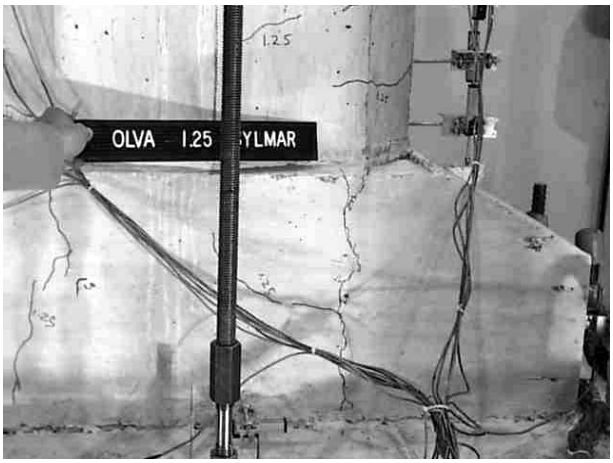

Figure 3. As-built column after 1.25xSylmar.

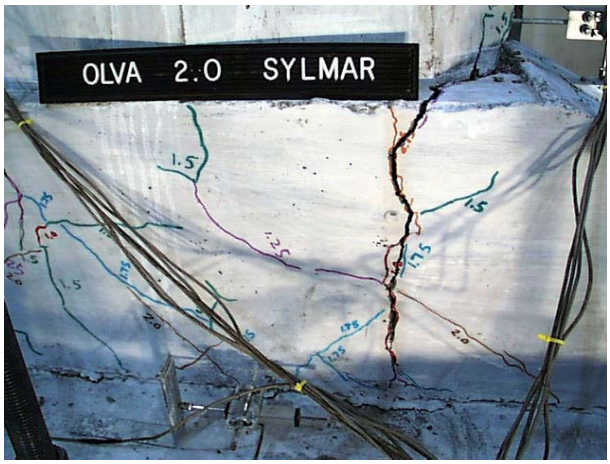

Figure 4. As-built column after 2.0xSylmar.

Very little damage could be observed in the column until 0.75xSylmar when vertical pedestal cracking began on the east side of the column in line with column edge. During the 1.0xSylmar test, the vertical cracks propagated to the top of the pedestal and connected out of plane. At 1.25xSylmar the vertical pedestal cracks became more pronounced (Fig. 3) and could be seen on all sides of the column. Also at 1.25xSylmar, flexural cracking began to show on the east side of the column. Additional vertical and horizontal cracks were developed mostly in the pedestal in subsequent runs. Figure 4 shows the failure crack pattern at the end of 2.0xSylmar (failure). The most severe cracks were the vertical pedestal cracks that had initiated during 0.75xSylmar. It appeared that the side stubs of the pedestal had separated from the column. Severe out of plane displacement could be seen in the column after 2.0xSylmar.

The column tie bars recorded a maximum strain of 630με. This strain level is far below the measured yield strain of 1380με. No diagonal tension cracks were observed in the column indicating that the shear performance was adequate. The embedment lengths of the column bars into the pedestal and the footing bars into the pedestal meet the current code requirement. Because the pedestal has a small amount of steel for confinement, and cracking of the pedestal was observed, this was still an area of concern. Load-strain envelopes at the pedestal-footing interface showed yielding of longitudinal bars at 0.75xSylmar and increased strains in subsequent runs indicating that the bars did not pull out.

The main concern with pedestal cracking is that it began at the relatively small amplitude of 0.75xSylmar (0.45 g). The amplitude of 0.75xSylmar only caused a displacement ductility of

0.63. The large cracking at 1.25xSylmar (0.76 g) happened at a displacement ductility of 1.46. Both of these values are relatively small when compared to the overall ductility capacity of 6.9. The column pedestals in the ramp structure are below ground. This leads to a possibility of damage not being detected during inspection. Undetected cracking of the pedestal and exposure of steel to moisture even under a small earthquake would lead to corrosion and further pedestal deterioration.

RETROFITTED SPECIMENS

Based on shake table testing of OLVA, it was determined that the primary deficiency of the as-built column is in horizontal pedestal reinforcement. Other deficiencies of the as-built such as shear and confinement did not surface from the tests. Two retrofit methods were attempted on two additional specimens, OLVR-1 (for octagonal Las Vegas column, retrofit 1), and OLVR-2 (for octagonal Las Vegas column, retrofit 2). In OLVR-1, only the pedestal was retrofitted, whereas in OLVR-2 both the pedestal and the column base were retrofitted.

Retrofit 1 (OLVR-1)

Retrofit Design

OLVR-1 was the first of two columns for retrofit testing. The retrofit applied to OLVR-1 was designed to strengthen the pedestal in its long direction to make it work as an integral part of the column. The pedestal retrofit design consisted of two stages. The first was to extend the pedestal, increasing the moment capacity of the pedestal base to assure a diversion of failure into the column. The second was to laterally reinforce the pedestal to provide sufficient pedestal strength for preventing pedestal separation from the column. To calculate the design force for the required lateral pedestal reinforcement, a two-dimensional strut-and-tie model (Ref. 6) of the column that included an extended pedestal was created. To account for variability in lateral force demand after retrofit, a safety factor of 1.5 was applied to determine the design force.

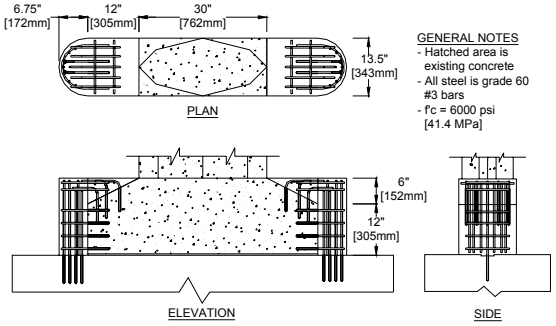

Figure 5. Pedestal extension plans.

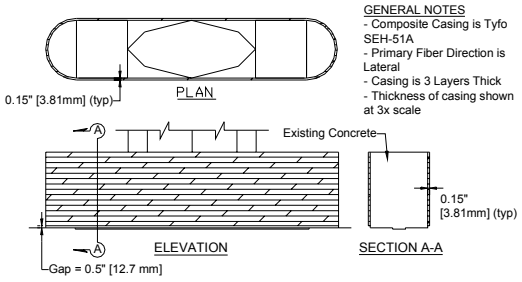

Figure 6. Pedestal wrap plans.

Extension of the pedestal was designed in two phases. The first was to design overlays to level out the pedestal stubs with the top of the pedestal. This was needed because the ends of the as-built pedestal are only 2/3 the height of the pedestal at the column-pedestal interface where cracking occurred. The shear friction method was used to design the reinforcement for the overlays. The second phase was to design a semicircular extension of the pedestal. The purpose

of the extension was to provide sufficient capacity in the strong direction of the one-way hinge to prevent failure at the pedestal base. The extension also needed to preserve the weak direction hinge response. A semicircular extension of the pedestal ends with a diameter equivalent to the pedestal width was determined to be the best solution. The bar configuration selected provided a failure safety factor of 1.35 for the lateral force demand at the column base. This was sufficiently larger than the as-built column safety factor of 0.84. Plans resulting from the design process are shown in Figs. 5 and 6.

Design of the lateral pedestal reinforcement was based on a GFRP fabric by the Fyfe co. called Tyfo SEH-51. It is a unidirectional fiber and was applied to the pedestal oriented in the horizontal direction. The design was based purely on a tensile force applied to the layers on each face of the long direction of the pedestal. Design values were based on Caltrans Memo to Designers (Ref. 2) and Federal Highway Specifications (Ref. 7). The values are for 0.6% strain and 75% of the specified modulus of elasticity. A permissible strength was calculated from these design values and used to determine the required number of layers. The design ultimate strain, however, was reduced to 0.4 percent to prevent excessive expansion and reduce crack width of the pedestal. The required number of layers was 2.85, leading to three layers in the actual retrofit (Fig. 6).

Test Results

No damage was observed in OLVR-1 until 0.75xSylmar when flexural cracking began to appear on the south side of the column. Flexural cracking steadily increased throughout the lower two-thirds of the column until 1.25xSylmar. During 1.5xSylmar, shear cracks began to appear on both sides of the column. From 1.75xSylmar to 2.25xSylmar, the shear and flexural cracks both expanded and widened steadily. At 2.25xSylmar, spalling was observed at the base of the north side of the column. The number and length of shear cracks continued to increase during 2.5xSylmar and the cracks propagated to the base of the column. During 2.75xSylmar the column failed in shear (Fig 9).

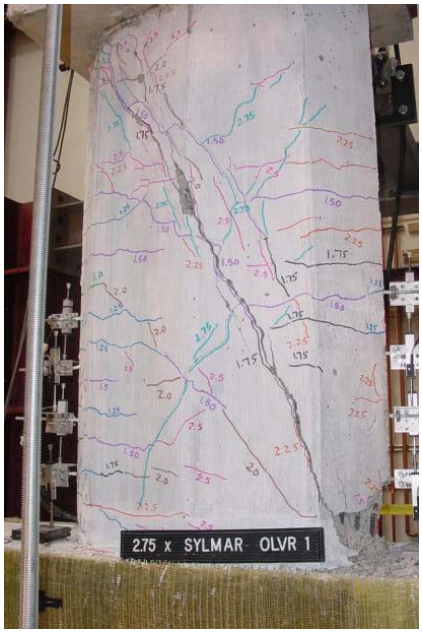

Figure 7. OLVR-1 after 2.75xSylmar.

The performance of OLVR-1 was evaluated to determine if the retrofit was effective and what actions if any would be needed to further modify the column performance. The GFRP provided adequate reinforcement to keep the column and pedestal integrated. Strains in the longitudinal direction of the jacket only reached 75 percent of the design strain. Restraining the column to the pedestal allowed all of the longitudinal pedestal steel to play a role in flexural resistance. Despite the larger forces that OLVR-1 was subjected to when compared to OLVA no signs of anchorage problems were shown. At both the pedestal-footing and the column-pedestal interfaces the bars were able to reach strains well beyond their yield point.

Because the pedestal in OLVA acted as a fuse, no signs of susceptibility to column shear damage could be seen in OLVA. In OLVR-1, the pedestal was strengthened, allowing the column to be subjected to much larger forces. Shear cracking began in OLVR-1 during 1.5xSylmar at a displacement ductility of only 1.7. Yielding of the lateral steel was measured during 2.0xSylmar. Because the shear demand on the column was greater than the capacity the the poorly reinforced column could provide, the column failed in shear during 2.75xSylmar The shear failure of OLVR-1 caused the column to reach a displacement ductility of only 4.6, approximately 34 percent lower than the ductility capacity of the as-built specimen OLVA. The pedestal retrofit was a success because it brought plastic hinging into the column. A ductile plastic hinge was indeed formed in the column. However, the low ductility capacity and increase of shear demand indicated that the retrofit required improvement. This was the consideration for the retrofit of OLVR-2

Retrofit 2 (OLVR-2)

Retrofit Design

Priorities for the retrofit of OLVR-2 included increasing column ductility and lowering the column plastic shear demand to that of the as-built. Given that no pedestal damage was seen in the retrofit of OLVR-1, efforts to retrofit column response were undertaken. Two options and a combination of the two options were considered. The first was to sever some of the bars at the base of the column to lower the shear demand and to increase ductility. The second was to apply a jacket to the column for an increase in shear capacity. Both of these options were to include the retrofit of the pedestal as it was applied to OLVR-1. For the retrofit of OLVR-2, it was decided to try to increase ductility without placing a jacket on the column by severing some of the longitudinal steel at the column base. Satisfactory performance of the model column without a jacket could reduce the retrofit cost in the actual bridge significantly.

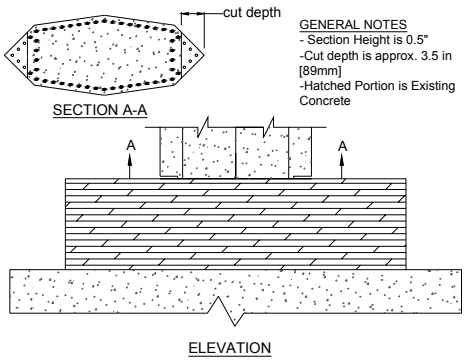

Figure 8. Plans for column cut.

To reduce the plastic shear demand, it was decided to reduce the cross section of the column immediately above the pedestal. This was accomplished by severing some of the extreme bars and removing the associated concrete. A configuration with 10 bars severed at the ends of the column was chosen because it provided a safety factor of 1.3 for the shear strength of OLVR-1 without cutting too far into the column. The gap thickness of the cut was 12.7 mm (0.5 in), which was calculated by plastic rotation at failure. Plans for the cut are shown in Fig. 8.

Test Results

Cracking of OLVR-2 began during 1.0xSylmar in the form of flexural cracks on the north and south sides of the column base. During 1.25xSylmar, the flexural cracks increased, propagating through the depth of the column. Also, diagonal cracks formed in the region of the cuts at the base of the column. At 1.5xSylmar, flexural cracks increased and were spread

throughout the lower half of the column. A diagonal shear crack began to form in the upper half of the column. The 1.75xSylmar run caused slight increases in both the shear and flexural cracking. Through 2.25xSylmar, new shear and flexural cracks were formed. By the end of 2.5xSylmar, the column had significant shear and flexural cracking. During 2.5xSylmar compression spalling was seen at the inside of the cut on the north side of the column. Tension cracking occurred in the region of the cut on the south side of the column. The column failed during the 2.75xSylmar run. The diagonal shear cracks opened, spalling the cover concrete from both sides and rupturing multiple ties (Fig. 9). The shear failure caused the top half of the column to slide down and close the gap on the north side of the column (Fig 10).

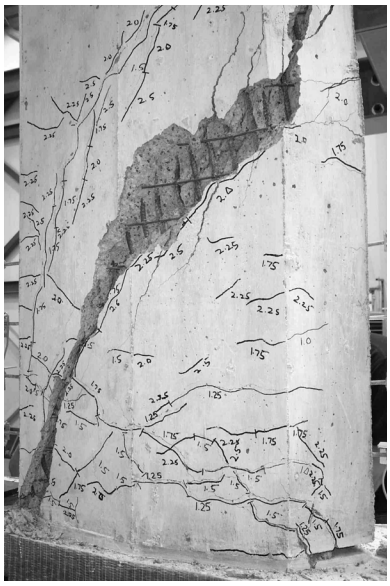

Figure 9. OLVR-2 after failure.

Similar to the retrofitted pedestal in OLVR-1, the pedestal of OLVR-2 remained intact and undamaged throughout testing. Strains in the fiber direction of the jacket reached only 45 percent of the recommended jacket design strain of 6000με. The displacement transducers at north and south ends for pedestal uplift, and the east and west ends for pedestal slippage showed negligible signs of any pedestal movement. Extensive yielding in the longitudinal steel of both the pedestal and the column bars, and strain increase of bars in progressive runs, indicated that despite the lack of hooks, anchorage of the longitudinal bars was effective.

Shear cracking began in OLVR-2 during 1.5xSylmar (Fig. 5-46) at a displacement ductility of 2.2. OLVR-1 shear cracking occurred during the same run but at a lower ductility value of 1.7. Two of the gauges on lateral steel in OLVR-2 showed signs of yielding during 1.75xSylmar. Extent of yielding steadily increased and began to show in most of the other lateral steel gauges until the last run of 2.75xSylmar where the column failed in shear. It was determined by the data and by observation that the failure was caused by the column ductility increase, and by an increase of the inclination of the crack angle, which propagated into the cut (Fig 10).

OLVR-2 testing reassured that the pedestal retrofit of OLVR-1 was successful, and showed that the cut at the base of the column of OLVR-2 was effective in moving the plastic shear of the column closer to the capacity of the as-built. Though OLVR-2 reached larger displacement ductility than OLVR-1, and the base of the column underwent more extensive plastic hinging, OLVR-2 still failed in shear, proving that in addition to the OLVR-2 retrofit the column requires further modification.

Figure 10. OLVR-2 gap closure.

COMPARISON OF RESULTS

Measured Load and Deflection

Load-deflection hysteresis curves for each specimen is plotted in Fig. 12. The maximum measured lateral load and deflection for each column is compared in Fig. 11. All of the curves were idealized as elasto-plastic to compare yield point, stiffness, and column ductility. The idealized yield force of OLVR-2 is within 10 percent of that from the as-built OLVA. Also, the yield force of OLVR-2 is substantially lower than that of OLVR-1 proving that the column cut was effective. OLVR-1 is approximately 16 percent stiffer than the as-built column. The stiffness of OLVR-2 is approximately 18 percent less than that of the as-built. The increase of stiffness for OLVR-1 was because the column is slightly stiffer than the combination of the column and a cracked pedestal. The stiffness reduction of OLVR-2 is because of the cut section, and was responsible for the somewhat lower value of ductility reached by OLVR-2 than for the as-built. The measured as-built displacement ductility capacity was 6.9. However, the unacceptable pedestal cracks began at a ductility of only 1.46. The measured displacement ductility demands for OLVR-1 and OLVR-2 were 4.6 and 5.9, respectively. The cut retrofit of OLVR-2 showed a ductility improvement of 28 percent over OLVR-1. Had the OLVR-2 shear failure been postponed, and the column base been allowed to fail in flexure, a significant ductility improvement would be seen as was predicted by the analytical results.

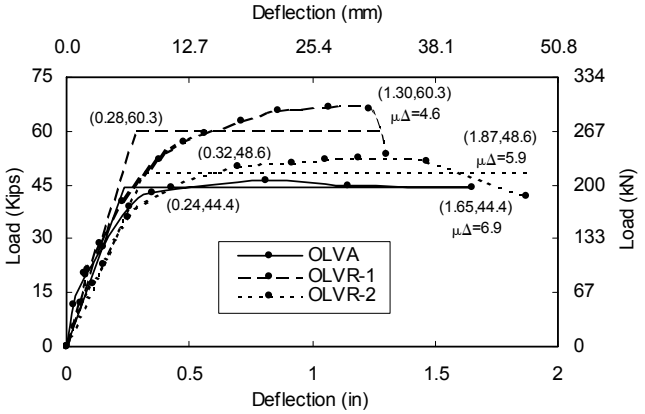

Figure 11. Load-deflection envelope comparison.

SHEAR CAPACITY

Due to the brittle nature of a shear failure, consideration of its avoidance holds an important role in seismic design. All of the specimens that were tested in this study included strong consideration of margin against shear failure. For this reason, the shear capacity of the columns was compared to that predicted by equations from Caltrans and the Federal Highway Administration (FHWA). These equations were chosen because they both include ductility as a parameter. Specimens OLVR-1 and OLVR-2 were both included in this comparison because they failed in shear. OLVA was not included because the pedestal separation prevented a shear failure from surfacing.

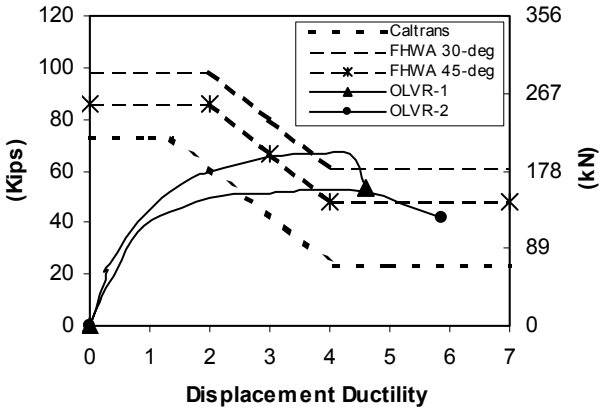

Figure 13. Shear Capacity Comparison.

The Caltrans method for nominal shear capacity is presented in Ref. 2. The nominal shear capacity calculated from the FHWA method is outlined in Ref. 7. FHWA and Caltrans recommend using a shear crack angle of 30 and 45 degrees, respectively. For consistency of comparison, the FHWA values were calculated for both angles. A comparison of capacities predicted by Caltrans and FHWA with the experimental results from the retrofitted columns is shown in Fig. 13. The plots in the figure show force for a given displacement ductility. The yield stress of the steel used in the equations was modified for the average strain rate effect of OLVR-1 and OLVR-2 (Ref. 5). Shear capacity from both equations is constant for small displacement ductility and changes linearly until it is constant at larger displacement ductility. The variation of shear capacity with ductility comes from the calculated contribution of concrete strength. The mark at the end of each load-deflection diagram is the point where the columns failed in shear. The intersections of the measured and calculated curves indicate that for OLVR-1 the Caltrans and FHWA methods predict shear failure at displacement ductility of 2.1 and 3.0 or 3.7 (depending on the crack angle), respectively. The measured ductility at shear failure was 4.6. For OLVR-2, the Caltrans and FHWA methods predict shear failure for a 45-degree shear crack at displacement ductility of 2.7 and 3.7, respectively. For a 30-degree shear crack, FHWA predicts that the shear capacity is not reached. The measured ductility at shear failure for OLVR-2 was 5.9. For 45-degree shear crack the Caltrans and FHWA methods are very conservative.

The measured crack angle for both columns was substantially lower than the 45-degree Caltrans estimate. For OLVR-1, and OLVR-2 the measured angles were 31.0 degrees and 28.8 degrees, respectively. For OLVR-1, Caltrans and FHWA methods predicted failure at displacement ductility values of 2.5 and 3.7, respectively. For OLVR-2, the Caltrans method calculated failure at a ductility of 3.3. The FHWA method calculated a shear capacity greater than measured. Calculated shear capacity values for the actual crack angle of each specimen were closer than those for the estimated angle of 45-degrees. Between the two methods, the FHWA method seems to be more accurate. However, in most cases both equations were still very conservative.

CONCLUSIONS

(1) The embedment of the longitudinal reinforcement at the column-pedestal interface and pedestal-footing interface for columns in Ramp DW is sufficient for adequate development. (2) The lateral reinforcement of the pedestals was highly deficient and could not provide the strength to make the column and pedestal work as an integral unit. (3) Design of the pedestal extension retrofit and the addition of reinforcement outside pedestal were sufficient to prevent pedestal deterioration and to integrate the pedestal with the column. (4) When plastic hinging was shifted to the columns above the pedestal, the plastic shear demand was increased and exceeded the shear capacity of the column under moderate displacement ductilities. (5) Severing select longitudinal bars at the base of the column adequately reduced the plastic shear demand. (6) Severing of longitudinal bars to reduce the shear demand, without the addition of shear reinforcement was not sufficient to prevent a column shear failure. It became clear that a column jacket is necessary to change the failure mode to flexure. (7) A column retrofit including pedestal extension, pedestal reinforcement, severed bars, and sufficient shear reinforcement should be effective to dramatically improve the column response.

ACKNOWLEDGEMENTS

The study presented in this paper was funded by grants from the Nevada Department of Transportation and Federal Highway Administration. The opinions expressed in this article belong solely to the authors and do not necessarily represent the views of others. The valuable support and comments of Mr. Bill Crawford, Mr. Troy Martin and other Bridge Division staff members are appreciated. The authors would also like to thank Dr. Patrick Laplace, Mr. Paul Lucas, and Mrs. Rita Johnson for their help in the construction and testing of the scaled columns. Mr. Ed Fyfe and Mr. Scott Arnold of Fyfe Co. are thanked for their interaction in selection and application of the fiber reinforced plastic composites

REFERENCES

1. American Association of State Highway and Transportation Officials," AASHTO LRFD Bridge Design Specifications", AASHTO, Washington D.C., 1998.
2. Caltrans (California Department of Transportation), "Caltrans Seismic Design Criteria Version 1.2," Engineering Service Center, Earthquake Engineering Branch, California, December 2001.
3. Johnson, N., Saiidi, M., Itani, A., and Ladkany, S., "Seismic Retrofit of Octagonal Columns with Pedestal and One-way Hinge at the Base," Civil Engineering Department, Report No. CCEER-03-05, University of Nevada, Reno, 2003.
4. Kulkarni, S.M., and Shah, S.P., "Response of Reinforced Concrete Beams at High Strain Rates," ACI Structural Journal, Vol. 95, No. 6, pp. 705-715, Nov.-Dec. 1998.
5. Laplace, P., Sanders, D., Douglas, B., and Saiidi, M., "Shake Table Testing of Flexure Dominated Reinforced Concrete Bridge Columns," Civil Engineering Department, Report No. CCEER-99-13, University of Nevada, Reno, 1999.
6. Nawy, E., Reinforced Concrete A Fundamental Approach, Prentice Hall, 2003.
7. U.S. Department of Transportation, "Seismic Retrofitting Manual for Highway Bridges," Federal highway Administration, Pub. No. FHWA-RD-94-052, May 1995.

Hydrodynamic Effect on Seismic Response of Bridges

Jun-jie Wang[1], Wei Lai[1], Xiao Wei[2], Shide Hu[1]

ABSTRACT

A semi-analytical and semi-numerical approach for earthquake induced hydrodynamic pressure on pier was developed. Trefftz-complete functions were used to form the potential of rigid movement and that of elastic vibration. The coupling kinetic equations were solved by FEM with beam element. This method is a relatively simple and efficient approach, retaining the gravity waves on the water surface and the compressibility of the fluid. Examples were presented to discuss the influence of earthquake induced hydrodynamic pressure on pier and the accuracy of this method was illustrated. Based on the potential theory, hydrodynamic pressure on the side of circular pile cap was also investigated. An efficient semi-analytical and semi-numerical approach for harmonic earthquake induced hydrodynamic pressure on the side of circular pile cap was developed, as well as coefficient of added mass. This method is not only able to consider gravity waves on the water surface, but also able to be applied to pile cap in arbitrary depth of water. Results of analysis illustrated that for pile cap near the surface of water, surface wave would have significant effect on hydrodynamic pressure in the case of low frequency of movement, while there is little effect of surface wave induced by high frequency of movement. Besides, using coefficient of added mass in modified Morison equation will over-evaluate the hydrodynamic pressure on pile cap. To investigate the importance of hydrodynamic pressure on seismic response of bridge, shaking table tests of bridge models have been carried out.

[1]State Key Laboratory for Disaster Reduction in Civil Engineering, Tongji University, Shanghai 200092, PRC
[2]Department of Earthquake Hazard Prevention, Seismological Bureau of Shanghai, 200062, PRC

INTRODUCTION

Some bridges crossing sea bays or sea straits have been constructed, or are in the design and planning stage in home and abroad, two examples are shown in Figure 1 and Figure2. The Bohai bay has a width of 145km, and a mean water depth of 40m; the Qiongzhou strait has a shortest width of 20km, and a mean water depth of 60m. Solutions of bridges and tunnels have been proposed. The earthquake-resistance of bridges surrounded by water requires special considerations, while it does not need such considerations for bridges on the land.

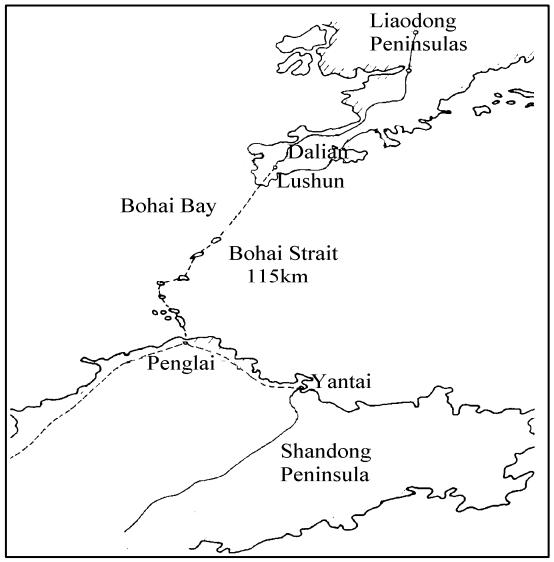

Figure 1. The Bohai Bay in China

Figure2 The Qiongzhou Strait

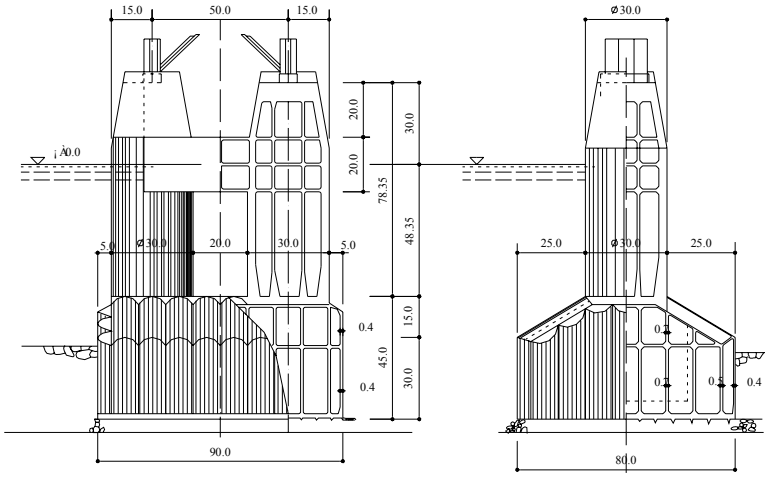

Figure3 A suggested design for the bridge piers for Qiongzhou Strait

For decades, most of the researches on dynamics of structures surrounded by water has focused on dams[3-6], platforms[7-12], and tower structures[13-17], etc. For vibration of structures surrounded by water, various methods may be used, e.g., FEM, BEM, and analytical method. However, for complex cases, an analytical method is rather difficult to process mathematically. To solve such a problem numerically with FEM or BEM would involve a large number of degrees of freedom and much computer time.

To the knowledge of the authors, there have been few research papers[18-22] that deal with the response characteristics of bridges surrounded by water up to now. Furthermore, in most papers about bridges, the pier was reduced to a cantilever beam in water. For a circular cylinder surrounded by water, [23-25] which has given analytical or semi-analytical solutions based on vibration equation and mode functions of cantilever beam in water. But those solutions are limited to single cylinder, being not convenient to be coupled with other parts of a structure for vibration analysis of the whole structure. To overcome the above problems, a semi-analytical and semi-numerical method is introduced herein based on Trefftz complete function and FEM. The gravity waves on the water surface and the compressibility are retained in the method for extremely low frequency and high frequency. The hydrodynamic pressure is expressed in the form of virtual mass as the Morison's equation does.

For pile foundation, Morison equation is preferable to calculate the added mass on piles with small radius. But for pile cap under free surface of water, regular coefficient of added mass in Morison equation is not suitable anymore. Thus in this paper, earthquake induced horizontal hydrodynamic pressure are also obtained for pile cap, as well as coefficient of added mass for pile cap.

MORISON'S EQUATION

Seismic action will produce relative motion between the bridge pier and the sea water. This relative motion acts on the bridge pier in two manners, the first is the inertia action because of the change of the water, and the second is the viscosity action of the water. For a slender column (eg. pile) with small diameter, the water dynamic effects on the pier can be expressed by Morision equation:

$$\mathbf{F} = \rho \mathbf{V}\ddot{\mathbf{u}} + (C_M - 1)\rho \mathbf{V}(\ddot{\mathbf{u}} - \ddot{\mathbf{x}} - \ddot{\mathbf{x}}_g) + \frac{1}{2} C_D \rho \mathbf{A}_P [(\dot{\mathbf{u}} - \dot{\mathbf{x}} - \dot{\mathbf{x}}_g) \,|\, (\dot{\mathbf{u}} - \dot{\mathbf{x}} - \dot{\mathbf{x}}_g)\,|] \qquad (1)$$

where ρ is the density of the water; $\dot{\mathbf{u}}$、$\ddot{\mathbf{u}}$ are the absolute velocity and acceleration of the water respectively; $\mathbf{x}$、$\dot{\mathbf{x}}$ and $\ddot{\mathbf{x}}$ are the relative displacement, velocity and acceleration respectively; $\ddot{\mathbf{x}}_g$ is the seismic ground motion; C_M is the inertia factor, and C_D is the viscosity factor. In this study, C_D is equal to 2，and C_M is equal to 2.0.

When the water is still, i.e., $\dot{\mathbf{u}} = \ddot{\mathbf{u}} = 0$, equation (1) can be rewritten as,

$$\mathbf{F} = -(C_M - 1)\rho \mathbf{V}(\ddot{\mathbf{x}} + \ddot{\mathbf{x}}_g) - \frac{1}{2} C_D \rho \mathbf{A}_P [(\dot{\mathbf{x}} + \dot{\mathbf{x}}_g) \,|\, (\dot{\mathbf{x}} + \dot{\mathbf{x}}_g)\,|] \qquad (2)$$

then one can obtain the motion equation of a bridge under seismic action with the water effects,

$$\mathbf{M}\ddot{\mathbf{x}} + \mathbf{C}\dot{\mathbf{x}} + \mathbf{K}\mathbf{x} = -\mathbf{M}\ddot{\mathbf{x}}_g - (C_M - 1)\rho \mathbf{V}(\ddot{\mathbf{x}} + \ddot{\mathbf{x}}_g) - \frac{1}{2} C_D \rho \mathbf{A}_P [(\dot{\mathbf{x}} + \dot{\mathbf{x}}_g) \,|\, (\dot{\mathbf{x}} + \dot{\mathbf{x}}_g)\,|] \qquad (3)$$

The third term in the right hand is nonlinear, by adopting the linearization technique[5] to this term, one can obtain the following linearized equation,

$$[\mathbf{M} + \mathbf{M}_w]\ddot{\mathbf{x}} + [\mathbf{C} + \mathbf{C}_w]\dot{\mathbf{x}} + \mathbf{K}\mathbf{x} = -[\mathbf{M} + \mathbf{M}_w]\ddot{\mathbf{x}}_g - \mathbf{C}_w \dot{\mathbf{x}}_g \qquad (4)$$

where

$$\mathbf{M}_w = (C_M - 1)\rho\mathbf{V}, \qquad \mathbf{C}_w = \frac{1}{2} C_D \rho \mathbf{A}_P \sigma_{\dot{\mathbf{x}}+\dot{\mathbf{x}}_g} \sqrt{\frac{8}{\pi}} \tag{5}$$

In equations (5), $\sigma_{\dot{\mathbf{x}}+\dot{\mathbf{x}}_g}$ is the variance response of absolute accelerations of the bridge. $\sigma_{\dot{\mathbf{x}}+\dot{\mathbf{x}}_g}$ is a unknown vector, the computation of sub-matrix of concerns the unknown $\sigma_{\dot{\mathbf{x}}+\dot{\mathbf{x}}_g}$, an iterative procedure is needed.

If the effect of water viscosity is neglected, the motion equation of a bridge under the seismic action can be simplified,

$$[\mathbf{M} + \mathbf{M}_w]\ddot{\mathbf{x}} + \mathbf{C}\dot{\mathbf{x}} + \mathbf{K}\mathbf{x} = -[\mathbf{M} + \mathbf{M}_w]\ddot{\mathbf{x}}_g \tag{7}$$

In this simple case, the effects of the water are equivalent to that of an additional mass matrix. The additional mass matrix changes the dynamic characteristics of the analyzed bridge, and then changes the seismic responses of the analyzed bridge. In this paper only the inertia effect of water is taken into account.

HYDRODYNAMIC PRESSURE ON PIERS DUE TO EARTHQUAKES

It is assumed that the seabed moves in a harmonic way with frequency of ω. The column surrounded by water will be acted by hydrodynamic pressure because of the column-water interaction. The hydrodynamic pressure can be expressed as a sum of two terms, $P^{(1)}(a,z,t)$ and $P^{(2)}(a,z,t)$, the first term, $P^{(1)}(a,z,t)$, for the rigid motion of column, and the second term, $P^{(2)}(a,z,t)$, for the elastic vibration of column.

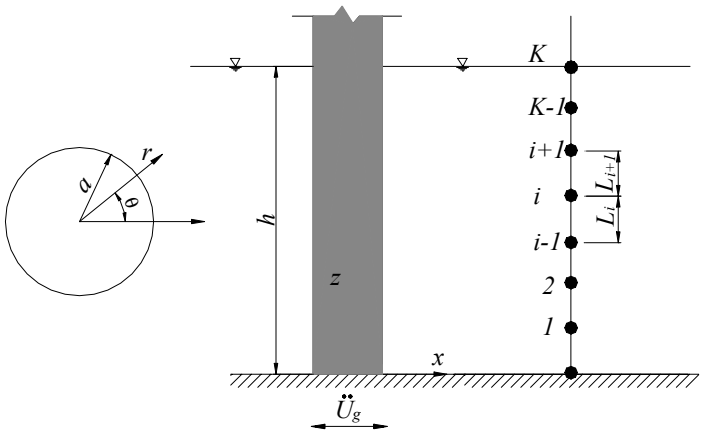

Figure 4 a circular-section cantilever surrounded by water

The hydrodynamic pressure along unit length of the column for the rigid motion of the column, $P^{(1)}(a,z,t)$, can be written,

$$P^{(1)}(a,z,t) = 2a\rho\ddot{U}_g(t)\left\{\frac{\sinh(\lambda_0 h)\cosh(\lambda_0 z)}{\beta_0\lambda_0\left(h + \sigma^{-1}\sinh^2(\lambda_0 h)\right)}\frac{H_1^{(2)}(\beta_0 a)}{H_1^{(2)'}(\beta_0 a)}\right.$$

$$+\sum_{m=1}^{\infty}\frac{\sin(\lambda_m h)\cos(\lambda_m z)}{\beta_m\lambda_m\left(h-\sigma^{-1}\sin^2(\lambda_m h)\right)}\frac{R_m(\beta_m a)}{R_m'(\beta_m a)}\Bigg\} \tag{1}$$

To obtain $P^{(2)}(a,z,t)$ in a general way, the column is discretised using beam finite elements, the number of nodes is k, and the number of elements below water is k-1. After complex derivation, the hydrodynamic pressures on unit length of column due to elastic vibration of column, $P^{(2)}(a,z,t)$, can be expressed as,

$$P^{(2)}(a,z,t)=2a\rho\Bigg\{\frac{\cosh(\lambda_0 z)}{\beta_0\left(h+\sigma^{-1}\sinh^2(\lambda_0 h)\right)}\frac{H_1^{(2)}(\beta_0 a)}{H_1^{(2)'}(\beta_0 a)}\sum_{i=1}^{K-1}\cosh(\lambda_0 z_i)L_i\ddot{U}_s(z_i,t)$$
$$+\sum_{m=1}^{\infty}\left(\frac{\cos(\lambda_m z)}{\beta_m\left(h-\sigma^{-1}\sin^2(\lambda_m h)\right)}\frac{R_m(\beta_m a)}{R_m'(\beta_m a)}\sum_{i=1}^{K-1}\cos(\lambda_m z_i)L_i\ddot{U}_s(z_i,t)\right)\Bigg\} \tag{2}$$

where a is the radium of the column, ρ is density of the fluid, h is the depth of water, z_i is the coordinate of z at the ith node, $\ddot{U}_s(z_i,t)$ is the vibrational acceleration of column at node I, L_i is the length of element I, $\sigma=\omega^2/g$, λ_0 and λ_m is the solution of the following equation,

$$\begin{cases}\tanh(\lambda_0 h)=\dfrac{\omega^2}{g\lambda_0}\\ \tan(\lambda_m h)=-\dfrac{\omega^2}{g\lambda_m}\end{cases} \tag{3}$$

in equation (2),

$$\beta_m=\sqrt{\left|k^2-(\lambda_m)^2\right|},\quad m=1,2,\cdots,\infty \tag{4}$$

$$\begin{cases}R_m(r)=H_1^{(2)}(r) & \text{当} k^2\geq(\lambda_m)^2\\ R_m(r)=K_1(r) & \text{当} k^2<(\lambda_m)^2\end{cases},\quad m=1,2,\cdots,\infty \tag{5}$$

where $k=\omega/c$, c is the sound velocity in water, $H_1^{(2)}(\cdot)$ is the Hankel function of the second kind of order 1, $K_1(\cdot)$ is the modified Bessel function of second kind of order 1.

Finish the integrals of $P^{(1)}(a,z,t)$ and $P^{(2)}(a,z,t)$ in the range of element I, the vectors of hydrodynamic forces $\mathbf{P}^{(1)}$ and $\mathbf{P}^{(2)}$ acting on the discrete nodes can be expressed as,

$$\mathbf{P}^{(1)}=-\mathbf{M}^{(1)}\ddot{\mathbf{U}}_g,\quad \mathbf{P}^{(2)}=-\mathbf{M}^{(2)}\ddot{\mathbf{U}}_s \tag{6}$$

where $\mathbf{M}^{(1)}$ is the added mass matrix corresponding to the rigid motion of the column, and $\mathbf{M}^{(2)}$ is the added mass matrix corresponding to the elastic vibration of the column. $\mathbf{M}^{(1)}$ is a diagonal one, and $\mathbf{M}^{(2)}$ may has non-diagonal elements. The elements of $\mathbf{M}^{(1)}$ and $\mathbf{M}^{(2)}$ are calculated as follows,

$$m_i^{(1)}=-2a\rho\int_{\Gamma_i}\Bigg\{\frac{\sinh(\lambda_0 h)\cosh(\lambda_0 z)}{\beta_0\lambda_0\left(h+\sigma^{-1}\sinh^2(\lambda_0 h)\right)}\frac{H_1^{(2)}(\beta_0 a)}{H_1^{(2)'}(\beta_0 a)}$$

$$+\sum_{m=1}^{\infty}\frac{\sin(\lambda_m' h)\cos(\lambda_m' z)}{\beta_m\lambda_m'\left(h-\sigma^{-1}\sin^2(\lambda_m' h)\right)}\frac{R_m(\beta_m a)}{R_m'(\beta_m a)}\Bigg\}dz \qquad i=1,2,\cdots K-1 \tag{7}$$

$$m_{ij}^{(2)}=-2a\rho\int_{\Gamma_i}\Bigg\{\frac{\cosh(\lambda_0 z)\cosh(\lambda_0 z_j)L_j}{\beta_0\left(h+\sigma^{-1}\sinh^2(\lambda_0 h)\right)}\frac{H_1^{(2)}(\beta_0 a)}{H_1^{(2)'}(\beta_0 a)}$$
$$+\sum_{m=1}^{\infty}\frac{\cos(\lambda_m' z)\cos(\lambda_m' z_j)L_j}{\beta_m\left(h-\sigma^{-1}\sin^2(\lambda_m' h)\right)}\frac{R_m(\beta_m a)}{R_m'(\beta_m a)}\Bigg\}dz \qquad i,j=1,2,\cdots K-1 \tag{8}$$

where Γ_i is the integral range of node i.

It can be seen from the above direction, matrices $\mathbf{M}^{(1)}$ and $\mathbf{M}^{(2)}$ are related to frequency ω with the considerations of surface waves and the compressibility of water, therefore we need to express the dynamic equation of the structure analyzed in frequency domain. From equations (7) and (8), the motion equation of bridge analyzed can be written as,

$$\left[\mathbf{K}+i\omega\mathbf{C}-\omega^2\left(\mathbf{M}+\mathbf{M}^{(2)}\right)\right]\mathbf{u}_s(\omega)=-\left(\mathbf{M}+\mathbf{M}^{(1)}\right)\ddot{\mathbf{u}}_g(\omega) \tag{9}$$

where $\mathbf{K}$, $\mathbf{C}$ and $\mathbf{M}$ are the stiffness matrix, damping matrix and mass matrix of bridge respectively.

$$\ddot{\mathbf{u}}_g(\omega)=\int_{-\infty}^{\infty}\ddot{\mathbf{u}}_g(t)e^{-i\omega t}dt \tag{10}$$

where $\ddot{\mathbf{u}}_g(t)$ is the seismic seabed motion vector.

From the equation (9), one can obtain the solution of $\mathbf{u}_s(\omega)$ in frequency domain. With the inverse Fourier transform one can obtain the solution of equation (9) in time domain,

$$\mathbf{u}_s(t)=\frac{1}{2\pi}\int_{-\infty}^{\infty}\mathbf{u}_s(\omega)e^{i\omega t}dt \tag{11}$$

If the effects of surface waves and the compressibility of water are ignored, then we have,

$$\sigma^{-1}=g/\omega^2=0,\quad k=\omega^2/c=0,\quad R_m(\beta_m r)=K_1(\beta_m r),\quad \beta_m=\lambda_m=\frac{(2m-1)\pi}{2h} \tag{12}$$

with equation (12), $\mathbf{M}^{(1)}$ and $\mathbf{M}^{(2)}$ are free of frequency, then equation (9) can be written in time domain,

$$\left(\mathbf{M}+\mathbf{M}^{(2)}\right)\ddot{\mathbf{u}}_s(t)+\mathbf{C}\dot{\mathbf{u}}(t)+\mathbf{K}\mathbf{u}(t)=-\left(\mathbf{M}+\mathbf{M}^{(1)}\right)\ddot{\mathbf{u}}_g(t) \tag{13}$$

To verify the equations derived in this section, an example is calculated and the results are compared with those given in previous references.

The example is a thin-wall column with a circular section. The depth of water is $h=150m$ (which is also the height of the column), the radium of section is $a=12.5m$, the wall thickness of the section is $t=1.5m$. The E1-Centro(recorded in 1941) seismic ground motion is used as seismic excitation, the maximum value of the excitation is scaled to $0.2g$. In computation, the effects of surface waves and compressibility of fluid are neglected. The calculated results are shown in Figue2-5.

From Figure 5-8, it can be seen that the method proposed in this paper is of higher precision, meanwhile it can be used with FEM as usual.

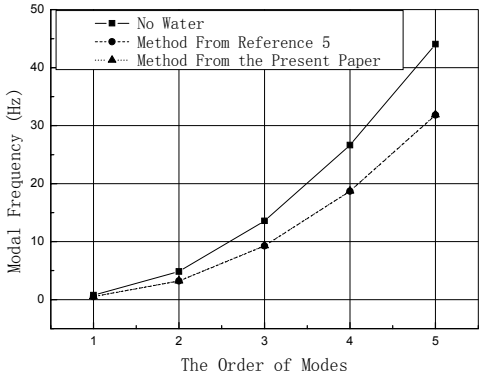

Figure 5 The First Lowest Modal Frequency

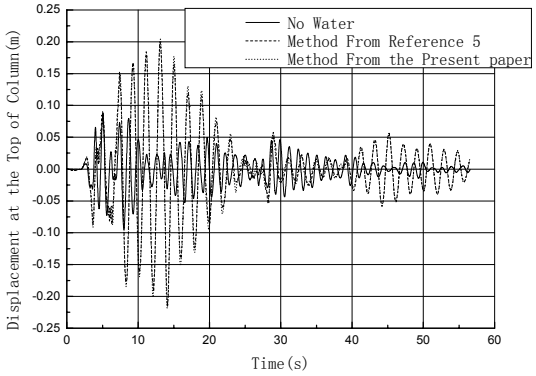

Figure 6 Displacement at Top of Column

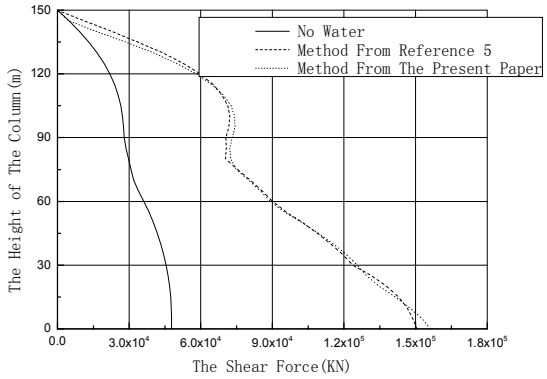

Figure 7 Envelope Shear Force

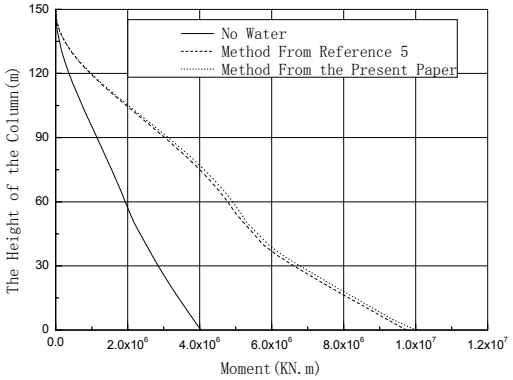

Figure 8 Envelope Moment

HYDRODYNAMIC PRESSURE ON PILE CAP DUE TO EARTHQUAKES

It is assumed that the global displacement motion of pile cap is $U(t) = u_0 e^{i\omega t}$, and then the hydrodynamic pressure along unit length of the pile cap is,

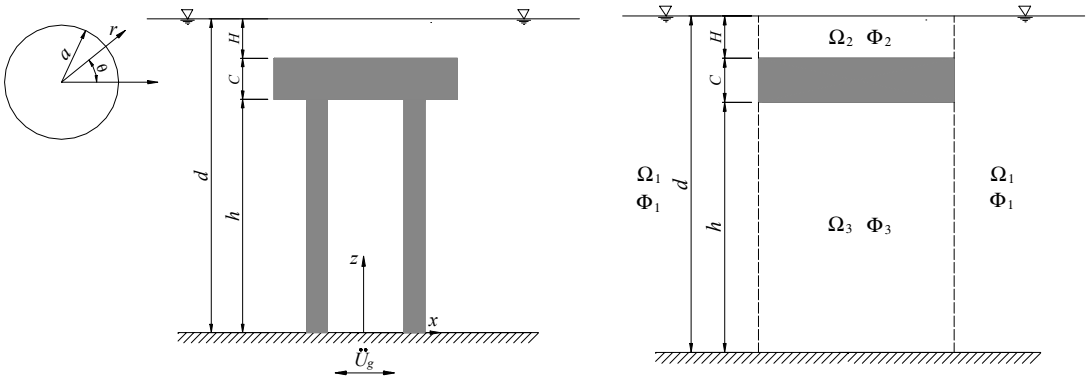

(a) the pile foundation (b) the domains of fluid

Figure 9 Model for Analysis of Hydrodynamic Pressure of Pile Cap

$$P(a,z,t)=\ddot{U}(t)\rho a\pi\left[Z_0(z)\overline{H}_1(\lambda_0 a)\int_h^{C+h}Z_0(z)dz+\sum_{m=1}^{\infty}Z_m(z)\overline{K}_1(\lambda_m a)\int_h^{C+h}Z_m(z)dz\right.$$
$$\left.+Z_0(z)\overline{H}_1(\lambda_0 a)\left(\sum_{n=0}^{\infty}\overline{\dot{V}}_{1n}P_{0n}^{(1)}+\sum_{s=0}^{\infty}\overline{\dot{V}}_{2s}P_{0s}^{(2)}\right)+\sum_{m=1}^{\infty}Z_m(z)\overline{K}_1(\lambda_m a)\left(\sum_{n=0}^{\infty}\overline{\dot{V}}_{1n}P_{mn}^{(1)}+\sum_{s=0}^{\infty}\overline{\dot{V}}_{2s}P_{ms}^{(2)}\right)\right] \tag{14}$$

in which

$$\overline{H}_1(ka)=\frac{H_1^{(2)}(ka)}{kH_1^{(2)'}(ka)},\quad \overline{K}_1(ka)=\frac{K_1(ka)}{kK_1'(ka)} \tag{15}$$

$$Z_0(z)=\frac{\sqrt{2}\cosh(\lambda_0 z)}{\sqrt{d+\sigma^{-1}\sinh^2(\lambda_0 d)}},\quad Z_m(z)=\frac{\sqrt{2}\cos(\lambda_m z)}{\sqrt{d-\sigma^{-1}\sin^2(\lambda_m d)}}\quad m=1,2,...\quad 0<z<d \tag{16}$$

where $\overline{\dot{V}}_{1n}$ and $\overline{\dot{V}}_{2s}$ are constants to be decided by the continuous conditions among velocity potentials of different fluid domain, other symbols have the same meaning as before. Constants of $P_{ij}^{(1)}$ and $P_{ij}^{(2)}$ are calculated respectively,

$$P_{ij}^{(1)}=\int_{C+h}^{d}Z_i(z)F_j(z)dz\quad i,j=0,1,2\cdots \tag{17a}$$

$$P_{ij}^{(2)}=\int_0^h Z_i(z)f_j(z)dz\quad i,j=0,1,2\cdots \tag{17a}$$

where,

$$\begin{cases}F_0(z)=\dfrac{\sqrt{2}\cosh[\partial_0(z-C-h)]}{\sqrt{H+\sigma^{-1}\sinh^2(\partial_0 H)}}\\ F_m(z)=\dfrac{\sqrt{2}\cos[\partial_m(z-C-h)]}{\sqrt{H-\sigma^{-1}\sin^2(\partial_m H)}}\quad m=1,2,...\end{cases}\quad C+h<z<d \tag{18}$$

$$\begin{cases}f_0(z)=1/\sqrt{h}\\ f_m(z)=\sqrt{\dfrac{2}{h}}\cos\left(\dfrac{m\pi z}{h}\right)\quad m=1,2,...\end{cases}\quad 0<z<h \tag{19}$$

in which, H is the displacement from the surface of cap to the water surface, ∂_0 and ∂_m are the solution of the following dispersion relation equations,

$$\begin{cases}\tanh(\partial_0 H)=\dfrac{\omega^2}{g\partial_0}\\ \tan(\partial_m H)=-\dfrac{\omega^2}{g\partial_m}\end{cases} \tag{20}$$

Finish the integral of $P(r,z,t)|_{r=a}$ along cap in z-direction, the horizontal hydrodynamic force F_a can be obtained,

$$F_a = \ddot{U}(t)\rho a\pi\left[\overline{H}_1(\lambda_0 a)\left(\int_h^{C+h} Z_0(z)dz\right)^2 + \sum_{m=1}^{\infty}\overline{K}_1(\lambda_m a)\left(\int_h^{C+h} Z_m(z)dz\right)^2\right.$$
$$\left. + \overline{H}_1(\lambda_0 a)\left(\sum_{n=0}^{\infty}\overline{\dot{V}}_{1n}P_{0n}^{(1)} + \sum_{s=0}^{\infty}\overline{\dot{V}}_{2s}P_{0s}^{(2)}\right)\int_h^{C+h} Z_0(z)dz + \sum_{m=1}^{\infty}\overline{K}_1(\lambda_m a)\left(\sum_{n=0}^{\infty}\overline{\dot{V}}_{1n}P_{mn}^{(1)} + \sum_{s=0}^{\infty}\overline{\dot{V}}_{2s}P_{ms}^{(2)}\right)\int_h^{C+h} Z_m(z)dz\right] \quad (21)$$

denote,

$$\mathrm{m}_a = -\rho a\pi\left[\overline{H}_1(\lambda_0 a)\left(\int_h^{C+h} Z_0(z)dz\right)^2 + \sum_{m=1}^{\infty}\overline{K}_1(\lambda_m a)\left(\int_h^{C+h} Z_m(z)dz\right)^2\right.$$
$$+ \overline{H}_1(\lambda_0 a)\left(\sum_{n=0}^{\infty}\overline{\dot{V}}_{1n}P_{0n}^{(1)} + \sum_{s=0}^{\infty}\overline{\dot{V}}_{2s}P_{0s}^{(2)}\right)\int_h^{C+h} Z_0(z)dz$$
$$\left. + \sum_{m=1}^{\infty}\overline{K}_1(\lambda_m a)\left(\sum_{n=0}^{\infty}\overline{\dot{V}}_{1n}P_{mn}^{(1)} + \sum_{s=0}^{\infty}\overline{\dot{V}}_{2s}P_{ms}^{(2)}\right)\int_h^{C+h} Z_m(z)dz\right] \quad (22)$$

then equation (21) can be written as,

$$F_a = -m_a\ddot{U}(t) \quad (23)$$

in which m_a is the added hydrodynamic mass on the cap in horizontal direction. Then the added hydrodynamic mass factor $C_a^{'}$ is,

$$C_a^{'} = m_a / C\rho\pi a^2 \quad (24)$$

From the above analysis, with the consideration of surface waves, $C_a^{'}$ is related to frequency ω, then the dynamic equation of bridge under seismic action should be written in frequency domain,

$$\left(\mathbf{K} + i\omega\mathbf{C} - \omega^2\mathbf{M}\right)\mathbf{u}_s(\omega) = -\mathbf{M}\ddot{\mathbf{u}}_g(\omega) - \mathbf{M}_a\left(\ddot{\mathbf{u}}_g(\omega) - \omega^2\mathbf{u}_s(\omega)\right) \quad (25a)$$

$$\left(\mathbf{K} + i\omega\mathbf{C} - \omega^2(\mathbf{M} + \mathbf{M}_a)\right)\mathbf{u}_s(\omega) = -(\mathbf{M} + \mathbf{M}_a)\ddot{\mathbf{u}}_g(\omega) \quad (25b)$$

where $\mathbf{K}$, $\mathbf{C}$ and $\mathbf{M}$ are the stiffness matrix, damping matrix and mass matrix of bridge respectively. $\ddot{\mathbf{u}}_g(\omega)$ is defined in equation (10), $\left[\ddot{\mathbf{u}}_g(\omega) - \omega^2\mathbf{u}_s(\omega)\right]$ is the absolute acceleration vector of bridge structure, $\mathbf{M}_a$ is the matrix of added hydrodynamic mass, which diagonal elements correspond to the part of bridge in water and zero elements correspond to other parts of bridge.

When the effects of surface waves are neglected, we have $\sigma^{-1} = g/\omega^2 = 0$, and λ_0 and ∂_0 do not exist, $\lambda_m = \dfrac{(2m-1)\pi}{2d}$, $Z_m(z) = \sqrt{\dfrac{2}{d}}\cos(\lambda_m z)$, $\partial_m = \dfrac{(2m-1)\pi}{2H}$, $F_m(z) = \sqrt{\dfrac{2}{H}}\cos(\partial_m z)$, meanwhile $\overline{\dot{V}}_{1n}$ and $\overline{\dot{V}}_{2s}$ are not related to ω, thus the added hydrodynamic mass is not related to ω. Then equation (25b) can be written in time domain,

$$(\mathbf{M} + \mathbf{M}_a)\ddot{\mathbf{u}}_s(t) + \mathbf{C}\dot{u}_s(t) + \mathbf{K}u_s(t) = -(\mathbf{M} + \mathbf{M}_a)\ddot{\mathbf{u}}_g(t) \quad (26)$$

As an example, assume the pile cap moves in an harmonic way, and $d = 30m$, $a = 6m$, $C = 3m$, $\theta = 0^{\circ}$. The results are shown in Figure 10 and 11. It is observed that the added mass factor is significantly increased or decreased by the surface waves in the range of lower frequency,

and with the increase of ω, the contribution of surface waves to $C_a^{'}$ decreases, finally reach the value without consideration of the effects of surface waves. From Figure 11, $C_a^{'}$ is related to the position of the cap in the water. Figure 12 gives the relationship between $C_a^{'}$ and d. It can be seen from Figure 12 that the depth of water d has an insignificant effect on $C_a^{'}$.

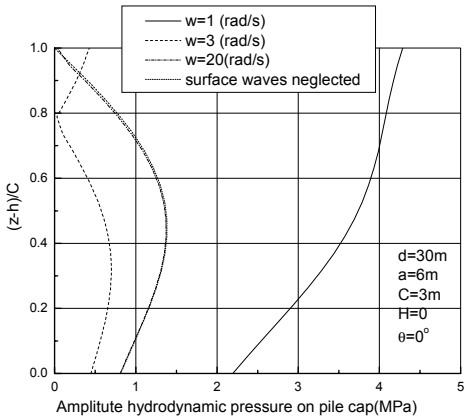

Figure 10 The Amplitute of Hydrodynamic Pressure on The lateral Side of The Pile Cap

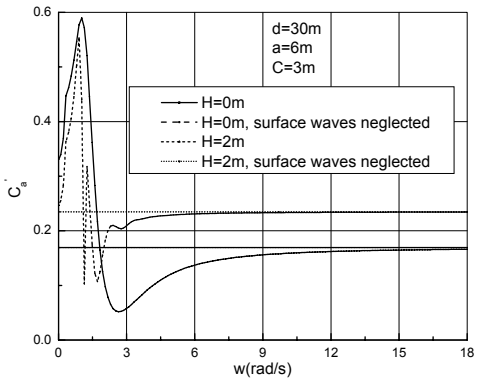

Figure 11 The Added mass Factor

Figure 13 gives the relationship between $C_a^{'}$ and C/d. Figure 13(a) is for $d = 20m$, and (b) is for $d = 40m$. It is observed that $C_a^{'}$ increases with C (the thickness of the cap) when d is a constant. One can see that $C_a^{'}$ vary with frequency ω, and reaches a peak at a frequency range of 0.5-1.5rad/s. It means that fluid motion with low frequency may lead to large hydrodynamic pressure.

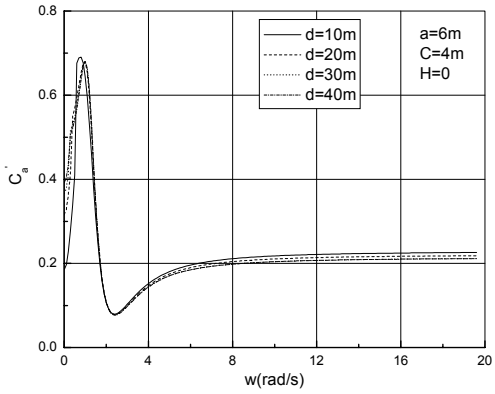

Figure 12 Relationship Between $C_a^{'}$ and d

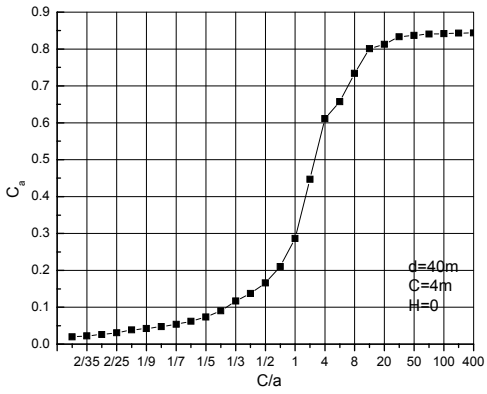

Figure 14 Relationship Between $C_a^{'}$ and a

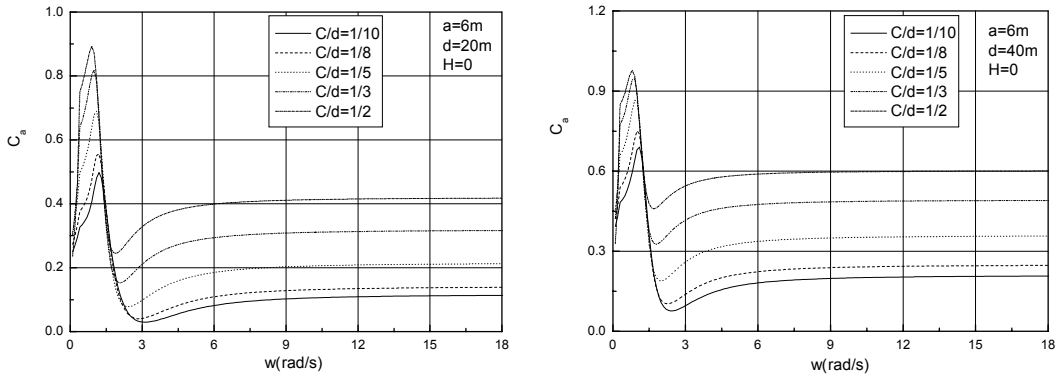

(a) d=20m (b) d=40m

Figure 13 Relationship Between $C_a^{'}$ and C/d

Figure 14 demonstrates that $C_a^{'}$ gets larger with the value of radius a. But $C_a^{'}$ is not more than 1. According to the modified Morison equation, the added mass factor for a circular cylinder with relative minor radius to water depth is $C_a = 1.0$. The results shown in Figure 14 mean that the Morison's equation would exaggerate the added hydrodynamic mass on the cap in horizontal direction.

SHAKING TABLE TESTS OF MODEL PIERS OF BRIDGE

To investigate the importance of hydrodynamic pressure on seismic response of bridge, and to verify the formulas derived in this paper, shaking table tests of model bridge piers were carried out. Two model bridge piers were designed. The first is a model of Pingtan Bridge(in Fujian province, China, see Figure 15) following the similarity laws，and the second one is an ideal model, which is the same in configuration, but with different mass density and different stiffness. The configurations of the model bridge pier are shown in Figure 16. Figure 17 shows the pictures of the model bridge piers. Figure 18 shows the arrangement of sensors for both model of Pingtan Bridge and the ideal one.

Some results of the shaking table tests for harmonic excitations are shown in Figure 19-25.

What one can observe from Figure 19-25 tell us that the hydrodynamic fluid pressures enlarge the seismic responses of the model bridges. Not much enlargement is observed in Figure 20 and 21 for model of Pingtan Bridge. But large enlargement for ideal model bridge is observed.

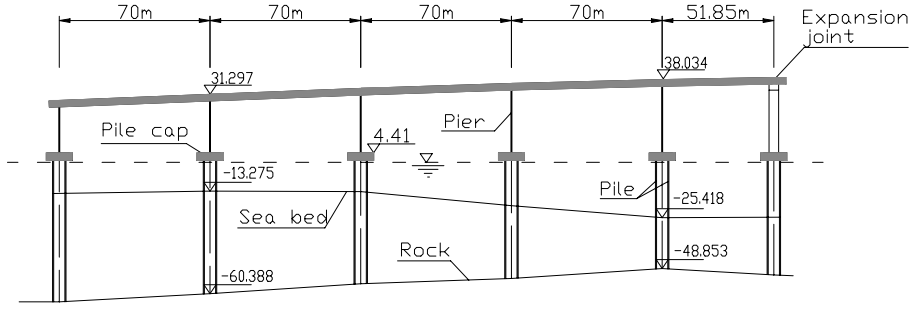

Figure 15 The Pingtan Bridge(approach spans)

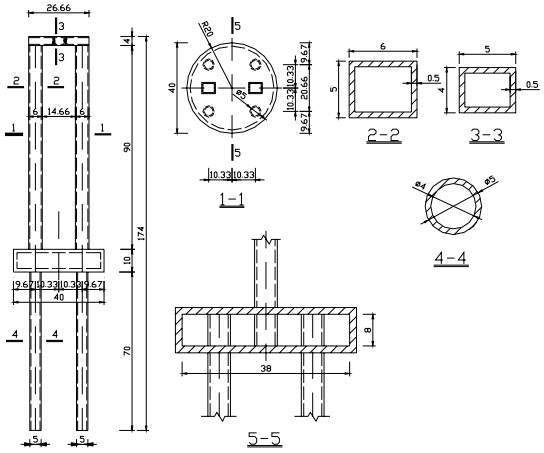

Figure 16 The Configuration of The Tested Model Bridge Piers

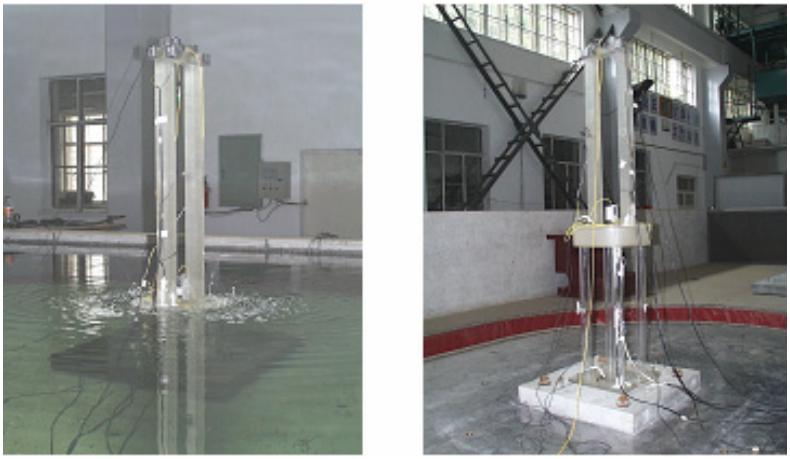

Figure 17 Example Photos of Bridge Models in Testing

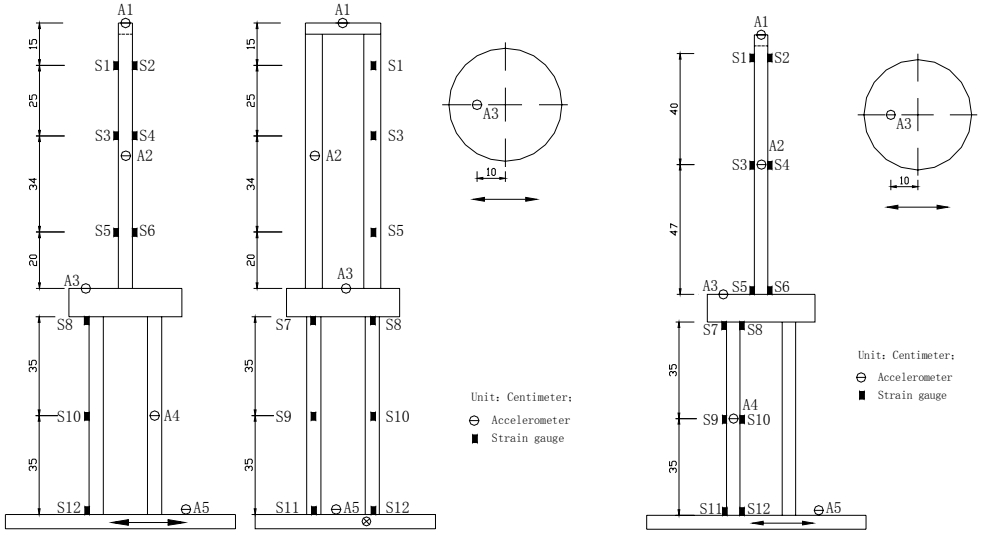

(a) Model for Pingtan Bridge (b) Ideal Model

Figure 18 The Arrangement of Sensors

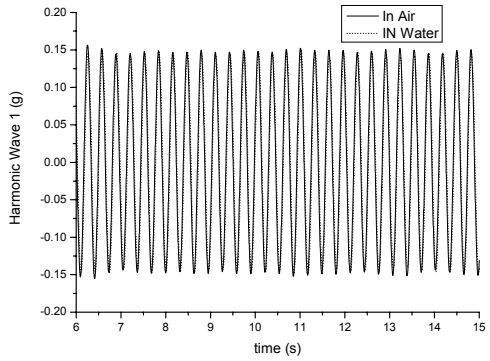

Figure 19 Harmonic Excitations (3.13Hz) For Model of Pingtan Bridge

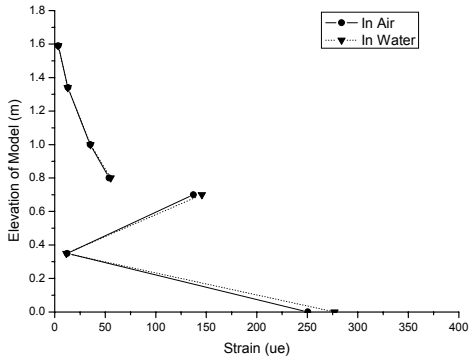

Figure 20 Strain envelope along the elevation For Model of Pingtan Bridge

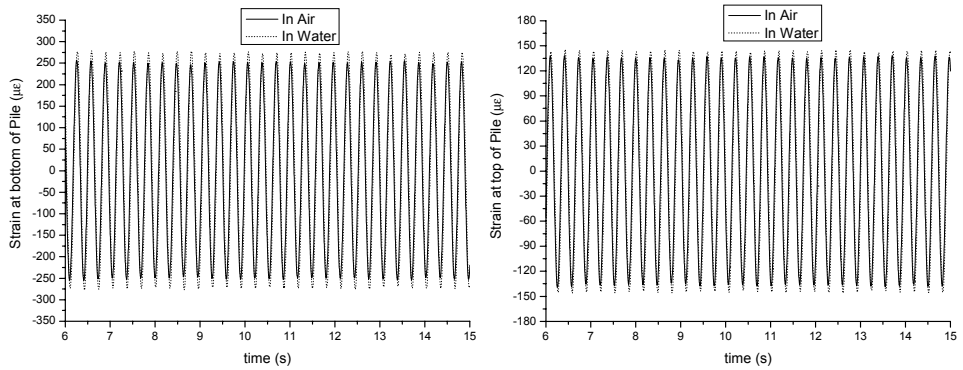

Figure 21 Time History of Strains(3.13Hz Harmonic excitation) For Model of Pingtan Bridge

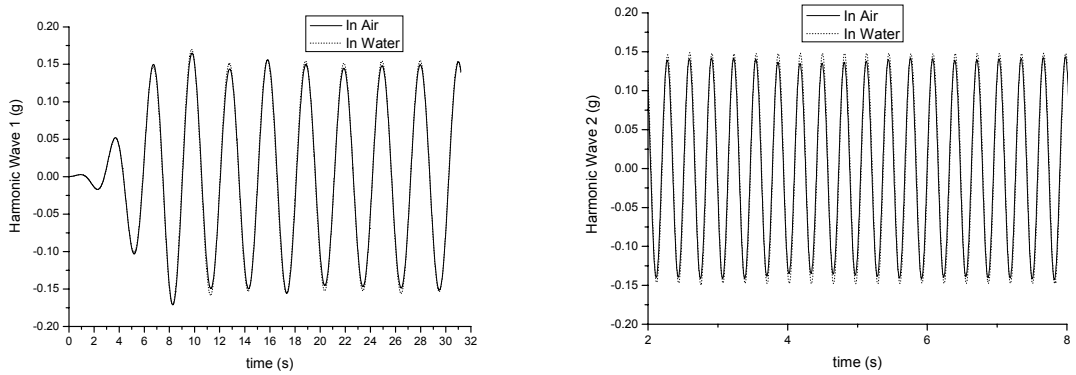

(a) 0.313Hz (b) 3.13Hz

Figure 22 Harmonic Excitations for Ideal Model Bridge

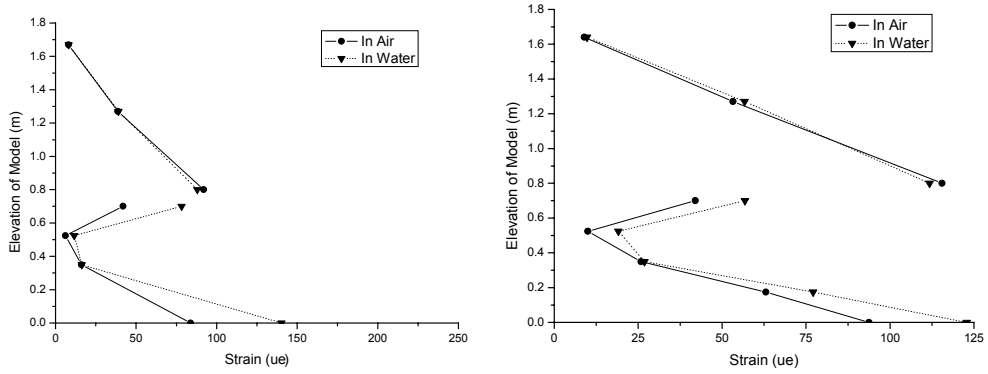

0.313Hz 3.13Hz

Figure 23 Strain envelope along the elevation for Ideal Model Bridge

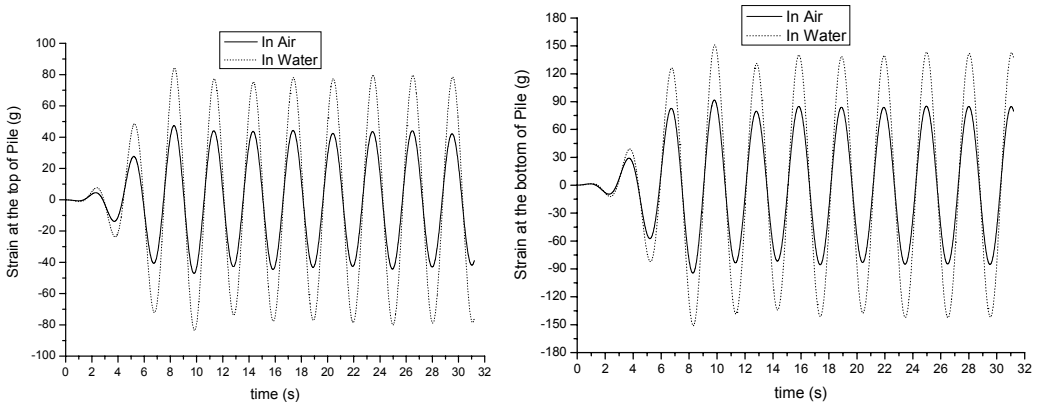

Figure 24 Time History of Strains(0.313Hz) for Ideal Model Bridge

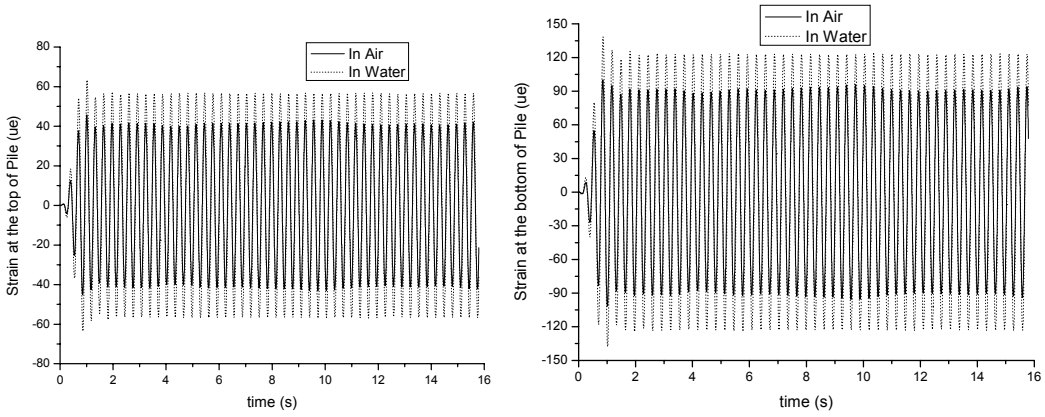

Figure 25 Time History of Strains(3.13Hz) for Ideal Model Bridge

DISCUSSIONS

Two examples are computed in this section. The first one is as the same as that in section 3. The E1-centro seismic ground motion is used as seismic excitation. The maximum value of the excitation is scaled to $0.2\,g$. The effects of surface waves and compressibility of fluid are neglected in computation. The calculated results are shown in Figue26-31.

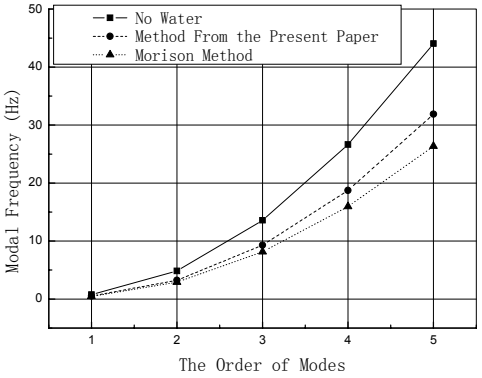

Figure 26 The First Lowest Modal Frequencies

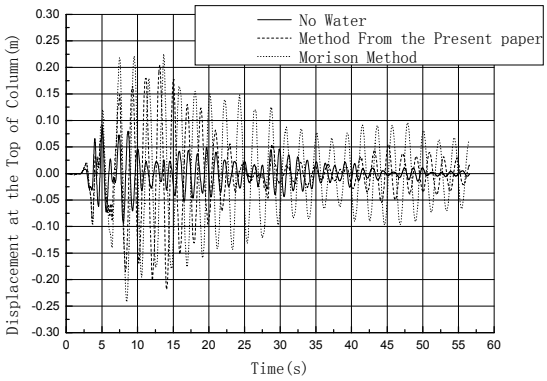

Figure 27 Displacement at Top of Column

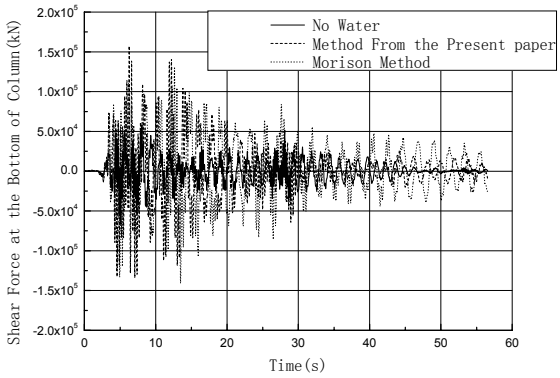

Figure 28 Shear Force at bottom of Column

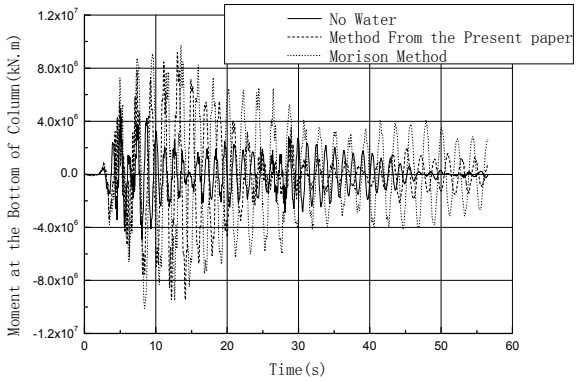

Figure 29 Moment at bottom of Column

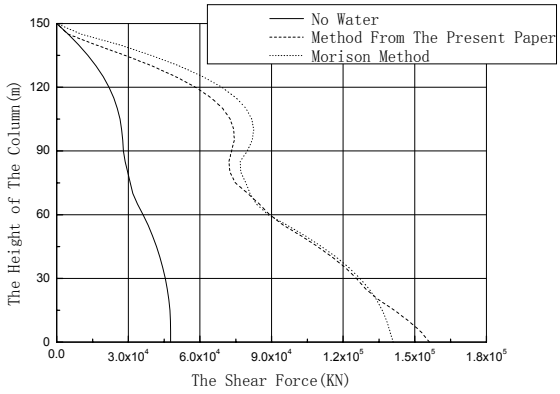

Figure 30 Envelope Shear Force

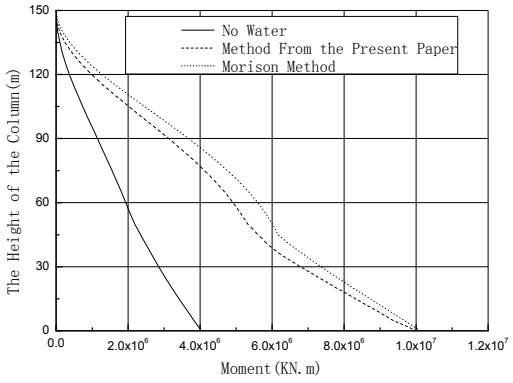

Figure 31 Envelope Moment

Figure 26 shows the lowest modal frequencies of cylinder. From the figure, it can be seen that the modal frequencies of cylinder vibrating in water by the methods both from the present paper and Morison equation are lower than those of cylinder vibrating in air. However, the results by Morison equation are lower than the corresponding modal frequencies by the method from the present paper. Figures 27-31 show the dynamic responses of cylinder vibrating in air and water. Significant differences were observed between the seismic responses of the column vibrating in air and those in water. Significant differences were also observed between the results from Morison's equation and those from the present method. The results mean that the hydrodynamic pressure might important to the seismic responses of some types of bridges surrounded by water, and it would be necessary to develop reasonable methods to estimate the effects of hydrodynamic pressure for typical bridge piers that may be used for sea-strait bridges.

The second example is the prototype of the Pingtan Bridge shown in figure 32. The calculated results are shown in Figure 32-37.

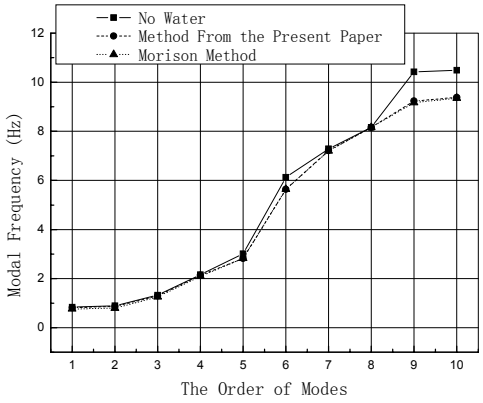

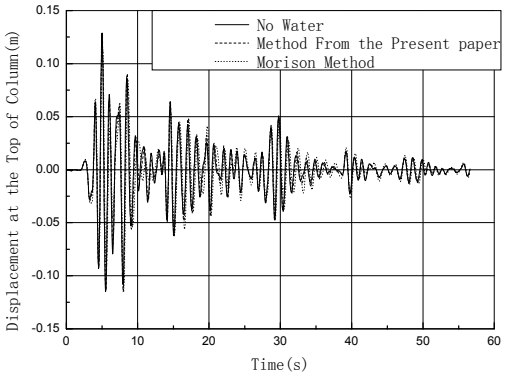

Figure 32 The First Lowest Modal Frequency Figure 33 Displacement at Top of Pier

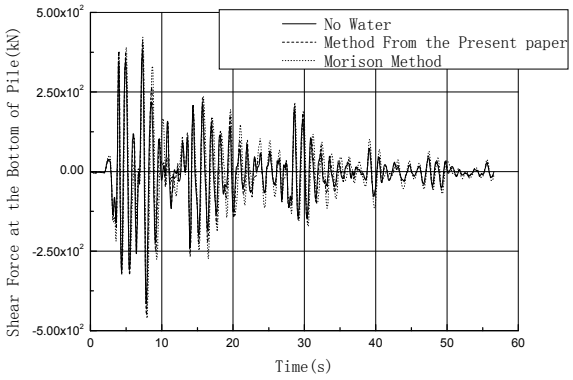

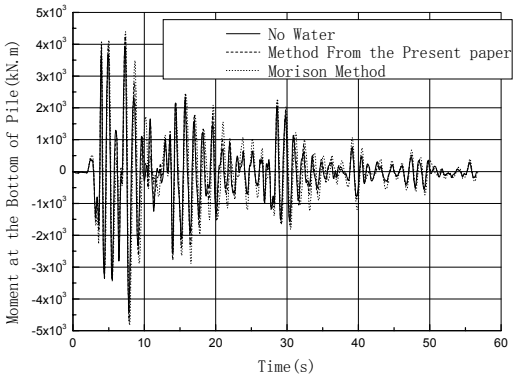

Figure 34 Shear Force at bottom of Pile Figure 35 Displacement at Top of Pile

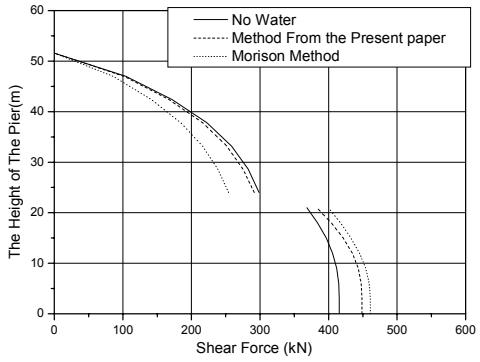

Figure 36 Envelope Shear Force

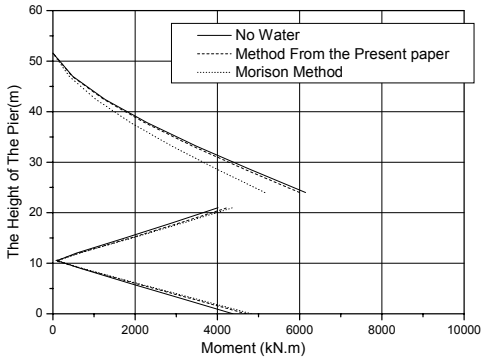

Figure 37 Envelope Moment

Figure 32 gives the first ten modal frequencies of pier vibrating in air and water. In figure, the lowest four modal frequencies of pier vibrating in water are almost the same as those in air. Moreover the results by two methods have minor difference. The dynamic responses of pier vibrating in air and water are compared in figure 33-37. Differences between the dynamic responses of pier vibrating in water and in air are observed, but the differences are not significant, not more than 10%. The reason is that the added masses for pile cap obtained by two methods are quite small with regard to the mass of pile cap. Accordingly, the effect of hydrodynamic pressures on dynamic characteristics of the computed pier is not obvious.

CONCLUSIONS

To estimate the seismic responses of bridges surrounded by water, a semi-analytical and semi-numerical approach for earthquake induced hydrodynamic pressure on pier was developed and shaking table tests of model bridge piers were finished. The following conclusions can be reached.

- The methods developed in this paper can easily be combined with FEM method, and then make it convenient to estimate the seismic responses of bridges surrounded by water;
- Hydrodynamic pressure may largely change the seismic responses of bridges which are of low modal frequencies or bridges which consist of thin-wall column piers;
- The results from shaking table tests show that hydrodynamic pressure may be important to seismic responses of some types of bridges surrounded by water. This conclusion agrees to that obtained by theoretical computation.

ACKNOWLEDGEMENT

This research is supported by the National Science Foundation of China at granted No. 40072088.

REFERENCES

Bridge and Offshore Engineering Association, Sea Strait Crossing, Vol.13, 47-53, 1998.

Fujian Highway Design Institute, The Pre-feasibility Study of Pingtan Bridge, 1999.

Chopra, A. K.; Gupta, S., Hydrodynamic and foundation interaction effects in frequency response functions for concrete gravity dams, Earthquake Engineering & Structural Dynamics, 10, 1, Jan.-Feb. 1982, pages 89-106

Fahjan, Y.M., Borekci, O.S., And Erdik, M, Earthquake-induced hydrodynamic pressures on a 3D rigid dam-reservoir system using DRBEM and a radiation matrix, Int. J. for Numerical Methods in Engineering, Vol.56, No.10, 2003, 1511-1532

Madabhushi, S. P. Gopal, Seismic behaviour of dams subjected to earthquake induced hydro-dynamic forces, Earthquake Geotechnical Engineering, Proceedings of the Second International Conference on, A.A. Balkema, Rotterdam, Vol. 2, 1999, pages 649-654

Proulx, Jean; et al., An experimental investigation of water level effects on the dynamic behaviour of a large arch dam, Earthquake Engineering & Structural Dynamics, 30, 8, 2001, 1147-1166

Aviles, Javier; Li, Xiangyue, Hydrodynamic pressures on axisymmetric offshore structures considering seabed flexibility, Computers & Structures, 79, 29-30, Nov. 2001, pages 2595-2606

Chen, Bang-Fuh, Dynamic responses of coastal structures during earthquakes including sediment-sea-structure interaction, Soil Dynamics and Earthquake Engineering, 20, 5-8, Dec. 2000, pages 445-467

Chen, B.-F., 3D nonlinear hydrodynamic analysis of vertical cylinder during earthquakes. I: rigid motion, Journal of Engineering Mechanics, 123, 5, May 1997, pages 458-465

Hu, Yuxia; Randolph, Mark F., Bearing capacity of caisson foundations on normally consolidated clay, Soils and Foundations, 42, 5, Oct. 2002, pages 71-77

Sun, K.; Nogami, T. 1991. Earthquake induced hydrodynamic pressure on axisymmetric offshore structures, Earthquake Engineering & Structural Dynamics, 20, 5, May, pages 429-440.

Yamada, Y.; et al. 1989. Seismic response of offshore structures in random seas, Earthquake Engineering & Structural Dynamics, 18, 7, Oct, pages 965-981.

Chopra A. K., Goyal, A. 1991. Simplified earthquake analysis of intake-outlet towers, Journal of Structural Engineering, 117, 3, Mar, pages 767-788.

Liaw, C.-Y., and Chopra, A.K., Dynamics of towers surrounded by water, Earthquake Engineering & Structural Dynamics, Vol.3, No.1, 1974, 33-49

Goyal, A.; Chopra, A. K. 1989. Hydrodynamic and foundation interation effects in dynamics of intake towers:earthquake responses, Journal of Structural Engineering, 115, 6, June, 1386-1395.

Goyal A., Chopra, A. K. 1989. Earthquake response spectrum analysis of intake-outlet towers, Journal of Engineering Mechanics, 115, 7, July, pages 1413-1433.

Spyrakos, C. C.; Xu, C., Soil-structure-water interaction of intake-outlet towers allowed to uplift, Soil Dynamics and Earthquake Engineering, 16, 2, 1997, 151-159.

Akkas, Demirci, Y., Dynamic response of a bridge pier within a fluid medium, Proceedings of the 8th European conference on Earthquake Engineering, Lab. Nacional de Engenharia Civil, Lisbon, 1986, 6.9/33-39, Vol.3

H. Goto and K. Toki. 1965. Vibration Characteristics and Aseismic Design of Submerged Bridge Piers, Proc. Third World Conf. On Earthq. Eng, Auckland, Welligton, New Zealand.

Kotsubo,S., and Takanoshi, T., Analysis of Hydrodynamic pressure on multi-piles foundation during earthquakes, (in Japanese) Proceedings of Japan Society of Civil Engineers, 276, 1978, 1-12

Rao, P.V., Hydrodynamic Earthquake Coefficients of Bridge Piers, Bulletin of the Indian Society of Earthquake Technology, Vol.8, No.4, 1971, 188-194

S.Kotsubo. 1965. Seismic force effect on submerged bridge piers with elliptic cross-section, Proc. Third World Conf. On Earthq. Eng., Auckland, Welligton, New Zealand.

Anthony N.Willians. 1986.Earthquake response of submerged circular cylinder. Ocean Engng, Vol.13.No.6,pp.569-585.

Keming Sun and Toyoaki Nogami, 1991, Earthquake induced hydrodynamic pressure on axisymmetric offshore structures., J.Earthquake Engng struct.Dynamics 20, pp.429-440

Yoshihiro Tanaka and Robert T.Hudspeth. 1988. Restoring forces on vertical circular cylinders forced by earthquakes. Earthquake Engng and Struc Dynamics, Vol.16.99-119

EVALUATION OF NCHRP PROJECT 12-49 PROVISIONS FOR SEISMIC DESIGN OF BRIDGES IN NEW JERSEY

Harry Capers, Husam Najm, and Hani Nassif

ABSTRACT

Current LRFD provisions are based on seismic design criteria and detailing provisions that are at least 10 to 20 years old. These provisions are mostly based on the Division I-A Seismic Design of the AASHTO Standard Specifications (1996) and NEHRP (1997). National Cooperative Highway Research Program (NCHRP) project known as NCHRP Project 12-49 "Comprehensive Specifications for the Seismic Design of Bridges" was initiated to address the inadequate performance of highway bridges in recent earthquakes and the deficiencies in the current seismic code. NCHRP Project 12-49 is intended to develop comprehensive specifications for seismic design of bridges considering all aspects of the design process including: (1) design philosophy and performance criteria, (2) seismic loads and site effects, (3) analysis and modeling, (4) design requirements, and (5) detailing. With the completion of NCHRP Project 12-49 "Comprehensive Specifications for the Seismic Design of Bridges", NCHRP Report 472, with the same name, was issued. Along with the report, a proposed new seismic design specification was issued. The new seismic design specification was to be considered by the American Association of State Highway and Transportation Officials (AASHTO) as a replacement for its existing aged seismic design provisions. While not adopted in the form presented, the new specifications are available for consideration by jurisdictions to use them in their bridge designs. New Jersey saw some value in utilizing the new specifications. Because of the several significant changes in the design criteria and approach provided in the new provisions, there are questions on how these new provisions will affect the design and performance of bridge in states nationwide as well as the retrofit of existing bridges. There are also questions on the impact of new provisions on the design of abutments and retaining walls an area beyond the scope of the original project. Hence, there was a need to evaluate the impact of the new seismic design for use in design and detailing of bridges in New Jersey. This paper provides an update on a project undertaken to do this evaluation.

Harry Capers, Jr., New Jersey Department of Transportation, Trenton, New Jersey, 08625, USA
Husam Najm, Rutgers, The State University of New Jersey, Piscataway, NJ 08854, USA
Hani Nassif, Rutgers, The State University of New Jersey, Piscataway, NJ 08854, USA

INTRODUCTION

In 1998 AASHTO-sponsored National Cooperative Highway Research Program (NCHRP) initiated a project to develop a new set of seismic design provisions for highway bridges intended to be compatible with AASHTO LRFD specifications. NCHRP Project 12-49 was conducted by a joint venture of Applied Technology Council (ATC) and the Multidisciplinary Center for Earthquake Engineering Research (MCEER). NCHRP 12-49 was intended to reflect experience gained during recent damaging earthquake and results of research work conducted in the United States and elsewhere over the last decade. With the completion of NCHRP Project 12-49 "Comprehensive Specifications for the Seismic Design of Bridges", NCHRP Report 472, with the same name, was recently issued. Along with the report, a proposed new seismic design specification was issued. The new seismic design specification was to be considered by the American Association of State Highway and Transportation Officials (AASHTO) as a replacement for its existing aged seismic design provisions. While not adopted in the form presented, the new specifications are available for consideration by jurisdictions to use them in their bridge designs. New Jersey saw some value in utilizing the new specifications. The proposed provisions for abutment and retaining structures in the NCHRP 12-49 report are essentially an upgrade of existing AASHTO LRFD provisions with few additional guidelines. The purpose of this study is to evaluate the impact of new seismic design provisions proposed in NCHRP Report 472 on the seismic design and detailing of bridges and the design of abutments in New Jersey. The purpose of the new NCHRP 472 provisions is to provide seismic guidelines and procedures for bridge design that ensures safety of the public and to minimize structural and non-structural damage. In recent years, several major bridges have collapsed and others sustained significant damage during an earthquake. Among the major changes in

the new provisions are the increased ground motion accelerations and soil amplification factors. These changes will have a major impact on seismic design of bridges in the Eastern United States. Several states including New Jersey are looking at the impact of these changes on their local, state, and federal bridges. The difference in ground motion acceleration between the expected earthquake (EXP) and the maximum considered earthquakes (MCE) in the Northeast is significant compared to those in the Western United States. Designing all bridges for the MCE in Eastern US would be too conservative and need to be evaluated. The soil amplification factors F_a and F_v are higher than those in the existing provisions, especially for soft soils. These factors are not site-specific to the Northeast and were based on soils mostly in the Western US (Nikolaou, 2001). These factors can be different for different soils in different states. The evaluation of these site factors for New Jersey soils is needed.

The current guidelines for seismic design of bridges in New Jersey are based on the 1998 LRFD Specifications (w/interims 1999-2003). These specs require Safety Evaluation performance level as well as Functional Evaluation level for "critical" bridges. Local road bridges over major facilities, including State and Federal Highways, are designed based on the lesser of the two events. Single-span bridges that are less than 2300 m^2 (25,000 ft^2) in deck area are designed using the 1997 NEHRP response spectra while those exceeding 2300 m^2 require site-specific evaluation. Site-specific is also required for soil profile types E and F (as defined by NEHRP) or when a time-history response analysis to be performed as part of the design/retrofit. Some states design their bridges such that the substructures are capable of resisting all the seismic loads without any contribution from the abutments. Other states use the abutments as key components of the ERS. Although the new NCHRP 472 provisions recognize the abutment can be an important part of the ERS and considerable attention should be given to their contribution to the global response of the bridge, more information and guidance is needed for their design and detailing. The new NCHRP 472 provisions have made significant improvements over the current LRFD Specifications. It provided more detailed performance and hazard level criteria that would be very helpful to bridge owners and state officials. It also gave the designer more flexibility in the analysis and design procedures and it provided more updated seismic maps. Two bridge configurations were chosen to evaluate the impact of new NCHRP 472 provisions on the seismic design and detailing of bridges in New Jersey. A three-span seat-type abutment bridge and three-span integral abutment bridge were modeled, analyzed, and designed using new and current provisions.

NEW SEISMIC DESIGN PROVISIONS (NCHRP REPORT 472)

The new seismic design provisions proposed in NCHRP Report 472 are substantially different and significantly more intricate than the existing provisions. It includes many new concepts and several major modifications compared to the existing provisions. Among the new concepts and major changes in the proposed NCHRP 472 provisions are: (1) *adoption of the 1996 USGS Maps* as basis for the rock ground motion of seismic design. The parameters obtained from these maps include the peak ground acceleration (PGA), elastic response ground acceleration for 0.2 sec, 0.3 sec, and 1.0 sec periods of vibrations. These values are available in three different probabilities: 10 percent in 50 years, 5 percent in 50 years, and 2 percent in 50 years (2 percent in 50 years is approximately 3 percent in 75 years), (2) *design earthquakes and performance criteria*: the proposed provisions provide two design earthquakes with definite performance objectives and design checks: an upper-level event termed the "rare" or Maximum Considered Earthquake (MCE) which has a 2% probability of occurrence in 50 years; and a lower-level event termed the "expected" earthquake, which has a 10 percent probability in 50 years. The "rare" earthquake or MCE governs the limits of inelastic deformations in the substructure and the design displacements in the superstructure while the "expected" earthquake event essentially assures an elastic response of the structure with minimum or no damage, (3) *new soil site factors*, where soil sites are classified based on the average shear wave velocity, SPT blow-count, and undrained shear strength in the upper 30 m of the site profile, (4) *new spectral shapes* where the long-portion of acceleration response spectrum is governed by a spectral shape that decays as $1/T$ rather than $1/T^{2/3}$, (5) *allowing ERS and ERE* that are not currently permitted in current AASHTO LRFD, (6*) four seismic hazardous levels I, II, III, and IV* based on the design earthquake response spectral acceleration values $S_{DS}= F_vS_1$ and $S_{D1}=F_aS_s$, (7) *five defined SDAP (Seismic Design and Analysis Procedures) A, B, C, D, and E* that reflect the variation in seismic risk are based on seismic hazard level, performance objective, structural configuration, and type of ERS and ERE concepts, (8) *seismic detailing requirements (SDR)*, and (9) *design incentives when performing "push over" analysis* in which higher values of the response modification factor, R are used. The new provisions did include procedures for including pile cap lateral load capacity and displacement evaluation. Liquefaction of soil is also addressed. Abutment design incorporated the research that has been done on bridge abutments over the past 10 years. The proposed LRFD limit state for seismic design is similar to the current LRFD limit state used for seismic design for foundations, which is Extreme Event I except that the γ_p factor for dead

loads and earth pressures is taken as 1.0. The resistance factor $\Phi = 1.0$. The load combination and load factors for this limit state is the following:

$$Ext\ Event\ I = 1.0(DC+DD+DW+EH+EV+ES)+\gamma_{E\Theta}(LL+IM+CE+BR+PL+LS+EL)+FR+EQ$$

NJDOT SEISMIC PERFORMANCE AND HAZARD LEVELS

The current guidelines for seismic design of bridges in New Jersey are based on the 1998 LRFD Specifications (w/interims 1999-2003). The specs also require Safety Evaluation performance level as well as Functional Evaluation level for "critical" bridges including bridges carrying Turnpike traffic. Local road bridges over major facilities, including State and Federal Highways, are designed based on the lesser of the two events. The proposed NJDOT seismic performance and hazard levels based on the new NCHRP provisions are shown in Table 1.

Table 1- Proposed NJDOT seismic performance and hazard levels based on New provisions NCHRP 472

Importance Category	Hazard Level	Seismic Event	Return Period	Performance Criteria (Service and Dam	
				Operational	Life Safety
Critical Bridge (TPK & Special Bridges)	Upper Level (MCE)	2% PE in 50 years	2500 Years	Service - Immediate Damage- Minimal	Significant Disrup Significant
	Lower Level (EXP)	10% PE in 50 years	500 Years	Service - Immediate Damage- Minimal	Immediate Minimal
Essential Bridge	Single Level (2/3 of MCE)	2/3 (2% PE in 50 years	2500 Years	Service - Immediate Damage- Minimal	Significant Disrup Significant
Other Bridges	Lower Level (EXP)	PE 10 % in 50 Years	500 Years	Service - Immediate Damage - Minimal	Significant Disrup Significant

The proposed seismic performance criteria and hazard levels are based on new NCHRP provisions and are consistent with NJDOT current philosophy in seismic design of bridges in New Jersey. The proposed criteria will also be consistent with NYCDOT seismic design criteria (NYCDOT, 2000).

Acceleration Coefficients and Design Response Spectra

The acceleration coefficients for various return periods and various locations in New Jersey are summarized in Table 2. Short period acceleration S_s and long period acceleration S_1 are tabulated for the maximum earthquake (2% PE in 50 years) and for the expected earthquake (10% PE in 50 years). Also tabulated are acceleration coefficients for 2/3 of 2500 years event and the 1000 years event (5% PE in 50 years).

Table 2. Acceleration Coefficients in New Jersey for various earthquake events

Location	Accel Coeff (%g)	10% PE in 50 years 500 Years Event (EXP)	2% PE in 50 years 2500 Years Event (MCE)	2/3 of 2% PE in 50 years ~ 1500 Years Event	5% PE in 50 years 1000 Years Event
New NCRP 12- 49 Provisions					
North NJ	S_s =	0.11 - 0.13	0.38 - 0.48	0.25 - 0.32	0.20 - 0.23
Central NJ	S_s =	0.09 - 0.11	0.32 - 0.38	0.21 - 0.25	0.15 - 0.20
South NJ	S_s =	0.06 - 0.09	0.18 - 0.32	0.12 - 0.21	0.10 - 0.15
North NJ	S_1 =	0.025 - 0.027	0.09 - 0.10	0.06 - 0.07	0.048 - 0.052
Central NJ	S_1 =	0.023 - 0.025	0.08 - 0.09	0.05 - 0.06	0.042 - 0.048
South NJ	S_1 =	0.02 - 0.023	0.06 - 0.08	0.04 - 0.05	0.03 - 0.042
Existing LRFD Specifications *					
North NJ	A =	0.18 - 0.20			
Central NJ	A =	0.16 -0.18			
South NJ	A =	0.08 - 0.16			
** PGA Maps*					

The design spectral accelerations for various return periods in North New Jersey in soil type E is shown in Figure 1. Also shown are the spectral accelerations from the current LRFD specifications. The 2/3 of 2500 years return period accelerations are considered for the essential bridges. For local and ordinary bridges, designs will be based on the lower level (expected) earthquake.

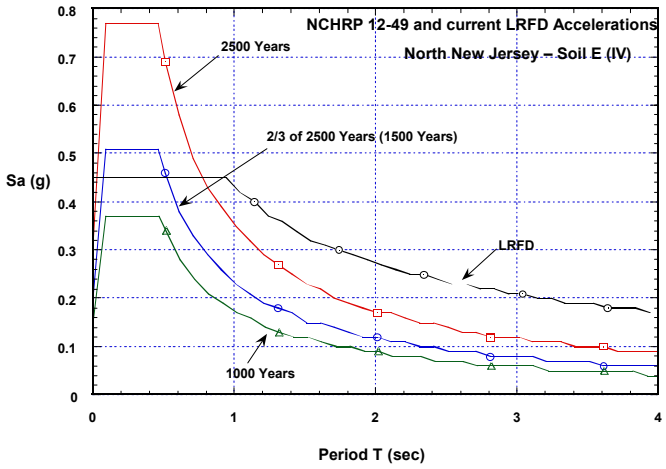

Figure 1. Design response spectra for various return periods in North NJ

The design response spectra for a bridge located in North New Jersey based on the new provisions is shown in Figures 2 and 3 for different soil sites. Figure 2 shows the spectra for the upper level earthquake (MCE) and Figure 3 shows the spectra for lower level earthquake (EXP). A comparison of the response spectra from the new and existing provisions for a bridge located in New Brunswick, NJ in soil type E is shown in Figure 4. In Figure 4 and for this particular location, the short period acceleration form the new provisions is approximately 60% higher than that of the existing provisions while the long period acceleration is smaller beyond the 1 sec period. Several plots were developed for various locations in New Jersey. For very stiff soil conditions, the existing provisions could result in higher short period accelerations compared to the new provisions. The soil type has a major effect on the

design response spectra in the new provisions. This effect is more significant in the new provisions compared to the current provisions. The combination of higher return period and soft soil conditions will result in higher design accelerations in New Jersey and in the Northeast in general. The 2500 year return period could be applied to critical bridges, however, for essential and ordinary bridges in the state, lower return periods need to be considered.

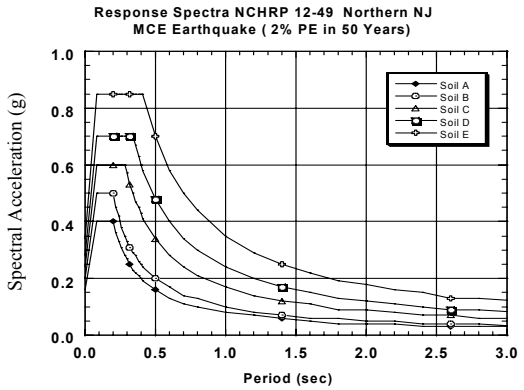

Figure 2. MCE response spectra for different soils.

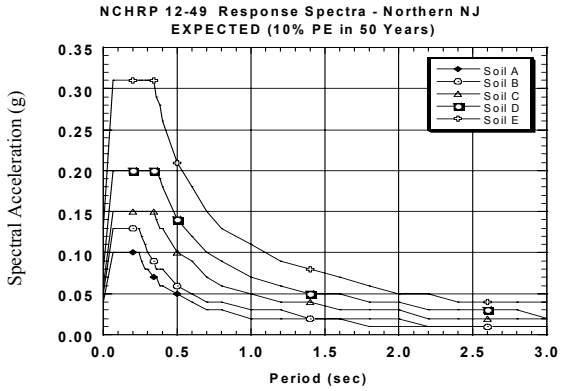

Figure 3. EXP response spectra for different soils.

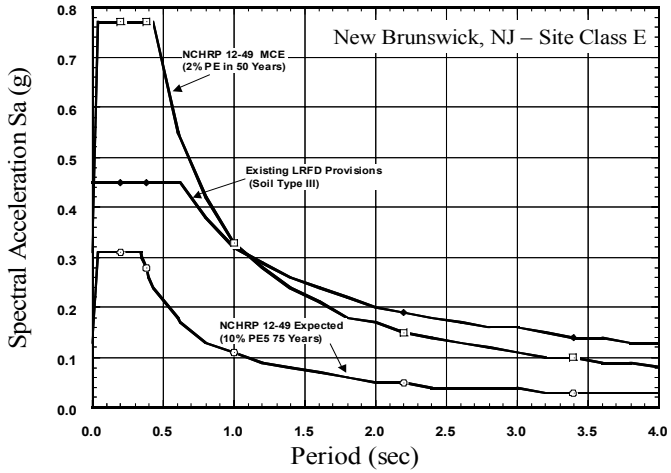

Figure 4. Design response spectra from new NCHRP and existing LRFD provisions.

CASE STUDIES – DESIGN EXAMPLES

Bridge Description and Analysis Results

The structures considered in this study are: 1) a three-span integral abutment bridge with fixed bearings on two-column piers, and 2) a three-span seat-type abutment bridge with fixed bearings on two-column piers. The piers are supported on pile foundations. Figures 5 and 6 show plans, elevations, and sections of the two structures. The span lengths are 24.5 m (80 ft), 30.5 m (100 ft), and 24.5 m (80 ft). The columns are 1.22 m (4 ft) in diameter. The footing dimensions are 9.1x4.6 mxm (30x15 ftxft). Integral abutment piles are HP 360x152 (HP14x73).

Two computer models were created to model the two structures. These models are shown in Figures 7 and 8. Translation springs are used to model the pile foundations under the piers as well as the passive pressure behind the integral abutments. Springs were also used to model the transverse stiffness of the abutments. The height of abutment walls was taken as 3.05 m (10 ft) and the effective width of wing walls equal to 1.52 m (5 ft). The design response spectra from both provisions were input in the program. The soil chosen in this investigation was soft soil (V<180m/s). This soil is classified as Type E in the new NCHRP provisions and Type IV in the existing LRFD provisions.

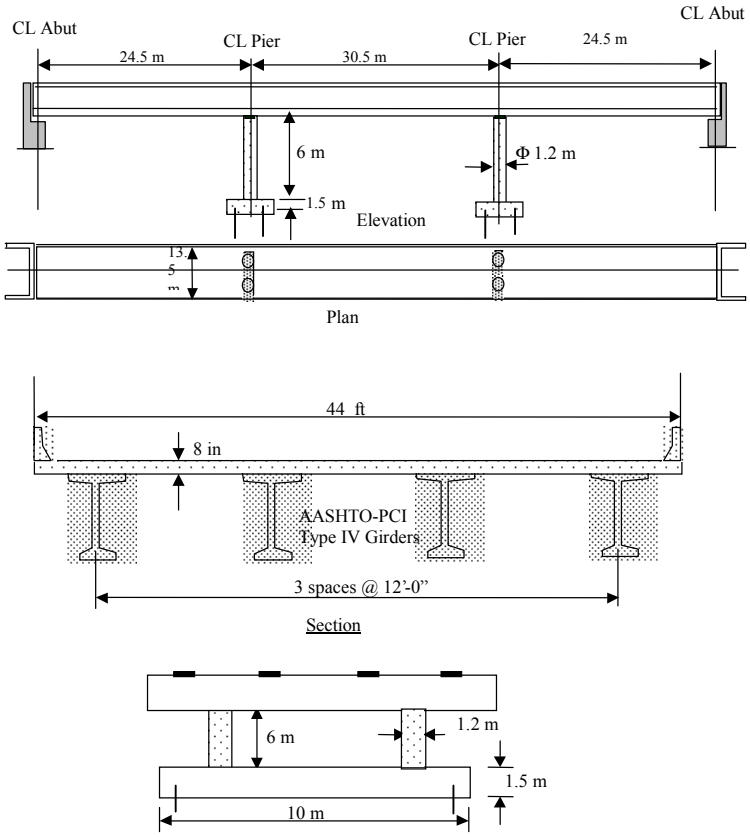

Figure 5. Plan, elevation, and sections of seat-type abutment example.

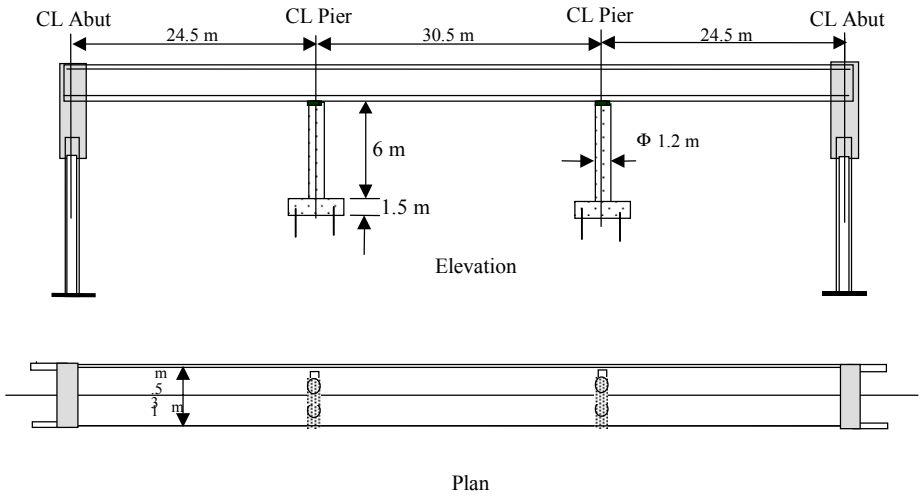

Figure 6. Plan and elevation of integral abutment example.

Modeling

The two bridges were modeled as shown in Figures 7 and 8. The pile foundations at the pier were replaced by two translation springs. In the transverse direction, the abutment restraints were two transverse springs that account for abutment piles and effective length of wing walls. The expansion bearings at the seat abutments were free to move with no soil resistance. In the integral abutment model, similar springs were used at the piers and in the transverse direction. In the longitudinal direction, the passive resistance of the soil was represented by a translation spring in the longitudinal direction. The spring stiffness was calculated using the guidelines in the new provisions. For the existing provisions, the spring constant was computed using passive resisting force of the soil and a certain prescribed soil movement.

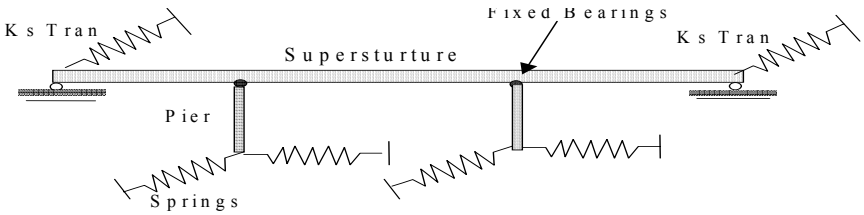

Figure 7. Model of seat-type abutment example.

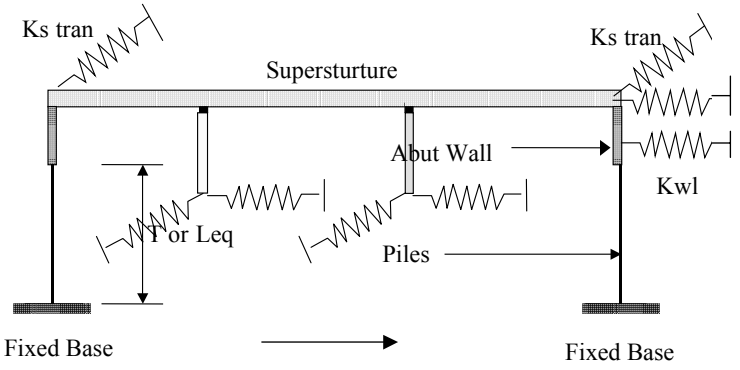

Leq = Pile Equiv Length to Point of Fixity

Figure 8. Model for integral abutment example.

Table 3. Summary of forces, moments, and deflections from elastic spectrum analysis

Seat -Type Abutment SDAP D - Elastic Response Spectrum Ananlysis I eff = 0.4 Ig

T 1 = 0.967 sec T 2 = 0.485 sec

Provisions	Location	Column shears and moments				Piles shears and moments				Displacements				Abutment forces		Long Soil Pressure
		V L	V T	M T	ML	V L	V T	M T	ML	Abut x	Abut y	Pile x	Pile y	Px	Py	
Exisiting	South NJ	1370	351	8264	2143	1392	378	10480	2705	58.7	14.2	9.7	2.8	-	1010	0
LRFD 1998	Central NJ	2055	525	12547	3214	2091	569	15727	4057	86.6	22.4	14.5	4.2	-	1517	0
	North NJ	2469	632	15051	3855	2509	685	18866	4597	105.7	27.2	17.3	5.1	-	1824	0
New	South NJ	1632	818	9956	4909	374	890	40913	6296	69.1	34.8	11.7	6.6	-	2335	0
NCHRP	Central NJ	1859	916	11327	5597	427	996	46535	7060	78.5	37.3	13.5	7.6	-	2624	0
12-49	North NJ	2046	1023	12463	6253	470	1116	51196	7888	90.2	41.9	14.7	8.4	-	2927	0

Integral Abutment SDAP D - Elastic Response Spectrum Ananlysis I eff = 0.4 Ig

T 1 = 0.485 sec T 2 = 0.358 sec

Provisions	Location	Column shears and moments				Piles shears and moments				Displacements				Abutment forces		Long Soil Pressure
		V L	V T	M T	ML	V L	V T	M T	ML	Abut x	Abut y	Pile x	Pile y	Px	Py	
Exisiting	South NJ	182	351	1121	2156	227	383	1474	2720	8.4	14.5	1.8	2.8	2397	1010	0
LRFD 1998	Central NJ	276	529	1695	3234	338	574	2227	4082	12.4	21.6	2.8	4.3	3590	1512	0.669
	North NJ	334	636	2027	3878	409	689	2673	4898	15.0	25.9	3.3	5.3	4315	1819	0.805
New	South NJ	600	818	3648	4990	374	890	15172	6296	25.9	34.0	5.3	6.6	5800	2335	1.078
NCHRP	Central NJ	716	916	4459	5597	427	996	18544	7061	31.8	37.8	6.6	7.6	7086	2624	1.317
12-49	North NJ	810	1027	4795	6253	470	1116	20470	7888	35.1	44.2	7.4	8.4	7828	2927	1.454

Units: Shears in KN, Moments in KN-m, Displacemnts in mm, Soil Pressure in KN/m^2

Analysis Results

The two bridges were analyzed using both the new NCHRP provisions and the existing LRFD provisions. The bridges were also analyzed for three different geographic locations in the state of New Jersey – North, Central, and South. Results of the seismic analysis of the two models are shown in Table 3. Table 3 shows base shears, bending moments, and displacements in the longitudinal and the transverse directions. Also tabulated are abutment forces and soil pressures. Table 4 shows the response modification factors from both provisions used to modify the earthquake loads obtained from the analysis. For the bridge configuration chosen in this study, the maximum displacement under the maximum earthquake (2500 years event) for the structure located in (4.13 in) North New Jersey was about 90 mm (3.54 in) using the new NCHRP provisions and about 105 mm using the current LRFD specifications. For the integral abutment bridge, these displacements were 15 mm (0.6 in) and 35 mm (1.7 in) respectively. The passive soil pressure behind the abutment wall increased the stiffness of the bridge and reduced its period of vibration ($T_1 = 0.485$ sec) compared to the seat-type abutment bridge ($T_1 = 0.967$ seconds). The maximum soil pressure behind the integral abutment wall was 1.45 KN/m^2 (3.5 ksf) for the 2500 years event. This value was less than the maximum value specified by NCHRP 472 provisions, however, it was about three times the pressure resulting from temperature variations.

Table 4. Comparisons of R-Factors for both provisions

Location	Substructure Element	Existing LRFD			New NCHRP 12-49 SDAP D			
		Critical	Essen	Others	T	T_s	R_B	R
Seat Type Abutment								
South NJ	Multipl Column bent	**1.5**	**3.5**	**5.0**	0.967	0.443	4.0	**4.0**
	Vertical Piles	**1.0**	**1.75**	**2.5**	0.967	0.443	2.0	**2.0**
Central NJ	Multipl Column bent	**1.5**	**3.5**	**5.0**	0.967	0.409	4.0	**4.0**
	Vertical Piles	**1.0**	**1.75**	**2.5**	0.967	0.409	2.0	**2.0**
North NJ	Multipl Column bent	**1.5**	**3.5**	**5.0**	0.967	0.412	4.0	**4.0**
	Vertical Piles	**1.0**	**1.75**	**2.5**	0.967	0.412	2.0	**2.0**
Integral Abutments								
South NJ	Multipl Column bent	**1.5**	**3.5**	**5.0**	0.485	0.443	4.0	**3.6**
	Vertical Piles	**1.0**	**1.75**	**2.5**	0.485	0.443	2.0	**1.9**
Central NJ	Multipl Column bent	**1.5**	**3.5**	**5.0**	0.485	0.409	4.0	**3.8**
	Vertical Piles	**1.0**	**1.75**	**2.5**	0.485	0.409	2.0	**1.9**
North NJ	Multipl Column bent	**1.5**	**3.5**	**5.0**	0.485	0.412	4.0	**3.8**
	Vertical Piles	**1.0**	**1.75**	**2.5**	0.485	0.412	2.0	**1.9**

Design Procedures in NCRP 472 Provisions

The five SDAP (Seismic Design and Analysis Procedure) given in the new provisions are: A1, A2, B, C, D, and E depending on the seismic hazard and performance levels. In the two examples, the seismic hazard levels were III for Central and South New Jersey and IV for North New Jersey for the safety level performance of the MCE earthquake (2% PE in 50 years). Based on Table 3.7-2 in NCHRP 472, SDAP B, C, D, and E can be used for level III and SDAP C, D, and E can be used for level IV. The SDR (Seismic Detailing Requirements) was 3 for Central and South New Jersey and 4 for North New Jersey. SDAP C is a Capacity Design Spectrum Method (CDSM) in which demand and capacity analyses are combined. This SDAP can only be used in bridges that satisfy the

requirements of Section 4.4.2 of the new provisions. The examples analyzed here satisfy these limitations and hence this SDAP can be used in both directions. Capacity Design Spectrum Method is a relatively simple procedure and should be used whenever applicable. SDAP D is an Elastic Response Spectrum Method (ERSM). This procedure is a one step procedure using elastic (cracked section properties) analysis. Either the Uniform Load or Multimode method of analysis may be used. These two examples were analyzed and designed using SDAP D. Results of the analysis are shown in Table 3. R-factors and the design summary of columns and piles are shown in Tables 4 and 5 respectively. SDAP E is an Elastic Response Spectrum Method with displacement capacity verification (pushover analysis). This SDAP is similar to SDAP D except that-the response modification factors R are increased. This SDAP was not used in the two design examples.

Table 5. Column and Pile Design – SDAP D

Seat Type Abutment							
Provisions	Location	Column Design				Piles	
		ρ_{long}	Pu	Mu	Φ Mn	V_{EQ}/R	N_{piles}
Exisiting LRFD	South NJ	1%	2313	2712	2712	721	12
	Central NJ	1.5%	2313	3390	3390	1083	24
	North NJ	2%	2313	4068	4068	1299	28
New NCHRP 12-49	South NJ	1.2%	2,313	2,780	2,983	943	20
	Central NJ	1.5%	2,313	3,159	3,390	1072	24
	North NJ	2%	2,313	3,485	4,068	1183	26
Integral Abutment							
Exisiting LRFD	South NJ	1%	2268	651	2712	254	6
	Central NJ	1%	2268	1037	2712	379	8
	North NJ	1%	2268	1252	2712	689	16
New NCHRP 12-49	South NJ	1%	2268	1718	2712	588	14
	Central NJ	1%	2268	1882	2712	684	16
	North NJ	1%	2268	2075	2712	761	18

Units: Shears in KN, Moments in KN-m

V_{EQ}/R = design earthquake load on piles

Transverse Column Reinforcement in Plastic Hinge Zones

The requirements for column design in the new provisions are more complicated than those in the current LRFD provisions. Column design based on the new NCHRP provisions showed that the design was controlled by the requirements to restrain longitudinal bars in plastic hinge zones. In the current LRFD provisions, column transverse reinforcement was also controlled by confinement in the plastic hinge zones. Table 6 shows comparison of transverse reinforcement requirements for the new provisions and the existing provisions. In the new provisions, these requirements are usually governed by the need to restrain longitudinal reinforcement in plastic hinge zones. The required transverse reinforcement is dependent on the longitudinal steel ratio, diameter of the column, and strength of steel but independent of the strength of concrete. In the current LRFD provisions, the transverse reinforcement in plastic hinge zones is independent of the longitudinal steel ratio and column diameter. The table shows that for 0.91 m (3 ft) and 1.22 m (4 ft) diameter columns with 1% steel ratio, the existing provisions require about 10% - 20% more confining reinforcement than the new provisions. For 0.91 m (3 ft) and 1.22 m (4 ft) diameter columns with 2% steel or more and for larger column sizes, the new provisions require more confining reinforcement than the existing provisions. A 50% to 100% increase in transverse reinforcement could be expected for 1.52 m (5 ft) and 1.83 m (6 ft) diameter column with 2% steel when using the new NCHRP provisions.

Table 6. Comparison of transverse reinforcement for new and existing provisions

Column	Long steel	NCHRP Project 12-49[1]			Existing LRFD[2]		
Diameter	ρ_t	ρ_s	spiral size	spacing mm	ρ_s	spiral size	spacing mm
0.9 m	1%	0.0058	# 13	98	0.008	# 13	71
(3' - 0")	# 25 bars	0.0058	# 16	152	0.008	# 16	109
	(# 8 bars)	0.0058	# 19	216	0.008	# 19	155
	2%	0.0102	# 13	55	0.008	# 13	71
	# 29 bars	0.0102	# 16	85	0.008	# 16	109
	(# 9 bars)	0.0102	# 19	121	0.008	# 19	155
1.2 m	1%	0.0068	# 13	62	0.008	# 13	53
(4' - 0")	# 29 bars	0.0068	# 16	96	0.008	# 16	82
	(# 9 bars)	0.0068	# 19	136	0.008	# 19	116
	2%	0.0121	# 13	35	0.008	# 13	53
	# 32 bars	0.0121	# 16	54	0.008	# 16	82
	(# 10 bars)	0.0121	# 19	77	0.008	# 19	116
1.52 m	1%	0.0085	# 16	62	0.008	# 16	66
(5' - 0")	# 29 bars	0.0085	# 19	87	0.008	# 19	93
	(# 9 bars)	0.0085	# 22	119	0.008	# 22	127
	2%	0.0136	# 19	55	0.008	# 19	93
	# 36 bars	0.0136	# 22	75	0.008	# 22	127
	(# 11 bars)	0.0136	# 25	98	0.008	# 25	167
1.83 m	1%	0.0091	# 16	48	0.008	# 16	55
(6' - 0")	# 32 bars	0.0091	# 19	68	0.008	# 19	78
	(# 10 bars)	0.0091	# 22	93	0.008	# 22	106
	2%	0.0163	# 22	52	0.008	# 22	106
	# 36 bars	0.0163	# 25	68	0.008	# 25	139
	(# 11 bars)	0.0163	# 29	86	0.008	# 29	176

ρ_s = ratio of transverse reinforcement ρ_t = ratio of longitudinal reinforcement

1 $\rho_s = 0.016*(D/s)*(s/d_b)* \rho_t (f_y/f_{yh})$ 2 $\rho_s = 0.12*(f'_c/f_y)$

$f'_c = 27.5$ MPa, $f_{yh} = 413$ MPa

Discussion of Results

Seat-Type Abutments

For the bridge configuration considered and for this abutment type, the maximum long seismic displacement for soil class E in North New Jersey was approximately 105 mm (4.13 in) without abutment resistance (K = 0). For a typical expansion gap, the soil behind the abutment wall is not likely to be mobilized and the passive pressure resistance will not be significant. In Central and South New Jersey, the maximum long seismic displacements for soil class E in were 58 mm (2.3 in) and 86 mm (3.4 in) respectively. Hence no passive soil pressure behind abutment and the only resistance to lateral loads will be provided by the piers. For this bridge configuration, both the existing LRFD and the new NCHRP provisions gave comparable displacements for North and Central NJ, however, for South New Jersey, the new NCHRP 472 gave higher forces and displacements.

Integral Abutments

For the bridge configuration considered and for this abutment type, the soil is engaged in resisting the seismic loads and, hence, longitudinal as well as transverse springs are used. The displacements and forces from new NCHRP 472 provisions were higher than those of existing LRFD provisions. This can be attributed to higher accelerations and soil amplification factors. The higher displacements from NCHRP will result in higher forces on the embankment behind the diaphragm. In both provisions, the soil seismic loads did not exceed the 2.75 KN/m^2 (6.67 ksf) ultimate passive pressure specified in the new NCHRP 472 provisions for this abutment height. Because of the larger displacements from new NCHRP 472 provisions, more soil movement behind abutment wall is expected. The longitudinal forces in the piers in the integral abutment were less than those of a seat-type abutment because of soil participation in resisting seismic loads. Engaging the soil behind the abutment will make the structure stiffer because

of the added soil stiffness. This increased stiffness reduces the period of bridge and may result in higher seismic loads depending on the soil class and earthquake intensity.

CONCLUSIONS

1. The new NCHRP 472 provisions does not necessarily result in higher seismic loads compared to existing LRFD provisions. For example, relatively long span bridges on stiff soils can have lower seismic forces using NCHRP 472 provisions compared to the existing LRFD provisions.

2. The 2500 year return period for the MCE earthquake is very conservative compared to other extreme events such as vessel impact and floods. While this maximum earthquake can exceed the expected earthquakes by 50% in the Western United States, it could exceed the expected earthquake by 4 times in the Eastern United States. A lower return period would more reasonable in the Eastern United States. A return period of 1500 years is being considered, however no USGS maps are available. Accelerations equal to 2/3 of the 2500 year event would be reasonable for certain bridges. The 2/3 of the 2500 event is adopted in the IBC seismic design provisions fro buildings.

3. Soil amplification factors F_a and F_v are high for medium to soft soils and they have a major impact on the design response spectra and the selection of the seismic hazard level. Also they have an impact on the R-factors. The soil factors were based on soils from a specific region in the US (mostly the Western US). These factors need to be evaluated for states in the Eastern United States.

4. The new NCHRP 472 provisions provide information on the analysis of integral and seat abutments and on foundation stiffness. It also gives more options in analysis and design procedures. For example, SDAP C, D, and E could be used in most cases. Reduction factors of elastic seismic loads (R) are tabulated in more details for various cases. Allowing larger R-values when SDAP E is used rewards pushover analysis.

5. Because a large number of bridges can qualify under the category where the Capacity Design Spectrum Analysis (SDAP C) can be used, this procedure should be used because it is relatively simple and does not require complicated analyses. Design aids for this procedure can also be prepared to further simplify the procedure.

6. Transverse column reinforcement in plastic hinge zones are significantly affected by the bar size of longitudinal steel. This reinforcement is independent of the longitudinal steel in the existing provisions. For 0.91 m (3 ft) and 1.22 m (4 ft) diameter columns with 1% longitudinal reinforcement, the existing specifications require 10% to 20% more transverse reinforcement. For larger size columns with 2% steel, the new NCHRP provisions require approximately 50% to 100% more transverse reinforcement.

REFERENCES

1. AASHTO, 1998, *LRFD Bridge Design Specifications*, Second Edition, American Association of State Highway Transportation Officials, Washington, D.C.

2. AASHTO, 2002*, Standard Specifications for Highway Bridges*. , 17^h Edition, American Association of State Highway Transportation Officials, Washington, D.C.

3. ATC and BSSC, 1997, Applied Technology Council and Building Seismic Safety Council, NEHRP Guidelines for the Seismic Rehabilitation of Buildings, Federal Emergency management Agency Report FEMA-273.

4. ATC Report 32, 1996, *Improved Seismic Design Criteria for California Bridges: Provisional Recommendations,* Applied Technology Council, Redwood City, CA.

5. ATC Report 32-1, 1996, *Improved Seismic Design Criteria for California Bridges: Resource Document,* Applied Technology Council, Redwood City, CA.

6. BSCE Seminar, 1999, *Design and construction of Integral Abutment Bridges*, ASCE, Boston, MA.

7. Caltrans, 1986, *Bridge Design Manual*, California Department of Transportation, Sacramento, California.

8. Massachusetts Highway Department, Bridge Manual-Part I and II, 1995, Boston, MA.

9. ATC/MCEER Joint Venture, 2002 "NCHRP Report 472 – Comprehensive Specification for the Seismic Design of Bridges", Transportation Research Board, National Research Council, 2101 Constitution Avenue, NW, Washington, DC 20418

10. Nikolaou, S., Mylonkis, G., and Edinger, P., 2001, " Evaluation of Site Factors for Seismic Bridge Design in the New York City Area'", Journal of Bridge Engineering, Vol 6, No. 6, Nov-Dec., pp. 564-576.

11. New Jersey Department of Transportation, Bridge Design Manual, 1997, Trenton, NJ.

12. Proceedings of The Third National Seismic Conference and Workshop on Bridges and Highways, Advances in Engineering and Technology for the Seismic Safety of Bridges in the New Millennium, 2002, sponsored by FHWA, ODOT, and WSDOT, Edited by Roland Nimis and Michel Bruneau, April-May, 2002.

PERFORMANCE BASED DESIGN FOR THE SEISMIC RETROFITTING OF LONG-SPAN STEEL TRUSS HIGHWAY BRIDGES

Charles Seim

ABSTRACT

We can define long-span truss bridges as spans exceeding 150 m., according to AASHTO Specifications. Many of these long-span truss bridges were designed according to older design codes, which did not specify realistic seismic forces. Many of these older bridges still have remaining service life and now require seismic retrofitting to current design standards. This paper discusses seismic retrofitting for long-span steel truss highway bridges based on seismic performance criteria and the vulnerabilities of long-span steel truss highway bridges to earthquakes. The paper presents methods of seismic analysis and the range of retrofit strategies available to the seismic retrofit designer of existing long-span truss bridges

To safely fulfill the remaining life of a long-span truss bridge, the structure needs to be seismically retrofitted to current performance criteria that are developed in cooperation between the bridge owner and the engineer. The minimum performance criterion is no-collapse in an upper level earthquake**,** to preserve life safety. However, a long-span truss that is costly to replace, has special value to the community, is located on an emergency corridor, or is a structure of historical importance, should be seismically retrofitted for essentially elastic response with little or no damage after an upper level event**.**

Charles Seim, Vice President, T. Y. Lin International, 825 Battery Street, San Francisco, CA 94111, USA

INTRODUCTION

The major turning point in modern seismic engineering of bridges in the United States began with the 1971 earthquake in the San Fernando Valley of California. In 1973, the California Department of Transportation responded to public outcry to make highway bridges safe from earthquake collapse by issuing new seismic design criteria for bridges in California. This was the first attempt in the US to relate peak ground accelerations, as are shown on seismic hazard maps, to the different soil types at bridge sites; to the dynamic-response characteristics of the structure; and to the force-reduction factors that account for inelastic behavior. The California seismic design criteria formed the basis for the seismic provisions in the *1977 AASHTO Standard Specifications for Highway Bridges*. Each new edition of the AASHTO specifications has added or refined these seismic provisions.

However, AASHTO specifications cover only the design of new bridges and do not cover seismic retrofit of existing bridges. In 1983, FHWA published Report No. FHWA/RD-83/007**,** *Seismic Retrofitting Guidelines for Highway Bridges*. FHWA followed this first document by publishing, in 1987, Report No. FHWA-IP-87-6, *Seismic Design and Retrofit Manual for Highway Bridges,* which updated and expanded the 1983 work into a manual for the design and retrofit of highway bridges. This document was followed, in 1995, by the FHWA publication Report No. FHWA-IP-95-X, *Seismic Retrofitting Manual for Highway Bridges.*

The 1995 Retrofitting Manual has been revised, updated, and expanded by the Multidisciplinary Center for Earthquake Engineering Research (MCEER), University at Buffalo, State University of New York, as the two-volume *Seismic Retrofitting Manual for Highway Structures,* scheduled for publication in 2004, and sponsored by FHWA. Part 1, entitled *Seismic Retrofitting of Highway Bridges,* will incorporate experience gained from recent earthquakes and from the intense seismic-research effort that has recently been developed and conducted in several structural-testing laboratories.

STEEL TRUSS HIGHWAY BRIDGES

In the U. S., the most prolific long span bridge type used in the last 100 years for highway structures, in the span range of about 50-m to 500-m, is the steel truss. Since 1927, *AASHTO Standard Specifications for Highway Bridges* have governed the design of highway bridges for spans less than 150 m. Hence, long-span trusses are defined as spans exceeding 150 m**.**

In the last two decades, the cable-stayed girder bridge has been the long-span truss bridge of choice for highway bridges with spans above 150 m because the cable-stayed bridge is structurally efficient and, therefore, costs less than the traditional truss bridge. Many existing long-span steel truss highway bridges have many years of service life remaining but need seismic retrofitting to fulfill their function of safely carrying traffic for their remaining life.

Definition of Steel Truss Highway Bridges

Steel truss highway bridges are defined generally as a framework of straight steel members, forming triangular patterns, that are connected together to form a primary load-supporting system, the truss. Trusses contain upper and lower chords that act in compression or tension. Vertical members, called verticals, posts, or plumb posts, connect the upper and lower chords and act in tension or compression. Sloping members, called diagonals, frame between the

upper and lower chords and between the vertical members and act in tension or compression. The triangle is the characteristic basic unit of a truss bridge configuration because the triangle is the most inherently stable geometric figure. Another characteristic of a truss is that each straight member acts in tension or in compression. Small secondary bending stresses are induced into the truss members by dead load deflections, because the connections of the members have some stiffness.

Generally, two primary trusses are spaced apart by floor beam members framed into the vertical posts, or into the apex of the diagonals. The floor beams support longitudinal stringers, which support the concrete deck, on which vehicles travel. Secondary members fulfill important functions, such as forming a lateral bracing system in a horizontal plane at the upper and lower chord levels, and acting to carry transverse wind and seismic loads longitudinally to the truss supports. Secondary cross bracing in the vertical plane at the panel points acts to space the trusses apart to match the floor beam spacing, as well as acting to stiffen the rectangular cross-section against sway distortions. Tertiary bracing members fulfill the important function of bracing long compression members within the trusses and secondary members against buckling.

Most trusses have stiff sway-frames at each end of the truss, called portals or portal frames. The function of the portal frames is to carry wind and seismic loads from the lateral bracing system, in the plane of the upper chord, down to the bridge bearings that support the truss at each end. In the past, wind loading usually controlled the design of the portal frames, particularly in high seismic areas, since seismic forces, until about the 1990's, were greatly underestimated. However, in a seismic event, the portal frames will perform the same function as they do for wind; i.e. carry seismic lateral forces down to the truss bearings, provided the portal frames have sufficient capacity or were seismically retrofitted.

Classifications and Articulations of Steel Trusses used for Highway Bridges

Trusses are classified by the position of the deck within the cross section of the bridge. If the deck is in the plane of the top chords, the bridge is referred to as a deck truss; when the deck is in the plane of the lower chord, the bridge is referred to as a through truss. If the deck is between the top and bottom chords, the bridge is referred as a half-through truss.

Trusses are also classified by the articulation of the truss at its support points and inter-span hinged points. A cantilever truss refers to a construction method in which the truss is erected by balanced cantilevering out from each of two center towers. A suspended span is used to join the two cantilever arms. The suspended span is usually connected to the tips of the cantilever arms by eye bars or by hanger plates and the suspended span functions as a simple span. A continuous truss is, as its name implies, continuous over each of the piers that support the truss. Continuous trusses are generally limited to two, three, or, rarely, four spans. The position of the deck, as denoted by the terms "through" or "deck" is usually placed after the truss classification term, i.e., Cantilever Deck Truss, or Cantilever Through Truss.

DESIGN METHODS AND COMMONLY USED STEELS FOR TRUSSES

Materials in a bridge respond to the laws and forces of nature and not to the methods of design**.** The method and year in which the bridge was designed can be important to the retrofit analysis of the bridge since different design methods and the year of the design specification produce slightly different amounts and placements of material and different force levels within

the structure. Over the years, the AASHTO *Standard Specifications for Highway Bridges* have undergone three significant changes of design methods in its approach to bridge design practice: Allowable Stress Design, Load Factor Design, and Load and Factor Resistance Design.

Allowable Stress Design

Starting with the first edition in 1927, the AASHTO bridge design specifications were historically based on the Allowable Stress Design (ASD) philosophy. Many truss bridges were designed using the ASD method, because this was the only design method available during the time when truss bridges were the structure of choice for highway bridges.

Load Factor Design

In 1967, AASHTO introduced the Load factor Design (LFD), an alternative design method using load factors and a limit-state design approach. Designers slowly adopted the changeover from ASD to LFD. Although the LFD method was available to designers, many truss bridges continued to be designed by ASD.

Load and Resistance Factor Design

In 1994, AASHTO introduced its third alternative design procedure called Load and Resistance Factor Design (LRFD), which is an extension of the LFD limit-state design philosophy with load and resistance factors developed through a statistical approach. Load Factors and Resistance Factors are calibrated to achieve a uniform reliability index for span lengths, bridge types, and the statistical variability of the loads and materials. LRFD is the current recommended design method of choice.

Steels used for Truss Highway Bridges

Older bridges were constructed from cast iron, wrought iron, and steels of unknown type and strength. In the early 1900's, before the development of ASTM specifications, most of the steels used in bridges were called "medium steels," for nominal strength levels, and "high-carbon steels" for higher strength requirements. In about this same period high-strength silicon and nickel steels were also developed. Steel "eyebars" were forged from higher strength steel. Most of these early steels are considered unweldable.

Around the 1920's, steel plates and rolled sections, conforming to ASTM specifications began to be supplied by steel mills. The ASTM specifications produced standards that steel manufactures were required to meet and that bridge designers could specify with reliability.

After the Second World War, low-alloy steels with higher strengths became available and some were formulated for welding. In the 1950's, welded, high-yield-strength, quenched, and tempered steels were developed and were used as tension members in place of eyebars. In the 1970's and 1980's, several bridges developed brittle fractures, resulting in collapses or closures for bridge repairs. As a result Steels with stated toughness requirements are now part of ASTM A 709.

The seismic retrofit designer should attempt to determine what steels were used in the various members of the truss. If construction plans or specifications are not available, steel

samples can be cut from the truss in low-stressed areas for laboratory testing of physical properties.

TRUSS MEMBERS AND CONNECTIONS

Members

Older truss bridge members usually were small rolled sections, round rods, flat bars, and eyebars. Eyebars were used for tension members exclusively because the pins allowed easily made connections to the gusset plates. When larger members were required, flat plates, rolled sections, and angles were riveted together, usually in the form of I beams or H-shapes or in an open box-shape with plates on three sides and the fourth side covered with a lattice of bars or angles.

After the Second World War, truss plate units were usually welded together to form members with an H-shape or a box-shape with plates on all four sides. Generally one, and sometimes two, plates on opposite sides to each other were perforated with large rectangular cutouts to allow the painting of inside surfaces. In the last 25 years the box sections were often welded with solid plates and with welded diaphragms at each end, which sealed the box to prevent inside corrosion

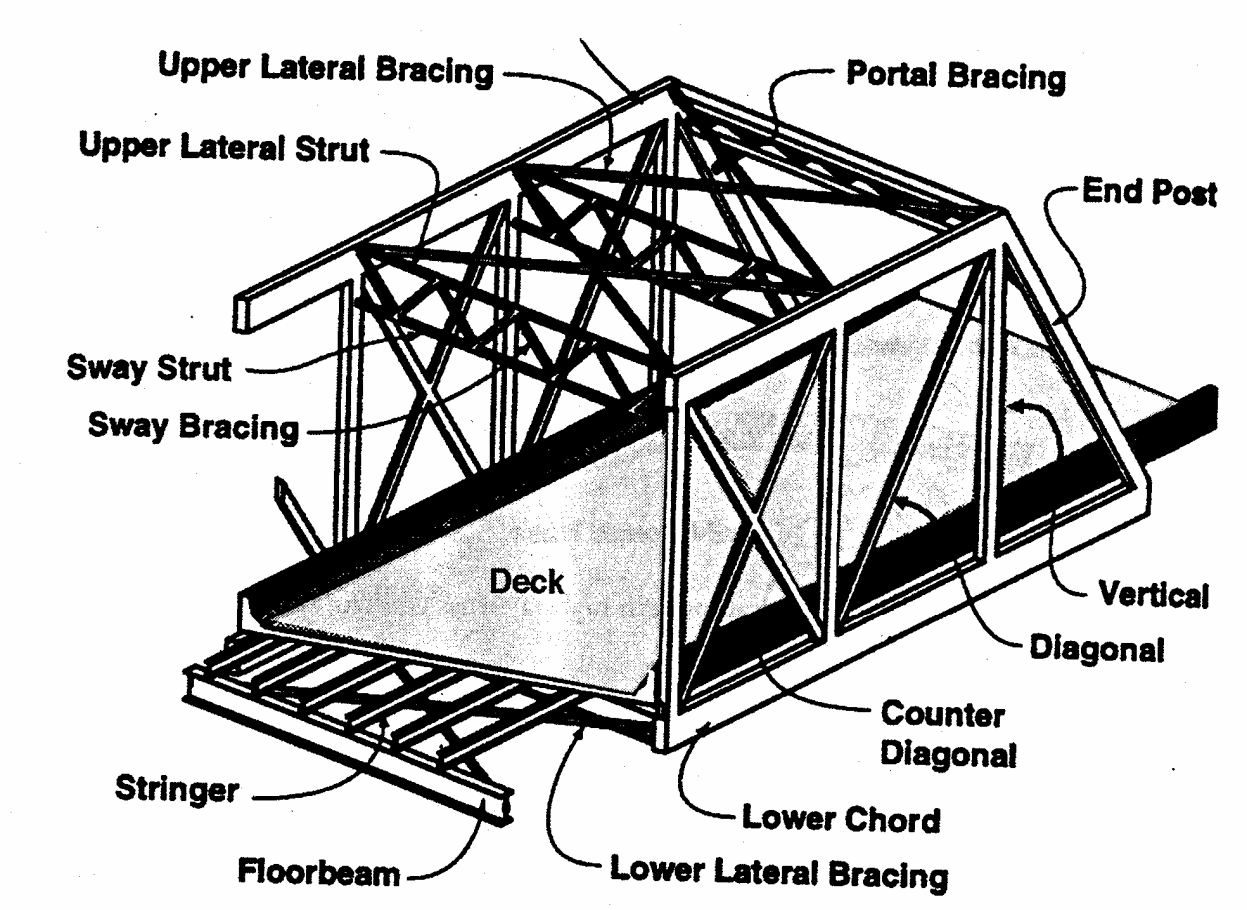

STEEL TRUSS HIGHWAY BRIDGE COMPONENTS

Connections

Truss bridges constructed before the Second World War used riveted connections between the truss members and the gusset plates. After the war rivets continued to be used, but high strength bolts were developed which could be tightened with an easy-to-use pneumatic wrench, so bolts gradually replaced rivets. By the 1960's, the art of riveting had ended and bolting was used exclusively.

Truss Bearings

Bridge bearings installed on long-span truss bridges are usually fabricated structural steel devices. Bridge designers of these long, heavy spans usually designed the bridge bearings and detailed them on the design drawings as part of the design process. A seismic retrofit analysis may demonstrate that an existing bearing does not have the capacity to carry seismic demands or displacement and so requires replacement. While a number of bridge bearing types and devices are available today from bearing manufactures, few will have the vertical load or seismic capacity for a long-span structure. Some long span trusses may be too heavy to lift or there is no space for placing jacks. In such cases, the existing bearings must be retrofitted to provide capacity for the seismic demands obtained from the seismic analysis.

Expansion Joints

Expansion joints, placed at each end of the truss, bridge the gap between the bridge deck and the abutments to allow thermal movements. For joints with large movements, two intermeshing fingerplates are usually employed. Occasionally, the original expansion joints wear out under the passage of millions of wheel-loads; they can be replaced with modular expansion joints that are readily available today.

Often expansion joints are placed in the concrete deck of the truss span to break up participation by composite action between the concrete deck and the chords of the truss. For seismic analysis these deck expansion joints need to be modeled for the demand-evaluation of the truss. Field measurements of a few truss bridges indicate that the floor system and the concrete deck can participate in load sharing at least partly with the truss chords.

CHARACTERISTICS OF THROUGH-TRUSS BRIDGES

The most prevalent long span truss type is the Through Truss. The Through Truss type is characterized by the placing of the trusses and bracing system above the roadway with the vehicles driving through the array of steel. The Through Truss type is often used for long truss spans over navigation channels because the structural depth of the deck system from the top of the deck to the lower chord clearance line is smaller than for Deck Truss types. This reduces the height of the main span, which reduces the height and length of the approach spans and that reduces the initial cost of the crossing.

Through trusses are usually configured as a cantilever span with two back spans, though some use Gerber framing, and some are fully continuous over several spans. The three-span cantilever configuration usually has a suspended span hinged in the center of the main span, or it can be continuous over the three spans. The structural depth of most cantilever trusses is

increased at the two center supports, giving these bridges their characteristic up-swooping curves at the towers.

Lateral Force Resisting Elements

The backbone**s** of lateral force-resisting elements in Through Trusses are the horizontal lateral bracing systems placed within the plane of the upper and lower chords. The upper lateral bracing system usually carries the forces by truss action to the ends of the suspended span or toward the towers of the cantilevers, or of the continuous spans. At these points, the forces are transmitted down to the lower lateral bracing system through portal frames placed at the end of the suspended spans at the end of the cantilevers, or by portal frames placed in the plane of the two diagonals that frame into the truss supports. The portal frames have cross bracing only at the top of the frames, because the lower portion of the frames is open for the passage of vehicles.

The lower lateral bracing system in the suspended span carries the forces by truss action to each end and then transmits these forces, and the forces from the end portals, through wind tongues, sometimes called wind locks, to the cantilever arms. The lower lateral bracing systems in the cantilever arms carry the forces by truss action to the truss support-point bearings. In continuous spans, there are no suspended spans or wind locks; hence the forces are carried directly to the support-point bearings by the lower lateral bracing systems.

Potential Seismic Vulnerabilities

In the past, all of the lateral bracing systems and wind tongues were designed for static wind forces because wind forces always controlled over seismic forces until the seismic codes changed to reflect the higher demands imposed on bridges by dynamic actions of earthquakes. The mass of non-composite concrete decks and supporting systems contributes inertia demands on the lateral bracing system, but contributes little lateral resisting capacity. The lateral bracing systems, the wind tongues, and the portal systems are the most vulnerable systems within a long-span truss. These systems, as well as the truss members, connections, and bearings, must be carefully modeled to evaluate their capacity-demand ratios to determine their vulnerabilities.

DECK SYSTEMS

The predominant deck system for most highway truss bridges is a reinforced concrete deck supported on longitudinal steel stringers connected to, or supported on, transverse floor beams. In Deck Trusses, the transverse floor beams connect to the top chords; in Through Trusses, the transverse floor beams connect to the bottom chords.

The floor beams are connected to the chords at the panel-point gusset plates by clip angles that are riveted or bolted to the web of the floor beam. This type of connection transmits shear and little moment in the vertical plane and is completely flexible in the horizontal plane. The same type of connection connects the stringers to the floor beams in deck systems that have the stringers framing into the floor beams. For deck systems that have the stringers supported on the top flange of the floor beam, the connections are usually rivets or bolts connecting the bottom flange of the stringer directly to the top flange of the floor beam. A lateral bracing system is usually placed under the plane of the stringers and framed into the intersections of the floor beam and the chord.

The concrete deck is supported directly on the top flanges of the floor beams and the stringers, which are usually spaced four to six feet apart. The deck is generally not connected to

the stringers, to achieve composite action. Deck joints, placed over the floor beams, are spaced along the bridge-length from one to four floor beams. These deck joints are placed in the deck to eliminate any frictional composite-action participation from the differential expansion and contraction of the concrete deck with the chords of the truss. Usually the only connection holding the deck in place laterally is a concrete lip, or fillet, bearing against the top flanges of the stringers and the bonding of the concrete on the steel supports. Bonding of the concrete to the steel on the top flanges of the stringers will also provide partial composite action. However, this type of bonding is accidental and the bond may break during service.

Potential Seismic Vulnerabilities

The concrete deck is a heavy mass concentrated in the plane of the lower or upper chord along the length of the bridge. Under strong seismic excitation, the truss is deflected in a horizontal plane, with the amount of deflection controlled by the effectiveness of the lateral bracing system. The concrete deck is forced to follow these deflections and it structurally participates with the horizontal truss action until the concrete lips, or fillets, holding the deck in place are sheared off. The concrete deck panels then float free and collide with one another and the truss members. This may lead to cracking of the concrete deck, destruction of the deck joints, and damage to the truss members, leaving the deck displaced. The seismically damaged deck may need extensive repair or complete replacement.

SUBSTRUCTURES FOR STEEL TRUSS HIGHWAY BRIDGES

Most substructures for long-span bridges can be classified into the following substructure types:

- Spread footings
- Timber piles
- Reinforced Concrete piles
- Prestressed Concrete piles
- Steel piles
- Steel and Concrete Caissons

The substructure needs seismic evaluation either separately or as part of the global analysis. For important long span bridges in high seismic areas, a soil-foundation-structure interaction analysis is warranted.

Steel Truss Highway Bridges are usually supported on concrete pier shafts, on steel towers of cellular construction, on steel braced frames, and, occasionally, on unreinforced masonry piers. Concrete pier shafts are fixed to the concrete substructure with embedded reinforcing bars that generally were spliced at the base of the pier shafts for ease of construction. The reinforcing bars are usually confined with small, widely spaced stirrups.

Steel towers, steel towers of cellular construction, or steel braced-frames are usually attached to the concrete pile caps or the caissons by steel anchor bolts. Towers of steel cellular construction are usually shop-connected in older structures by riveting, and, in newer structures by shop welding. Field connections are typically riveted on older structures or are bolted with high strength bolts on newer bridges. Welded field connections are rarely used. Steel braced frames are usually used to support older structures and are usually made up of rolled sections that are field-riveted together.

Most of these types of concrete piers and steel towers will require some form of seismic retrofitting. Usually the original concrete reinforcement was lap-spliced at the base in the plastic hinging zone and inadequately confined with stirrups. Braced frame members can buckle and are usually inadequately sub-braced and inadequately anchored to the substructure.

HISTORICAL TRUSS BRIDGES

Long-span truss bridges older than 50 years are eligible for listing as an historical structure. The rehabilitation and retrofit of historic bridges must be done in a way that respects the historic nature of the structure**.** The first step in the rehabilitation of a historic building is to identify, retain, and preserve the materials and features that define the historic character of the building

Rehabilitation and repair then follows a hierarchy wherever possible:

- Protect and maintain the structure and original materials.
- Replace members with identical new members.
- Replace missing historic features.

SEISMIC PERFORMANCE LEVELS

When a bridge is identified as seismically deficient and is scheduled for retrofitting, the owner, with the help of the bridge engineer, should choose one of the three performance levels listed below, to which their bridge should be seismically retrofitted.

The three Performance Levels for the seismic retrofitting of an existing bridge are:

Performance Level 1 (PL1): Life Safety
Sustained damage is *significant* after a large earthquake and service is significantly disrupted, but life safety is assured. The Bridge may need to be replaced after a large earthquake.

Performance Level 2 (PL2): Limited Performance
Sustained damage is *minimal* and limited service for emergency vehicles is available after inspection and clearance of debris. The Bridge is repairable, but with restrictions on traffic flow during repair.

Performance Level 3 (PL3): Full Performance
Sustained damage is *negligible* and full service to all traffic is available after inspection and clearance of debris. Damage that does occur is repairable without interruption to traffic flow.

Generally, the assignment of performance criteria varies with earthquake level, bridge importance, replacement cost, and anticipated service life.

Objectives of Retrofitting and Acceptable Damage

The objective of retrofitting a bridge is to ensure that it will perform satisfactorily in the design earthquake. .

Performance Levels 1 and 2 permit some structural damage as long as the bridge does not collapse. For Performance Level 3, damage is negligible and the response of the bridge to an earthquake is essentially elastic.

Selecting the preferred retrofit strategy is a multi-faceted problem. Not only is it often a challenge to find the right technical solution, it is also a challenge to satisfy a multitude of socio-economic constraints.

RETROFIT STRATEGIES, RETROFIT APPROACH, AND RETROFIT MEASURES

Retrofit Strategy is the overall plan for the seismic retrofit of a bridge. This plan can employ more than one retrofit approach and several different retrofit measures.

Retrofit Approach is a method of improving or correcting the seismic deficiencies of the bridge. Strengthening and Isolation are examples of retrofit approaches. One or more retrofit approaches may be employed in the seismic retrofit of a bridge.

Retrofit Measure is the physical modification of a component in a bridge for the purpose of improving or correcting seismic deficiencies of the bridge.

EARTHQUAKE LEVELS

The *lower level* earthquake is the largest earthquake that has a reasonable probability of occurrence within the lifetime of the bridge. However, rather than the assigning of a probability of occurrence, common practice uses a probability of exceedance to characterize the event. The lower level earthquake has a relatively high probability of exceedance within the life of a bridge and a return period of about 500 years is generally used.

The *upper level* earthquake is an earthquake that has a finite probability of occurrence within the life of the bridge and represents a large and rare event. A return period of 1000 to 1500 years is generally selected. The selection of the upper level event for retrofitting bridges is therefore a compromise between the need to provide safety and adequate performance for these less frequent events and the limited resources of the owner of the long-span bridge in need of seismic retrofitting.

SELECTING A RETROFIT STRATEGY

Step 1: Conduct a detailed as-built evaluation. The goal of this step is to assess the performance of the bridge during the design earthquake and to identify deficiencies that are correctable by retrofitting. Structural and Geotechnical specialists and the Owner should be involved in this evaluation.

Step 2: Identify alternative retrofit strategies. Often there is more than one way to improve the performance of an existing bridge, and it is important that the designer identify as many options as possible. Many will be quickly eliminated because of excessive cost, constructability or other problems.

Step 3: Evaluate alternative retrofit strategies. Perform detailed analytical evaluations of each viable retrofit strategy. This step should also include the preliminary design of the elements of the proposed retrofit so that a preliminary cost estimate can be prepared for each alternative.

Step 4: Conduct a strategy meeting. Since seismic retrofitting involves many complex issues, consensus must be achieved on the most appropriate strategy. Representatives of all agencies interested in the project should attend this meeting, including the bridge owner, utility companies, Federal, State and Local government agencies, structural and geotechnical engineering specialists, environmental and citizens groups.

Step 5: Document the strategy selection. Document the retrofit decision in a strategy report that becomes part of the permanent record for the project. This report should include all the calculations of the as-built and as-retrofitted structure, preliminary plans and sketches showing the proposed retrofit, a summary of conclusions and recommendations, preliminary cost estimates, and a summary of the discussions from the strategy meeting.

SEISMIC EVALUATION METHODS AND STEPS

When preliminary evaluation of a long-span truss bridge shows seismic deficiency, the next step is the performance of a detailed seismic evaluation. The detailed seismic evaluation of a long-span truss bridge is a two-part process. A demand analysis is first required to determine the forces and displacements imposed on the existing structure by the design-earthquake. This demand analysis is followed by an assessment of the capacity of the truss and its components to withstand this demand. A capacity/demand ratio above 1.0 implies essentially elastic resistant action, whereas a capacity/demand ratio below 1.0 implies some inelastic damage and a possible need to retrofit the component or the structure.

Three evaluation methods are required for a fully detailed evaluation of the truss bridge. All three methods are based on capacity-demand principles. They are listed below in order of increasing complexity and rigor.

Method A: Elastic component capacity-demand method. Determine seismic demands by an elastic analysis on simplified models, using a multi-mode response spectrum method. Capacity values are determined from simplified bilinear lateral strength curves. If the results of this simplified method indicate that the capacity/demand ratios are comfortably above 1, then it will not be necessary to use more complex evaluation methods.

Method B: Elastic structure capacity-demand method and pushover analysis. Determine seismic demands by elastic methods on a detailed model by either a multi-mode response spectrum method, or an elastic time history method, and an elastic pushover analysis. Capacity assessment of the structure and its components are based on the displacement capacity as is determined from the response spectrum analysis, and by a lateral load-displacement pushover analysis. The results of this elastic evaluation will determine whether the structure must be re-analyzed using the more complex and rigorous Method C.

Method C: Nonlinear dynamic time-history analysis and quasi-static nonlinear pushover analysis. Seismic demands are determined by a nonlinear dynamic analysis, using time-recorded histories of earthquake ground motions and a quasi-static non-linear pushover analysis, to evaluate the displacement and force demands. Capacities of individual components are explicitly modeled in the demand analysis.

The choice of methods to use for a seismic evaluation is based on two principles. First, as the seismic hazard increases, improved modeling and analysis for the seismic demands is necessary because bridge response is sensitive to increasing demand. Second, as the complexity of the bridge increases, models that are more complex are required to capture both the demand and the capacity with certainty. Note that a higher level of analysis may always be used in place of a lower-level method.

SUMMARY

The paper discusses seismic retrofitting for long-span steel truss highway bridges based on seismic performance criteria and the vulnerabilities of long-span steel truss highway bridges to earthquakes. The paper presents methods of seismic analysis and the range of retrofit strategies available to the seismic retrofit designer of existing long-span truss bridges

REFERENCES

Beginning in the 1990s, a number of truss bridges have been designed for seismic retrofitting and a few are currently undergoing seismic retrofit construction. Several excellent papers have been published on these projects and will provide a resource for retrofit examples. The papers can be obtained from the organization the produced them.

- Design Criteria and Construction Plans, Golden Gate Bridge (California) Seismic Retrofit Design, TYLI, San Francisco, CA.

- Design Criteria and Construction Plans San Francisco-Oakland Bay Bridge West Spans (California) Seismic Retrofit, Caltrans, Sacramento, CA.

- Design Criteria and Construction Plans, Carquinez Bridge (California) Seismic Retrofit, CH2M-Hill, Oakland, CA.

- Design Criteria and Construction Plans, Benicia-Martinez Bridge (California) Imbsen and Associates, Inc., Sacramento, CA.

- A Guideline for Seismic Retrofit Evaluation and Design for Latticed Members and their Connections on San Francisco-Oakland Bay Bridge, Caltrans, Sacramento, CA.

Development of Damage-based Limit States in Performance-based Seismic Design for Steel Bridges

George C. Lee, Zach Liang, and Yu-Chen Ou
Multidisciplinary Center for Earthquake Engineering Research
University at Buffalo

Introduction

Performance-based seismic design enables engineers to explicitly consider the functionality or performance level of a structure under a prescribed seismic hazard. Quantifying performance levels into engineering limit states is a very challenging issue. Qualitative descriptions of damage-based limit states that correspond to various performance levels have been given in ATC-32 (1996) for bridges, as shown in Table 1, and in Vision 2000 (1995) and FEMA 356 (2000) for buildings. Damage indices allow designers to directly address the process of damage accumulation in a structure during an earthquake and its resulting post-earthquake damage state. Therefore, damage indices can be employed to quantify damage-based limit states associated with various performance levels. A variety of damage indices for concrete and steel structures have been developed. This paper first gives a brief review of the concepts and developments of damage indices, with a focus given on those for steel structural components. It is followed by describing observations from a pilot experimental study on structural steel bars with respect to their change in dynamic properties (period, damping ratio and transfer function).

This pilot study is the initial phase of a research program to quantitatively establish the damage accumulation process of bridge components.

Characteristics of cumulative damage in RC and steel structures

Due to the difference in material behavior, the processes of damage accumulation under seismic loading reversals for RC and steel structures are different. In RC structures, the damage can be categorized into two types: the maximum ductility demand sustained by a structure, and the energy dissipated resulting from repeated loading reversals (Park and Ang 1985). For steel structures, damage accumulation due to strong ground motions is mainly associated with fatigue, especially low-cycle fatigue (Krawinkler 1983). A low-cycle fatigue model has also been applied to predict the damage accumulation in RC bridge columns, when reinforcing steel becomes the dominant source of damage accumulation (Kunnath 1997).

For steel structural members, local and overall buckling are typical failure modes. Large inelastic strain reversal in the post local buckling range can accelerate the fatigue-based damage accumulation of steel structural members. For instance, tests of coupons without local buckling show that mild steel can resist more than 400 cycles with strain cycling between $\pm 2.43\%$. On the other hand, flange local buckling in a beam subjected to bending reversals with a flange width-thickness ratio of 10.5 occurred after only half cycles at strain cycling between $\pm 2.5\%$, and

the beam fractured after 16 cycles (Bertero 1965). This was the basis for specifying a smaller limiting value of width-thickness ratios λ_{ps} in the AISC seismic provisions (2002) for certain structural components.

Damage indices and damage spectra

Damage indices have been used as a useful tool to quantitatively describe the damage in a structure. For local damage indices, non-cumulative damage indices are primarily based on ductility or stiffness (Banon 1981; Powell 1988; Cosenza 1993), while cumulative damage indices are categorized into fatigue-based (Krawinkler 1983; Chung 1987; Azevedo 1994; Mander 1994; Mehanny 2001; Liu 2002), energy-based (Fajfar 1992; Kratzig 1997) and ductility-energy-based (Park and Ang 1985; Chai 1995; Reinhorn 1996; Bozorgnia 2003). For global damage indices, some models use the weighted average of the local indices (Park 1985a; Chung 1990) whereas others use the change of the modal parameters (Dipasquale 1988). Bozorgnia and Bertero (2003) have recently extended the application of damage indices into damage spectra where the seismic damage potential of a SDOF system in terms of a proposed damage index can be obtained.

Furthermore, most of the damage indices developed to date are focused on flexural failure mode only.

For steel structures, a fatigue-based damage model is the most widely used for cumulative damage. The original Coffin and Manson equation of fatigue life of a steel member under constant amplitude cycling is of the form

$$\varepsilon_{ap} = \frac{\Delta\varepsilon_p}{2} = \varepsilon_f^{'}(2N_f)^c \tag{1}$$

in which ε_{ap} is the plastic strain amplitude; $\varepsilon_f^{'}$ and c are constants depending on properties of structural component; and $2N_f$ is the number of reversals to failure. Assuming linear damage accumulation, the total cumulative damage can be expressed as

$$D = \sum_{i=1}^{n} \frac{1}{N_{fi}} \tag{2}$$

D=1 denotes failure of the structural component whereas D=0 means no damage. This model addresses the cumulative effect of repeated cycles while taking into account the amplitude of loading cycles. It is noted that the fatigue life of the steel is exponentially proportional to the plastic strain amplitude. The constants $\varepsilon_f^{'}$ and c in Eq. (1) are calibrated against the experimental results in specific applications.

Therefore, local buckling with inelastic strain reversal has the most importance in the damage accumulation process for steel components. Krawinkler (1983) intentionally induced local buckling after a small number of loading reversals, and studied the process of damage accumulation in terms of deterioration of stiffness, strength, and hysteretic energy. These conditions are described in three stages, as shown in Fig. 1. For each stage, the correlation

between deterioration per reversal Δd and plastic deformation range $\Delta\delta_p$ was established as

$$\Delta d = A(\Delta\delta_p)^a \tag{3}$$

Where A and a are parameters that depend on structural properties. If structural failure occurred after local buckling, it is defined as the attainment of a certain level of total deterioration x. The fatigue life under constant amplitude cycling is given by

$$N_f = xA^{-1}(\Delta\delta_p)^{-a} = c^{-1}(\Delta\delta_p)^{-c} \tag{4}$$

Eq. (4) is essentially of the same form as Eq. (1). This indicated that the forms of fatigue life models for the fatigue of material itself and for the fatigue due to local buckling are the same. Furthermore, assuming linear damage accumulation, the total accumulated damage can also be represented by Eq. (2). The experimental result is therefore based on structural steel section W6×9 with a width-thickness ratio of $b/t = 18.9$.

Experimental Program

A pilot experimental program using shaking table was carried out to develop damage-based limit states in performance-based seismic design for steel bridges. This paper describes the initial phase of this study to investigate damage accumulation in terms of the changing dynamic characteristics (period, damping ratio and transfer function), while local and global buckling were prevented.

The seismic damage behavior of reinforced concrete bridge column in terms of effective stiffness, energy dissipation, residual displacement and frequency content of displacement response has been investigated (Park et al 2001). In this pilot study, three steel columns, see Fig. 2, with lump mass were tested by using the shaking table and the El-Centro ground motion. A SDOF system is assumed for the columns in the analyses. The magnitude of the ground motion was increased up to the onset of yielding at the base of the column and then kept at the same level for 10 cycles. The loading history is given in Table 2. The yielding of the column base was confirmed by strain gauges that were applied on the surface of column. The intent of such loading history is to observe the damage accumulation of steel columns in the elastic and inelastic ranges, while preventing buckling. An HSS3×1 section with yield stress of 70ksi, determined by material coupon tests, was selected to avoid premature local buckling. Shaking about the weak axis of the cross section was to prevent global instability and to minimize the cross-effect between the two principal directions (Liang and Lee 2002, 2003). In order to capture the change in damping ratio and frequency of the structure, free vibration tests within the elastic range and white noise vibration tests, with frequency content 0~10Hz were performed, respectively, between every two consecutive ground motion events. The acceleration transfer function was calculated by using the data from accelerometers installed on the specimen and shaking table. The displacement response was recorded by a linear potentiometer installed at the top of the column.

Results

Three identical specimens were used. They were tested sequentially with identical test

protocol. The experimental results were very similar. Therefore, the results, in terms of change of period, damping ratio and transfer function, are presented for only one of the specimens. Again, it is noted that for this initial phase, local and/or overall instability of the specimens were not permitted by design.

Damage evolution: change of period

The period change of the specimen was observed from free vibration tests within the elastic range of the structure after each ground motion event. As shown in Fig. 3, the period of the structure increases as the magnitude of the ground motion event increases. This suggests a decrease in structural stiffness. Although the period continues to increase throughout the test, the total change is only 1% at the end of test. It may be concluded that the damage accumulation in terms of stiffness degradation is relatively insignificant. This implies that stiffness degradation as a measure of damage accumulation may be inappropriate for steel structures. Typical hysteresis loop models for steel elements, often acquired by quasi-static cyclic loading, reinforce this observation. On the other hand, local or overall buckling reversals in the inelastic range will soften the structural resistance. Thus, without buckling, the slopes of unloading and reloading curves will exhibit no signs of reduction regardless of the amount of ductility experienced by the structure. This is different from the hysteresis behavior of RC structures, where stiffness degradation is one of the three indications of damage accumulation.

Damage evolution: change of damping ratio

Free-vibration decay was utilized to obtain the damping ratio of the structure. Results of the variation of damping ratio versus ground motion intensity variation are shown in Fig. 4. For each free-vibration test, the column top was held and released from the same position, since the damping ratio increases as the amplitude of response increases. The change of damping ratio in Fig. 4 is approximately doubled at the end of the test. This implies that a certain level of damage had occurred in the structure. Furthermore, in Fig. 4, the damping ratio changed substantially during ground motion events 2-5, during which the structure was supposed to respond only within the elastic range. Most likely this is the effect of yielding due to welding residual stress.

Free-vibration testing is a simple yet accurate method to estimate the linear viscous damping ratio. However, it is not practical to perform free vibration tests on actual structures. An alternative approach to experimentally estimate the modal damping ratio of an actual structure is to apply the half-power bandwidth technique to the frequency response curves obtained by forced vibration. This observation of changing damping ratio suggests that it may be used to quantify damage accumulation, although it has been questioned in some publications (e.g., Williams 1995).

Damage evolution: change of transfer function

The acceleration transfer function is obtained through estimating the cross spectral density functions of the acceleration time history data at the column top and the shaking table. The results are shown in Fig. 5, where the amplitude is plotted versus the frequency. It can be seen that the

abscissa of the peak of transfer function, the fundamental frequency of the column is shifted from 1.13 to 1.12 Hz, when the magnitude is increased from 135% to 179% of the El-Centro ground motions. This change can also be confirmed by the frequency change observed in Fig. 3, where the corresponding frequencies for 135% and 179% of the El-Centro ground motion are 1.127 Hz and 1.124 Hz, respectively. This demonstrates the accuracy of the transfer function in estimating the frequency of a structure. The decrease in amplitude of the transfer function as the magnitude of the ground motion increases implies an increase in the damping ratio. This fact is further supported by the change in damping ratio shown in Fig. 4. However, it is difficult to estimate the damping ratio from the transfer functions using methods such as the half-power bandwidth technique, since the peak value of the transfer function is hard to obtain experimentally. Furthermore, the peak values vary as the length of FFT changes.

It is interesting to note that the transfer functions near the end of the testing sequence exhibit two peaks, as shown with the dotted line in Fig. 5. A more detailed view of the evolution of transfer functions of the final 10 repeated ground motions is shown in Fig. 6. It is shown that the two-peak transfer function appeared suddenly when the ground motion with the same magnitude was repeated 7 times. The boundary condition of the column setup had not changed after careful inspection at the end of the test. This sudden change from single to double peak might be an indication of a certain level of damage occurring in the column. A similar phenomenon has been observed for RC columns tested by using the shaking table (Park and Yen 2001). Since the profile of the transfer function greatly depends on the length of the Fast Fourier Transform, the profile change of the transfer function most likely can be utilized as a qualitative description of the level of damage in a structure, if the baseline transfer function of the structure with no damage is given in advance.

Summary

The dynamic characteristics that affect damage accumulation in steel members without buckling were examined via shake table testing. It was found that changes in period or structural stiffness are not appropriate quantities to describe the cumulative damage of steel structural members, because the stiffness degradation is negligible. It was also observed that accumulated damage to a steel member can result in an increase in the damping ratio. Once the correlation between the increase in damping ratio and the level of structural damage is established, the damping ratio may be used to quantitatively describe cumulative damages. However, the damping ratio is only a global parameter. Its changing value will not provide information on the distribution of damage in a structure. The transfer function is shown to provide an accurate estimation of the frequencies of a structure. In addition, the profile change of transfer function can be used to qualitatively describe the level of damage, provided that the baseline transfer function of the structure with no damage is recorded in advance.

Various types of damage indices have been attempted and reported in the literature to quantify the process of damage accumulation and to predict the collapse state of a structure. Many studies have been directed to establishing the damage-based limit state of RC specimens. The most widely used damage index for steel structural elements is the fatigue-based damage index, which is not well established, by considering the low cycle fatigue failure resulting from inelastic strain reversals due to strong earthquake ground motions. Such failures are mostly the

result of local and/or overall buckling of the structural elements. The results presented in this paper have clarified several issues needed for the next phase. This focuses on the investigation of damage accumulations of low cycle fatigue failure of steel structural elements when inelastic strain reversals (due to buckling) control the useful life span of the structure.

Acknowledgments

This pilot investigation is jointly funded by a FHWA grant (No. DTFH61-03-P-00434) and an NSF grant (No. CMS-0346674) to the University at Buffalo. The advice and encouragement of Dr. Philip Yen and Dr. Steve McCabe are sincerely acknowledged.

Seismic hazard level	Performance level	
	Ordinary bridges	**Important bridges**
Functional-evaluation ground motion	Immediate service level Repairable damage	Immediate service level Minimal damage
Safety-evaluation ground motion	Limited service level Significant damage	Immediate service level Reparable damage

Table. 1. Seismic performance objectives for bridges (ATC-32, 1996)

Ground motion events	% magnitude of El-Centro earthquake
1	66
2	99
3	135
4	179
5	214
6	251
7	280
8	304 (yielding)
:	304 (yielding)
17	304 (yielding)

Table. 2. Ground motion events used in the experimental program

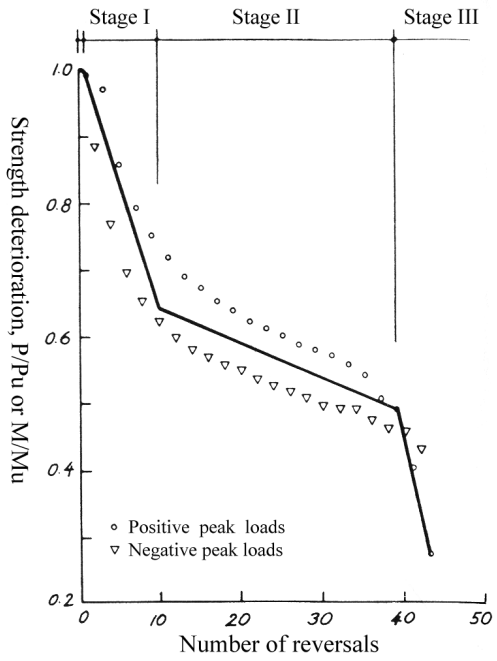

Fig. 1. Three stages of damage accumulation after local buckling has occurred (Krawinkler 1983)

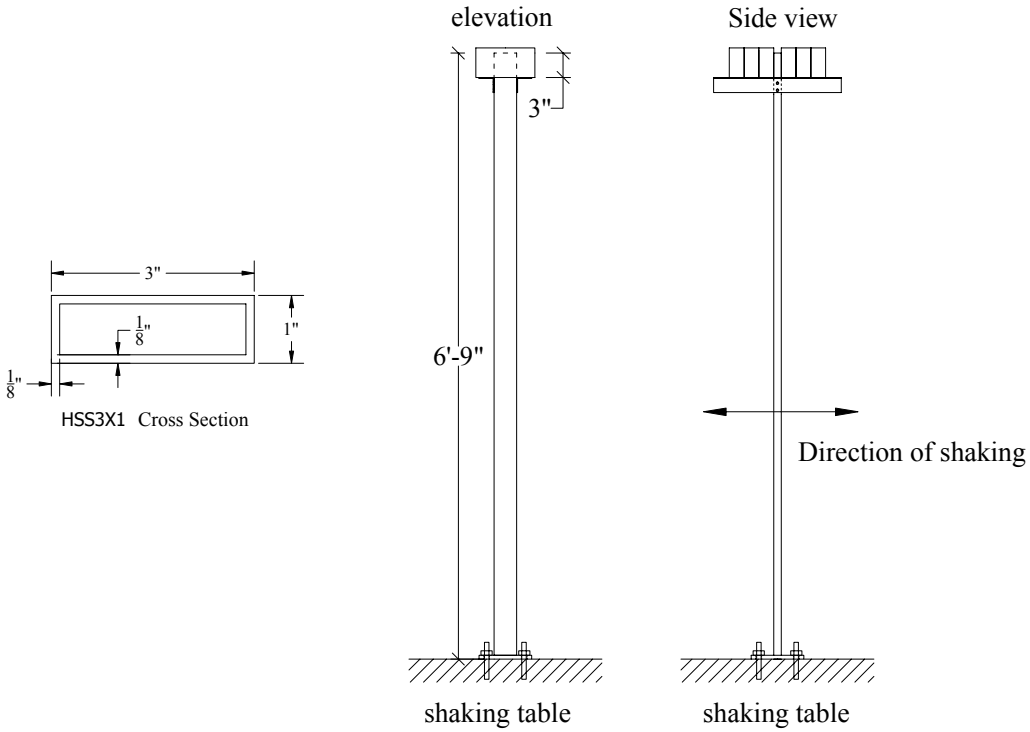

Fig. 2. Experimental setup

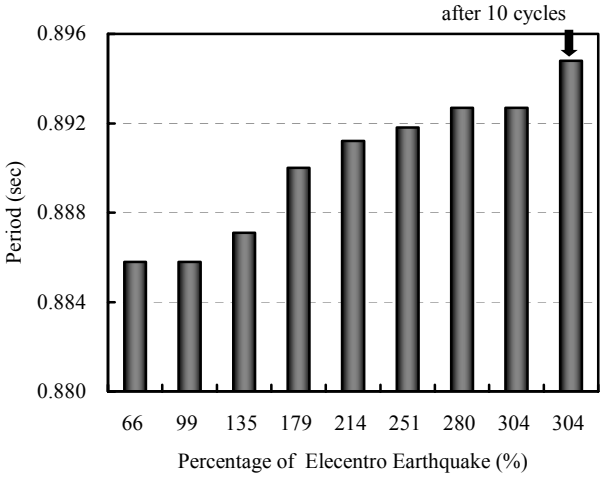

Fig. 3. Experimental results:
Damage evolution: Period of the structure

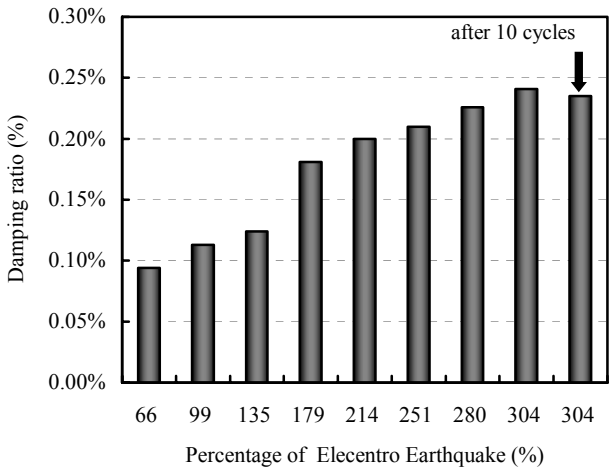

Fig. 4. Experimental results:
Damage evolution: Damping ratio of the structure

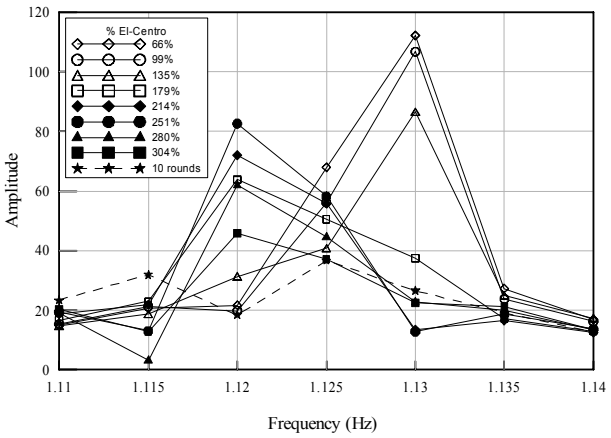

Fig. 5. Experimental results:
Damage evolution: acceleration transfer function

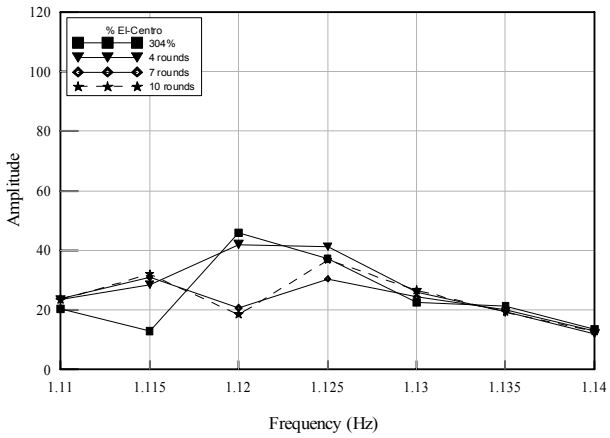

Fig. 6. Experimental results:
Damage evolution: acceleration transfer function – details of the last 11 events

References

American Institute of Steel Construction (AISC). (2001). *AISC manual of steel construction, load and resistance factor design, 3rd Ed.*, Chicago, I.L.

Applied Technology Council (ATC). (1996). *ATC-32 – Improved seismic design guidelines for bridges*. Redwood city, C.A.

Azevedo, J., and Calado, L. (1994) "Hysteretic behavior of steel members: Analytical models and experimental tests." *J. Construct. Steel Res.*, 29, 71-94.

Ballio, G., and Castiglioni, C. A. (1994) "Seismic behavior of steel sections." *J. Construct. Steel Res.*, 29, 21-54.

Banon, H., Biggs, J. M., and Irvine, H. M. (1981). "Seismic damage in reinforced concrete frames." *J. Struct. Eng.*, 107(9), 1713-1729.

Bertero, V. V., and Popov, E. P. (1965). "Effect of large alternating strains of steel beams." *J. Struct. Div., ASCE*, 91(ST1).

Bozorgnia, Y., and Bertero, V. V. (2003). ''Damage spectra: Characteristic and applications to seismic risk reduction.'' *J. Struct. Eng.*, 129(10), 1330-1340.

Bruneau, M., Uang, C. M., and Whittaker, A. (1998). *Ductile design of steel structures*. McGraw-Hill, New York, N.Y.

Chai, Y. H., Romstad, K. M., and Bird, S. M. (1995). ''Energy-based linear damage model for high-intensity seismic loading.'' *J. Struct. Eng.*, 121(5), 857–864.

Chung, Y. S., Meyer, C., and Shinozuka, M. (1987). ''Seismic damage assessment of reinforced concrete members.'' *Technical Rep. NCEER 87-0022*, National Center for Earthquake Engineering Research, State University of New York, Buffalo, N.Y.

Chung Y. S., Meyer C., and Shinozuka M. (1990). "Automatic seismic design of reinforced concrete building frames." *ACI Struct. J.,* 87(3), 326-340.

Cosenza, E., Manfredi, G., and Ramasco, R. (1993). ''The use of damage functionals in earthquake engineering: A comparison between different methods.'' *Earthquake Eng. Struct. Dyn.*, 22, 855–868.

Dipasquale E., and Cakmak A. S. (1988). "Identification of the serviceability limit state and detection of seismic structural damage." *Technical Rep. NCEER 88-0022*, National Center for Earthquake Engineering Research, State University of New York, Buffalo, N.Y.

Fajfar, P. (1992). ''Equivalent ductility factors, taking into account low-cycle fatigue.'' *Earthquake Eng. Struct. Dyn.*, 21, 837–848.

Federal Emergency Management Agency (FHWA). (2000). "Prestandard and commentary for the seismic rehabilitation of buildings." *Rep. No. FEMA 356*, Washington, D.C.

Ghobarah, A., Abou-Elfath, H., and Biddah, A. (1999). ''Response-based damage assessment of structures.'' *Earthquake Eng. Struct. Dyn.*., 28, 79–104.

Gupta, V. K., Nielsen, S. R. K., and Kirkegaard, P. H. (2001). "A preliminary prediction of seismic damage-based degradation in RC structures." *Earthquake Eng. Struct. Dyn.*, 30, 981–993.

Kratzig, W. B., and Meskouris, K. (1997). ''Seismic damage evaluation treated as a low-cycle fatigue process.'' *Seismic design methodologies for the next generation of codes*, P. Fajfar and H. Krawinkler, eds., Balkema, Rotterdam, The Netherlands, 139–149.

Krawinkler, H., and Zohrei, M. (1983). ''Cumulative damage in steel structures subjected to earthquake ground motion.'' *Comput. Struct.*, 16, 531–541.

Kunnath, S. K., EI-Bahy A., Taylor, A. W., and Stone, W. C. (1997). "Cumulative seismic damage of reinforced concrete bridge piers." *NISTIR-6075*, National Institute of Standards and Technology, Gaithersburg, M.D.

Lehman, D. E., and Moehle, J. P. (2000). "Seismic performance of well-confined concrete bridge columns." *Rep. No. UCB/PEER 1998/01*, Pacific Earthquake Engineering Research Center, University of California, Berkeley, C.A.

Liang, Zack, Lee, G. C. (2002). “Principal axes of M-DOF structures Part I: Static loading.” *Earthquake engineering and engineering vibration*, 293-302.
Liang, Zack, Lee, G. C. (2003). “Principal axes of M-DOF structures Part II: Dynamic loading.” *Earthquake engineering and engineering vibration*, 39-50.
Liu, W. C., Liang, Z., and Lee, G. C. (2002). *Low-cycle bending-fatigue of steel bars under random excitation*. Ph.D. Dissertaion, CSEE at State University of New York, Buffalo, N.Y.
Mander, J. B., Panthaki, F. D., and Kasalanati, A. (1994). “Low-cycle fatigue behavior of reinforcing steel.” *J. Mater. Civ. Eng.*, 6(4), 453-468.
Mehanny, S. S. F., and Deierlein, G. G. (2001). ‘‘Seismic damage and collapse assessment of composite moment frames.’’ *J. Struct. Eng.*, 127(9), 1045-1053.
Park, S. W., Yen, W. P., Cooper, J. D., and O’Fallon, J. D. (2001). “Seismic Performance of RC Bridge Column under Repeated Ground Motions.” *J. Bridge Eng.*, 6(6), 461-467.
Park, Y. J., and Ang, A. H.-S. (1985). ‘‘Mechanistic seismic damage model for reinforced concrete.’’ *J. Struct. Eng.*, 111(4), 722–739.
Park, Y. J., Ang, A. H.-S., and Wen, Y. K. (1985a). ‘‘Seismic damage analysis of reinforced concrete buildings.’’ *J. Struct. Eng.*, 111(4), 740–757.
Powell, G. H., and Allahabadi, R. (1988). ‘‘Seismic damage prediction by deterministic methods: Concepts and procedures.’’ *Earthquake Eng. Struct. Dyn.*, 16, 719–734.
Structural Engineers Association of California (SEAOC). (1995). *Vision 2000 - Performance based seismic engineering of buildings*. Sacramento, C. A.
Valles, R. E., Reinhorn, A. M., Kunnath, S. K., Li, C., and Madan, A. (1996). ‘‘IDARC Version 4.0—A computer program for the inelastic damage analysis of buildings.’’ *Technical Rep. NCEER 96-0010*, National Center for Earthquake Engineering Research, State University of New York, Buffalo, N. Y.
Williams, M. S., and Sexsmith, R. G. (1995). ‘‘Seismic damage indices for concrete structures: A state-of-the-art review.’’ *Earthquake Spectra*, 11(2), 319–349.

Aseismic performance of base-isolated bridges using lead-rubber bearings

Guiping Yan [1], Guanyuan Zhao [1], Tieyi Zhong [1]

ABSTRACT

Aseismic performance of a base-isolated simply-supported bridge using lead-rubber bearings (LRB) and laminated rubber bearings (RB) is compared through nonlinear dynamic time history analysis, using 20 pieces of earthquake records representing A-type and C-type site conditions as input motions. The effect of lead diameter, height and cross section of pier on aseismic performance of bridge attached with LRB is investigated. At the same time, the parametric study of a multi-span continuous base-isolated bridge is performed through nonlinear dynamic analysis using El Centro earthquake record. The effect of LRB parameters and bridge dynamic characteristics on seismic performance is discussed thoroughly.

[1] College of Civil Engineering & Architecture Beijing Jiaotong University, Beijing, P.R.China,100044

INTRODUCTION

The lead-rubber bearing (LRB), a new and effective seismic isolation system, was developed by W. H. Robinson in 1975. It has both enough vertical load bearing capacity and large lateral displacement capacity. At the same time , the plastic deformation of lead core used in LRB can dissipate earthquake energy greatly. So LRB is economic and effective equipment in base isolation. In New Zealand, Japan, America and Italy, LRB has been used in newly built structures and retrofit of old structures broadly, some of which have suffered severe earthquakes. During the Los Angeles earthquake in 1994, LRB successfully protected the University of Southern California Teaching Hospital, a seven-story hospital, from damage while the ten nearby hospitals were badly damaged. In Great Hanshin Earthquake, Kobe, occurred in 1995, the Computer Center of the Ministry of Post and Telecommunications isolated with LRB system survived with no damage. During this earthquake, six base-isolated bridges using LRB all showed good aseismic performance. These examples of isolated structures in real earthquakes illustrate the advantages of LRB clearly [1].

When isolation systems are used in newly built bridges or old ones, the seismic forces sustained by piers can be reduced greatly so that the ductile requirement on piers are lessened and the cost of piers and foundation is decreased [2]. For multi-span continuous beam bridges, base isolation system can balance seismic forces distributed on piers, especially for those piers which the heights of piers differ greatly. However, for base-isolated bridges using LRB, the parameters of LRB, dynamic characteristics of bridges and earthquake motions, affect aseismic performance in a great deal. At the same time, LRB and bridges would enter into nonlinear states when severe earthquakes occur and that will makes the responses of isolated bridges very complex. So, it's a very important task to study the effect of parameters for isolated bridge of using LRB on aseismic performance.

The research group leaded by the primary author has carried out the study systemically on the design and analysis of base-isolated bridges using LRB in recent years and some important results have been got. The main content in this paper includes the followings. Aseismic performance of a base-isolated simply-supported bridge using LRB and laminated rubber bearings (RB) is compared through nonlinear dynamic time history analysis, using 20 pieces of earthquake records representing A-type and C-type site conditions as input motions. The effect of lead diameter, height and cross section of pier on aseismic performance of bridge attached with LRB is investigated. The parameters study of a multi-span continuous beam base-isolated bridge is performed through nonlinear dynamic analysis using El Centro earthquake record. The effect of LRB parameters and bridge dynamic characteristics on aseismic performance is discussed.

ASEISMIC PERFORMANCE ANALYSIS

Structural model

Structural model used here is a reinforced concrete simply-supported bridge, whose the pier height is 10 meters and the span is 24 meters (Fig. 1). Rectangle piers, whose dimensions are all 3m×1.1m, are used. Seismic response in longitudinal direction is considered in this paper. The weight of the superstructure is taken as 10 ton per meter. The main parameters of piers in longitudinal direction are described as follows.

Effective inertia moment $I_{eff} = 0.139\ \mathrm{m}^4$

Yield moment $M_y = 0.67 \times 10^4\ \mathrm{kN.m}$

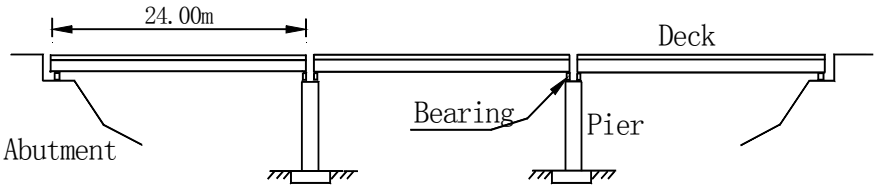

Fig. 1. Configuration of an isolated simply-supported bridge

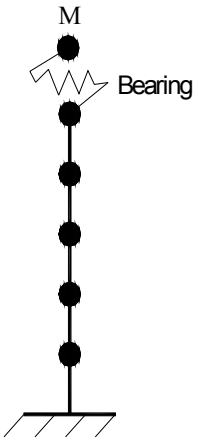

Fig. 2. FEM model

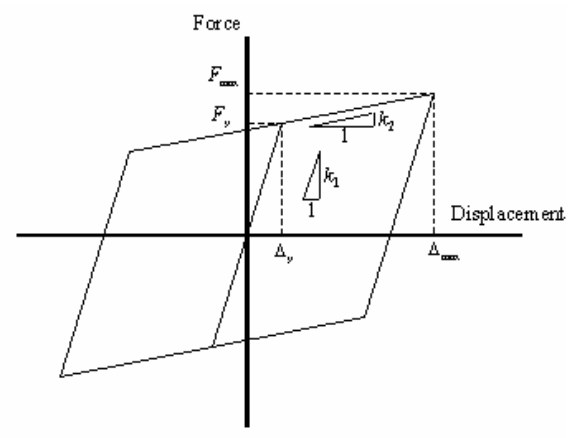

Fig. 3. Bilinear force-displacement of LRB

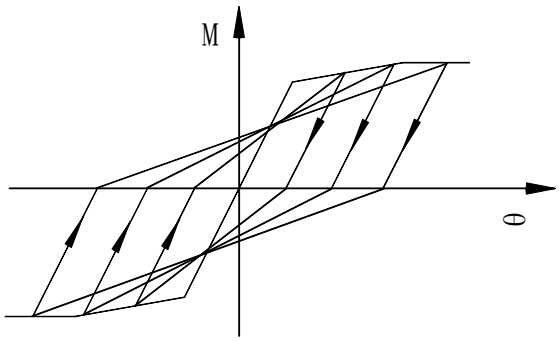

Fig. 4 Takeda trilinear model

TABLE I. EARTHQUAKE RECORDS USED IN THE ANALYSIS

(a) A-type site records

NO.	Earthquake	Component	Intensity	Maximum acceleration (cm/s^2)	Date
A-1	San Fernando	S16E	9	1148.1	02/09/1971
A-2	Helena Montana	N00E	8	143.5	10/21/1935
A-3	W.Washington	S04E	8	161.6	04/13/1949
A-4	San Francisco	N81E	7	102.8	03/22/1957.
A-5	Parkfield Calif	S65W	7	264.3	06/27/1966
A-6	San Fernando	N52W	7	147.1	02/09/1971
A-7	San Fernando	N50W	7	126.5	02/09/1971
A-8	San Fernando	S00W	7	158.2	02/09/1971
A-9	San Fernando	S62E	7	64.2	02/09/1971
A-10	San Fernando	N00E	7	164.2	02/09/1971

(b) C-type earthquake records

NO.	Earthquake	Component	Intensity	Maximum acceleration (cm/s^2)	Date
C-1	Imperial Valley	S90W	8	210.1	05/18/1940
C-2	Long Beach	S82E	7	151.5	03/10/1933
C-3	San Jose	N59E	7	105.8	09/04/1955
C-4	Borrego Mt	S00W	7	127.8	04/08/1968
C-5	San Fernando	S00W	7	167.3	02/09/1971
C-6	San Fernando	S00W	7	113.9	02/09/1971
C-7	San Fernando	S61E	7	83.4	02/09/1971
C-8	Imperial Valley	E	6	48.8	04/12/1938
C-9	Torrance-Gardena	E	6	53.7	11/04/1941.
C-10	Imperial County	N	6	62.5	12/16/1955

For regular base-isolated simply-supported bridge, its seismic response can be described as a single pier model (Fig. 2). The bilinear force-displacement of LRB shown in Fig. 3 is used in the analysis. Nonlinear element is used at the bottom of pier, and Takeda trilinear hysteretic model shown in Fig. 4 is adopted.

20 pieces of earthquake records representing A-type and C-type site are taken as input motions, whose parameters are listed in Table 1. The acceleration time histories of records are modified according to the absolute difference between the record's intensity and design earthquake intensity. The acceleration would be amplified or reduced 2 times when intensity difference is 1. Design earthquake intensity in this section is 9.

Aseismic effectiveness of LRB

LRB is manufactured by pouring lead core into laminated rubber bearing (RB). Compared with RB, LRB has better hysteretic energy dissipating ability due to the plastic deformation of lead core. In this paper, as a comparison, aseismic performance of RB whose amount is same as LRB is analyzed. The dimension of RB used here is $300mm \times 300mm \times 52mm$, and the stiffness is $2.43 \times 10^3 kN/m$. Diameter of lead core of LRB is 60mm, and the initial stiffness of LRB equals

3.27×10^4 kN/m and the post-yield stiffness equals 0.1 times of the initial stiffness.

Nonlinear dynamic analysis is performed using earthquake records representing two site types. The peak displacement at pier top and beam for two site types earthquakes are shown in Fig. 5 and Fig. 6 respectively.

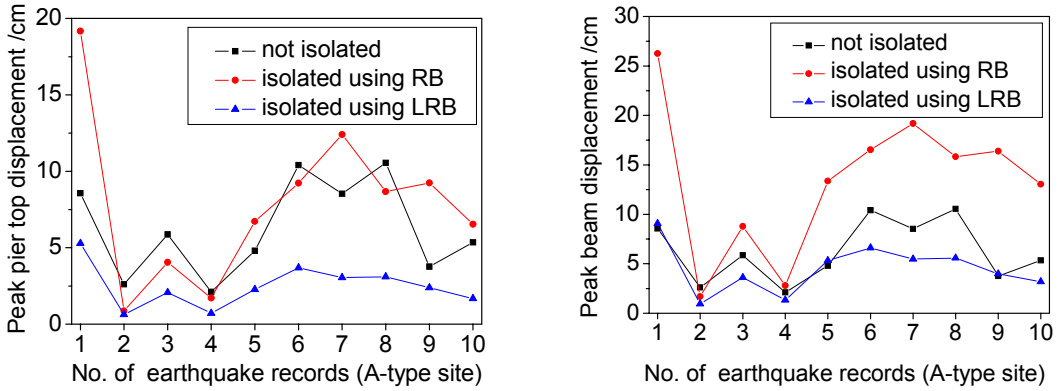

(a) Peak displacement of pier top (b) Peak displacement of beam

Fig. 5 Comparison of seismic responses under the excitation of A-site earthquakes

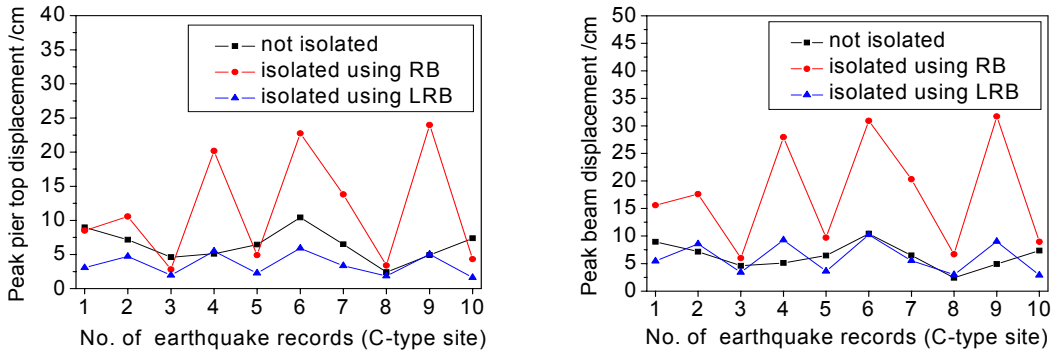

(a) Peak displacement of pier top (b) Peak displacement of beam

Fig. 6. Comparison of seismic responses under the excitation of C-site earthquakes

It shows that, when the isolated bridge using LRB suffers A-type earthquakes, the pier top displacement is reduced greatly, and beam displacement keeps in a reasonable range except for three earthquake records (e.g. A-1, A-5 and A-9). When such an isolated bridge using LRB suffers C-type earthquakes, the aseismic performance is not so effective, and the displacement at pier top and beam is greater than that of the bridge without bearings under the excitation of some earthquake records.

Compared with LRB, RB is not so effective for aseismic performance. Under several earthquake records of both site types, the displacement at pier top and beam is more than that of the bridge without bearings.

Even RB can prolong the period of the structure, it almost has no energy dissipating capacity, and its aseismic mechanism is only to cut off transfer path of earthquake without changing the dynamic characteristics of the structure. In addition, the beam displacement and the deformation of RB are too large. Under several records (e.g. C-4、C-6 and C-9), the deformation

of RB itself has exceeded its ultimate displacement. But LRB can enhance the damping of the structure a lot so that the displacement at beam can be controlled effectively.

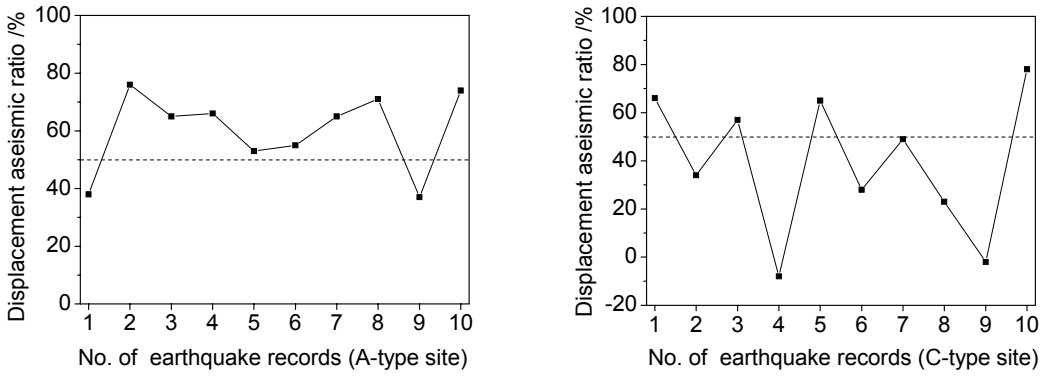

(a) A-type site (b) C-type site

Fig. 7. Displacement reduction ratio of LRB

In this paper, aseismic ratio of the base-isolated structure η is defined by Eq.(1).

$$\eta = \frac{D_O - D_I}{D_O} \tag{1}$$

where， D_O is the maximum displacement of pier top without isolation,

and D_I is the maximum displacement of pier top with isolation.

Aseismic ratio of the isolated bridge using LRB under the excitation of 20 earthquake records is shown in Fig. 7. For A-type site, there are 3 pieces of earthquake records for which aseismic ratio is over 70%, and 2 pieces of earthquake records for which aseismic ratio is less 50%. For C-type site, there is only 1 pieces of earthquake records for which aseismic ratio is over 70%, but 5 pieces of earthquake records for which aseismic ratio is less 50%. It can be seen that aseismic performance of isolated bridge using LRB on C-type site is not so good as that on A-type site.

The isolated bridge shows worse performance under the excitation of A-7, A-9, C-2, C-4, C-6, C-7, and C-9. By means of frequency domain analysis on these records, it's found that they are all typical low-frequency impulse type earthquakes. So when base-isolated bridges are built on sites where low frequency impulse type earthquakes occurs frequently, more attention should be paid when designing isolator.

Effect of lead core diameter

Five diameter sizes of lead cores are considered, 30, 40, 50, 60 and 70mm. The parameters of LRB are listed in Table II.

TABLE II. PARAMETERS OF LRB

Diameter /mm	30	40	50	60	70
k_1 /kN/m	9247	15150	23650	35680	51850
k_2 /kN/m	2642	2806	3016	3273	3576

Under the excitation of earthquakes, the ratio of the pier top acceleration with LRB to that of without LRB is shown in Fig. 8. As seen, with increasing of LRB diameter, the reduction degree of acceleration at pier top is increased. That is because the energy dissipated by LRB improves with the increase of LRB diameter (see Fig. 9). However, with increasing of LRB diameter, reduction degree decreases a little. The ratio of beam displacement with LRB to that of without LRB is shown in Fig. 10. As seen, beam displacement is also reduced greatly with the increase of LRB diameter.

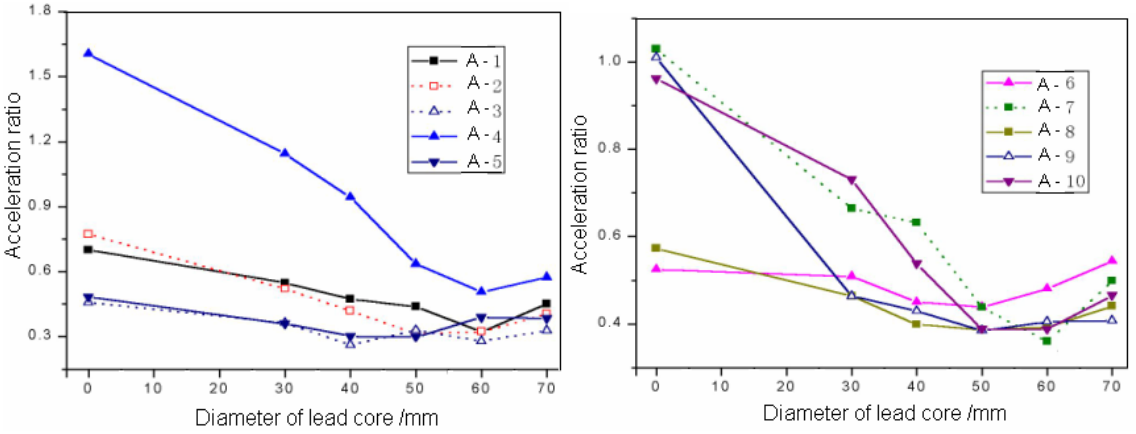

Fig. 8. Acceleration ratio with the variation of lead core diameter

Though the acceleration at the pier top and base shear at pier bottom are reduced greatly due to LRB, the beam displacement is more than that without bearings, which may give rise to adjacent beams colliding or falling to the ground. To prevent such accident, the shear stiffness of LRB should be higher, and that need to choose a larger diameter of lead core. However, acceleration at pier top decreases firstly, and then increases a little with increasing of LRB diameter (Fig. 8).

Generally speaking, the larger the lead core diameter is, the better energy dissipating capacity LRB has. However, when the lead core is enlarged, the initial stiffness or yield strength of LRB will decrease. When the initial stiffness or yield strength of LRB is too small, it is just like a linear spring, whose stiffness equals its post-yield stiffness approximately. In addition, if yield strength of LRB is too low, isolation system may yield even under service loads. On the contrary, when the diameter of lead core is too small, LRB is just like RB having no energy dissipating capacity. So the diameter of LRB has an optimized value for a specified structure.

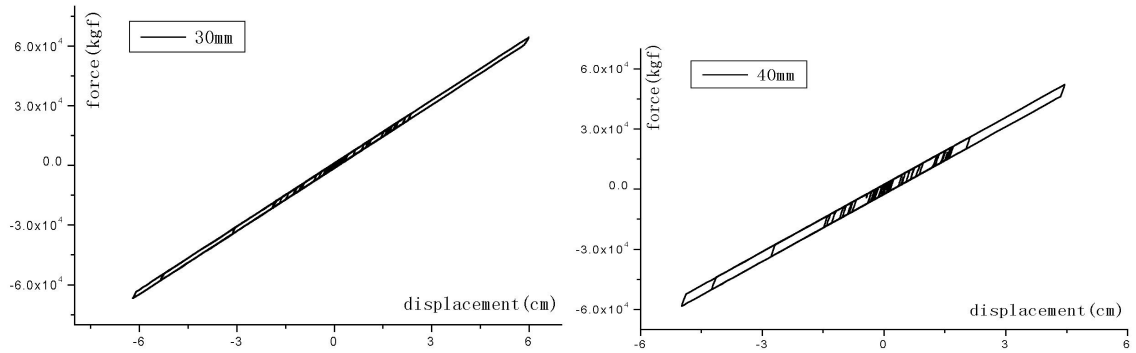

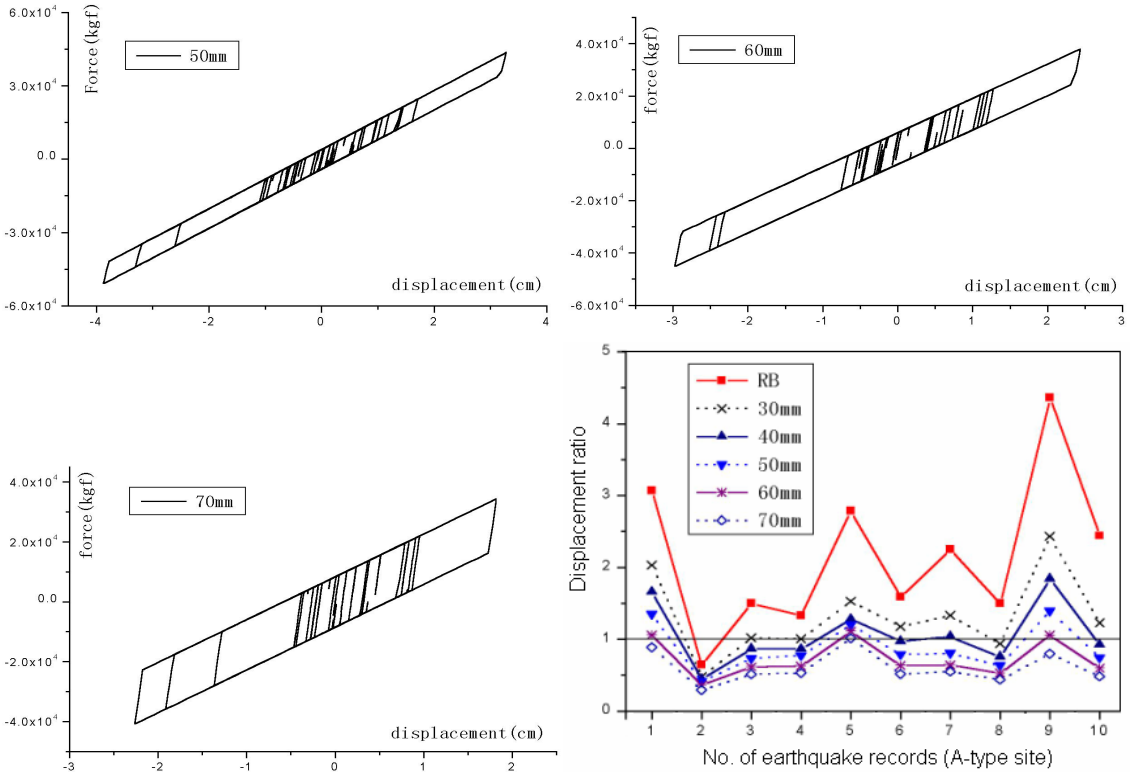

Fig. 9. Hysteretic energy dissipated by LRB under the excitation of A-6

Fig.10. Beam displacement ratio (A-type site)

Effect of pier stiffness

The pier sections from 3×0.9 to 3×1.4 are considered, whose design parameters are listed in Table III. Pier height is 10 meters. The superstructure is same as before. The diameter of lead core is 60mm. Using three pieces of A-type site earthquake records A-1, A-4, A-8, and three pieces of C-type site earthquake records C-3, C-4, C-10 as input motions, nonlinear dynamic analysis is performed.

TABLEIII. PARAMETERS OF PIER SECTIONS

Dimension /m	3×0.9	3×1.0	3×1.1	3×1.2	3×1.3	3×1.4
Inertial moment /m^4	0.0726	0.1022	0.1389	0.1835	0.2367	0.2994
Yield moment /kN.m	4371	5487	6732	8104	9603	11230

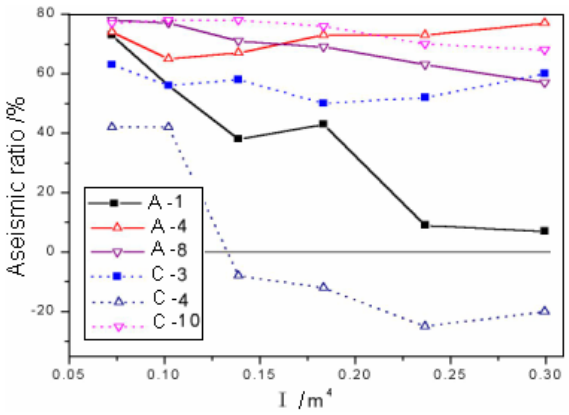

Fig. 11. Pier top displacement reduction ratio of LRB

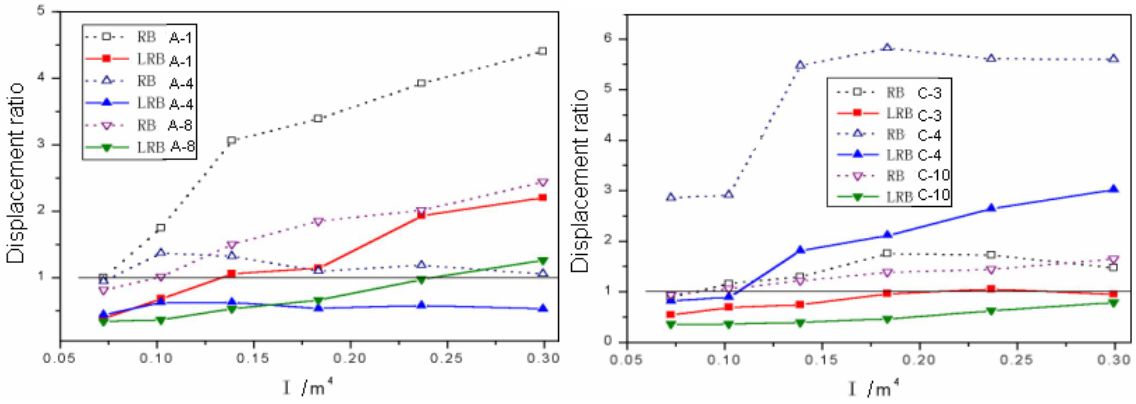

(a) A-type site (b) C-type site

Fig. 12. Beam displacement ratio

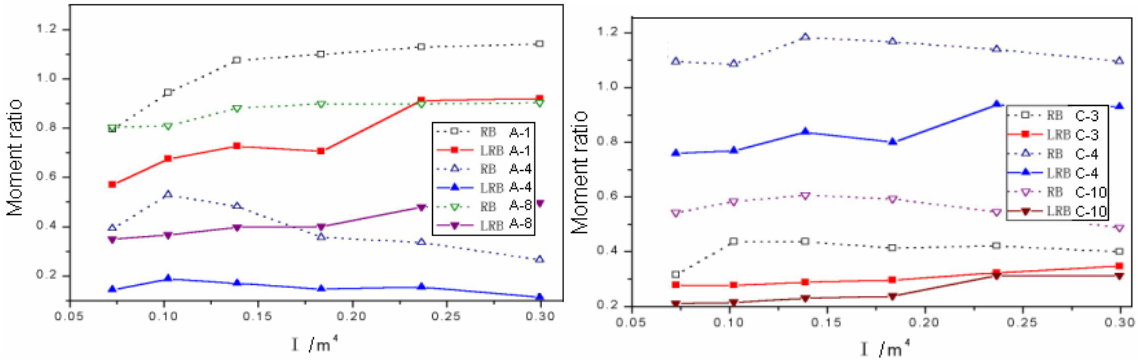

(a) A-type site (b) C-type site

Fig. 13. Flexural moment ratio

As seen from Fig. 11, the effect of pier stiffness on pier top displacement of bridges with LRB is very little, for the excitation of two site-type earthquakes, except for A-1 and C-4.

From Fig. 12, with increasing of the pier stiffness, the ratio of beam displacement with LRB or RB to that of without bearings increases except for the excitation of A-4 and C-3. This is because with increasing of the pier stiffness, the first vibration mode of isolated structure is characterized by the movement of beam mainly.

It can be seen from Fig. 13, the pier stiffness has little effect on the flexural moment at pier bottom, but for the excitation of different earthquake, the structural responses differ greatly.

Compared with RB, The pier top displacement and beam displacement responses of isolated bridges using LRB are less than those of isolated bridges using LRB. That shows that, LRB may attain good aseismic performance for different pier stiffness. For the isolated bridge using LRB, with the increase of pier stiffness, the pier top displacement changes a little, but beam displacement increase a lot. So when the pier height and bearing parameters keep unchangeable, the increase of pier stiffness is neither economic nor effective.

PARAMETERS STUDY

Analytical model

A multi-span continuous bridge is taken as analytical model, whose span is 20m (Fig. 14). The weight of superstructure is 10 tons per meter. And the weight of pier P-1 and P-2 is 2.04 tons per meter, and P-3 is 2.47 tons per meter.

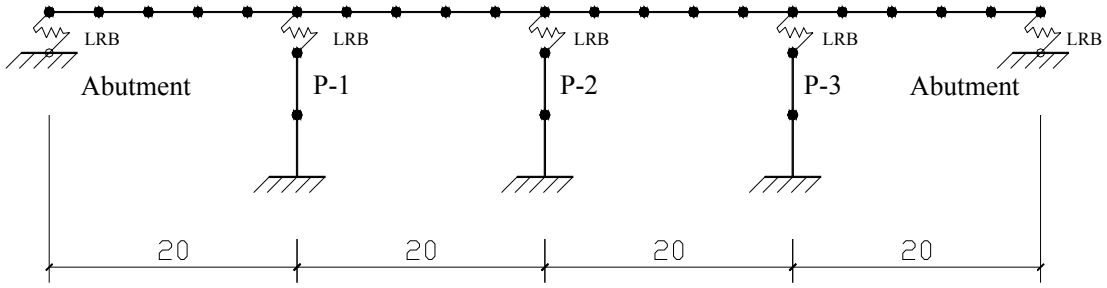

Fig. 14. FEM model of an isolated continuous bridge using LRB

Effect of yield strength of LRB

Define a dimensionless factor,

$$\beta = Q_{\Delta} / W \tag{2}$$

where, Q_{Δ} is the sum of yield strength of LRB equipped at all abutments and all piers, and W is the weight of superstructure.

Nonlinear dynamic analysis of the isolated continuous bridge using LRB is performed by using El Centro (1940, N-S) as input motion, and β varies from 2% to 12%.

The peak displacement responses of beam and tops of P-1 and P-2 are shown in Fig. 15 (a). It can be seen that when the factor β increases from 2% to 6%, the beam displacement decreases. After β reaches 6%, the beam displacement changes little. The factor β has little effect on the displacement on pier top.

Peak base shears of P-1 and P-2 are shown in Fig. 15 (b) considering the piers linear and nonlinear respectively. It can be seen that, for linear isolation system, there is an optimized value for the factor β to make base shear of piers minimum. For nonlinear isolation system, with the increase of β, the base shear increases firstly, and then keeps at a steady level.

Considering the reduction of both displacement and base shear, for El Centro type earthquakes, when β equals 6% approximately, better aseismic performance can be attained.

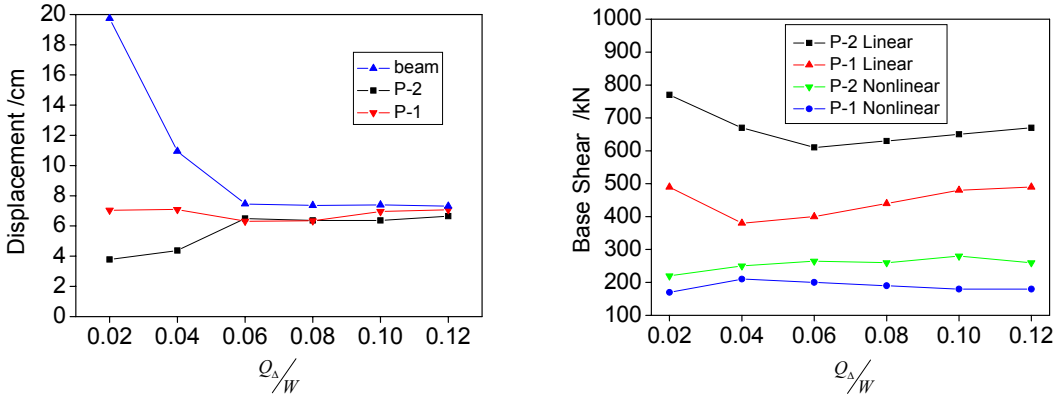

a) Peak displacement (b) Peak base shear

Fig. 15. Effect of yield strength of LRB

Effect of damping and initial stiffness of LRB

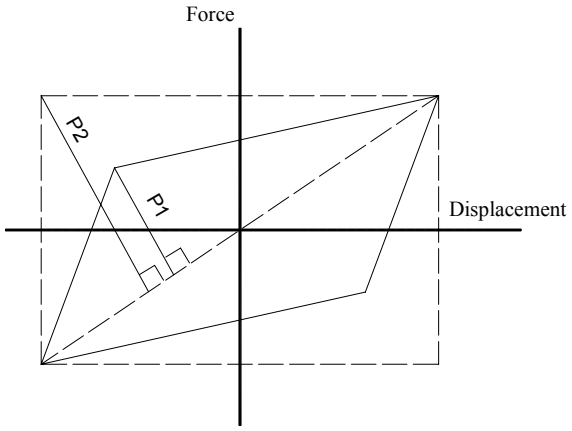

Fig. 16. Definition of NL

For bilinear hysteretic model of LRB shown in Fig. 3, a nonlinear factor NL can be used to describe its hysteretic damping factor [1],

$$\underline{\text{NL}} = P_1 / P_2 \tag{3}$$

Where, P_1 and P_2 are the distances shown in Fig. 16.

When the shape of hysteretic changes from a rhombus whose area is zero to a rectangle, NL increases from 0 to 1. So this factor equals the ratio of the area of hysteretic loop to the area of rectangle, and it's proportional to the hysteretic damping factor of LRB.

$$\underline{\text{NL}} = A_h / (4F_{\max}\Delta_{\max}) = F_y / F_{\max} - \Delta_y / \Delta_{\max} \tag{4}$$

Consider the following cases in this paper.

(1) NL = 0.32， $k_1 = 5\times10^6$ N/m ；

(2) NL = 0.32， $k_1 = 2.5\times10^6$ N/m；

(3) NL = 0.32， $k_1 = 10^7$ N/m；

(4) NL = 0.16， k_1 is same as the first case, and increase the maximum displacement of LRB；

(5) NL = 0.16， k_1 is same as the first case, and decrease the maximum displacement of LRB；

(6) NL = 0.16， k_1 is same as the first case, and increase the post-yield strength of LRB；

(7) NL = 0.48， k_1 is same as the first case, and decrease the post-yield strength of LRB；

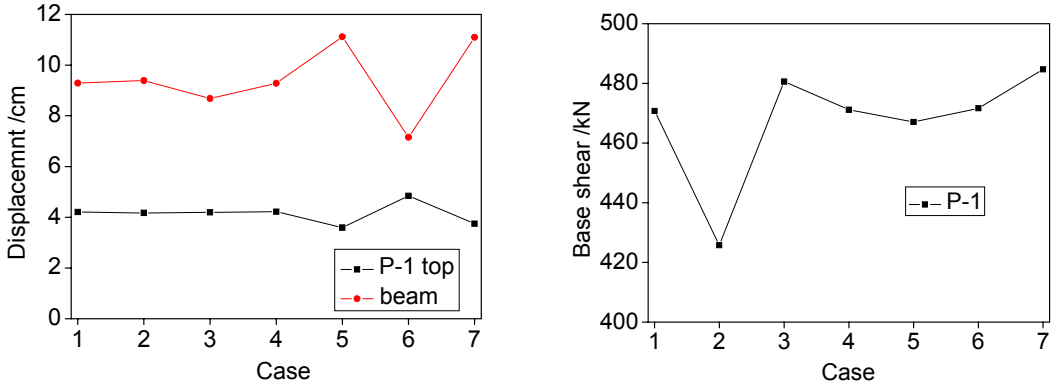

（a）Peak displacement (b) Peak base shear

Fig. 17. Effect of damping and initial stiffness of LRB

The dynamic responses of isolated bridge under the excitation of El Centro earthquake are shown in Fig. 17. It can be seen from the comparison of case 1, case 2 and case 3, when the hysteretic damping of LRB remains constant, seismic responses of the isolated bridge change little with the change of initial stiffness. It shows that hysteretic damping affects seismic response of isolated bridge greater. From the comparison of case 1, case 4, case 5, case 6 and case 7, it can be seen that higher hysteretic damping of LRB will make the beam displacement response larger, for the deformation of LRB become larger, so more earthquake energy is dissipated and base shear of piers is reduced. From the comparison of case 1 and case 4, it can be seen that seismic response of piers varies little if NL is increased by modifying the maximum displacement of LRB.

Effect of stiffness degrading factors of LRB

For bilinear hysteretic model of LRB, the stiffness degrading factor can be defined in Eq.(5).

$$\alpha = k_2 / k_1 \tag{5}$$

In this analysis, α equals 0.08, 0.1, 0.13, 0.17 and 0.25 respectively, and the initial stiffness of LRB k_1 keeps constant.

It can be seen from Fig.18, the stiffness degrading factor has very less effect on the displacement at pier tops, but it has more effect on the base shear of piers.

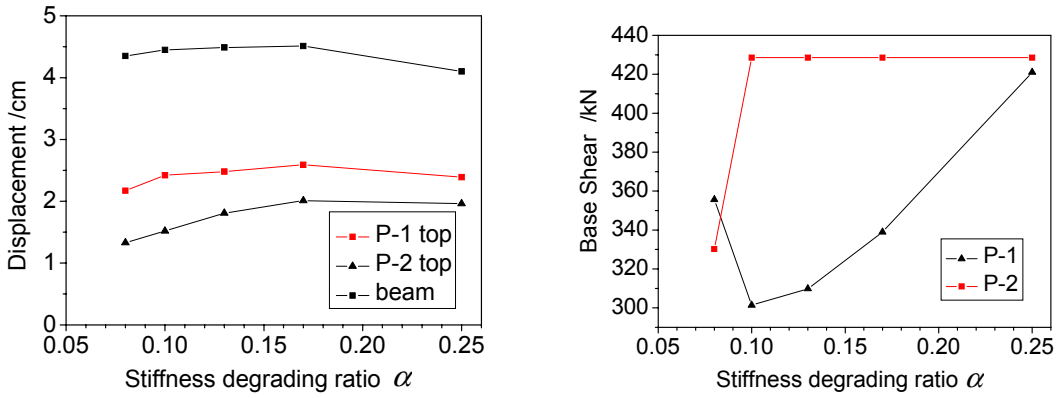

（a）Peak displacement (b) Peak base shear

Fig. 18. Effect of stiffness degrading factors of LRB

Effect of dynamic characteristics of pier

In this analysis, the sections and reinforcement of piers remain unchangeable, but the height of piers is taken as 5m, 10m and 15m. That makes fundamental frequencies of piers changed a lot. In actual design of isolated bridges, LRB should be designed according to specific dynamic parameters of piers. In this study, the goal is to analyze aseismic performance of LRB under the conditions of different characteristics of piers, so when the pier height varies, the parameters of LRB remain unchangeable.

It can be seen from Fig. 19, when piers are in linear states, LRB can reduce displacement at pier top and beam more greatly for stiffer piers whose height are shorter. With the decrease of pier's stiffness, the reduction degree of the displacement responses decreases.

When piers are in nonlinear states, the deformation of LRB decreases with the decrease of pier stiffness, and the displacement at pier top and flexural moment at pier bottom increase. So for those isolated bridges, which are designed using elastic analysis, the aseismic performance is uncertain when piers undergo inelastic deformation.

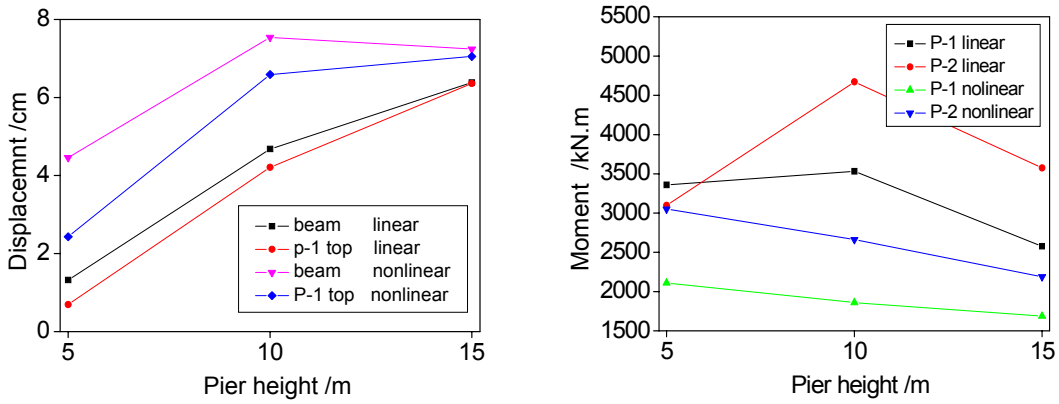

（a）Peak displacement (b) Peak base shear

Fig. 19. Effect of dynamic characteristics of piers

Effect of LRB distribution along the whole bridge

Define a factor λ in order to describe the distribution of LRB along the whole bridge.

$$\lambda = \frac{Q_p}{Q_\Delta} \tag{6}$$

where, Q_p is the sum of the yield strength of LRB used in all piers, and Q_Δ is the sum of the yield strength of LRB used in the whole bridge.

When the factor λ equals zero, it means LRBs are all equipped on abutments. When the factor λ equals 1, it means LRBs are all equipped on piers. In this analysis, assume that Q_Δ / W keeps 8%. When λ equals different values, the base shear responses of isolated bridge under the excitation of El Centro earthquake, is shown in Fig. 20.

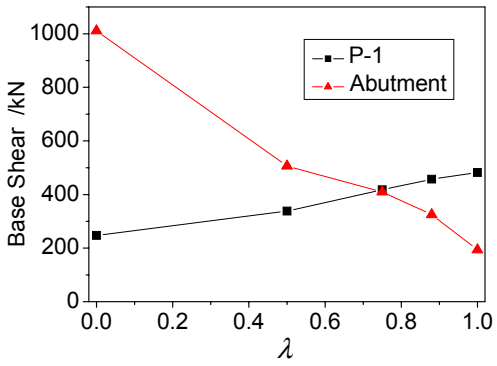

Fig. 20. Effect of LRB distribution along the whole bridge

It can be seen that, when λ equals 0.75, seismic forces can be distributed to abutments and piers evenly. When λ equals zero, the base shear sustained by the abutment is 4.1 times that sustained by P-1. When λ equals 1, the base shear sustained by the abutment is 0.4 times that sustained by P-1. So the distribution of LRB along the whole bridge has a very much effect on the seismic force distribution to abutments and piers. Through choosing an appropriate value of λ, seismic force can be distributed to piers or abutments at expected ratio.

CONCLUSIONS

(1) Compared with RB, LRB can reduce displacement at pier top and beam at the same time.

(2) The frequency composite of earthquake wave affects aseismic performance of isolated bridges greatly. Generally speaking, aseismic performance of the isolated bridge on A-site would be better than that on C-type site. When base-isolated bridges are built on sites where low-frequency impulse type earthquakes may occur, more attention should be paid in designing isolator.

(3) Excessive increase of the lead core diameter is not favored. The diameter of lead core has an optimized value for a specified structure.

(4) When pier's height and LRB parameters keep unchangeable, the increase of pier

stiffness is neither economic nor effective, as far as aseismic performance is concerned.

(5) The calculation results of using El Centro earthquakes record show that the better aseismic performance can be attained when Q_{Δ} / W equals 6% approximately.

(6) Greater hysteretic damping of LRB will make the beam displacement response larger, and the deformation of LRB becomes larger also, and more earthquake energy is dissipated, and base shear of piers is reduced.

(7) The stiffness degrading factor of LRB has very little effect on the displacement responses of piers, but it has much effect on the base shear of piers.

(8) For those isolated bridges, which are designed using elastic analysis, the aseismic performance is uncertain when piers undergo inelastic deformation, because the interaction between LRB and the structure becomes complex.

(9) The distribution of LRB along the whole bridge has a large effect on the seismic force distribution to abutments and piers. Through distributing LRB appropriately, seismic force can be distributed to piers or abutments at expected ratio.

ACKNOWLEDGEMENTS

The research was funded by the National Natural Science Foundation of China (NSFC) (No. 59978002). The financial support is gratefully acknowledged. Computation work in this paper was accomplished by MS. Zhang Jun, MS. Zeng Pan , MS. Wang Li and MS. Zhang Zhenge. They are gratefully acknowledged by authors.

REFERENCES

R. I. Skinner, W. H. Robison, and G. H. McVerry. An introduction to seismic isolation. John Wiley & Sons Ltd. 1993

I. G. Buckle, R. L. Mayes. Seismic retrofit of bridge using mechanical energy dissipaters. Proceedings of Fourth U.S. National Conference on Earthquake Engineering, vol.3, 1990

Seismic Behavior of CFST Bridges in China

Yan Xu[1] , Shi-de Hu[2] , Bao-chun Chen[1]

ABSTRACT

In recent 10 years, CFST (Concrete-Filled-Steel-Tubular) arch bridges have been widely built in china owing to its high bearing capacity, good plastic behavior and convenient construction. However, compared with its prosperous engineering application, its computing theory has lagged behind. Therefore, large quantities of research work have been carried out in this field, and have made phased achievements on its static behavior, while studies on its dynamic behavior is at the start. Actually, as a new type of bridge, CFST arch bridges have a very short construction history and few have experienced the earthquake excitation. This paper introduces the theoretical progress that have been made in recent years with focus on the seismic behavior of CFST arch bridges and also provides discussions on several important issues of CFST arch bridges that still need to be further studied.

[1]College of Civil Engineering And Architecture, Fuzhou University, Fuzhou, Fujian, 350002,PRC
[2]State Key Laboratory for Disaster Reduction in Civil Engineering, Tongji University, Shanghai, 200092,PRC

INTRODUCTION

High strength material and no-false work construction have restricted the development of arch bridges toward large span. With the application of CFST in bridge Engineering, which solved the two problems successfully, arch bridges were injected into new energy and refreshed a new look. Since the first CFST arch bridge, Wangchang Bridge in Sichuan, built in 1990, CFST arch bridges have been developed quickly in china. According to a rough investigation, there are more than 200 CFST bridges already existed and being completed in china, and with the main span of 460m,Wu Xia Yangtze river which is under the construction will become the world 's record of this kind of bridge. With the breakthrough in spans and innovation in structures, CFST arch bridges show us a strong life force and prosperous prospective.

Due to its new material and construction method, there are obvious differences in material and structure system between CFST arch bridges and the traditional concrete arch bridges, therefore both its static behavior and its dynamic behavior have its own characteristics, which need to be studied systematically. However, compared to its prosperous Engineering application, its computing theory has lagged behind. Therefore, large quantities of research work have been carried out in this field, and have made phased achievements on its static behavior(Baochun Chen. 2000), while studies on its dynamic behavior is at the start.

As we all know, the existed CFST arch bridges are distributed all over the country, with quite a lot of them are in the seismic zone. Furthermore, CFST arch bridges vary great in structure types. It is needless to say that researches on dynamic behavior of CFST arch bridges are urgently required. But actually, as a new type of bridge, CFST arch bridges have a very short construction history and few have experienced the earthquake excitation.

Therefore, both theoretical research and shake table test are important methods to investigate their dynamic behavior. This paper introduces the theoretical progress and the shaking table test that have been made in recent years with focus on the seismic behavior of CFST arch bridges, and also provides discussions on several important issues of CFST arch bridges which still need to be further studied.

DYNAMIC CHARACTERISTICS

Fundamental frequency and mode shape

Dynamic characteristics are the basis to carry out seismic response analysis and to evaluate the seismic performance of CFST arch bridges. According to dynamic field test and the finite element analysis (Baochun Chen etc. 2001,Jiashu Zheng etc. 2003,Yunshen Li 1997), table I and II show the fundamental frequency of several CFST bridges.

TABLE I. FIRST FREQUENCY OF CFST BRIDGES RESULTED FROM TESTED IN FIELD

Bridge name	Location	Span (m)	Structure type	frequency（Hz）	
				Out-plane	In-plane
Liuzhou wenhui bridge	Guangxi	108	Half-through arch bridge	1.0625～1.9375	
Liantuo bridge	Hubei	114	Half-through arch bridge	0.976	___
Cidu bridge	Jiangxi	150	Half-through arch bridge	0.98	1.27
Jiuwanxi bridge	Hubei	160	Deck arch bridge	___	0.637
Shanshanxi bridge	Guangzhou	200	Half-through arch bridge with rigid tie bar	___	1.125

TABLE II. FIRST FREQUENCY OF CFST BRIDGES RESULTED FROM FEM ANALYIS

Bridge name	Location	Span (m)	Structure type	frequency（Hz）	
				Out-plane	In-plane
Fuzhou liberation bridge	Fuzhou	80	Half-through arch bridge	0.72	1.56
Liantuo bridge	Hubei	114	Half-through arch bridge with rigid tie bar	0.88	1.03
Shitanxi bridge	Fuqing	136	Half-through arch bridge	1.24	1.25
Cidu bridge	Jiangxi	150	Half-through arch bridge	1.04	1.32
Shenzhen north station bridge	Shenzhen	150	Through arch bridge	0.33	0.55
Huangbo river bridge	Henan	160	Deck arch bridge	1.02	1.22
Tianjing rainbow bridge	Tianjing	160	Through arch bridge with rigid tie bar	0.40	1.07
Jiuwanxi bridge	Hubei	160	Deck arch bridge	____	0.60
Longtan river bridge	Hubei	208	Half-through arch bridge	0.36	2.55
Meixi river bridge	Sichuan	288	Deck truss arch bridge	0.20	0.45
Yaji sha bridge	Guangzhou	360	Half-through arch bridge with rigid tie bar	0.33	0.44
Wu gorge Yangtze bridge	Sichuan	400	Deck truss arch bridge	0.17	0.35

Seen from table I and II, the fundamental frequency of CFST arch bridges is considerably influenced by bridge span and structural type. The fundamental frequency decreases as the span increases, and is lowest for through arch bridges and highest for deck arch bridges, with half-through arch bridges in the middle. For most CFST arch bridges (except very large span like Meixi river bridge and Wu Gorge Yangtze bridge), its fundamental frequency both out-plane (0.16Hz-2.72Hz) and in-plane (0.35Hz-1.49Hz) are higher than that of cable-stayed bridge and suspension bridge which is usually lower than 0.2Hz(for instance, 0.1486 Hz for Nanpu bridge, 0.078Hzfor Yangpu bridge, 0.05Hz for Jiangyin Yangtze bridge and 0.091Hz for Humen bridge), while lower than that of the common rigid arch bridges (2.5-3.3Hz).

With corresponding to its fundamental frequency, mode shapes are also important characteristics to understand the dynamic behavior of CFST arch bridges. The first mode shape for the bridges listed in table II is lateral bending symmetrically, the second is in-plane bending antisymmetrically, which indicate that the out-plane stiffness is weaker than the in-plane stiffness and the lateral stability should be paid attention for most CFST arch bridges, especially for large spans. And for very large spans, such as Wu gorge Yangtze bridge and Meixi river bridge, the second mode shape is coupled bending-twisting out-plane. Therefore, 3-dimenstion FEM model should be used to perform further seismic response analysis.

In additional to the above mentioned bridges, there is another type of bridges with basket ribs inclined inward as shown in figure 1 (Haigen Cheng etc. 2002, Canhui Zhao, 2001). The suspenders could be either vertical or oblique. Table III shows the influence of oblique angle on vibration frequency.

Table III indicates that the frequency increases with the increasing of inclined angle, which means the increase of the globe stiffness. When the angle exceeds 10^o, the influence becomes weak while the static load carrying capacity decreases (Yongqing yang 1998). Therefore, 10^o is a favorable inclined angle for the consideration of both static behavior and dynamic property.

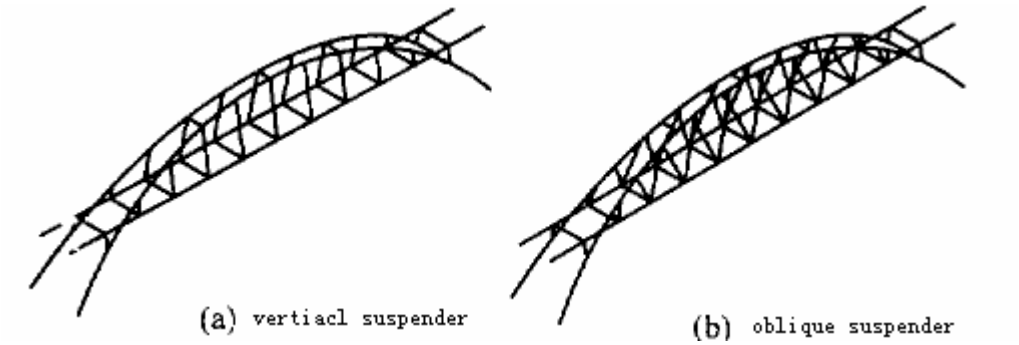

Figure 1 Model for CFST Basket arch bridge

TABLE III. INFLUENCE OF INCLINED ANGLE ON VIBRATION FREQUENCY.

Inclined angle (°)	Frequency				
	1st order	2st order	3st order	4st order	5st order
0(vertical suspender)	1.0513	2.6806	2.7575	2.9796	4.8414
0(oblique suspender)	1.0009	1.4756	2.3302	2.5331	3.3322
5	1.2172	2.4760	2.5728	2.9717	4.1909
10	1.6089	2.4897	2.7443	2.9586	4.7076
12	1.7879	2.5783	2.7730	2.7907	4.7766

Influence of lateral bracings on basic frequency

In order to improve the lateral stability, increasing the number of bracings, optimizing the locations of bracings and strengthening the stiffness of arch ribs are the available strategies.

Take Cidu bridge as example, four straight bracings and two K shape bracings are set on the vault, one K shape bracings and one location cross beam are set at each side of spring originally. Now we take off two straight bracings at the vault and one K shape bracing at the spring, the corresponding FEM analysis shows that the basic frequency out-plane and in-plane changes from 1.043/1.320 to 1.011/1.282 and 1.042/1.320, respectively, which also indicates that the effect of changes on bracing numbers at the vault are more obvious than that at the spring. Arch ribs are the important components of arch bridges, however, changes on rib stiffness have little effect on the fundamental frequency. Therefore, for most half-through CFST arch bridges, the layout of setting weaker bracings on the vault and stronger K shape or X shape bracings at the spring is appropriate design proposal, for which can both meet the requirement of the lateral stability and obtain good architectural configuration.

SEISMIC RESPONSE ANAYSIS

Three-dimension FEM analysis

As mentioned before, CFST arch bridges have a very short construction history, and few have experienced the earthquake excitation. However, China is a country with its northwest, southwest and Taiwan Strait lying in the strong seismic zone. But only a small part of CFST arch bridges have been analyzed on their seismic response at the beginning, which caused the lag of its seismic theory to some extent. However, with the progress on the static theory of CFST arch

bridges, its seismic theory has also advanced from the linear analysis to nonlinear analysis in recent years.

Linear seismic response analysis

Huangbo river bridge and Shitanxi bridge are the first two bridges that had been made seismic response analysis. The former used response spectrum method and the latter used dynamic history method. But due to the lag of theory of CFST arch bridges, the characteristic of composite material was not considered and was converted to concrete, which still includes seismic analysis of Yaji sha bridge(Shenqiao Xu 2000) and Longtan river bridge(Jiashu Zheng.2000). The conversion principle is: $A=A_c+nA_s$, $I=I_c+ n'I$, $I_p=I_{pc}+nI_{ps}$, in which $n=E_s/E_c$,$n'=G_s/G_c$. Therefore, the analysis was actually the same as RC or steel arch bridges, but the results as shown in TableIV could still disclosure some preliminary seismic behavior of this bridges.

TABLE IV. SESIMIC RESPONSE OF CFST ARCH BRIDGES

Section		N(KN)		M(KN.m)	
		Seismic response	Live load	Seismic response	Live load
Huangbo river bridge	vault	559.9	2295.6	315.2	7902.8
	spring	367.6	2831.3	395.7	9889.5
Shitanxi bridge	vault	4673	13480	424.4	1103
	spring	3726	17150	473.8	1531

The seismic analysis of the two bridges indicated that the seismic response was relatively smaller than that of the live load, which showed the advantages of light-weighted and high -strength of CFST arch bridges. However, this result obtained from only two bridges, general principles should be obtained through more case studies.

Current seismic response analytical methods of CFST arch bridges include section conversion method as used above and double elements method that treated concrete and steel as separated element while keeping their nodes the same. In order to reflect the material behavior of CFST and get more accurate result, a seismic response analytical FEM method based on CFST unified theory that treated CFST composite material as mono-material and its mechanics performance named CFST element method was proposed (Hong Su etc. 2003). Seismic response analysis indicated that although differences could be obtained by using different analytical method, the maximum difference in inner force would not exceed 20%. The reason implied could be explained by Table V, which shows the stiffness of the arch rib calculated from three methods.

TABLE V. STIFFENSESS USED IN DIFFERENT METHODS

Method	EA/KN	EI/(KN.m^2)	GI_p(KN.m^2)
Double elements method	210	10.60	8.48
Section conversion method	210	10.60	8.48
CFST element method	186	7.97	4.84

It can be seen that double element method and section conversion method have nearly the same stiffness, which led to the same seismic responses computed by the two methods. However, stiffness calculated from CFST element method is relatively smaller than that of the other two methods, which explained why the seismic response resulted from this method differenced from the other two methods. Because the case study was in the elastic phase, the difference was not that

obvious, but as could be anticipated, it will become obvious when the material goes into plastic phase. CFST element method, with the advantages of clear concept and relative accuracy, was proved to be a simple and convenient seismic response analytical method that is worthy of further development.

Nonlinear seismic response analysis

For CFST bridges with large spans, nonlinear effect should be taken in consideration, which mainly includes geometric nonlinearity and material nonlinearity. But the study(Jiashu Zheng 2000) shows that geometric nonlinearity has little effect on both displacement response and inner force response, there is no more difference except that at the peak value. While another study (Canhui Zhao 2001)shows that geometric nonlinearity has effect on seismic response to some extent with the maximum difference 17.1% in axial force. Actually, due to the random of earthquake waves and the structure types the bridges designed, the seismic responses may vary greatly with the waves and could not get consistent conclusion. However, so long as the effect on seismic response caused by geometric nonlinearity could be considerable under one certain wave, we should take this effect into consideration in seismic response analysis of large span CFST arch bridges.

To consider the geometric nonlinearity in FEM analysis is to include geometric stiffness matrix $[K]_\sigma$ and large displacement stiffness matrix $[K]_L$ in the general stiffness matrix[K]. That is $[K]=[K]_0+[K]_\sigma+[K]_L$, in which $[K]_\circ=[Kgs]_\circ+[Kgd]_\circ$, $[K]_L=[Kgs]_L+[Kgd]_L$, the first item in the two equations denotes the stiffness arose from static load, usually the dead load, the second item denotes the stiffness resulted from dynamic load, like earthquake excitation, which is usually a minor part of the stiffness matrix while becomes more important when strong seismic response is inspired. Table VI compares the axial forces resulted from earthquake with that of dead load of a CFST arch bridge with the span of 336.28m and the height of 77.27m(Canhui Zhao 2001), it can be seen that the seismic response is about 50% of the dead load, therefore the effect of axial force caused by earthquake on geometric stiffness can not be ignored. This study also points out that the seismic behavior of basket CFST arch bridge is not better than that of parallel CFST arch bridge when geometric nonlinear is considered.

TABLE VI. COMPARISON OF AXIAL FORCES

Axial force resulted from dead load			Axial force resulted from earthquake		
Sping	L/4	vault	Sping	L/4	vault
31296.3	20296.8	29992.2	18503.1	14310.4	12100.5

As for the material nonlinearity is considered, it is the key point in developing the theory of CFST arch bridges. The rapid and wide application of CFST in arch bridges should first owe to its material advantages of light-weighted, high-strength and good ductility. Generally speaking, there are two layers to consider the material nonlinearity, one is on the section layer, which means constitutive equation and Gauss integral method should be used to form the stiffness matrix of CFST components, however since the constitutive relationship used herein is followed by that used for column under axial compression, while the arch ribs are usually subjected to eccentric compression, the corresponding result may showed a certain deviation from that of the experiment in the evening of stress. Therefore, much endeavor has been made to develop suitable constitutive relationship for CFST arch bridges (Baochun Chen 2003). The other is on the component layer, which means the model of restoring force resulted from experiment of CFST components was

used to simulate the mechanical behavior of CFST arch ribs. A method for seismic response analysis based on CFST unified theory is presented by introducing the CFST plastic-elastic beam-column element with the application of lumped plastic hinge model, and which validity is proved through a planar arch model by using DRAIN-2D program(Hong Su 2002). Studies on material nonlinearity(Chanhui Zhao 2001,Hong Su 2002)of CFST arch bridges show that the bridge with large span is not likely to be destroyed because of strength due to the relatively flexible stiffness, while those with small spans may experience the plastic phase and be destroyed partly by loss of the strength of some components.

Shaking table test

Although FEM analysis is a very useful method to study seismic response of CFST arch bridges, and which can provide us nearly everything we want. But as we know, earthquake is a very complicated phenomenon with great randomness, the FEM analysis are processed based on a series of assumptions, especially on the earthquake input. Usually, the best way is to learn from the practical engineering cases attacked by real earthquake. However, as a new kind of bridge, any information on seismic response obtained by disaster or field experiment is not available. Fortunately, shaking table test could offer us an alternative to investigate the seismic behavior of CFST arch bridges. Supported by the open-subject — *research on seismic behavior of CFST arch bridges* of SLDRCE in 1999 (State Key Laboratory for Disaster Reduction in Civil Engineering), shaking table test of CFST arch model was carried out at Tongji university. The model consists of 5 bracings and two ribs with uniform circular section, and is 6m in span, 1m in height. The section dimensions for bracings and ribs are Φ 76×1mm and Φ 60×1mm,respectively.Both were filled with C30 concrete to form CFST material.

Figure 1 shows the model completed on the shaking table. The model showed good seismic behavior during the test even when El-centro record scaled to 1.6g was input to excite the model. In order to investigate the collapse state of CFST arch bridges, removing all the bracings, Shanghai artificial wave scaled to 0.8g was input transversely to excite the model, which eventually caused the collapse of the model as shown in figure 2.

Figure 1. CFST arch model installed on shaking table

Figure 2. Model collapse during shaking table test

During the test, we can see that the model collapsed to one side suddenly, local buckling with convex steel tube could be found at the springs, but the strain gauges pasted to the rib's surface showed that the rib did not yield except at the vault. Therefore preliminary study on the test

phenomenon drew the conclusion that CFST bridges have very good seismic performance, and was influenced more severely by spectrum distribution of earthquake wave than by the peak acceleration, the loss of lateral dynamic stability is probably the main reason to cause globe collapse (Feng Xiong 2001).

Dynamic stability is a very complicated problem, which has been made progress only on simple structure like beam and column under periodic excitation. Where it's a parametric resonance problem in Engineering and a solution to Mathieu or Mathieu-Hill equation in mathematics. While for the complicated structures under the excitation of earthquake, it's coupled with parametric resonance and forced vibration under the random excitation and more complicated than the parametric resonance, which can be solved only through FEM analysis (Zhongxue Li 1998).

As for CFST arch bridges, it is actually a double nonlinear problem processed by FEM analysis. And the key point of this problem lies in establishing reasonable criterion identifying the instability, which is the key point in *research on seismic theory of CFST arch bridges* anticipating solution under the support of National Science Foundation of China.

SUMMARY AND DISCUSSION

Several aspects of the seismic behavior of CFST bridges are being introduced herein. Although the study on seismic behavior is at the start, some progress has been made through many researchers' endeavor. But as a new type of bridges, compared with its prosperous engineering application, its computing theory has lagged behind, there are still many problems need to be studied urgently, which includes:

1. Field experiment on dynamic characteristics of CFST arch bridges, which can offer an overall and deeper understanding of different types of CFST arch bridges.
2. Shaking table test on seismic behavior of CFST arch bridges with truss ribs.
3. Mechanical behavior of CFST material under dynamic load, the hysteretic curves of CFST under repeated load is the basis of FEM analysis.
4. Dynamic stability of CFST arch bridges and the relationship between the lateral stability and lateral seismic response.

ACKNOWLEDGEMENT

This study is supported by the 2001 National Science Foundation of China - *research on seismic theory of CFST arch bridges* at grant number 50078016, which is gratefully acknowledged. And part of the results in this study came from the general report of *research on seismic behavior of CFST arch bridges* supported by the open-subject of SLDRCE in 1999. The authors would like to thank those researchers contributed to this subject.

REFERENCES

Baochun Chen. 2000. "Design and Construction of Concrete Filled Steel Tubular Arch Bridges", People's Communications Press, Beijing

Baochun Chen, Shuisheng Chen, Yuqing Liu. 2001.Preliminary Analysis of Natural Vibriation Characteristics and Anti-seismic Behavior of Concrete Filled Steel Tubular Arch Bridges, Theories and Applying of Structural En gineering (Proceedings of the Sixth International Symposium on Structural Engineering for Youth Experts), Y unan Science and Technology Press, 136-146

Jiashu Zheng.2000. "Three-dimensional Seismic Responses of Long-span CFST Arch Bridges" Journal. of Southwest Jiaotong University ,vol.38 No.1,Feb 53-56

Yunshen Li.1997. "Spatial dynamic Characteristics analysis of CFST arch bridges",Journal of Shijiazhuang Raiwaiy Insititute, vol.10 No.4,Dec 21-26

Haigen Chen, Shizhong Qiang.2002. "Dynamic Property Analysis of CFST X arch bridges", Journal of Highway and Transportation Research and Development, Vol.19. No.3,Jun 63-65

Shenqiao Xu.2000. "Seismic Response of the Main Bridge of Yaji Sha Bridge", Railway Standered Design, vol.20 No.12,Dec 8-11

Hong Su, Shide Hu. 2003. "Methods of Seismic Response Analysis of Concrete-filled-tube Arch Bridges", Journal of Tongji university,vol.31 No.4,Apr 404-407

Jiashu Zheng.2000. "Longitudinal seismic Response Analysis of Longtan river Arch Bridges", Journal of Engineering Mechanics(supplement),300-305

Chanhui Zhao.2001. "Researches on Seismic Response of long-span Concrete Filled Steel Tubular Arch Bridges", Dissertation for the Degree of Doctor of Philosophy in Engineering, Southwest Jiaotong University, Chengdu

Hong Su .2002. "Seismic Response Analysis of Concrete-Filled-tube Arch Bridges", Dissertation for the Degree of Master of Philosophy in Engineering, Tongji University, Shanghai

Feng Xiong.2001. "Study on Seismic Behavior of Concrete Filled Steel Tubular Arch Bridges", Dissertation for the Degree of Doctor of Philosophy in Engineering, Sichuan University, Chengdu

Report. 2003. "Study on Seismic Behavior of Concrete Filled Steel Tubular Arch Bridges", supported byopen-subject of SLDRCE in 1999

Zhongxue Li, Yuanqi li etc.2000. "Discussion on Key points of Research on Strucuture Nonlinear Dynamic Stability " Jouranl of Spatial Strucuture, Vol.6. No.4. Dec 29-35

Workshop Recommendations

The participants thought that this second workshop was very successful and provided a useful exchange of valuable technical information and construction experience in the seismic design and performance of special highway bridges.

There are many areas of common technical interest between the PRC and US that require urgent research in order to refine the design of special bridges (revise definition 'special:' tall piers of varying height, special foundations or sub or super, when site-specific required?) and protect the public from the catastrophic effects of earthquakes.

Research needs include:

- Ground motions (selection of return period): spatial distribution, near fault.
- Systems issues: conceptual seismic design for large bridges, network analysis, simplified analysis of irregular MDOF systems, nonlinear analysis, retrofitting strategies and measures, PBD application related to safety, reliability, security), multi-hazard design.
- Component issues: RMDs, SFSI, curved and irregular bridges, high piers and varying height, deep foundations (pile groups, caissons, large diameter piles).
- Damage modeling and bridge vulnerability analysis: NDE, sensors, post-earthquake evaluation.
- Emerging technologies for long term health monitoring (i.e., isolators, dampers, smart materials, hybrid systems, etc.).
- Durability, longevity of emerging technologies, quality assurance.
- Other research needs such as post-event response, construction technologies, etc.

The participants agreed that it would be useful to compile a database of researchers and practitioners in PRC and US who are interested in working together on cooperative projects. The database would include (at a minimum):

- Name.
- Organization.
- Expertise (structural/geotechnical/analyst/experimentalist/designer, etc.).
- Research topics of interest.

Furthermore, the participants wish to thank Professors George Lee and Lichu Fan for their skillful organization of this successful meeting, and to recognize the US and PRC sponsors of this workshop for their generous support.

Finally, the third workshop in this series should be held in 2004 in PRC, with a broader range of participants.

Agenda

WEDNESDAY, DECEMBER 3RD

Salon A

6:15 pm – 8:00 pm **Welcoming Reception**

THURSDAY, DECEMBER 4TH

Ballroom 2

7:30 am – 8:15 am **Continental Breakfast/Registration**

8:15 am – 8:30 am **Introductory Remarks (*Drs. Bruneau, Li and Lee*)**

8:30 am – 10:00 am **Session I**

R. Land , "Caltrans' Seismic Design Criteria"
Professor Fan, Presented by Professor Li "A Brief Introduction on China Code for Seismic Design of Urban Bridges (2nd Draft)"
L. Marsh, "Recommended LRFD Guidelines for the Seismic Design of Highway Bridges"

10:00 am – 10:30 am **BREAK (Photo Session)**

10:30 am – 12:30 pm **Session II**

J. Kulicki and T.P. Murphy, "Impacts of Seismic Requirements on the Design of the I-70 Cable Stayed Bridge at St. Louis"
J. Li, "Seismic Performance of a Double-deck Viaduct"
J. Sun and M-C Tang, "Chongqing CaiYuanBa Yangtze River Crossing"
M. Shinozuka, S-H Kim and Y. Zhou, "Effect of Retrofit, Skew and Number of Spans on Bridge Fragility"

Ballroom 3

12:30 pm – 1:30 pm **LUNCH**

1:30 pm – 3:30 pm **Session III**

X. Zhu, "Seismic Pounding Behavior of Simply Supported Girder Bridges"
R. DesRoches and S. Muthukumar, "Implications of Seismic Pounding on the Response of Bridges – An Analytical Perspective"
Q. Yang, "Analysis Models and Methods for Structural Response of Spatially Varying Ground Motions"
M. Bruneau and M. Pollino, "Controlled Rocking System for Seismic Retrofit of Steel Truss Bridge Piers"

3:30 pm – 3:50 pm **BREAK**

3:50 pm – 5:50 pm **Session IV**

I. Buckle, P. Dusicka and A. Itani, "Development of Built-up Shear Links as Energy Dissipators for the Seismic Protection of Long Span Bridges"
A. Ye, "The Implementation of Dampers on Several Large Bridges in China"
M. Constantinou and P. Roussi, "Performance of Seismic Isolation System of Bolu Viaduct in the 1999 Duzce Earthquake"
M. Feng, D.K. Kim, J-H Yi and Y. Chen, "Instrumentation and Baseline Modeling for Long-Term Performance Evaluation of Highway Bridges"

Salon C-D (Second Floor)

6:30 pm	**BANQUET**
8:15 pm	**Special Presentation – "Seismic Design of the New San Francisco Oakland Bay Bridge Self Anchored Suspension Span" By M. Nader, T.Y. Lin International**

FRIDAY, DECEMBER 5, 2003

Salon C-D (Second Floor)

7:30 am – 8:30 am	**Continental Breakfast**
8:30 am – 10:30 am	**Session V** **N. Johnson, S. Saiidi and A. Itani, "Seismic Retrofit Strategies for Substandard Single-Column Bents Supported on Pedestals"** **J. Wang, "Hydrodynamic Effect on Seismic Response of Bridges"** **H. Capers, H. Najm and H. Hassif, "Evaluation of NCHRP 12-49 Provisions for Seismic Design of Bridges in New Jersey"** **C. Seim, "Performance Based Design for Seismic Retrofitting of Long-Span Steel Truss Highway Bridges"**
10:30 am – 10:50 am	**BREAK**
10:50 am – 12:30 pm	**Research Need and Summary** **P. Yen, "New Initiative of Bridge Research in Federal Highway Administration"** **G. Lee, "Summary of Research Needs Statements From Participants"** **Others/Discussion** **I. Buckle, "Workshop Recommendations"**

CLOSING

12:30 pm – 1:30 pm	**LUNCH**
1:30 pm – 2:00 pm	**M. Bruneau, UB NEES NODE**
2:30 pm – 3:30 pm	**Tour of Ketter Hall Laboratory**

Participants List

PRC

Li, Jianzhong
University of Tongji
Department of Bridge Engineering
Siping Road, 1239#,
200092, Shanghai, China
e-mail: lijianzh@mail.tongji.edu.cn

Wang, Junjie
University of Tongj
Department of Bridge Engineering
Siping Road, 1239#,
200092, Shanghai, China
e-mail: jjwang@mail.tongji.edu.cn

Wang, Zhiqiang
University of Tongji
Department of Bridge Engineering
Siping Road, 1239#,
200092, Shanghai, China
e-mail: wangshiq@mail.tongji.edu.cn

Xu, Weiliang
University of Tongji
Department of Bridge Engineering
Siping Road, 1239#,
200092, Shanghai, China

Yan, Guiping
Northern Beijing Jiaotong University
College of Engineering and Architecture
Beijing, 100044, PRC
e-mail: Gpyanq1101@hotmail.com

Yang, Qingshan
Beijing Jiaotong University
Northern Beijing Jiaotong University
College of Engineering and Architecture
Beijing, 100044, PRC
e-mail: Qshyang6620@sina.com

Ye, Aijun
University of Tongji
Department of Bridge Engineering
Siping Road, 1239#,
200092, Shanghai, China
e-mail: yeaijun@mail.tongji.edu.cn

Zhu, Xi
Northern Beijing Jiaotong University
College of Engineering and Architecture
Beijing, 100044, PRC

US

Bruneau, Michel
University at Buffalo
Multidisciplinary Center for
Earthquake Engineering Research
Red Jacket Quadrangle
Buffalo, NY 14261
e-mail: bruneau@mceermail.buffalo.edu

Buckle, Ian
University of Nevada, Reno
Department of Civil Engineering
MS 258
Reno, NV 89557
e-mail: igbuckle@unr.edu

Capers, Harry
New Jersey Department of Transportation
Structural Engineering
P.O. Box 615
Trenton, NJ 08625-0615
e-mail: harry.capers@dot.state.nj.us

Constantinou, Michael
University at Buffalo
Department of Civil Engineering
Ketter Hall
Buffalo, NY 14260
e-mail: constan1@eng.buffalo.edu

DesRoches, Reginald
Georgia Institute of Technology
School of civil & Environ. Engr.
Atlanta, GA 30332-00355
e-mail: reginald.desroches@ce.gatech.edu

Feng, Maria
University of California, Irvine
Civil & Environ. Engr. Department
Engineering Gateway 4139
Irvine, CA 92697-2175
e-mail: mfeng@uci.edu

Kulicki, John
Modjeski and Masters, Inc.
4909 Louise Drive
Mechanicsburg, PA 17055
e-mail: jmkulicki@modjeski.com

Land, Richard
California Department of Transportation
Div. of Engineering Services-Structures Div.
1801 30th Street, MS 9/4-11G
P.O. Box 168041
Sacramento, CA 95816-8041
e-mail: richard_land@dot.ca.dogv

Lee, George
University at Buffalo
Multidiscplinary Center for
Earthquake Engineering Research
Red Jacket Quadrangle
Buffalo, NY 14261
e-mail: gclee@mceermail.buffalo.edu

Marsh, Lee
Berger/Abam Engineering, Inc.
33301 9th Avenue S.
Suite 300
Federal Way, WA 98003-6395
e-mail: marsh@abam.com

Nader, Marwan
T Y Lin International
825 Battery Street
San Francisco, CA 94111
e-mail: mnader@tylin.com

O'Connor, Jerome
Multidisciplinary Center for
Earthquake Engineering Research
Red Jacket Quadrangle
Buffalo, NY 14261
e-mail: jso7@buffalo.edu

Saiidi, M. Saiid
University of Nevada, Reno
Civil Engineering Department
Mail Stop 258
Reno, NV 89557-0030
e-mail: saiidi@unr.edu

Seim, Charles
T Y Lin International
825 Battery Street
San Francisco, CA 94111
e-mail: cseim@tylin.com

Shinozuka, M.
University of California, Irvine
Department of Civil & Environ. Engr.
E/4150 Engineering Gateway
Irvine, CA 92697-2175
e-mail: shino@uci./edu

Stoyle, Jane
Multidisciplinary Center for
Earthquake Engineering Research
Red Jacket Quadrangle
Buffalo, NY 14261
e-mail: jestoyle@mceermail.buffalo.edu

Sun, John
T Y Lin International
825 Battery Street
San Francisco, CA 94111
e-mail: jsun@tylin.com

Yen, Phillip
Federal Highway Administration
Office of Infrastructure R & D
Bridge Design & Hazard Mitigation T-111
6300 Georgetown Pike
McLean, VA 22101
e-mail: wen-huei.yen@fhwa.dot.gov

Multidisciplinary Center for Earthquake Engineering Research
List of Technical Reports

The Multidisciplinary Center for Earthquake Engineering Research (MCEER) publishes technical reports on a variety of subjects related to earthquake engineering written by authors funded through MCEER. These reports are available from both MCEER Publications and the National Technical Information Service (NTIS). Requests for reports should be directed to MCEER Publications, Multidisciplinary Center for Earthquake Engineering Research, State University of New York at Buffalo, Red Jacket Quadrangle, Buffalo, New York 14261. Reports can also be requested through NTIS, 5285 Port Royal Road, Springfield, Virginia 22161. NTIS accession numbers are shown in parenthesis, if available.

NCEER-87-0001 "First-Year Program in Research, Education and Technology Transfer," 3/5/87, (PB88-134275, A04, MF-A01).

NCEER-87-0002 "Experimental Evaluation of Instantaneous Optimal Algorithms for Structural Control," by R.C. Lin, T.T. Soong and A.M. Reinhorn, 4/20/87, (PB88-134341, A04, MF-A01).

NCEER-87-0003 "Experimentation Using the Earthquake Simulation Facilities at University at Buffalo," by A.M. Reinhorn and R.L. Ketter, to be published.

NCEER-87-0004 "The System Characteristics and Performance of a Shaking Table," by J.S. Hwang, K.C. Chang and G.C. Lee, 6/1/87, (PB88-134259, A03, MF-A01). This report is available only through NTIS (see address given above).

NCEER-87-0005 "A Finite Element Formulation for Nonlinear Viscoplastic Material Using a Q Model," by O. Gyebi and G. Dasgupta, 11/2/87, (PB88-213764, A08, MF-A01).

NCEER-87-0006 "Symbolic Manipulation Program (SMP) - Algebraic Codes for Two and Three Dimensional Finite Element Formulations," by X. Lee and G. Dasgupta, 11/9/87, (PB88-218522, A05, MF-A01).

NCEER-87-0007 "Instantaneous Optimal Control Laws for Tall Buildings Under Seismic Excitations," by J.N. Yang, A. Akbarpour and P. Ghaemmaghami, 6/10/87, (PB88-134333, A06, MF-A01). This report is only available through NTIS (see address given above).

NCEER-87-0008 "IDARC: Inelastic Damage Analysis of Reinforced Concrete Frame - Shear-Wall Structures," by Y.J. Park, A.M. Reinhorn and S.K. Kunnath, 7/20/87, (PB88-134325, A09, MF-A01). This report is only available through NTIS (see address given above).

NCEER-87-0009 "Liquefaction Potential for New York State: A Preliminary Report on Sites in Manhattan and Buffalo," by M. Budhu, V. Vijayakumar, R.F. Giese and L. Baumgras, 8/31/87, (PB88-163704, A03, MF-A01). This report is available only through NTIS (see address given above).

NCEER-87-0010 "Vertical and Torsional Vibration of Foundations in Inhomogeneous Media," by A.S. Veletsos and K.W. Dotson, 6/1/87, (PB88-134291, A03, MF-A01). This report is only available through NTIS (see address given above).

NCEER-87-0011 "Seismic Probabilistic Risk Assessment and Seismic Margins Studies for Nuclear Power Plants," by Howard H.M. Hwang, 6/15/87, (PB88-134267, A03, MF-A01). This report is only available through NTIS (see address given above).

NCEER-87-0012 "Parametric Studies of Frequency Response of Secondary Systems Under Ground-Acceleration Excitations," by Y. Yong and Y.K. Lin, 6/10/87, (PB88-134309, A03, MF-A01). This report is only available through NTIS (see address given above).

NCEER-87-0013 "Frequency Response of Secondary Systems Under Seismic Excitation," by J.A. HoLung, J. Cai and Y.K. Lin, 7/31/87, (PB88-134317, A05, MF-A01). This report is only available through NTIS (see address given above).

NCEER-87-0014 "Modelling Earthquake Ground Motions in Seismically Active Regions Using Parametric Time Series Methods," by G.W. Ellis and A.S. Cakmak, 8/25/87, (PB88-134283, A08, MF-A01). This report is only available through NTIS (see address given above).

NCEER-87-0015 "Detection and Assessment of Seismic Structural Damage," by E. DiPasquale and A.S. Cakmak, 8/25/87, (PB88-163712, A05, MF-A01). This report is only available through NTIS (see address given above).

NCEER-87-0016 "Pipeline Experiment at Parkfield, California," by J. Isenberg and E. Richardson, 9/15/87, (PB88-163720, A03, MF-A01). This report is available only through NTIS (see address given above).

NCEER-87-0017 "Digital Simulation of Seismic Ground Motion," by M. Shinozuka, G. Deodatis and T. Harada, 8/31/87, (PB88-155197, A04, MF-A01). This report is available only through NTIS (see address given above).

NCEER-87-0018 "Practical Considerations for Structural Control: System Uncertainty, System Time Delay and Truncation of Small Control Forces," J.N. Yang and A. Akbarpour, 8/10/87, (PB88-163738, A08, MF-A01). This report is only available through NTIS (see address given above).

NCEER-87-0019 "Modal Analysis of Nonclassically Damped Structural Systems Using Canonical Transformation," by J.N. Yang, S. Sarkani and F.X. Long, 9/27/87, (PB88-187851, A04, MF-A01).

NCEER-87-0020 "A Nonstationary Solution in Random Vibration Theory," by J.R. Red-Horse and P.D. Spanos, 11/3/87, (PB88-163746, A03, MF-A01).

NCEER-87-0021 "Horizontal Impedances for Radially Inhomogeneous Viscoelastic Soil Layers," by A.S. Veletsos and K.W. Dotson, 10/15/87, (PB88-150859, A04, MF-A01).

NCEER-87-0022 "Seismic Damage Assessment of Reinforced Concrete Members," by Y.S. Chung, C. Meyer and M. Shinozuka, 10/9/87, (PB88-150867, A05, MF-A01). This report is available only through NTIS (see address given above).

NCEER-87-0023 "Active Structural Control in Civil Engineering," by T.T. Soong, 11/11/87, (PB88-187778, A03, MF-A01).

NCEER-87-0024 "Vertical and Torsional Impedances for Radially Inhomogeneous Viscoelastic Soil Layers," by K.W. Dotson and A.S. Veletsos, 12/87, (PB88-187786, A03, MF-A01).

NCEER-87-0025 "Proceedings from the Symposium on Seismic Hazards, Ground Motions, Soil-Liquefaction and Engineering Practice in Eastern North America," October 20-22, 1987, edited by K.H. Jacob, 12/87, (PB88-188115, A23, MF-A01). This report is available only through NTIS (see address given above).

NCEER-87-0026 "Report on the Whittier-Narrows, California, Earthquake of October 1, 1987," by J. Pantelic and A. Reinhorn, 11/87, (PB88-187752, A03, MF-A01). This report is available only through NTIS (see address given above).

NCEER-87-0027 "Design of a Modular Program for Transient Nonlinear Analysis of Large 3-D Building Structures," by S. Srivastav and J.F. Abel, 12/30/87, (PB88-187950, A05, MF-A01). This report is only available through NTIS (see address given above).

NCEER-87-0028 "Second-Year Program in Research, Education and Technology Transfer," 3/8/88, (PB88-219480, A04, MF-A01).

NCEER-88-0001 "Workshop on Seismic Computer Analysis and Design of Buildings With Interactive Graphics," by W. McGuire, J.F. Abel and C.H. Conley, 1/18/88, (PB88-187760, A03, MF-A01). This report is only available through NTIS (see address given above).

NCEER-88-0002 "Optimal Control of Nonlinear Flexible Structures," by J.N. Yang, F.X. Long and D. Wong, 1/22/88, (PB88-213772, A06, MF-A01).

NCEER-88-0003 "Substructuring Techniques in the Time Domain for Primary-Secondary Structural Systems," by G.D. Manolis and G. Juhn, 2/10/88, (PB88-213780, A04, MF-A01).

NCEER-88-0004 "Iterative Seismic Analysis of Primary-Secondary Systems," by A. Singhal, L.D. Lutes and P.D. Spanos, 2/23/88, (PB88-213798, A04, MF-A01).

NCEER-88-0005 "Stochastic Finite Element Expansion for Random Media," by P.D. Spanos and R. Ghanem, 3/14/88, (PB88-213806, A03, MF-A01).

NCEER-88-0006 "Combining Structural Optimization and Structural Control," by F.Y. Cheng and C.P. Pantelides, 1/10/88, (PB88-213814, A05, MF-A01).

NCEER-88-0007 "Seismic Performance Assessment of Code-Designed Structures," by H.H-M. Hwang, J-W. Jaw and H-J. Shau, 3/20/88, (PB88-219423, A04, MF-A01). This report is only available through NTIS (see address given above).

NCEER-88-0008 "Reliability Analysis of Code-Designed Structures Under Natural Hazards," by H.H-M. Hwang, H. Ushiba and M. Shinozuka, 2/29/88, (PB88-229471, A07, MF-A01). This report is only available through NTIS (see address given above).

NCEER-88-0009 "Seismic Fragility Analysis of Shear Wall Structures," by J-W Jaw and H.H-M. Hwang, 4/30/88, (PB89-102867, A04, MF-A01).

NCEER-88-0010 "Base Isolation of a Multi-Story Building Under a Harmonic Ground Motion - A Comparison of Performances of Various Systems," by F-G Fan, G. Ahmadi and I.G. Tadjbakhsh, 5/18/88, (PB89-122238, A06, MF-A01). This report is only available through NTIS (see address given above).

NCEER-88-0011 "Seismic Floor Response Spectra for a Combined System by Green's Functions," by F.M. Lavelle, L.A. Bergman and P.D. Spanos, 5/1/88, (PB89-102875, A03, MF-A01).

NCEER-88-0012 "A New Solution Technique for Randomly Excited Hysteretic Structures," by G.Q. Cai and Y.K. Lin, 5/16/88, (PB89-102883, A03, MF-A01).

NCEER-88-0013 "A Study of Radiation Damping and Soil-Structure Interaction Effects in the Centrifuge," by K. Weissman, supervised by J.H. Prevost, 5/24/88, (PB89-144703, A06, MF-A01).

NCEER-88-0014 "Parameter Identification and Implementation of a Kinematic Plasticity Model for Frictional Soils," by J.H. Prevost and D.V. Griffiths, to be published.

NCEER-88-0015 "Two- and Three- Dimensional Dynamic Finite Element Analyses of the Long Valley Dam," by D.V. Griffiths and J.H. Prevost, 6/17/88, (PB89-144711, A04, MF-A01).

NCEER-88-0016 "Damage Assessment of Reinforced Concrete Structures in Eastern United States," by A.M. Reinhorn, M.J. Seidel, S.K. Kunnath and Y.J. Park, 6/15/88, (PB89-122220, A04, MF-A01). This report is only available through NTIS (see address given above).

NCEER-88-0017 "Dynamic Compliance of Vertically Loaded Strip Foundations in Multilayered Viscoelastic Soils," by S. Ahmad and A.S.M. Israil, 6/17/88, (PB89-102891, A04, MF-A01).

NCEER-88-0018 "An Experimental Study of Seismic Structural Response With Added Viscoelastic Dampers," by R.C. Lin, Z. Liang, T.T. Soong and R.H. Zhang, 6/30/88, (PB89-122212, A05, MF-A01). This report is available only through NTIS (see address given above).

NCEER-88-0019 "Experimental Investigation of Primary - Secondary System Interaction," by G.D. Manolis, G. Juhn and A.M. Reinhorn, 5/27/88, (PB89-122204, A04, MF-A01).

NCEER-88-0020 "A Response Spectrum Approach For Analysis of Nonclassically Damped Structures," by J.N. Yang, S. Sarkani and F.X. Long, 4/22/88, (PB89-102909, A04, MF-A01).

NCEER-88-0021 "Seismic Interaction of Structures and Soils: Stochastic Approach," by A.S. Veletsos and A.M. Prasad, 7/21/88, (PB89-122196, A04, MF-A01). This report is only available through NTIS (see address given above).

NCEER-88-0022 "Identification of the Serviceability Limit State and Detection of Seismic Structural Damage," by E. DiPasquale and A.S. Cakmak, 6/15/88, (PB89-122188, A05, MF-A01). This report is available only through NTIS (see address given above).

NCEER-88-0023 "Multi-Hazard Risk Analysis: Case of a Simple Offshore Structure," by B.K. Bhartia and E.H. Vanmarcke, 7/21/88, (PB89-145213, A05, MF-A01).

NCEER-88-0024 "Automated Seismic Design of Reinforced Concrete Buildings," by Y.S. Chung, C. Meyer and M. Shinozuka, 7/5/88, (PB89-122170, A06, MF-A01). This report is available only through NTIS (see address given above).

NCEER-88-0025 "Experimental Study of Active Control of MDOF Structures Under Seismic Excitations," by L.L. Chung, R.C. Lin, T.T. Soong and A.M. Reinhorn, 7/10/88, (PB89-122600, A04, MF-A01).

NCEER-88-0026 "Earthquake Simulation Tests of a Low-Rise Metal Structure," by J.S. Hwang, K.C. Chang, G.C. Lee and R.L. Ketter, 8/1/88, (PB89-102917, A04, MF-A01).

NCEER-88-0027 "Systems Study of Urban Response and Reconstruction Due to Catastrophic Earthquakes," by F. Kozin and H.K. Zhou, 9/22/88, (PB90-162348, A04, MF-A01).

NCEER-88-0028 "Seismic Fragility Analysis of Plane Frame Structures," by H.H-M. Hwang and Y.K. Low, 7/31/88, (PB89-131445, A06, MF-A01).

NCEER-88-0029 "Response Analysis of Stochastic Structures," by A. Kardara, C. Bucher and M. Shinozuka, 9/22/88, (PB89-174429, A04, MF-A01).

NCEER-88-0030 "Nonnormal Accelerations Due to Yielding in a Primary Structure," by D.C.K. Chen and L.D. Lutes, 9/19/88, (PB89-131437, A04, MF-A01).

NCEER-88-0031 "Design Approaches for Soil-Structure Interaction," by A.S. Veletsos, A.M. Prasad and Y. Tang, 12/30/88, (PB89-174437, A03, MF-A01). This report is available only through NTIS (see address given above).

NCEER-88-0032 "A Re-evaluation of Design Spectra for Seismic Damage Control," by C.J. Turkstra and A.G. Tallin, 11/7/88, (PB89-145221, A05, MF-A01).

NCEER-88-0033 "The Behavior and Design of Noncontact Lap Splices Subjected to Repeated Inelastic Tensile Loading," by V.E. Sagan, P. Gergely and R.N. White, 12/8/88, (PB89-163737, A08, MF-A01).

NCEER-88-0034 "Seismic Response of Pile Foundations," by S.M. Mamoon, P.K. Banerjee and S. Ahmad, 11/1/88, (PB89-145239, A04, MF-A01).

NCEER-88-0035 "Modeling of R/C Building Structures With Flexible Floor Diaphragms (IDARC2)," by A.M. Reinhorn, S.K. Kunnath and N. Panahshahi, 9/7/88, (PB89-207153, A07, MF-A01).

NCEER-88-0036 "Solution of the Dam-Reservoir Interaction Problem Using a Combination of FEM, BEM with Particular Integrals, Modal Analysis, and Substructuring," by C-S. Tsai, G.C. Lee and R.L. Ketter, 12/31/88, (PB89-207146, A04, MF-A01).

NCEER-88-0037 "Optimal Placement of Actuators for Structural Control," by F.Y. Cheng and C.P. Pantelides, 8/15/88, (PB89-162846, A05, MF-A01).

NCEER-88-0038 "Teflon Bearings in Aseismic Base Isolation: Experimental Studies and Mathematical Modeling," by A. Mokha, M.C. Constantinou and A.M. Reinhorn, 12/5/88, (PB89-218457, A10, MF-A01). This report is available only through NTIS (see address given above).

NCEER-88-0039 "Seismic Behavior of Flat Slab High-Rise Buildings in the New York City Area," by P. Weidlinger and M. Ettouney, 10/15/88, (PB90-145681, A04, MF-A01).

NCEER-88-0040 "Evaluation of the Earthquake Resistance of Existing Buildings in New York City," by P. Weidlinger and M. Ettouney, 10/15/88, to be published.

NCEER-88-0041 "Small-Scale Modeling Techniques for Reinforced Concrete Structures Subjected to Seismic Loads," by W. Kim, A. El-Attar and R.N. White, 11/22/88, (PB89-189625, A05, MF-A01).

NCEER-88-0042 "Modeling Strong Ground Motion from Multiple Event Earthquakes," by G.W. Ellis and A.S. Cakmak, 10/15/88, (PB89-174445, A03, MF-A01).

NCEER-88-0043 "Nonstationary Models of Seismic Ground Acceleration," by M. Grigoriu, S.E. Ruiz and E. Rosenblueth, 7/15/88, (PB89-189617, A04, MF-A01).

NCEER-88-0044 "SARCF User's Guide: Seismic Analysis of Reinforced Concrete Frames," by Y.S. Chung, C. Meyer and M. Shinozuka, 11/9/88, (PB89-174452, A08, MF-A01).

NCEER-88-0045 "First Expert Panel Meeting on Disaster Research and Planning," edited by J. Pantelic and J. Stoyle, 9/15/88, (PB89-174460, A05, MF-A01).

NCEER-88-0046 "Preliminary Studies of the Effect of Degrading Infill Walls on the Nonlinear Seismic Response of Steel Frames," by C.Z. Chrysostomou, P. Gergely and J.F. Abel, 12/19/88, (PB89-208383, A05, MF-A01).

NCEER-88-0047 "Reinforced Concrete Frame Component Testing Facility - Design, Construction, Instrumentation and Operation," by S.P. Pessiki, C. Conley, T. Bond, P. Gergely and R.N. White, 12/16/88, (PB89-174478, A04, MF-A01).

NCEER-89-0001 "Effects of Protective Cushion and Soil Compliancy on the Response of Equipment Within a Seismically Excited Building," by J.A. HoLung, 2/16/89, (PB89-207179, A04, MF-A01).

NCEER-89-0002 "Statistical Evaluation of Response Modification Factors for Reinforced Concrete Structures," by H.H-M. Hwang and J-W. Jaw, 2/17/89, (PB89-207187, A05, MF-A01).

NCEER-89-0003 "Hysteretic Columns Under Random Excitation," by G-Q. Cai and Y.K. Lin, 1/9/89, (PB89-196513, A03, MF-A01).

NCEER-89-0004 "Experimental Study of `Elephant Foot Bulge' Instability of Thin-Walled Metal Tanks," by Z-H. Jia and R.L. Ketter, 2/22/89, (PB89-207195, A03, MF-A01).

NCEER-89-0005 "Experiment on Performance of Buried Pipelines Across San Andreas Fault," by J. Isenberg, E. Richardson and T.D. O'Rourke, 3/10/89, (PB89-218440, A04, MF-A01). This report is available only through NTIS (see address given above).

NCEER-89-0006 "A Knowledge-Based Approach to Structural Design of Earthquake-Resistant Buildings," by M. Subramani, P. Gergely, C.H. Conley, J.F. Abel and A.H. Zaghw, 1/15/89, (PB89-218465, A06, MF-A01).

NCEER-89-0007 "Liquefaction Hazards and Their Effects on Buried Pipelines," by T.D. O'Rourke and P.A. Lane, 2/1/89, (PB89-218481, A09, MF-A01).

NCEER-89-0008 "Fundamentals of System Identification in Structural Dynamics," by H. Imai, C-B. Yun, O. Maruyama and M. Shinozuka, 1/26/89, (PB89-207211, A04, MF-A01).

NCEER-89-0009 "Effects of the 1985 Michoacan Earthquake on Water Systems and Other Buried Lifelines in Mexico," by A.G. Ayala and M.J. O'Rourke, 3/8/89, (PB89-207229, A06, MF-A01).

NCEER-89-R010 "NCEER Bibliography of Earthquake Education Materials," by K.E.K. Ross, Second Revision, 9/1/89, (PB90-125352, A05, MF-A01). This report is replaced by NCEER-92-0018.

NCEER-89-0011 "Inelastic Three-Dimensional Response Analysis of Reinforced Concrete Building Structures (IDARC-3D), Part I - Modeling," by S.K. Kunnath and A.M. Reinhorn, 4/17/89, (PB90-114612, A07, MF-A01). This report is available only through NTIS (see address given above).

NCEER-89-0012 "Recommended Modifications to ATC-14," by C.D. Poland and J.O. Malley, 4/12/89, (PB90-108648, A15, MF-A01).

NCEER-89-0013 "Repair and Strengthening of Beam-to-Column Connections Subjected to Earthquake Loading," by M. Corazao and A.J. Durrani, 2/28/89, (PB90-109885, A06, MF-A01).

NCEER-89-0014 "Program EXKAL2 for Identification of Structural Dynamic Systems," by O. Maruyama, C-B. Yun, M. Hoshiya and M. Shinozuka, 5/19/89, (PB90-109877, A09, MF-A01).

NCEER-89-0015 "Response of Frames With Bolted Semi-Rigid Connections, Part I - Experimental Study and Analytical Predictions," by P.J. DiCorso, A.M. Reinhorn, J.R. Dickerson, J.B. Radziminski and W.L. Harper, 6/1/89, to be published.

NCEER-89-0016 "ARMA Monte Carlo Simulation in Probabilistic Structural Analysis," by P.D. Spanos and M.P. Mignolet, 7/10/89, (PB90-109893, A03, MF-A01).

NCEER-89-P017 "Preliminary Proceedings from the Conference on Disaster Preparedness - The Place of Earthquake Education in Our Schools," Edited by K.E.K. Ross, 6/23/89, (PB90-108606, A03, MF-A01).

NCEER-89-0017 "Proceedings from the Conference on Disaster Preparedness - The Place of Earthquake Education in Our Schools," Edited by K.E.K. Ross, 12/31/89, (PB90-207895, A012, MF-A02). This report is available only through NTIS (see address given above).

NCEER-89-0018 "Multidimensional Models of Hysteretic Material Behavior for Vibration Analysis of Shape Memory Energy Absorbing Devices, by E.J. Graesser and F.A. Cozzarelli, 6/7/89, (PB90-164146, A04, MF-A01).

NCEER-89-0019 "Nonlinear Dynamic Analysis of Three-Dimensional Base Isolated Structures (3D-BASIS)," by S. Nagarajaiah, A.M. Reinhorn and M.C. Constantinou, 8/3/89, (PB90-161936, A06, MF-A01). This report has been replaced by NCEER-93-0011.

NCEER-89-0020 "Structural Control Considering Time-Rate of Control Forces and Control Rate Constraints," by F.Y. Cheng and C.P. Pantelides, 8/3/89, (PB90-120445, A04, MF-A01).

NCEER-89-0021 "Subsurface Conditions of Memphis and Shelby County," by K.W. Ng, T-S. Chang and H-H.M. Hwang, 7/26/89, (PB90-120437, A03, MF-A01).

NCEER-89-0022 "Seismic Wave Propagation Effects on Straight Jointed Buried Pipelines," by K. Elhmadi and M.J. O'Rourke, 8/24/89, (PB90-162322, A10, MF-A02).

NCEER-89-0023 "Workshop on Serviceability Analysis of Water Delivery Systems," edited by M. Grigoriu, 3/6/89, (PB90-127424, A03, MF-A01).

NCEER-89-0024 "Shaking Table Study of a 1/5 Scale Steel Frame Composed of Tapered Members," by K.C. Chang, J.S. Hwang and G.C. Lee, 9/18/89, (PB90-160169, A04, MF-A01).

NCEER-89-0025 "DYNA1D: A Computer Program for Nonlinear Seismic Site Response Analysis - Technical Documentation," by Jean H. Prevost, 9/14/89, (PB90-161944, A07, MF-A01). This report is available only through NTIS (see address given above).

NCEER-89-0026 "1:4 Scale Model Studies of Active Tendon Systems and Active Mass Dampers for Aseismic Protection," by A.M. Reinhorn, T.T. Soong, R.C. Lin, Y.P. Yang, Y. Fukao, H. Abe and M. Nakai, 9/15/89, (PB90-173246, A10, MF-A02). This report is available only through NTIS (see address given above).

NCEER-89-0027 "Scattering of Waves by Inclusions in a Nonhomogeneous Elastic Half Space Solved by Boundary Element Methods," by P.K. Hadley, A. Askar and A.S. Cakmak, 6/15/89, (PB90-145699, A07, MF-A01).

NCEER-89-0028 "Statistical Evaluation of Deflection Amplification Factors for Reinforced Concrete Structures," by H.H.M. Hwang, J-W. Jaw and A.L. Ch'ng, 8/31/89, (PB90-164633, A05, MF-A01).

NCEER-89-0029 "Bedrock Accelerations in Memphis Area Due to Large New Madrid Earthquakes," by H.H.M. Hwang, C.H.S. Chen and G. Yu, 11/7/89, (PB90-162330, A04, MF-A01).

NCEER-89-0030 "Seismic Behavior and Response Sensitivity of Secondary Structural Systems," by Y.Q. Chen and T.T. Soong, 10/23/89, (PB90-164658, A08, MF-A01).

NCEER-89-0031 "Random Vibration and Reliability Analysis of Primary-Secondary Structural Systems," by Y. Ibrahim, M. Grigoriu and T.T. Soong, 11/10/89, (PB90-161951, A04, MF-A01).

NCEER-89-0032 "Proceedings from the Second U.S. - Japan Workshop on Liquefaction, Large Ground Deformation and Their Effects on Lifelines, September 26-29, 1989," Edited by T.D. O'Rourke and M. Hamada, 12/1/89, (PB90-209388, A22, MF-A03).

NCEER-89-0033 "Deterministic Model for Seismic Damage Evaluation of Reinforced Concrete Structures," by J.M. Bracci, A.M. Reinhorn, J.B. Mander and S.K. Kunnath, 9/27/89, (PB91-108803, A06, MF-A01).

NCEER-89-0034 "On the Relation Between Local and Global Damage Indices," by E. DiPasquale and A.S. Cakmak, 8/15/89, (PB90-173865, A05, MF-A01).

NCEER-89-0035 "Cyclic Undrained Behavior of Nonplastic and Low Plasticity Silts," by A.J. Walker and H.E. Stewart, 7/26/89, (PB90-183518, A10, MF-A01).

NCEER-89-0036 "Liquefaction Potential of Surficial Deposits in the City of Buffalo, New York," by M. Budhu, R. Giese and L. Baumgrass, 1/17/89, (PB90-208455, A04, MF-A01).

NCEER-89-0037 "A Deterministic Assessment of Effects of Ground Motion Incoherence," by A.S. Veletsos and Y. Tang, 7/15/89, (PB90-164294, A03, MF-A01).

NCEER-89-0038 "Workshop on Ground Motion Parameters for Seismic Hazard Mapping," July 17-18, 1989, edited by R.V. Whitman, 12/1/89, (PB90-173923, A04, MF-A01).

NCEER-89-0039 "Seismic Effects on Elevated Transit Lines of the New York City Transit Authority," by C.J. Costantino, C.A. Miller and E. Heymsfield, 12/26/89, (PB90-207887, A06, MF-A01).

NCEER-89-0040 "Centrifugal Modeling of Dynamic Soil-Structure Interaction," by K. Weissman, Supervised by J.H. Prevost, 5/10/89, (PB90-207879, A07, MF-A01).

NCEER-89-0041 "Linearized Identification of Buildings With Cores for Seismic Vulnerability Assessment," by I-K. Ho and A.E. Aktan, 11/1/89, (PB90-251943, A07, MF-A01).

NCEER-90-0001 "Geotechnical and Lifeline Aspects of the October 17, 1989 Loma Prieta Earthquake in San Francisco," by T.D. O'Rourke, H.E. Stewart, F.T. Blackburn and T.S. Dickerman, 1/90, (PB90-208596, A05, MF-A01).

NCEER-90-0002 "Nonnormal Secondary Response Due to Yielding in a Primary Structure," by D.C.K. Chen and L.D. Lutes, 2/28/90, (PB90-251976, A07, MF-A01).

NCEER-90-0003 "Earthquake Education Materials for Grades K-12," by K.E.K. Ross, 4/16/90, (PB91-251984, A05, MF-A05). This report has been replaced by NCEER-92-0018.

NCEER-90-0004 "Catalog of Strong Motion Stations in Eastern North America," by R.W. Busby, 4/3/90, (PB90-251984, A05, MF-A01).

NCEER-90-0005 "NCEER Strong-Motion Data Base: A User Manual for the GeoBase Release (Version 1.0 for the Sun3)," by P. Friberg and K. Jacob, 3/31/90 (PB90-258062, A04, MF-A01).

NCEER-90-0006 "Seismic Hazard Along a Crude Oil Pipeline in the Event of an 1811-1812 Type New Madrid Earthquake," by H.H.M. Hwang and C-H.S. Chen, 4/16/90, (PB90-258054, A04, MF-A01).

NCEER-90-0007 "Site-Specific Response Spectra for Memphis Sheahan Pumping Station," by H.H.M. Hwang and C.S. Lee, 5/15/90, (PB91-108811, A05, MF-A01).

NCEER-90-0008 "Pilot Study on Seismic Vulnerability of Crude Oil Transmission Systems," by T. Ariman, R. Dobry, M. Grigoriu, F. Kozin, M. O'Rourke, T. O'Rourke and M. Shinozuka, 5/25/90, (PB91-108837, A06, MF-A01).

NCEER-90-0009 "A Program to Generate Site Dependent Time Histories: EQGEN," by G.W. Ellis, M. Srinivasan and A.S. Cakmak, 1/30/90, (PB91-108829, A04, MF-A01).

NCEER-90-0010 "Active Isolation for Seismic Protection of Operating Rooms," by M.E. Talbott, Supervised by M. Shinozuka, 6/8/9, (PB91-110205, A05, MF-A01).

NCEER-90-0011 "Program LINEARID for Identification of Linear Structural Dynamic Systems," by C-B. Yun and M. Shinozuka, 6/25/90, (PB91-110312, A08, MF-A01).

NCEER-90-0012 "Two-Dimensional Two-Phase Elasto-Plastic Seismic Response of Earth Dams," by A.N. Yiagos, Supervised by J.H. Prevost, 6/20/90, (PB91-110197, A13, MF-A02).

NCEER-90-0013 "Secondary Systems in Base-Isolated Structures: Experimental Investigation, Stochastic Response and Stochastic Sensitivity," by G.D. Manolis, G. Juhn, M.C. Constantinou and A.M. Reinhorn, 7/1/90, (PB91-110320, A08, MF-A01).

NCEER-90-0014 "Seismic Behavior of Lightly-Reinforced Concrete Column and Beam-Column Joint Details," by S.P. Pessiki, C.H. Conley, P. Gergely and R.N. White, 8/22/90, (PB91-108795, A11, MF-A02).

NCEER-90-0015 "Two Hybrid Control Systems for Building Structures Under Strong Earthquakes," by J.N. Yang and A. Danielians, 6/29/90, (PB91-125393, A04, MF-A01).

NCEER-90-0016 "Instantaneous Optimal Control with Acceleration and Velocity Feedback," by J.N. Yang and Z. Li, 6/29/90, (PB91-125401, A03, MF-A01).

NCEER-90-0017 "Reconnaissance Report on the Northern Iran Earthquake of June 21, 1990," by M. Mehrain, 10/4/90, (PB91-125377, A03, MF-A01).

NCEER-90-0018 "Evaluation of Liquefaction Potential in Memphis and Shelby County," by T.S. Chang, P.S. Tang, C.S. Lee and H. Hwang, 8/10/90, (PB91-125427, A09, MF-A01).

NCEER-90-0019 "Experimental and Analytical Study of a Combined Sliding Disc Bearing and Helical Steel Spring Isolation System," by M.C. Constantinou, A.S. Mokha and A.M. Reinhorn, 10/4/90, (PB91-125385, A06, MF-A01). This report is available only through NTIS (see address given above).

NCEER-90-0020 "Experimental Study and Analytical Prediction of Earthquake Response of a Sliding Isolation System with a Spherical Surface," by A.S. Mokha, M.C. Constantinou and A.M. Reinhorn, 10/11/90, (PB91-125419, A05, MF-A01).

NCEER-90-0021 "Dynamic Interaction Factors for Floating Pile Groups," by G. Gazetas, K. Fan, A. Kaynia and E. Kausel, 9/10/90, (PB91-170381, A05, MF-A01).

NCEER-90-0022 "Evaluation of Seismic Damage Indices for Reinforced Concrete Structures," by S. Rodriguez-Gomez and A.S. Cakmak, 9/30/90, PB91-171322, A06, MF-A01).

NCEER-90-0023 "Study of Site Response at a Selected Memphis Site," by H. Desai, S. Ahmad, E.S. Gazetas and M.R. Oh, 10/11/90, (PB91-196857, A03, MF-A01).

NCEER-90-0024 "A User's Guide to Strongmo: Version 1.0 of NCEER's Strong-Motion Data Access Tool for PCs and Terminals," by P.A. Friberg and C.A.T. Susch, 11/15/90, (PB91-171272, A03, MF-A01).

NCEER-90-0025 "A Three-Dimensional Analytical Study of Spatial Variability of Seismic Ground Motions," by L-L. Hong and A.H.-S. Ang, 10/30/90, (PB91-170399, A09, MF-A01).

NCEER-90-0026 "MUMOID User's Guide - A Program for the Identification of Modal Parameters," by S. Rodriguez-Gomez and E. DiPasquale, 9/30/90, (PB91-171298, A04, MF-A01).

NCEER-90-0027 "SARCF-II User's Guide - Seismic Analysis of Reinforced Concrete Frames," by S. Rodriguez-Gomez, Y.S. Chung and C. Meyer, 9/30/90, (PB91-171280, A05, MF-A01).

NCEER-90-0028 "Viscous Dampers: Testing, Modeling and Application in Vibration and Seismic Isolation," by N. Makris and M.C. Constantinou, 12/20/90 (PB91-190561, A06, MF-A01).

NCEER-90-0029 "Soil Effects on Earthquake Ground Motions in the Memphis Area," by H. Hwang, C.S. Lee, K.W. Ng and T.S. Chang, 8/2/90, (PB91-190751, A05, MF-A01).

NCEER-91-0001 "Proceedings from the Third Japan-U.S. Workshop on Earthquake Resistant Design of Lifeline Facilities and Countermeasures for Soil Liquefaction, December 17-19, 1990," edited by T.D. O'Rourke and M. Hamada, 2/1/91, (PB91-179259, A99, MF-A04).

NCEER-91-0002 "Physical Space Solutions of Non-Proportionally Damped Systems," by M. Tong, Z. Liang and G.C. Lee, 1/15/91, (PB91-179242, A04, MF-A01).

NCEER-91-0003 "Seismic Response of Single Piles and Pile Groups," by K. Fan and G. Gazetas, 1/10/91, (PB92-174994, A04, MF-A01).

NCEER-91-0004 "Damping of Structures: Part 1 - Theory of Complex Damping," by Z. Liang and G. Lee, 10/10/91, (PB92-197235, A12, MF-A03).

NCEER-91-0005 "3D-BASIS - Nonlinear Dynamic Analysis of Three Dimensional Base Isolated Structures: Part II," by S. Nagarajaiah, A.M. Reinhorn and M.C. Constantinou, 2/28/91, (PB91-190553, A07, MF-A01). This report has been replaced by NCEER-93-0011.

NCEER-91-0006 "A Multidimensional Hysteretic Model for Plasticity Deforming Metals in Energy Absorbing Devices," by E.J. Graesser and F.A. Cozzarelli, 4/9/91, (PB92-108364, A04, MF-A01).

NCEER-91-0007 "A Framework for Customizable Knowledge-Based Expert Systems with an Application to a KBES for Evaluating the Seismic Resistance of Existing Buildings," by E.G. Ibarra-Anaya and S.J. Fenves, 4/9/91, (PB91-210930, A08, MF-A01).

NCEER-91-0008 "Nonlinear Analysis of Steel Frames with Semi-Rigid Connections Using the Capacity Spectrum Method," by G.G. Deierlein, S-H. Hsieh, Y-J. Shen and J.F. Abel, 7/2/91, (PB92-113828, A05, MF-A01).

NCEER-91-0009 "Earthquake Education Materials for Grades K-12," by K.E.K. Ross, 4/30/91, (PB91-212142, A06, MF-A01). This report has been replaced by NCEER-92-0018.

NCEER-91-0010 "Phase Wave Velocities and Displacement Phase Differences in a Harmonically Oscillating Pile," by N. Makris and G. Gazetas, 7/8/91, (PB92-108356, A04, MF-A01).

NCEER-91-0011 "Dynamic Characteristics of a Full-Size Five-Story Steel Structure and a 2/5 Scale Model," by K.C. Chang, G.C. Yao, G.C. Lee, D.S. Hao and Y.C. Yeh," 7/2/91, (PB93-116648, A06, MF-A02).

NCEER-91-0012 "Seismic Response of a 2/5 Scale Steel Structure with Added Viscoelastic Dampers," by K.C. Chang, T.T. Soong, S-T. Oh and M.L. Lai, 5/17/91, (PB92-110816, A05, MF-A01).

NCEER-91-0013 "Earthquake Response of Retaining Walls; Full-Scale Testing and Computational Modeling," by S. Alampalli and A-W.M. Elgamal, 6/20/91, to be published.

NCEER-91-0014 "3D-BASIS-M: Nonlinear Dynamic Analysis of Multiple Building Base Isolated Structures," by P.C. Tsopelas, S. Nagarajaiah, M.C. Constantinou and A.M. Reinhorn, 5/28/91, (PB92-113885, A09, MF-A02).

NCEER-91-0015 "Evaluation of SEAOC Design Requirements for Sliding Isolated Structures," by D. Theodossiou and M.C. Constantinou, 6/10/91, (PB92-114602, A11, MF-A03).

NCEER-91-0016 "Closed-Loop Modal Testing of a 27-Story Reinforced Concrete Flat Plate-Core Building," by H.R. Somaprasad, T. Toksoy, H. Yoshiyuki and A.E. Aktan, 7/15/91, (PB92-129980, A07, MF-A02).

NCEER-91-0017 "Shake Table Test of a 1/6 Scale Two-Story Lightly Reinforced Concrete Building," by A.G. El-Attar, R.N. White and P. Gergely, 2/28/91, (PB92-222447, A06, MF-A02).

NCEER-91-0018 "Shake Table Test of a 1/8 Scale Three-Story Lightly Reinforced Concrete Building," by A.G. El-Attar, R.N. White and P. Gergely, 2/28/91, (PB93-116630, A08, MF-A02).

NCEER-91-0019 "Transfer Functions for Rigid Rectangular Foundations," by A.S. Veletsos, A.M. Prasad and W.H. Wu, 7/31/91, to be published.

NCEER-91-0020 "Hybrid Control of Seismic-Excited Nonlinear and Inelastic Structural Systems," by J.N. Yang, Z. Li and A. Danielians, 8/1/91, (PB92-143171, A06, MF-A02).

NCEER-91-0021 "The NCEER-91 Earthquake Catalog: Improved Intensity-Based Magnitudes and Recurrence Relations for U.S. Earthquakes East of New Madrid," by L. Seeber and J.G. Armbruster, 8/28/91, (PB92-176742, A06, MF-A02).

NCEER-91-0022 "Proceedings from the Implementation of Earthquake Planning and Education in Schools: The Need for Change - The Roles of the Changemakers," by K.E.K. Ross and F. Winslow, 7/23/91, (PB92-129998, A12, MF-A03).

NCEER-91-0023 "A Study of Reliability-Based Criteria for Seismic Design of Reinforced Concrete Frame Buildings," by H.H.M. Hwang and H-M. Hsu, 8/10/91, (PB92-140235, A09, MF-A02).

NCEER-91-0024 "Experimental Verification of a Number of Structural System Identification Algorithms," by R.G. Ghanem, H. Gavin and M. Shinozuka, 9/18/91, (PB92-176577, A18, MF-A04).

NCEER-91-0025 "Probabilistic Evaluation of Liquefaction Potential," by H.H.M. Hwang and C.S. Lee," 11/25/91, (PB92-143429, A05, MF-A01).

NCEER-91-0026 "Instantaneous Optimal Control for Linear, Nonlinear and Hysteretic Structures - Stable Controllers," by J.N. Yang and Z. Li, 11/15/91, (PB92-163807, A04, MF-A01).

NCEER-91-0027 "Experimental and Theoretical Study of a Sliding Isolation System for Bridges," by M.C. Constantinou, A. Kartoum, A.M. Reinhorn and P. Bradford, 11/15/91, (PB92-176973, A10, MF-A03).

NCEER-92-0001 "Case Studies of Liquefaction and Lifeline Performance During Past Earthquakes, Volume 1: Japanese Case Studies," Edited by M. Hamada and T. O'Rourke, 2/17/92, (PB92-197243, A18, MF-A04).

NCEER-92-0002 "Case Studies of Liquefaction and Lifeline Performance During Past Earthquakes, Volume 2: United States Case Studies," Edited by T. O'Rourke and M. Hamada, 2/17/92, (PB92-197250, A20, MF-A04).

NCEER-92-0003 "Issues in Earthquake Education," Edited by K. Ross, 2/3/92, (PB92-222389, A07, MF-A02).

NCEER-92-0004 "Proceedings from the First U.S. - Japan Workshop on Earthquake Protective Systems for Bridges," Edited by I.G. Buckle, 2/4/92, (PB94-142239, A99, MF-A06).

NCEER-92-0005 "Seismic Ground Motion from a Haskell-Type Source in a Multiple-Layered Half-Space," A.P. Theoharis, G. Deodatis and M. Shinozuka, 1/2/92, to be published.

NCEER-92-0006 "Proceedings from the Site Effects Workshop," Edited by R. Whitman, 2/29/92, (PB92-197201, A04, MF-A01).

NCEER-92-0007 "Engineering Evaluation of Permanent Ground Deformations Due to Seismically-Induced Liquefaction," by M.H. Baziar, R. Dobry and A-W.M. Elgamal, 3/24/92, (PB92-222421, A13, MF-A03).

NCEER-92-0008 "A Procedure for the Seismic Evaluation of Buildings in the Central and Eastern United States," by C.D. Poland and J.O. Malley, 4/2/92, (PB92-222439, A20, MF-A04).

NCEER-92-0009 "Experimental and Analytical Study of a Hybrid Isolation System Using Friction Controllable Sliding Bearings," by M.Q. Feng, S. Fujii and M. Shinozuka, 5/15/92, (PB93-150282, A06, MF-A02).

NCEER-92-0010 "Seismic Resistance of Slab-Column Connections in Existing Non-Ductile Flat-Plate Buildings," by A.J. Durrani and Y. Du, 5/18/92, (PB93-116812, A06, MF-A02).

NCEER-92-0011 "The Hysteretic and Dynamic Behavior of Brick Masonry Walls Upgraded by Ferrocement Coatings Under Cyclic Loading and Strong Simulated Ground Motion," by H. Lee and S.P. Prawel, 5/11/92, to be published.

NCEER-92-0012 "Study of Wire Rope Systems for Seismic Protection of Equipment in Buildings," by G.F. Demetriades, M.C. Constantinou and A.M. Reinhorn, 5/20/92, (PB93-116655, A08, MF-A02).

NCEER-92-0013 "Shape Memory Structural Dampers: Material Properties, Design and Seismic Testing," by P.R. Witting and F.A. Cozzarelli, 5/26/92, (PB93-116663, A05, MF-A01).

NCEER-92-0014 "Longitudinal Permanent Ground Deformation Effects on Buried Continuous Pipelines," by M.J. O'Rourke, and C. Nordberg, 6/15/92, (PB93-116671, A08, MF-A02).

NCEER-92-0015 "A Simulation Method for Stationary Gaussian Random Functions Based on the Sampling Theorem," by M. Grigoriu and S. Balopoulou, 6/11/92, (PB93-127496, A05, MF-A01).

NCEER-92-0016 "Gravity-Load-Designed Reinforced Concrete Buildings: Seismic Evaluation of Existing Construction and Detailing Strategies for Improved Seismic Resistance," by G.W. Hoffmann, S.K. Kunnath, A.M. Reinhorn and J.B. Mander, 7/15/92, (PB94-142007, A08, MF-A02).

NCEER-92-0017 "Observations on Water System and Pipeline Performance in the Limón Area of Costa Rica Due to the April 22, 1991 Earthquake," by M. O'Rourke and D. Ballantyne, 6/30/92, (PB93-126811, A06, MF-A02).

NCEER-92-0018 "Fourth Edition of Earthquake Education Materials for Grades K-12," Edited by K.E.K. Ross, 8/10/92, (PB93-114023, A07, MF-A02).

NCEER-92-0019 "Proceedings from the Fourth Japan-U.S. Workshop on Earthquake Resistant Design of Lifeline Facilities and Countermeasures for Soil Liquefaction," Edited by M. Hamada and T.D. O'Rourke, 8/12/92, (PB93-163939, A99, MF-E11).

NCEER-92-0020 "Active Bracing System: A Full Scale Implementation of Active Control," by A.M. Reinhorn, T.T. Soong, R.C. Lin, M.A. Riley, Y.P. Wang, S. Aizawa and M. Higashino, 8/14/92, (PB93-127512, A06, MF-A02).

NCEER-92-0021 "Empirical Analysis of Horizontal Ground Displacement Generated by Liquefaction-Induced Lateral Spreads," by S.F. Bartlett and T.L. Youd, 8/17/92, (PB93-188241, A06, MF-A02).

NCEER-92-0022 "IDARC Version 3.0: Inelastic Damage Analysis of Reinforced Concrete Structures," by S.K. Kunnath, A.M. Reinhorn and R.F. Lobo, 8/31/92, (PB93-227502, A07, MF-A02).

NCEER-92-0023 "A Semi-Empirical Analysis of Strong-Motion Peaks in Terms of Seismic Source, Propagation Path and Local Site Conditions, by M. Kamiyama, M.J. O'Rourke and R. Flores-Berrones, 9/9/92, (PB93-150266, A08, MF-A02).

NCEER-92-0024 "Seismic Behavior of Reinforced Concrete Frame Structures with Nonductile Details, Part I: Summary of Experimental Findings of Full Scale Beam-Column Joint Tests," by A. Beres, R.N. White and P. Gergely, 9/30/92, (PB93-227783, A05, MF-A01).

NCEER-92-0025 "Experimental Results of Repaired and Retrofitted Beam-Column Joint Tests in Lightly Reinforced Concrete Frame Buildings," by A. Beres, S. El-Borgi, R.N. White and P. Gergely, 10/29/92, (PB93-227791, A05, MF-A01).

NCEER-92-0026 "A Generalization of Optimal Control Theory: Linear and Nonlinear Structures," by J.N. Yang, Z. Li and S. Vongchavalitkul, 11/2/92, (PB93-188621, A05, MF-A01).

NCEER-92-0027 "Seismic Resistance of Reinforced Concrete Frame Structures Designed Only for Gravity Loads: Part I - Design and Properties of a One-Third Scale Model Structure," by J.M. Bracci, A.M. Reinhorn and J.B. Mander, 12/1/92, (PB94-104502, A08, MF-A02).

NCEER-92-0028 "Seismic Resistance of Reinforced Concrete Frame Structures Designed Only for Gravity Loads: Part II - Experimental Performance of Subassemblages," by L.E. Aycardi, J.B. Mander and A.M. Reinhorn, 12/1/92, (PB94-104510, A08, MF-A02).

NCEER-92-0029 "Seismic Resistance of Reinforced Concrete Frame Structures Designed Only for Gravity Loads: Part III - Experimental Performance and Analytical Study of a Structural Model," by J.M. Bracci, A.M. Reinhorn and J.B. Mander, 12/1/92, (PB93-227528, A09, MF-A01).

NCEER-92-0030 "Evaluation of Seismic Retrofit of Reinforced Concrete Frame Structures: Part I - Experimental Performance of Retrofitted Subassemblages," by D. Choudhuri, J.B. Mander and A.M. Reinhorn, 12/8/92, (PB93-198307, A07, MF-A02).

NCEER-92-0031 "Evaluation of Seismic Retrofit of Reinforced Concrete Frame Structures: Part II - Experimental Performance and Analytical Study of a Retrofitted Structural Model," by J.M. Bracci, A.M. Reinhorn and J.B. Mander, 12/8/92, (PB93-198315, A09, MF-A03).

NCEER-92-0032 "Experimental and Analytical Investigation of Seismic Response of Structures with Supplemental Fluid Viscous Dampers," by M.C. Constantinou and M.D. Symans, 12/21/92, (PB93-191435, A10, MF-A03). This report is available only through NTIS (see address given above).

NCEER-92-0033 "Reconnaissance Report on the Cairo, Egypt Earthquake of October 12, 1992," by M. Khater, 12/23/92, (PB93-188621, A03, MF-A01).

NCEER-92-0034 "Low-Level Dynamic Characteristics of Four Tall Flat-Plate Buildings in New York City," by H. Gavin, S. Yuan, J. Grossman, E. Pekelis and K. Jacob, 12/28/92, (PB93-188217, A07, MF-A02).

NCEER-93-0001 "An Experimental Study on the Seismic Performance of Brick-Infilled Steel Frames With and Without Retrofit," by J.B. Mander, B. Nair, K. Wojtkowski and J. Ma, 1/29/93, (PB93-227510, A07, MF-A02).

NCEER-93-0002 "Social Accounting for Disaster Preparedness and Recovery Planning," by S. Cole, E. Pantoja and V. Razak, 2/22/93, (PB94-142114, A12, MF-A03).

NCEER-93-0003 "Assessment of 1991 NEHRP Provisions for Nonstructural Components and Recommended Revisions," by T.T. Soong, G. Chen, Z. Wu, R-H. Zhang and M. Grigoriu, 3/1/93, (PB93-188639, A06, MF-A02).

NCEER-93-0004 "Evaluation of Static and Response Spectrum Analysis Procedures of SEAOC/UBC for Seismic Isolated Structures," by C.W. Winters and M.C. Constantinou, 3/23/93, (PB93-198299, A10, MF-A03).

NCEER-93-0005 "Earthquakes in the Northeast - Are We Ignoring the Hazard? A Workshop on Earthquake Science and Safety for Educators," edited by K.E.K. Ross, 4/2/93, (PB94-103066, A09, MF-A02).

NCEER-93-0006 "Inelastic Response of Reinforced Concrete Structures with Viscoelastic Braces," by R.F. Lobo, J.M. Bracci, K.L. Shen, A.M. Reinhorn and T.T. Soong, 4/5/93, (PB93-227486, A05, MF-A02).

NCEER-93-0007 "Seismic Testing of Installation Methods for Computers and Data Processing Equipment," by K. Kosar, T.T. Soong, K.L. Shen, J.A. HoLung and Y.K. Lin, 4/12/93, (PB93-198299, A07, MF-A02).

NCEER-93-0008 "Retrofit of Reinforced Concrete Frames Using Added Dampers," by A. Reinhorn, M. Constantinou and C. Li, to be published.

NCEER-93-0009 "Seismic Behavior and Design Guidelines for Steel Frame Structures with Added Viscoelastic Dampers," by K.C. Chang, M.L. Lai, T.T. Soong, D.S. Hao and Y.C. Yeh, 5/1/93, (PB94-141959, A07, MF-A02).

NCEER-93-0010 "Seismic Performance of Shear-Critical Reinforced Concrete Bridge Piers," by J.B. Mander, S.M. Waheed, M.T.A. Chaudhary and S.S. Chen, 5/12/93, (PB93-227494, A08, MF-A02).

NCEER-93-0011 "3D-BASIS-TABS: Computer Program for Nonlinear Dynamic Analysis of Three Dimensional Base Isolated Structures," by S. Nagarajaiah, C. Li, A.M. Reinhorn and M.C. Constantinou, 8/2/93, (PB94-141819, A09, MF-A02).

NCEER-93-0012 "Effects of Hydrocarbon Spills from an Oil Pipeline Break on Ground Water," by O.J. Helweg and H.H.M. Hwang, 8/3/93, (PB94-141942, A06, MF-A02).

NCEER-93-0013 "Simplified Procedures for Seismic Design of Nonstructural Components and Assessment of Current Code Provisions," by M.P. Singh, L.E. Suarez, E.E. Matheu and G.O. Maldonado, 8/4/93, (PB94-141827, A09, MF-A02).

NCEER-93-0014 "An Energy Approach to Seismic Analysis and Design of Secondary Systems," by G. Chen and T.T. Soong, 8/6/93, (PB94-142767, A11, MF-A03).

NCEER-93-0015 "Proceedings from School Sites: Becoming Prepared for Earthquakes - Commemorating the Third Anniversary of the Loma Prieta Earthquake," Edited by F.E. Winslow and K.E.K. Ross, 8/16/93, (PB94-154275, A16, MF-A02).

NCEER-93-0016 "Reconnaissance Report of Damage to Historic Monuments in Cairo, Egypt Following the October 12, 1992 Dahshur Earthquake," by D. Sykora, D. Look, G. Croci, E. Karaesmen and E. Karaesmen, 8/19/93, (PB94-142221, A08, MF-A02).

NCEER-93-0017 "The Island of Guam Earthquake of August 8, 1993," by S.W. Swan and S.K. Harris, 9/30/93, (PB94-141843, A04, MF-A01).

NCEER-93-0018 "Engineering Aspects of the October 12, 1992 Egyptian Earthquake," by A.W. Elgamal, M. Amer, K. Adalier and A. Abul-Fadl, 10/7/93, (PB94-141983, A05, MF-A01).

NCEER-93-0019 "Development of an Earthquake Motion Simulator and its Application in Dynamic Centrifuge Testing," by I. Krstelj, Supervised by J.H. Prevost, 10/23/93, (PB94-181773, A-10, MF-A03).

NCEER-93-0020 "NCEER-Taisei Corporation Research Program on Sliding Seismic Isolation Systems for Bridges: Experimental and Analytical Study of a Friction Pendulum System (FPS)," by M.C. Constantinou, P. Tsopelas, Y-S. Kim and S. Okamoto, 11/1/93, (PB94-142775, A08, MF-A02).

NCEER-93-0021 "Finite Element Modeling of Elastomeric Seismic Isolation Bearings," by L.J. Billings, Supervised by R. Shepherd, 11/8/93, to be published.

NCEER-93-0022 "Seismic Vulnerability of Equipment in Critical Facilities: Life-Safety and Operational Consequences," by K. Porter, G.S. Johnson, M.M. Zadeh, C. Scawthorn and S. Eder, 11/24/93, (PB94-181765, A16, MF-A03).

NCEER-93-0023 "Hokkaido Nansei-oki, Japan Earthquake of July 12, 1993, by P.I. Yanev and C.R. Scawthorn, 12/23/93, (PB94-181500, A07, MF-A01).

NCEER-94-0001 "An Evaluation of Seismic Serviceability of Water Supply Networks with Application to the San Francisco Auxiliary Water Supply System," by I. Markov, Supervised by M. Grigoriu and T. O'Rourke, 1/21/94, (PB94-204013, A07, MF-A02).

NCEER-94-0002 "NCEER-Taisei Corporation Research Program on Sliding Seismic Isolation Systems for Bridges: Experimental and Analytical Study of Systems Consisting of Sliding Bearings, Rubber Restoring Force Devices and Fluid Dampers," Volumes I and II, by P. Tsopelas, S. Okamoto, M.C. Constantinou, D. Ozaki and S. Fujii, 2/4/94, (PB94-181740, A09, MF-A02 and PB94-181757, A12, MF-A03).

NCEER-94-0003 "A Markov Model for Local and Global Damage Indices in Seismic Analysis," by S. Rahman and M. Grigoriu, 2/18/94, (PB94-206000, A12, MF-A03).

NCEER-94-0004 "Proceedings from the NCEER Workshop on Seismic Response of Masonry Infills," edited by D.P. Abrams, 3/1/94, (PB94-180783, A07, MF-A02).

NCEER-94-0005 "The Northridge, California Earthquake of January 17, 1994: General Reconnaissance Report," edited by J.D. Goltz, 3/11/94, (PB94-193943, A10, MF-A03).

NCEER-94-0006 "Seismic Energy Based Fatigue Damage Analysis of Bridge Columns: Part I - Evaluation of Seismic Capacity," by G.A. Chang and J.B. Mander, 3/14/94, (PB94-219185, A11, MF-A03).

NCEER-94-0007 "Seismic Isolation of Multi-Story Frame Structures Using Spherical Sliding Isolation Systems," by T.M. Al-Hussaini, V.A. Zayas and M.C. Constantinou, 3/17/94, (PB94-193745, A09, MF-A02).

NCEER-94-0008 "The Northridge, California Earthquake of January 17, 1994: Performance of Highway Bridges," edited by I.G. Buckle, 3/24/94, (PB94-193851, A06, MF-A02).

NCEER-94-0009 "Proceedings of the Third U.S.-Japan Workshop on Earthquake Protective Systems for Bridges," edited by I.G. Buckle and I. Friedland, 3/31/94, (PB94-195815, A99, MF-A06).

NCEER-94-0010 "3D-BASIS-ME: Computer Program for Nonlinear Dynamic Analysis of Seismically Isolated Single and Multiple Structures and Liquid Storage Tanks," by P.C. Tsopelas, M.C. Constantinou and A.M. Reinhorn, 4/12/94, (PB94-204922, A09, MF-A02).

NCEER-94-0011 "The Northridge, California Earthquake of January 17, 1994: Performance of Gas Transmission Pipelines," by T.D. O'Rourke and M.C. Palmer, 5/16/94, (PB94-204989, A05, MF-A01).

NCEER-94-0012 "Feasibility Study of Replacement Procedures and Earthquake Performance Related to Gas Transmission Pipelines," by T.D. O'Rourke and M.C. Palmer, 5/25/94, (PB94-206638, A09, MF-A02).

NCEER-94-0013 "Seismic Energy Based Fatigue Damage Analysis of Bridge Columns: Part II - Evaluation of Seismic Demand," by G.A. Chang and J.B. Mander, 6/1/94, (PB95-18106, A08, MF-A02).

NCEER-94-0014 "NCEER-Taisei Corporation Research Program on Sliding Seismic Isolation Systems for Bridges: Experimental and Analytical Study of a System Consisting of Sliding Bearings and Fluid Restoring Force/Damping Devices," by P. Tsopelas and M.C. Constantinou, 6/13/94, (PB94-219144, A10, MF-A03).

NCEER-94-0015 "Generation of Hazard-Consistent Fragility Curves for Seismic Loss Estimation Studies," by H. Hwang and J-R. Huo, 6/14/94, (PB95-181996, A09, MF-A02).

NCEER-94-0016 "Seismic Study of Building Frames with Added Energy-Absorbing Devices," by W.S. Pong, C.S. Tsai and G.C. Lee, 6/20/94, (PB94-219136, A10, A03).

NCEER-94-0017 "Sliding Mode Control for Seismic-Excited Linear and Nonlinear Civil Engineering Structures," by J. Yang, J. Wu, A. Agrawal and Z. Li, 6/21/94, (PB95-138483, A06, MF-A02).

NCEER-94-0018 "3D-BASIS-TABS Version 2.0: Computer Program for Nonlinear Dynamic Analysis of Three Dimensional Base Isolated Structures," by A.M. Reinhorn, S. Nagarajaiah, M.C. Constantinou, P. Tsopelas and R. Li, 6/22/94, (PB95-182176, A08, MF-A02).

NCEER-94-0019 "Proceedings of the International Workshop on Civil Infrastructure Systems: Application of Intelligent Systems and Advanced Materials on Bridge Systems," Edited by G.C. Lee and K.C. Chang, 7/18/94, (PB95-252474, A20, MF-A04).

NCEER-94-0020 "Study of Seismic Isolation Systems for Computer Floors," by V. Lambrou and M.C. Constantinou, 7/19/94, (PB95-138533, A10, MF-A03).

NCEER-94-0021 "Proceedings of the U.S.-Italian Workshop on Guidelines for Seismic Evaluation and Rehabilitation of Unreinforced Masonry Buildings," Edited by D.P. Abrams and G.M. Calvi, 7/20/94, (PB95-138749, A13, MF-A03).

NCEER-94-0022 "NCEER-Taisei Corporation Research Program on Sliding Seismic Isolation Systems for Bridges: Experimental and Analytical Study of a System Consisting of Lubricated PTFE Sliding Bearings and Mild Steel Dampers," by P. Tsopelas and M.C. Constantinou, 7/22/94, (PB95-182184, A08, MF-A02).

NCEER-94-0023 “Development of Reliability-Based Design Criteria for Buildings Under Seismic Load,” by Y.K. Wen, H. Hwang and M. Shinozuka, 8/1/94, (PB95-211934, A08, MF-A02).

NCEER-94-0024 “Experimental Verification of Acceleration Feedback Control Strategies for an Active Tendon System,” by S.J. Dyke, B.F. Spencer, Jr., P. Quast, M.K. Sain, D.C. Kaspari, Jr. and T.T. Soong, 8/29/94, (PB95-212320, A05, MF-A01).

NCEER-94-0025 “Seismic Retrofitting Manual for Highway Bridges,” Edited by I.G. Buckle and I.F. Friedland, published by the Federal Highway Administration (PB95-212676, A15, MF-A03).

NCEER-94-0026 “Proceedings from the Fifth U.S.-Japan Workshop on Earthquake Resistant Design of Lifeline Facilities and Countermeasures Against Soil Liquefaction,” Edited by T.D. O’Rourke and M. Hamada, 11/7/94, (PB95-220802, A99, MF-E08).

NCEER-95-0001 "Experimental and Analytical Investigation of Seismic Retrofit of Structures with Supplemental Damping: Part 1 - Fluid Viscous Damping Devices," by A.M. Reinhorn, C. Li and M.C. Constantinou, 1/3/95, (PB95-266599, A09, MF-A02).

NCEER-95-0002 "Experimental and Analytical Study of Low-Cycle Fatigue Behavior of Semi-Rigid Top-And-Seat Angle Connections," by G. Pekcan, J.B. Mander and S.S. Chen, 1/5/95, (PB95-220042, A07, MF-A02).

NCEER-95-0003 "NCEER-ATC Joint Study on Fragility of Buildings," by T. Anagnos, C. Rojahn and A.S. Kiremidjian, 1/20/95, (PB95-220026, A06, MF-A02).

NCEER-95-0004 "Nonlinear Control Algorithms for Peak Response Reduction," by Z. Wu, T.T. Soong, V. Gattulli and R.C. Lin, 2/16/95, (PB95-220349, A05, MF-A01).

NCEER-95-0005 "Pipeline Replacement Feasibility Study: A Methodology for Minimizing Seismic and Corrosion Risks to Underground Natural Gas Pipelines," by R.T. Eguchi, H.A. Seligson and D.G. Honegger, 3/2/95, (PB95-252326, A06, MF-A02).

NCEER-95-0006 "Evaluation of Seismic Performance of an 11-Story Frame Building During the 1994 Northridge Earthquake," by F. Naeim, R. DiSulio, K. Benuska, A. Reinhorn and C. Li, to be published.

NCEER-95-0007 "Prioritization of Bridges for Seismic Retrofitting," by N. Basöz and A.S. Kiremidjian, 4/24/95, (PB95-252300, A08, MF-A02).

NCEER-95-0008 "Method for Developing Motion Damage Relationships for Reinforced Concrete Frames," by A. Singhal and A.S. Kiremidjian, 5/11/95, (PB95-266607, A06, MF-A02).

NCEER-95-0009 "Experimental and Analytical Investigation of Seismic Retrofit of Structures with Supplemental Damping: Part II - Friction Devices," by C. Li and A.M. Reinhorn, 7/6/95, (PB96-128087, A11, MF-A03).

NCEER-95-0010 "Experimental Performance and Analytical Study of a Non-Ductile Reinforced Concrete Frame Structure Retrofitted with Elastomeric Spring Dampers," by G. Pekcan, J.B. Mander and S.S. Chen, 7/14/95, (PB96-137161, A08, MF-A02).

NCEER-95-0011 "Development and Experimental Study of Semi-Active Fluid Damping Devices for Seismic Protection of Structures," by M.D. Symans and M.C. Constantinou, 8/3/95, (PB96-136940, A23, MF-A04).

NCEER-95-0012 "Real-Time Structural Parameter Modification (RSPM): Development of Innervated Structures," by Z. Liang, M. Tong and G.C. Lee, 4/11/95, (PB96-137153, A06, MF-A01).

NCEER-95-0013 "Experimental and Analytical Investigation of Seismic Retrofit of Structures with Supplemental Damping: Part III - Viscous Damping Walls," by A.M. Reinhorn and C. Li, 10/1/95, (PB96-176409, A11, MF-A03).

NCEER-95-0014 "Seismic Fragility Analysis of Equipment and Structures in a Memphis Electric Substation," by J-R. Huo and H.H.M. Hwang, 8/10/95, (PB96-128087, A09, MF-A02).

NCEER-95-0015 "The Hanshin-Awaji Earthquake of January 17, 1995: Performance of Lifelines," Edited by M. Shinozuka, 11/3/95, (PB96-176383, A15, MF-A03).

NCEER-95-0016 "Highway Culvert Performance During Earthquakes," by T.L. Youd and C.J. Beckman, available as NCEER-96-0015.

NCEER-95-0017 "The Hanshin-Awaji Earthquake of January 17, 1995: Performance of Highway Bridges," Edited by I.G. Buckle, 12/1/95, to be published.

NCEER-95-0018 "Modeling of Masonry Infill Panels for Structural Analysis," by A.M. Reinhorn, A. Madan, R.E. Valles, Y. Reichmann and J.B. Mander, 12/8/95, (PB97-110886, MF-A01, A06).

NCEER-95-0019 "Optimal Polynomial Control for Linear and Nonlinear Structures," by A.K. Agrawal and J.N. Yang, 12/11/95, (PB96-168737, A07, MF-A02).

NCEER-95-0020 "Retrofit of Non-Ductile Reinforced Concrete Frames Using Friction Dampers," by R.S. Rao, P. Gergely and R.N. White, 12/22/95, (PB97-133508, A10, MF-A02).

NCEER-95-0021 "Parametric Results for Seismic Response of Pile-Supported Bridge Bents," by G. Mylonakis, A. Nikolaou and G. Gazetas, 12/22/95, (PB97-100242, A12, MF-A03).

NCEER-95-0022 "Kinematic Bending Moments in Seismically Stressed Piles," by A. Nikolaou, G. Mylonakis and G. Gazetas, 12/23/95, (PB97-113914, MF-A03, A13).

NCEER-96-0001 "Dynamic Response of Unreinforced Masonry Buildings with Flexible Diaphragms," by A.C. Costley and D.P. Abrams," 10/10/96, (PB97-133573, MF-A03, A15).

NCEER-96-0002 "State of the Art Review: Foundations and Retaining Structures," by I. Po Lam, to be published.

NCEER-96-0003 "Ductility of Rectangular Reinforced Concrete Bridge Columns with Moderate Confinement," by N. Wehbe, M. Saiidi, D. Sanders and B. Douglas, 11/7/96, (PB97-133557, A06, MF-A02).

NCEER-96-0004 "Proceedings of the Long-Span Bridge Seismic Research Workshop," edited by I.G. Buckle and I.M. Friedland, to be published.

NCEER-96-0005 "Establish Representative Pier Types for Comprehensive Study: Eastern United States," by J. Kulicki and Z. Prucz, 5/28/96, (PB98-119217, A07, MF-A02).

NCEER-96-0006 "Establish Representative Pier Types for Comprehensive Study: Western United States," by R. Imbsen, R.A. Schamber and T.A. Osterkamp, 5/28/96, (PB98-118607, A07, MF-A02).

NCEER-96-0007 "Nonlinear Control Techniques for Dynamical Systems with Uncertain Parameters," by R.G. Ghanem and M.I. Bujakov, 5/27/96, (PB97-100259, A17, MF-A03).

NCEER-96-0008 "Seismic Evaluation of a 30-Year Old Non-Ductile Highway Bridge Pier and Its Retrofit," by J.B. Mander, B. Mahmoodzadegan, S. Bhadra and S.S. Chen, 5/31/96, (PB97-110902, MF-A03, A10).

NCEER-96-0009 "Seismic Performance of a Model Reinforced Concrete Bridge Pier Before and After Retrofit," by J.B. Mander, J.H. Kim and C.A. Ligozio, 5/31/96, (PB97-110910, MF-A02, A10).

NCEER-96-0010 "IDARC2D Version 4.0: A Computer Program for the Inelastic Damage Analysis of Buildings," by R.E. Valles, A.M. Reinhorn, S.K. Kunnath, C. Li and A. Madan, 6/3/96, (PB97-100234, A17, MF-A03).

NCEER-96-0011 "Estimation of the Economic Impact of Multiple Lifeline Disruption: Memphis Light, Gas and Water Division Case Study," by S.E. Chang, H.A. Seligson and R.T. Eguchi, 8/16/96, (PB97-133490, A11, MF-A03).

NCEER-96-0012 "Proceedings from the Sixth Japan-U.S. Workshop on Earthquake Resistant Design of Lifeline Facilities and Countermeasures Against Soil Liquefaction, Edited by M. Hamada and T. O'Rourke, 9/11/96, (PB97-133581, A99, MF-A06).

NCEER-96-0013 "Chemical Hazards, Mitigation and Preparedness in Areas of High Seismic Risk: A Methodology for Estimating the Risk of Post-Earthquake Hazardous Materials Release," by H.A. Seligson, R.T. Eguchi, K.J. Tierney and K. Richmond, 11/7/96, (PB97-133565, MF-A02, A08).

NCEER-96-0014 "Response of Steel Bridge Bearings to Reversed Cyclic Loading," by J.B. Mander, D-K. Kim, S.S. Chen and G.J. Premus, 11/13/96, (PB97-140735, A12, MF-A03).

NCEER-96-0015 "Highway Culvert Performance During Past Earthquakes," by T.L. Youd and C.J. Beckman, 11/25/96, (PB97-133532, A06, MF-A01).

NCEER-97-0001 "Evaluation, Prevention and Mitigation of Pounding Effects in Building Structures," by R.E. Valles and A.M. Reinhorn, 2/20/97, (PB97-159552, A14, MF-A03).

NCEER-97-0002 "Seismic Design Criteria for Bridges and Other Highway Structures," by C. Rojahn, R. Mayes, D.G. Anderson, J. Clark, J.H. Hom, R.V. Nutt and M.J. O'Rourke, 4/30/97, (PB97-194658, A06, MF-A03).

NCEER-97-0003 “Proceedings of the U.S.-Italian Workshop on Seismic Evaluation and Retrofit,” Edited by D.P. Abrams and G.M. Calvi, 3/19/97, (PB97-194666, A13, MF-A03).

NCEER-97-0004 "Investigation of Seismic Response of Buildings with Linear and Nonlinear Fluid Viscous Dampers," by A.A. Seleemah and M.C. Constantinou, 5/21/97, (PB98-109002, A15, MF-A03).

NCEER-97-0005 "Proceedings of the Workshop on Earthquake Engineering Frontiers in Transportation Facilities," edited by G.C. Lee and I.M. Friedland, 8/29/97, (PB98-128911, A25, MR-A04).

NCEER-97-0006 "Cumulative Seismic Damage of Reinforced Concrete Bridge Piers," by S.K. Kunnath, A. El-Bahy, A. Taylor and W. Stone, 9/2/97, (PB98-108814, A11, MF-A03).

NCEER-97-0007 "Structural Details to Accommodate Seismic Movements of Highway Bridges and Retaining Walls," by R.A. Imbsen, R.A. Schamber, E. Thorkildsen, A. Kartoum, B.T. Martin, T.N. Rosser and J.M. Kulicki, 9/3/97, (PB98-108996, A09, MF-A02).

NCEER-97-0008 "A Method for Earthquake Motion-Damage Relationships with Application to Reinforced Concrete Frames," by A. Singhal and A.S. Kiremidjian, 9/10/97, (PB98-108988, A13, MF-A03).

NCEER-97-0009 "Seismic Analysis and Design of Bridge Abutments Considering Sliding and Rotation," by K. Fishman and R. Richards, Jr., 9/15/97, (PB98-108897, A06, MF-A02).

NCEER-97-0010 "Proceedings of the FHWA/NCEER Workshop on the National Representation of Seismic Ground Motion for New and Existing Highway Facilities," edited by I.M. Friedland, M.S. Power and R.L. Mayes, 9/22/97, (PB98-128903, A21, MF-A04).

NCEER-97-0011 "Seismic Analysis for Design or Retrofit of Gravity Bridge Abutments," by K.L. Fishman, R. Richards, Jr. and R.C. Divito, 10/2/97, (PB98-128937, A08, MF-A02).

NCEER-97-0012 "Evaluation of Simplified Methods of Analysis for Yielding Structures," by P. Tsopelas, M.C. Constantinou, C.A. Kircher and A.S. Whittaker, 10/31/97, (PB98-128929, A10, MF-A03).

NCEER-97-0013 "Seismic Design of Bridge Columns Based on Control and Repairability of Damage," by C-T. Cheng and J.B. Mander, 12/8/97, (PB98-144249, A11, MF-A03).

NCEER-97-0014 "Seismic Resistance of Bridge Piers Based on Damage Avoidance Design," by J.B. Mander and C-T. Cheng, 12/10/97, (PB98-144223, A09, MF-A02).

NCEER-97-0015 “Seismic Response of Nominally Symmetric Systems with Strength Uncertainty,” by S. Balopoulou and M. Grigoriu, 12/23/97, (PB98-153422, A11, MF-A03).

NCEER-97-0016 “Evaluation of Seismic Retrofit Methods for Reinforced Concrete Bridge Columns,” by T.J. Wipf, F.W. Klaiber and F.M. Russo, 12/28/97, (PB98-144215, A12, MF-A03).

NCEER-97-0017 “Seismic Fragility of Existing Conventional Reinforced Concrete Highway Bridges,” by C.L. Mullen and A.S. Cakmak, 12/30/97, (PB98-153406, A08, MF-A02).

NCEER-97-0018 “Loss Asssessment of Memphis Buildings,” edited by D.P. Abrams and M. Shinozuka, 12/31/97, (PB98-144231, A13, MF-A03).

NCEER-97-0019 “Seismic Evaluation of Frames with Infill Walls Using Quasi-static Experiments,” by K.M. Mosalam, R.N. White and P. Gergely, 12/31/97, (PB98-153455, A07, MF-A02).

NCEER-97-0020 “Seismic Evaluation of Frames with Infill Walls Using Pseudo-dynamic Experiments,” by K.M. Mosalam, R.N. White and P. Gergely, 12/31/97, (PB98-153430, A07, MF-A02).

NCEER-97-0021 “Computational Strategies for Frames with Infill Walls: Discrete and Smeared Crack Analyses and Seismic Fragility,” by K.M. Mosalam, R.N. White and P. Gergely, 12/31/97, (PB98-153414, A10, MF-A02).

NCEER-97-0022 "Proceedings of the NCEER Workshop on Evaluation of Liquefaction Resistance of Soils," edited by T.L. Youd and I.M. Idriss, 12/31/97, (PB98-155617, A15, MF-A03).

MCEER-98-0001 "Extraction of Nonlinear Hysteretic Properties of Seismically Isolated Bridges from Quick-Release Field Tests," by Q. Chen, B.M. Douglas, E.M. Maragakis and I.G. Buckle, 5/26/98, (PB99-118838, A06, MF-A01).

MCEER-98-0002 "Methodologies for Evaluating the Importance of Highway Bridges," by A. Thomas, S. Eshenaur and J. Kulicki, 5/29/98, (PB99-118846, A10, MF-A02).

MCEER-98-0003 "Capacity Design of Bridge Piers and the Analysis of Overstrength," by J.B. Mander, A. Dutta and P. Goel, 6/1/98, (PB99-118853, A09, MF-A02).

MCEER-98-0004 "Evaluation of Bridge Damage Data from the Loma Prieta and Northridge, California Earthquakes," by N. Basoz and A. Kiremidjian, 6/2/98, (PB99-118861, A15, MF-A03).

MCEER-98-0005 "Screening Guide for Rapid Assessment of Liquefaction Hazard at Highway Bridge Sites," by T. L. Youd, 6/16/98, (PB99-118879, A06, not available on microfiche).

MCEER-98-0006 "Structural Steel and Steel/Concrete Interface Details for Bridges," by P. Ritchie, N. Kauhl and J. Kulicki, 7/13/98, (PB99-118945, A06, MF-A01).

MCEER-98-0007 "Capacity Design and Fatigue Analysis of Confined Concrete Columns," by A. Dutta and J.B. Mander, 7/14/98, (PB99-118960, A14, MF-A03).

MCEER-98-0008 "Proceedings of the Workshop on Performance Criteria for Telecommunication Services Under Earthquake Conditions," edited by A.J. Schiff, 7/15/98, (PB99-118952, A08, MF-A02).

MCEER-98-0009 "Fatigue Analysis of Unconfined Concrete Columns," by J.B. Mander, A. Dutta and J.H. Kim, 9/12/98, (PB99-123655, A10, MF-A02).

MCEER-98-0010 "Centrifuge Modeling of Cyclic Lateral Response of Pile-Cap Systems and Seat-Type Abutments in Dry Sands," by A.D. Gadre and R. Dobry, 10/2/98, (PB99-123606, A13, MF-A03).

MCEER-98-0011 "IDARC-BRIDGE: A Computational Platform for Seismic Damage Assessment of Bridge Structures," by A.M. Reinhorn, V. Simeonov, G. Mylonakis and Y. Reichman, 10/2/98, (PB99-162919, A15, MF-A03).

MCEER-98-0012 "Experimental Investigation of the Dynamic Response of Two Bridges Before and After Retrofitting with Elastomeric Bearings," by D.A. Wendichansky, S.S. Chen and J.B. Mander, 10/2/98, (PB99-162927, A15, MF-A03).

MCEER-98-0013 "Design Procedures for Hinge Restrainers and Hinge Sear Width for Multiple-Frame Bridges," by R. Des Roches and G.L. Fenves, 11/3/98, (PB99-140477, A13, MF-A03).

MCEER-98-0014 "Response Modification Factors for Seismically Isolated Bridges," by M.C. Constantinou and J.K. Quarshie, 11/3/98, (PB99-140485, A14, MF-A03).

MCEER-98-0015 "Proceedings of the U.S.-Italy Workshop on Seismic Protective Systems for Bridges," edited by I.M. Friedland and M.C. Constantinou, 11/3/98, (PB2000-101711, A22, MF-A04).

MCEER-98-0016 "Appropriate Seismic Reliability for Critical Equipment Systems: Recommendations Based on Regional Analysis of Financial and Life Loss," by K. Porter, C. Scawthorn, C. Taylor and N. Blais, 11/10/98, (PB99-157265, A08, MF-A02).

MCEER-98-0017 "Proceedings of the U.S. Japan Joint Seminar on Civil Infrastructure Systems Research," edited by M. Shinozuka and A. Rose, 11/12/98, (PB99-156713, A16, MF-A03).

MCEER-98-0018 "Modeling of Pile Footings and Drilled Shafts for Seismic Design," by I. PoLam, M. Kapuskar and D. Chaudhuri, 12/21/98, (PB99-157257, A09, MF-A02).

MCEER-99-0001 "Seismic Evaluation of a Masonry Infilled Reinforced Concrete Frame by Pseudodynamic Testing," by S.G. Buonopane and R.N. White, 2/16/99, (PB99-162851, A09, MF-A02).

MCEER-99-0002 "Response History Analysis of Structures with Seismic Isolation and Energy Dissipation Systems: Verification Examples for Program SAP2000," by J. Scheller and M.C. Constantinou, 2/22/99, (PB99-162869, A08, MF-A02).

MCEER-99-0003 "Experimental Study on the Seismic Design and Retrofit of Bridge Columns Including Axial Load Effects," by A. Dutta, T. Kokorina and J.B. Mander, 2/22/99, (PB99-162877, A09, MF-A02).

MCEER-99-0004 "Experimental Study of Bridge Elastomeric and Other Isolation and Energy Dissipation Systems with Emphasis on Uplift Prevention and High Velocity Near-source Seismic Excitation," by A. Kasalanati and M. C. Constantinou, 2/26/99, (PB99-162885, A12, MF-A03).

MCEER-99-0005 "Truss Modeling of Reinforced Concrete Shear-flexure Behavior," by J.H. Kim and J.B. Mander, 3/8/99, (PB99-163693, A12, MF-A03).

MCEER-99-0006 "Experimental Investigation and Computational Modeling of Seismic Response of a 1:4 Scale Model Steel Structure with a Load Balancing Supplemental Damping System," by G. Pekcan, J.B. Mander and S.S. Chen, 4/2/99, (PB99-162893, A11, MF-A03).

MCEER-99-0007 "Effect of Vertical Ground Motions on the Structural Response of Highway Bridges," by M.R. Button, C.J. Cronin and R.L. Mayes, 4/10/99, (PB2000-101411, A10, MF-A03).

MCEER-99-0008 "Seismic Reliability Assessment of Critical Facilities: A Handbook, Supporting Documentation, and Model Code Provisions," by G.S. Johnson, R.E. Sheppard, M.D. Quilici, S.J. Eder and C.R. Scawthorn, 4/12/99, (PB2000-101701, A18, MF-A04).

MCEER-99-0009 "Impact Assessment of Selected MCEER Highway Project Research on the Seismic Design of Highway Structures," by C. Rojahn, R. Mayes, D.G. Anderson, J.H. Clark, D'Appolonia Engineering, S. Gloyd and R.V. Nutt, 4/14/99, (PB99-162901, A10, MF-A02).

MCEER-99-0010 "Site Factors and Site Categories in Seismic Codes," by R. Dobry, R. Ramos and M.S. Power, 7/19/99, (PB2000-101705, A08, MF-A02).

MCEER-99-0011 "Restrainer Design Procedures for Multi-Span Simply-Supported Bridges," by M.J. Randall, M. Saiidi, E. Maragakis and T. Isakovic, 7/20/99, (PB2000-101702, A10, MF-A02).

MCEER-99-0012 "Property Modification Factors for Seismic Isolation Bearings," by M.C. Constantinou, P. Tsopelas, A. Kasalanati and E. Wolff, 7/20/99, (PB2000-103387, A11, MF-A03).

MCEER-99-0013 "Critical Seismic Issues for Existing Steel Bridges," by P. Ritchie, N. Kauhl and J. Kulicki, 7/20/99, (PB2000-101697, A09, MF-A02).

MCEER-99-0014 "Nonstructural Damage Database," by A. Kao, T.T. Soong and A. Vender, 7/24/99, (PB2000-101407, A06, MF-A01).

MCEER-99-0015 "Guide to Remedial Measures for Liquefaction Mitigation at Existing Highway Bridge Sites," by H.G. Cooke and J. K. Mitchell, 7/26/99, (PB2000-101703, A11, MF-A03).

MCEER-99-0016 "Proceedings of the MCEER Workshop on Ground Motion Methodologies for the Eastern United States," edited by N. Abrahamson and A. Becker, 8/11/99, (PB2000-103385, A07, MF-A02).

MCEER-99-0017 "Quindío, Colombia Earthquake of January 25, 1999: Reconnaissance Report," by A.P. Asfura and P.J. Flores, 10/4/99, (PB2000-106893, A06, MF-A01).

MCEER-99-0018 "Hysteretic Models for Cyclic Behavior of Deteriorating Inelastic Structures," by M.V. Sivaselvan and A.M. Reinhorn, 11/5/99, (PB2000-103386, A08, MF-A02).

MCEER-99-0019 "Proceedings of the 7th U.S.- Japan Workshop on Earthquake Resistant Design of Lifeline Facilities and Countermeasures Against Soil Liquefaction," edited by T.D. O'Rourke, J.P. Bardet and M. Hamada, 11/19/99, (PB2000-103354, A99, MF-A06).

MCEER-99-0020 "Development of Measurement Capability for Micro-Vibration Evaluations with Application to Chip Fabrication Facilities," by G.C. Lee, Z. Liang, J.W. Song, J.D. Shen and W.C. Liu, 12/1/99, (PB2000-105993, A08, MF-A02).

MCEER-99-0021 "Design and Retrofit Methodology for Building Structures with Supplemental Energy Dissipating Systems," by G. Pekcan, J.B. Mander and S.S. Chen, 12/31/99, (PB2000-105994, A11, MF-A03).

MCEER-00-0001 "The Marmara, Turkey Earthquake of August 17, 1999: Reconnaissance Report," edited by C. Scawthorn; with major contributions by M. Bruneau, R. Eguchi, T. Holzer, G. Johnson, J. Mander, J. Mitchell, W. Mitchell, A. Papageorgiou, C. Scaethorn, and G. Webb, 3/23/00, (PB2000-106200, A11, MF-A03).

MCEER-00-0002 "Proceedings of the MCEER Workshop for Seismic Hazard Mitigation of Health Care Facilities," edited by G.C. Lee, M. Ettouney, M. Grigoriu, J. Hauer and J. Nigg, 3/29/00, (PB2000-106892, A08, MF-A02).

MCEER-00-0003 "The Chi-Chi, Taiwan Earthquake of September 21, 1999: Reconnaissance Report," edited by G.C. Lee and C.H. Loh, with major contributions by G.C. Lee, M. Bruneau, I.G. Buckle, S.E. Chang, P.J. Flores, T.D. O'Rourke, M. Shinozuka, T.T. Soong, C-H. Loh, K-C. Chang, Z-J. Chen, J-S. Hwang, M-L. Lin, G-Y. Liu, K-C. Tsai, G.C. Yao and C-L. Yen, 4/30/00, (PB2001-100980, A10, MF-A02).

MCEER-00-0004 "Seismic Retrofit of End-Sway Frames of Steel Deck-Truss Bridges with a Supplemental Tendon System: Experimental and Analytical Investigation," by G. Pekcan, J.B. Mander and S.S. Chen, 7/1/00, (PB2001-100982, A10, MF-A02).

MCEER-00-0005 "Sliding Fragility of Unrestrained Equipment in Critical Facilities," by W.H. Chong and T.T. Soong, 7/5/00, (PB2001-100983, A08, MF-A02).

MCEER-00-0006 "Seismic Response of Reinforced Concrete Bridge Pier Walls in the Weak Direction," by N. Abo-Shadi, M. Saiidi and D. Sanders, 7/17/00, (PB2001-100981, A17, MF-A03).

MCEER-00-0007 "Low-Cycle Fatigue Behavior of Longitudinal Reinforcement in Reinforced Concrete Bridge Columns," by J. Brown and S.K. Kunnath, 7/23/00, (PB2001-104392, A08, MF-A02).

MCEER-00-0008 "Soil Structure Interaction of Bridges for Seismic Analysis," I. PoLam and H. Law, 9/25/00, (PB2001-105397, A08, MF-A02).

MCEER-00-0009 "Proceedings of the First MCEER Workshop on Mitigation of Earthquake Disaster by Advanced Technologies (MEDAT-1), edited by M. Shinozuka, D.J. Inman and T.D. O'Rourke, 11/10/00, (PB2001-105399, A14, MF-A03).

MCEER-00-0010 "Development and Evaluation of Simplified Procedures for Analysis and Design of Buildings with Passive Energy Dissipation Systems," by O.M. Ramirez, M.C. Constantinou, C.A. Kircher, A.S. Whittaker, M.W. Johnson, J.D. Gomez and C. Chrysostomou, 11/16/01, (PB2001-105523, A23, MF-A04).

MCEER-00-0011 "Dynamic Soil-Foundation-Structure Interaction Analyses of Large Caissons," by C-Y. Chang, C-M. Mok, Z-L. Wang, R. Settgast, F. Waggoner, M.A. Ketchum, H.M. Gonnermann and C-C. Chin, 12/30/00, (PB2001-104373, A07, MF-A02).

MCEER-00-0012 "Experimental Evaluation of Seismic Performance of Bridge Restrainers," by A.G. Vlassis, E.M. Maragakis and M. Saiid Saiidi, 12/30/00, (PB2001-104354, A09, MF-A02).

MCEER-00-0013 "Effect of Spatial Variation of Ground Motion on Highway Structures," by M. Shinozuka, V. Saxena and G. Deodatis, 12/31/00, (PB2001-108755, A13, MF-A03).

MCEER-00-0014 "A Risk-Based Methodology for Assessing the Seismic Performance of Highway Systems," by S.D. Werner, C.E. Taylor, J.E. Moore, II, J.S. Walton and S. Cho, 12/31/00, (PB2001-108756, A14, MF-A03).

MCEER-01-0001 "Experimental Investigation of P-Delta Effects to Collapse During Earthquakes," by D. Vian and M. Bruneau, 6/25/01, (PB2002-100534, A17, MF-A03).

MCEER-01-0002 "Proceedings of the Second MCEER Workshop on Mitigation of Earthquake Disaster by Advanced Technologies (MEDAT-2)," edited by M. Bruneau and D.J. Inman, 7/23/01, (PB2002-100434, A16, MF-A03).

MCEER-01-0003 "Sensitivity Analysis of Dynamic Systems Subjected to Seismic Loads," by C. Roth and M. Grigoriu, 9/18/01, (PB2003-100884, A12, MF-A03).

MCEER-01-0004 "Overcoming Obstacles to Implementing Earthquake Hazard Mitigation Policies: Stage 1 Report," by D.J. Alesch and W.J. Petak, 12/17/01, (PB2002-107949, A07, MF-A02).

MCEER-01-0005 "Updating Real-Time Earthquake Loss Estimates: Methods, Problems and Insights," by C.E. Taylor, S.E. Chang and R.T. Eguchi, 12/17/01, (PB2002-107948, A05, MF-A01).

MCEER-01-0006 "Experimental Investigation and Retrofit of Steel Pile Foundations and Pile Bents Under Cyclic Lateral Loadings," by A. Shama, J. Mander, B. Blabac and S. Chen, 12/31/01, (PB2002-107950, A13, MF-A03).

MCEER-02-0001 "Assessment of Performance of Bolu Viaduct in the 1999 Duzce Earthquake in Turkey" by P.C. Roussis, M.C. Constantinou, M. Erdik, E. Durukal and M. Dicleli, 5/8/02, (PB2003-100883, A08, MF-A02).

MCEER-02-0002 "Seismic Behavior of Rail Counterweight Systems of Elevators in Buildings," by M.P. Singh, Rildova and L.E. Suarez, 5/27/02. (PB2003-100882, A11, MF-A03).

MCEER-02-0003 "Development of Analysis and Design Procedures for Spread Footings," by G. Mylonakis, G. Gazetas, S. Nikolaou and A. Chauncey, 10/02/02, (PB2004-101636, A13, MF-A03, CD-A13).

MCEER-02-0004 "Bare-Earth Algorithms for Use with SAR and LIDAR Digital Elevation Models," by C.K. Huyck, R.T. Eguchi and B. Houshmand, 10/16/02, (PB2004-101637, A07, CD-A07).

MCEER-02-0005 "Review of Energy Dissipation of Compression Members in Concentrically Braced Frames," by K.Lee and M. Bruneau, 10/18/02, (PB2004-101638, A10, CD-A10).

MCEER-03-0001 "Experimental Investigation of Light-Gauge Steel Plate Shear Walls for the Seismic Retrofit of Buildings" by J. Berman and M. Bruneau, 5/2/03, (PB2004-101622, A10, MF-A03, CD-A10).

MCEER-03-0002 "Statistical Analysis of Fragility Curves," by M. Shinozuka, M.Q. Feng, H. Kim, T. Uzawa and T. Ueda, 6/16/03, (PB2004-101849, A09, CD-A09).

MCEER-03-0003 "Proceedings of the Eighth U.S.-Japan Workshop on Earthquake Resistant Design f Lifeline Facilities and Countermeasures Against Liquefaction," edited by M. Hamada, J.P. Bardet and T.D. O'Rourke, 6/30/03, (PB2004-104386, A99, CD-A99).

MCEER-03-0004 "Proceedings of the PRC-US Workshop on Seismic Analysis and Design of Special Bridges," edited by L.C. Fan and G.C. Lee, 7/15/03, (PB2004-104387, A14, CD-A14).

MCEER-03-0005 "Urban Disaster Recovery: A Framework and Simulation Model," by S.B. Miles and S.E. Chang, 7/25/03, (PB2004-104388, A07, CD-A07).

MCEER-03-0006 "Behavior of Underground Piping Joints Due to Static and Dynamic Loading," by R.D. Meis, M. Maragakis and R. Siddharthan, 11/17/03.

MCEER-03-0007 "Seismic Vulnerability of Timber Bridges and Timber Substructures," by A.A. Shama, J.B. Mander, I.M. Friedland and D.R. Allicock, 12/15/03.

MCEER-04-0001 "Experimental Study of Seismic Isolation Systems with Emphasis on Secondary System Response and Verification of Accuracy of Dynamic Response History Analysis Methods," by E. Wolff and M. Constantinou, 1/16/04.

MCEER-04-0002 "Tension, Compression and Cyclic Testing of Engineered Cementitious Composite Materials," by K. Kesner and S.L. Billington, 3/1/04.

MCEER-04-0003 "Cyclic Testing of Braces Laterally Restrained by Steel Studs to Enhance Performance During Earthquakes," by O.C. Celik, J.W. Berman and M. Bruneau, 3/16/04.

MCEER-04-0004 "Methodologies for Post Earthquake Building Damage Detection Using SAR and Optical Remote Sensing: Application to the August 17, 1999 Marmara, Turkey Earthquake," by C.K. Huyck, B.J. Adams, S. Cho, R.T. Eguchi, B. Mansouri and B. Houshmand, 6/15/04.

MCEER-04-0005 "Nonlinear Structural Analysis Towards Collapse Simulation: A Dynamical Systems Approach," by M.V. Sivaselvan and A.M. Reinhorn, 6/16/04.

MCEER-04-0006 "Proceedings of the Second PRC-US Workshop on Seismic Analysis and Design of Special Bridges," edited by G.C. Lee and L.C. Fan, 6/25/04.

MULTIDISCIPLINARY CENTER FOR EARTHQUAKE ENGINEERING RESEARCH

A National Center of Excellence in Advanced Technology Applications

University at Buffalo, State University of New York
Red Jacket Quadrangle ▪ Buffalo, New York 14261
Phone: (716) 645-3391 ▪ Fax: (716) 645-3399
E-mail: *mceer@mceermail.buffalo.edu* ▪ WWW Site *http://mceer.buffalo.edu*

University at Buffalo *The State University of New York*